Modeling Pile Behavior in Large Pile Groups under Lateral Loading

by

Andrew M. Dodds and Geoffrey R. Martin

NOTICE

Modeling Pile Behavior in Large Pile Groups Under Lateral Loading

by

Andrew M. Dodds[1] and Geoffrey R. Martin[2]

1   Senior Project Engineer, Golder Associates, Inc.; Formerly Project Engineer, Earth Mechanics, Inc.
2   Professor, Department of Civil Engineering, University of Southern California

MCEER
University at Buffalo, The State University of New York
Red Jacket Quadrangle, Buffalo, NY 14261
Phone: (716) 645-3391; Fax (716) 645-3399
E-mail: *mceer@buffalo.edu*; WWW Site: *http://mceer.buffalo.edu*

Preface

The Multidisciplinary Center for Earthquake Engineering Research (MCEER) is a national center of excellence in advanced technology applications that is dedicated to the reduction of earthquake losses nationwide. Headquartered at the University at Buffalo, State University of New York, the Center was originally established by the National Science Foundation in 1986, as the National Center for Earthquake Engineering Research (NCEER).

Comprising a consortium of researchers from numerous disciplines and institutions throughout the United States, the Center's mission is to reduce earthquake losses through research and the application of advanced technologies that improve engineering, pre-earthquake planning and post-earthquake recovery strategies. Toward this end, the Center coordinates a nationwide program of multidisciplinary team research, education and outreach activities.

MCEER's research is conducted under the sponsorship of two major federal agencies, the National Science Foundation (NSF) and the Federal Highway Administration (FHWA), and the State of New York. Significant support is also derived from the Federal Emergency Management Agency (FEMA), other state governments, academic institutions, foreign governments and private industry.

The Center's Highway Project develops improved seismic design, evaluation, and retrofit methodologies and strategies for new and existing bridges and other highway structures, and for assessing the seismic performance of highway systems. The FHWA has sponsored three major contracts with MCEER under the Highway Project, two of which were initiated in 1992 and the third in 1998.

Of the two 1992 studies, one performed a series of tasks intended to improve seismic design practices for new highway bridges, tunnels, and retaining structures (MCEER Project 112). The other study focused on methodologies and approaches for assessing and improving the seismic performance of existing "typical" highway bridges and other highway system components including tunnels, retaining structures, slopes, culverts, and pavements (MCEER Project 106). These studies were conducted to:

- assess the seismic vulnerability of highway systems, structures, and components;
- develop concepts for retrofitting vulnerable highway structures and components;
- develop improved design and analysis methodologies for bridges, tunnels, and retaining structures, which include consideration of soil-structure interaction mechanisms and their influence on structural response; and
- develop, update, and recommend improved seismic design and performance criteria for new highway systems and structures.

The 1998 study, "Seismic Vulnerability of the Highway System" (FHWA Contract DTFH61-98-C-00094; known as MCEER Project 094), was initiated with the objective of performing studies to improve the seismic performance of bridge types not covered under Projects 106 or 112, and to provide extensions to system performance assessments for highway systems. Specific subjects covered under Project 094 include:

- development of formal loss estimation technologies and methodologies for highway systems;
- analysis, design, detailing, and retrofitting technologies for special bridges, including those with flexible superstructures (e.g., trusses), those supported by steel tower substructures, and cable-supported bridges (e.g., suspension and cable-stayed bridges);
- seismic response modification device technologies (e.g., hysteretic dampers, isolation bearings); and
- soil behavior, foundation behavior, and ground motion studies for large bridges.

In addition, Project 094 includes a series of special studies, addressing topics that range from non-destructive assessment of retrofitted bridge components to supporting studies intended to assist in educating the bridge engineering profession on the implementation of new seismic design and retrofitting strategies.

Large pile groups were examined using a three-dimensional finite-difference based numerical modeling approach. The specific case of a large pile group subject to only translational loading at the groundline was considered. Research efforts focused on local pile-soil interaction using p-y curves as the primary assessment tool and p-multipliers to characterize group effects. Rationalization of a large pile group into a two-pile in-line configuration and a single pile with periodic boundaries was undertaken, representing typical leading and immediately trailing piles, and internal piles, respectively. Factors considered were: (a) soil type; (b) pile type; (c) initial soil stress states; (d) pile head restraint; and (e) pile spacing. Isolated pile models provided a benchmark for both the in-line and periodic models. A total of 30 analyses were completed. Overall, the large pile group study indicated that initial stress state, pile type and pile head restraint resulted in some differences, but these were relatively weak compared with the influence of soil behavior and movement. Marked decreases in lateral resistance for interior piles were attributed to the different stiffness and strength characteristics of the soil models, and effects resulting from the boundary conditions employed. Much lower p-multipliers compared with current small pile group recommendations are therefore recommended for large pile groups, implying a comparatively softer translational stiffness for design. Various related issues such as installation effects, pile, pile head and soil conditions require further research.

ABSTRACT

Large pile groups, defined as pile groups containing a large number of closely spaced vertical piles, were examined using a three-dimensional finite-difference based numerical modeling approach. The specific case of a large pile group subject to only translational loading at the groundline was considered, assuming that a rigid pile cap, whose base is located at the groundline, was present to enforce equal horizontal displacements of all pile heads. Research efforts focused on local pile-soil interaction using *p-y* curves as the primary assessment tool and *p*-multipliers to characterize group effects. Analysis efforts were preceded by an extensive review on lateral pile-soil interaction to provide an assessment of the existing state of knowledge, and a critical review of the three-dimensional modeling approach in terms of its formulation and application to simulating laterally loaded piles and pile groups.

Rationalization of a large pile group into a two-pile in-line configuration and a single pile with periodic boundaries was undertaken for the purpose of the research, representing typical leading and immediately trailing piles, and internal piles, respectively. Factors considered were: (a) soil type; (b) pile type; (c) initial soil stress states; (d) pile head restraint; and (e) pile spacing. Isolated pile models provided a benchmark for both the in-line and periodic models. A total of 30 analyses were completed.

Overall, the large pile group study indicated that initial stress state, pile type and pile head restraint resulted in some differences, but these were relatively weak compared with the influence of soil behavior and movement. Marked decreases in lateral resistance for interior piles were attributed to the different stiffness and strength characteristics of the soil models, and effects resulting from the boundary conditions employed. Much lower *p*-multipliers compared with current small pile group recommendations are therefore recommended for large pile groups, implying a comparatively softer translational stiffness for design. While the study enabled greater insight into the mechanics of large pile group lateral stiffness, various issues such as installation effects, pile, pile head and soil conditions remain, ensuring that the task of assessing lateral group stiffness remains a challenging endeavor.

TABLE OF CONTENTS

LIST OF ILLUSTRATIONS

LIST OF TABLES

SECTION 1
INTRODUCTION

1.1   Background

Piled foundations are most often designed in a group configuration, and piled foundations that support long span bridges are no exception. Such a foundation configuration typically contains a large number of closely spaced piles cast into a substantial pile cap, referred to here as a "large pile group." In the case of a large pile group, the individual responses of piles within the group are certainly influenced by the presence and actions of neighboring piles, and thus pile group effects become an important design consideration. For lateral load design of long span bridges, such as is required for seismic loading, it is a question of how to adequately characterize this group interaction and the effect it has on the lateral stiffness of the foundation group as a whole.

An example of a large pile group is given in Figure 1-1, used as a foundation component for the support of the Vincent Thomas Bridge located in Los Angeles, California. The "forest" of piles apparent is a distinct feature of large pile groups, and while a reasonable understanding of the basic mechanisms and issues involved with single pile and small pile group (up to 16 piles) lateral load behavior is emerging (e.g., Reese and Van Impe, 2001), very limited knowledge on the behavior of large pile groups exists. Field data is lacking given that full-scale load testing is obviously not feasible, and instrumentation of constructed large pile groups rare. Model tests in the laboratory or centrifuge has offered some insight, but these are few in number, group configurations are still limited in size, and interpretation of results marred by scaling issues and lack of case histories validating the observed behavior. Given there are no specific design procedures for large pile groups (Law and Lam, 2001), current practice is therefore forced to rely mainly on numerical predictions to assess large pile group behavior, with the knowledge gained from testing and analysis of single piles and small pile groups providing some guidance in terms of behavioral trends.

Performing numerical predictions of lateral pile-soil behavior has seen the use of the discrete load-transfer method, employing p-y curves to simulate soil response and representing a pile as a discretized line element, emerge as a practicable means of analysis. This approach is popular in design practice, offering the effectiveness of p-y curves in simulating the non-linear behavior of soil, and versatility given the relative ease in which adjustment factors such as p-multipliers and y-multipliers can be incorporated to assess group effects. In the case of small pile groups, the growing pool of instrumented field and centrifuge tests are consolidating the state of p-y multiplier knowledge (e.g., Zhang and McVay, 1999; Mokwa and Duncan, 2001). However, in the case of large pile groups, the current lack of empirical knowledge requires that recourse to numerical models is the only feasible means of developing appropriate p-y multipliers for use in design.

In terms of research, the fundamental nature of the laterally loaded pile problem is three-dimensional, demanding the use of three-dimensional numerical models in order to properly assess behavior. Previous numerical studies of this nature indicate that such a numerical approach is capable of providing a realistic assessment of pile-soil behavior, thus allowing a rational means for assessing the mechanics at play. Furthermore, the utility of three-dimensional models to perform "instrumented" lateral load tests similar to those undertaken in the field has been demonstrated, enabling an assessment of p-y characteristics that can be applied to their empirical counterparts. Assessment of pile groups in this way is restricted from a computational standpoint, but employment of modeling economies can relieve the computational burden. Law and Lam (2001) applied such a technique for the specific case of large pile groups, and this preliminary work initiated the current research.
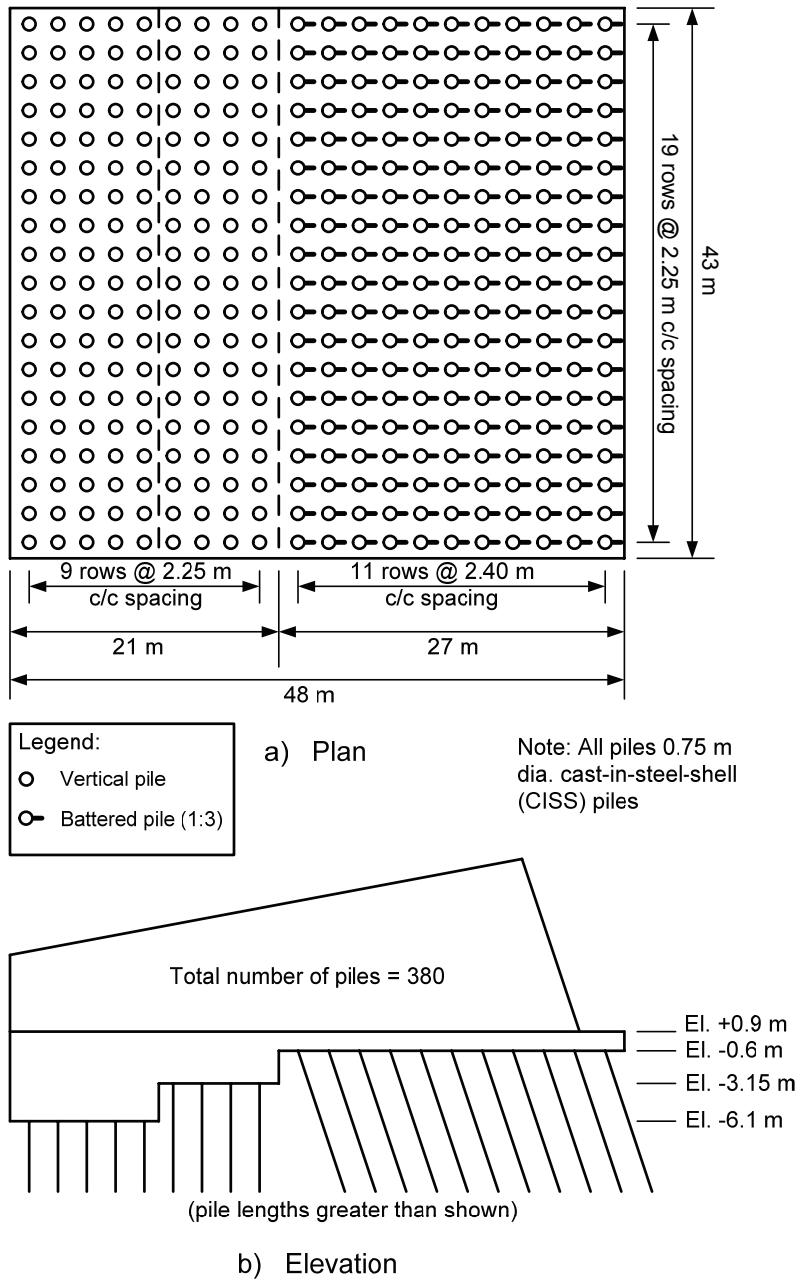
Figure 1-1: Example of a large pile group

The current research was performed as part of the highway research project "Seismic Vulnerability of the Highway System," a Federal Highway Administration sponsored project administered through the Multidisciplinary Center for Earthquake Engineering Research (MCEER). Research efforts were conducted as doctoral studies undertaken by Andrew Dodds under the supervision of Dr. Geoffrey R. Martin at the University of Southern California, Los Angeles, California. The doctoral dissertation produced from these research efforts (Dodds, 2005) provided the basis for the information provided in the immediate report.

1.2   Scope and Objectives

The lack of design guidance and quantitative information on large pile groups prompted the numerical approach undertaken here. Idealized numerical pile-soil models depicting the behavior of piles within a group are used to rationalize large pile group behavior. $FLAC^{3D}$, a three-dimensional computer program with nonlinear geometric and material capabilities (Itasca, 1997), provides the analysis means for such purposes. Analysis efforts are preceded by extensive reviews on lateral pile-soil interaction to provide an assessment of the existing state of knowledge, and a critical review of $FLAC^{3D}$ in terms of its formulation and application to simulating laterally loaded piles and pile groups.

Given the relative success and prevalence of p-y curves, emphasis on determination of appropriate p-y multipliers for a given pile spacing is considered as the most appropriate means to characterize group behavior. Research efforts therefore focus on local pile-soil interaction using p-y curves as the primary assessment tool and p-multipliers to characterize group effects. The group models represent square or rectangular pile groups of vertical piles equally spaced in each orthogonal direction, and a respective isolated pile model is also considered in order to establish p-multipliers. Factors considered include pile spacing, pile-head conditions, initial stress states of the soil, pile type, and soil type. Comparison with empirical p-multipliers is also made in order to assess the numerical findings in the context of design practice.

The research will help address the current lack of design guidance and quantitative information on large pile groups, and help clarify issues surrounding large pile group behavior. The ultimate objective is to improve the characterization of large pile group foundation systems based on an understanding of the mechanics of interaction. In doing so, the research will serve the need of designers involved with the design of vast piled foundations, such as used with long span bridges.

1.3   Organization of Report

The report comprises seven sections that form the body of the report, and two appendices that tabulate pile group observations for ease of reference (Appendix A), and information on constitutive models used to model soil behavior (Appendix B). The body of the report is organized in a progressive fashion such that information in each section generally serves as background information for subsequent sections.

Sections 2 and 3 present a comprehensive review of pile-soil interaction from both theoretical and empirical perspectives. Single pile response to lateral loading is considered in Section 2, beginning with an essentially historical account of numerical developments from linear subgrade reaction approaches through to the more sophisticated continuum approaches in the form of boundary element and finite element pile-soil models. Insights afforded by each approach are discussed throughout. This is followed by a review of the more empirical-based discrete load-transfer approach utilizing p-y curves, documenting the development of the approach and the various p-y curve formulations in existence. Discussion of various issues affecting p-y curve formulations completes the review of single pile response.

Section 3 discusses pile group effects under lateral loading, beginning with elastic-based interaction and the insights afforded by this approach. Attention is then turned to observation-based interaction that encompasses the p-y analysis framework using p-y multipliers to assess group effects. Insights gleaned from field and centrifuge testing are discussed and supplemented by detailed summaries of key field and centrifuge tests as tabulated in Appendix A. Latest p-multiplier design recommendations are then presented. A review of past three-dimensional modeling work follows, discussing the insights gained and merits of using such an approach. Identification and discussion of various group-related p-y issues completes the section, including a final brief commentary on design approaches.

Section 4 introduces the three-dimensional numerical modeling technique chosen to undertake the research analyses, namely $FLAC^{3D}$ (Itasca, 1997). Given the unique formulation of $FLAC^{3D}$ and its relative infancy compared with finite elements, a detailed explanation of the formulation is provided. Important concepts and formulation aspects of $FLAC^{3D}$ are discussed using physical analogies and comparisons to aid in the understanding of its modus operandi. Specific details on the component providing separation and sliding capabilities at the interface of the pile and soil are also included. Important information regarding the application of $FLAC^{3D}$ to the research completes the section.

Section 5 documents a most essential component of the research, namely the verification, validation and calibration of $FLAC^{3D}$ for the purpose of the research undertaken. Procedures developed to justify the pile-soil model configurations used in the research models are described and results reported. Findings are deliberated in relation to the research intentions of assessing large pile group effects, identifying restrictions and particular analysis procedures required when undertaking lateral pile analyses with $FLAC^{3D}$. Limitations of $FLAC^{3D}$ are also addressed.

Section 6 describes the research approach and presents research results. The research methodology is first explained followed by details on pile-soil parameters, configurations and analysis factors adopted (soil model details are provided in Appendix B). Procedures developed for data integrity and data interpretation purposes are then described. Typical results are then presented to illustrate the behavioral trends identified from the research models, and indicate the magnitude of group effects relative to isolated pile behavior.

Section 7 provides a critical discussion of the research results and the conclusions that can be drawn from them. Recommendations for large pile group *p*-multipliers to be used in design are then presented, followed by recommendations for future studies and research.

SECTION 2
SINGLE PILE BEHAVIOR

2.1   Introduction

When a pile is subjected to lateral loading, the interaction that ensues between the pile and the surrounding soil is a topic replete with issues. The nature of soil is an obvious source of complexity, but so too are the pile and the dependence of its behavior on the nature of the soil present. Introduction of other piles nearby, or in other words consideration of pile groups, provides further complexity through pile-soil-pile interaction and the physical repercussions of the group configuration. Further modification is possible due to construction-related issues such as the installation process, and this is to say nothing of other factors that can affect lateral response, such as the pile head fixity.

In answer to these various issues a basic framework of mathematical models supplemented with empirical rules has emerged. Playing a key role has been the understanding of single pile behavior, serving to identify both general pile-soil interaction issues as well as providing a benchmark from which group behavior can be assessed. Single pile behavior will therefore be reviewed in the current section, followed by a review of lateral group effects in the next section.

2.2   Linear Subgrade Reaction Theory

The response of an isolated, single pile to lateral loading is a typical soil-structure interaction problem whereby appreciation of both components and their dependence on each other is required in order to properly assess behavior. This basic need to consider the properties of both the soil and pile combined is epitomized by the classical beam-on-elastic-foundation problem as illustrated in Figure 2-1.
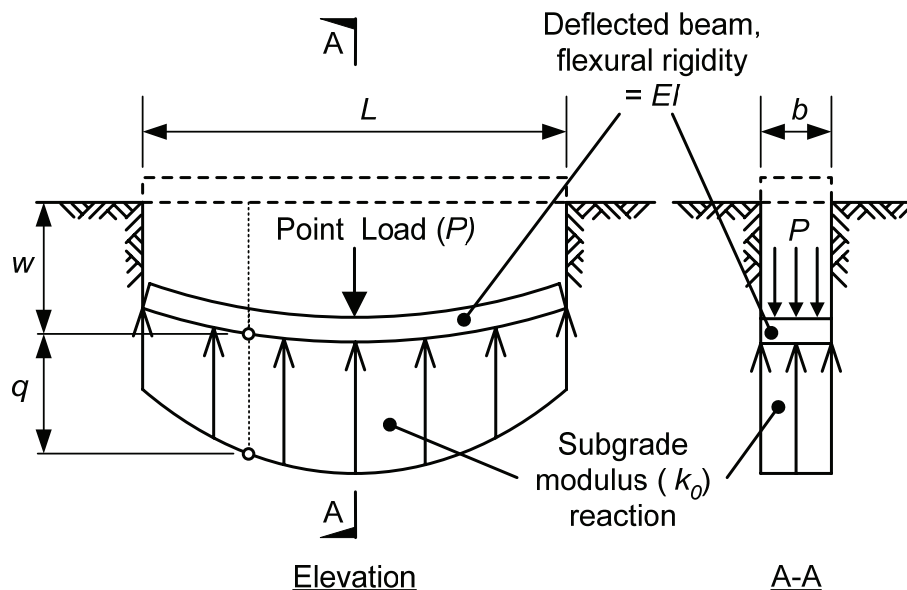
Figure 2-1:   Beam-on-elastic-foundation problem (after Terzaghi, 1955)

Idealizing the soil foundation as a Winkler foundation, consisting of a bed of infinitely closely spaced, independent springs each possessing a linear vertical pressure q per unit area versus vertical deflection w relationship as follows,

$$\frac{q}{w} = k_0 \ \text{ or } \ \frac{qb}{w} = k \tag{2.1}$$

where $k_0 =$ subgrade modulus (FL^{-3} dimensions),

$b =$ width of beam,

$k =$ subgrade modulus for beam (FL^{-2} dimensions),

the general deflection solution for such a case is

$$w = \left(C_1 \cos \lambda x + C_2 \sin \lambda x\right)e^{\lambda x} + \left(C_3 \cos \lambda x + C_4 \sin \lambda x\right)e^{-\lambda x} \tag{2.2}$$

where C_1 through $C_4 =$ constants, and

$\lambda = \sqrt[4]{\dfrac{k}{4EI}}$ (L^{-1} dimensions).

The parameter λ is dependent on the properties of both the "soil" and beam, and its reciprocal represents a characteristic length of the soil-beam system. In this way λ defines the interaction of the soil and beam: If the beam is very stiff compared with the soil then the characteristic length is large and a load applied to the beam will cause vertical deflections of the soil for a considerable distance from the point of load application; conversely, a beam that is very soft compared with the soil (i.e., a very stiff soil) will result in a small characteristic length and only cause vertical deflections in the immediate vicinity of the point load (Scott, 1981). Although use of subgrade reaction theory to depict soil is far removed from real soil behavior, identification of λ as an interactive measure dependent on the relative stiffness of the soil and structure, and in turn the dependency of behavior on such a measure, is a fundamental aspect of soil-structure interaction.

In the context of laterally loaded piles, the dependence of behavior on relative stiffness has resulted in the need to distinguish between "short" (rigid) and "long" (flexible) piles. These definitions acknowledge a somewhat intuitive sense of pile behavior whereby a very short and relatively stiff pile (e.g., a fence strainer-post) would be expected to deflect in a rigid manner when laterally loaded, whereas a very long pile in the same situation would be expected to exhibit a different type of behavior due to the increased embedment and accompanying fixity that this implies. Reese (1986) discussed this dependence of lateral behavior on pile length, noting that short piles can deflect a large amount at the groundline given movement of the pile tip, but with increasing depth of penetration the soil resistance at the pile tip increases until a point is reached at which groundline deflection reaches a limiting value. This type of behavior is depicted in Figure 2-2 for the case of both lateral load (P_t) and moment (M_t) applied at the groundline, assuming an elastic ($E_p I_p$) pile model and constant horizontal subgrade modulus (k_h) soil model. As shown, a so called "critical length" l_c exists, beyond which any additional pile length has no further influence on the pile head response.

6
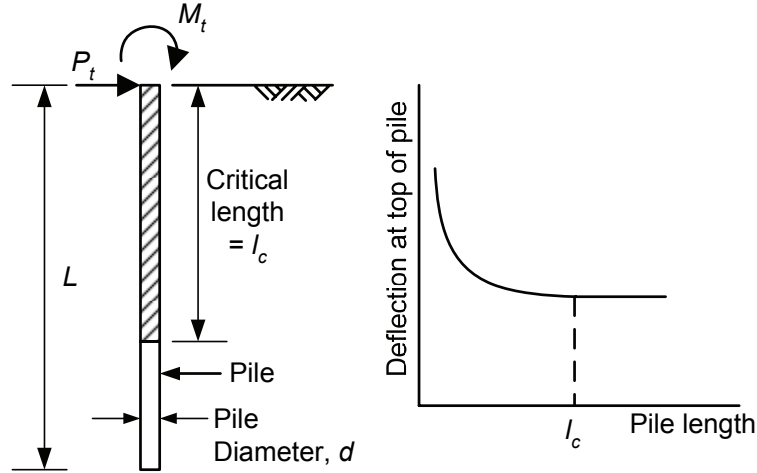
Figure 2-2: Critical length for a laterally loaded pile (after Reese and Van Impe, 2001)

Thus a flexible pile is defined as a pile whose length equals or exceeds its critical length. In subgrade reaction terms such critical lengths have been established for the case of a horizontal subgrade modulus (k_h) that is constant with depth (as in Figure 2-2), in which case

$$l_c = \frac{4}{\lambda} \tag{2.3}$$

where $\lambda = \sqrt[4]{\dfrac{k_h}{4 E_p I_p}}$,

k_h = subgrade modulus for pile (FL^{-2} dimensions),

E_p = Young's modulus for pile,

I_p = Second moment of area for pile,

and for the case of a horizontal subgrade modulus increasing linearly with depth, in which case

$$l_c = 4T \tag{2.4}$$

where $T = \sqrt[5]{\dfrac{E_p I_p}{n_h}}$,

n_h = constant of horizontal subgrade reaction (FL^{-3} dimensions), given

$k_h = n_h z$ (FL^{-2} dimensions), where z = depth.

While these critical length values are subject to the limitations inherent in idealizing the pile-soil system in such a simplistic way, the concept of a critical length is nevertheless of general validity and acknowledges the dependence of lateral behavior on a certain mobilized depth of soil that may or may not extend the entire length of the pile. As a comment aside, this physical attribute of lateral behavior is also suggestive of some form of normalization, an early example of which was the non-dimensional linear solutions derived by Matlock and Reese (1960) using principles of dimensional analysis.

7

The initial preference towards subgrade reaction theory to assess lateral pile-soil interaction was understandable given that readily obtainable solutions were possible, but the selection of an appropriate subgrade modulus presented a real problem. Terzaghi (1955) expressed such concern in the now classic paper that serves as a reminder of both the basic limitations involved with subgrade reaction theory, and the difficulty of obtaining an appropriate value for the subgrade modulus. Besides his all-important remark that the theory was only approximately valid for pile-soil contact pressures less than about one-half the ultimate bearing capacity of the soil under lateral load, Terzaghi also emphasized the importance of soil type and the dimensions of the pile. These issues were considered as shown in Figure 2-3, where stiff (overconsolidated) clay and sand subgrade characteristics were idealized by constant and linearly increasing subgrade reaction models respectively, and pile dimensions were addressed utilizing the notion of differing horizontal pressure bulbs mobilized by different pile widths. These simple ideas underlined the need to appreciate both the different deformation characteristics of soils, and possible size effects due to differing volumes of the surrounding soil mass being affected by different loaded areas.

The issue of flexural rigidity of a structure, such as a pile, and its effect on the subgrade modulus was only briefly mentioned by Terzaghi (1955), and only then in the context of theoretical work. Rowe (1956), on the other hand, specifically pursued the response of a laterally loaded single pile in real sand and noted significant differences in the back-calculated values of subgrade modulus depending on whether the pile was considered to be rigid or flexible. Though weakened somewhat by use of some data from scaled-down 1g laboratory pile-soil models and thus subject to scaling errors, this work by Rowe was of particular value given that it utilized subgrade reaction theory in conjunction with experimentally observed data. In doing so it served to demonstrate the highly variable nature of the subgrade modulus during lateral loading as a result of the actual nonlinear interplay between pile and soil. This resulted in a rather convoluted analysis procedure, relying on various assumptions and approximations in order to adapt the underlying subgrade reaction theory to agree with observed behavior.

That subgrade reaction theory is limited from both a physical and theoretical point of view is a fact that has long been recognized: Terzaghi himself expressed reservations in publishing his 1955 paper and only did so after numerous requests (Reese, 1986). Jamiolkowski and Garassino (1977) acknowledged this limitation in their review of soil moduli for laterally loaded piles, noting the important observation made earlier by McClelland and Focht (1958a) that the subgrade modulus is not a property exclusively of the soil, but simply a convenient mathematical parameter that expresses the ratio of soil reaction to pile deflection. In doing so, such a parameter depends on the characteristics of the pile (i.e., pile geometry, flexural rigidity, boundary conditions at the top and bottom of the pile, etc.), the soil, and the manner in which the pile and soil characteristics change with the level of lateral loading applied.

In response to this complex state of affairs, two general categories of design approaches for single piles have emerged: a) Those that retain the basic qualities of subgrade reaction theory in the form of discrete, nonlinear load-transfer mechanisms along the pile length depicting the soil reaction to pile deflection relationship; and b) those that represent the soil as a continuum. These approaches will be referred to here as the Discrete Load-Transfer and Continuum approaches, respectively. Prior to discussing these approaches, however, mention must also be made of limit equilibrium approaches, exemplified by the work of Broms (1964a, 1964b, 1965). This type of approach, representing a limit analysis, is confined to ultimate (failure) conditions where reasonable assumptions of lateral soil pressures can be made and solutions readily found by use of the equations of statics. While largely redundant now given the versatility and capabilities of the continuum and discrete load-transfer approaches, a brief account of the work of Broms will be given as it provides an instructive account of lateral soil-pile interaction and is an appropriate precursor to the more advanced continuum and discrete load-transfer approaches.

a) Soil type:

y = lateral deflection

Deflected pile

Idealized distribution of soil resistance

Stiff (Overconsolidated) Clay   Sand

Horizontal pressure bulbs mobilized
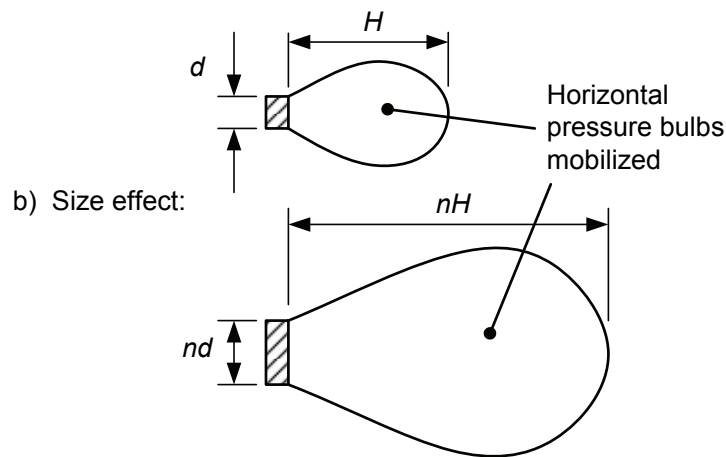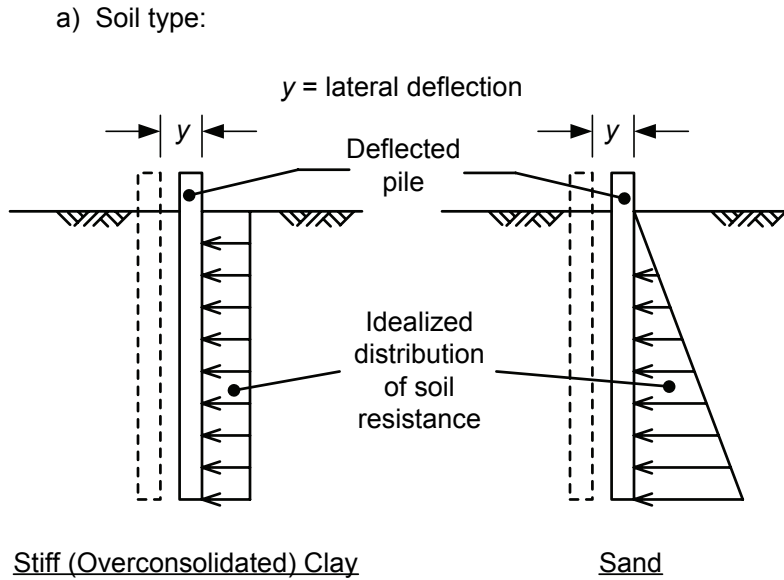
b) Size effect:

Figure 2-3: Idealized soil type and size effects (after Terzaghi, 1955)

2.3   Broms Design Method

Restricting his work to driven piles, Broms (1964a, 1964b) presented methods for the design of laterally loaded piles in uniform soil profiles consisting of cohesive ("clay") and cohesionless ("sand") material, and for unrestrained (free-head) and restrained (fixed-head) pile-head conditions. In doing so, failure modes involving either the pile (formation of plastic hinges) or the soil (mobilization of ultimate lateral resistance) were proposed for short and long piles as shown in Figure 2-4. These failure modes recognized the relative importance of either pile or soil strength in governing the ultimate capacity of long or short piles, respectively.

In considering the ultimate lateral soil pressures acting against a laterally loaded pile, Broms (1964a, 1964b) considered the general behavior at ultimate conditions to be as shown in Figure 2-5. This depicts different deformation patterns of the soil in front of the laterally loaded pile depending on depth: Soil

9

towards the surface exhibits upwards movement, while soil at depth only moves horizontally around the pile. Also, separation of the soil from the back of the deflected pile is shown for the cohesive soil case, while downwards movement of soil to fill the gap created at the back of the deflected pile is depicted for the cohesionless case. Such kinematic behavior indicates the need to distinguish between surficial and at-depth soil resistance because of the relative freedom of soil near the surface to move upwards when loaded horizontally. Consequently, the surficial soil offers lesser resistance compared with the resistance at-depth which is derived from only horizontal movement as a result of overburden weight suppressing any upward movement. Both resistances are three-dimensional in nature, as is the soil behavior at the back of the pile, reminding one that lateral pile behavior is a consequence of soil resistance mechanisms that vary around, as well as along, the pile.
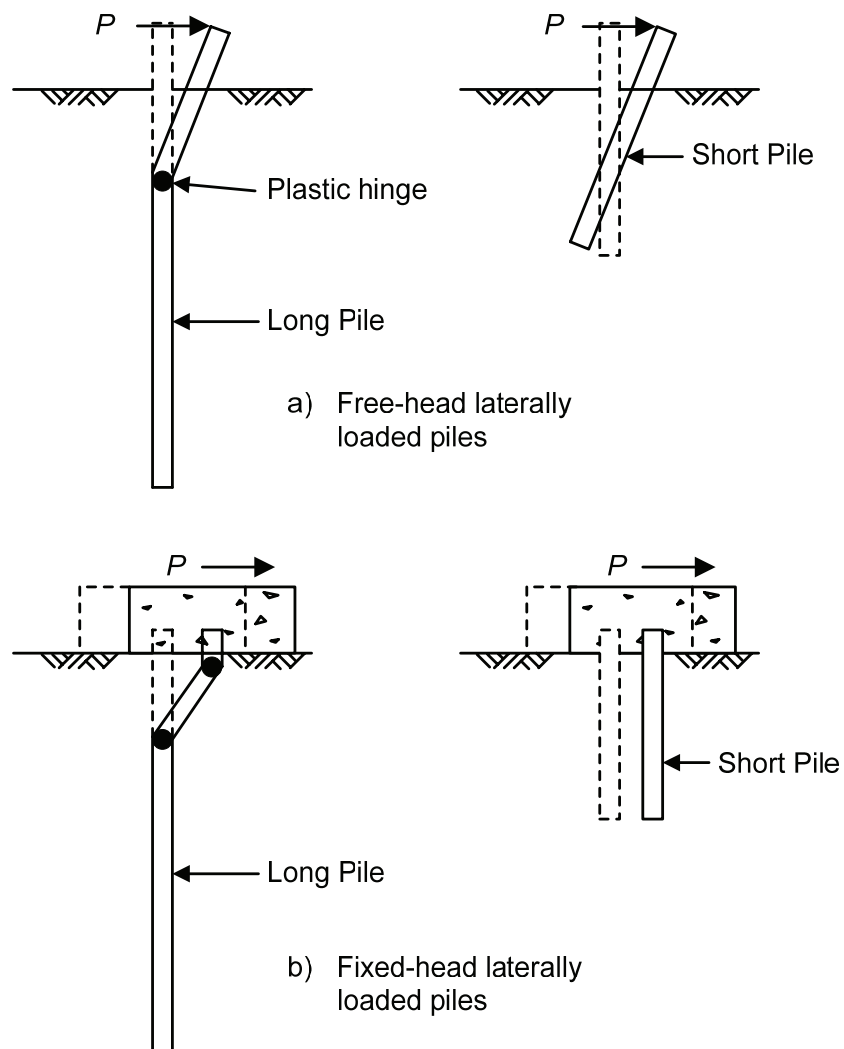
Figure 2-4: Failure modes proposed for short and long piles (after Broms, 1964a, 1964b)
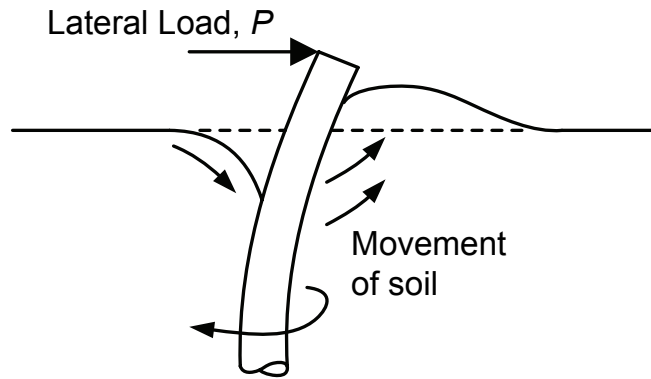
a) Ultimate behavior for
cohesionless (sand) conditions
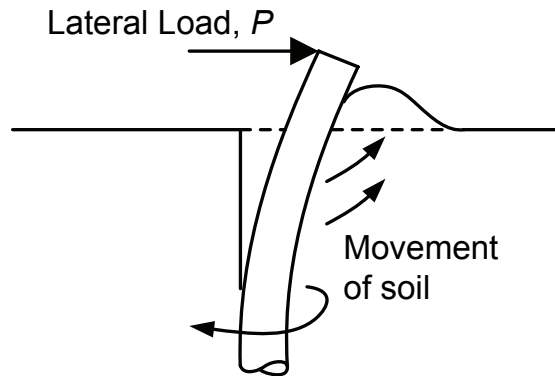
b) Ultimate behavior for
cohesive (clay) conditions

Figure 2-5: General behavior for ultimate conditions (after Broms, 1964a, 1964b)

In addition to ultimate behavior, Broms (1964a, 1964b) considered design at working loads and made some other noteworthy observations. As deflection was considered to govern working load design, linear subgrade reaction theory was utilized to produce dimensionless groundline lateral deflection versus dimensionless length plots for restrained and unrestrained pile-head conditions. These are shown in Figure 2-6 for a lateral load P applied at the groundline only, for both "cohesive" (constant subgrade modulus = k_h) and "cohesionless" (linearly increasing subgrade modulus = $n_h z$) soil conditions. Immediately apparent is the significant reduction in lateral deflection as a result of restraining the pile-head.

11
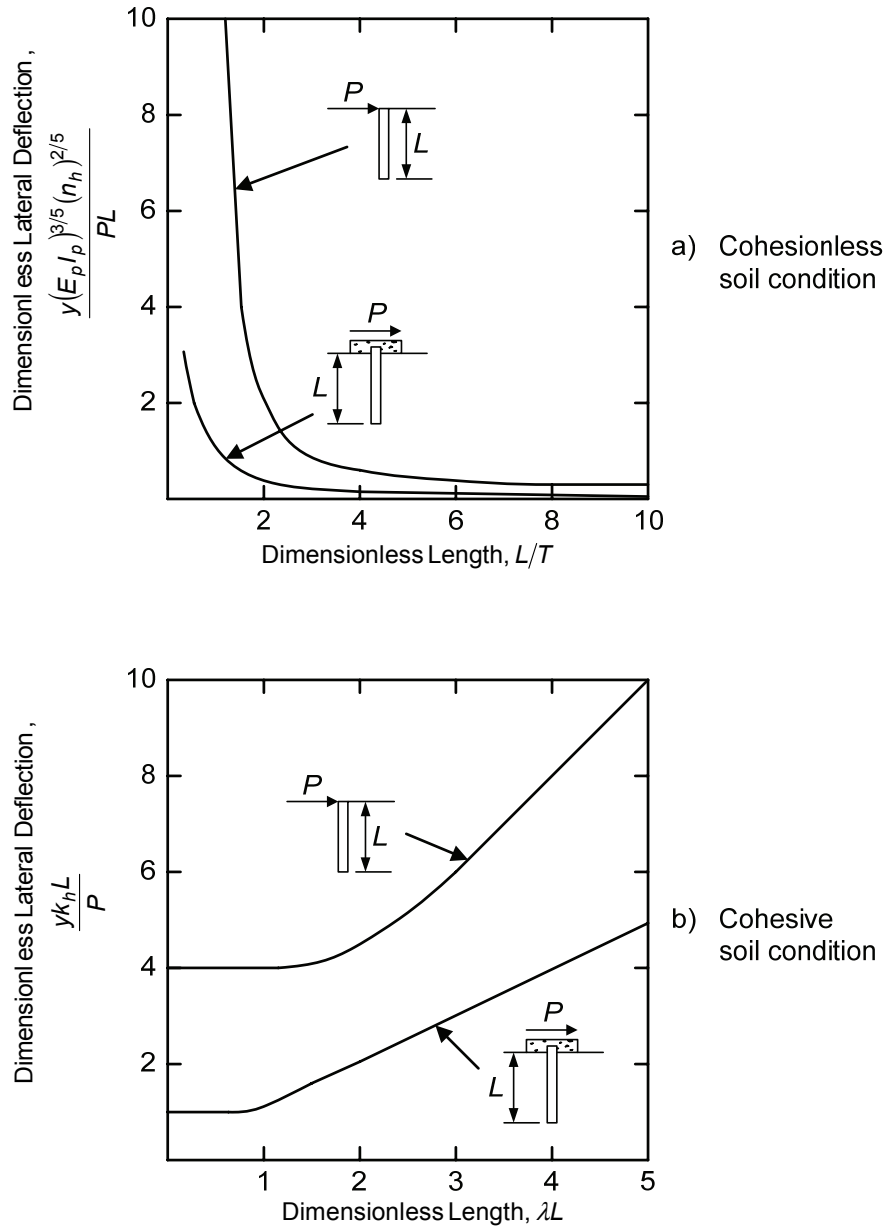
Figure 2-6: Broms (1964a, 1964b) lateral deflection design charts

Based on deflection behavior, rigid and flexible piles were as defined in Table 2-1.

Table 2-1: Rigid and flexible pile criteria from Broms (1964a, 1964b)

Soil Condition	Rigid Pile Criteria		Flexible Pile Criteria	
	Free-Head	**Fixed-Head**	**Free-Head**	**Fixed-Head**
Cohesive	$\lambda L < 1.5$	$\lambda L < 0.5$	$\lambda L > 2.5$	$\lambda L > 1.5$
Cohesionless	$L/T < 2.0$		$L/T > 4.0$	

12

In connection with this deflection behavior, reference was made to a "critical depth" for the cohesive soil condition case, in that the subgrade reaction within this depth was considered to control the groundline deflection of the pile. Such critical depths equal to dimensionless depths (λL) of 2.0 and 1.0 were given for fixed-head and free-head piles respectively, based on the observation from Figure 2-6(b) that groundline deflections at these lengths are approximately the same as those assuming the pile is long (within 10%). This indicates that the way lateral soil resistance is mobilized is a function of the deflected shape of a pile, and the reduced deflection of a fixed-head pile compared with a similarly loaded free-head pile is due in part to the greater depth of soil mobilized by the deflected shape.

The work of Broms (1964a, 1964b) and subsequent design summary (Broms, 1965) provided greater insight into lateral pile-soil interaction with the use of suitable models and reasonable assumptions. Practicably, its use in the design of rigid piles was widespread (Allen, 1985) and capable application to the design of drilled shafts demonstrated (Kulhawy and Chen, 1995). Nevertheless, the approach required the assignment of problems into particular categories that necessarily approximate behavior, and with the advent of computer technology analytical improvements were possible (Matlock and Grubbs, 1965). One such improvement was to model the soil using elasticity and plasticity theory in order to depict the continuous nature of soil in a more realistic way.

2.4   Continuum Approaches

A weakness of the subgrade reaction approach is the independence of each soil "spring", whereby the response of any one spring is assumed to have no influence on the response of others. Real soil is inherently a particulate material and thus derives its resistance through innumerable load paths that can generally be considered in a continuous, interactive sense. As a result, mathematical elastic and plastic continuums have been applied extensively in modeling soil behavior with much success. Applied to laterally-loaded piles, the replacement of soil with a continuous elastic or elastic-plastic model therefore stands to reason, providing a more fundamental approach to modeling the actual interaction between the pile and soil entities. While of value from a fundamental point of view, the success of such an approach relies on the ability to model the soil, pile and the pile-soil interface behavior appropriately. This aspect is still a subject in need of further research, but the work undertaken to date has served to strengthen the general understanding of lateral pile-soil interaction, and more importantly provide an appropriate basis for consideration of pile-soil-pile interaction effects that characterize lateral pile-group behavior.

Continuum approaches, as defined here, comprise an assortment of solution techniques utilizing either the theory of elasticity alone or both the theory of elasticity and plasticity. These include fully three-dimensional analyses and simplifications using two-dimensional analyses (plane strain or plane stress). Three-dimensional analyses offer the most realistic approach to assessing pile-soil interaction, and are divided into integral equation (or boundary element) method and differential method analysis categories. Boundary element analysis work will be discussed first given that this approach is considered to have been most useful in providing a framework in which to synthesize single pile lateral behavior from a general standpoint.

2.4.1   Boundary Element Single Pile Models

An advantage of the boundary element method over other methods is its use of surface discretization that provides for the greatest numerical efficiency when dealing with three-dimensional problems possessing low surface area to volume ratios, as is the case with pile foundation problems (Banerjee, 1976; Banerjee and Driscoll, 1976). This enables a three-dimensional solution with the least computational effort, and is certainly a redeeming feature of the method. Boundary element methods use the Mindlin (1936) solution for lateral displacement induced by a horizontal point load (refer Figure 2-7) as the mechanism

responsible for interdependency. Through numerical integration of this solution over a discretized pile surface, equating lateral displacements from the elastic soil (Mindlin's solution) and elastic pile (Bernoulli-Euler beam theory), and imposing equilibrium conditions, a simultaneous equation solution ensues to solve for unknown forces that then allows determination of pile actions.

Introducing this type of approach to assess lateral response of piles, Spillers and Stoll (1964) noted that the purely elastic solution generated very high lateral pressures against the pile near the surface that would result in yielding of real soil. Nonlinear behavior of the soil model was therefore introduced by specifying maximum permissible pressures mobilized against the pile based on plastic yield criteria, considered a "first modifying effect" (p. 5) towards reconciling results with observed behavior. This reiterated the need for attention to surficial soils when assessing lateral load behavior, and the need of non-linearity in the pile- soil system. Subsequent work developed the boundary element principle put forward by Spillers and Stoll to produce useful design information for various pile-soil configurations, albeit from a mostly linear-elastic perspective. Notable was the work of Poulos (1971a), Banerjee and Davies (1978), Davies and Budhu (1986), and Budhu and Davies (1987, 1988).

u_R = lateral displacement at point R due to point load P
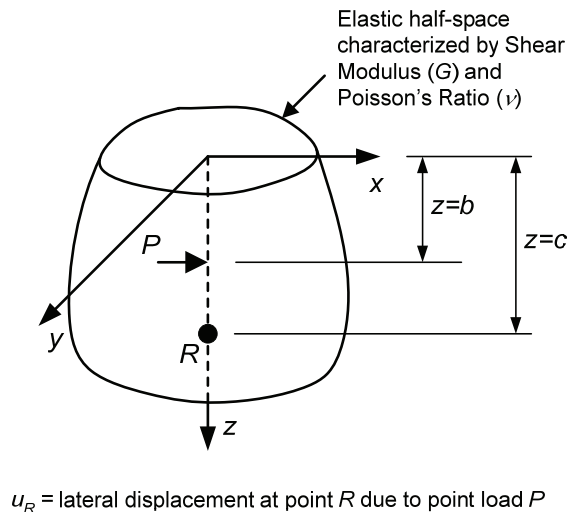
where

$$u_R = \frac{P}{16\pi G(1-v)}\left[\frac{3-4v}{|b-c|}+\frac{1+2(1-v)(1-2v)}{b+c}+\frac{2bc}{(b+c)^3}\right]$$

Figure 2-7: Mindlin (1936) solution

Poulos (1971a) chose a somewhat crude approach, starting with the depiction of a pile as a thin rectangular strip of width equal to the pile diameter (d), and possessing a length (L) and flexibility (E_pI_p) corresponding to that of the pile. A linear-elastic continuum with Young's modulus (E_s) constant with depth was used to represent the surrounding soil, and no separation between the pile and soil allowed. Any shear stresses at the pile edges were neglected, pile-soil interaction derived solely from uniform distribution of normal stress assumed across each pile-segment width, where pile lengths were discretized into standard 21 equal-length segments. Although a very crude approximation of actual behavior, the approach provided a consistent framework in which to assess the behavior of both rigid and flexible piles.

Such behavior was presented using the concept of pile head influence factors of the form given by (2.5), where rotational influence factors were similarly defined to obtain rotation at the pile head.

$$\delta_h = I_{\delta P} \frac{P}{E_s L} + I_{\delta M} \frac{M}{E_s L^2}$$

(2.5)

where δ_h = lateral deflection at pile head,

$\quad I_{\delta P}$ = displacement influence factor for horizontal load only,

$\quad\quad P$ = horizontal load (applied at pile head),

$\quad I_{\delta M}$ = displacement influence factor for moment only, and

$\quad\quad M$ = moment (applied at pile head).

Typical trends observed are shown in Figure 2-8, where the parameter K_R represents a relative pile-soil stiffness measure, and the length-to-diameter (or slenderness) ratio, L/d, an appropriate parameter for distinguishing between rigid and flexible piles. In effect, K_R accounts for non-rigidity of the pile foundation and L/d accounts for embedment (Kuhlemeyer, 1979). Poulos (1972) noted that displacement and rotation at the pile head are virtually unaffected by the boundary condition at the pile tip when K_R values are less than about 0.01. Kuhlemeyer (1979) noted that this translates to an effective slenderness ratio at which flexbile pile behavior can be assumed to apply, and such effective slenderness ratio values are plotted in Figure 2-9 against the ratio of the pile to soil modulus, E_p/E_s. Shown are slenderness ratios corresponding to K_R values of 0.01 and 0.05. Kuhlemeyer considered that $K_R = 0.01$ was appropriate for displacement behavior at the pile head, but $K_R = 0.05$ more appropriate for rotation behavior.

The work of Banerjee and Davies (1978) mainly served to provide a more rigorous boundary element technique whereby both normal and shear stresses around a cylindrical pile-soil interface were incorporated into the solution scheme using an a priori numerical procedure. Results for the soil modulus linearly increasing at the ground surface from both zero and half the pile tip modulus (i.e., triangular and trapezoidal distributions respectively) were also obtained, although these required an approximate solution scheme given that the Mindlin (1936) solution is strictly only valid for a constant modulus distribution with depth. These non-homogenous modulus cases exhibited a relative increase in the values of influence factors and transfer of pile actions to greater depths compared with the homogeneous modulus case. Relatively higher bending moments in the pile were also noted in the non-homogeneous cases.

Davies and Budhu (1986) and Budhu and Davies (1987, 1988) advanced on Banerjee and Davies (1978) by acknowledging different soil resistance patterns around a pile. Assuming a solid cylindrical elastic beam for the pile (as used by Banerjee and Davies), limiting soil stresses were assigned at the front, sides and back of the pile. These were based on conventional bearing capacity values for the normal stresses acting against the front face of the pile, empirical adhesion values for shear stresses acting along the sides of the pile, and limiting the decrease in normal stresses at the back of the pile to be no greater than in situ horizontal stresses derived from assumed lateral earth pressure coefficients. The latter served to prevent tensile stresses and thus convey a pile-soil separation effect. While only an approximate account of soil non-linearity, this approach emphasized the significant increase in pile displacements, rotations and bending moments as a result of soil yielding. This effect was shown to increase as the level of loading increased, and was most apparent with flexible piles.
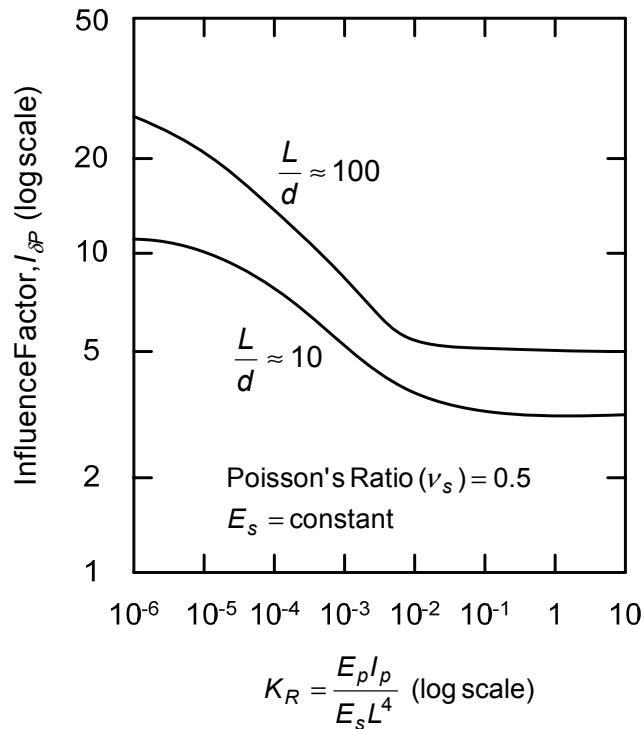
a) Influence factor for free-head piles
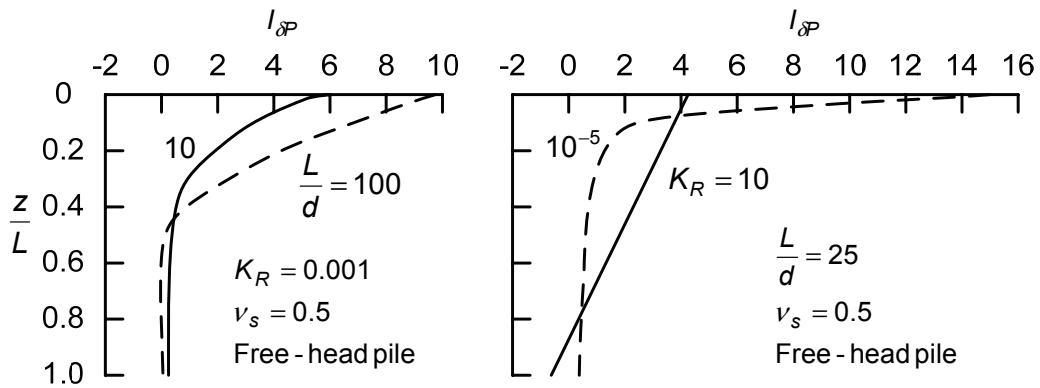
b) Typical displacement profiles showing effect of L/d and K_R

Figure 2-8: Typical trends for rigid and flexible piles (after Poulos and Davis, 1980)
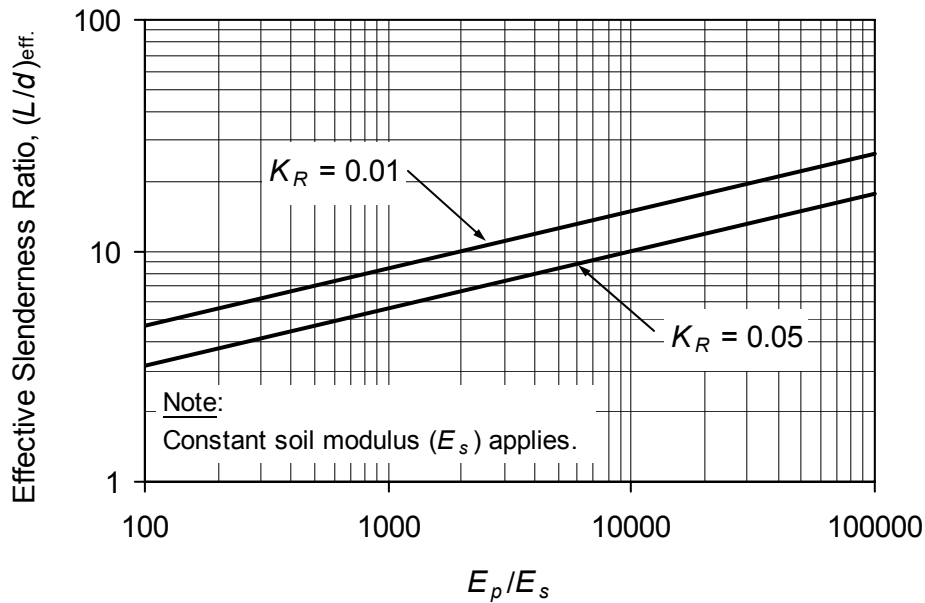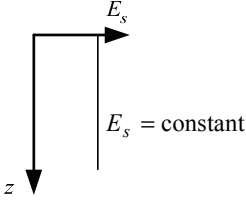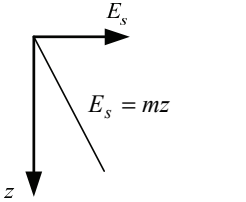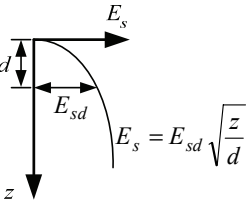
Figure 2-9: Apparent effective slenderness ratios for flexible pile behavior

Besides emphasizing the importance of nonlinear soil effects, the work of Davies and Budhu (1986) and Budhu and Davies (1987, 1988) also improved on prior elastic boundary element solutions by providing algebraic expressions to directly calculate pile head behavior for flexible piles. This approach was initiated by Kuhlemeyer (1979), who showed that, given flexible pile and elastic conditions, the independence of pile head displacement and rotation to pile length leads to behavior that is only a function of the pile-soil stiffness ratio. The algebraic expressions together with appropriate critical pile lengths for constant and linearly increasing distributions of Young's modulus with depth, as determined by Davies and Budhu and Budhu and Davies, are indicated in Table 2-2. Also given are expressions for a parabolic distribution of Young's modulus with depth, as determined by Pender (1993) using the work reported by Gazetas (1991). Such information can be used as a means of back-calculating equivalent elastic soil moduli at small deflections using real load-deflection behavior. This is an important consideration when modeling pile load tests because the initial stiffness assigned to a soil model, particularly an elastic-plastic soil model, is one of the key parameters that control the nonlinear response of a modeled pile.

Although useful from a general design standpoint, the boundary element technique suffers in that its underlying elastic nature limits its applicability and allows for soil non-linearity in only an approximate manner (i.e., introduction of limiting pressures that are strictly out of place in an elastic system). Idealization of the pile as a line element, necessary to avoid otherwise prohibitively expensive numerical computations, is also restrictive. This is because the governing integral equations can be satisfied only at the centerline of the pile, which in turn enforces limitations on the nature of surface tractions (i.e., normal and shear stresses) acting around the mathematical pile circumference (Banerjee and Driscoll, 1976). To this end recourse to differential methods in the form of finite elements, and use of elastic-plastic soil models, affording a more rational representation of soil non-linearity, has provided a powerful alternative for modeling pile-soil interaction.

17

Table 2-2: Elastic pile head solutions for flexible piles

Type of Variation of Elastic Soil Modulus with Depth	Critical length (l_c)	Horiz. displ. at pile head, $u = f_{uP}P + f_{uM}M$ Rotation at pile head, $\theta = f_{\theta P}P + f_{\theta M}M$		
		f_{uP}	$f_{uM} = f_{\theta P}$	$f_{\theta M}$
Constant[1]: $E_s = $ constant	$l_c = 0.5dK^{4/11}$ $K = \dfrac{E_p}{E_s}$	$\dfrac{1.3K^{-2/11}}{E_s d}$	$\dfrac{2.2K^{-5/11}}{E_s d^2}$	$\dfrac{9.2K^{-8/11}}{E_s d^3}$
Linear[2]: $E_s = mz$	$l_c = 1.3dK^{2/9}$ $K = \dfrac{E_p}{md}$	$\dfrac{3.2K^{-3/9}}{md^2}$	$\dfrac{5.0K^{-5/9}}{md^3}$	$\dfrac{13.6K^{-7/9}}{md^4}$
Parabolic[3]: $E_s = E_{sd}\sqrt{\dfrac{z}{d}}$	l_c between constant and linear modulus critical lengths $K = \dfrac{E_p}{E_{sd}}$	$\dfrac{2.14K^{-0.29}}{E_{sd} d}$	$\dfrac{3.43K^{-0.53}}{E_{sd} d^2}$	$\dfrac{12.16K^{-0.77}}{E_{sd} d^3}$

Note: d = pile diameter, E_s = soil modulus, E_p = pile modulus, P = lateral load applied at the groundline, M = moment applied at the groundline.

References: [1] Davies and Budhu (1986); [2] Budhu and Davies (1987); [3] Pender (1993)

2.4.2   Finite Element Single Pile Models

The finite element method is a well-established numerical framework that has been utilized in various three-dimensional studies of laterally loaded piles. Unlike the boundary element approach, the finite element framework is theoretically qualified to model both linear and nonlinear behavior, thus providing a more correct numerical environment in which to study the nonlinear interaction between the pile and soil. Finite elements also offer the ability to model the pile and soil in detail, and to account for possible separation and slippage between the pile and soil using interface elements. A greater degree of realism is therefore possible with a three-dimensional finite element approach, and the studies that have been undertaken have enabled a greater appreciation of some of the more complex issues that exist.

Two of the most critical of such issues are separation between the pile and the soil, and soil nonlinearity. Trochanis, Bielak and Christiano (1988, 1991a, 1991b) examined these factors for the flexible pile model configuration given in Table 2-3, investigating the case of a free-head pile subject to a maximum lateral load of 216 kN applied at the pile head.

A series of three axisymmetric analyses were undertaken: The first adopted an elastic soil bonded to the pile, the second an elastic soil but allowing pile-soil separation when tensile normal stresses developed at the pile-soil interface, and the third allowing such separation as well as modeling soil nonlinearity using an elastic-plastic (i.e., Drucker Prager) soil model employing the friction angle and cohesion plasticity parameters indicated in Table 2-3. Separation was modeled using two-dimensional interface elements possessing zero tensile capacity, but allowing for controlled slippage using stiffness and shear strength properties characterized by the linear-elastic and Coulomb friction parameters, respectively, given in Table 2-3.

Comparison of the analysis runs indicated a 60 percent increase in pile head deflection due to separation alone, and a 30 percent increase at peak load due solely to nonlinear (i.e., plastic) soil behavior. This highlighted the significance of both geometric and material nonlinearities when modeling lateral load behavior. Furthermore, in both the second and third analysis runs, the depth to which separation occurred was observed to be about three meters, or six pile widths. This extent of separation is noteworthy in light of the fact that the theoretical critical length for such a pile model, obtained using the constant modulus expression given in Table 2-2. (which applies to the case of elastic soil bonded to the pile), is also about six pile widths. Thus separation readjusts the pile-soil system in that the critical length is increased, causing a greater depth of soil resistance, or interaction, to be mobilized.

Table 2-3: Trochanis et al. (1988) single pile parameters

Pile Parameters		Soil Parameters	
Type:	Concrete	Description:	Typical Mexico City subsoil
Cross-Sectional Shape:	Square	Submerged Unit Weight (γ'):	11.8 kN/m^3
Length (L):	10 m	Young's Modulus (E_s)[1]:	20000 kPa
Diameter/Width (d):	0.5 m	Poisson's Ratio (v_s):	0.45
Young's Modulus (E_p):	20 GPa	Undrained Shear Strength (s_u):	34 kPa
Poisson's Ratio (v_p):	0.3	Friction Angle (ϕ'):	16.7º
Interface Parameters			
Elastic Stiffness: 6800 kN/m^2/m			
Coulomb Friction Coefficient (μ)[2]: 0.7			
Pile - Soil Parameters			
L/d = 20		E_s/s_u = 588	
K_R = 5x10^{-4}		E_p/E_s = 1000	
Notes:	1. Modulus constant with depth.		
	2. Maximum shear stress = μ x normal stress.		

In addition to the increased pile displacements with separation, Trochanis et al. (1988, 1991a, 1991b) also observed a more concentrated pattern of horizontal displacements of the soil surface closer to the pile, compared with a more evenly spread distribution around the pile without separation (both assuming elastic soil behavior). Furthermore, when separation was allowed the rate of decay of the displacement with distance away from the pile was greater in the direction normal to loading compared with the direction in line with loading. An additional increase in the rate of decay was noted with the incorporation of the inelastic Drucker Prager soil model, although this additional increase was not as significant as that due to separation alone. Such displacement trends reflect the transferal of lateral load resistance to the soil region around the front of the pile once separation occurs. The corresponding surface deformation patterns indicate concentrated soil movement near the pile face, brought on by geometrical effects and exacerbated by soil nonlinearity. The differing rates of displacement decay also suggest that the region of soil affected by lateral loading is greater in the direction of loading, implying more pronounced interaction in this direction for pile groups.

Other three-dimensional studies substantiate and augment these findings. Bhowmik and Long (1991), modeling a lateral load test on a steel pipe pile in overconsolidated clay (Dunnavant and O'Neill, 1989), found good agreement with pile-head load-deflection and bending moment behavior only by allowing for separation. Brown, Shie and Kumar (1989) and Brown and Shie (1990a, 1991b), in a series of papers advocating three-dimensional modeling as a useful parametric tool, also emphasized the need to include for separation and slippage. Furthermore, Brown and Shie (1990a) showed that significant soil deformation, represented as plastic strain, is not just confined to a surficial area in front of the pile, but also extends with depth in a diminishing fashion. This zone of plastic strain propagated laterally and to greater depths with increasing pile displacement, and differed in extent depending on whether a constant failure strength ("clay") or pressure-dependent failure strength ("sand") was used as a plastic failure criterion.

Given the complexity of nonlinear pile-soil interaction, it would appear that modeling lateral behavior in any way other than with three-dimensional models using nonlinear soil models and interface elements must constitute a compromise. However, consideration of the ratio of pile to soil stiffness, commonly in the region of several orders of magnitude, suggests benefit in viewing pile-soil interaction more from the standpoint of pile behavior. Trochanis et al. (1988, 1991a, 1991b), for example, noted that inclusion of their inelastic soil model increased pile deflections but did not change the deflected shape of the pile when plotted relative to the pile length and maximum displacement. The so called normalized deflected shape was considered to depend only on the elastic properties of the pile and soil, and for the case of equal soil properties was controlled solely by the slenderness ratio of the pile. Well-behaved pile behavior was thus exhibited regardless of the soil behavior.

Yang and Jeremić (2002), using a three-dimensional finite element model with separation and slippage capabilities, noted similar behavior when modeling lateral response in layered elastic-plastic soils. Two layered-soil cases were considered: One depicting a medium dense sand layer within a soft clay deposit, the other depicting a soft clay layer within a medium dense sand deposit. In both cases the top of the distinct layer was located at a depth of four pile diameters, and was four pile diameters in thickness. The top of the pile was unrestrained and loaded horizontally, but located above the ground surface so that both moment and horizontal loading applied at the groundline. Under lateral loading the two cases developed significantly different distributions of soil pressures along the pile length, but the pile displacement profiles and pile-head displacements were almost the same.

Consideration of pile curvature is also instructive. Disregarding pile failure and the associated excessive local rotations, the radius of curvature of a pile is large with respect to its diameter. Even in the extreme case of a magnitude 8 earthquake, Margason and Holloway (1977) estimated the radius of curvature to be of the order of 60 m (200 feet). Given that pile diameters are in the order of one meter (3 feet), the large

ratio of radius of curvature to diameter demands highly continuous horizontal displacements along the length of a pile. Therefore, in terms of behavior along the pile at and in the vicinity of a given depth, practically constant behavior is implied and suggests the possibility of assessing pile-soil interaction in a more local form.

Combining the qualities of greater emphasis on pile behavior and employment of local pile-soil interaction mechanisms is indeed the essence of the Discrete Load-Transfer approach. This approach is an empirical approach to pile-soil interaction, but it recognizes some of the more decisive elements of pile-soil interaction. It also draws on theoretical means, in conjunction with empirical data, to formulate pile-soil interaction mechanisms. Thus it represents an interconnection of sorts, utilizing both theoretical and empirical observations to resolve lateral load behavior. Consequently, much of the three-dimensional continuum work already discussed also serves the discrete load-transfer approach. In terms of two-dimensional (plane strain and plane stress) continuum work that has been undertaken, this is certainly the case given the local form of pile-soil interaction demanded by such an analysis. Discussion of this work is therefore left for the following sections.

2.5   Discrete Load-Transfer Approach

The Discrete Load-Transfer (DLT) approach maintains the subgrade reaction idea of replacing the soil with discrete soil reaction mechanisms, but enables a far more realistic depiction of lateral pile-soil interaction through specification of soil reaction behavior of a form that mimics the reaction behavior that has been observed in full-scale field tests. A basis for obtaining soil reaction behavior in the field is evident from the beam theory relations given in Table 2-4.

Table 2-4: Beam theory relations (after Ting, 1987)

Displacement (2nd Integral)	Slope (1st Integral)	Moment	Shear (1st Derivative)	Loading (2nd Derivative)
y $\leftarrow$	$\dfrac{dy}{dz}$ $\leftarrow$	$E_p I_p \dfrac{d^2 y}{dz^2}$ $\rightarrow$	$E_p I_p \dfrac{d^3 y}{dz^3}$ $\rightarrow$	$E_p I_p \dfrac{d^4 y}{dz^4}$

In terms of the lateral soil loads mobilized against a laterally loaded pile, this translates to the relation given by (2.6), whereby soil loads are established from bending moments induced in the pile.

$$p = \frac{d^2 M_p}{dz^2} = E_p I_p \frac{d^4 y}{dz^4} \tag{2.6}$$

where $M_p = E_p I_p \dfrac{d^2 y}{dz^2}$ = moment in pile at depth z,

$\quad\quad y$ = lateral deflection of the pile at depth z,

$\quad E_p I_p$ = flexural rigidity of pile, and

$\quad\quad p$ = soil reaction at depth z expressed as a force per unit depth (FL^{-1} units).

McClelland and Focht (1958a) formalized the procedure for obtaining p and y by twice differentiating and twice integrating, respectively, moment diagrams determined using strain-gauge measurements on a full-scale test pile. By determining moment diagrams at successive stages of their lateral load test, and obtaining corresponding p and y values at various depths, McClelland and Focht derived p versus y

relationships appropriate to their pile-soil system. In doing so, they introduced the so called *p-y* curves that have become a well-established means of representing soil resistance behavior for the purpose of establishing laterally loaded pile behavior.

Since the initial work of McClelland and Focht (1958a), numerous studies have been undertaken to develop appropriate formulations for *p-y* curves taking into consideration the various factors affecting them. This quest has drawn on instrumented full-scale field tests, soil testing, and numerical and analytical studies. Featuring prominently are what may be termed "conventional" *p-y* curve formulations that have essentially developed the McClelland and Focht idea to a stage fit for practice. In the process various mechanistic models and principles have been developed that form a basis for *p-y* curve construction, and serve as a general framework that has helped to rationalize and improve the understanding of lateral pile-soil interaction.

2.5.1 Conventional Formulations

In the same way that the response behavior of a laterally loaded pile depends on the stiffness and strength qualities of the surrounding soil, establishing *p-y* curves requires the assignment of appropriate stiffness and strength qualities that are a function of the pile-soil system. A generic *p-y* curve is shown in Figure 2-10, indicating soil resistance versus pile deflection behavior typically exhibited for monotonic static loading. A secant stiffness measure (E_{py}) is used to denote the obvious variation of stiffness with deflection. While nonlinear behavior is apparent as a whole, rationalization of the curve identifies an initial tangent stiffness ($E_{py\text{-max}}$), representing an upper limit of *p-y* stiffness, an ultimate soil resistance (p_u), representing an upper limit of *p-y* resistance, and a transitional section in between giving the curve a shape.
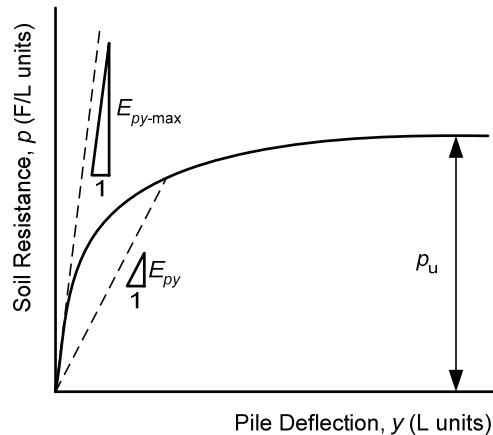
Figure 2-10: Generic *p-y* curve for static loading conditions

2.5.1.1 Initial Stiffness

The initial stiffness of a *p-y* curve is a matter of small strain where behavior is essentially linear. Thus $E_{py\text{-max}}$ can be considered as a horizontal subgrade modulus (k_h), as used in linear subgrade reaction theory, and both terms are used interchangeably hereafter. The behavior of soil itself at small strains is reasonably approximated by a linear elastic continuum, characterized by elastic parameters in the form of Young's Modulus (E_s) and Poisson's Ratio (v_s), in this case both E_s and v_s denoting values appropriate for

22

soil at small strain. Consideration of lateral pile-soil behavior using a k_h and E_s, ν_s representation of soil reveals a strong kinship between k_h ($E_{py\text{-max}}$) and E_s, but an elusive definitive relation due to the nature of the laterally loaded pile problem.

Biot (1937) offered a means of obtaining a basis for such a relation by solving the problem of an infinite elastic beam resting on a linearly elastic (E_s, ν_s) continuum and acted upon by a point load. Matching the maximum bending moment in the beam with that obtained using a subgrade reaction model, Biot determined that an equivalent subgrade modulus was given by

$$k_\infty = \frac{1.23 E_s}{(1 - \nu_s)^2} \left[\frac{E_s b}{(1 - \nu_s^2)(E_b I_b)} \right]^{0.11} \tag{2.7}$$

where k_∞ = subgrade modulus for an infinite beam (FL^{-2} dimensions)

b = width of the beam

$E_b I_b$ = flexural rigidity of the beam

Vesić (1961) improved on Biot's work by also considering an infinite elastic beam acted upon by a couple, and evaluating an appropriate subgrade modulus for both loading cases in more general terms by comparing differences in maximum bending moment, deflection and subgrade pressure. In this way Vesić determined that average differences between elastic continuum and subgrade reaction solution values of less than 10 percent were obtained by using

$$k_\infty = \frac{0.65 E_s}{1 - \nu_s^2} \sqrt[12]{\frac{E_s b^4}{E_b I_b}} \tag{2.8}$$

Given typical values of ν_s (0.1 to 0.3 for sands and 0.5 for a saturated clay behaving undrained), and noting that the twelfth root of any reasonable number inside the radical sign (as would be the case for typical beam and soil values) is close to unity (Scott, 1981), the relation given by (2.8) indicates that $k_\infty \approx E_s$.

Applied to laterally loaded piles, a seemingly simple relationship between $E_{py\text{-max}}$ and E_s could be construed from (2.8), but there are various issues that confound such a proposition. The finite, rather than infinite length of a structural element, be it a pile or beam, is a first consideration. Vesić (1961) addressed this issue by computing the difference in maximum bending moments in beams of different bending stiffness using both subgrade reaction and elastic continuum soil approaches, and showed that negligible difference resulted provided the beam was "sufficiently long". Vesić defined sufficiently long as when $\lambda L > 2.25$ (λ being defined as in Equation 2.2), and in terms of a pile translates to the requirement of a flexible pile. Given that most piles in practice fall into this category (e.g., Randolph, 1981; Reese and Van Impe, 2001), the effect of an infinite length basis is likely to be of minor importance.

It is with regards to the fact that pile-soil interaction varies with depth that application of (2.8) requires significant qualification. As is already apparent, the orientation of a pile compared with a beam resting on the ground surface demands more complex soil reaction mechanisms in response to structurally-imposed deflections. This is especially the case when a linearly elastic continuum depicts the soil surrounding a pile, because the ensuing elastic displacements in the soil continuum pose a far more pervasive picture of interaction. The consequence of such pervasiveness has been noted in the case of a

soil continuum with E_s constant with depth, where it was found that the stiffness of the corresponding elastic p-y curves (i.e., an $E_{py\text{-}max}$ value) was not constant, but in fact decreased with depth (Baguelin, Frank and Saïd, 1977; Baguelin and Frank, 1980; Bransby, 1999). At play are significant far-field continuum displacements that are a result of elastic interaction, or coupling, causing p-y response at any one depth to be significantly affected by load-deflection behavior elsewhere along the pile (Bransby, 1999).

In fact, Baguelin et al. (1977) noted that the condition of E_s and an $E_{py\text{-}max}$ value both constant with depth can only occur for the case of a fixed-head rigid pile translated horizontally through the soil continuum. Otherwise a constant $E_{py\text{-}max}$ value does not exist but must vary with depth depending on the relative soil-pile stiffness, pile-head loading and fixity conditions. A "unique" $E_{py\text{-}max}$ value can only exist in the sense of an equivalent value that results in the same pile action, just as Biot (1937) and Vesić (1961) determined for the specific case of a beam of infinite length acted upon by either a point load or moment. Baguelin and Frank (1980) reported such equivalent $E_{py\text{-}max}$ values[†] for laterally loaded piles based on compatibility of pile-head displacements using constant horizontal subgrade modulus (k_h = Equivalent $E_{py\text{-}max}$) and finite element continuum (E_s) soil representations. These are shown in Figure 2-11, where it is apparent that even a "unique" equivalent $E_{py\text{-}max}$ value is dependent on pile, loading and soil characteristics.
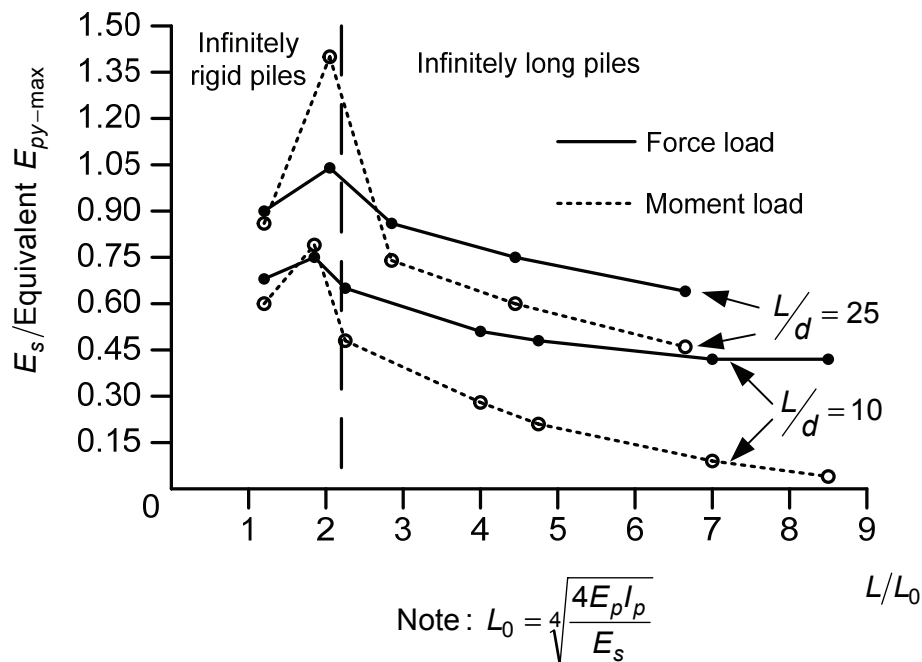
Figure 2-11: Equivalent Epy-max for various soil, pile and loading conditions (after Baguelin and Frank, 1980)

[†] Baguelin and Frank (1980) used the term "reaction modulus" in their work, denoted as E_{si}

24

The variation of $E_{py\text{-}max}$ with depth is also important for determining structural actions. Lam and Cheang (1995), evaluating *p-y* criteria using field data on a laterally loaded 610 mm diameter steel pile ($L/d = 16$) in submerged sand, assessed free-head and fixed-head *p-y* solutions assuming an initial *p-y* stiffness either increasing linearly with depth or with the square root of depth (i.e., a parabolic increase). While both *p-y* formulations indicated reasonable agreement with measured maximum moments, only the parabolic formulation showed reasonable agreement with the observed distribution of moment below a depth of five diameters (5*d*). Moreover, the parabolic formulation indicated soil reactions below this depth approximately half those derived from the linear formulation, resulting in greater pile rotation and increased displacement at the ground line. Thus cognizance of initial *p-y* stiffness over the entire pile length was required to fully appreciate the structural actions observed.

The complexity in relating $E_{py\text{-}max}$ and E_s, and the need to be cognizant of initial stiffness variation with depth, obviously adds to the difficulty of establishing accurate *p-y* curves for lateral loading. However, the need of a precise value of initial *p-y* stiffness is tempered by the fact that lateral single pile behavior is generally least sensitive to this parameter and more affected by the nonlinear characteristics of *p-y* curves (e.g., Meyer, 1979; Murchison and O'Neill, 1984; Gazioglu and O'Neill, 1984). Reese and Van Impe (2001) also appointed minor relevance to the initial stiffness of *p-y* curves, suggesting that it may only be important in special cases such as vibratory loading (i.e., small strain applications), and considered it unlikely that initial stiffness would play an important role even for working load conditions. Furthermore, Gazioglu and O'Neill considered that the use of *p-y* curves could not be assumed to apply in the case of "extremely low-displacement pile response" (p. 203), implying little confidence in the $E_{py\text{-}max}$ aspect of *p-y* curve formulations.

In terms of appointing an initial stiffness to *p-y* curves in practice, it has been common to simply adopt an $E_{py\text{-}max}$ value that increases linearly with depth and with the gradient a function of density and shear strength for sands and clays, respectively. The usual form of the equation is given by (2.9), and typical values for k_{py} are indicated in Figure 2-12 for sands and Figure 2-13 for clays.

$$E_{py-\max} = k_{py} z \qquad\qquad (2.9)$$

where k_{py} = gradient of initial *p-y* stiffness with depth (FL^{-3} dimensions)

z = depth below ground surface

2.5.1.2   Curve Shape

A certain observation is that in terms of behavioral characteristics there is clearly much in common between the $E_{py\text{-}max}$ and E_s stiffness measures. This sentiment is certainly apparent beyond small strains, Reese and Van Impe (2001) having noted that the relationship between E_{py} and E_s (where E_s now denotes a secant modulus value for soil) is "undoubtedly close" (p. 50), and that their decay with deflection "is certainly due to the same phenomenon, a decrease in stiffness of an element of soil with increased strain" (p. 51). This similarity in response traits was first exploited by Skempton (1951) to relate the load-settlement response of rigid footings resting on saturated clay and the undrained triaxial compression test response of the same saturated clay. The essence of the approach is illustrated in Figure 2-14, comprising the theoretical solution for settlement of a rigid circular footing resting on an elastic foundation, that is combined with clever mathematical manipulations to relate the footing settlement (*w*) and triaxial strain (ε) via an assumed equivalency of applied to ultimate stress ratio experienced in each case. A general correlation between laboratory and field response is then implied in the form of multiplicative coefficients

combined with the footing width to convert the triaxial stress and strain variables into comparable field variables.
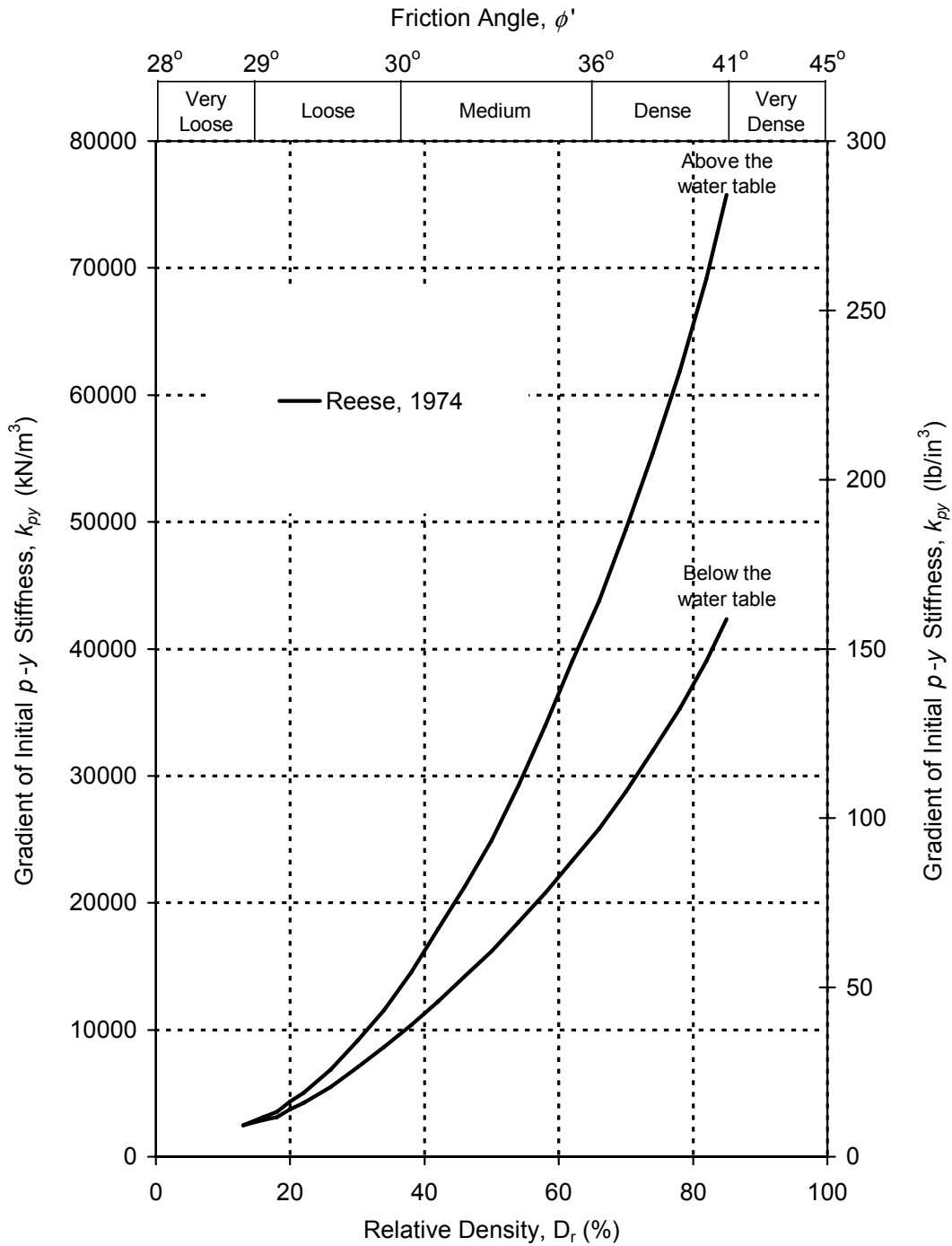
Figure 2-12: Typical k_{py} values for sands
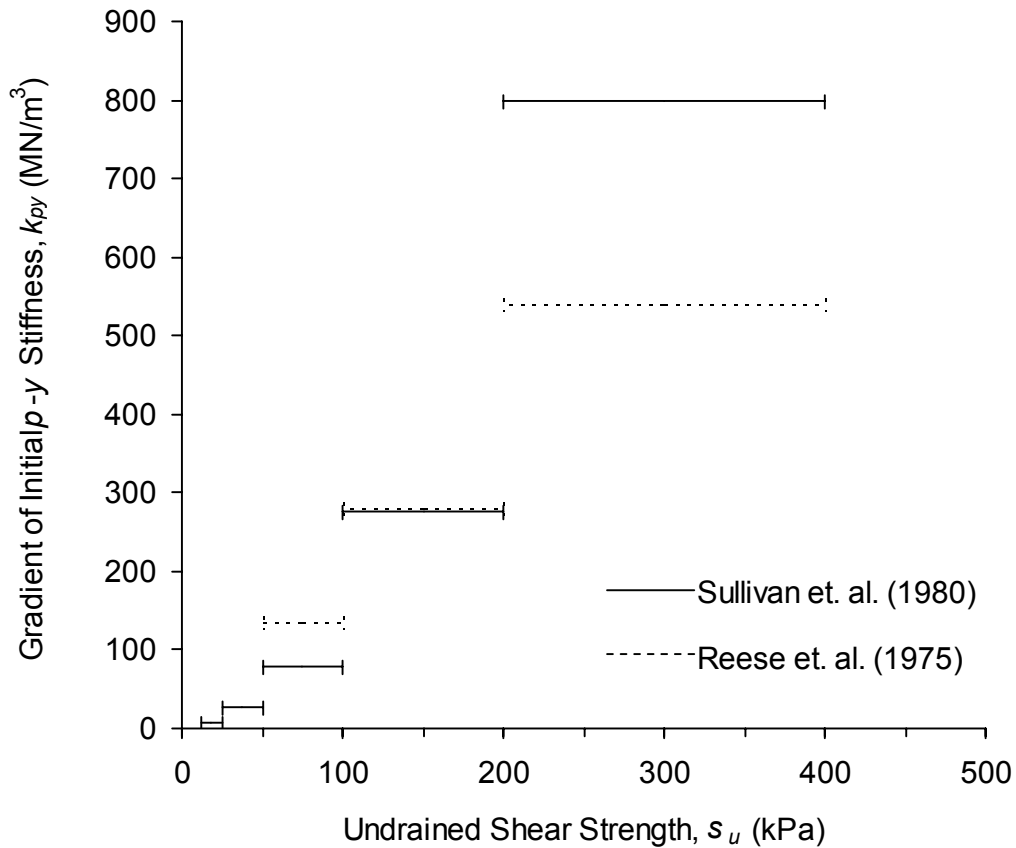
Figure 2-13: Typical k_{py} values for clays

The case of a vertically loaded footing suffers in the same way that a beam on elastic foundation fails to portray depth-dependent lateral pile-soil interaction, but the relationship derived by Skempton (1951) nevertheless provided a mechanistic basis for developing *p-y* curves from the laboratory stress-strain response of soil, at least for saturated clays under undrained conditions. Empirical evidence in support of this theoretical deduction was demonstrated in the pioneering work of McClelland and Focht (1958a), where the following field and laboratory (i.e., consolidated-undrained triaxial) relationships were established for a 610mm diameter steel pipe pile (*L/d* = 37) driven into soft clay and laterally loaded with a free-head condition to a maximum static load of 500 kN (corresponding to lateral deflections up to 4% of the pile diameter):

$$p = 5.5d(\sigma_1 - \sigma_3) \quad \text{and} \tag{2.10a}$$

$$y = 0.5d\varepsilon \tag{2.10b}$$

These relationships were not conclusive given the limitations of the experimental techniques used to obtain them, and nor were they general given the specific pile-soil system used to establish them (Peck, Davisson and Hansen, 1958; Lundgren, 1958; Matlock, 1958; McClelland and Focht, 1958b). However, they introduced *p-y* curves that were at least of the correct order of magnitude (Allen, 1985), and promoted a practical means of characterizing the shape of *p-y* curves for engineering purposes.

In fact the combined approach of field instrumentation to measure pile behavior and laboratory measurement of soil behavior has dominated the development of empirical *p-y* curves since the initial work by McClelland and Focht (1958a). Well known work of this nature were the series of instrumented field tests undertaken on single piles in the 1970's, developing recommendations to construct *p-y* curves for soft, plastic clays in the presence of free water (Matlock, 1970), stiff, brittle clays in the presence of free water (Reese, Cox and Koop, 1975), stiff clay with no free water (Reese and Welch, 1975), and medium dense to dense sands (Reese, Cox and Koop, 1974). The curve shapes produced by these formulations are illustrated in Figure 2-15 through Figure 2-18 for static loading conditions. Each shape reflects the influence of the pile-soil-loading system(s) used to establish the *p-y* behavior, and highlight the importance that soil type has in characterizing *p-y* curves.

Laboratory

$$\sigma_1 - \sigma_3$$

$$E_s$$

$$(\sigma_1 - \sigma_3)_f = 2c_u$$

$$\varepsilon \text{ (triaxial strain)}$$

$$\varepsilon = \frac{\sigma_1 - \sigma_3}{E_s}\left[\frac{2c_u}{(\sigma_1 - \sigma_3)_f}\right]$$

$$\Rightarrow \frac{\sigma_1 - \sigma_3}{(\sigma_1 - \sigma_3)_f} = \frac{\varepsilon E_s}{2c_u}$$

Field

Diam., *b*

Loading, *q*

Circular, rigid footing

Soil (E_s, v_s, c_u)

Settlement, *w*

$$w = \frac{\pi}{4} qb \frac{1 - v_s^2}{E_s}$$

and $q_{ult.} = 6.8c_u$, $v_s = 0.5$ (undrained)

$$\therefore w = \frac{\pi}{4} qb \frac{0.75}{E_s}\left[\frac{6.8c_u}{q_{ult.}}\right]$$

$$\Rightarrow \frac{q}{q_{ult.}} = \frac{wE_s}{4c_u b}$$

If $\dfrac{\sigma_1 - \sigma_3}{(\sigma_1 - \sigma_3)_f} = \dfrac{q}{q_{ult.}}$ then $\boxed{2b\varepsilon = w}$

Implies the following correlation:

Triaxial Test Response

$$(\sigma_1 - \sigma_3)$$

$$\varepsilon$$

Load-Settlement Response

$$q = Mb(\sigma_1 - \sigma_3)$$

$M \& N$ = conversion factors

$$w = Nb\varepsilon$$
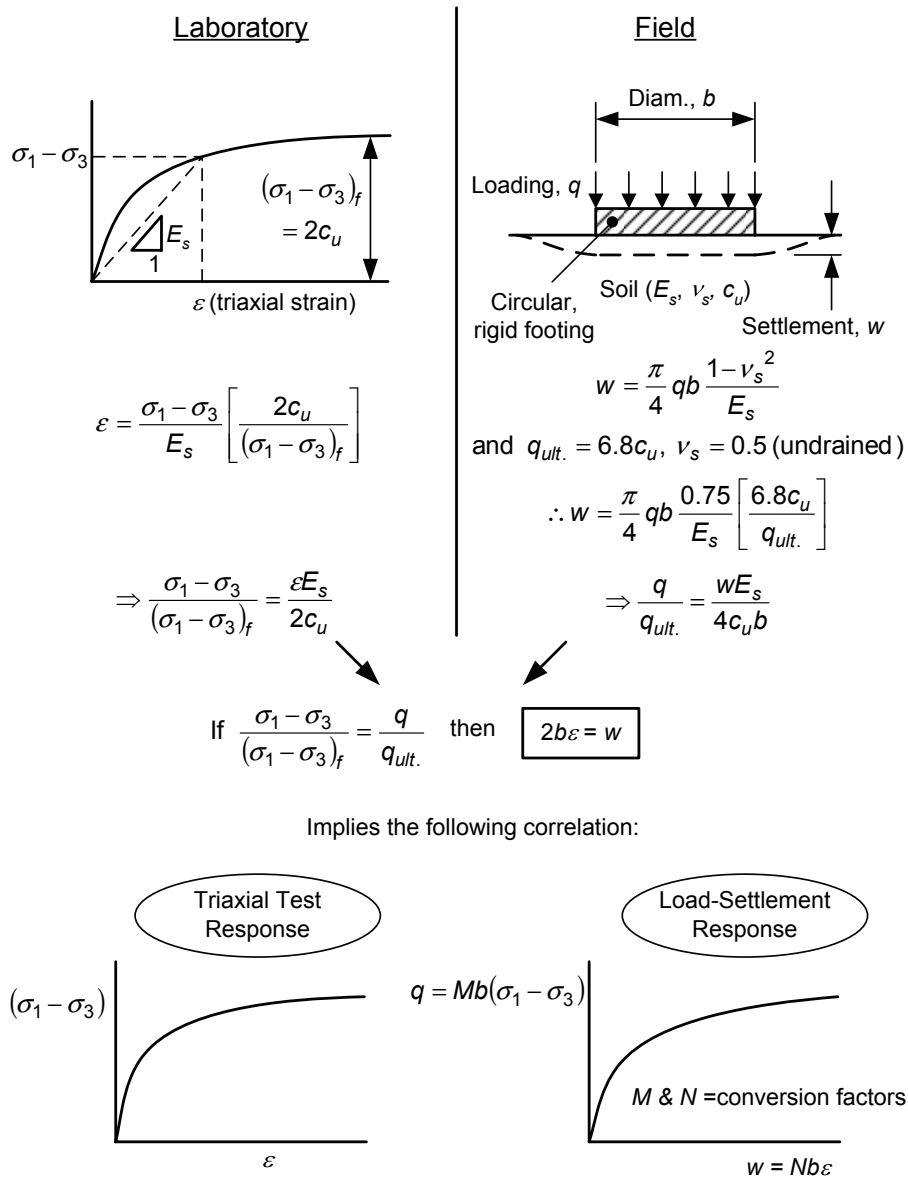
Figure 2-14: Field and laboratory correlation for saturated clays (after Skempton, 1951)

$$\frac{p}{p_u} = 0.5$$

$$p = 0.5 p_u \left(\frac{y}{y_{50}}\right)^{1/3}$$

p_u

y_{50}

$8y_{50}$

Pile Deflection, y (L units)

Soil Resistance, p (F/L units)
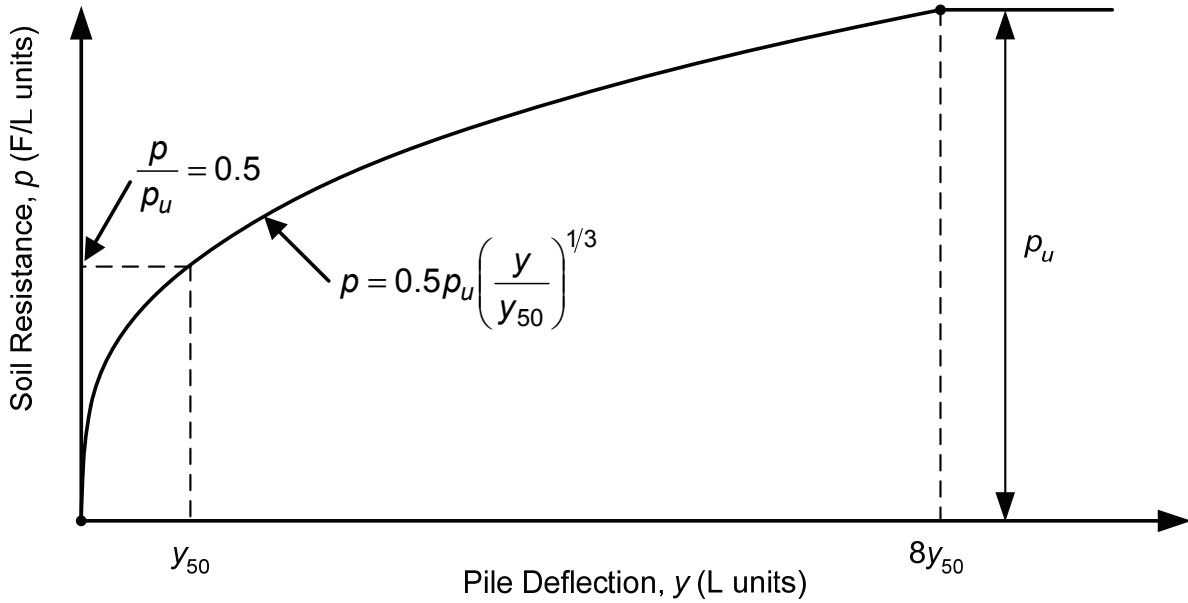
Figure 2-15: Soft clay by Matlock (1970)

$p_m = B_s p_s$

$$m = \frac{p_u - p_m}{y_u - y_m}$$

$p = Cy^{1/n}$

$k_{py}z = E_{py-max}$

$p_u = A_s p_s$

Notes:

$$n = \frac{p_m}{my_m} \text{ and } C = \frac{p_m}{y_m^{1/n}}$$

A_s and $B_s =$
empirical factors

$$y_m = \frac{d}{60}$$

$$y_u = \frac{3d}{80}$$

Pile Deflection, y (L units)

Soil Resistance, p (F/L units)
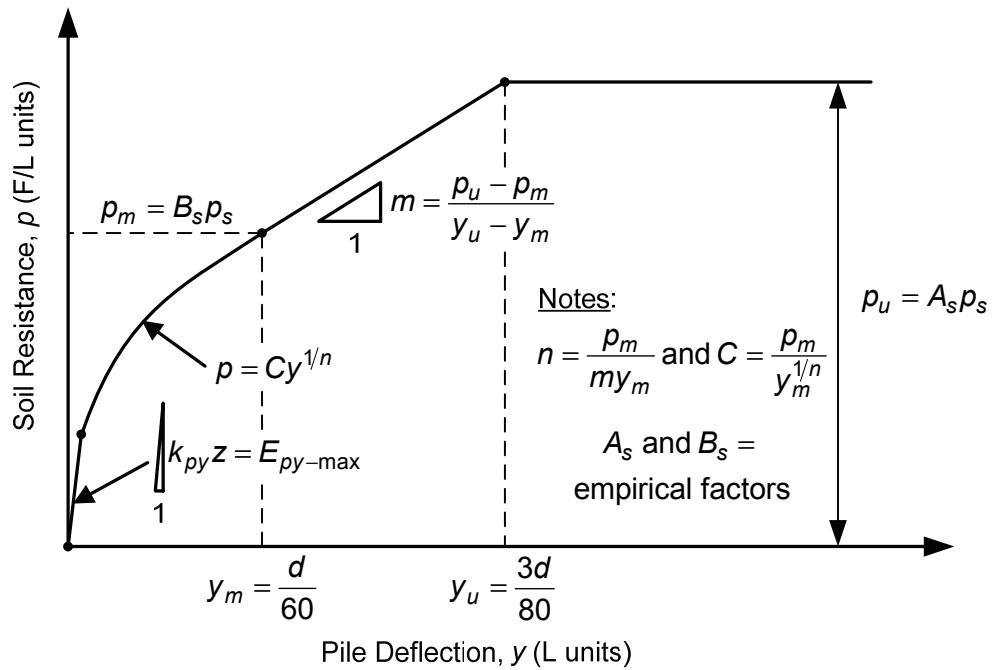
Figure 2-16: Sand by Reese et al. (1974)

29

$$\text{Offset} = 0.055p_c\left[\frac{y - A_sy_{50}}{A_sy_{50}}\right]^{1.25}$$

$$p = 0.5p_c\left(\frac{y}{y_{50}}\right)^{1/2}$$

$$\text{Slope} = \frac{-0.0625p_c}{y_{50}}$$

Note:

A_s = empirical factor

$k_{py}z = E_{py-\text{max}}$

1

Soil Resistance, p (F/L units)

A_sy_{50} $6A_sy_{50}$ $18A_sy_{50}$

Pile Deflection, y (L units)
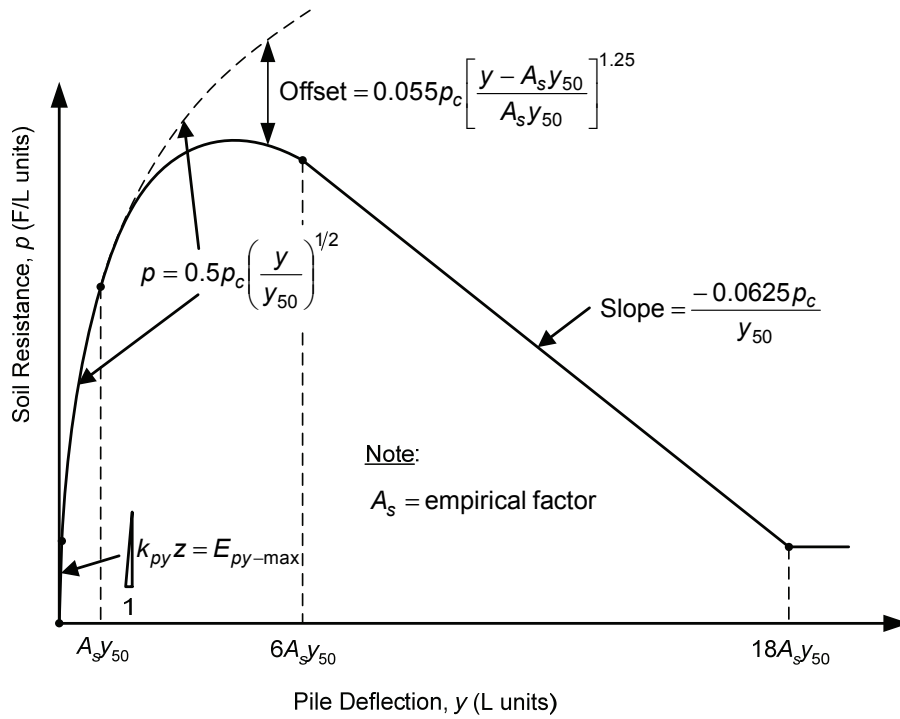
Figure 2-17: Stiff clay in the presence of free water (Reese et al., 1975)

$$p = 0.5p_u\left(\frac{y}{y_{50}}\right)^{1/4}$$

p_u

$k_{py}z = E_{py-\text{max}}$

Soil Resistance, p (F/L units)

$16y_{50}$

Pile Deflection, y (L units)
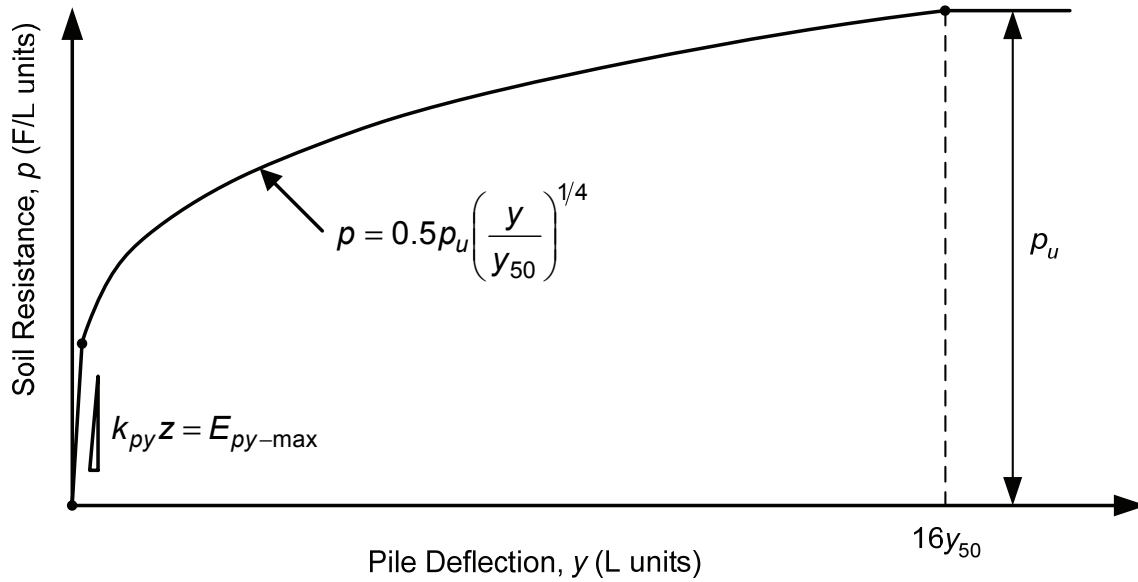
Figure 2-18: Stiff clay with no free water (Reese and Welch, 1975)

30

Apparent with each of the *p-y* formulations shown in Figure 2-15 through Figure 2-18 is the use of specific pile deflection values to anchor the various straight and parabolic portions forming each *p-y* curve. The anchor points are shown as solid circles with corresponding deflection values that are given in terms of the deflection at one-half the ultimate soil resistance (denoted as y_{50}) in the clay cases, or as a specific ratio of the pile diameter for the sand case. Definitions of y_{50} for the clay curves are given in Table 2-5, requiring associated values of triaxial strain at one-half the maximum principal stress difference (denoted as ε_{50}).

Table 2-5: Definitions of y_{50} for clays

Soil Type	y_{50}	Reference
Soft Clay in the presence of free water	$2.5\varepsilon_{50}d$	Matlock (1970)
Stiff Clay in the presence of free water (Stiff Clay A)	$\varepsilon_{50}d$	Reese et. al. (1975)
Stiff Clay with no free water (Stiff Clay B)	$2.5\varepsilon_{50}d$	Reese and Welch (1975)

Suggested values of ε_{50} are given in Table 2-6 in the absence of direct triaxial measurement.

Table 2-6: Recommended values of ε_{50} for clays

Undrained Shear Strength, kPa	ε_{50} (decimal)
Soft Clay in the presence of free water (Matlock, 1970)	
< 50	0.020
50 - 100	0.010
100 - 200	0.005
Stiff Clay A (Reese et. al., 1975)	
50 - 100	0.007
100 - 200	0.005
200 - 400	0.004
Stiff Clay B (Reese and Welch, 1975)	
Obtain ε_{50} from laboratory stress-strain curve, otherwise use 0.010 or 0.005[1].	

[1] Refer Reese and Van Impe (2001), p. 82.

The use of characteristic deflection values dependent on ε_{50} and/or *d* recognized a laboratory and field relationship in the spirit of Skempton (1951), but did not go so far as establishing a direct relationship between the *p-y* curve and the shape of the laboratory stress-strain curve, as did (2.10).

Other *p-y* curve shapes based on the combined field and laboratory approach have been proposed since the 1970's with various intentions in mind. An attempt to amalgamate the soft and stiff clay recommendations by Matlock (1970) and Reese et al. (1975), respectively, was made by Sullivan, Reese and Fenske (1980) with the "Unified Method". The curve shape for the Unified Method is shown in Figure and, as noted by Gazioglu and O'Neill (1984), was essentially a restatement of the prior clay recommendations once the choice of conversion parameters *A* and *F* were made.
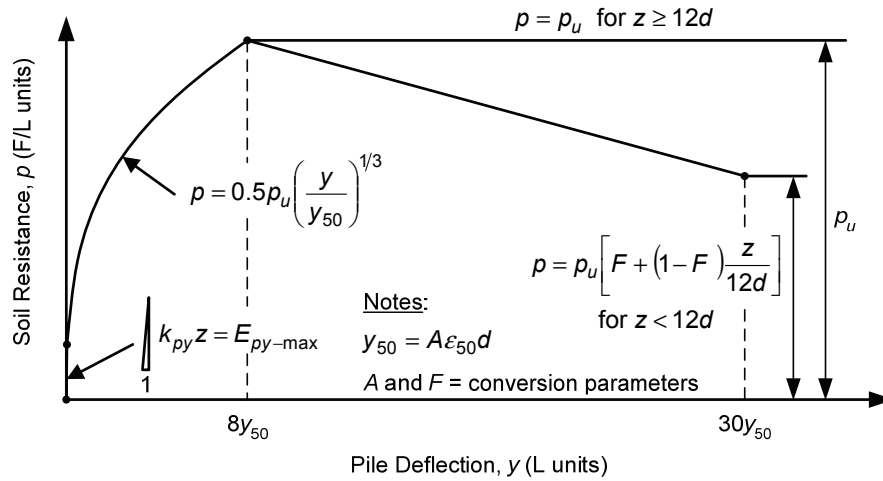
Figure 2-19: Unified clay by Sullivan et al. (1980)

Reese and Van Impe (2001) noted that these parameters have no rational basis and further work would be required in that respect. A more advanced method for clays was put forward by Gazioglu and O'Neill, termed the "Integrated Clay Method" as illustrated in Figure 2-20.
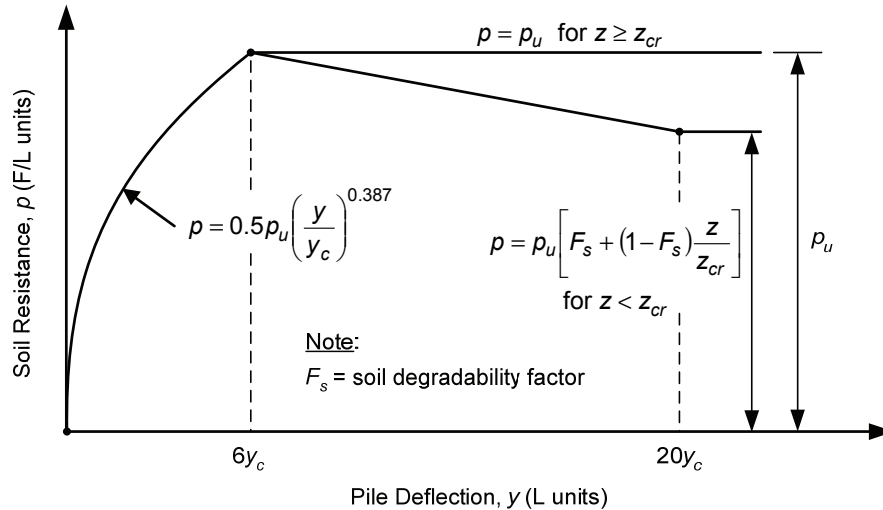
Figure 2-20: Integrated clay method by Gazioglu and O'Neill (1984)

While the Integrated Clay Method curve shape still resembled the curve shapes of the previous clay recommendations, the method addressed a possible effect of the pile, as well as the soil, on the characteristic deflection parameter and hence the curve shape. The characteristic deflection value was denoted by y_c as shown in Figure 2-20, and given by

$$y_c = 0.8\varepsilon_{50}\sqrt{d}\left(\frac{E_p I_p}{E_s}\right)^{0.125} \tag{2.11}$$

32

where recommended values of E_s were as given in Table 2-7. Gazioglu and O'Neill (1984) noted that although relative pile-soil stiffness was implicitly accounted for in the previous empirical *p-y* formulations, there was no assurance that a pile-soil system different to those used to establish the previous *p-y* formulations would produce the same *p-y* curve response. Hence the relative pile-soil stiffness measure incorporated in (2.11) recognized possible differences in *p-y* curve response for pile-soil systems with different pile to soil stiffness ratios. The use of the square root of the pile diameter in (2.11) is discussed in Section 2.5.3.1.

Table 2-7: Recommended values of E_s for the integrated clay method (from Gazioglu and O'Neill, 1984)

Undrained Shear Strength (kPa)	Soil Modulus, E_s (kPa)
< 25	350
25 - 50	350 - 1,000
50 - 100	1,000 - 3,000
100 - 200	3,000 - 10,000
200 - 400	10,000 - 35,000
> 400	> 35,000

Dunnavant and O'Neill (1989) also incorporated a relative pile-soil stiffness measure in their *p-y* recommendation for submerged, stiff clays. This work drew on free-head lateral load tests on a 273 mm diameter driven steel pipe pile (L/d = 43), a 1.22 m diameter driven steel pipe pile (L/d = 9.3), and a 1.83 m diameter bored reinforced concrete pile (L/d = 6.2). Testing was undertaken in an overconsolidated (stiff) clay soil site located at the University of Houston Foundation Test Facility, providing a soil that was different in geological character to that used by Reese et al. (1975). This was an intended change to address suspicions that the Reese et al. (1975) stiff clay had exhibited unusual strength degradation in connection with its well-developed joint structure. While not proven conclusively, the joint structure was suspected of producing a peculiar softening effect by imbibing free water (Gazioglu and O'Neill, 1984).

The *p-y* curve shape deduced by Dunnavant and O'Neill (1989) for static loading is illustrated in Figure 2-21. The characteristic deflection value (y_{50}) was given by

$$y_{50} = 0.0063\varepsilon_{50}d(K_R)^{-0.875} \tag{2.12}$$

where
$$K_R = \left(\frac{E_p I_p}{E_s L^4}\right)$$

and E_s values were as recommended in Table.

The parameter K_R (as introduced in Section 2.4.1) represented a more refined relative pile-soil stiffness measure compared with (2.11), and implied that y_{50} was not linearly dependent on d as also recognized in (2.11) and as discussed further in Section 2.5.3.1. Also apparent in Figure 2-21 was the use of a hyperbolic tangent function to describe the majority of the curve shape, providing the necessary qualities of high initial stiffness, a resistance at large deflections approaching a limiting value, and intervening continuous nonlinear behavior.

$$p = p_u \text{ for } y \geq 8y_{50}$$

$$p = 1.02 p_u \tanh\left[0.537\left(\frac{y}{y_{50}}\right)^{0.7}\right]$$
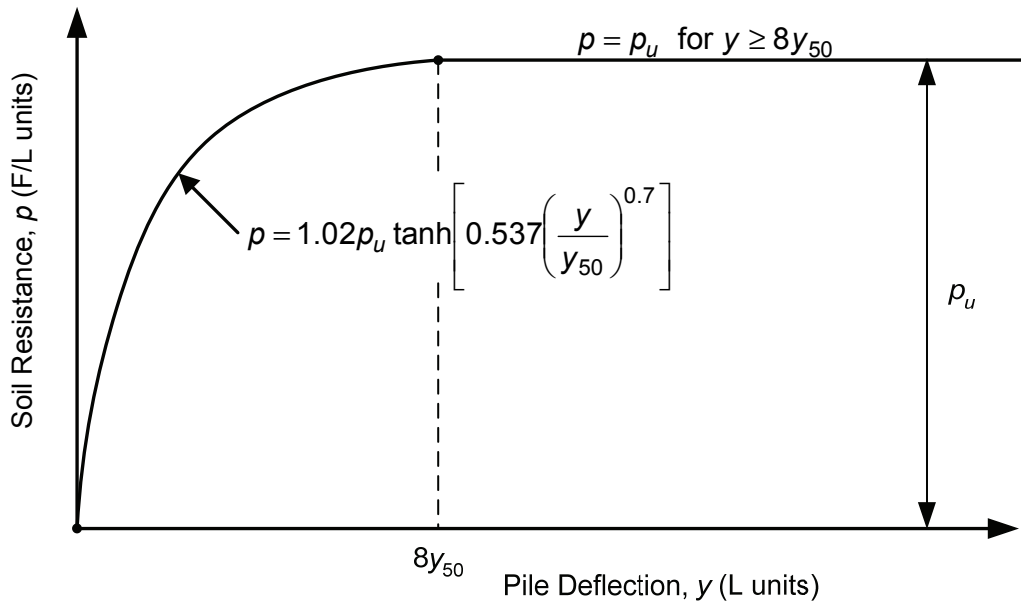
Figure 2-21: Submerged stiff clay by Dunnavant and O'Neill (1989)

Indeed the hyperbolic tangent function has also been recommended for sands in the form as indicated in Figure 2-22 (Murchison and O'Neill, 1984; API, 1993).

Hyperbolic tangent function

Hyperbolic function

$$p = A p_u \tanh\left[\left(\frac{k_{py}z}{A p_u}\right)y\right]$$

Note:

$$A = \sup\left\{3 - 0.8\frac{z}{d}, 0.9\right\}$$

$$p = \frac{y}{\dfrac{1}{k_{py}z} + \dfrac{y}{p_u}}$$
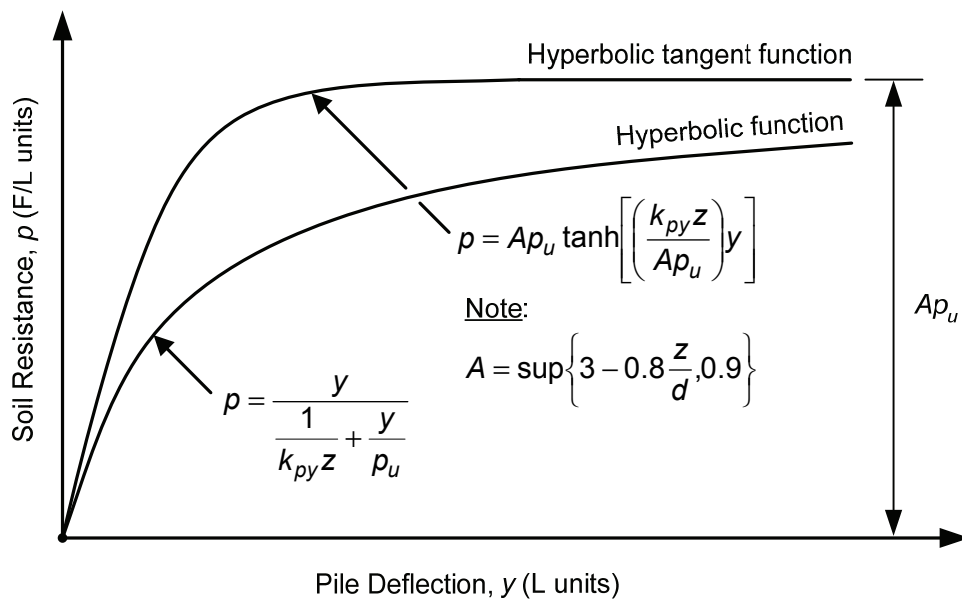
Figure 2-22: Hyperbolic and hyperbolic tangent functions

34

This formulation provided greater economy in that it described the entire curve with just one analytical function, and achieved an initial stiffness value that retained a $k_{py}z$ depth-wise characterization (using k_{py} values as per Figure 2-12), given that, in general,

$$\left[\frac{d(\tanh By)}{dy}\right]_{y=0} = B \quad \text{where } B = \text{a constant} \tag{2.13}$$

so that for the particular hyperbolic tangent p-y formulation shown in Figure 2-22,

$$\left[\frac{dp}{dy}\right]_{y=0} = Ap_u \left[\frac{d\left\{\tanh\left(\frac{k_{py}z}{Ap_u}\right)y\right\}}{dy}\right]_{y=0} = k_{py}z \tag{2.14}$$

Also shown in Figure 2-22 is a hyperbolic version of the same curve (i.e., a curve shape described by the hyperbolic function that is indicated in Figure 2-22, using the same values of initial stiffness and ultimate resistance as used in the hyperbolic tangent function), illustrating the similar utility of this function in describing the shape. Examples of the use of hyperbolic functions to describe the shape of sand and clay p-y curves are given by Vesić (1977), Allen (1985), Lam and Martin, (1986), Fedorovsky, Kurillo, Levachev and Kolesnikov (1986), Wu, Broms and Choa (1988), and Rajashree and Sitharan (2001).

In the case of sands, Murchison and O'Neill (1984) also interpreted a bilinear curve shape from centrifuge pile research undertaken by Scott (1980). Pyke and Beikae (1984) noted that although Scott checked the Reese et al. (1974) sand p-y formulation against his centrifuge results and found reasonable agreement, he concluded that the formulation was unduly complicated and suggested that a simple bilinear formulation would serve the purpose just as well. The bilinear formulation interpreted by Murchison and O'Neill is shown in Figure 2-23, where the initial stiffness value ($E_{py\text{-max}}$) was as determined from (2.9). Given this value the beginning of the second straight line segment was established using the following empirical expression for p_k:

$$p_k = \frac{\sigma_h' d}{\frac{1}{\pi}\left(\frac{1}{\sin^2\phi} + \frac{1}{3-4\nu}\right)^{0.5}} \tag{2.15}$$

where $\sigma_h' = $ effective lateral stress in the soil

$\quad\quad d = $ pile diameter

$\quad\quad \phi = $ interal angle of friction for sand

$\quad\quad \nu = $ Poisson's Ratio for sand
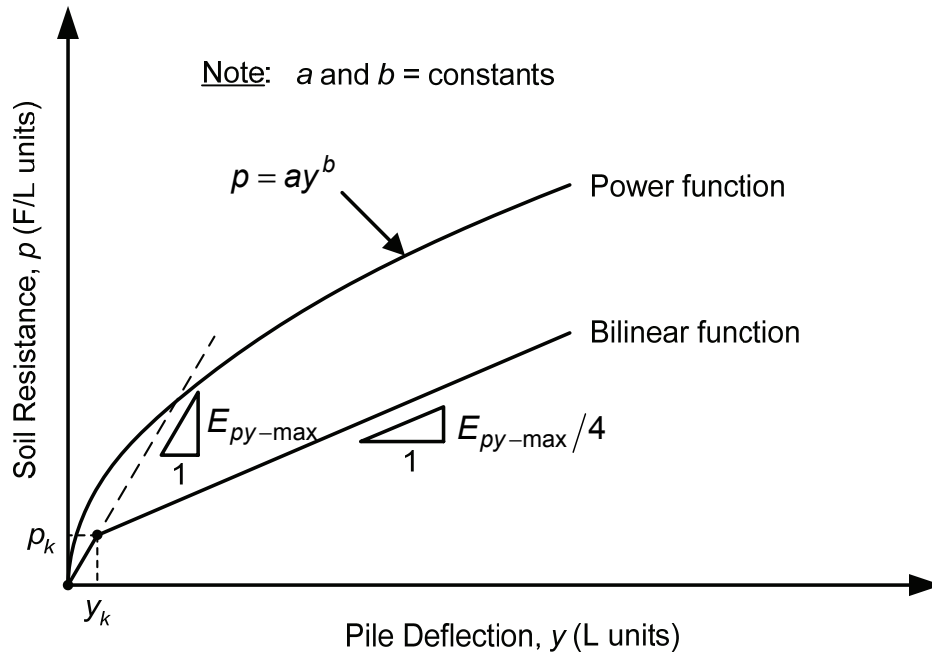
Figure 2-23: Bilinear and power functions

Similar behavior in the centrifuge was noted by Dyson and Randolph (2001) for the case of calcareous sands, where a power law relationship (the basic form of which is shown in Figure 2-23 for comparison) was found to fit experimental results with good agreement. In addition to centrifuge research, Kishida and Nikai (1977) utilized an elastic-perfectly plastic bilinear *p-y* relationship (i.e., a curve shape possessing a horizontal second straight-line segment) for both sand and clay to predict field behavior, and Bransby (1999) advocated the use of a power law relationship to describe *p-y* curves for undrained serviceability conditions.

Pender (1993) considered that some of the existing forms of *p-y* curves were becoming rather complex and in the interest of simplicity offered the following nonlinear relationship instead:

$$y = \frac{p}{E_{py-\max}} \left(\frac{p_u}{p_u - p} \right)^n \tag{2.16}$$

where n = parameter to control the extent of nonlinearity

Resultant *p-y* curve shapes for values of n equal to 0.1 and 1.0 are shown in Figure 2-24, and it is apparent that n was essentially a shape factor. Pender implemented such curves into a finite element pile model and back-analyzed full scale field tests in order to obtain appropriate n values. In this way Pender reported that an n value equal to 1.0 was appropriate for sands, while values in the range 0.2 to 0.3 appeared appropriate for clays. It is noted that the curve shapes in Figure 2-24 are similar to those given by the hyperbolic and hyperbolic tangent shapes shown in Figure 2-22, as all assume a curve shape in the form of a hyperbola.

36

The various *p-y* curve shapes that have been presented are justified in their own right, but the variety of forms that are apparent are suggestive of some leeway in specifying the manner in which soil resistance is developed with increasing pile deflection. In terms of pile behavior this is suggestive of some tolerance of structural actions to the shape of the curve. However, as indicated in most of the *p-y* formulations that have been presented, the curve shape is of no use without the specification of an appropriate ultimate resistance value that serves to bound the curve in conjunction with its lower (initial stiffness) limit. Given that Reese and Van Impe (2001) considered that stress will control in most designs, this is perhaps the most important component of *p-y* curves.

2.5.1.3   Ultimate Resistance

A complete *p-y* specification requires the determination of appropriate ultimate values of soil resistance mobilized against a pile with depth. In this respect, and as was the case when determining initial *p-y* stiffness values, the influence of soil type and the presence of a stress-free ground surface play a significant role. Broms (1964a, b), as discussed in Section 2.3, exemplified such dependence in establishing different design criteria for determining the ultimate lateral resistance of driven piles in cohesive ("clay") and cohesionless ("sand") soils. Implicit in these criteria was acknowledgement of the differing deformation characteristics of clay and sand in response to pile loading (Figure 2-5), as reflected in the ultimate resistance distributions that were adopted, as shown in figure 2-25.

Curve Function:

$$y = \frac{p}{E_{py-\max}} \left(\frac{p_u}{p_u - p} \right)^n$$
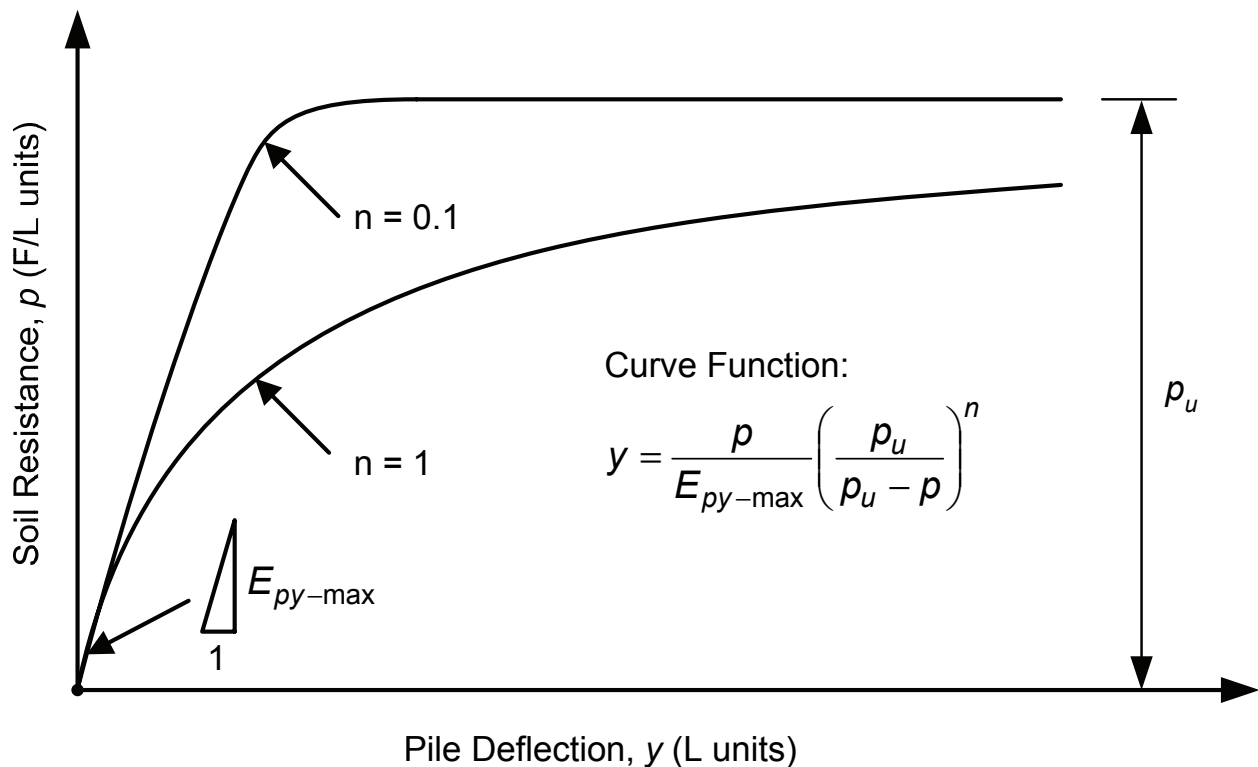
Figure 2-24: Nonlinear p-y function proposed by Pender (1993)

37

a) Clay Case   b) Sand Case

$2s_u d$

$1.5d$

$3d$

z

(8 to 12)$s_u d$ $9s_u d$ $3d\gamma z K_p$

Probable   Adopted   Adopted
Distribution   Distribution   Distribution
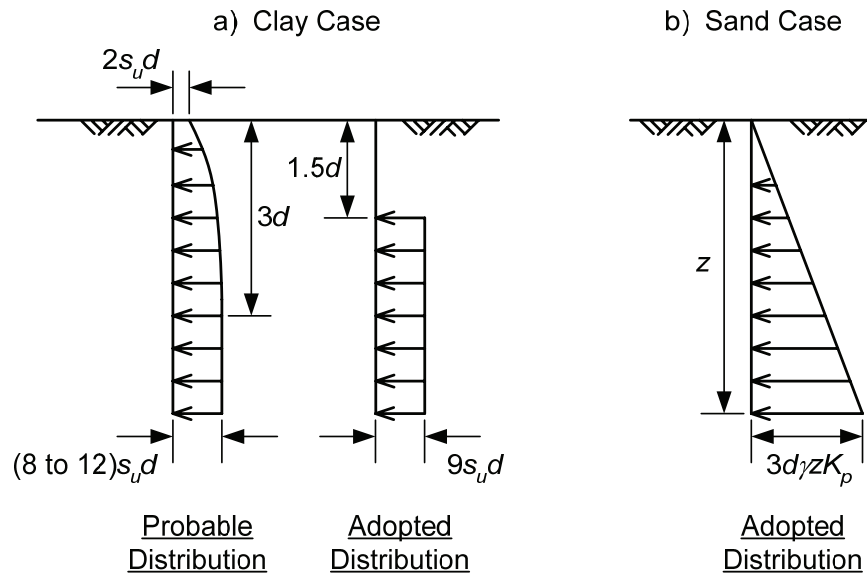
Notes: s_u = undrained shear strength
           K_p = Rankine passive earth
                   pressure coefficient
           d = pile diameter
           γ = unit weight of soil

Figure 2-25: Ultimate resistance (p_u) distributions according to Broms (1964a, b)

Broms (1964a, b) reasoned ultimate resistance values based on theoretical models, load test data and judgment. A similar state of affairs applies to the *p-y* framework, where demarcation between cohesive and cohesionless soil conditions, together with surficial and at-depth distinctions, forms a basis for the various *p-y* formulations that have been presented. Reese (1958) was instrumental in this effort, proposing idealized mechanistic models to rationalize ultimate soil resistance exerted against a pile at shallow and deep depths. In order to characterize shallow resistance, Reese envisaged a mobilized wedge of soil being moved up and out of the ground in response to a laterally deflected pile. At sufficiently deep depths, a transformation to only horizontal movement was surmised, where overburden was assumed to be sufficient to confine the region of resistance to a mobilized horizontal slice of soil acting to flow around the pile. These ideas are illustrated in Figure 2-26.

The forces acting on the free body surficial wedge shown in Figure 2-26(b) consist of the following: *W* is the body force; F_ϕ is the reaction force mobilized on the sloping underside of the wedge; F_s is the shear force mobilized along the sides of the wedge; F_n is the normal force acting on the sides of the wedge; and F_{pile} is the force imposed by the pile over the contact height *h*. The angles α and β completely define the wedge geometry. It is instructive to consider the case when $\phi = 0$ and $\alpha = 0$ as depicted in Figure 2-27(a), where this case has been used to represent cohesive (clay) soil conditions with the assumptions that the soil is saturated and a total stress (undrained) approach applies (Reese and Van Impe, 2001).
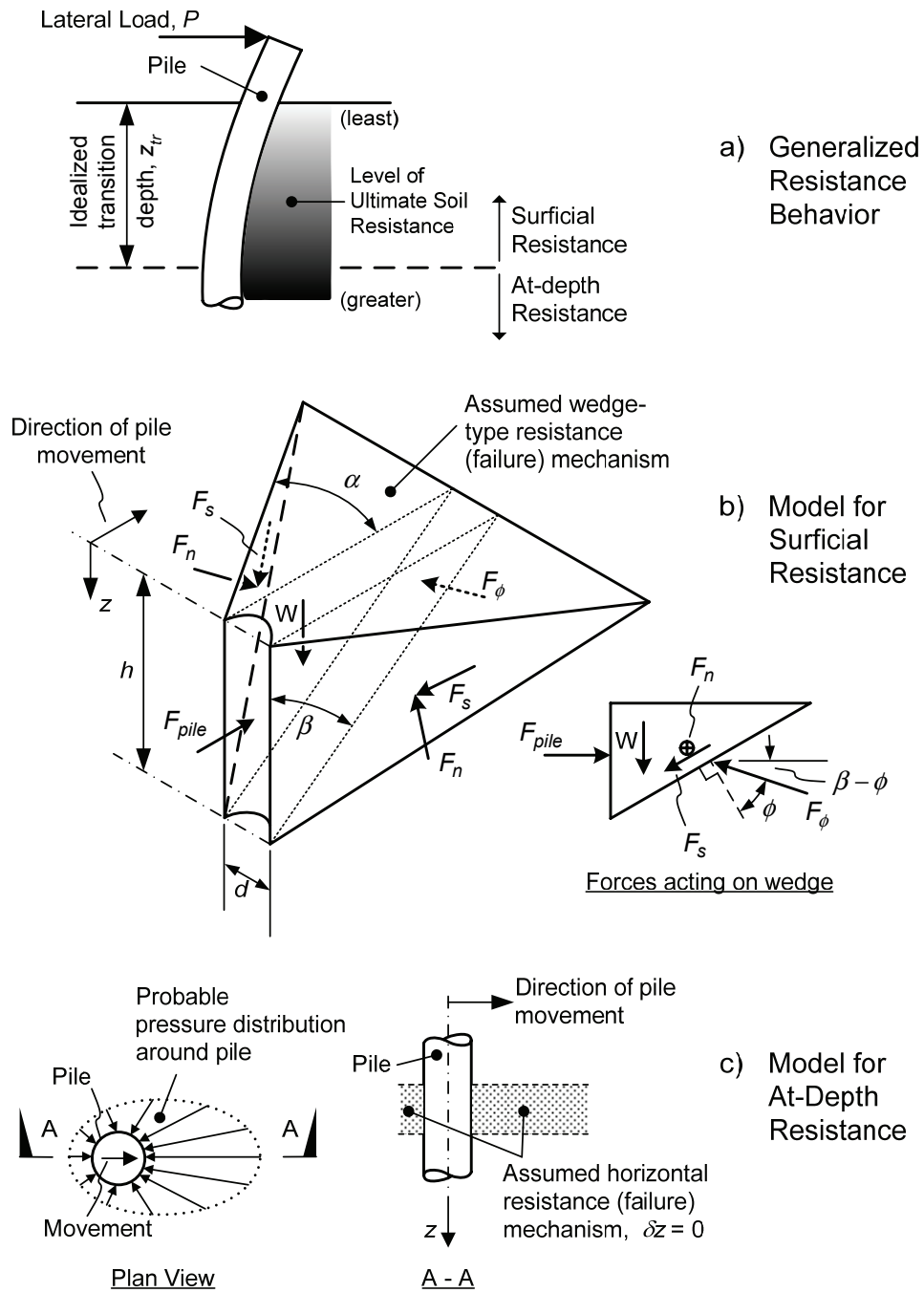
Figure 2-26: Ultimate resistance behavior and models (after Reese and Van Impe, 2001)
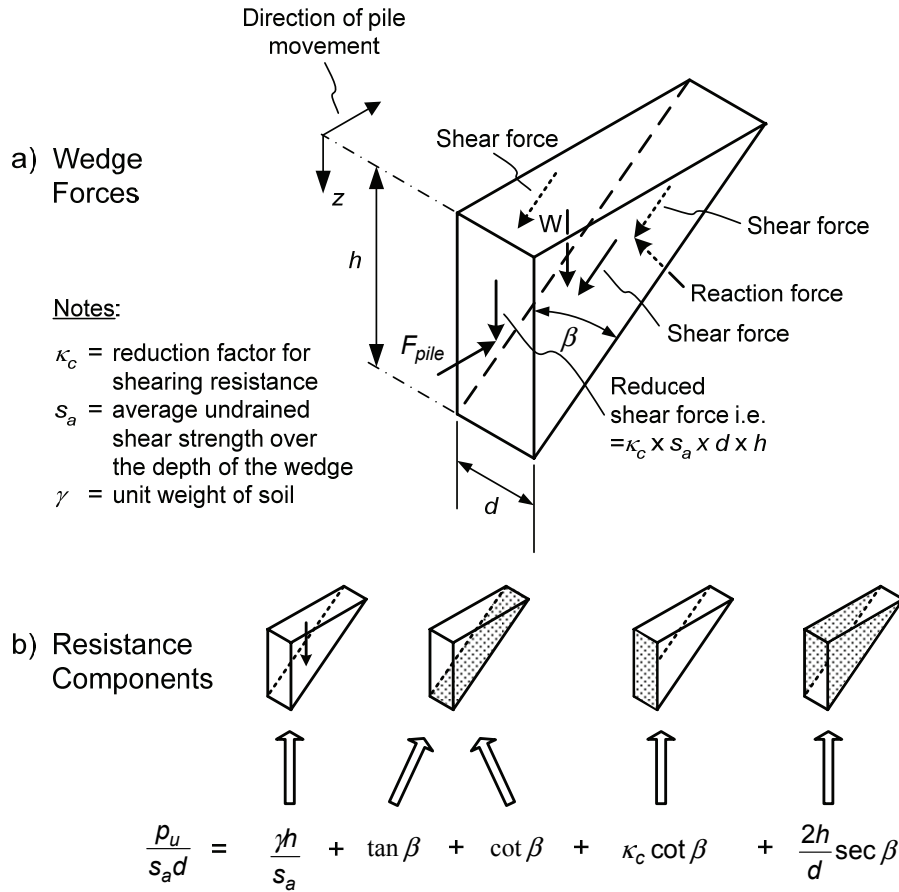
Figure 2-27: Surficial wedge model for cohesive soil conditions

Following Reese (1958) and Thompson (1977), consideration of both vertical and horizontal static equilibrium of the wedge shown in Figure 2-27(a) leads to the following:

$$F_{pile} = \frac{1}{2}\gamma dh^2 + (1 + \kappa_c)s_a d\cot\beta + s_a dh\tan\beta + s_a h^2 \sec\beta \qquad (2.17)$$

Differentiating this expression with respect to h (assuming β to be fixed) defines the ultimate resistance (p_u), that can then be normalized by dividing by the average undrained shear strength and pile diameter to give

$$\frac{p_u}{s_a d} = \frac{\gamma h}{s_a} + (1 + \kappa_c)\cot\beta + \tan\beta + \frac{2h}{d}\sec\beta \qquad (2.18)$$

40

The expansion of (2.18) is given in Figure 2-27(b), with the resistance component that is associated with each term shown pictorially. In this way the right hand side of (2.18) is clearly synonymous with a bearing capacity factor for cohesion such that

$$\frac{p_u}{s_a d} = N_p \tag{2.19}$$

where N_p = lateral ultimate resistance factor

If an appropriate angle is assigned to β and the depth term h is replaced with the variable z, a generalized form of N_p for surficial resistance is evident from (2.18) as follows

$$N_p = A + \frac{\sigma'_z}{s_u} + B\frac{z}{d} \tag{2.20}$$

where A, B = constants

$\quad\sigma'_z = \gamma' z$ = vertical effective stress

$\quad s_u$ = undrained shear strength value for wedge

$\quad z$ = depth

$\quad d$ = pile diameter

Utilization of this form of equation is evident in Table 2-8 that lists the various surficial N_p expressions that have been recommended for the clay p-y curve formulations presented. These indicate differences in detail reflecting the different pile-soil systems used to derive the relationships, and the differing empiricism employed to fit the results to agree with observed behavior. The latter is also reflected in the use of some additional empirical adjustment factors that are indicated with the curve shape information given in Figure 2-15 through Figure 2-21. These adjustment factors were necessary given that the theoretical wedge model is only considered to be an appropriate indicator of the form, rather than the magnitude, of ultimate resistance that is actually developed (Reese and Van Impe, 2001).

Once a sufficient depth is reached in a cohesive soil, a limiting value of N_p is considered to exist in conjunction with the at-depth resistance mechanism illustrated in Figure 2-26(c). This case has been the subject of various investigations with varying degrees of sophistication (Reese, 1958; Hansen, 1961; Broms, 1964a; Yegian and Wright, 1973; Thompson, 1977; Stevens and Audibert, 1979; Randolph and Houlsby, 1984). The notion of soil flowing around the pile in horizontal planes is well suited to plasticity theory, so that most of the work cited is seated in two-dimensional plasticity solutions using either classical (slip-line) or numerical (finite element) analysis means. These encompass variations due to considering whether or not separation of the soil from the pile occurs, the extent of the undrained shear strength of the soil that is mobilized in shear around the pile perimeter, and differences in pile shape. Reese employed the most simplistic approach by considering the stress states of discrete soil blocks representing the soil around a pile (refer Figure 2-28a for concept), whereas Stevens and Audibert back-calculated N_p values from field test data. In any case the magnitude of at-depth N_p values lie in the range 8 to 12, with Kulhawy and Chen (1995) having noted that a unique value of $N_p = 9$ for driven piles would be a fair simplification, whereas for drilled shafts with much rougher surfaces a value of $N_p = 12$ may be more appropriate.

Table 2-8: Surficial N_p expressions for cohesive soil conditions

N_p	Notes	Reference
$3+\dfrac{\sigma_z}{s_u}+J\dfrac{z}{d}$	$J = 0.25$ or 0.5 s_u = value at depth z	Matlock (1970)
$2+\dfrac{\sigma_z'}{s_u}+2.83\dfrac{z}{d}$	s_u = average value over depth z	Reese et al. (1975)
$3+\dfrac{\left(\sigma_z'\right)_{ave.}}{s_u}+0.5\dfrac{z}{d}$	$\left(\sigma_z'\right)_{ave.}$ and s_u = average values over depth z	Reese and Welch (1975)
$2+\dfrac{\left(\sigma_z'\right)_{ave.}}{s_u}+0.833\dfrac{z}{d}$ or $3+0.5\dfrac{z}{d}$	As per immediately above for first expression. Second expression uses s_u value at depth z to calculate p_u. Lesser p_u derived from both expressions used in design.	Sullivan et al. (1980)
$3+6\left(\dfrac{z}{z_{cr}}\right)$	$z_{cr}=L_c/4$ where $L_c=3d\left(\dfrac{E_pI_p}{E_s d^4}\right)^{0.286}$ = critical length measure	Gazioglu and O'Neill (1984)
$2+\dfrac{\sigma_z'}{s_u}+0.4\dfrac{z}{d}$	s_u = average value over depth z	Dunnavant and O'Neill (1989)

The surficial wedge and horizontal at-depth mechanisms depicted in Figure 2-26 also apply for the case of sands, as was utilized by Reese et al. (1974). This work employed the wedge configuration shown in Figure 2-26(b) to determine surficial resistance, and the block flow model depicted in Figure 2-28 for at-depth resistance.
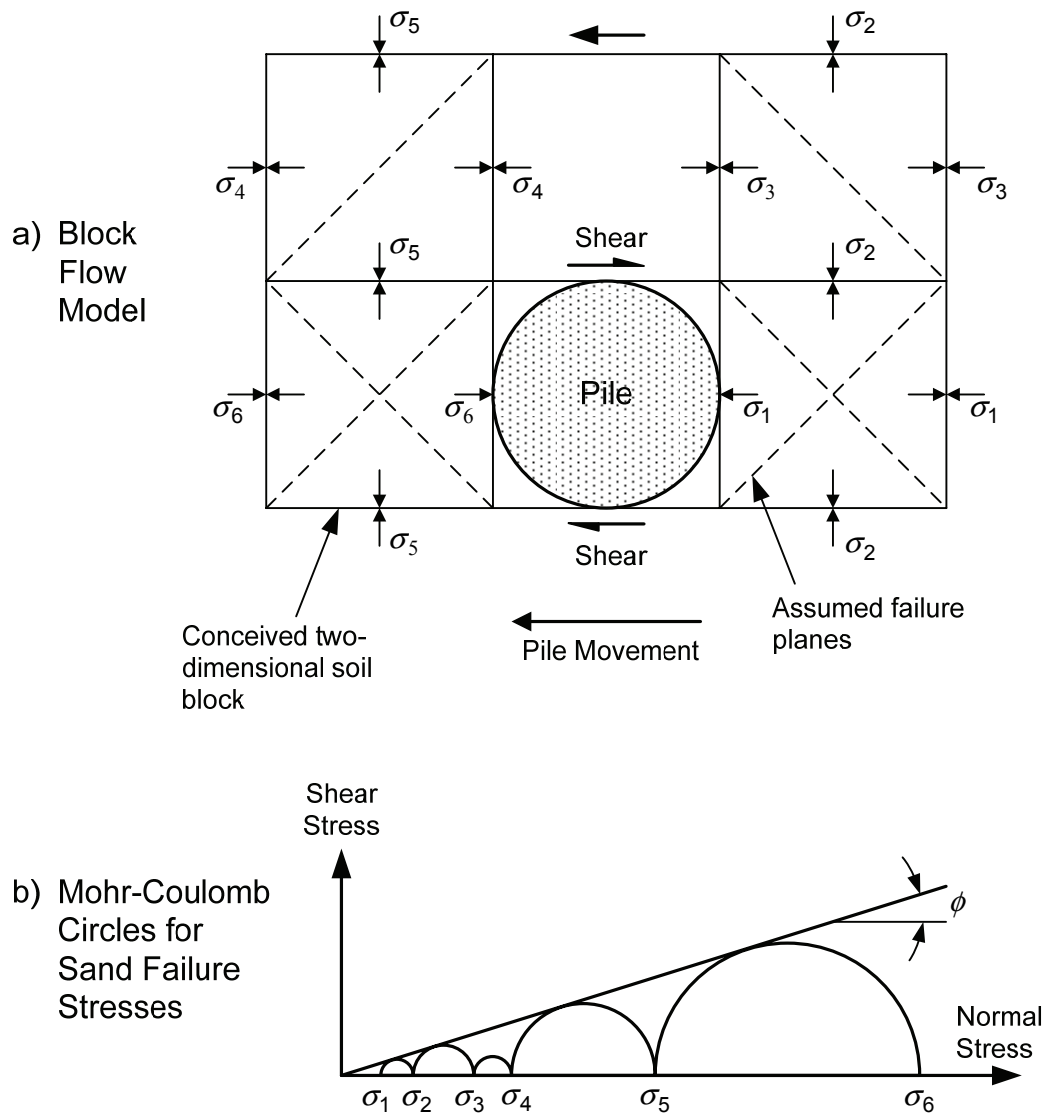
Figure 2-28: At-depth ultimate resistance model for case of cohesionless soil (after Reese et al., 1974; Reese and Van Impe, 2001)

Establishing and differentiating the pile force acting on the free body wedge shown in Figure 2-26(b) in the same fashion as was done for the cohesive soil case, and deriving mobilized soil stresses for the block flow model in Figure 2-28(a) based on physical arguments and the Mohr-Coulomb failure states depicted in Figure 2-28(b), expressions for surficial and at-depth ultimate resistances were derived as given by (2.21) and (2.22), respectively.

$$(p_u)_{\text{surf.}} = \gamma z \left[\frac{K_0 z \tan \phi \sin \beta}{\tan(\beta - \phi)\cos \alpha} + \frac{\tan \beta}{\tan(\beta - \phi)}(d + z \tan \beta \tan \alpha) \right]$$

$$+ \gamma z [K_0 z \tan \beta (\tan \phi \sin \beta - \tan \alpha) - K_a d] \qquad (2.21)$$

$$(p_u)_{\text{at-depth}} = K_a d \gamma z (\tan^8 \beta - 1) + K_0 d \gamma z \tan \phi \tan^4 \beta \qquad (2.22)$$

where K_0 = coefficient of earth pressure at rest

K_a = minimum coefficient of active earth pressure

These expressions are far more complex compared with the cohesive soil case, a result of the frictional nature of the cohesionless (sand) soil and the assumed drained conditions (i.e., effective stress analysis) that demand more complex failure geometry and associated forces in the surficial case, and more complex failure stresses in the at-depth case.

Once again (2.21) and (2.22) are only considered to be appropriate indicators of the form of ultimate resistance, as Reese et al. (1974) found it necessary to apply depth-dependent empirical adjustment factors A_s and B_s (as indicated on the curve shape shown in Figure 2-16) in order to agree with observed behavior. A similar approach applied to the hyperbolic tangent *p-y* formulation for sands shown in Figure 2-22, where the determination of p_u was as per (2.21) and (2.22), and the parameter *A* represented a depth-dependent empirical adjustment factor similar to the factor A_s used in the Reese et al. procedure.

In addition to the ultimate resistance work of Broms (1964b) and Reese et al. (1974), the limit analysis work of Hansen (1961) is also applicable to sands given that it catered for soils with both cohesion and friction (i.e., a *c-φ* soil). This work invoked mechanistic models similar to those used by Reese et al. to develop expressions for ultimate resistance as a function of *φ* and depth, but given that only rigid piles applied its use has been limited. However, Hansen's expressions have been implemented within a *p-y* framework to assess drilled shaft response in partially saturated silts and clays with good results (Mokwa, Duncan and Helmers, 2001). Comparison of Hansen's ultimate resistance with the Broms and Reese et al. criteria (Evans and Duncan, 1982; Kulhawy and Chen, 1995) indicates they are all comparable at shallower depths, but deviate with increasing depth in that Hansen's values are generally lower compared to Reese et. al., and higher compared to Broms.

There are various *p-y* curve formulations apparent from the above discussion, but in terms of practice the use of the 1970's *p-y* formulations for sand and clay have tended to be the industry standards, at least in the United States. This has been encouraged by commercial programs such as LPILE (Ensoft, 1999), where these *p-y* curve formulations have been implemented as "standard" clay and sand options for assessing laterally loaded behavior. To provide a more physical appreciation of such formulations, Figure 2-29 shows an illustrative comparison of the ultimate resistance with depth for a 600 mm diameter pile embedded in either clay or sand, calculated using the formulations according to Matlock (1970) and Reese et al. (1974), respectively. Illustrative comparisons of the various *p-y* curve formulations for clay and sand at various depths are then provided in Figure 2-30 and Figure 2-31. In all cases a groundwater table at the ground surface applied.
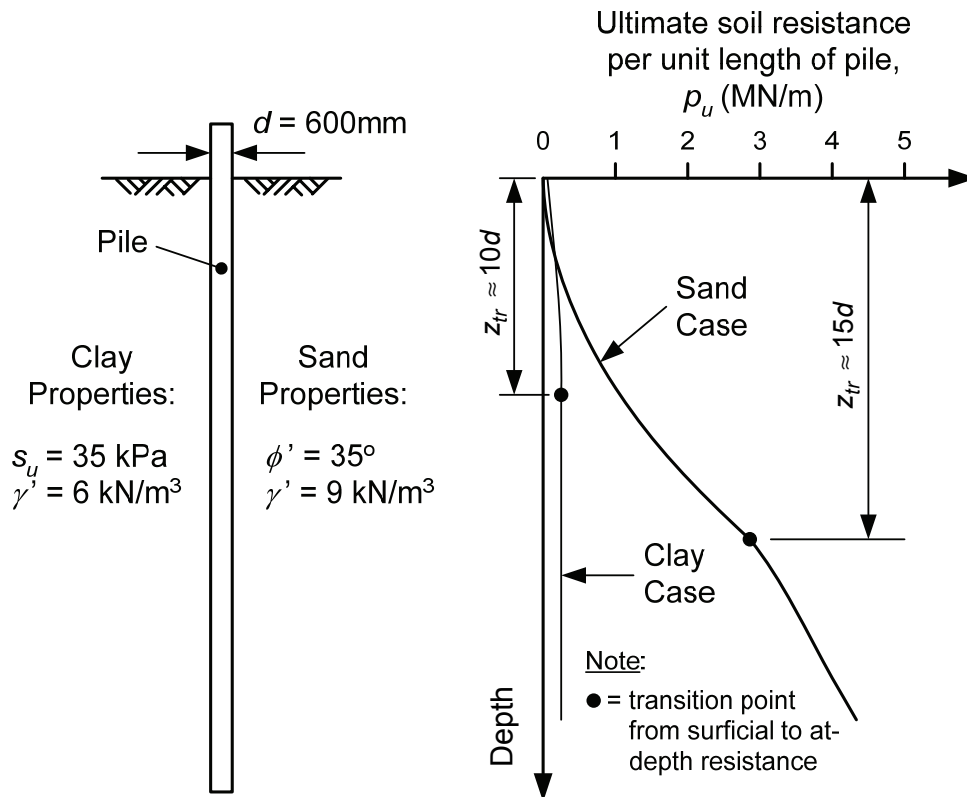
Figure 2-29: Illustrative comparison of sand and clay ultimate resistance with depth

2.5.2   Alternative *p-y* Approaches

Although the *p-y* approaches based on full-scale, instrumented pile testing coupled with laboratory soil testing can be considered as somewhat of the mainstream in U.S. practice, a case for alternative approaches is emerging. In this alternative category are field-based methods utilizing the pressuremeter, flat dilatometer or cone penetrometer testing devices, and a theory-based method utilizing the so-called "Strain Wedge" model.

2.5.2.1   Field-Based Methods

An in situ test is particularly worthy if it can be compared, to some extent, with the design element for which it is providing information. In the case of the pressuremeter and flat dilatometer tests, this is apparent in terms of laterally loaded pile design. The pressuremeter test presents a strong analogy to the problem of a laterally loaded pile as illustrated in Figure 2-32. As shown, the all-round pressure (p') developed against the radially expanded pressuremeter resembles the soil resistance (p) developed against the front of a laterally loaded pile. Furthermore, the ability of the pressuremeter to measure both the resistance and deformation of the soil (the latter recorded in terms of radial strain), enables a direct comparison to be made between the pressuremeter response curve and the *p-y* curve for a pile.

45

Depth = d
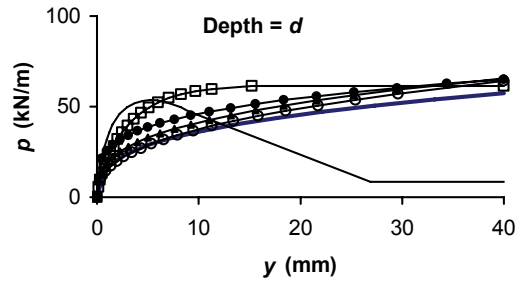
Notes:

d = 0.5 m
s_u = 50 kPa
γ = 6 kN/m^3
L = 10 m
$E_p I_p$ = 92,000 kN-m^2
E_s = 1000 kPa

Key:

Unified Clay	:	Sullivan et al. (1980)
Stiff Clay A	:	Reese et al. (1975)
Soft Clay	:	Matlock (1970)
Stiff Clay B	:	Reese and Welch (1975)
Integrated Clay	:	Gazioglu and O'Neill (1984)
Stiff Clay C	:	Dunnavant and O'Neill (1989)

Depth = 3d

— Unified Clay
— Stiff Clay A
▲ Soft Clay
♦ Stiff Clay B
○ Integrated Clay
□ Stiff Clay C

Depth = 6d

Depth = 9d
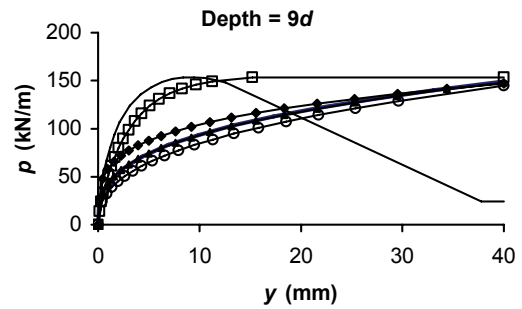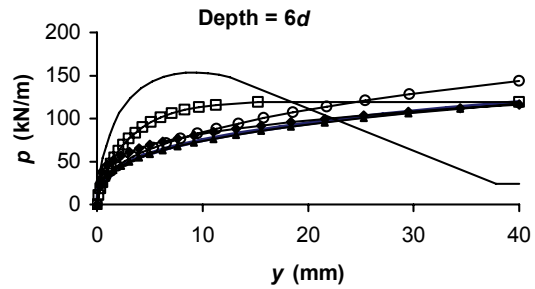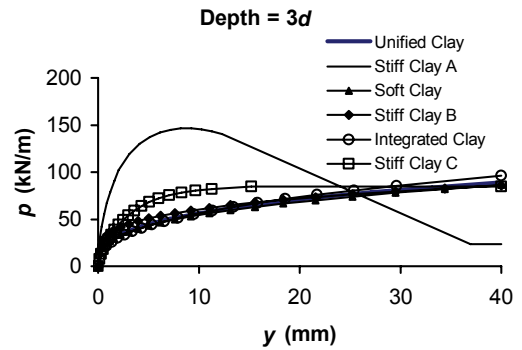
Figure 2-30: Illustrative comparison of clay *p-y* curves at various depths

46

Depth = _d_

Depth = 3_d_

Depth = 6_d_

Depth = 9_d_

Notes:

d = 0.5 m
ϕ = 35 degrees
γ = 9 kN/m^3
K_0 = 1.0

Key:

Hyperbolic Sand : API (1993)

Bilinear Sand : Murchison and O'Neill (1984)
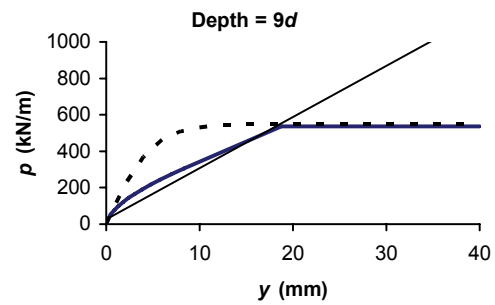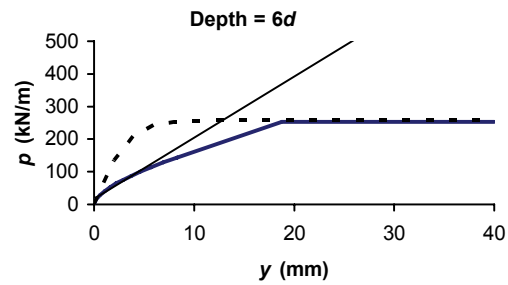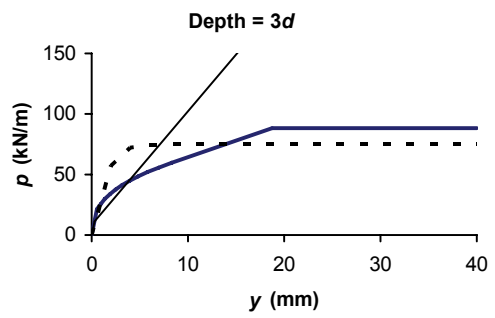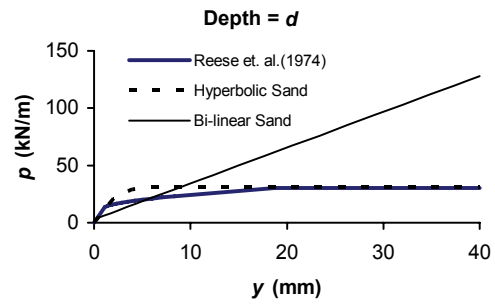
Figure 2-31: Illustrative comparison of sand _p-y_ curves at various depths

a) Laterally loaded pile

b) Pressuremeter test
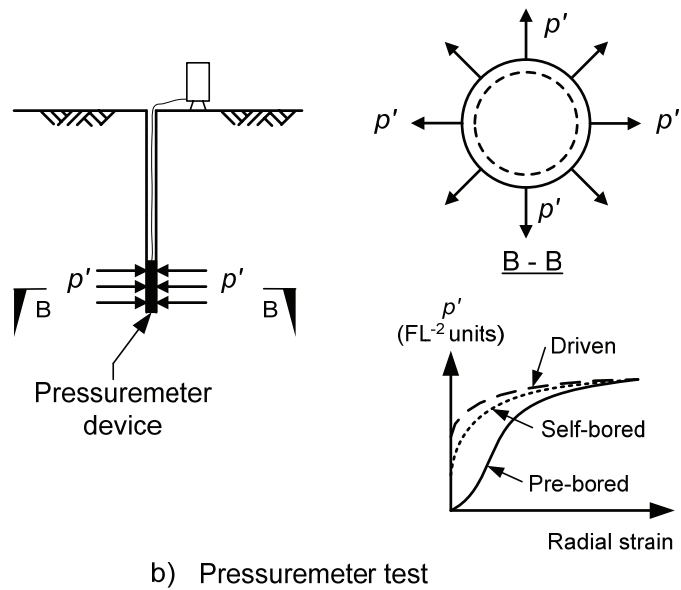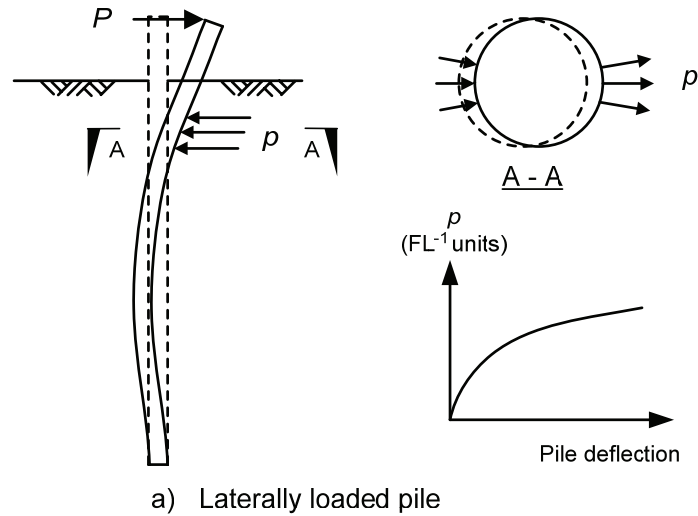
Figure 2-32: Laterally loaded pile and pressuremeter analogy (after Briaud et al., 1984; Robertson et al., 1984)

Pressuremeter methods to derive *p-y* curves have been presented for the case of prebored pressuremeter tests (Briaud, Smith and Meyer, 1984; Briaud, Smith and Tucker, 1985) and pushed-in (driven) pressuremeter tests (Robertson, Hughes, Campanella and Sy, 1984). Briaud et al. (1984) also noted four other methods for prebored tests and two methods for self-bored tests. The method by Briaud et al. also served to provide additional insight into the laterally loaded problem with identification of what was termed the "critical depth". The concept is illustrated in Figure 2-33, where Figure 2-33(a) first depicts the distribution of soil resistance that would be expected to be mobilized against a laterally loaded pile at a given deflection. Briaud et al. defined the instantaneous critical depth (z_c) as the distance below the ground surface at which the maximum soil resistance was developed at a given pile deflection, and noted that it defined the zone of reduced lateral soil resistance due to the presence of the ground surface.

a) Instantaneous critical depth (z_c)

b) Ultimate critical depth (D_c)

c) Critical depth versus pile-soil stiffness measure

Notes:

p_L^* = pressuremeter net limit pressure
d = pile diameter
E_p = Young's modulus for pile
I_p = Second moment of area for pile
D_c = critical depth

Legend:

● Clay site
○ Sand site
■ Silt site

$$\text{Relative Rigidity } (RR) = \frac{1}{d}\sqrt[4]{\frac{E_p I_p}{p_L^*}}$$
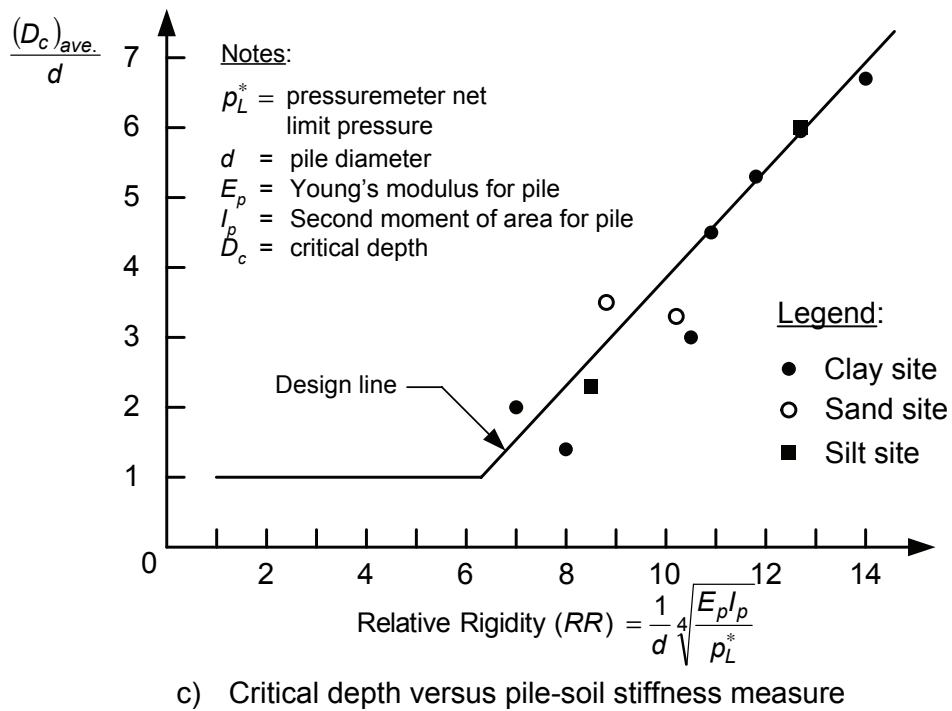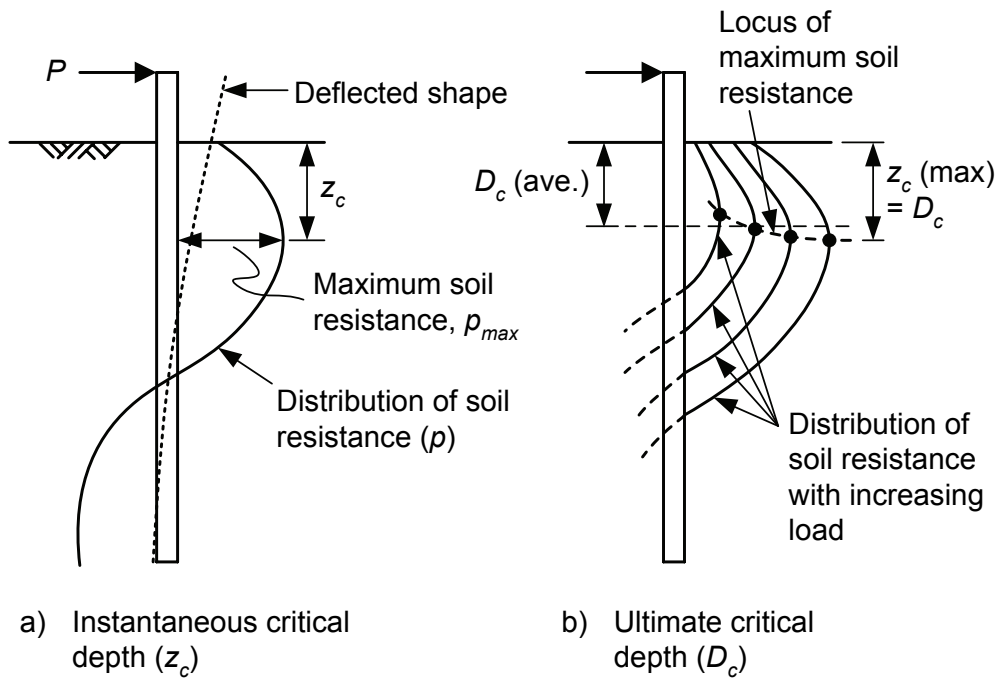
Figure 2-33: Critical depth and relative rigidity concepts (after Briaud et al., 1984, 1985)

Drawing on documented field test data as evidence, the progressive deepening of instantaneous critical depth values to a maximum value with increased loading was noted (refer Figure 2-33b), and the critical depth, denoted by D_c, defined as such. Recognizing the influence of a critical depth in both the pile and pressuremeter cases, empirical soil resistance reduction factors within the critical depth were then established for both cases. To determine the appropriate critical depth of a pile, an empirical relationship was developed between the average critical depth, denoted by $(D_c)_{ave.}$ and indicated in Figure 2-33(b), and a relative pile-soil stiffness measure termed the relative rigidity (RR), as given in Figure 2-33 (c). The RR measure incorporated the pressuremeter value p_L^*, where this represented the average net limit pressure measured within the critical depth of each pile in the field-test database.

The data and design line shown in Figure 2-33(c) served as another reminder of the need to account for relative pile-soil stiffness when assessing laterally loaded pile behavior, but more importantly highlighted the pressuremeter as a useful in situ tool capable of directly characterizing a pile-soil system. This included the ability of the pressuremeter to produce *p-y* curves, as validated by Briaud et al. (1984, 1985) and Robertson et al. (1984) by conducting pressuremeter tests at load test sites to derive relevant *p-y* curves. These curves were then implemented in standard DLT models to derive pile actions, and the results compared with those measured, indicating good agreement. Anderson, Townsend and Grajales (2003) also reported successful predictions of case histories using pressuremeter-derived *p-y* curves, although they noted caution with saturated clays, recommending that pressuremeter tests be performed slowly in this case in order to minimize pore pressure effects.

The flat dilatometer has also found use in establishing *p-y* curves, although its capabilities are not to the same extent as the pressuremeter. In the flat dilatometer test, the technique of inflating a 60 mm diameter steel membrane into the soil in the horizontal direction to achieve 1 mm of deflection at the center, can only reasonably be expected to correlate well with the initial stiffness of *p-y* curves. Robertson, Davies and Campanella (1989) and Gabr, Lunne and Powell (1994) provided evidence in this respect, successfully predicting field test data using *p-y* curves that utilized dilatometer data to characterize the stiffness, and the conventional mechanistic approaches to establish ultimate resistance values. Anderson et al. (2003) also compared case histories against computer predictions using dilatometer-derived *p-y* curves, but recommended a restrictive application to low load levels (25% of ultimate), as predictions at higher load levels were too stiff.

The cone penetration test (CPT) is an attractive alternative given its ability to provide practically continuous profiling of soil behavior in terms of cone resistance and shaft friction correlations. Given that the behavior of the soil near the ground surface plays the most important role in defining laterally loaded pile behavior, obtaining detailed knowledge in this zone to characterize *p-y* curves is an improvement. Evidence of this improvement was suggested by the findings of Anderson et al. (2003), who concluded that *p-y* curves using friction angle and undrained shear strength input parameters derived from standard CPT correlations produced the best prediction of field behavior, compared with *p-y* curves using input parameters from standard penetration test (SPT) correlations, or *p-y* curves derived from pressuremeter and flat dilatometer methods. Another CPT approach is the centrifuge work by Dyson and Randolph (2001), where the cone resistance was used to quantify the resistance component of a *p-y* curve described by a power law relationship.

2.5.2.2   Strain Wedge Method

The notion of a mobilized passive wedge of soil resisting a laterally loaded pile forms the hypothesis of the Strain Wedge (SW) approach. Initially presented in connection with a laterally loaded pile in sand (Norris, 1986), the SW model has subsequently been applied to clay soils, layered soils, and pile groups (Ashour, Pilling and Norris, 1997; Ashour, Norris and Pilling, 1998; Ashour, Pilling and Norris, 2001;

Ashour, Pilling and Norris, 2004). A defining feature of the SW model is an interdependent formulation that accounts for the varying flexibility and size of a passive wedge necessary to resist a laterally deflected flexible pile of certain dimensions and bending stiffness. Consequently, possible output from the model includes *p-y* curves generated over the depth of the mobilized passive wedge for a particular pile-soil system. In this way a theory-based *p-y* approach is apparent.

Geometry of the assumed passive soil wedge is shown in Figure 2-34(a), characterized by the spread of its fan angle (assumed equal to the mobilized effective friction angle, ϕ_m'), a height *h* corresponding to the mobilized depth of the passive wedge, and a mobilized base angle $\beta_m = 90 - \theta_m$, where θ_m is assumed equal to $45 - \phi_m'/2$. The resistance mechanism to an applied line load acting on a unit depth of pile (i.e., *p*) is considered to exist in the form of shear resistance mobilized along the side of the pile (τ) and a constant increment in horizontal stress $\Delta\sigma_h$ mobilized across the width of the wedge. These are illustrated in Figure 2-34(b), for a horizontal wedge slice of unit thickness at an arbitrary depth *z*. As indicated, the length *AB* represents the width of the wedge over which $\Delta\sigma_h$ acts, and the assumed geometry of the wedge results in the opposing side forces *F* canceling out so that no contribution to lateral resistance results.

Recognizing that effective stress increases with depth and thus the response characteristics of the soil at different depths will be different, the passive wedge is envisioned to consist of horizontal sublayers whereby each sublayer represents a specific state of the soil (refer Figure 2-34c). In this way the SW model can easily cater for layered soil profiles or equally a uniform soil that differs with depth according to effective stress states. In order to characterize the response characteristics of the passive soil wedge, the assumption of initial isotropic stress conditions is made and an analogy drawn between a horizontal soil element located at the wedge boundary, and a vertical isotropically consolidated triaxial compression test sample, as illustrated in Figure 2-34(c). The horizontal stress change $\Delta\sigma_h$ is thus considered equal to the deviatoric stress in the triaxial test, and the effective overburden stress (σ_{v0}') equal to the confining pressure imposed in the triaxial test. A solution process is then required to relate the distortion of the strain wedge to triaxial strain, ε.

The solution process first considers the shear distortion of the passive wedge as depicted in Figure 2-35(a), where it is noted that small-strain shear strain (γ) is constant over the height of the wedge. Furthermore, the stress system is assumed such that the induced horizontal stress change $\Delta\sigma_h$ is in the direction of the major principal effective stress and the stress changes in all other directions are zero. Given the constant value of $\Delta\sigma_h$ over the width of the wedge, a constant state of strain then applies within the wedge in the horizontal direction. The associated Mohr circle of strain for this case provides the following relationship (Norris, 1986):

$$\delta = \frac{\gamma}{2} = \frac{(1+\nu)}{2}\sin 2\theta_m \varepsilon \qquad (2.23)$$

where δ = deflection pattern,

γ = shear strain,

ν = Poisson's ratio of soil,

θ_m = current wedge angle, and

ε = axial strain in triaxial test.

Using (2.23) as a theoretical link between wedge distortion and triaxial test distortion, the deflected shape of the flexible pile that accompanies the wedge distortion is linearized in the manner shown in Figure 2-35(b), in order to assign appropriate values of stress change $\Delta\sigma_h$ to each sublayer (as illustrated in Figure 2-35c).

a) Strain wedge geometry

b) Wedge slice at depth z indicating forces

Plan View

c) Stress system equivalency

Triaxial Test

Sublayers

$\theta_m = 45 - \dfrac{\phi'_m}{2}$

A - A
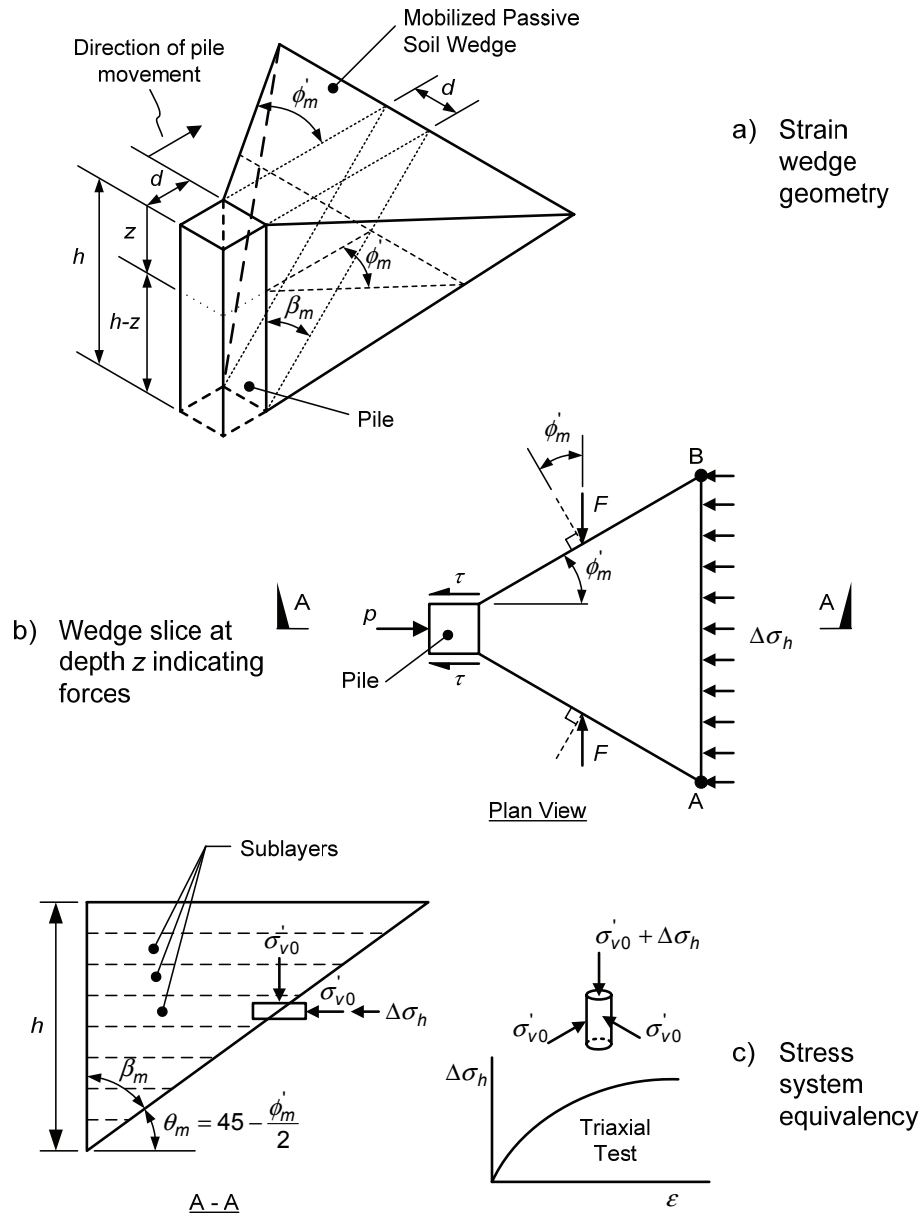
Figure 2-34: Strain wedge model concepts (after Norris, 1986)

a) Shear distortion of strain wedge

b) Pile deflection (exaggerated)

c) Strain - stress response at different depths z_1 and z_2
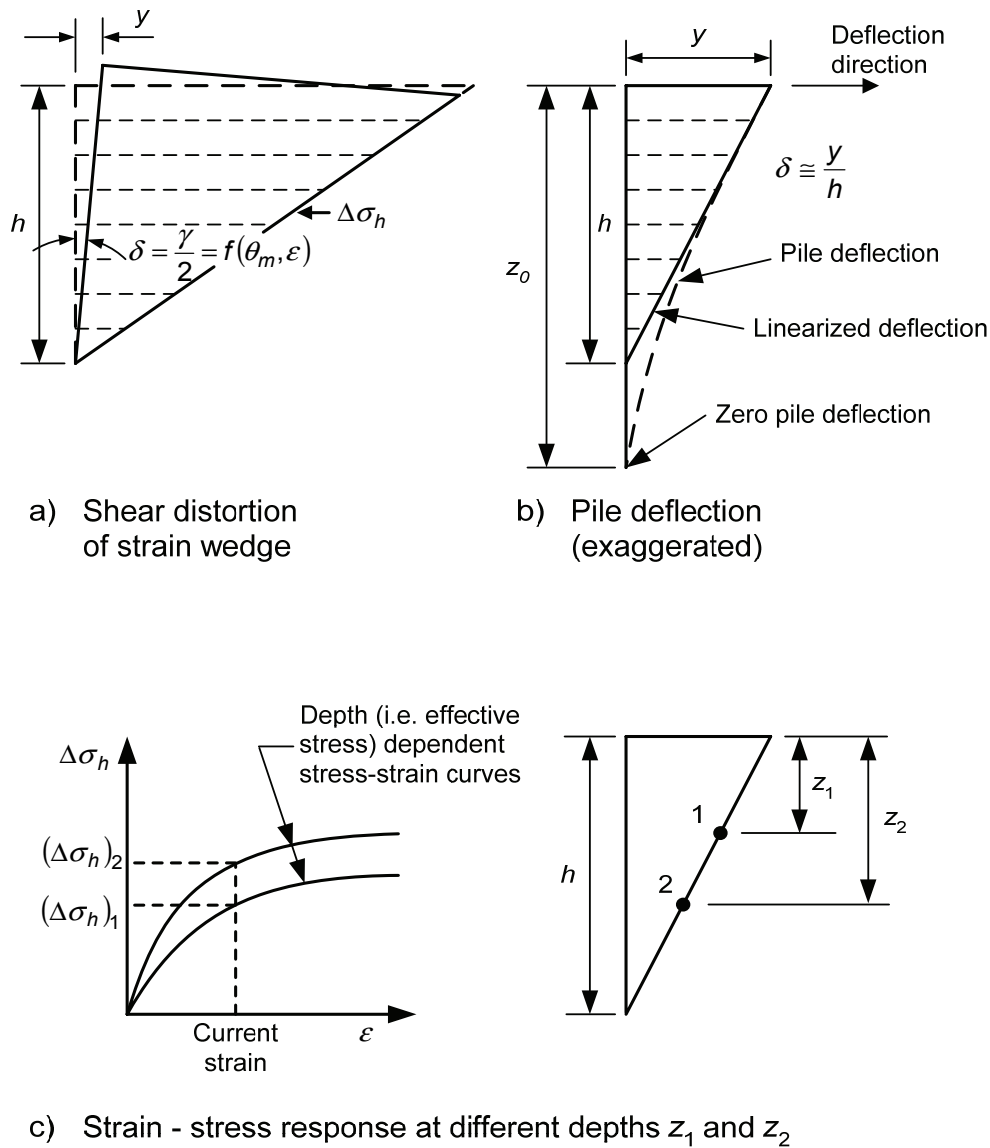
Figure 2-35: Strain-stress relationships for the SW model (after Ashour et al., 1998)

As detailed in Ashour et al. (1998), empirical relationships are utilized to describe triaxial response (i.e., $\Delta\sigma_h$ versus ε behavior), and similarly side shear (τ) versus pile deflection (y) behavior, in order to establish equivalent linear springs for each sublayer. The stiffness of each spring represents a secant value [i.e., $E_s(z) = p(z)/y(z)$] appropriate to the current deflection of the pile-soil system. These springs are then considered as an elastic foundation for the flexible pile, and a one-dimensional beam-on-elastic-foundation (BEF) solution technique employed to identify a depth (z_0) at which zero deflection occurs (refer Figure 2-35b). If z_0 and h are not compatible, an iterative scheme ensues whereby a revised wedge height is selected (based on z_0), and the solution process repeated until h and z_0 achieve compatibility.

Whilst various assumptions and idealizations are apparent with the SW methodology, comparison with field test behavior indicates the SW model is capable of predicting field behavior (e.g., Ashour et al.,

1997). Hence the *p-y* curves extracted from such a theoretical analysis can be justified. Ashour and Norris (2000) have described SW *p-y* curves for clay and sand, both characterized by the shape as shown in Figure 2-36(a). This shape was largely influenced by the empirical stress-strain relationship used to describe both clay and sand $\Delta\sigma_h$ - ε behavior, as presented in Figure 2-36(b) in normalized form using the stress level (*SL*) parameter, defined as

$$SL = \frac{\Delta\sigma_h}{\Delta\sigma_{hf}} \qquad (2.24)$$

where $\Delta\sigma_{hf}$ = maximum stress change.
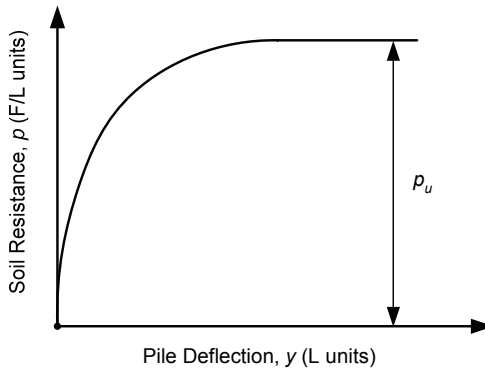
a) Characteristic shape of *p-y* curve in SW model
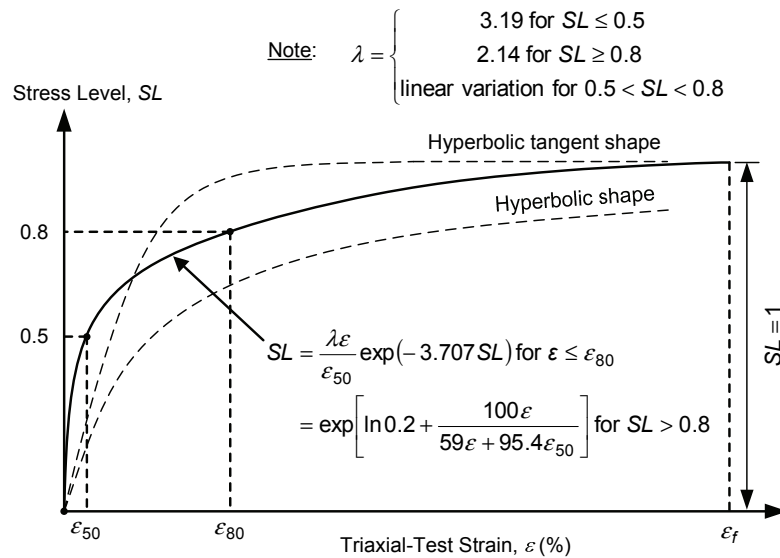
b) Empirical stress level vs. strain relationship to
    characterize stress-strain behavior of wedge soil

Figure 2-36: *p-y* and soil characteristics for SW model (after Ashour and Norris, 2000)

Limits to SW *p-y* resistance apply in the form of at-depth values similar to those discussed in Section 2.5.1.3, and another form of reduction is possible due to the geometry of the passive wedge relative to the pile (i.e., a form of a relative pile-soil stiffness effect). Given the ability of the SW approach to also account for *p-y* influences such as fixed or free pile-head restraint conditions, pile bending stiffness, and pile-head embedment, it therefore incorporates key aspects necessary to characterize *p-y* curves in detail. Thus, provided the hypothesis of a passive wedge forming is appropriate, the proposed wedge configuration a reasonable one, and the prescribed stress-strain behavior an acceptable characterization for the soil types present, the SW *p-y* approach represents a promising numerical tool.

2.5.3 *p-y* Issues

The *p-y* curves introduced in the 1970's and subsequent developments that have been discussed provide an insightful basis for understanding and assessing laterally loaded pile behavior, but issues remain.

2.5.3.1 Diameter Effect

An issue that has received some attention from various investigators is what has been termed the "diameter effect". This is often deliberated in connection with the work of Terzaghi (1955), where a diameter effect was implied in terms of pressure bulbs whose dimensions were in direct proportion to the pile width (refer Figure 2-3). Terzaghi assumed that deflection was linearly proportional to the dimensions of a pressure bulb, and thus linearly proportional to pile width. Hence, given a pile of width d_1 applying a pressure q per unit area with an associated deflection y_1, and a pile of width d_2 (= nd_1) applying the same pressure q per unit area with an associated deflection y_2 (= ny_1), the following relationship applied:

$$(k_h)_2 = \frac{qd_2}{y_2} = \frac{q}{ny_1} nd_1 = \frac{qd_1}{y_1} = (k_h)_1 \tag{2.25}$$

where $(k_h)_1$ = subgrade modulus for pile of width $d_1 (FL^{-2}$ dimensions), and

$(k_h)_2$ = subgrade modulus for pile of width $d_2 (FL^{-2}$ dimensions).

Thus a subgrade modulus for a pile was considered to be independent of the pile diameter, a conclusion inconsistent with observations.

Evidence that laterally loaded pile response appears to become stiffer with increasing diameter has been reported in several cases, based on comparison of observed lateral deflections of field piles of varying diameter with DLT model predictions (e.g., Stevens and Audibert, 1979; Pender, 1993; Curras, Hutchinson, Boulanger, Chai and Idriss, 2001). In terms of *p-y* formulations this has lead to modifications to the characterization of *p-y* stiffness, such as the various suggestions for determining characteristic deflection values in clay as shown in Table 2-9 (refer Section 2.5.1.2 for definitions of parameters), or the findings from Pender that the initial horizontal subgrade modulus for a pile is linearly proportional to the pile diameter, viz:

$$(k_h)_2 = (k_h)_1 \frac{d_2}{d_1} \tag{2.26}$$

Table 2-9: Deflection parameters addressing apparent diameter effects for clay *p-y* curves

Characteristic Deflection Parameter	Reference
$y_c = 8.9\varepsilon_{50}\sqrt{d}$	Stevens and Audibert (1979)
$y_c = 0.8\varepsilon_{50}\sqrt{d}\left(\dfrac{E_p I_p}{E_s}\right)^{0.125}$	Gazioglu and O'Neill (1984)
$y_{50} = 0.0063\varepsilon_{50}d(K_R)^{-0.875}$	Dunnavant and O'Neill (1989)

However, Ashford and Juirnarongrit (2003) reported no such diameter effects when modeling low-amplitude vibration response of cast-in-drilled-hole (CIDH) piles of various diameters in cemented sand. As shown in Figure 2-37, model response favored a horizontal subgrade modulus independent of the pile diameter ($k_{h-\text{ind}}$), rather than a horizontal subgrade modulus linearly proportional to pile diameter ($k_{h-\text{dep}}$), calculated as per (2.26).
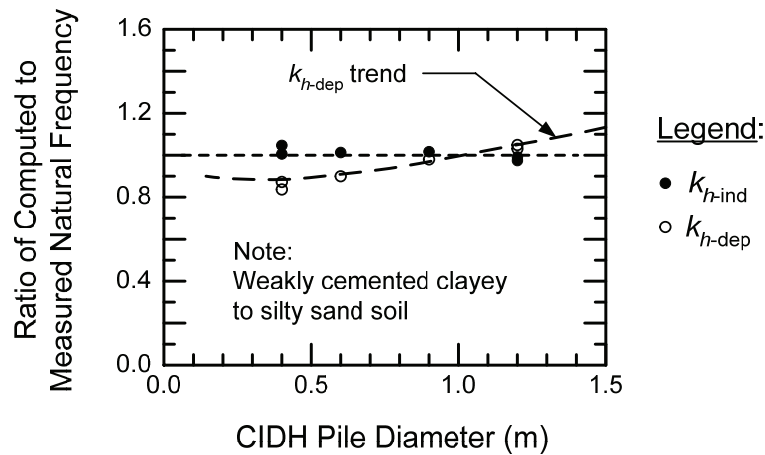
Figure 2-37: Comparative CIDH vibration response predictions (after Ashford and Juirnarongrit, 2003)

Lam and Martin (1986) provided a possible mechanistic explanation of these varying observations through a more detailed account of laterally loaded behavior. In addition to translational resistance in the form of *p-y* curves, Lam and Martin considered rotational resistance associated with pile rotation, as illustrated in Figure 2-38. For larger diameter piles (especially drilled shafts), this additional rotation-induced moment resistance can become significant, requiring additional "moment-rotation" (*m-θ*) curves as depicted in Figure 2-38 to fully account for soil resistance. Consequently, pile models utilizing *p-y* curves alone may predict softer than measured load-deflection behavior if rotational resistance contributions are significant and have not been accounted for in the *p-y* curves themselves.

Hence the presence of soil resistance in addition to that represented by *p-y* curves must be respected, particularly when applying *p-y* curves derived from one pile-soil system to a different pile-soil system. In terms of diameter effects, the rotation-induced soil resistance speculated by Lam and Martin (1986) can

explain seemingly stiffer pile response with increasing diameter, as well as lack of diameter effects in cases of negligible rotation.
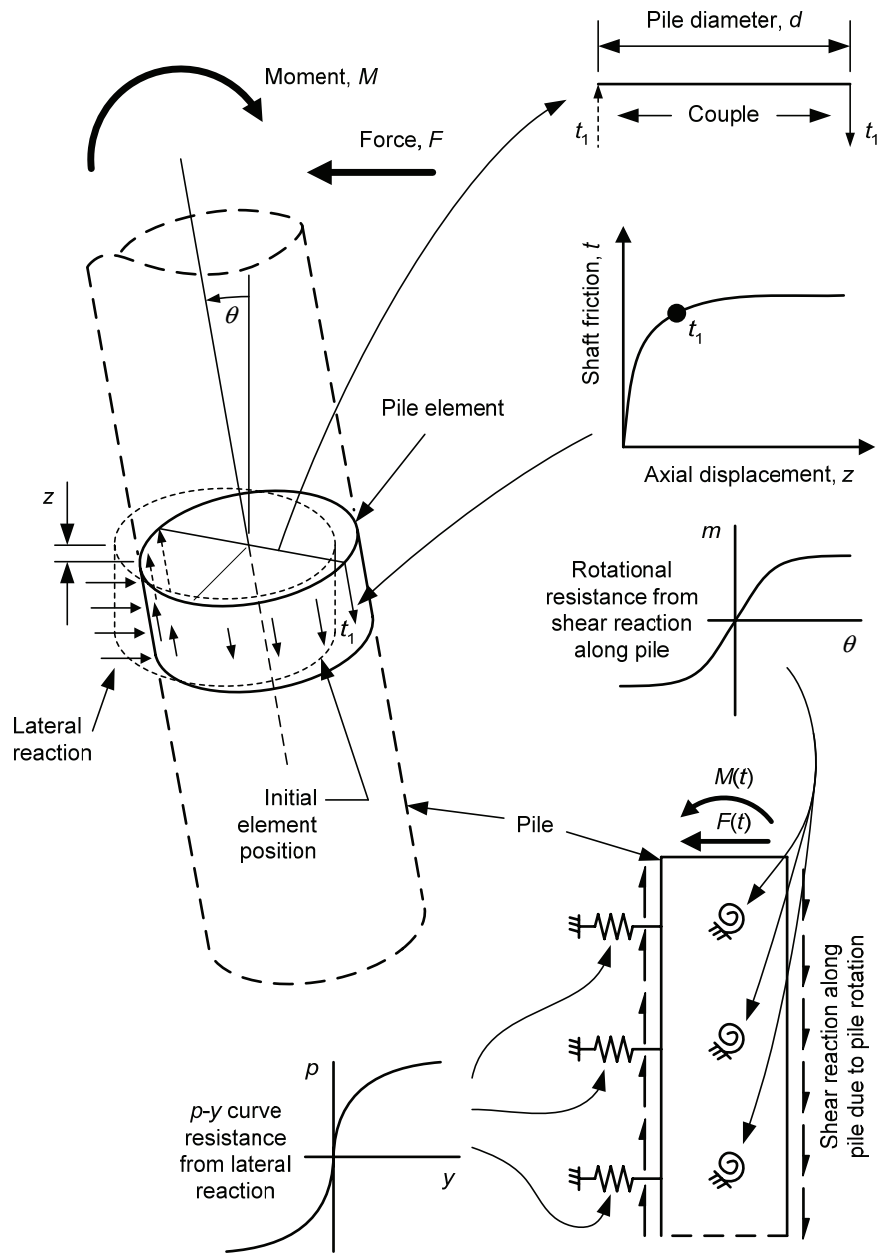
Figure 2-38: Forms of soil resistance during lateral pile loading (after Lam and Cheang, 1995)

Unfortunately, the characterization of such additional resistance is complicated by soil, loading and boundary conditions: A greatly diminished significance of rotational resistance for cohesionless (sand) soil cases compared with cohesive (clay) cases was noted by Lam and Martin, attributed to the differing *t-z* characteristics of each; while Lam and Cheang (1995) and Lam, Kapuskar and Chaudhuri (1998) noted mobilized rotational resistance as a function of loading level and pile-head fixity conditions, pointing out

that the so called diameter effects observed in empirical pile load tests were accentuated by the free-head fixity condition that applied in most cases, allowing rotation rather than restraint as in a fixed-head case.

Pender (2004) has also offered another possible explanation of diameter effects by considering the real possibility of soil modulus distributions increasing either linearly with depth or with the square root of the depth, as opposed to constant with depth (refer Table 2-2). Drawing on pile-head stiffness trends derived from the solutions given in Table 2-2, Pender pointed out that the ratio of unrestrained lateral pile head stiffness to pile diameter remains constant with changes in diameter for the case of a constant soil modulus profile, whereas the ratio increases with increasing diameter for the non-constant soil modulus cases. By doubling the pile diameter in the linear modulus case, for example, the lateral stiffness increased by a factor greater than two. Thus a seemingly stiffer response with increasing pile diameter was attributed to a varying soil modulus distribution with depth.

2.5.3.2   Installation Effects

The fact that soil surrounding a pile experiences physical changes due to the installation process has certainly been appreciated for some time. Taylor (1948) described the case of a displacement pile driven into clay, depicting an annulus of disturbed soil around the pile experiencing decreasing strength loss with distance away from the pile, accompanied by the development of excess pore water pressures leading to flow-induced consolidation and subsequent strength increase with time. Broms (1964a, 1964b) considered that driven piles affected the soil within a distance of approximately one pile diameter of the pile surface, causing increases in the relative density of cohesionless soils and immediate decreases of stiffness and strength as a result of remolding in cohesive soils. Broms noted further changes with time were expected in cohesive soils, ranging from increases in strength and stiffness as a result of consolidation in normally or lightly overconsolidated clays, to possible decreases in strength and stiffness in highly overconsolidated clays. Poulos and Davis (1980) also noted possible strength regain in clays due to thixotropic effects, and possible decreases in density alongside driven pile shafts in sands. Vesić (1977) described the case of bored piles where most of the change was considered to occur in a thin annulus immediately adjacent to the pile, accompanied by lateral stress relief due to soil removal.

More recent investigations (Hwang, Liang and Chen, 2001; Pestana, Hunt and Bray, 2002; Hunt, Pestana, Bray and Riemer, 2002) have provided more detailed accounts of installation effects. Hwang et al. used a network of piezometers, inclinometers, level posts and velocity sensors to investigate the effects of installing 800 mm diameter precast concrete driven piles in a soil profile consisting of sandy and clayey layers in Taiwan. This revealed radial soil displacements up to 4% of the pile diameter at a distance of 3 pile diameters from the pile center (i.e., 2.5 pile diameters from the pile surface), gradually decreasing to insignificant movement at a distance of 12 pile diameters from the pile center. A maximum ground heave of 36 mm was detected at a distance of 1.5 pile diameters from the pile center. Substantial excess pore water pressures were detected within a distance of approximately 3 pile diameters from the pile center, reaching values equal to 1.5 times the effective overburden pressure in a sandy layer and 3.5 times the effective overburden pressure in a clayey layer. Negligible excess pore water pressures were detected beyond a distance of 15 pile diameters from the pile center, with a rapid decrease in excess pore water pressure buildup noted beyond the 3 pile diameter zone of substantial buildup. Dissipation of excess pore water pressures was the order of minutes for the sandy layer, whereas almost a day applied to the clayey layer.

Pestana et al. (2002) and Hunt et al. (2002) utilized field piezometers, inclinometers, and downhole shear wave measurements, and laboratory consolidation, triaxial and direct simple shear testing, to investigate the effects of installing a 600 mm diameter closed-ended steel pipe pile driven into a thick soft clay deposit (San Francisco Bay Mud). This study reaffirmed the general process for driven displacement pile installation in soft clays, involving outward soil movement of a disturbed annulus of soil immediately

adjacent to the pile upon installation, transferal of installation pressures via increased pore water pressures, and then inward soil movement with time following consolidation of the disturbed annulus. However, while shear wave velocity measurements over time and the various laboratory tests on pre-pile and post-pile soil samples revealed a definite increase of soil stiffness and strength as a result of the installation process, they also indicated a more detailed level of complexity associated with the disturbed soil zone. In particular, retarded regain of shear wave velocity at distances less than one pile diameter from the pile surface were observed, suspected as being the result of severe remolding and destruction of soil fabric in this zone as opposed to primarily radial distortion elsewhere. In the laboratory, anistropically consolidated undrained triaxial testing indicated much higher ductility from post-pile samples compared with pre-pile samples (both consolidated to in situ stresses), and post-pile samples also exhibited a marked change in response from pre-pile samples beyond approximately 2% axial strain, suspected as being representative of anisotropic conditions brought about by the driving of the pile. Apparent independence of shear strength to sample orientation was also observed with post-pile samples in the direct simple shear device, whereas pre-pile samples exhibited a definite strength difference depending on sample orientation.

Such detailed accounts of installation effects are of course specific to the particular pile types used and ground conditions encountered, but are evidence that changes to the soil system do (and must) occur as a result of pile installation. Reese and Van Impe (2001) provided further examples of changed soil conditions as the result of installation of various pile types, but noted that "no comprehensive attack has been mounted by geotechnical engineers to allow the prediction of the effects of pile installation on soil properties" (p. 139). Indeed, assessment of pile installation effects in connection with *p-y* curves is scarce. Jamiolkowski and Garassino (1977) could only note qualitative differences between displacement and bored piles, stating that *p-y* data derived from one could not be used to assess the other. Gabr et al. (1994), in connection with a 153 mm diameter closed-ended pipe pile jacked into a medium clay deposit, attempted to quantify installation effects by applying a strength correction factor to *p-y* ultimate resistance values based on measurement of pre-installation and post-installation undrained shear strengths at varying depths and distances away from the pile wall. In their case, a general reduction in shear strength applied in order to account for installation effects.

To date, perhaps the best assessment of installation effects in terms of *p-y* curves is in regards to the lateral load tests on bored pile and driven pile groups conducted for the Taiwan High Speed Rail Authority, as reported by Huang, Hsueh, O'Neill, Chern and Chen (2001) and also Brown, O'Neill, Hoit, McVay, El Naggar and Chakraborty (2001). Soil conditions were predominantly loose to medium-dense silty sands, and pre-installation and post-installation CPT and flat dilatometer (DMT) tests served to provide soil stiffness and strength indicators. The subject of pile group analysis and assessment is left for the following section, but it suffices to say that installation effects were evident from the pre-installation and post-installation CPT and DMT test results. Using these test results to develop site specific pre-installation and post-installation *p-y* curves, the curves were then implemented into a DLT pile group analysis model to compare pre-installation and post-installation computed behavior with measured behavior.

In each case a good match between computed and measured behavior was achieved by using an adjustment factor that scaled *p-y* curve ordinates in a uniform manner. Assessment of installation effects was therefore achieved through comparison of the adjustment factor values required in each case. In this way a reduction in resistance (for a given displacement) in the order of 20% was attributed to the installation process for the bored pile group (i.e., softening of the pile-soil system), whereas a 30% increase applied to the driven pile group (i.e., stiffening of the pile-soil system). Thus the significance of the installation process on *p-y* curve behavior was clearly demonstrated, but what is more is the distinction afforded to installation technique. Noting the impact that the installation process can have on

ground conditions, examples of which have been given, the implications for existing *p-y* curve formulations are obvious.

2.5.3.3 Pile Head Restraint

In current practice the selection of *p-y* curves is independent of the pile head condition, the underlying assumption being that *p-y* curve characteristics are the same whether a free-head or fixed-head pile applies. Matlock (1970) observed such behavior when undertaking free-head and fixed-head lateral load tests on a steel pipe pile in soft clay ($d = 320$ mm; $L/d = 40$; $E_pI_p \approx 31150$ kN-m^2; $s_u \approx 15$ kPa), concluding, "within practical ranges, the fundamental resistance-deflection characteristics of the soil appear to be independent of the degree of pile-head restraint" (p. 581). Reese and Van Impe (2001) were of a similar opinion, stating "the experimental *p-y* curves that were obtained from experiments with fully instrumented piles will predict within reasonable limits the response of a pile whose head is free to rotate or fixed against rotation" (p. 47). However, suggestions to the contrary are evident.

Jamiolkowski and Garassino (1977), in discussing the ultimate resistance for *p-y* curves (p_u), noted a suggestion from E. E. de Beer that "the value of P_u [where P_u denoted p_u] which can be mobilized in front of laterally loaded piles may strongly depend on pile rigidity and boundary conditions at the top of the pile" (p. 54). It was therefore considered that p_u would not correspond to an absolute ultimate soil resistance, but rather some limiting value appropriate to a specific pile-soil system. This implied different *p-y* curves for different pile head restraint conditions, and more recent work by Ashour and Norris (2000), using the SW model, supports such a viewpoint as shown in Figure 2-39. Significantly different trends in *p-y* curves are apparent for more competent soil conditions, suggesting that pile head restraint may need to be considered as a variable in terms of the formulation of *p-y* curves.

a) SW *p-y* trends in sand

Key:
– – Free-head
—— Fixed-head

b) SW *p-y* trends in clay
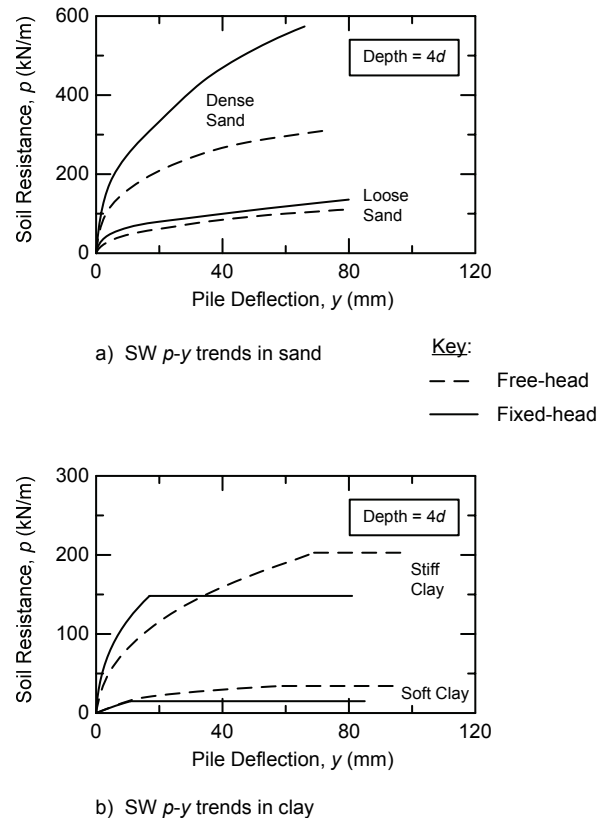
Figure 2-39: Effect of pile head restraint on SW *p-y* trends in sand and clay (after Ashour and Norris, 2000)

60

2.5.3.4   Pile Nonlinearity

In contrast to soil conditions that are brought about by mostly natural processes, the conditions of a pile are the result of manufactured processes that often allow the pile to be idealized as a linear (elastic) element in the pile-soil system. This is generally the case for steel pipe piles that behave in an essentially linear fashion up to high load levels (unless driving stresses dictate otherwise). However, in the case of reinforced concrete piles, the issue of nonlinear behavior must be considered given the very low tensile strength of concrete, causing cracking at much lower levels of loading. This produces highly nonlinear moment-curvature behavior that can cause significant changes in response behavior.

An appreciation of the need for nonlinear pile behavior was demonstrated by Kramer and Heavey (1988), who analyzed a full-scale lateral load test on a 0.46 m diameter drilled shaft in stiff expansive clay using a DLT model. To analyze the problem they pointed out that the governing differential equation for the "standard" case of constant pile bending stiffness (i.e., a linear moment-curvature relationship) was

$$E_p I_p \frac{d^4 y}{dz^4} + Q \frac{d^2 y}{dz^2} - p = 0 \qquad (2.27)$$

where $Q = $ axial load,

whereas the case of variable bending stiffness (i.e., a nonlinear moment-curvature relationship) required solution of the following governing differential equation:

$$(E_p I_p)_s \frac{d^4 y}{dz^4} + 2 \frac{d(E_p I_p)_s}{dz} \frac{d^3 y}{dz^3} + \left[\frac{d^2 (E_p I_p)_s}{dz^2} + Q \right] \frac{d^2 y}{dz^2} - p = 0 \qquad (2.28)$$

where $(E_p I_p)_s = $ a secant pile bending stiffness.

In physical terms (2.28) required a pile-soil system simultaneously satisfying lateral displacement (y) compatible with p-y curve behavior with depth, and curvature ($d^2 y / dz^2$) compatible with moment-curvature behavior with depth. Adopting the Reese and Welch (1975) stiff clay p-y curves to represent soil response, Kramer and Heavey only found agreement between predicted and observed pile-head load-deflection behavior by implementing (2.28) in conjunction with an elastic-plastic moment-curvature relationship to represent pile flexural behavior.

While recognizing that nonlinear pile behavior influenced lateral load response, Kramer and Heavey (1988) did not address the influence of nonlinear pile behavior on p-y curve characteristics given that their p-y curves were predefined. However, in using the SW model that is not restricted in this way, Ashour, Norris and Shamsabadi (2001) demonstrated that changes to p-y curve behavior can occur in the presence of nonlinear pile behavior. Given the incremental SW solution procedure that is well suited to modeling the actual progressive interplay occurring between pile and soil, they found that changes in p-y response were conditional upon the level of bending moment experienced by the pile and the extent of soil resistance mobilized. In zones of maximum bending moment of sufficient magnitude to mobilize nonlinear moment-curvature behavior of the pile, and providing p-y resistance was not governed by soil failure, appreciable reductions in p-y resistance were noted at higher levels of load/deflection.

2.5.3.5   Circumferential Behavior

Soil resistance defined by a *p-y* curve represents the collective actions of soil in front of a pile ("frontal" resistance) and soil around the pile ("side friction" resistance). Smith (1989) emphasized the need to account for horizontal side friction resistance in addition to frontal resistance, citing lack of force and moment equilibrium of laterally loaded bored piles otherwise. Briaud et al. (1985) noted similar need of side resistance in conjunction with pressuremeter-derived frontal resistance. Furthermore, Briaud (1984) considered the side friction to represent 50% of the lateral resistance at working loads, decreasing to 20 to 30% at ultimate loads. Yegian and Wright (1973), predicting at-depth behavior with a two-dimensional plane stress finite element model, indicated differences in ultimate resistance of 37% with and without side friction.   Thus circumferential behavior is another aspect of the *p-y* approach that needs to be appreciated, especially given that other piles will interfere with such behavior in the pile group case.

The use of two-dimensional studies, where an imaginary horizontal, unit thickness slice of a pile and surrounding soil is analyzed, has offered some understanding of circumferential behavior. Such was the case with the two-dimensional study by Baguelin, Frank and Saïd (1977). The model used by Baguelin et al. is shown in Figure2-40, consisting of a circular continuum of elastic soil (characterized by *E* and *v*) that forms an annulus around a central rigid circular section of radius r_0 that represents the pile. Fixed against movement at radial distance *R*, the continuum of soil includes an inner zone immediately adjacent to the pile of radius r_1 that depicts disturbance brought about by installation of the pile. Such disturbance was characterized by a reduced Young's modulus as defined in Figure 2-40.
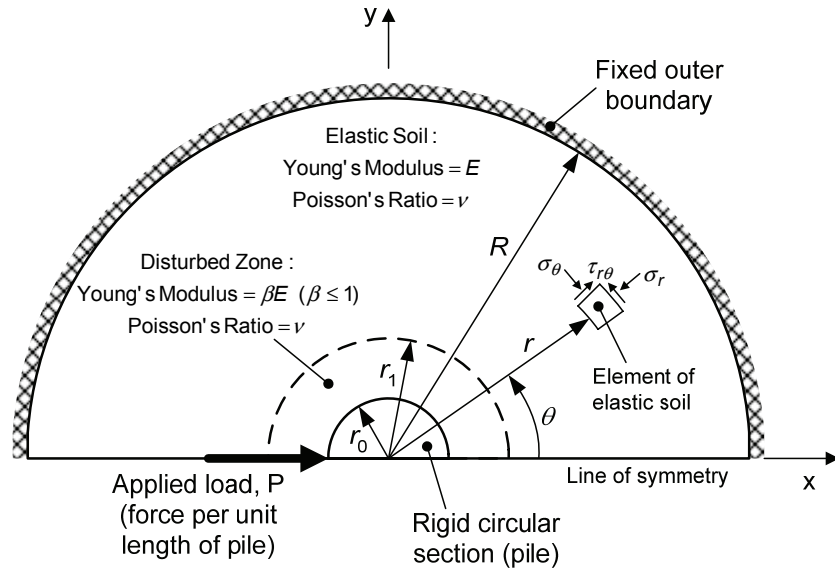
Figure 2-40: Two-dimensional pile-soil model (from Baguelin et al., 1977)

Assuming perfect adhesion of the soil to the pile (i.e., no separation) and no disturbance, sufficiently accurate analytical expressions were derived for normal (radial) and shear stresses near the pile as given by (2.13) and (2.14) respectively.

$$\sigma_r \approx \frac{P}{4\pi r_0} \frac{1}{(1-v)}\left[(3-2v)\frac{r_0}{r}-\left(\frac{r_0}{r}\right)^3\right]\cos\theta \qquad (2.29)$$

$$\tau_{r\theta} \approx -\frac{P}{4\pi r_0}\frac{1}{(1-v)}\left[(1-2v)\frac{r_0}{r}+\left(\frac{r_0}{r}\right)^3\right]\sin\theta \qquad (2.30)$$

In the case of disturbance ($\beta < 1$), expressions (2.15) and (2.16) similarly applied.

$$\sigma_r \approx \frac{P}{4\pi r_0}\frac{1}{(1-v)}\left[(3-2v)\frac{r_0}{r}-\left(\frac{r_0}{r}\right)^3 CF+\frac{1}{(3-4v)}\frac{r_0}{r}(1-CF)\right]\cos\theta \qquad (2.31)$$

$$\tau_{r\theta} \approx -\frac{P}{4\pi r_0}\frac{1}{(1-v)}\left[(1-2v)\frac{r_0}{r}+\left(\frac{r_0}{r}\right)^3 CF-\frac{1}{(3-4v)}\frac{r_0}{r}(1-CF)\right]\sin\theta \qquad (2.32)$$

$$\text{where } CF = \frac{(3-4v)\left[1-\left(\frac{r_0}{r_1}\right)^2(1-\beta)\right]+\beta}{(3-4v)\left[1-\left(\frac{r_0}{r_1}\right)^4(1-\beta)\right]+\beta}.$$

In terms of the distribution of the soil reaction around the pile due to the applied lateral load P, expressions (2.29) through (2.32) resulted in the distributions shown in Figure 2-41. This indicated that the annulus of reduced Young's modulus increased radial stress and decreased shear stress acting around the pile circumference, resulting in a pile reaction drawing more from the continuum directly in front of the pile and less from the sides.
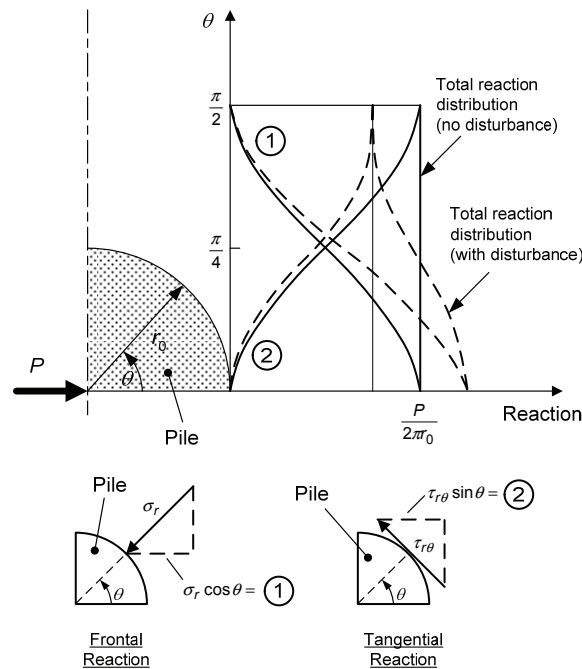
Figure 2-41: Distribution of the reaction around the pile without pile-soil separation (after Baguelin et al., 1977)

63

Baguelin et al. (1977) also considered an elastic-plastic soil continuum for the model shown in Figure 2-40, using a finite element method of analysis. This case predicted rapid development of plastic flow originating at the pile sides and progressing towards the front of the pile in a narrow band with increasing load, followed by expansion of plastic zones outwards from the front of the pile and in the direction of loading with further loading. The plastic flow was observed to affect stresses and displacements only in the immediate vicinity of the pile, behavior at a distance being the same regardless of whether elastic, elastic-plastic, undisturbed or disturbed soil conditions applied.

Obviously the findings of Baguelin et al. (1977) are limited given the assumed plain strain conditions, the models used for soil behavior, and the inability for soil to separate away from the pile. However, the findings illustrated the different ways in which soil resistance is mobilized around a pile, highlighting yet another dimension to the characterization of *p-y* curves.

2.5.4   Closing Comments

It is now apparent that *p-y* curves are the culmination of various factors. Some of the factors have been characterized to a fair degree of certainty, while others remain far less certain but nevertheless included either explicitly or implicitly in some shape or form in existing *p-y* curve formulations. This state of affairs gives rise to different viewpoints. On the one hand, significant uncertainty should be considered to exist when using existing *p-y* curve formulations, as has already been demonstrated in a probabilistic sense for the case of soft clays (Esteva and Ruiz, 1982; Ruiz, 1986), and from the very wide scatter of predictions apparent when utilizing existing sand and clay *p-y* curve formulations to predict observed pile behavior (Murchison and O'Neill, 1984; Gazioglu and O'Neill, 1984). Various instances where existing *p-y* curve formulations required modification to fit observed pile behavior also attest to this uncertainty (Stevens and Audibert, 1979; Hariharan and Kumarasamy, 1982; Nogami and Paulson, 1985; Curras et al., 2001; Huang et al., 2001).

On the other hand, assessing the affect a pile group configuration has on *p-y* curves is primarily a matter of assessing the relative differences between single (isolated) pile behavior and behavior of the same pile in a group. Thus uncertainties in an absolute sense still exist, but in terms of pile group effects these uncertainties play a far lesser role given the emphasis on assessing relative behavior. There is also comfort in that uncertainties in *p-y* curves affect pile actions far less than they do the *p-y* curves themselves. Lam et al. (1998) noted that uncertainties in the maximum pile moment versus pile load "are relatively minor and are relatively insensitive to many sources of uncertainty" (p. 56). Such insensitivity was also noted by Meyer (1979), and is reflected in simplified approaches to lateral load analysis, such as the Characteristic Load Method (Evans and Duncan, 1982; Duncan, Evans and Ooi, 1994; Brettmann and Duncan, 1996), where normalization of pile behavior was possible for a relatively wide range of *p-y* soil conditions.

In either case the uncertainty of existing *p-y* curve formulations still remains, and this adds weight to the use of more controlled assessment procedures for studying pile-soil behavior. Numerical modeling can provide this control, and is further incentive for the numerical approach undertaken in the current study.

SECTION 3
LATERAL GROUP EFFECTS

3.1   Introduction

The introduction of additional piles into a pile-soil system creates the common case of a pile group configuration, the nomenclature of which is shown in Figure 3-1. O'Neill (1983) noted two classes of pile groups, widely spaced and closely spaced, distinguishing a closely spaced pile group as when "the piles are situated closely enough to each other that the individual responses of the pile are influenced by the presence of and loadings upon neighboring piles" (p 25). In the case of a laterally loaded pile group, such "pile-soil-pile" interaction leads to lateral "group effects", whereby a typical pile in the group experiences greater deflection and reduced lateral load capacity compared with behavior of the same pile in isolation. The inference to isolated (single) pile lateral behavior is important in that isolated behavior has served to establish an appropriate benchmark from which lateral group effects have been assessed.

Characterization of pile-soil-pile interaction has therefore remained closely aligned to single pile behavior, utilizing the same analysis approaches and frameworks in which to assess pile-soil-pile interaction.   Assessment of lateral group effects draws heavily on recent test-based empirical observations, in addition to traditional elastic-based theory. Review and discussion of key pile group tests to date is therefore included. Given the more advanced numerical means of investigating pile group effects in the current research, past efforts of similar nature are also reviewed and assessed. As was the case with single piles, application of elastic-based continuum approaches initially predominated in the assessment of pile-soil-pile interaction.

3.2   Elastic-Based Interaction

The essence of elastic-based interaction is illustrated in Figure 3-2, and the Mindlin (1936) solution has been used to represent the mechanism I_{ij} that quantifies the influence lateral loading on one pile has on another pile.

The form of interaction portrayed by the Mindlin solution is strain superposition, or increased displacement to a pile brought about by the accumulation of load-induced strains from all other piles within a group, and lends itself to elastic-based continuum methods. Most widely known of the elastic-based approaches was the two-pile interaction approximation developed by Poulos (1971b), representing an extension of the analysis framework used for single pile behavior (Poulos, 1971a). The approach was formulated in terms of lateral interaction factors (denoted by α and applying at the pile head) that represented the elastic interaction between a pair of identical piles (depicted as in Figure 3-2), defined as

$$\alpha = \frac{\text{additional movement caused by adjacent pile}}{\text{movement of pile caused by its own loading}} \qquad (3.1)$$

a) In-line arrangement
(3 x 1 shown)

b) Side-by-side arrangement
(1 x 3 shown)

P_g

s

Pile

P_g

s'
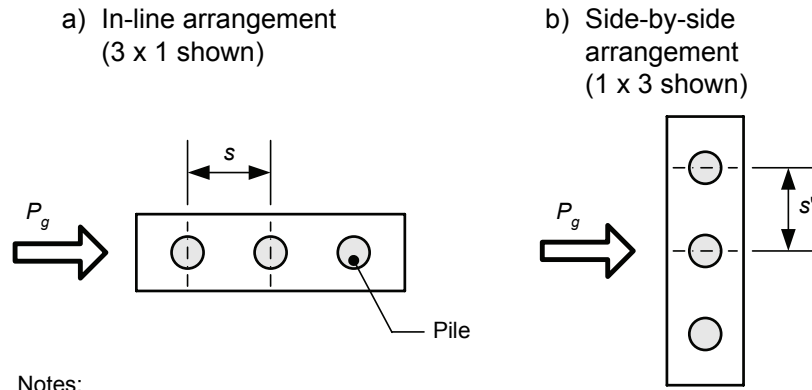
Notes:

s = center to center (c/c) spacing in direction of load

s' = c/c spacing perpendicular to direction of load

P_g = horizontal load applied to pile group

3rd trailing row

2nd trailing row

1st trailing row

leading row

P_g

s'

s
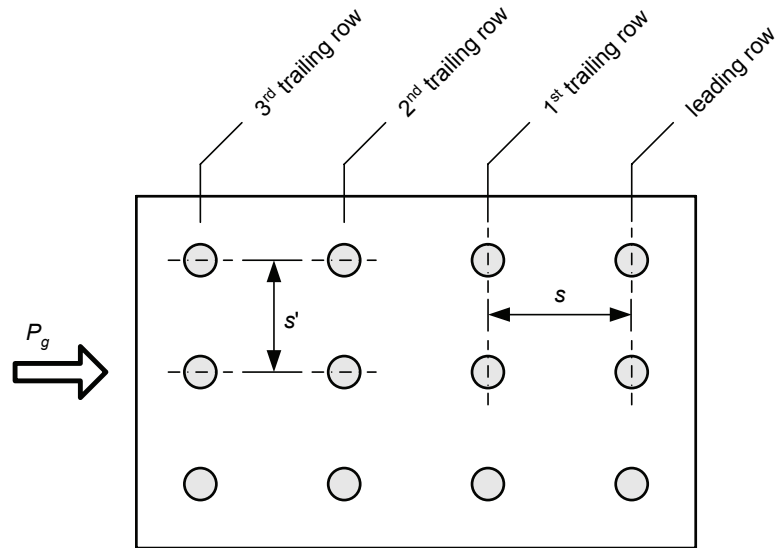
c) Box (square or rectangular) arrangement
(rectangular 4 x 3 shown)

Figure 3-1: Pile group nomenclature according to plan configurations (after Mokwa, 1999)
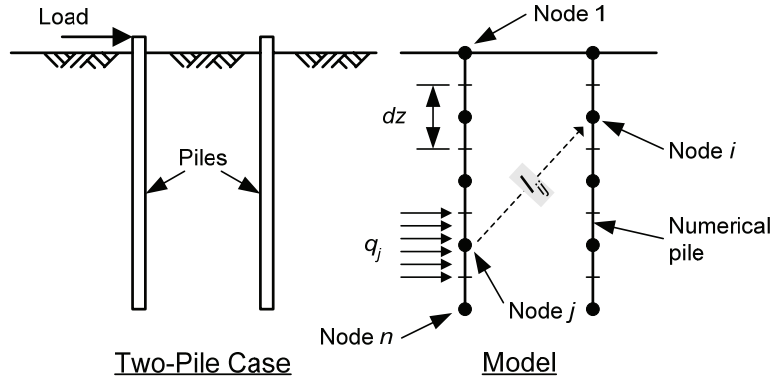
$$p_j = q_j dz \text{ and } u_i = \sum_{j=1}^{n} I_{ij} p_j$$

where:

dz = tributary length for nodes of numerical pile
q_j = lateral pressure acting over tributary length for node j
p_j = lateral load acting at node j
I_{ij} = elastic interaction factor defining influence of load at node j on node i
u_i = additional lateral displacement at node i from adjacent pile

Figure 3-2: Essence of elastic-based pile-soil-pile interaction

Charts of interaction factors for either displacement or rotation movement were developed as functions of pile-head restraint (fixed-head or free-head), loading direction, ratio of center to center pile spacing (s) to pile diameter (d), and relative pile-soil stiffness (K_R), all assuming symmetrical, vertical pile groups. Pile group action was then determined by assuming superposition of interaction factors, expressed mathematically by (noting that rotation interaction was similarly defined)

$$\delta_j = \overline{\delta}_P \left(\sum_{\substack{k=1 \\ k \neq j}}^{m} P_k \alpha_{\delta Pjk} + P_j \right) \tag{3.2}$$

where

δ_j = deflection of the *jth* pile,

$\overline{\delta}_P$ = displacement of a single pile under unit horizontal load (refer Eq. 2.5),

P_i = lateral load on pile i,

$\alpha_{\delta Pjk}$ = influence factor of node j on node k for horizontal loading,

P_j = lateral load on pile j, and

m = number of piles in the group.

This implied a pile group whose individual piles, at any given load per pile, would exhibit greater lateral deflection compared with an equivalent isolated pile subjected to the same load. In terms of the *p-y*

framework this translates to a multiplying factor ("*y*-multiplier") that increases the deflection values of each point on a *p-y* curve, or in other words represents a curve stretching parameter (Reese and Van Impe, 2001).

Banerjee and Driscoll (1976a, 1976b) improved on the Poulos (1971b) approach by using a more rigorous boundary element formulation that considered the elastic interaction of all the elements of all the numerical piles within a group simultaneously. Other enhancements included use of single pile solutions that recognized nonlinear soil behavior in the form of limiting pressures (Poulos, 1975, 1980), and consideration of soil non-homogeneity in the form of a soil modulus linearly increasing with depth (Banerjee, 1978; Poulos, 1979). An alternative means of deriving two-pile interaction factors was also undertaken using finite element modeling (Randolph, 1981), indicating good agreement with interaction factors obtained using the Poulos approach (Randolph; Randolph and Poulos, 1982; Poulos and Randolph, 1983). Randolph expressed the finite element interaction factors in the form of algebraic expressions as indicated in Figure 3-3, where it is noted that a restriction to flexible piles applied.

Use of elastic interaction factors provided some insight into lateral group effects: Interaction in the direction normal to loading was noted as being in the order of half that in the direction of loading; significantly reduced interaction was observed for the case of the soil modulus increasing with depth; and the importance of pile spacing was emphasized given that the interaction factors were approximately inversely proportional to pile spacing (Poulos, 1971b; Poulos, 1979; Randolph, 1981). Elastic-based interaction can also be justified to some extent, for example Pecker and Pender (2000) noted that for 3 x 3 pile groups subjected to static lateral loads corresponding to deflections up to 3% of the pile diameter, observed load distributions between piles followed those predicted using elastic interaction factors. However, there are shortcomings associated with the approach, such as difficulty in establishing an appropriate modulus for the elastic soil, and the tendency to over-predict interaction given the purely elastic interaction mechanism.

A most serious shortcoming, however, is the fact that load distribution amongst piles of a laterally loaded pile group is not symmetrical for all levels of loading, whereas an elastic-based interaction analysis would indicate this to be the case. The fact that non-symmetrical load distribution exists has come about primarily as a result of observation of full-scale lateral load testing. Indeed, observations have revealed a far more complex picture of laterally loaded pile group behavior than elastic-based interaction would appear to indicate. This has required the need to modify and augment elastic-based interaction approaches to help reconcile results with observed behavior, resulting in a form of interaction that has been categorized here as observation-based interaction.

3.3 Observation-Based Interaction

A tabulated summary of the key full-scale lateral load tests undertaken on pile groups to date is provided in Appendix A. Included are pertinent details of the tests and key observations that have contributed to the current understanding of lateral pile group effects, at least for "small" pile group configurations. The various issues that are apparent from such observations are numerous, and are not only concerned with pile-soil-pile interaction. Nevertheless, pile-soil-pile interaction plays an important role and its consideration is vital for properly characterizing group effects. A most basic issue in this regard has been the need to address nonlinear pile-soil effects in the immediate vicinity of each pile in a group.

a) Geometry

$$L_c = d\left(\frac{E_p^*}{G_c}\right)^{0.286}$$

L

d

Pile

:Elevation

Pile

Direction of load

β

t

:Plan

Pile

b) Definition of terms

$$\rho = \frac{G(\text{avg. of } L)}{G(\text{at depth} = L)}$$

$$G_c = G(\text{avg. of } L_c)$$

$$\rho_c = \frac{G(\text{at depth} = L_c/4)}{G(\text{at depth} = L_c)}$$

E_p = Young's modulus of pile

G = Shear modulus of soil x 1.35

$$\lambda = \frac{E_p}{G(\text{at depth} = L_c)}$$

$$E_p^* = \frac{E_p I_p}{\pi d^4/64} = \text{equivalent modulus}$$
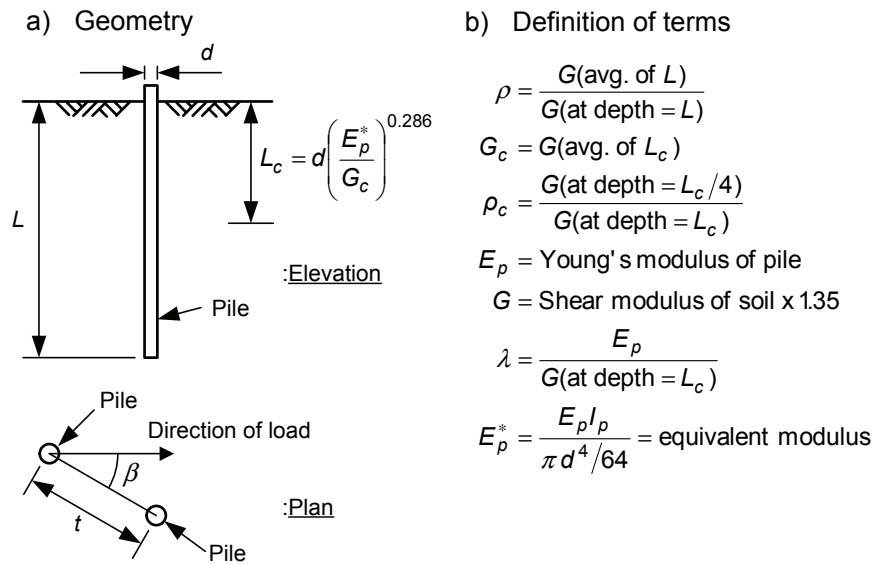
c) Interaction factors

Mode of Interaction	Symbol	Equation
Lateral deflection with fixed pile head	α_{uf}	$\alpha_{uf} = 0.6\rho_c\left(\dfrac{E_p^*}{G_c}\right)^{0.143}\left(\dfrac{d}{2t}\right)\left(1+\cos^2\beta\right) \le \dfrac{1}{3}$ $= 1 - \dfrac{2}{\sqrt{27\alpha_{uf}}} > \dfrac{1}{3}$
Lateral deflection due to shear (free head)	α_{uH}	$\alpha_{uH} \approx 0.7\alpha_{uf}$
Rotation due to moment	$\alpha_{\theta M}$	$\alpha_{\theta M} \approx \alpha_{uH}{}^3$
Lateral deflection due to moment or rotation due to shear	$\alpha_{uM} = \alpha_{\theta H}$	$\alpha_{uM} = \alpha_{\theta H} \approx \alpha_{uH}{}^2$

Figure 3-3: Lateral interaction factors for groups with flexible piles (after O'Neill, 1983; Randolph and Poulos, 1982)

Focht and Koch (1973) surmised that both "elastic" pile-soil-pile interaction and "plastic" local failure close to the pile contributed to overall behavior, and proposed a combined approach utilizing the Poulos (1971b) approach to represent pile-soil-pile interaction, and the *p-y* (single pile) approach to represent local behavior. The approach was embodied by a revised form of (3.2) as follows

$$\delta_j = \bar{\delta}_P \left(\sum_{\substack{k=1 \\ k \neq j}}^{m} P_k \alpha_{\delta Pjk} + RP_j \right) \tag{3.3}$$

where $R = \dfrac{\text{pile - head deflection using } p\text{ - }y \text{ curves}}{\text{pile - head deflection using Poulos (1971a)}}$.

This implied the simplistic notion of superposition of local and more global mechanisms associated with the individual piles in the group and the group as a whole, respectively. Such a rationalization has proven effective, with O'Neill (1983) noting the main advantage of the approach over elastic-based interaction, in that separate stiffness relationships can be used for individual pile action and for pile-soil-pile interaction.

However, the Focht and Koch (1973) notion of group effects is still not without its problems. Horsnell, Aldridge and Erbrich (1990) pointed out the basic inconsistencies in deformed shapes of piles that can arise from solutions using *p-y* and elastic representations of the soil. Reese, Wright and Aurora (1984) also noted the importance of choosing an appropriate soil modulus value when calculating $\bar{\delta}_P$ given the sole reliance on *R* to "marry" the local and group mechanisms together. Such incompatibilities between different mechanisms can be diminished by considering interaction along the piles instead of condensing it at the pile-head, an example of which was proposed by O'Neill, Ghazzaly and Ha (1977). Above all, however, is the marked difference in tension and compression behavior of soils that limits the effectiveness of elastic interaction (Reese and Van Impe, 2001).

Irrespective of any rational qualities that the aforementioned "hybrid" approaches possess through the Focht and Koch (1973) supposition, observations have also identified the "shadowing effect", or reduction in lateral resistance of piles trailing (or in the shadow of) the front row (leading) piles[†]. This is a geometrical effect associated with local reduction in lateral support of the soil in front of a pile as the pile positioned forward of it moves in the same direction (Ochoa and O'Neill, 1989). The shadowing effect has been observed to be primarily a function of row position in the group and the pile spacing, and is a local phenomenon that the elastic-based interaction methods do not recognize. Utilization of *p-y* curves can provide the necessary means to account for such behavior, using so called "p-multipliers" that scale *p-y* resistances according to row position (Brown, Morrison and Reese, 1988).

The *p*-multiplier concept is illustrated in Figure 3-4(a), and the process for establishing *p*-multiplier values (denoted here by f_m) has mainly drawn on experimental means using suitably instrumented full-scale laterally loaded group tests with an accompanying lateral load test on an isolated single "control" pile. The control pile is assumed to be representative of the soil and structural conditions that apply to the piles in the group, thereby providing a measurement basis from which group effects can be identified. Calculation of *p*-multipliers is undertaken by modeling the behavior of the control pile utilizing *p-y* curve formulations as described in Section 2, and then making any necessary adjustments to

---

[†] In fact Focht and Koch (1973) also recognized the need to adjust the resistance portion of *p-y* curves to account for shadowing, suggesting what were termed "P" factors of between 0.7 and 1.0 for offshore conditions.

the curves to obtain sufficiently accurate agreement between calculated and measured response. Such "site-specific" *p-y* curves are then assigned to a model of the pile group, and further adjustments made by way of trial and error f_m values on a row-by-row basis until sufficiently accurate agreement is obtained between the calculated and measured response of the pile group.

a) *p*-multiplier Concept

b) *y*-multiplier Concept
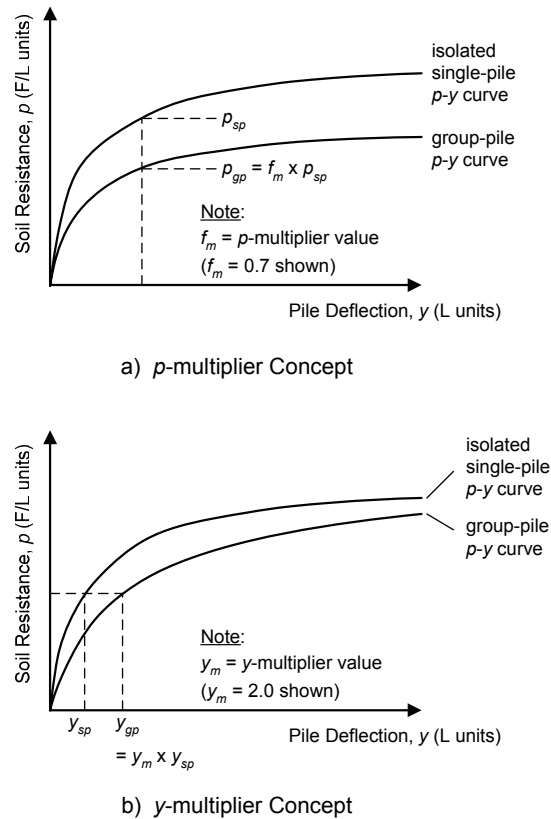
Figure 3-4: Illustration of *p-y* multipliers used for assessing group effects

A reduction in *p-y* resistance (i.e. "squashing" *p-y* curves with a *p*-multiplier) instead of an increase in *p-y* deflection (i.e. "stretching" *p-y* curves using a *y*-multiplier[‡]) to account for group effects has been preferred given the prominence of shadowing effects in pile group tests. Moreover, use of experimentally determined *p*-multipliers avoids the need of *y*-multipliers as any elastic-based interaction should already be included (Mokwa, 1999). In mechanistic terms the reduction in soil resistance characterized by *p*-multipliers has been explained by way of overlapping shear zones of surficial (wedge) resistance mechanisms associated with piles in a group, illustrated in Figure 3-5. The regions of overlap effectively diminish the resistance potential of the surrounding soil, leading to reductions in pile shears. A similar overlap mechanism has also been utilized with the strain wedge model to assess group response with successful results (Ashour, Pilling and Norris, 2001; Ashour et al., 2004), lending support to the existence of mechanistic interference via wedge-type mechanisms.

A compilation of *p*-multipliers derived from full-scale instrumented pile-group tests is provided in Figure 3-6 and Figure 3-7, demarcated on a row-by-row basis and given as a function of pile spacing expressed in pile diameter units. This follows the review of group effects undertaken in the dissertation by Mokwa (1999) and subsequently reported in Mokwa and Duncan (2001). Additional data is shown from more

---

[‡] The *y*-multiplier concept was previously mentioned in connection with elastic-based interaction and is also shown in Figure 3-4 (b) for comparative purposes.

recent full-scale *p*-multiplier findings reported in Brown et al. (2001). Also shown are design curves recommended by Mokwa and Duncan, as will be discussed further below. Significant scatter of *p*-multiplier values is apparent and reflects the various issues (discussed in section 3.5) that come into play when deriving *p*-multipliers based on field test and numerical modeling procedures. Nevertheless, *p*-multiplier design values have been proposed as shown in Figure 3-8.

The design curves indicated in Figure 3-8 (and shown individually in Figure 3-6 and Figure 3-7) were obtained by fitting data points from full-scale, 1*g* model and centrifuge tests using engineering judgment. These were considered by Mokwa (1999) to be conservative, but it is apparent from Figure 3-6 and Figure 3-7 that the design curves predict *p*-multipliers generally greater than the bulk of the updated full-scale data indicate. It should be noted that when the curves were developed they depicted an average measure of the entire data set (refer Mokwa or Mokwa and Duncan, 2001), suggesting that 1*g* model and centrifuge tests predict *p*-multipliers generally greater than full-scale tests. As noted by Mokwa and Duncan, effects of pile-head fixity, soil type and density, and pile displacement were considered a secondary issue that "for most engineering purposes, need not be considered" (p. 740).

In contrast, Zhang and McVay (1999) distinguished between sand and clay soil types in their recommendations for *p*-multipliers (based on full-scale, centrifuge and 1*g* model data), denoted by the individual data points as indicated in Figure 3-8. Zhang and McVay cited the presence of gaps and cracks around piles in clay that would prevent the transfer of stresses and thus diminish the shadowing effect for trailing rows. More uniform *p*-multipliers were therefore considered appropriate in clay compared with sand. This is evident in Figure 3-8 for the 3 x 3 pile group configuration considered, in that equal *p*-multiplier values are predicted for the middle row (first trailing row) and back row (second trailing row) in the clay case, whereas in the sand case (where recommendations were only given for s = 3*d*), the values are different and much smaller relative to the leading row value.
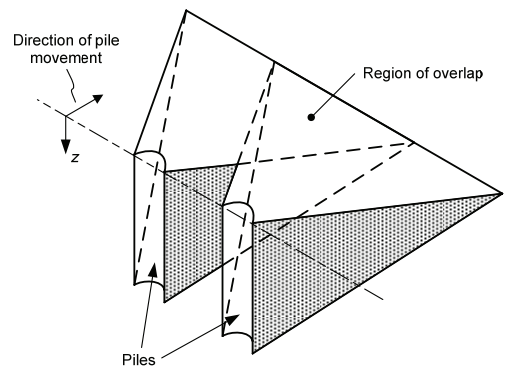
a) Possible overlapping for leading rows (isometric view)
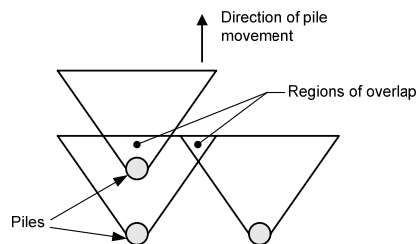
b) Possible overlapping for interior rows (plan view)

Figure 3-5: Overlapping shear zones associated with surficial resistance mechanisms for pile groups (after Brown et al., 1988)
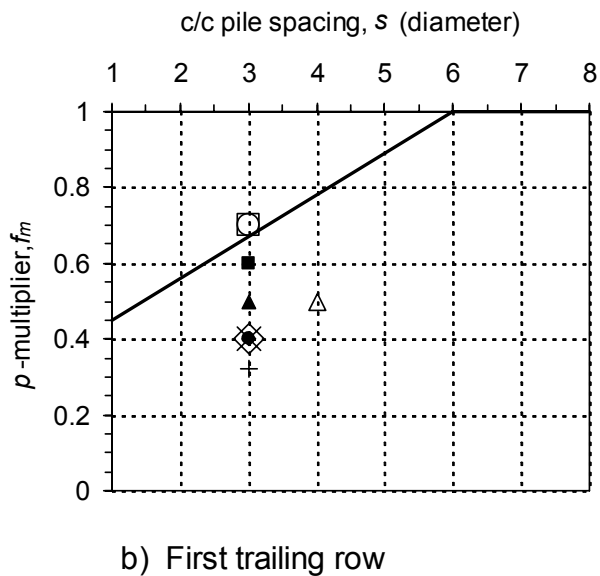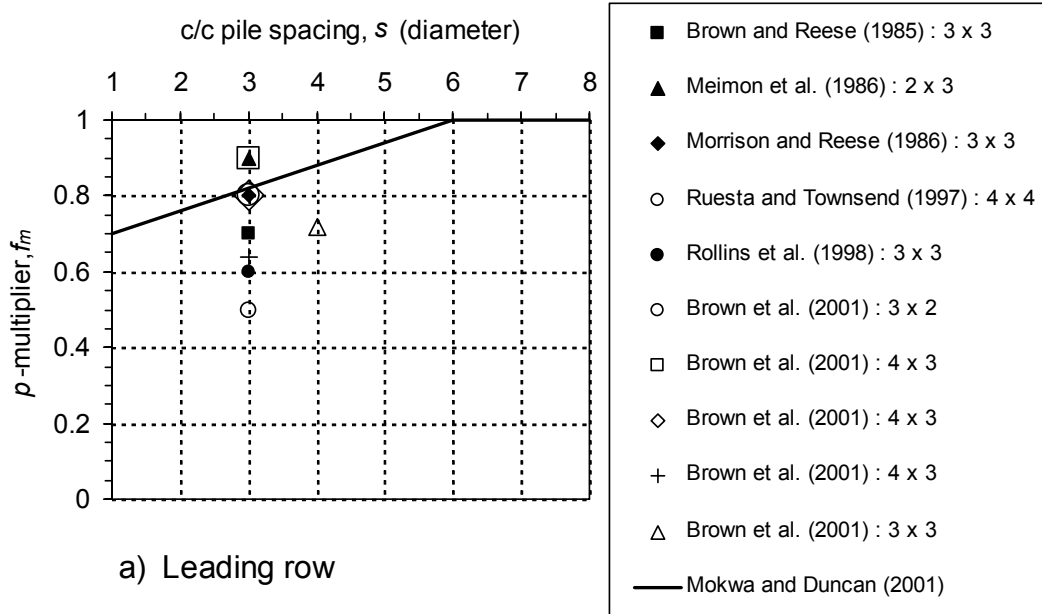
Figure 3-6: Empirical *p*-multipliers as a function of pile spacing for leading row and first trailing row (after Mokwa, 1999)

c) Second trailing row

Legend:
- ■ Brown and Reese (1985) : 3 x 3
- ▲ Meimon et al. (1986) : 2 x 3
- ◆ Morrison and Reese (1986) : 3 x 3
- ○ Ruesta and Townsend (1997) : 4 x 4
- ● Rollins et al. (1998) : 3 x 3
- ✕ Brown et al. (2001) : 3 x 2
- □ Brown et al. (2001) : 4 x 3
- ◇ Brown et al. (2001) : 4 x 3
- + Brown et al. (2001) : 4 x 3
- △ Brown et al. (2001) : 3 x 3
- —— Mokwa and Duncan (2001)

d) Third and greater trailing rows
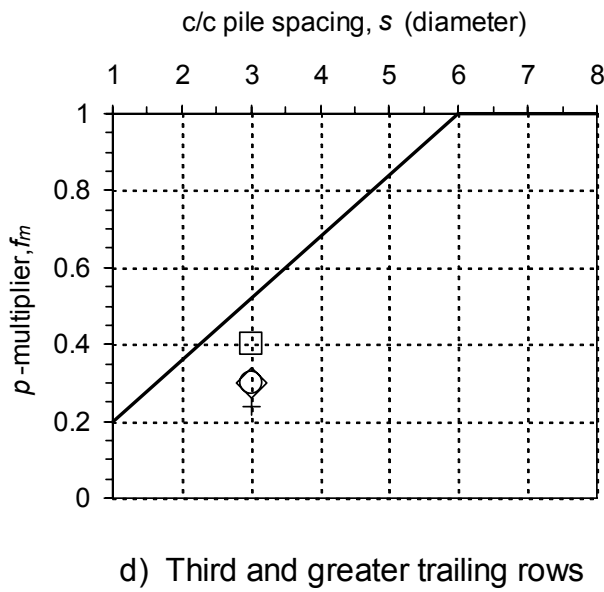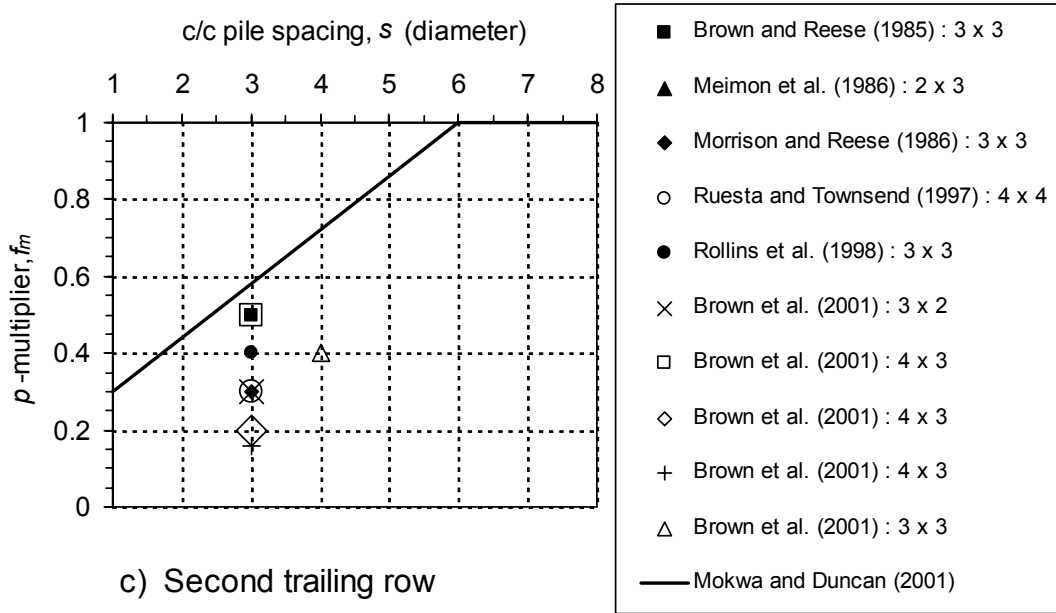
Figure 3-7: Empirical *p*-multipliers as a function of pile spacing for the second and third trailing rows (after Mokwa, 1999)
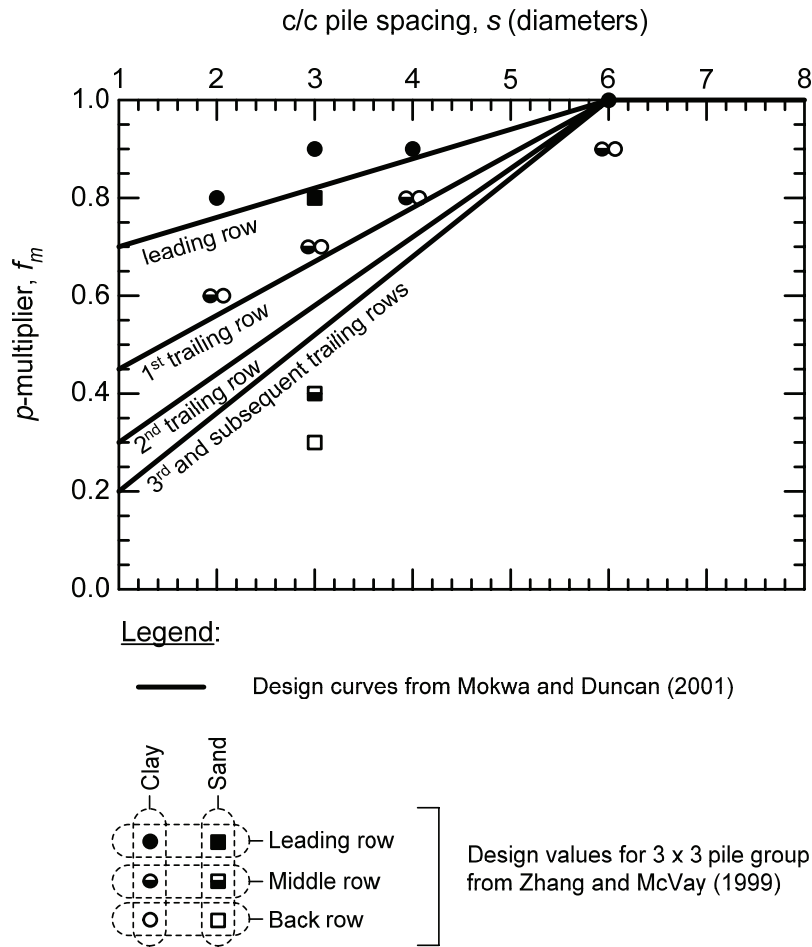
Figure 3-8: Suggested *p*-multiplier design values from Zhang and McVay (1999) and Mokwa and Duncan (2001)

It is noted that quantitative use of 1*g* model and centrifuge pile group test results is apparent from the work of Mokwa and Duncan (2001) and Zhang and McVay (1999). Venturing as to whether this is appropriate is unclear. Due credit to both of these testing techniques for providing useful information has certainly been acknowledged (Reese and Van Impe 2001, p. 303), but experimental errors associated with scaling and boundary effects are also certainly appreciated (e.g., O'Neill, 1983; Garnier and König, 1998; Foray, Balachowski and Rault, 1998; Mokwa, 1999). Sand is particularly relevant in the latter regard, Prevost (1982) having noted the real possibility of particulate difficulties with sand in the centrifuge, and Brown, Morrison and Reese (1990) expressing reservations "with respect to the use of 1*g* model tests in sand as a quantitative basis for predicting group effects" (p. 1282). Mokwa (1999) has also noted difficulties in modeling the state of clayey soils in the centrifuge.

Finally, Prevost (1982) offered a general philosophy for centrifuge testing, preferring its application more as a tool to calibrate numerical approaches. Hence, in view of the limitations of 1*g* model and centrifuge testing, data obtained from such means is considered in the current study in qualitative terms only. On this basis, observations from selected centrifuge group tests are included in Appendix A. These tests were considered the most relevant to the study at hand, and provide insight into some of the issues surrounding group effects as discussed in section 3.5.

75

3.4 Three-Dimensional Finite Element Group Models

While the use of full-scale tests to establish design parameters must remain the ultimate choice in pile group design, the significant scatter apparent in the above findings indicates obvious difficulties in being able to clearly assess pile-soil-pile interaction in the complex environment that nature presents. Continuum approaches utilizing a three-dimensional finite element framework have circumvented this problem to some extent, being able to provide a well defined group pile-soil system from which observations of pile-soil-pile interaction can be inferred. Of course, and as was the case with isolated single pile behavior, the degree of realism afforded by a finite element approach relies on the ability to model the soil, pile and pile-soil components appropriately. Furthermore, pile groups also present a far more demanding problem computational wise compared with the single pile problem.

Given that modeling pile groups is computationally intensive, a frequent approach has been to examine elements of the group in isolation using appropriate boundary conditions. An example of this type of approach is shown in Figure 3-9, used by Tamura, Ozawa, Sunami and Murakami (1982) to examine group effects for 3 x 3 and 5 x 5 configurations. Tamura et al. utilized a nonlinear (hyperbolic) stress-strain soil model in conjunction with a three-dimensional finite element framework, but no account of pile-soil separation is evident from the study. Nevertheless, the analyses confirmed the observation that the leading row attracts a disproportionately greater portion of the total applied lateral load, allowing some confidence in the ability of such an approach to provide insight into group effects. The analyses suggested that group effects increase at a decreasing rate with increasing number of rows, and that the effect is more pronounced with inner piles than with outer piles.

Trochanis et al. (1988, 1991a, 1991b) utilized an in-line pair of piles as a means of assessing the main features of group action. This extended on the single pile axisymmetric model discussed in section 2.4.2, adopting the same pile-soil-interface properties (refer Table 2-3) and loading as used for the single pile analysis, and performing the same series of three analyses (i.e. bonded/elastic soil, separation/elastic soil, separation/inelastic soil) as described in section 2.4.2. Imposing equal loads to the pair of piles spaced at two and three pile diameters (i.e. $s = 2d$ and $3d$), a shadowing effect was clearly demonstrated by much larger deflections experienced by the trailing pile. Assessment of results from the analysis series provided further insight: It was considered that separation caused an outright reduction of interaction, whereas soil plasticity caused a progressive reduction of interaction, dependent on the level of loading applied. The role of separation and soil nonlinearity was also noted as governing the absolute amount of interaction, however the rate that interaction decayed with distance was considered to be primarily an elastic phenomenon.

Brown and Shie (1990b, 1991a) also utilized an in-line pair of piles to assess group effects, but adopted a rectangular model configuration with symmetry boundaries following the modeling approach shown in Figure 3-9(c). This represented two rows of piles loaded in-line and extending to infinity in the direction perpendicular to loading. Group spacing of $3d$ and $5d$ were investigated, and a single row of piles with $10d$ spacing was used to simulate isolated single pile behavior. Two soil model cases were analyzed to depict "clay" (constant strength) and "sand" (frictional) conditions, details of which are given in Table 3-1 and Table 3-2, respectively. The sand model utilized a non-associated flow rule such that constant volume behavior applied, and was governed by a strength criterion in deviatoric space that closely approximated the Mohr-Coulomb failure criterion. All analysis cases simulated free-headed piles simultaneously loaded at the pile-head (located at the groundline), causing horizontal displacements of between 10% to 15% of the pile diameter. Interface elements provided for gapping and slippage at the pile-soil interface.
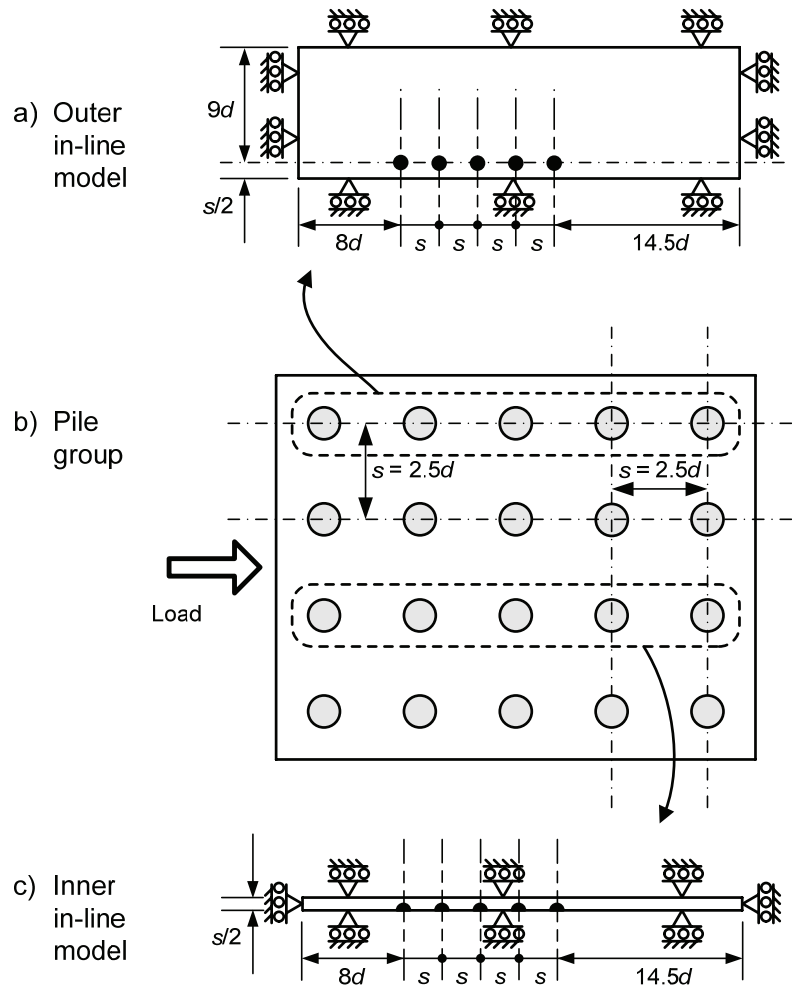
Figure 3-9: Plan views of in-line analysis models used by Tamura et al. (1982)

The work by Brown and Shie (1990b, 1991a) reaffirmed general observations from field testing, such as reduced shears for trailing piles leading to higher moment to shear ratios, and the occurrence of maximum bending moments in trailing piles at greater depths compared with the leading piles. Comparison of both cases also indicated more significant shadowing effects in the sand case, attributed to its stress-dependent shear strength. The latter was thought to have also affected leading pile behavior, in that increased shear strength near the sides of the pile, induced by increased confining stress imposed by load transfer from the trailing pile, served to "hold back" the pile and partially offset any additional displacement from strain superposition effects. Leading pile behavior was therefore considered as being comparable with an isolated single pile in both the sand and clay cases.

A most significant aspect of the Brown and Shie (1990b, 1991a) work was the additional step taken of extracting *p-y* curves from each analysis and deriving *p*-multipliers and *y*-multipliers to represent group effects. This was undertaken by fitting discrete bending moment values along the pile (obtained via stress values at the pile element centroids) to a fifth degree polynomial and then twice differentiating to obtain *p* values (*y* values being extracted directly). A practice-orientated assessment in the form of *p-y* multipliers was thus achieved, providing a more rational basis for comparison with full-scale tests. In this way good correlation with field test results was demonstrated using numerical experiments.

Table 3-1: Brown and Shie (1990b, 1991a) model parameters for clay case

Pile Parameters		Soil Parameters	
Type:	Steel	Description:	Saturated Clay (undrained)
Cross-Sectional Shape:	Pipe	Total Unit Weight (γ):	Not given
Length (L):	4 m[2]	Young's Modulus (E_s)[1]:	11000 kPa
Diameter/Width (d):	0.273 m	Poisson's Ratio (ν_s):	0.45
Young's Modulus (E_p):	200 GPa	Undrained Shear Strength (s_u):	27.5 kPa
Poisson's Ratio (ν_p):	Not given	Friction Angle (ϕ'):	0º

Interface Parameters
Elastic Stiffness: Not specified but provided
Coulomb Friction Coefficient (μ):   0.42

Pile - Soil Parameters	
$L/d \approx 15$[2]	$E_s/s_u = 400$
$K_R \approx 4.5\text{x}10^{-3}$	$E_p/E_s = 18000$

Notes:	1. Modulus constant with depth.
	2. Piles extended to base of model and were pinned at this point.

Table 3-2: Brown and Shie (1990b, 1991a) model parameters for sand case

Pile Parameters		Soil Parameters	
Type:	Steel	Description: Drained Sand [3]	
Cross-Sectional Shape:	Pipe	Total Unit Weight (γ):	18.9 kN/m^3
Length (L):	4 m[2]	Young's Modulus (E_s):	Varied[1]
Diameter/Width (d):	0.273 m	Poisson's Ratio (ν_s):	Not given
Young's Modulus (E_p):	200 GPa	Undrained Shear Strength (s_u):	13.8 kPa
Poisson's Ratio (ν_p):	Not given	Friction Angle (ϕ'):	23º

Notes:	1. Modulus 87 kPa at surface, increasing by 51 kPa per meter depth.
	2. Piles extended to base of model and were pinned at this point.
	3. Constant volume condition.
	4. Refer Table 3-1 for interface parameters.

Three-dimensional modeling economies, such as the two-pile in-line approach used by Brown and Shie (1990a, 1991a), have proven effective in assessing pile group behavior, but advances in computer technology are making the case of analyzing pile groups in their entirety a more feasible possibility. For example, Wakai, Gose and Ugai (1999) have presented a fully three-dimensional simulation of a full-scale laterally loaded test on a 3 x 3 pile group, details of which are shown in Figure 3-10. Soil behavior was modeled using an elastic-plastic framework employing the Mohr-Coulomb failure criterion and a non-associated flow rule allowing for volume change. Gapping was not accounted for explicitly, however thin elastic-plastic brick elements between the pile and soil elements considered possible slippage, and a scheme adopted to disallow tensile stresses in the soil elements and thus convey a separation effect. Piles were constructed from mainly brick elements and possessed the same diameter and flexural rigidity as the full-scale piles.

$s = 2.5d$

a) Plan view

$s' = 2.5d$

Load

b) Elevation

Footing (providing full fixity at pile heads)

Load

$10d$

14.5 m

Steel pipe piles:
Outside diameter (d) = 318.5 mm
Thickness = 6.9 mm

Soil Parameters

c' (kPa)	ϕ (deg.)	γ (kN/m^3)	E'_{50} (kPa)	v'
29.4	20	12.7	8829	0.3
0	39	8.63	25560	0.3
27.5	39	8.63	29160	0.3
74.6	0	7.36	2600	0.49
8.44	45	8.83	35280	0.3
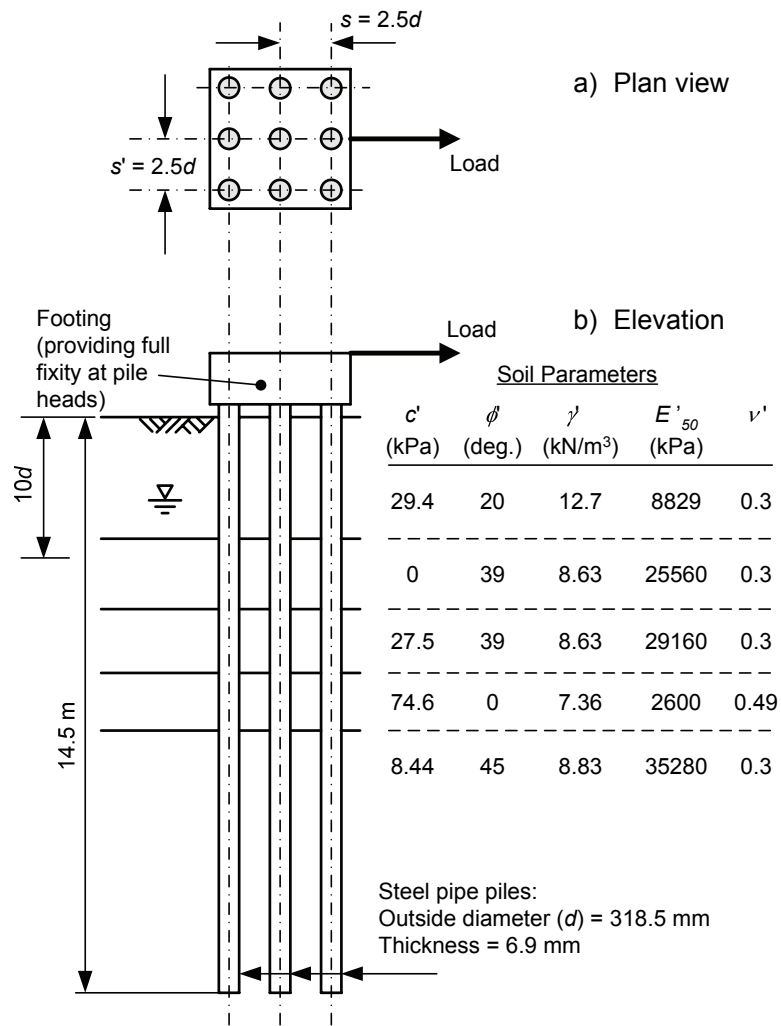
Notes: c' = Mohr-Coulomb cohesion.

ϕ = Mohr-Coulomb friction angle.

γ = submerged unit weight.

E'_{50} = secant Young's modulus @ 50% strain.

v' = Poisson's ratio.

Figure 3-10: Group test modeled by Wakai et al. (1999)

Comparison of observed and calculated load-deflection response and pile bending behavior with depth indicated reasonable agreement between field test and model behavior, although some discrepancy in load distribution trends amongst inner and outer piles at lateral displacements greater than 0.1d suggested modeling inadequacy at higher load levels. Nevertheless, good correlation with behavior was apparent and application of the same modeling technique to a 1g model test on a similar 3 x 3 group configuration in uniform dense sand exhibited some notable behavioral characteristics:

- The middle pile in the leading row experienced appreciable resisting soil pressures on its leading side faces as well as its leading face, and soil pressures serving to push it in the direction of movement on its trailing face.
- The middle pile in the back row only experienced appreciable resisting soil pressures on its leading face (where they extended to a greater depth compared with the middle pile in the leading row), and soil pressures reduced to zero to increasing depths with increased lateral displacement on the trailing face.
- *p-y* curves extracted for the middle pile in the back row exhibited strain softening behavior.
- Load sharing amongst inner and outer piles of a given row became more uniform with increasing lateral displacement.

In addition to these local observations, consideration of the pile group as a whole also identified rotational characteristics for fixed-head pile groups, whereby downward axial movements in leading row piles and upward axial movements in back row piles were induced as a result of pile cap rotation. This highlighted the need for appreciation of pile group behavior in a more global sense, in addition to pile-soil-pile interaction that serves to affect piles within the group on a more individual basis.

Other three-dimensional efforts to the same extent and level of numerical sophistication as Wakia et al. (1999) are not apparent from the existing literature, indicating such an approach is relatively rare. In terms of very large pile groups, being the topic of the current study, three-dimensional approaches are necessarily restricted given the substantial number of piles typically involved, and a three-dimensional large group analysis to the totality of Wakia et al. is certainly beyond current computational standards. A partial three-dimensional finite element analysis undertaken by Ono, Shimamura, Kasai and Omoto (1991) is likely to represent one of the largest problems investigated numerically, consisting of a circular tank 44 m in diameter, supported on 421 steel pipe piles (d = 700 mm; L/d = 43) spaced at 2.9 pile diameters.

Invoking symmetry to reduce the problem by half for modeling purposes, three-dimensional soil elements were governed by the hyperbolic Duncan and Chang (1970) constitutive formulation, and piles modeled using one-dimensional beam ("stick") elastic elements (fixed-head conditions applying at the pile heads). Modeling up to 23 rows of piles at the center of the group, analysis results indicated piles in the leading third portion of the group attracted a greater share of the lateral load imposed (up to 4.9 times the average load of all the piles for the leading piles), while the remaining piles attracted a fairly uniform share of between 60% to 80% of the average load of all the piles. Bending moments in piles were similarly distributed, and deepening of the zone of significant pile-soil interaction apparent with trailing piles. In the case of the 23 piles located along the center of the group in the line of loading, an increasing depth of interaction was apparent to the seventh trailing pile, reaching a maximum depth at this point and then maintaining the same depth over the remaining trailing piles.

While the analysis by Ono et al. (1991) is obviously limited by the simplistic portrayal of piles as line elements, and furthermore provision for separation does not appear to have been made, the results nevertheless reflect a somewhat intuitive sense that uniform behavior should prevail for a large portion of

the piles in a large pile group. Such a notion has been adopted by Law and Lam (2001) in the form of a three-dimensional modeling economy employing periodic boundary conditions. The so called periodic boundary concept, which results from viewing a large pile group as recurring rows of infinite number of piles, is illustrated in Figure 3-11. The notion of infinite bounds is a fair approximation, at least for piles located in the interior region of a large pile group. As depicted in Figure 3-11, this is seen to enforce periodic displacement conditions between piles, necessary in order to satisfy displacement compatibility between each tributary region.
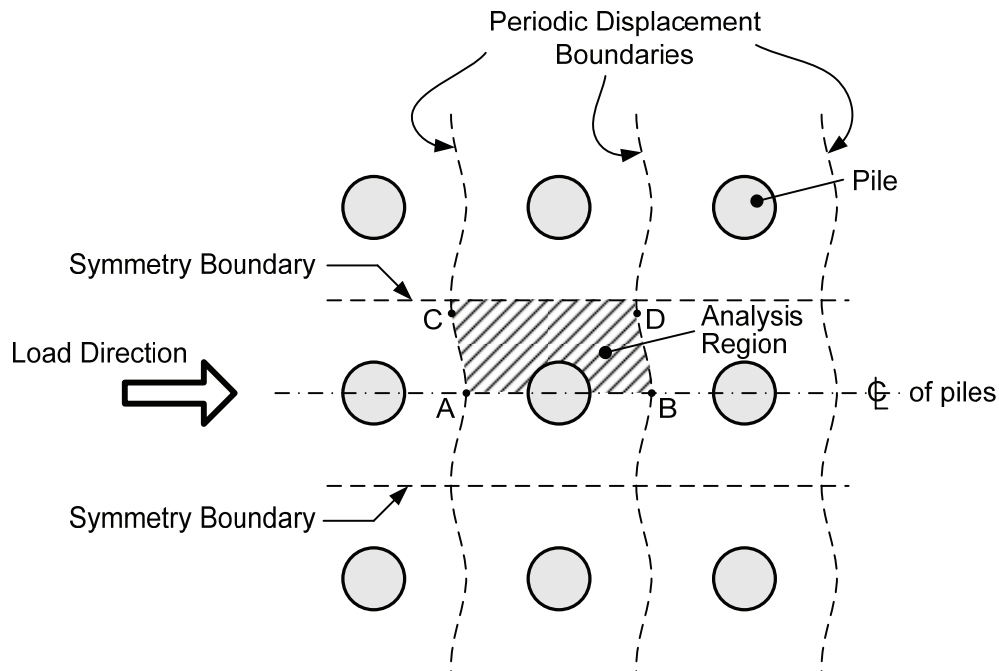
Figure 3-11: Periodic boundary analysis approach for large pile groups (after Law and Lam, 2001)

Deformations at adjacent points along periodic boundaries are therefore identical. For example, deformations at points A and B on Figure 3-11 are identical, likewise for points C and D. Further simplification arises by making use of symmetry boundaries through the centerline of the piles and through the midpoint between piles, also shown on Figure 3-11. The resultant analysis model can therefore be reduced to the analysis region indicated in Figure 3-11, with adjacent nodes along each periodic boundary slaved together to enforce the periodic displacement condition. Law and Lam (2001) utilized such a three-dimensional finite element model to assess the lateral behavior of 0.75 m diameter fixed-head cast-in-steel-shell piles ($L/d = 30$) forming a large pile group (380 piles) in soft clay soil conditions. By comparing the pile-head load-deflection behavior of the finite element model with an isolated single pile DLT model employing Matlock (1970) soft clay p-y curves, Law and Lam established appropriate p-multiplier and y-multiplier values as shown in Table 3-3. These results indicated the periodic boundary analysis approach was successful in portraying group effects, with increasingly lower lateral resistances mobilized at greater deflections for reduced pile spacing.

Table 3-3: Values of *p-y* multipliers suggested by Law and Lam (2001) for large pile groups in soft clay soil conditions

Large Pile Group Spacing (center to center)	*p*-multiplier	*y*-multiplier
3-pile diameters (3*d*)	0.5	4
6-pile diameters (6*d*)	0.75	2

3.5   Group *p-y* Issues

The review of pile group behavior in the preceding sections indicates that the *p-y* framework can provide a means to assess pile-soil-pile interaction through *p-y* multipliers. However, in addition to the various issues surrounding *p-y* curves themselves (discussed in Section 2), it is apparent that the group environment introduces issues of its own. A schematic depiction of pile group resistance is shown in Figure 3-12, indicating various factors and conditions that can influence pile group behavior. Assimilating *p-y* behavior in the presence of so many influences is no easy task, and this state of affairs helps to explain the significant scatter of *p*-multiplier data that has been observed from full-scale testing.
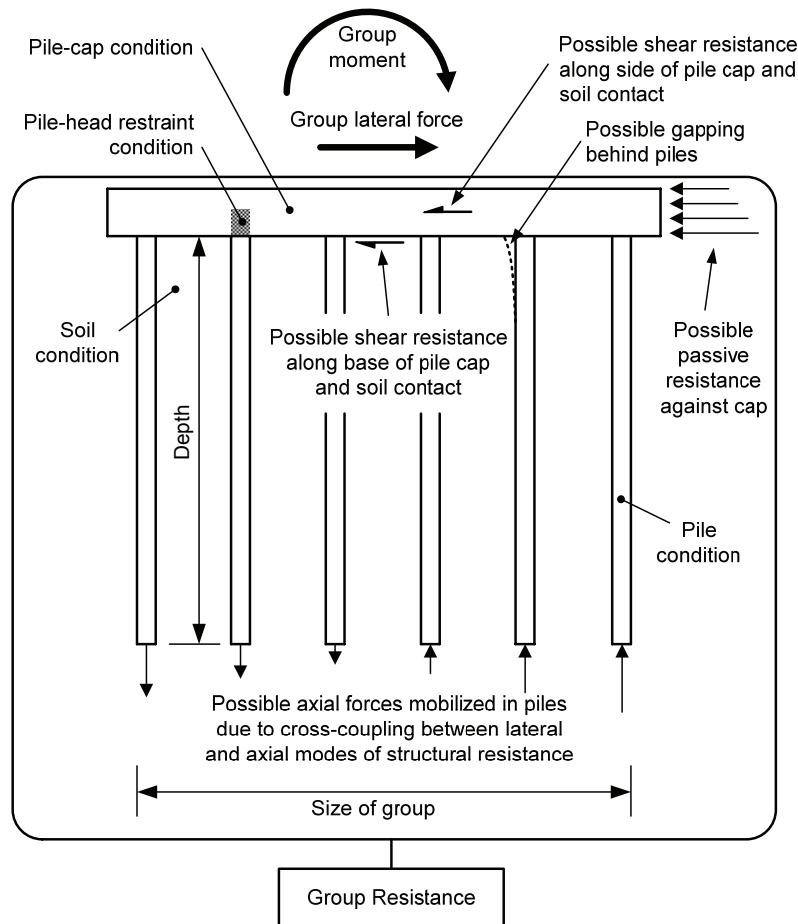
Figure 3-12: Schematic of pile group resistance

Pile-soil-pile interaction is therefore multi-faceted, and the following excerpt from the salient review of pile group action by O'Neill (1983) is timely:

> The nature of pile-soil-pile interaction is both complex and poorly understood. Simply put, it consists of two components: (a) alteration of soil stress states, densities, and perhaps grain size distributions, when piles are installed in close proximity to each other, in a manner different from those alterations that occur with the installation of single piles ("installation effects"), and (b) superposition of strains and alteration of failure zones … in the soil mass due to simultaneous loading of two or more neighboring piles ("mechanical effects"). These two components are interdependent. (p. 27)

Such installation and mechanical effects are already apparent from the discussion thus far, and are used here as general categories to discuss group *p-y* issues.

3.5.1   Installation Effects

Softening and stiffening of a loose to medium-dense silty sand site in Taiwan, attributed to the construction of a bored pile and driven pile group, respectively, was reported by Huang et al. (2001) [A-12][§], as discussed in Section 2. This study provided clear quantitative evidence that adjustments to group *p-y* curves as a result of the installation process are necessary in order to predict group behavior correctly. Changes to *p-y* curves in sands due to installation processes were also noted by Holloway, Moriwaki, Finno and Green (1982) [A-3], and Ruesta and Townsend (1997) [A-9] strongly suspected the pile driving sequence as causing appreciable differences in the loads of inner and outer piles of rows in sand. Evidence of installation effects on group *p-y* curves in clays is lacking in the literature, but given the possible installation effects as discussed in Section 2, and the tendency for even greater excess pore pressure generation within pile groups (O'Neill, 1983), modification to *p-y* curves cannot be discounted.

The basis for judging the amount that *p-y* curves should be adjusted to account for installation effects is currently highly empirical and draws on meager full-scale assessments. Application of an installation adjustment also poses problems in terms of identifying an appropriate adjustment measure. This is apparent from the study by Huang et al. (2001), who chose to normalize the installation adjustment factor (which was in the form of a *p*-multiplier) for each group by the single pile *p*-multiplier adjustment factor used to obtain site-specific *p-y* curves. In doing so, Huang et al. recognized the variability of *p-y* curve formulations and possible errors that may occur from applying installation adjustment factors based on one group pile-soil system to another. Normalizing served to provide a relative measure of installation effects and thus minimize errors.

3.5.2   Mechanical Effects

This category presents an array of interrelated issues, of which most are also likely to be dependent on installation effects to some degree. A most definite mechanical effect is the shadowing effect, where the repeated observance of disproportionate, row-by-row load distribution in full-scale, 1*g*, centrifuge and numerical pile group experiments have established it beyond doubt. However, while its existence cannot be denied, its quantification is subject to various factors and conditions.

First of all, that row dependence of load distribution only exists on an average basis was stressed by Brown et al. (2001) [A-15, A-16], as they noted variations of pile-head shear forces for individual piles in each row that differed by a factor as much as two. Random soil variability within the group or possible

---

[§] The alphanumeric expression(s) in square brackets refers to the table(s) in Appendix A providing summary details and key observations pertaining to the relevant pile group test(s).

inaccuracy of shear values were considered likely causes in those cases. Less drastic, but nevertheless variations, of 20% about the average of all piles were reported by Brown, Reese and O'Neill (1987) [A-5], and within row variations have been noted in other full-scale tests (e.g., Rollins, Peterson and Weaver, 1998 [A-10], McVay, Zhang, Molnit and Lai, 1998 [A-19]). The recent centrifuge study by Ilyas, Leung, Chow and Budi (2004) [A-20] indicated that inner piles in the middle rows of 3 x 3 and 4 x 4 configurations carried 50% to 60% less shear than outer piles in the same rows. Such variations demand attention from an assessment standpoint, so as to ensure that observed actions are representative of row action.

Viewed in terms of p-multipliers, load distribution becomes clouded by other considerations. The pile-head fixity condition, be it free, fixed or somewhere in-between, will dictate the deformed shape of a pile and thus influence the determination of an appropriate p-multiplier. In addition, for the cases of fixity or partial fixity of the pile-head, any lateral displacement of a pile cap will mobilize the "fixing" moments and these will act to try and rotate the pile cap. In turn, rotation of the pile cap is a function of the axial stiffness of the piles given the "push-pull" resisting couple that is mobilized from compression and tension forces induced in the piles.

Such lateral and axial interaction denotes cross-coupling of stiffness modes for the pile group, meaning that axial stiffness of piles can affect the lateral stiffness of a group. Thus p-multipliers are sensitive to the conditions of the connection between the piles and pile cap and to axial pile stiffness (e.g., McVay, Hays and Hoit, 1996 [A-18]; Huang et al., 2001 [A-12]; Brown et al., 2001 [A-15; A-16]; Ng, Zhang, and Nip, 2001 [A-13]). Indeed, Huang et al. and Brown et al. emphasized the importance of assigning appropriate connection and axial stiffness conditions when modeling experimental fixed or partially fixed pile group tests, as extraction of p-multipliers is contingent on the model apportioning group resistance in a realistic way.

Geometry of a pile group may also influence p-multipliers, both from a depth and size perspective. Experimental variation of p-multipliers with depth, as observed by Brown et al. (1988) [A-6], are shown in Figure 3-13. Three-dimensional analyses by Brown and Shie (1990b, 1991a) also indicated variation with depth, but an average value was deemed acceptable. Mokwa and Duncan (2001) have noted that use of an average value is sound given that the back-calculation procedure to obtain p-multipliers implicitly accounts for variation with depth. However, this is not to say that application of p-multipliers to group pile-soil systems significantly different from those in which they were derived is also acceptable.

In terms of size, the variation of p-multipliers with number of rows needs consideration, and Table 3-4 lists experimental p-multiplier values (f_m) as a function of row position. A definite decrease in f_m for rows trailing the leading row is observed, but no other obvious trends are apparent. An appreciably lower and more uniform f_m for the rearward interior rows with increasing number of rows is suggested from the data, a trend in agreement with the numerical analyses by Tamura et al. (1982) and Ono et al. (1991), as discussed in section 3.4. It is noted that the study by Ilyas et al. (2004) also noted a similar trend and reported what were termed p-multipliers supporting as much. However, this data reflected the average lateral resistance developed in each pile of a row, rather than an adjustment procedure applied to p-y curves. Hence the reported values were not p-multiplier values as p-multipliers are generally not directly proportional to the lateral resistance developed by piles in each row (McVay et al., 1998).

Differing opinions as to the effect of soil type on p-multipliers has already been noted in relation to the suggested design values presented in section 3.3, and it remains an issue. Brown et al. (1988) [A-6] did note that the shadowing effect was more pronounced in sand compared with stiff clay, and given that this was based on the same pile group set-up it must be considered well-founded. Other soil-related examples include suspected pore pressure effects influencing the p-multiplier value of a back row (Rollins et al., 1998), and the dependence of p-multipliers on soil density for free-headed pile groups in

sands in the centrifuge (McVay, Casper and Shang, 1995). However, McVay et al. (1998) later found no such density dependence for the case of fixed-headed pile groups in sands in the centrifuge. In any case the tabulated data in Table 3-4 does not appear to support any particular pattern based on soil type.
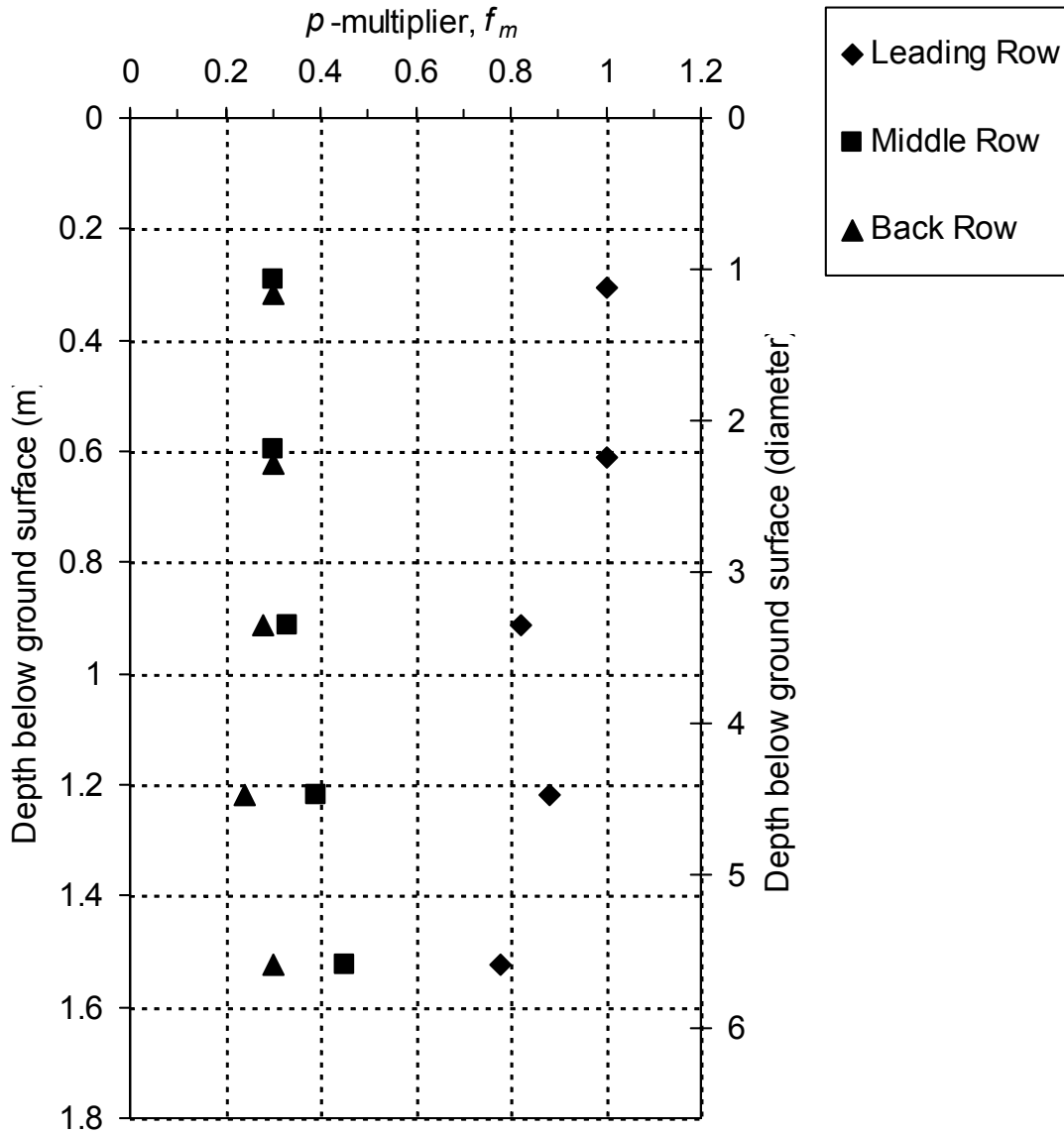
Figure 3-13: Observed variation of *p*-multipliers with depth (from Brown et al., 1988)

Table 3-4: Experimental *p*-multiplier data from full-scale and centrifuge tests

Pile Spacing, s*	Layout**	*p*-multiplier value, f_m							Maximum Deflection	Pile Head Condition***	Reference – Soil Type
		Leading Row	1st Trailing Row	2nd Trailing Row	3rd Trailing Row	4th Trailing Row	5th Trailing Row	6th Trailing Row			
Clay Soil Types											
3	3x3	0.7	0.6	0.5					0.23*d*	Fr	Brown et al. (1987) – stiff clay
3	2x3	0.9	0.5	0.5						Fr	Meimon et al. (1986) – stiff silty clay
3	3x3	0.6	0.4	0.4					0.19*d*	Fr	Rollins et al. (1998) – clayey silt
3	4x3	0.8	0.4	0.2	0.3				0.51*d*	Fi	Brown et al. (2001) – soft clay
3	4x3	0.64	0.32	0.16	0.24				0.20*d*	Fi-P	Brown et al. (2001) – sandy silts
Sand Soil Types											
3	3x3	0.8	0.4	0.3					0.23*d*	Fr	Brown et al. (1988) – med. dense sand
3	3x3	0.65	0.45	0.35					0.16*d*	Fr	McVay et al. (1995) – med. loose sand
3	3x3	0.8	0.4	0.3					0.18*d*	Fr	McVay et al. (1995) – med. dense sand
5	3x3	1.0	0.85	0.7					0.18*d*	Fr	McVay et al. (1995) – med. loose sand
5	3x3	1.0	0.85	0.7					0.2*d*	Fr	McVay et al. (1995) – med. dense sand
3	4x4	0.8	0.7	0.3	0.3				0.1*d*	Fr	Ruesta and Townsend (1997) – loose sand
3	3x3	0.8	0.4	0.3					0.2*d*	Fi	McVay et al. (1998) – med. dense sand
3	4x3	0.8	0.4	0.3	0.3				0.26*d*	Fi	McVay et al. (1998) – med. dense sand
3	5x3	0.8	0.4	0.3	0.2	0.3			0.27*d*	Fi	McVay et al. (1998) – med. dense sand
3	6x3	0.8	0.4	0.3	0.2	0.2	0.3		0.26*d*	Fi	McVay et al. (1998) – med. dense sand
3	7x3	0.8	0.4	0.3	0.2	0.2	0.2	0.3	0.26*d*	Fi	McVay et al. (1998) – med. dense sand
3	3x2	0.5	0.4	0.3					0.02*d*	P	Brown et al. (2001) – bored, silty sand
3	4x3	0.9	0.7	0.5	0.4				0.15*d*	Fr	Brown et al. (2001) – silty sand

Notes:

*   Expressed in pile diameter (*d*) units.

**   Refers to plan configuration (*a* rows x *b* columns)

***   Fr = Free; Fi = Fixed; P = Partial restraint

86

Finally, the issue of structural performance also requires due attention, both in terms of individual pile performance and overall group performance. Ruesta and Townsend (1997) noted the dominance that nonlinear characteristics of prestressed concrete piles had in ultimately assessing *p*-multipliers, and Brown et al. (2001) stated that "modeling of the structural properties of the piles is at least as important as modeling the resistance-deformation [i.e. *p-y*] behavior of the soil" (p. A-6). Not only is the modeling of individual piles in a group important, but also the group as a whole given that the performance of the structural system may overshadow that of the soil system. Brown et al. recognized this quality in conjunction with the 3 x 2 bored pile group test in Taiwan, as although softening of the pile-soil system was observed in connection with the installation process, the relatively high structural stiffness of the group demanded that a focus remain on correctly modeling the structural performance of the pile-soil-cap system. This is a return to the fundamental aspect of soil-structure interaction, whereby behavior is dependent on the relative stiffness of the soil and structure.

3.5.3   Concluding Comments

An appreciable amount of uncertainty is evident in relation to a *p-y* orientated assessment of lateral behavior for pile groups, arising from the uncertainties associated with the *p-y* curves themselves, and interrelated issues associated with the determination of group resistance. The pile-soil-pile interaction aspect of the problem certainly plays a significant role in the assessment process, but consideration of other contributing factors and appreciation of the problem as a whole are equally important aspects of the problem. In this respect, Lam et al. (1998) have emphasized the need for equable consideration of the various factors and conditions contributing to group action, pointing out that a *p*-multiplier of 0.5 may reduce pile-head stiffness by 50%, but this is relatively mild compared with the effect that other issues such as gapping, embedment, and cyclic loading can have on behavior. Altogether, judgment is clearly required and more guidance wanting, particularly in regards to large pile group behavior.

3.6   **Design Approaches**

The importance of lateral stiffness with respect to seismic design is the motivation for the current study, but design for ship impact, wind loading, and wave action are to be also noted from a lateral load design perspective. In terms of designing a laterally loaded pile group, there is a basic need to be able to adequately characterize the behavior of the group taking into account the various issues that have been discussed. In the course of the developments that have taken place towards understanding these issues, a progression of design approaches have naturally emerged. A summary of the prevalent design approaches is provided in Table 3-5.

Recent reviews of design methods used in practice (O'Neill, Brown, Anderson, El Naggar, Townsend and McVay, 1997; Walsh, Fréchette, Houston and Houston, 2000) indicate variations in the way design approaches are applied, but most revolve around the idea of applying a reduction to the soil system to account for group effects, and then examining the structural integrity of representative piles (or rows) in the group. A general move towards using *p-y* curves to represent the soil system is suggested, facilitated by the availability of commercial programs such as LPILE (Ensoft, 1999). Emergence of *p-y* based group programs GROUP (Ensoft, 2004) and FLPIER (McVay et al., 1996) are also influencing the assessment of small pile groups in this way.

Table 3-5: Prevalent design approaches for lateral pile groups

Design Method	Description	Comments	Reference for Guidance
Elastic Method	Utilizes superposition of elastic interaction factors (Poulos, 1971b) and a matrix formulation imposing displacement compatibility to derive individual pile forces.	Popular in the 1970's but now outdated by more non-linear methods.	Poulos, H.G. and Davis, E.H. (1980).
Linear Subgrade Modulus Methods	A discrete approach utilizing linear subgrade reaction theory to determine stiffness values. Charts provide lateral, rotational and cross-coupling stiffness for a range of piles and subgrade conditions. Group effects accounted for by subgrade reaction reduction factors.	A fairly straightforward hand method that provides a reasonable solution if site conditions are very simple. Otherwise recourse to iterative or computer orientated formulation appropriate.	Lam and Martin (1986).
Equivalent Cantilever Method	Represents pile group as an equivalent pile with properties of group as a whole. Either linear subgrade reaction or p-y approach can then be applied to assess "group" behavior.	Generally only used as a check against other methods.	Lam, I.P., Kapuskar, M., and Chaudhuri, D. (1998).
Discrete Load-Transfer Method	A discrete approach utilizing nonlinear p-y and "t-z" load-transfer curves to represent lateral and axial pile-soil stiffness respectively. Multipliers used to scale curves to take into account lateral group effects, in most cases using p-multipliers that reduce the ultimate lateral load capacity while keeping deflection the same.	A popular approach given availability of computer programs such as GROUP (Ensoft, 2004) and growing empirical test database.	Lam, I.P., Kapuskar, M., and Chaudhuri, D. (1998).
Coupled Method	A continuum approach utilizing a fully coupled continuum model that attempts to emulate inertial and kinematic response in some way.	Specialized approach generally undertaken on a case by case basis. However, Washington State DOT (WSDOT, 1997) has produced design guidelines incorporating coupled results for various site and pile group configurations considered typical.	Case by case.

The report by Lam et al. (1998) represents the most up-to-date authoritative reference on lateral pile group behavior, providing some design guidance on many of the issues that have been discussed. A design philosophy urging greater accountability of structural and soil nonlinearity is evident, and the use of *p-y* curves is the recommended basis for achieving this in the soil case. A key design principle advocated by Lam et al. is an uncoupled approach to account for pile-soil interaction in seismic design. This approach first determines the seismic response of the pile group utilizing linear elastic analysis methods. In this first step importance is given to characterizing a foundation stiffness that seeks to capture the average displacement behavior expected for the seismic conditions at play. If the foundation stiffness is either too high or too low there is a danger of force-displacement incompatibility because of the highly nonlinear nature of soil behavior. This is illustrated in Figure 3-14, which shows a general load-deflection representation of a pile foundation system together with an "average" design stiffness value.
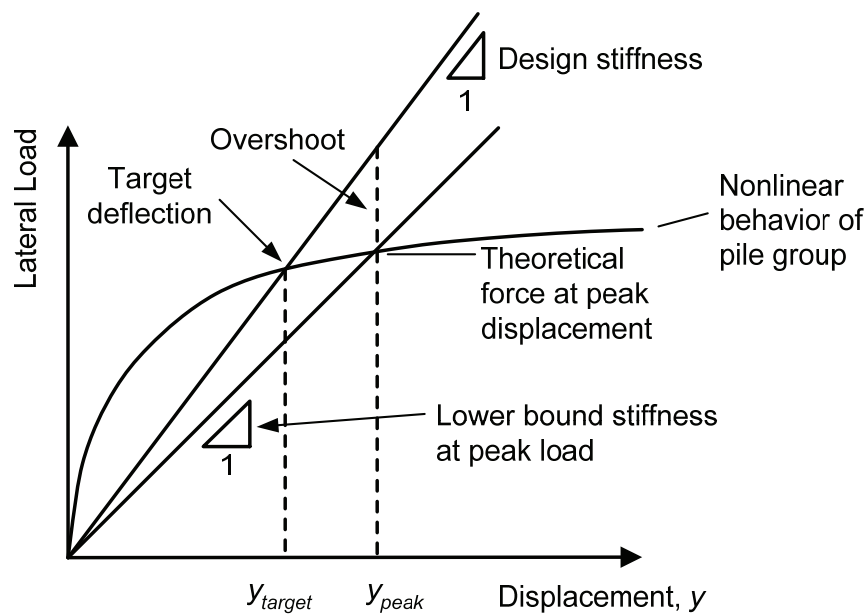
Figure 3-14:   General load-displacement relationship illustrating nonlinearity
(after Lam et al., 1998)

The second step of the design process involves a static nonlinear "pushover" analysis of the pile group foundation. This determines a realistic force that corresponds with the displacement calculated in the first step, taking into account nonlinearities of the system using discrete load-transfer modeling of the pile group. The second step is then a capacity analysis checking that ductility demand is within the capabilities of the system. In this way a compatible force-displacement regime is determined along with an appropriate stiffness for assessment of the entire system response.

Thus the *p-y* framework is serving a vital role in design and stands to represent the next standard for soil behavior in future pile foundation modeling, underlining the need of appropriate *p-y* multipliers to assess group effects.

SECTION 4
THREE-DIMENSIONAL NUMERICAL MODELING TECHNIQUE

4.1   Introduction

The use of mathematical models to idealize physical problems in civil engineering research and design is well-founded. Involved in such an undertaking is the important consideration of establishing whether one-dimensional (1-D), two-dimensional (2-D), or three-dimensional (3-D) numerical means are sufficient to characterize the problem. In the case of the laterally loaded pile group problem where pile-soil-pile interaction takes affect, it is clear from Section 3 that 3-D numerical modeling techniques are necessary from a research perspective to fully appreciate the mechanisms at play. Furthermore, the instance of pile-soil separation and appreciable loading of surficial soils demand both geometric and material nonlinearities be accounted for in the numerical formulation.

In previous numerical work the finite element computational framework has been the prevalent 3-D pile-soil modeling tool addressing such needs, as is apparent from the numerical work reviewed in the previous sections. Finite difference modeling techniques have generally not featured in this respect, having been applied instead to 1-D and 2-D problems where finite approximations are used to replace infinitesimal differences that form the components of governing differential equations. For example, the discrete load-transfer approach to pile-soil modeling has typically employed a finite difference solution to the differential equation governing pile behavior, as illustrated in Figure 4-1. Indeed, the term "finite difference" is often considered synonymous with this type of "classical" approach, where discretization is in the form of discrete calculation stations that are interrelated via a general finite difference equation, often depicted using finite difference "stencils", and unknown variables at each station are solved using matrix algebra.

Finite difference approaches are evident in other forms, however, particularly as applied to dynamic problems where they form a basis for direct integration methods that have been developed to solve the dynamic equations of equilibrium. The dynamic equations of equilibrium for a discretized numerical system can be succinctly expressed as

$$\mathbf{M\ddot{U} + C\dot{U} + KU = R} \tag{4.1}$$

where $\mathbf{M}$ = mass matrix,

$\mathbf{\ddot{U}}$ = acceleration vector,

$\mathbf{C}$ = damping matrix,

$\mathbf{\dot{U}}$ = velocity vector,

$\mathbf{K}$ = stiffness matrix,

$\mathbf{U}$ = displacement vector, and

$\mathbf{R}$ = vector of externally applied loads.

Application of finite difference expressions for acceleration, velocity and displacement in (4.1) lead to the various direct integration methods, for example the explicit central finite difference method, or the implicit Crank-Nicolson and Houbolt methods.

P_z = axial load

Notes:

- $\bullet$ = finite difference station
- h = discretization (increment) length for pile
- z = depth

Deflected pile

Pile characterized by E_pI_p line element

Soil characterized by springs, stiffness = $k = (p*h)/y$ i.e.

p-y curve resistance from lateral reaction

a) Finite difference model
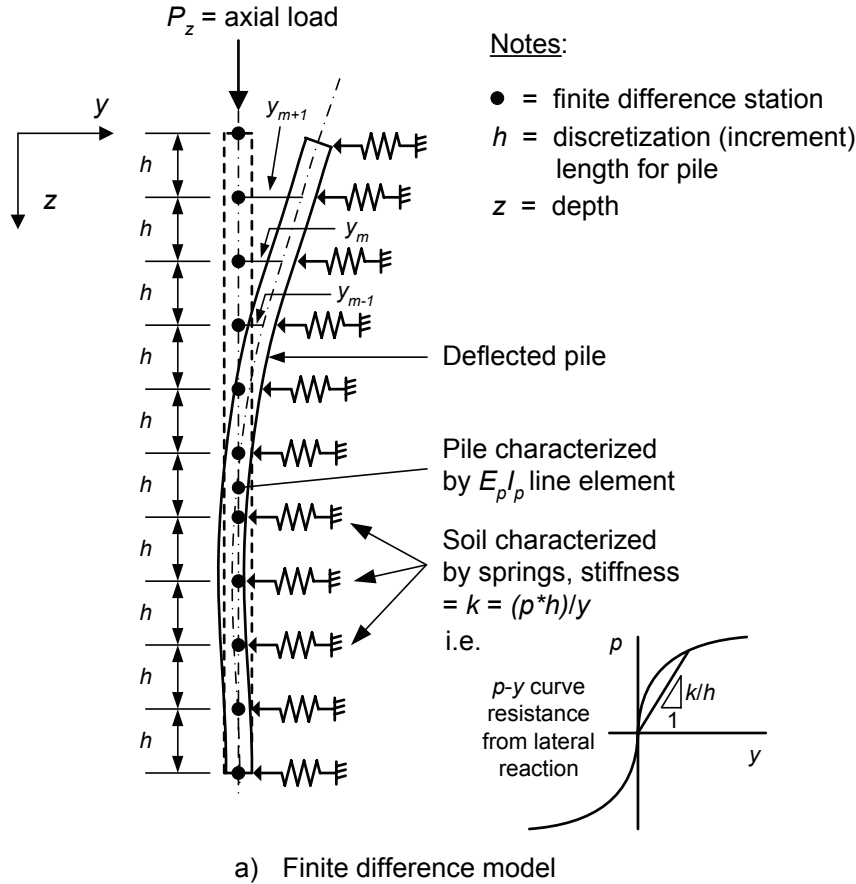
$$\frac{d^2}{dz^2}\left(E_pI_p\frac{d^2y}{dz^2}\right)+P_z\frac{d^2y}{dz^2}+ky=0$$

b) Governing differential equation

$$y_{m-2}(R_{m-1})+y_{m-1}\left(-2R_m-2R_{m-1}+P_xh^2\right)$$
$$+y_m\left(R_{m+1}+4R_m+R_{m-1}-2P_xh^2+k_mh^4\right)$$
$$+y_{m+1}\left(-2R_{m+1}-2R_m+P_xh^2\right)+y_{m+2}(R_{m+1})=0$$
where
$$R=E_pI_p$$

c) General finite difference equation

Figure 4-1: Finite difference solution scheme for pile-soil interaction problem utilizing the discrete load-transfer approach

Contrasting with the classical matrix-orientated finite difference techniques and distinctly temporal finite difference applications is the commercial 3-D explicit finite difference program *FLAC*[3D] (Itasca, 1997). Although drawing on finite difference computation to enable a solution, *FLAC*[3D] also relies on other modeling techniques and concepts to obtain a solution, thus it is best classified as a hybrid modeling technique when considered in the context of finite difference approaches in general. The *FLAC*[3D] formulation is therefore quite unique and represents a computational framework of a very different nature to that of the finite element approach. This demands particular care in the use of *FLAC*[3D] as a modeling tool, weighed down by its relative infancy that affords lack of familiarity and allows only a limited track record from which to assess its performance.

The current research adopted $FLAC^{3D}$ as the 3-D pile-soil modeling tool to undertake numerical studies on the lateral stiffness of pile groups. Given the emphasis of the research on pile groups, and the attendant actions around a pile that this implies, provision of a numerical formulation capable of modeling the pile-soil interface aspect of the problem was considered particularly important. The interface feature in $FLAC^{3D}$ provided such capabilities, allowing interface action to be implemented in a controlled manner that was considered appropriate to appreciate the mechanics at play. Hence, along with its 3-D formulation and the ability to account for geometric and material nonlinearities, $FLAC^{3D}$ met the necessary modeling requirements.

The current section thus serves to describe $FLAC^{3D}$ in sufficient detail to address both its capabilities and its uniqueness from a formulation standpoint.

4.2   FLAC³ᴰ

4.2.1   Overview

In broad terms $FLAC^{3D}$ (Fast Lagrangian Analysis of Continua in 3 Dimensions) is a three-dimensional, nonlinear, explicit finite difference program that can be used to simulate static and dynamic soil-structure interaction. The basis from which this is achieved is a unique explicit solution scheme that avoids a stiffness-based formulation common in finite element programs. Representing the chief solution "vehicle" of the explicit solution scheme is the central finite difference expression of Newton's Second Law of Motion:

$$v\left(t + \frac{\Delta t}{2}\right) = v\left(t - \frac{\Delta t}{2}\right) + \frac{\text{Force}}{\text{Mass}}\Delta t \qquad (4.2)$$

where v = velocity,

t = time, and

Δt = time step.

Use of the Second Law of Motion follows the "dynamic relaxation" connotations of $FLAC^{3D}$, the idea behind dynamic relaxation being that a dynamic formulation can be used to obtain a static solution based on the fact that the static solution is the steady state part of the transient response of a system (Underwood, 1983). Thus "time" only serves as a computational device for static problems in $FLAC^{3D}$.

Constructing the analysis domain using 3-D numerical building blocks (termed "zones" as opposed to "elements" used with finite elements), the solution procedure formulates (4.2) at discrete calculation points that locate the vertices of each 3-D zone (termed "gridpoints" as opposed to "nodes" used in finite elements). This is undertaken in terms of tetrahedral shapes, whereby the program considers each zone as consisting of pairs of tetrahedron sets, as shown in Figure 4-2. Consideration of each zone in terms of elemental tetrahedra enables the application of an efficient ("fast") computational algorithm, calling upon the divergence theorem, the principle of virtual work, and linearized velocity fields to apportion gridpoints with an equivalent force that represents the collective actions of forces derived from stress-strain behavior, body and inertial forces, and possible direct point loads applied in relation to boundary conditions. Such forces are collated at each gridpoint from all adjoining tetrahedra for both tetrahedron sets.

93
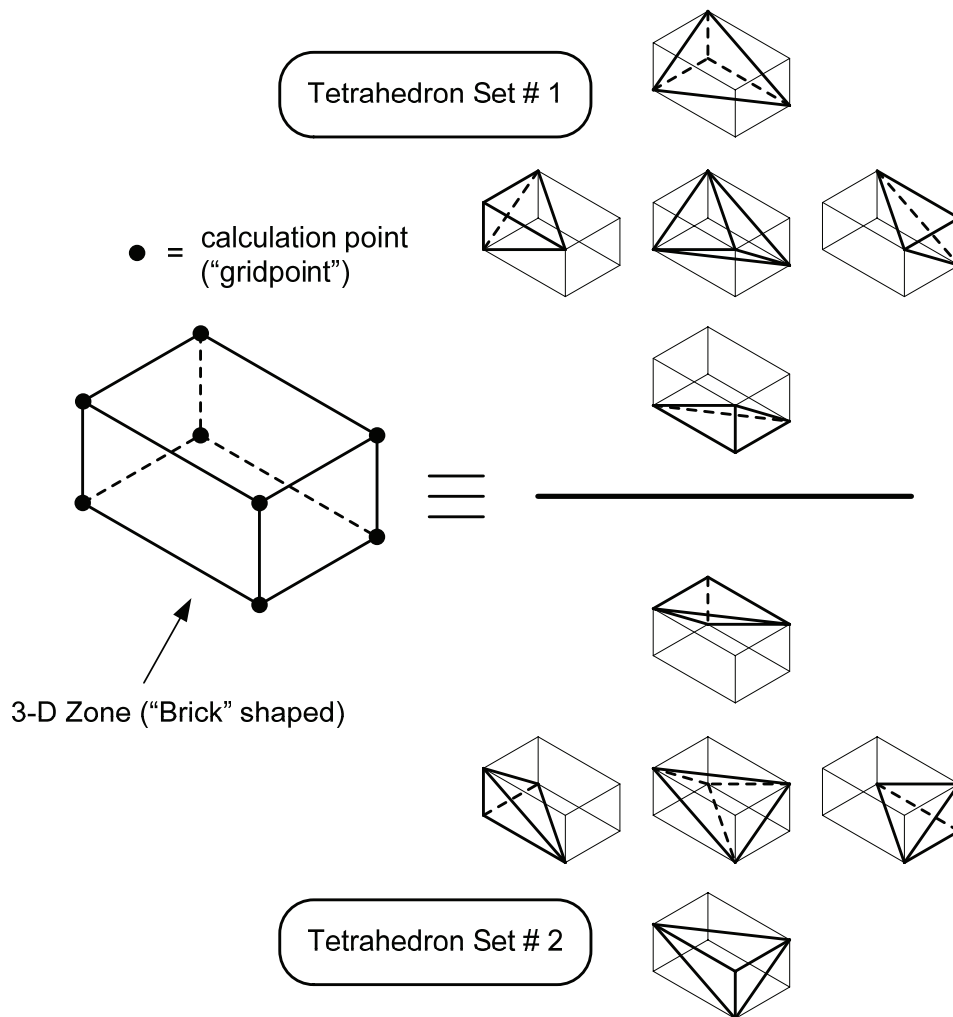
Figure 4-2: Internal tetrahedron sets used in FLAC3D formulation

An average of the forces obtained from both tetrahedron sets is used as the value of the gridpoint force to prevent possible directional bias in the solution, brought about by the different geometrical layout of each of the tetrahedron sets. Velocity and displacement are formulated at the gridpoints, while strain and stress tensors are formulated at the centroid of the zone. An illustration of this general analysis concept is illustrated in Figure 4-3.

Displacements are calculated at gridpoints by applying central finite difference approximation as follows,

$$u(t + \Delta t) = u(t) + v\left(t + \frac{\Delta t}{2}\right)\Delta t \qquad (4.3)$$
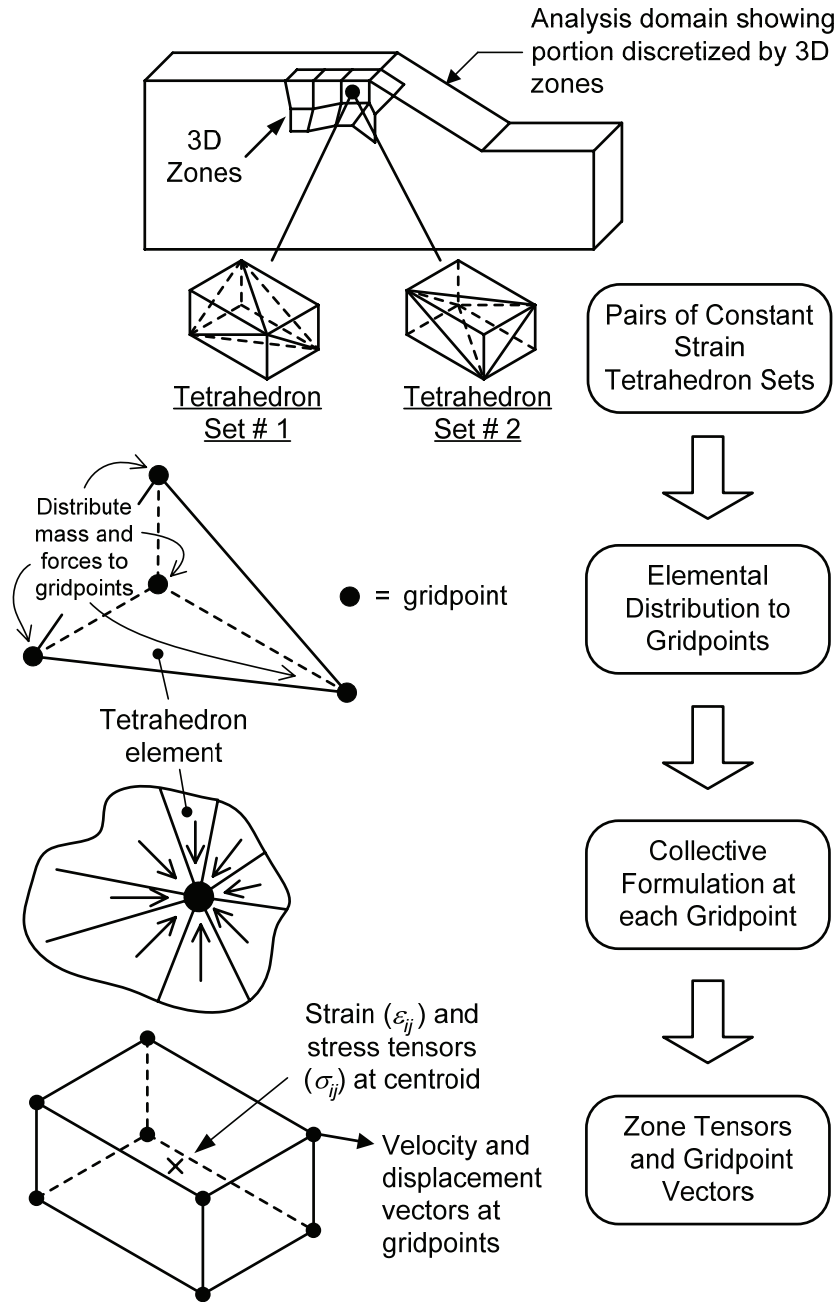
Figure 4-3: General analysis concept in FLAC3D

where u = displacement, and in this way the Lagrangian aspect of the formulation is seen to be a matter of course. Both (4.2) and (4.3) are successively applied to each gridpoint of every zone at each time step. The analysis sequence starts with (4.2) and (4.3) applied to obtain velocities and displacements, then velocity-induced strain increments are derived at element centroids, and ensuing stresses are derived via the stress-strain law appropriate to the constitutive model assigned to the zone. Conversion of stresses to gridpoint forces then completes the sequence in readiness for repeating the process for the next time step. This calculation cycle is illustrated in Figure 4-4.
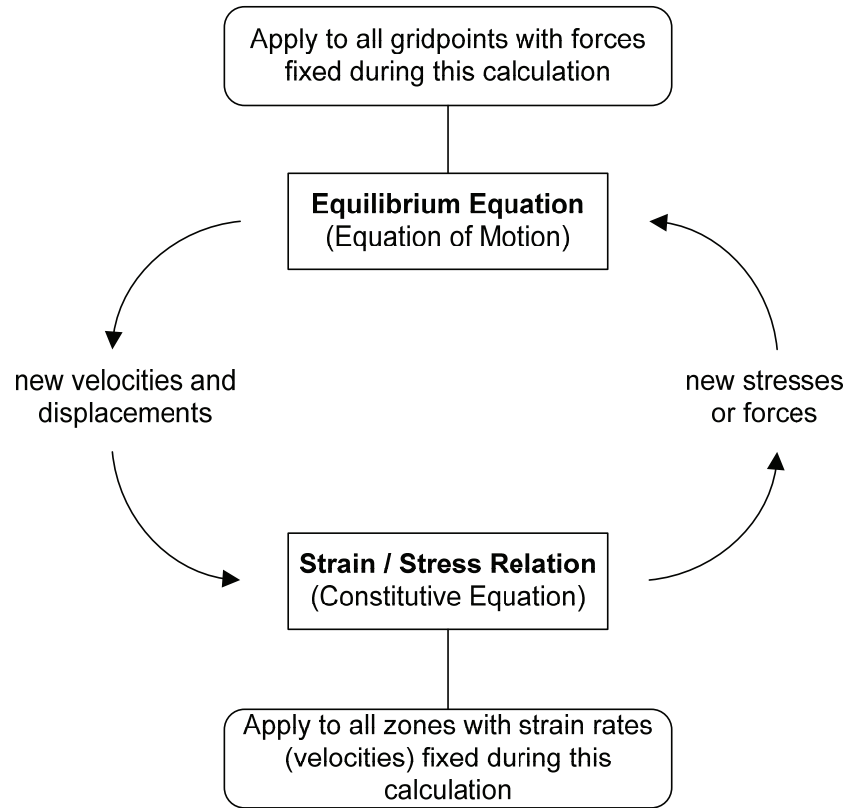
Figure 4-4: Basic calculation cycle in FLAC3D (Itasca, 1997)

Hence a physical interpretation of $FLAC^{3D}$ is that it is depicting a 3-D analysis problem as a system of interconnected but discrete masses and springs that propagate waves numerically using (4.2) as an approximation of the process. In doing so the $FLAC^{3D}$ formulation is removed from the encapsulated environment evident in finite elements, where the usual displacement-based approach enjoys the equivalency of invoking stationarity of the total potential of the discretized finite element system. Enforcing a system to obey such a well-founded principle serves as an effective theoretical assurance for the finite element approach, but in the $FLAC^{3D}$ case, existence of such an effective assurance is less apparent. This is where the nature of $FLAC^{3D}$ deviates from finite elements, shifting the focus instead to the transmission qualities of the system so that the attempt to approximate physical disturbance is made as realistic as possible.

Dynamic aspects are therefore of primary concern in the $FLAC^{3D}$ formulation, irrespective of whether a static or dynamic solution is being pursued. Forming the backbone for this dynamic framework are central finite difference and the spirit of dynamic relaxation. A brief review of these aspects will be undertaken prior to addressing the particulars of the $FLAC^{3D}$ formulation.

4.2.2   Central Finite Difference

An important consideration when utilizing finite differences is the issue of accuracy. In this way central finite difference performs well as can be demonstrated using Taylor series to obtain the order of accuracy:

$$u(t + \Delta t) = u(t) + \frac{\Delta t}{1!} \frac{du(t)}{dt} + \frac{(\Delta t)^2}{2!} \frac{d^2 u(t)}{dt^2} + \frac{(\Delta t)^3}{3!} \frac{d^3 u(t)}{dt^3} + \dots \qquad (4.4)$$

$$u(t - \Delta t) = u(t) - \frac{\Delta t}{1!} \frac{du(t)}{dt} + \frac{(\Delta t)^2}{2!} \frac{d^2 u(t)}{dt^2} - \frac{(\Delta t)^3}{3!} \frac{d^3 u(t)}{dt^3} + \dots \qquad (4.5)$$

Subtracting (4.5) from (4.4) and rearranging,

$$\frac{du(t)}{dt} = \frac{u(t + \Delta t) - u(t - \Delta t)}{2\Delta t} + O(\Delta t)^2 \qquad (4.6)$$

which implies that the central finite difference approximation has an error proportional to the square of Δt, and that halving the interval between sample points will reduce the error in the approximation to a quarter of its earlier value. A pictorial of the central finite difference approximation in relation to other finite difference approximations is indicated in Figure 4-5(a) to emphasize the accuracy it affords. Also shown in Figure 4-5(b) is the implication for interrelated variables, as is the case with velocity and displacement (refer Equations 4.2 and 4.3), where the order of accuracy is maintained if the sample points for each variable are offset.
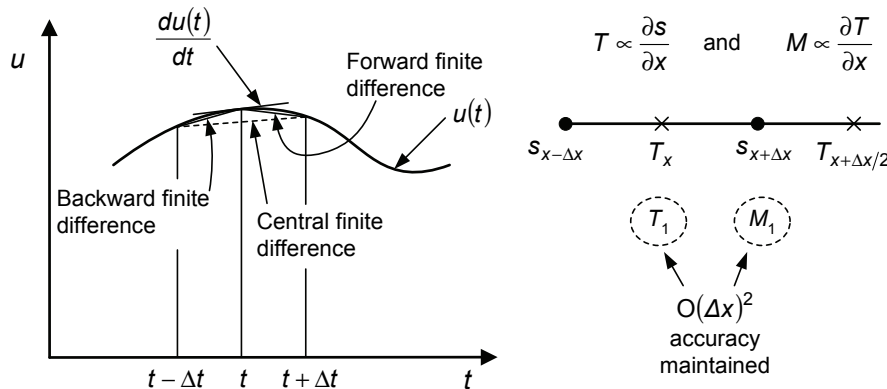
a) Finite difference pictorial

b) Accuracy for interrelated variables

Figure 4-5: Central finite difference approximation

4.2.3   Dynamic Relaxation

The spirit of the dynamic relaxation technique is best described by way of demonstration, and the 1-D problem of a bar subject to an axial stress at its free end and fixed at the other will be used for such purposes. This follows Otter, Cassell and Hobbs (1966) who used the problem as an introduction to the dynamic relaxation technique in the mid 1960's. Details of the problem are given in Figure 4-6, and the central finite difference equations for the governing equations indicated in Figure 4-6(b) are given as follows:

$$\sigma_k^{(r)} = \frac{E}{\Delta x}\left(u_{k+1}^{(r)} - u_k^{(r)}\right) \text{ and} \qquad (4.7)$$

$$\frac{\sigma_k^{(r)} - \sigma_{k-1}^{(r)}}{\Delta x} = \frac{\rho}{\Delta t}\left(\dot{u}_k^{(r+1)} - \dot{u}_k^{(r)}\right) + \frac{K\rho}{\Delta t}\frac{1}{2}\left(\dot{u}_k^{(r+1)} + \dot{u}_k^{(r)}\right) \qquad (4.8)$$

where the superscript (r) refers to a temporal sample point in computational time, and the subscript k refers to a spatial sample point (i.e., gridpoint). Definitions of terms are given in Figure 4-6.

Figure 4-6: Demonstrative example for dynamic relaxation technique (after Otter et al., 1966)

Rearrangement of (4.8) leads to

$$\dot{u}_k^{(r+1)} = \frac{1}{(1+K/2)}\left\{(1-K/2)\dot{u}_k^{(r)} + \frac{\Delta t}{\rho\Delta x}\left(\sigma_k^{(r)} - \sigma_{k-1}^{(r)}\right)\right\} \qquad (4.9)$$

and this provides a starting point for the solution scheme followed by the central finite difference expression for displacement,

$$u_k^{(r+1)} = u_k^{(r)} + \Delta t . \dot{u}_k^{(r+1)} \tag{4.10}$$

thus providing the means to calculate $\sigma_k^{(r+1)}$ from (4.7), whereupon the solution process is repeated for the next time step. A calculation flow as depicted in Figure (c) is therefore effected and this is applied to the gridpoints in succession (spatially) and with each time step (temporally) to seek a solution for the axial displacement, velocity and stress in the bar.

The nature of the solution process is typified by the behavior of the free-end of the bar as shown in Figure 4-7. The application of the external stress m disturbs the free-end and this disturbance is propagated numerically through the bar in an iterative fashion using (4.9), (4.10) and (4.7). Removal of kinetic energy is provided by inclusion of a viscous damping mechanism, the physical analogy being a dashpot that "consumes" a force that is proportional to the velocity of the dashpot. Coupled with enforcement of zero displacement at the fixed end of the bar, a progressive decline in dynamic tendencies is apparent with increasing number of iterations (i.e., computational time) until a static system (and thus solution) prevails.

Although a straightforward problem, a number of distinguishing features of the dynamic relaxation technique are evident from the 1-D bar example: (a) use of equations that express behavior in a most physical way, rather than more abstract forms such as derived in finite elements using the principle of virtual displacements; (b) offsetting sample points in both space and time in order to obtain a solution that maintains central finite difference accuracy; and (c) seeking a linear static solution in a progressive, iterative manner, instead of a direct manner such as when inverting a stiffness matrix to solve for unknown displacements. These attributes can be beneficial or detrimental to the cause in hand. In the case of linear static problems they are generally detrimental given the relative efficiency afforded by a displacement-based finite element approach utilizing the more direct stiffness matrix solution technique. A point in favor of dynamic relaxation for this case is less computer memory (storage) requirements, particularly for 3-D problems, however advances in computing power that continue today are serving to downgrade this distinction.

It is in the case of a nonlinear static problem where the dynamic relaxation technique stands to provide benefits. The relative simplicity of the computational scheme is obvious, but what is more is the relative ease in which geometric and material nonlinearities can be implemented. This is brought about through the combination of an explicit formulation and use of relatively basic numerical expressions of behavior. However, consideration of a nonlinear system also brings with it the most serious issue of load path dependency, and the associated question of uniqueness of solutions obtained using dynamic relaxation.

Load path dependency is an issue because introduction of a damping mechanism dictates the load path experienced by a discretized system when seeking static equilibrium using the dynamic relaxation technique. While a linear elastic system is essentially indifferent to the load path taken, a nonlinear elastic-plastic system will be highly dependent on a load path as this could be the difference between the occurrence of plastic "failure" or remaining elastic. The onset of plastic failure could conceivably lead to a static equilibrium state different to that obtained had the system remained elastic, or for that matter one that had experienced a different plastic failure regime. Hence one is faced with a possible erroneous static solution state for a nonlinear system when using dynamic relaxation, this being dependent on the performance of the damping mechanism utilized.
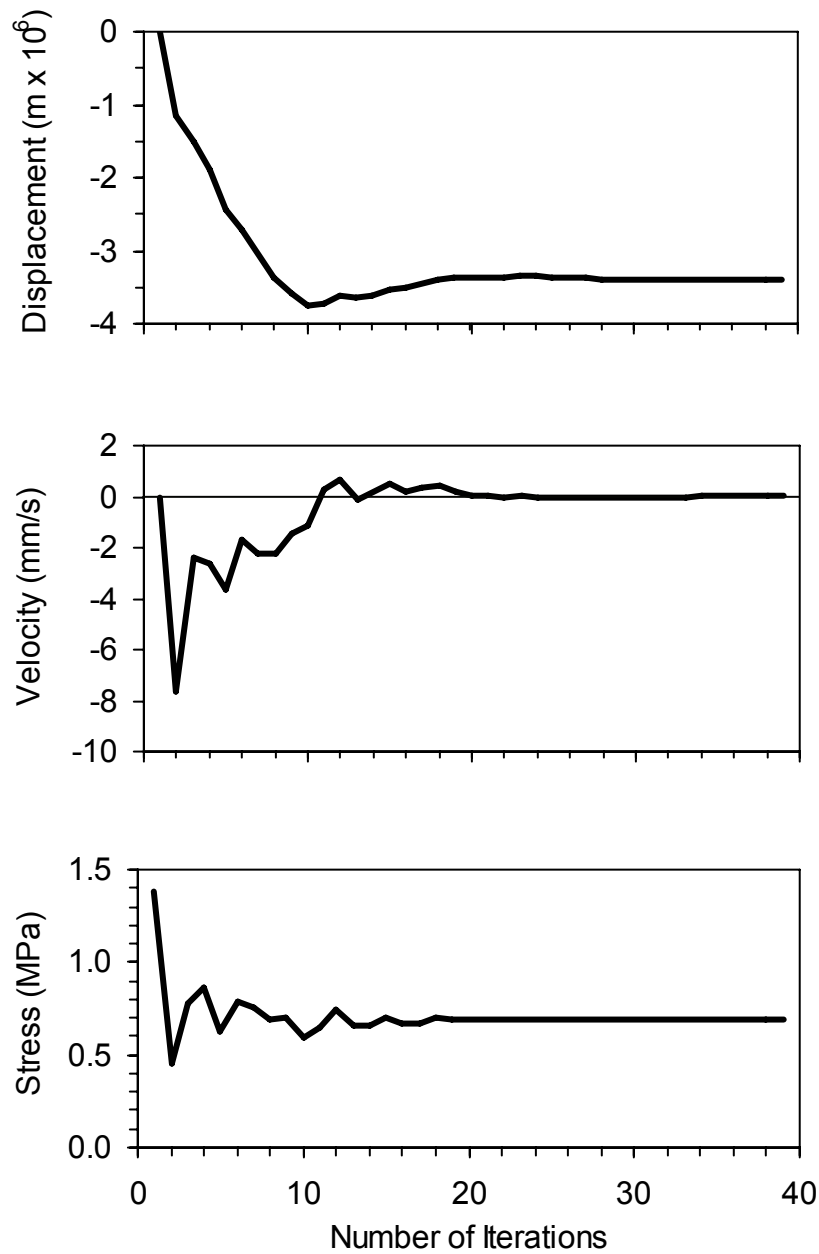
Figure 4-7: Behavior at free-end of 1-D bar during dynamic relaxation solution process (applied axial stress m = 0.7 MPa, K = 0.4)

This non-uniqueness aspect of dynamic relaxation invites criticism, and Cundall (1976, 1987) emphasized how deserved this criticism was for the case where velocity proportional damping (i.e. viscous dashpots) was utilized in the dynamic relaxation scheme. This damping mechanism introduces rate-dependent behavior that can only be treated with suspicion. Cundall (1976, 1982, 1987) suggested alternative forms of damping to help overcome some of the difficulties faced when using velocity proportional damping,

and this work served as a precursor to the approach employed in $FLAC^{3D*}$. Thus the $FLAC^{3D}$ formulation is mindful of the dangers that the dynamic relaxation technique can present, and works to minimize these while still maintaining the thrust of the dynamic relaxation idea to obtain a static solution.

4.2.4   Formulation Framework

4.2.4.1   Tetrahedral and Gridpoint Actions

The independent, or primary, variable in $FLAC^{3D}$ is velocity, and this is formulated at the gridpoints of 3-D zones that are considered internally as pairs of tetrahedral sets (refer Figure 4-2). A tetrahedron therefore serves as the elemental component for formulation purposes, and the nomenclature associated with this formulation is shown in Figure 4-8.

Notes: 1. $\hat{i}, \hat{j}$ & $\hat{k}$ = unit vectors in x, y and z directions, respectively.
2. Shaded face in figure corresponds to face number 2 (i.e. $f = 2$).
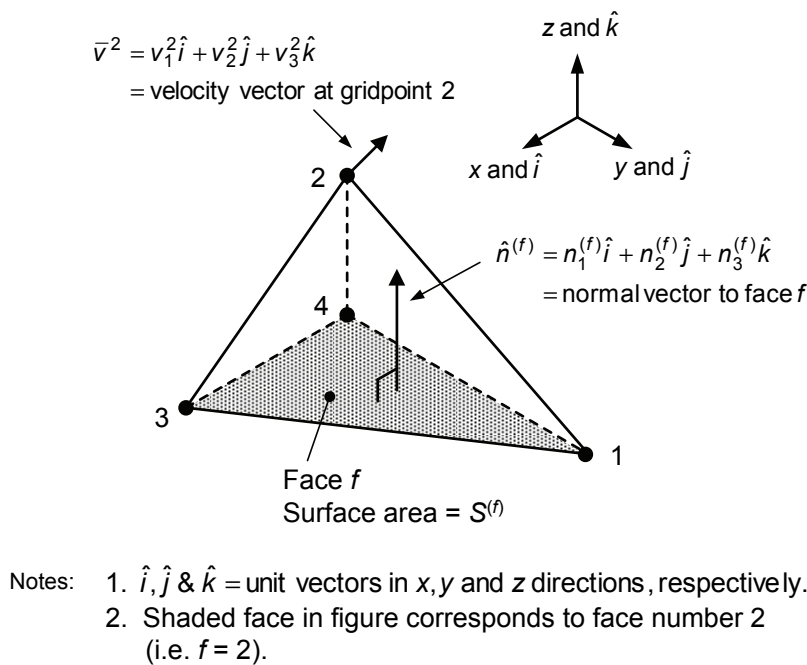
Figure 4-8: Tetrahedron nomenclature

A right-handed Cartesian system is utilized so that vectors (denoted here with an overbar) are expressed in terms of their x, y and z components and respective directions by $\hat{i}$, $\hat{j}$ and $\hat{k}$ unit vectors. Gridpoint vectors use superscripts to denote the gridpoint number (numbered 1 to 4), and subscripts to denote the Cartesian component ($1 = x$, $2 = y$ and $3 = z$). The planar faces that define a tetrahedron are denoted by the letter f and numbered such that the face number refers to the number of the gridpoint that does not lie in the plane of the face (refer note 2 in Figure 4-8). The geometry of each face is characterized by a unit vector $\hat{n}$ normal to the face, in which case bracketed superscripts are used to denote the face number, and subscripts denote the Cartesian components as per the gridpoint vector convention.

---

* Peter Cundall, together with Roger Hart, developed the $FLAC^{3D}$ and 2-D $FLAC$ programs.

An application of the divergence theorem serves to provide the means by which "volume" variables associated with a tetrahedron (i.e., stress and strain) are transformed into "discrete" variables (i.e. velocities, displacements and forces) associated with the gridpoints of the tetrahedron. This follows by considering velocity as a vector field, represented by a vector point function $\bar{v}(x, y, z)$ say, and noting the divergence theorem equality[†]

$$\text{div } \bar{v} = \lim_{V \to 0} \frac{\int_S (\hat{n} \bullet \bar{v}) dS}{V} \tag{4.11}$$

where $V = $ small volume about a point in the vector field,

$\quad S = $ surface area of V,

$\quad dS = $ differential surface area,

and div $\bar{v} = \dfrac{\partial v_1}{\partial x} + \dfrac{\partial v_2}{\partial y} + \dfrac{\partial v_3}{\partial z}$.

By expanding the RHS expression of (4.11),

$$\lim_{V \to 0} \frac{\int_S (\hat{n} \bullet \bar{v}) dS}{V} = \lim_{V \to 0} \frac{\int_S v_1 (\hat{n} \bullet \hat{i}) dS}{V} + \lim_{V \to 0} \frac{\int_S v_2 (\hat{n} \bullet \hat{j}) dS}{V} \\ + \lim_{V \to 0} \frac{\int_S v_3 (\hat{n} \bullet \hat{k}) dS}{V} \tag{4.12}$$

the following is then apparent,

$$\frac{\partial v_1}{\partial x} = \lim_{V \to 0} \frac{\int_S v_1 (\hat{n} \bullet \hat{i}) dS}{V} = \lim_{V \to 0} \frac{\int_S v_1 n_1 dS}{V} \tag{4.13}$$

and similarly for the y and z components.

Reverting to the more compact Einstein indicial notation, a general expression of (4.13) applicable to all components is given by

$$\frac{\partial v_i}{\partial x_j} = \lim_{V \to 0} \frac{\int_S v_i n_j dS}{V} \tag{4.14}$$

where $i, j = 1, 2, 3$.

In the case of the planar-faced tetrahedron, the integral in (4.14) becomes an exercise in summation, as follows:

[†] Refer Reddick and Miller (1955), pp. 350-352 for engineering proof of equality.

$$\int_S v_i n_j \, dS = \sum_{f=1}^{4} \widetilde{v}_i^{(f)} n_j^{(f)} S^{(f)} \tag{4.15}$$

where $\widetilde{v}_i^{(f)} = i^{th}$ component of average velocity over face f,

$\quad n_j^{(f)} = j^{th}$ component of unit vector normal to face f,

$\quad S^{(f)} =$ surface area of face f.

A linear distribution of velocity over each of the tetrahedron faces is assumed in $FLAC^{3D}$, so that, by virtue of the numbering system adopted for the gridpoints and faces, an expression for the average velocity over a face is

$$\widetilde{v}^{(f)} = \frac{1}{3} \sum_{h=1, h \neq f}^{4} v^h \tag{4.16}$$

Substituting (4.16) into (4.15) and performing some algebra, it can be shown that

$$\sum_{f=1}^{4} \widetilde{v}_i^{(f)} n_j^{(f)} S^{(f)} = \frac{-1}{3} \left[\sum_{h=1}^{4} v_i^h n_j^{(h)} S^{(h)} \right] \tag{4.17}$$

Hence the general expression given by (4.14) becomes

$$\frac{\partial v_i}{\partial x_j} = \frac{-1}{3V} \sum_{h=1}^{4} v_i^h n_j^{(h)} S^{(h)} \tag{4.18}$$

whereby the spatial rate of change of velocity throughout the volume of a tetrahedron (i.e., a "volume" variable) is expressed in terms of gridpoint velocities, unit normal vector components, and the surface area of faces (i.e., "discrete" variables). It is to be noted that (4.14) refers to an infinitesimal volume and so is an exact relationship, whereas (4.18) is an approximation given the finite volume associated with a tetrahedron. A connection with strain is made by recognizing that velocity is simply the rate of change of displacement per unit time, and from small deformation theory

$$\dot{\varepsilon}_{ij} = \frac{1}{2} \left(\frac{\partial v_i}{\partial x_j} + \frac{\partial v_j}{\partial x_i} \right) \tag{4.19}$$

where $\dot{\varepsilon}_{ij} =$ strain - rate tensor.

Substituting (4.18) into (4.19) leads to the following expression,

$$\dot{\varepsilon}_{ij} = \frac{-1}{6V} \sum_{h=1}^{4} \left(v_i^h n_j^{(h)} + v_j^h n_i^{(h)} \right) S^{(h)} \tag{4.20}$$

and this constitutes a key equation used in $FLAC^{3D}$, quantifying the interrelation between tetrahedral and gridpoint actions.

4.2.4.2 Gridpoint Formulation

Central to the approach in $FLAC^{3D}$ is formulation of the problem at the gridpoints. Defining gridpoint behavior are the dynamic equations of equilibrium that can be expressed in general form as follows:

$$\frac{\partial \sigma_{ij}}{\partial x_j} + \rho \left(b_i - \frac{dv_i}{dt} \right) = 0 \tag{4.21}$$

where $\sigma_{ij} = $ stress tensor,

$\rho = $ mass density,

$b_i = $ body force acceleration component, and

$\dfrac{dv_i}{dt} = $ inertia acceleration component.

In order to derive gridpoint expressions for the components of equilibrium, the theorem of virtual work is applied to a tetrahedron using the following expressions for external virtual work rate (E) and internal virtual work rate (I):

$$E = \sum_{h=1}^{4} \delta v_i^h f_i^h + \rho b_i \int_V \delta v_i \, dV - \int_V \rho \delta v_i \frac{dv_i}{dt} dV \tag{4.22a}$$

$$I = \int_V \delta \dot{\varepsilon}_{ij} \sigma_{ij} \, dV \tag{4.22b}$$

where $\delta v_i^h = i^{th}$ component of virtual velocity increment at gridpoint h,

$f_i^h = i^{th}$ component of force at gridpoint h,

$\delta v_i = i^{th}$ component of virtual velocity increment within volume V,

$\delta \dot{\varepsilon}_{ij} = $ incremental virtual strain - rate tensor.

Beginning with the body force component of the external virtual work rate (represented by the second term in the expression for E and denoted by E^b), the body force is assumed to be constant throughout the tetrahedron, hence both acceleration and mass density terms are brought outside the integrand. In order to describe δv_i in terms of gridpoint values (i.e. in terms of δv_i^h), a local co-ordinate system with an origin at the centroid of the tetrahedron is employed in conjunction with a linear shape function, as described in Figure 4-9.
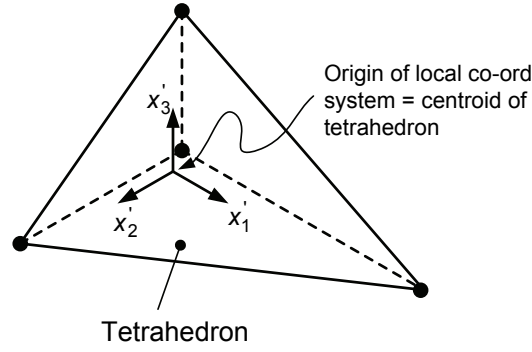
$$N^h = c_0^h + c_1^h x_1' + c_2^h x_2' + c_3^h x_3'$$

where N^h refers to a shape function with constant coefficients (c_0, c_1, c_2 and c_3) applied at gridpoint h to describe the linear variation of virtual velocity within the tetrahedron, viz.

$$c_0^1 + c_1^1 x_1'^1 + c_2^1 x_2'^1 + c_3^1 x_3'^1 = 1 \text{ @ Gridpoint No. 1,}$$

$$c_0^1 + c_1^1 x_1'^2 + c_2^1 x_2'^2 + c_3^1 x_3'^2 = 0 \text{ @ Gridpoint No. 2, etc.}$$

Figure 4-9: Local co-ordinate system and shape function to describe virtual velocity variation within tetrahedron

The body force component of the external work rate is then expressed as follows:

$$
\begin{aligned}
E^b &= \rho b_i \int_V \left(\sum_{h=1}^{4} \delta v_i^h N^h \right) dV \\
&= \rho b_i \sum_{h=1}^{4} \delta v_i^h \left\{ \int_V c_0^h dV + \int_V c_1^h x_1' dV + \int_V c_2^h x_2' dV + \int_V c_3^h x_3' dV \right\}
\end{aligned}
\tag{4.23}
$$

Given that the origin of the local co-ordinate system is at the centroid of the tetrahedron, the latter three terms in the second expression for E^b in (4.23) must equal zero, leading to

$$E^b = \rho b_i \sum_{h=1}^{4} \delta v_i^h c_0^h V \tag{4.24}$$

Consideration of the shape function applied to each gridpoint (refer Figure 4-9) lends itself to matrix representation, wherein Cramer's rule can be used to show that $c_0^h = 1/4$, giving the following desired expression for the body force external work rate component:

$$E^b = \sum_{h=1}^{4} \delta v_i^h \frac{\rho b_i V}{4} \tag{4.25}$$

Considering now the inertial force component of the external virtual work rate (represented by the third term in the expression for E and denoted by E^i), use of the shape function described in Figure 4-9 gives the following:

$$E^i = -\sum_{h=1}^{4} \delta v_i^h \int_V \rho N^h \frac{dv_i}{dt} dV \qquad (4.26)$$

An assumption is made that variations of acceleration within the tetrahedron are small enough to permit the acceleration term in (4.26) to be taken outside the integrand, and furthermore the term replaced by gridpoint values of acceleration, as follows:

$$E^i = -\sum_{h=1}^{4} \delta v_i^h \left(\frac{dv_i}{dt}\right)^h \int_V \rho N^h dV \qquad (4.27)$$

$$\text{where} \left(\frac{dv_i}{dt}\right)^h = \text{acceleration value at gridpoint } h.$$

Given that mass density is assumed to be constant throughout the tetrahedron and applying the findings that were evident in progressing from (4.23) to (4.25), the desired expression for the inertial force component of the external work rate is derived:

$$E^i = -\sum_{h=1}^{4} \delta v_i^h \left(\frac{dv_i}{dt}\right)^h \frac{\rho V}{4} \qquad (4.28)$$

The internal virtual work rate expression given by (4.22b) is converted into a gridpoint expression by first noting that from (4.20) the incremental virtual strain-rate tensor ($\delta \dot{\varepsilon}_{ij}$) can be expressed as follows:

$$\delta \dot{\varepsilon}_{ij} = -\frac{1}{6V} \sum_{m=1}^{4} \left(\delta v_i^h n_j^{(h)} + \delta v_j^h n_i^{(h)}\right) S^{(h)} \qquad (4.29)$$

Substituting (4.29) for $\delta \dot{\varepsilon}_{ij}$ in (4.22b) then gives the following,

$$I = -\frac{1}{6} \sum_{h=1}^{4} \left(\delta v_i^h \sigma_{ij} n_j^{(h)} + \delta v_j^h \sigma_{ji} n_i^{(h)}\right) S^{(h)} \qquad (4.30)$$

A force vector T_i^h is now defined as follows,

$$T_i^h = \sigma_{ij} n_j^{(h)} S^{(h)} \tag{4.31}$$

and given that the stress tensor is symmetric (i.e. $\sigma_{ij} = \sigma_{ji}$), the desired expression for the internal virtual work rate results:

$$I = -\frac{1}{3} \sum_{h=1}^{4} \delta v_i^h T_i^h \tag{4.32}$$

Equating E and I with use of the derived gridpoint expressions (4.25), (4.28) and (4.32) gives the following:

$$-\frac{1}{3} \sum_{h=1}^{4} \delta v_i^h T_i^h = \sum_{h=1}^{4} \delta v_i^h \left[f_i^h + \frac{\rho b_i V}{4} - \left(\frac{dv_i}{dt} \right)^h \frac{\rho V}{4} \right] \tag{4.33}$$

Rearranging (4.33) leads to,

$$\sum_{h=1}^{4} \delta v_i^h \left[f_i^h + \frac{\rho b_i V}{4} - \left(\frac{dv_i}{dt} \right)^h \frac{\rho V}{4} + \frac{T_i^h}{3} \right] = 0 \tag{4.34}$$

and, as the virtual velocity increment δv_i^h is finite, the expression in the brackets must equal zero, giving

$$-f_i^h = \frac{T_i^h}{3} + \frac{\rho b_i V}{4} - m^h \left(\frac{dv_i}{dt} \right)^h \tag{4.35}$$

where m^h is a modified gridpoint mass to ensure numerical stability, as is discussed in section 4.2.5.1.

The value of (4.35) is that it provides an equation for an equivalent tetrahedral gridpoint force in terms of discrete dynamic equilibrium components, providing the required basis for a discrete formulation at the gridpoints. The formulation is not complete, however, in that consideration must be given to the fact that gridpoints are associated with more than one tetrahedron. Also, it is possible that point loads are applied to gridpoints directly in connection with external or internal boundary conditions, representing an additional force that must be taken into account. The equation used for the gridpoint formulation in $FLAC^{3D}$ is therefore given as follows,

$$\left[\frac{T_i}{3} + \frac{\rho b_i V}{4} \right]^{<h>} + P_i^{<h>} = m^{<h>} \left(\frac{dv_i}{dt} \right)^{<h>} \tag{4.36}$$

107

where P_i refers to a possible point load applied at a gridpoint, and the bracketed superscript notation $<h>$ refers to the sum of contributions of the tetrahedra associated with the gridpoint h. A general summary of the terms is thus

$$\frac{T_i}{3} = \frac{\sigma_{ij} n_j^{(h)} S^{(h)}}{3} = \text{equivalent force vector at gridpoint from internal stress,}$$

$$\frac{\rho b_i V}{4} = \text{body force contribution to gridpoint,}$$

$$P_i = \text{possible point force applied at gridpoint, and}$$

$$m\left(\frac{dv_i}{dt}\right) = \text{inertial force contribution to gridpoint.}$$

4.2.4.3   Solution Vehicle

Equation 4.36 provides a statement of the equation of motion at each gridpoint in a form that is suitable for numerical implementation. However, a "solution vehicle" is still required to march through fictitious time to seek a static solution. This is where the explicit finite difference aspect of $FLAC^{\text{3D}}$ comes into play, utilizing central finite difference to provide an approximation of (4.36) in a temporal sense. Rearranging (4.36) as follows,

$$\left(\frac{dv_i}{dt}\right)^{<h>} = \frac{1}{m^{<h>}} \left\{ \left[\frac{T_i}{3} + \frac{\rho b_i V}{4} \right]^{<h>} + P_i^{<h>} \right\} \tag{4.37}$$

and given the central finite difference approximation

$$\left(\frac{dv_i}{dt}\right)^{<h>} = \left[v_i^{<h>}\left(t + \frac{\Delta t}{2}\right) - v_i^{<h>}\left(t - \frac{\Delta t}{2}\right) \right] \bigg/ \Delta t \tag{4.38}$$

then substituting (4.38) for $\left(\dfrac{dv_i}{dt}\right)^{<h>}$ in (4.37) leads to

$$v_i^{<h>}\left(t + \frac{\Delta t}{2}\right) = v_i^{<h>}\left(t - \frac{\Delta t}{2}\right) + \frac{\Delta t}{m^{<h>}} \left\{ \left[\frac{T_i}{3} + \frac{\rho b_i V}{4} \right]^{<h>} + P_i^{<h>} \right\} \tag{4.39}$$

which serves as the "solution vehicle" for marching through fictitious time.

It is to be noted that (4.39) maintains central finite difference accuracy by centering about time t, so that the velocities obtained are offset $\Delta t/2$ from the forces, and likewise the ensuing displacements are offset from the velocities $\Delta t/2$ using the following central finite difference approximation:

$$u_i^{<h>}(t + \Delta t) = u_i^{<h>}(t) + \Delta t . v_i^{<h>}\left(t + \frac{\Delta t}{2}\right)$$ (4.40)

Both (4.39) and (4.40) invoke another measure of approximation in that force, velocity and displacement quantities are determined at different points in fictitious time. This is a relatively insignificant issue, however, given that numerical stability requirements in $FLAC^{3D}$ restrict Δt to very small values, resulting in very small errors associated with offsetting solution variables.

4.2.5   Formulation Aspects

A framework providing a means to convey the solution technique in $FLAC^{3D}$ has been established, but associated with this framework are several aspects requiring attention. These concern numerical stability requirements, performance of the 3-D zones, and damping considerations.

4.2.5.1   Numerical Stability

The central finite difference approximation applied to the equation of motion in $FLAC^{3D}$ is an example of an explicit direct integration method, and the conditional stability of such a method is well known. Conditional stability is concerned with a critical time step Δt_c that must be sufficiently small to prevent artificial "numerical-made" response behavior polluting the system and rendering a computational solution scheme that is unstable. This artificial behavior is seated in the higher modes of vibration of a discrete system, so that knowledge of the period (T) or frequency (ω) of the highest mode is an important consideration in establishing a stability criterion. In $FLAC^{3D}$ this issue is addressed by drawing on the similarities between the gridpoint framework used to formulate behavior, and a configuration of lumped masses interconnected by springs.

A single mass-spring system of such kind is depicted in Figure 4-10(a), together with its dynamic characteristics. The critical time step to be used when calculating the response of this system using the central finite difference technique is also indicated (Bathe, 1996), so that $\Delta t \leq \Delta t_c = T/\pi = 2\sqrt{m/k}$. By setting $\Delta t = 1$ (allowed given the fictitious nature of the computational time) and letting $\Delta t = \Delta t_c$, it follows that

$$\left(\frac{1}{2}\right)^2 = \frac{m}{k} \text{ or } m = \frac{k}{4}$$ (4.41)

meaning that the magnitude of the lumped mass and stiffness of the spring for the single mass-spring system must satisfy the relationship given by (4.41) to ensure stability, if a value of unity is adopted for the time step. Considering now the mass-spring system shown in Figure 4-10(b), the infinite extent and symmetry that this demands leads to an equivalent single mass-spring system similar to that shown in Figure 4-10(a), except the spring stiffness is now $4k$.

Adopting a value of unity for the time step once again, it follows from (4.41) that stability is satisfied in this case if the magnitude of the lumped mass is made equal to or greater than the stiffness of the spring, or $m \geq k$.

a) One-degree-of-freedom (1-DOF) mass-spring system

Lumped mass, m

Spring stiffness, k

1-DOF Mass-Spring Dynamic Properties:

$$\omega = \sqrt{\frac{k}{m}} \ \text{ or } \ T = \frac{2\pi}{\sqrt{k/m}} \quad \text{and} \quad \Delta t_c = \frac{T}{\pi} = 2\sqrt{\frac{m}{k}}$$

where ω = natural frequency,
          T = natural period,
          Δt_c = critical time step.

b) Infinite mass-spring system

above equivalent to:

above equivalent to:
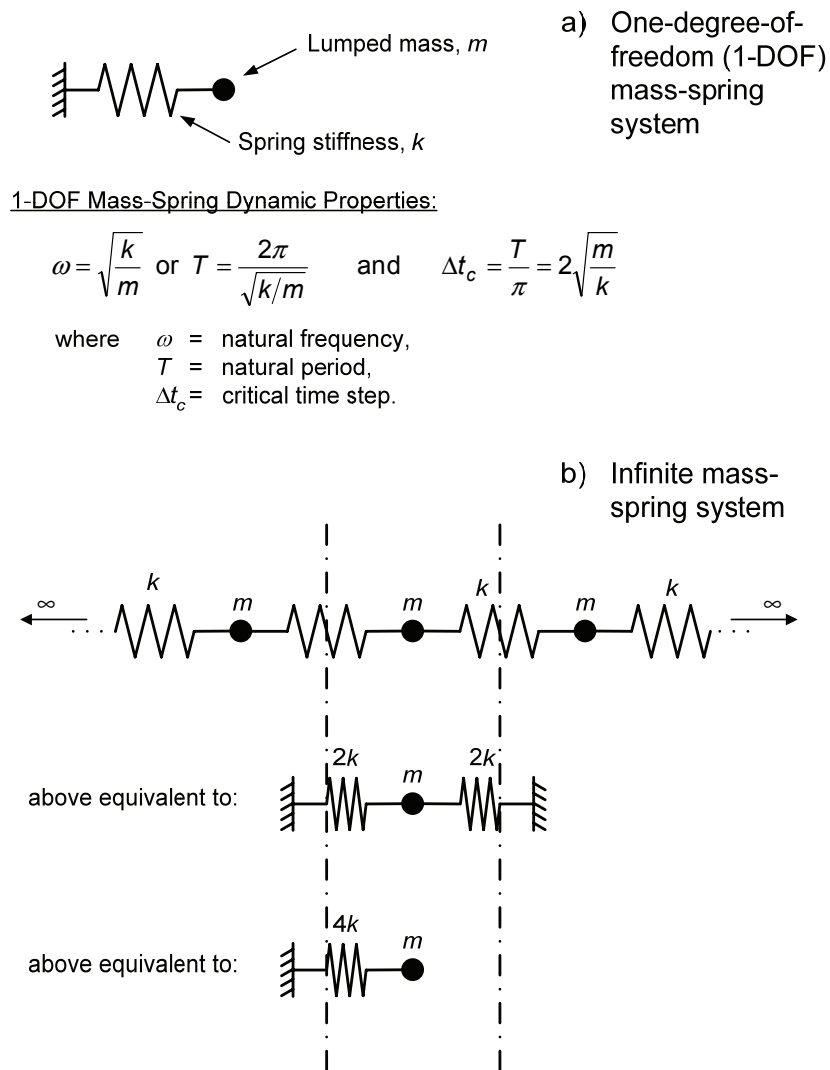
Figure 4-10. Mass-spring systems used for numerical stability analysis purposes (after Itasca, 1997)

If $\Delta t = 1$, the stability criterion $m \geq k$ for the infinite mass-spring system is rigorously correct given that the system has only one mode of vibration. It is also instructive to consider this system as a discretized, one-dimensional elastic bar of infinite extent in the x-direction, whereby the following equivalencies apply (Cundall, 2001):

$$k = \frac{EA}{\Delta x} \ \text{ and } \ m = \rho A \Delta x \qquad (4.42)$$

where E = Young's modulus of bar,
      A = cross - sectional area of bar,
      ρ = mass density of bar,
      Δx = discretization length.

110

Given that the critical time step for the infinite mass-spring system is

$$\Delta t_c = 2\sqrt{m/4k} = \sqrt{m/k} \qquad (4.43)$$

substituting the expressions for k and m given by (4.42) into (4.43) leads to

$$\Delta t_c = \Delta x \sqrt{\frac{\rho}{E}} = \frac{\Delta x}{C_L} \qquad (4.44)$$

where $C_L = \sqrt{\dfrac{E}{\rho}}$ = speed of compressional wave in bar.

Hence a physical interpretation of the stability criterion is that Δt must be small enough that the calculation speed does not exceed the transmission speed of the material being deformed.

Turning to a $FLAC^{3D}$ system, there are similarities with the infinite mass-spring system if a tetrahedron gridpoint h is considered as a lumped mass, the magnitude of which is an appropriate mass ($m^{<h>}$) as used in (4.39). The network of gridpoints that results from a 3-D model can therefore be considered as a vast array of interconnected lumped masses, the question being the nature of the "spring" that interconnects them. In $FLAC^{3D}$ a "spring" is derived by treating an increment in the equivalent force vector from internal stress as a force-stiffness relationship as follows:

$$\frac{dT_i^h}{3} = \frac{d\sigma_{ij}}{3} n_j^{(h)} S^{(h)} = -k_{ij}^h v_j^h dt \qquad (4.45)$$

where $k_{ij}^h = ij$ component of stiffness associated with gridpoint h.

Diagonal stiffnesses k_{11}, k_{22} and k_{33} can therefore be established by setting the velocity v_1, v_2 and v_3 acting at the gridpoint to unity, respectively, so that in general

$$k_{qq} dt = -\frac{d\sigma_{qq}}{3} n_q^{(h)} S^{(h)} \qquad (4.46)$$

where $qq = 11$, 22 or 33 (where no summation is implied on the repeated index).

Given a small increment in fictitious time, it is assumed that the increment in stress $d\sigma_{qq}$ is governed by Hooke's Law, or specifically

$$d\sigma_{qq} = M d\varepsilon_{qq} \qquad (4.47)$$

where M = constrained modulus = $K + \dfrac{4}{3} G$,

so that

$$k_{qq}dt = -\frac{\dot{\varepsilon}_{qq}Mdt}{3}n_q^{(h)}S^{(h)} \tag{4.48}$$

Now from (4.20)

$$\dot{\varepsilon}_{qq} = -\frac{1}{6V}\sum_{h=1}^{4}\left(v_q^h n_q^h + v_q^h n_q^h\right)S^{(h)} \tag{4.49}$$

and given that $v_q^h = 1$ at gridpoint q and $v_q^h = 0$ at the other gridpoints, then

$$\dot{\varepsilon}_{qq} = -\frac{1}{3V}n_q^{(h)}S^{(h)} \tag{4.50}$$

Substituting (4.50) for $\dot{\varepsilon}_{qq}$ in (4.48) leads to

$$k_{qq} = \frac{M}{9V}\left[n_q^{(h)}S^{(h)}\right]^2 \tag{4.51}$$

A measure of the stiffness of the "spring" interconnecting gridpoints is thus obtained from (4.51), and by adopting the stability criterion from the infinite mass-spring system (i.e. $m \geq k$ for $\Delta t = 1$), the form of stability criterion used in $FLAC^{3D}$ is given as follows

$$m^h = k^h = \frac{M}{9V}\max\left\{\left[n_i^{(h)}S^{(h)}\right]^2, \; i = 1,2,3\right\} \tag{4.52}$$

This requires that the greatest diagonal stiffness value is found for each gridpoint and this value is assigned as the magnitude of the mass of the gridpoint in order to satisfy stability requirements. Itasca (1997) note that the infinite mass-spring stability criterion provides an upper-bound value for the gridpoint mass, but it must be noted that use of a diagonal stiffness value deems (4.52) only an approximation from a stability standpoint. Indeed, the value obtained from (4.52) is multiplied by 6.75 in $FLAC^{3D}$ in recognition of the approximate nature of the approach, effectively applying a factor of safety of 2.6 on the time step, given that $m = k(\Delta t)^2$.

In physical terms the effective factor of safety applied to the time step ensures that information cannot propagate between gridpoints in one time step. This provides the justification for updating each gridpoint in turn at each time step in the $FLAC^{3D}$ formulation, given that each gridpoint is effectively isolated from its neighboring gridpoints during this time. An appreciation of the propagation behavior in $FLAC^{3D}$ can be gained by modeling the 1-D bar problem examined in section 4.2.3 and comparing the behavior at the free-end with that obtained using dynamic relaxation. The results are shown in Figure 4-11 and Figure 4-

11, where the $FLAC^{3D}$ model of the bar was constructed of five unit cube zones to maintain equivalency with the dynamic relaxation model shown in Figure 4-16. The significantly decreased velocity behavior reflects the more onerous propagation limits imposed in $FLAC^{3D}$, requiring more computational steps to obtain the static solution.
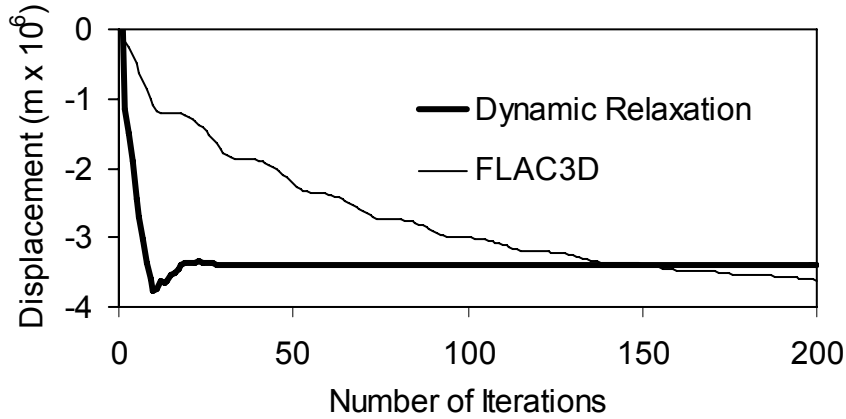
Figure 4-11: Comparison of $FLAC^{3D}$ and dynamic relaxation velocity behavior at free-end of 1-D bar analyzed in section 4.2.3
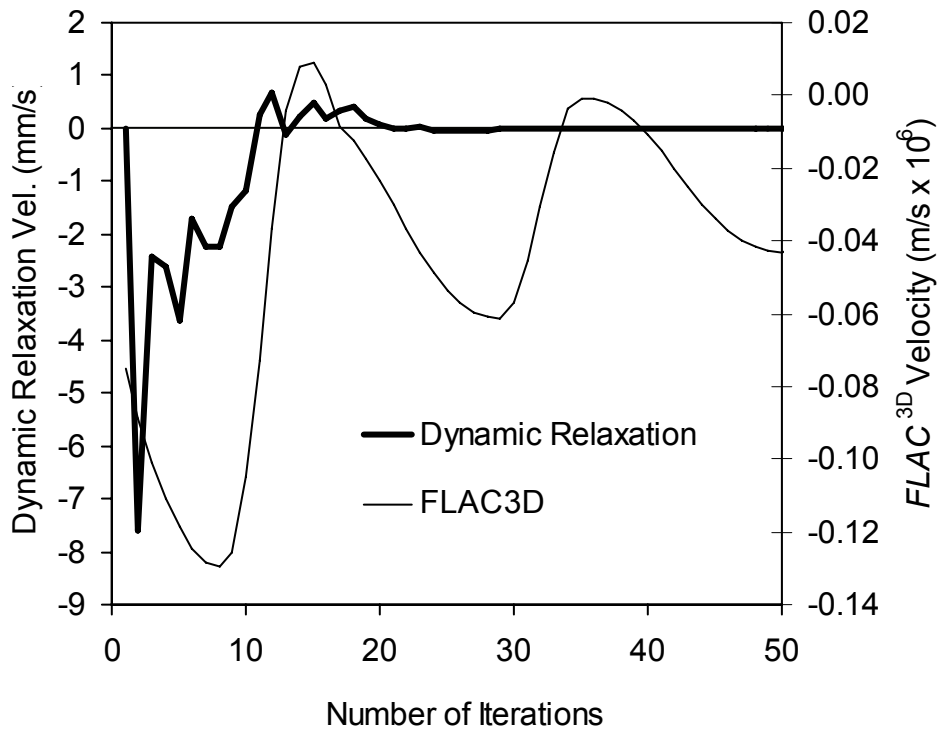
Figure 4-12: Comparison of $FLAC^{3D}$ and dynamic relaxation displacement behavior at free-end of 1-D bar analyzed in section 4.2.3

4.2.5.2   Damping Scheme

Instead of looking to a physical model for energy dissipation, the damping mechanism used in $FLAC^{3D}$ is a purely mathematical approach based on observed damping behavior.   Termed "local non-viscous damping", the idea relies on the assumption that a system will oscillate as a result of a disturbance being applied. This is usually a safe assumption, but in the case of flow failure, where a mass may move at a near constant velocity (e.g. ultimate bearing capacity failure), a variation on the idea, termed "combined damping", is utilized.   Cundall (1987) introduced the idea of local non-viscous damping, and a one-degree-of-freedom (1-DOF) mass and spring system (as per Figure 4-10a) will be used to illustrate the concept.

In the absence of energy dissipation, a 1-DOF mass-spring system will oscillate with energy being exchanged between kinetic and strain energy. Introduction of damping serves to add another form of energy interchange, and a schematic illustrating the interplay of system forces is shown in Figure 4-13. A point to note is the opposing sense of velocity and acceleration variation, but nevertheless an equal "area" of each quantity, during each quarter-cycle of oscillatory motion.   This opposing but equal sense of velocity and acceleration variation is suggestive of a damping force that can be made proportional to force rather than velocity, the latter being the case of viscous damping.
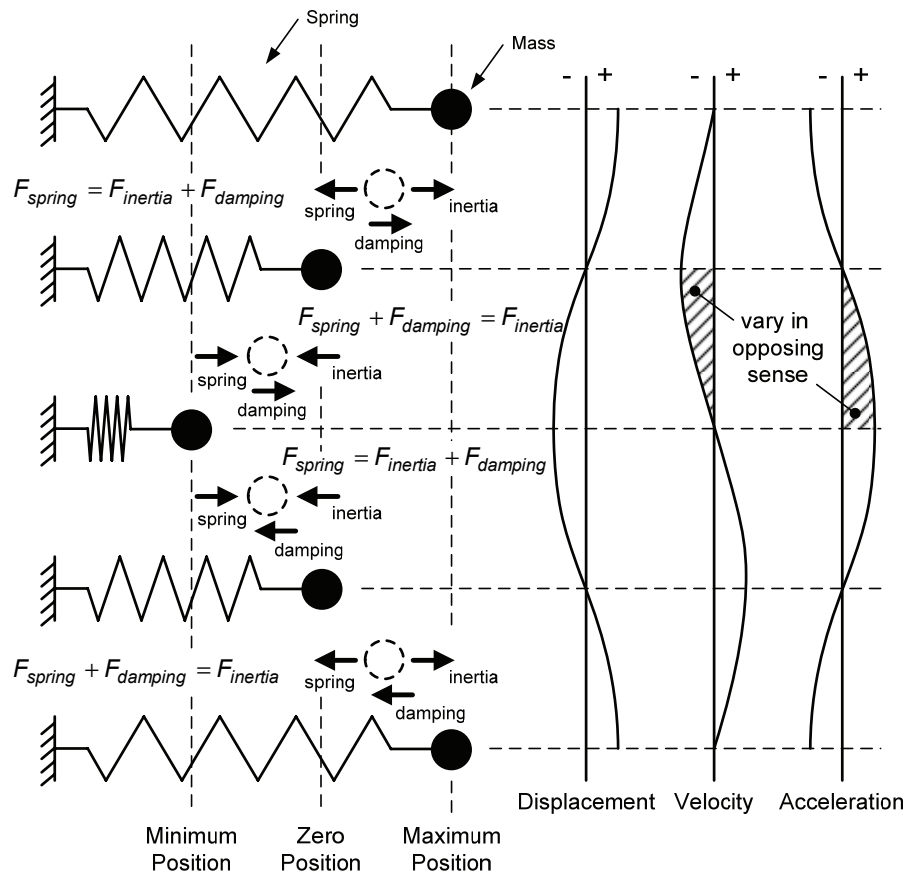
Figure 4-13: Oscillating 1-DOF mass-spring system

114

A damping force F_D is therefore introduced directly into Newton's Second Law of Motion as follows:

$$m\ddot{x}(t) = -kx(t) + F_D \tag{4.53}$$

where F_D is given by the following:

$$F_D = -\alpha |-kx(t)| \text{sgn}(v(t)) \tag{4.54}$$

where $\alpha =$ a damping constant, whose default value is 0.8,

and the sgn function is defined as follows:

$$\text{sgn}(v(t)) = \begin{cases} +1, \text{ if } v(t) > 0; \\ 0, \text{ if } v(t) = 0; \\ -1, \text{ if } v(t) < 0; \end{cases} \tag{4.55}$$

The effect of this formulation becomes apparent if one considers the oscillation of the 1-DOF mass-spring system when subjected to an initial displacement but no initial velocity. Acceleration (force) and velocity versus time are shown in Figure 4-14, where $F(t) = kx(t)$. By applying (4.54) and (4.55) to each of the intervals indicated on Figure 4-14, the following forms of (4.53) result:

Interval 1: $\quad -F(t) + \alpha F(t) = -m\ddot{x} \quad \text{or} \quad \ddot{x} = \dfrac{F(t)(1-\alpha)}{m} = \dfrac{F(t)}{m^+} \tag{4.56a}$

Interval 2: $\quad F(t) + \alpha F(t) = m\ddot{x} \quad \text{or} \quad \ddot{x} = \dfrac{F(t)(1+\alpha)}{m} = \dfrac{F(t)}{m^-} \tag{4.56b}$

Interval 3: $\quad F(t) - \alpha F(t) = m\ddot{x} \quad \text{or} \quad \ddot{x} = \dfrac{F(t)(1-\alpha)}{m} = \dfrac{F(t)}{m^+} \tag{4.56c}$

Interval 4: $\quad -F(t) - \alpha F(t) = -m\ddot{x} \quad \text{or} \quad \ddot{x} = \dfrac{F(t)(1+\alpha)}{m} = \dfrac{F(t)}{m^-} \tag{4.56d}$

where $m^+ = \dfrac{m}{(1-\alpha)}$ and $m^- = \dfrac{m}{(1+\alpha)}$.
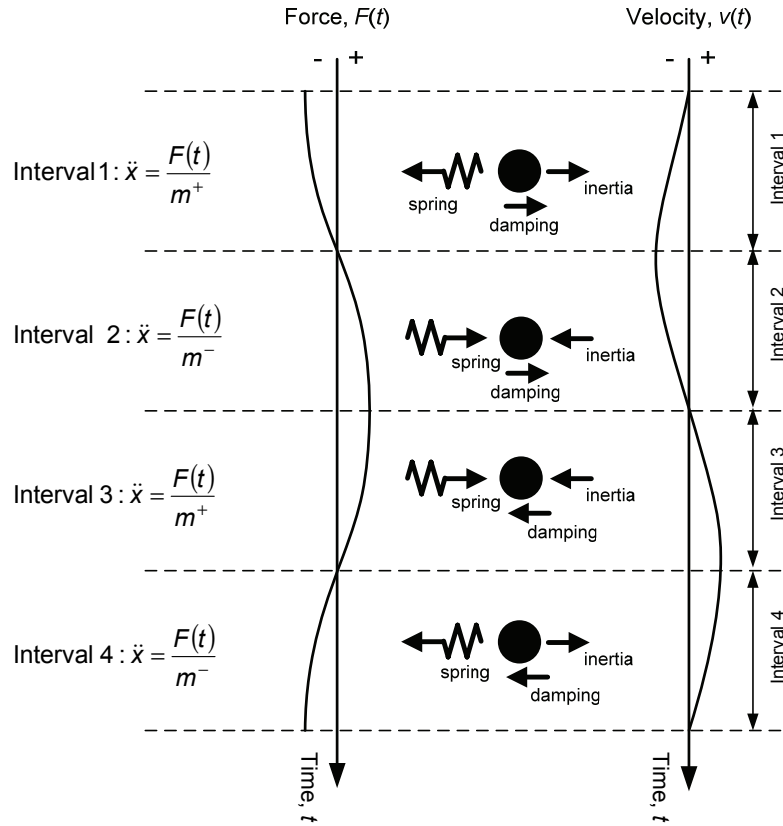
Figure 4-14: Temporal force and velocity relationship for oscillating 1-DOF mass-spring system

The nature of (4.53) and (4.54) guarantees that the damping force acts in the opposite direction to motion (i.e. velocity), just as is the case with viscous damping. However, instead of scaling the damping force to the magnitude of velocity, as is done with viscous damping, the technique simply scales it to the magnitude of the force at play via the α factor. The rightmost expressions in (4.56) and the definitions for m^+ and m^- provide an alternative interpretation in terms of an equivalent mass that the system thinks is present. In terms of kinetic energy, the effect is to extract energy at the peak velocity points, and for one complete cycle the amount extracted (ΔW) is given by

$$\Delta W = 2\left[\frac{1}{2}\left(m^+ - m^-\right)(v(t))^2\right] \tag{4.57}$$

where is to be noted that the addition of mass at zero velocity has no impact on kinetic energy. Given that this is a simple mass and spring system, the peak kinetic energy is equal to the peak strain energy stored in the spring. The peak kinetic energy (denoted by W) is the average of that produced by both of the equivalent masses i.e.

$$W = \frac{1}{4}\left(m^+ + m^-\right)(v(t))^2 \tag{4.58}$$

116

This enables a comparison with viscous damping, in that

$$\frac{\Delta W}{W} = \frac{4(m^+ - m^-)}{m^+ + m^-} = 4\alpha \qquad (4.59)$$

and given the following relationship for a viscous damping mechanism

$$\frac{\Delta W}{W} = 4\pi\xi \qquad (4.60)$$

where ξ = the viscous damping ratio, then

$$\xi = \frac{\alpha}{\pi} \qquad (4.61)$$

To demonstrate the concept, the case of free vibration was implemented via an Excel© spreadsheet utilizing central finite difference approximations of the governing equation of motion. The results are shown in Figure 4-15 and Figure 4-16, where a comparison with the viscous damping solution is also shown. Note that if $\alpha = 0.8$, then (4.61) gives $\xi \approx 0.25$. It is therefore apparent that the local non-viscous damping scheme acts in much the same way as viscous damping, but avoids the danger of velocity-dependent damping forces.
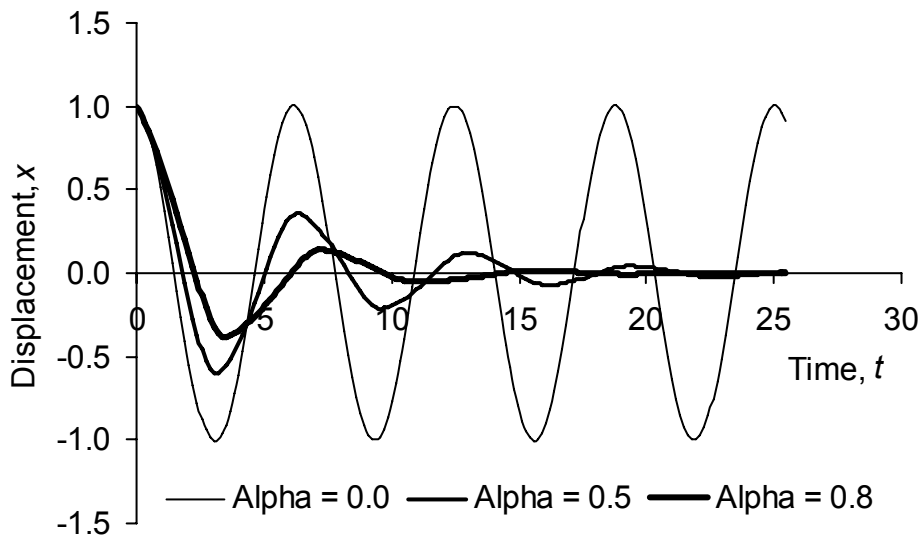
Figure 4-15: Free vibration behavior of local non-viscous damping mechanism for various α values

117
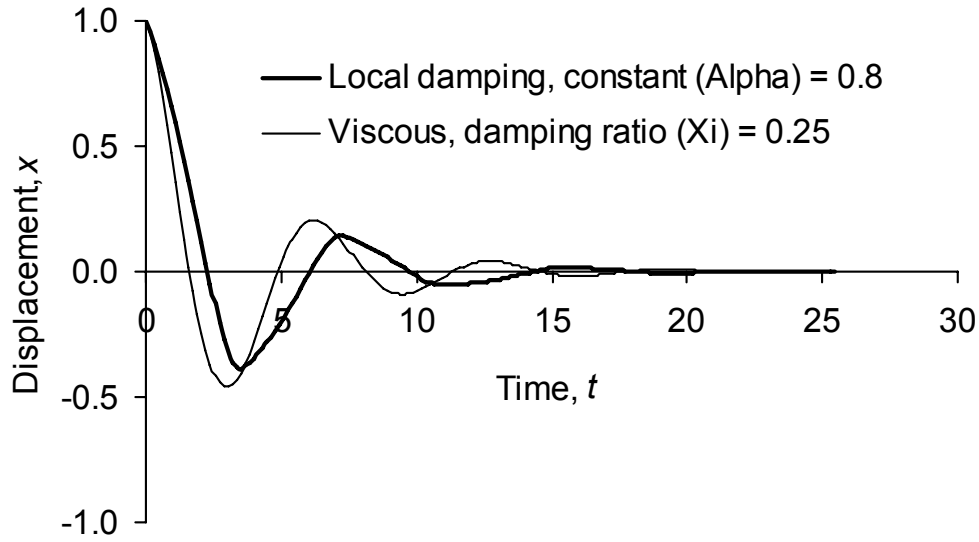
Figure 4-16: Comparison of free vibration behavior using local non-viscous damping and viscous damping mechanisms

Returning to the $FLAC^{3D}$ formulation, the local non-viscous damping scheme is easily incorporated by modifying (4.39) to include a damping force as follows:

$$v_i^{<h>}\left(t+\frac{\Delta t}{2}\right)=v_i^{<h>}\left(t-\frac{\Delta t}{2}\right)+\frac{\Delta t}{m^{<h>}}\left(F_i^{<h>}+F_D^{<h>}\right) \qquad (4.62)$$

where $F_i^{<h>}=\left[\dfrac{T_i}{3}+\dfrac{\rho b_i V}{4}\right]^{<h>}+P_i^{<h>}$,

$F_D^{<h>}=-0.8\left|F_i^{<h>}\right|\mathrm{sgn}\left(v_i^{<h>}\right)=$ gridpoint damping force.

In the "combined damping" case, where significant uniform motion exists in comparison to the magnitude of oscillations to be damped, use is made of the fact that the derivative of a harmonic force with respect to time is proportional to its harmonic velocity. Thus an additional term is added to the gridpoint damping force expression to accommodate constant velocity (rigid-body) motion equally, as follows:

$$F_D^{<h>}=\frac{\alpha\left|F_i^{<h>}\right|}{2}\left[\mathrm{sgn}\left(\frac{dF_i^{<h>}}{dt}\right)-\mathrm{sgn}\left(v_i^{<h>}\right)\right] \qquad (4.63)$$

118

4.2.5.3   Zone Performance

A zone in $FLAC^{3D}$ represents the basic numerical building block used to construct a 3-D analysis region to solve a physical problem using mathematical models. This process also applies to a 3-D finite element approach, except continuum "brick" elements would be used instead of zones. In displacement-based finite element analysis, the performance of such brick elements is concerned with shape functions and their ability to provide a state of strain that is appropriate to the type of deformation experienced by the element. Isoparametric continuum element formulations are typical in this respect, obtaining a strain measure through differentiation of the nodal shape functions so derived, and referring to sampling, or "integration" points, to establish element values.

In terms of the $FLAC^{3D}$ zone formulation, the means of obtaining a strain measure is different. First of all, rather than using shape functions to describe displacement spatially and then differentiating according to small deformation strain-displacement relations, a spatial derivative of displacement is obtained directly by application of the general integral expression given by (4.14), leading to the tetrahedron-specific formulation given by (4.18). This provides a spatial derivative of displacement (per unit of fictitious time) at the centroid of a tetrahedron, whereupon the small deformation strain-displacement relation given by (4.19) leads to the strain-tensor as given by (4.20), also applying at the centroid. A second difference is in use of the tetrahedron formulation itself, in that zone values of strain and stress (considered to apply at the centroid of the zone) are derived in terms of a weighted average calculation using tetrahedra volumes as the basis, i.e.

$$\text{Zone value} = \frac{\sum_{1}^{n} Q \times dVol}{\sum_{1}^{n} dVol} \tag{4.64}$$

where n = no. of tetrahedra in each zone,

$\qquad Q$ = stress or strain,

$\qquad dVol$ = volume of each tetrahedron.

Direct comparison of a $FLAC^{3D}$ zone with an equivalent finite element formulation is therefore obscured numerically, but the linear distribution of velocity over each tetrahedron face, as discussed in section 4.2.4.1, places a zone in the constant-strain finite element formulation category. Deformation experiments were therefore undertaken to provide a demonstration of the elastic performance of a $FLAC^{3D}$ zone in comparison with an 8-node 3-D brick element using 2x2x2 integration points, as shown in Figure 4-17.

The analysis program COSMOS/M (Structural Research & Analysis Corp., 1999) was used to undertake the finite element computations. Both a zone and 8-node brick element, shaped in the form of a unit cube and a bar, were tested for stress response by applying appropriate displacements to induce volumetric and shear deformation modes, as detailed in Figure 4-17. The results are shown in Table 4-1, and are in exact agreement as expected.
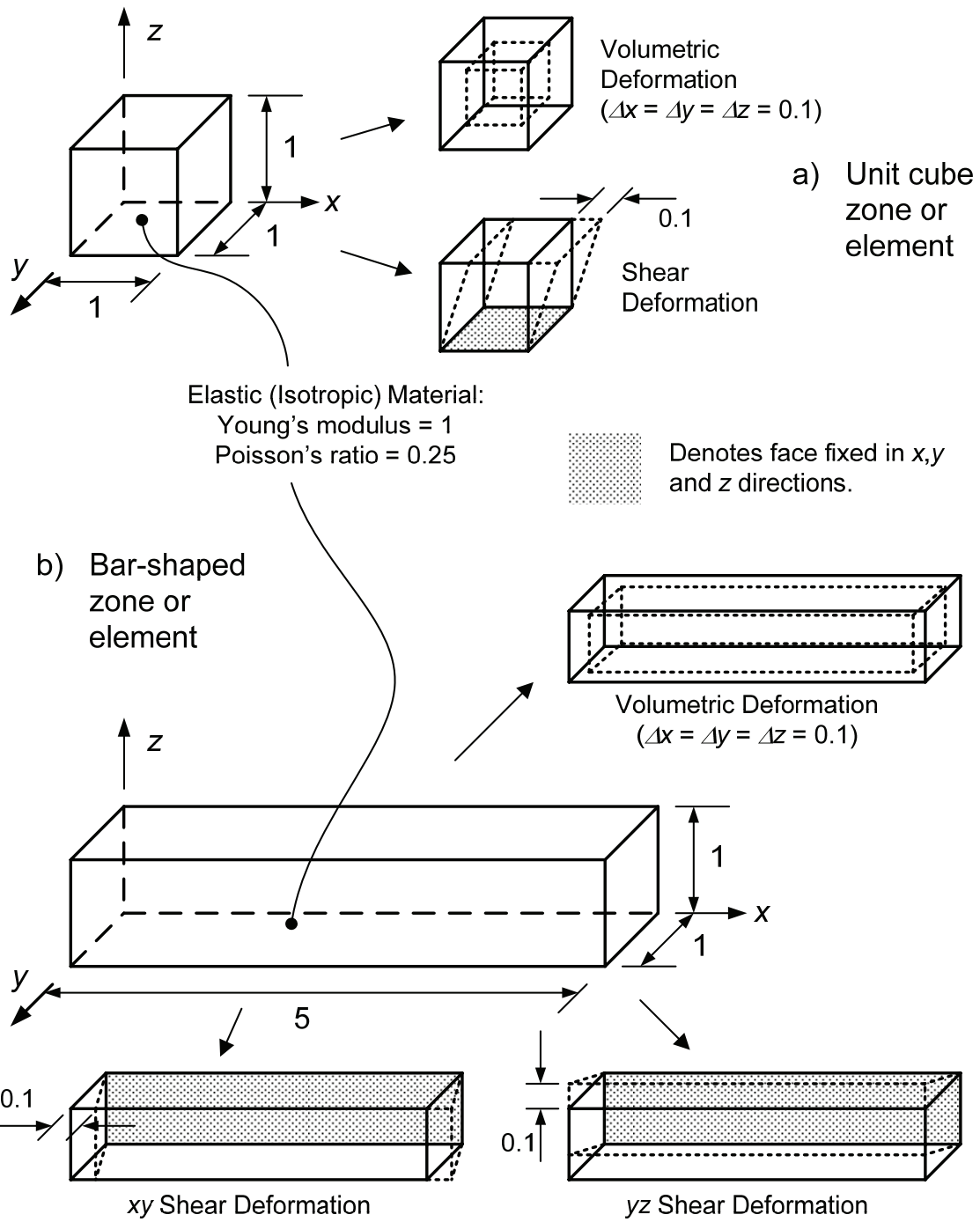
Figure 4-17: Experiments undertaken to compare *FLAC*[3D] and finite element elastic response

Table 4-1: Stress results from *FLAC*³ᴰ and COSMOS/M comparison

Stress Component	Unit Cube Shape (1x1x1)				Bar Shape (5x1x1)					
	Deformation Mode				Deformation Mode					
	Volumetric		Shear		Volumetric		*xy* Shear		*yz* Shear	
	A	B	A	B	A	B	A	B	A	B
σ_{xx}	0.4	0.4	0	0	0.208	0.208	0	0	0	0
σ_{yy}	0.4	0.4	0	0	0.336	0.336	0	0	0	0
σ_{zz}	0.4	0.4	0	0	0.336	0.336	0	0	0	0
σ_{xz}	0	0	0	0	0	0	0	0	0	0
σ_{xy}	0	0	0.022	0.022	0	0	0.038	0.038	0	0
σ_{yz}	0	0	0	0	0	0	0	0	0.023	0.023

Note: A = *FLAC*³ᴰ; B = COSMOS/M

A performance aspect of the tetrahedron-based formulation that certainly requires attention is the fact that a tetrahedron does not provide enough flexibility when volumetric restrictions associated with plastic flow conditions are imposed. Severe constraint resulting from the perfect plasticity requirement of zero volume change, leading to overly stiff behavior ("locking") and thus over-prediction of limit loads, was first explained by Nagtegaal, Parks and Rice (1974). This work used the ratio of total degrees of freedom to total number of incompressibility constraints to characterize the deficiency in volumetric flexibility, noting that a ratio greater than or equal to one was required to avoid locking, whereas a ratio of 3/5 applied to a tetrahedron. In *FLAC*³ᴰ, this flexibility deficiency is addressed by a procedure termed "mixed discretization" (Marti and Cundall, 1982).

The idea of the mixed discretization procedure is to increase the number of active degrees of freedom for volumetric action by discretizing volumetric strain at the zone level using a weighted average scheme as follows:

$$\varepsilon_v = \frac{\sum\limits_{h=1}^{n} \varepsilon_v^{(h)} V^{(h)}}{\sum\limits_{h=1}^{n} V^{(h)}} \tag{4.65}$$

where n = number of tetrahedra in a zone,

ε_v = volumetric strain for zone,

$\varepsilon_v^{(h)}$ = volumetric strain for each tetrahedron h,

$V^{(h)}$ = volume of tetrahedron h.

While similar in form to (4.64) used to report zone stress and strain values, (4.65) differs in that only the volume component is averaged, and is only invoked when plastic failure occurs. An adjusted strain tensor for each tetrahedron in a zone is then obtained as follows:

$$\varepsilon_{ij}^{(h)} = e_{ij}^{(h)} + \frac{\varepsilon_v}{3} \delta_{ij} \tag{4.66}$$

where $\varepsilon_{ij}^{(h)}$ = strain tensor for tetrahedron h,

$e_{ij}^{(h)}$ = "original" deviatoric strain tensor for tetrahedron h,

δ_{ij} = Kronecker delta.

Stress components are also adjusted in the same way for consistency. Applying the mixed discretization procedure overcomes locking problems while maintaining appropriate volumetric response, as demonstrated by Marti and Cundall (1982) and as evident in various verification problems provided in the $FLAC^{3D}$ documentation. It is noted that tetrahedra do not suffer from spurious zero-energy modes associated with the "hour-glass" modeling problem.

4.2.6   Interface Behavior

Separation and sliding capabilities at the common boundary, or "interface" of different materials, are provided in $FLAC^{3D}$ by so-called two-dimensional interface elements. The geometrical configuration of interface elements is indicated in Figure 4-18, comprising triangular elements that cover the faces of each zone that locate the planar boundary that forms the interface of differing materials. A "parent face" is defined as the face of each zone that the interface is imagined to be "wrapped" over, the terminology being adopted in light of a physical similarity to "shrink-wrap" that one could imagine to be stretched over the planar interface surface in order to protect one material from another material that it abuts up against (as per the situation depicted in Figure 4-18). In terms of the interface formulation, the material that the interface is wrapped over is termed the "parent" material, and each zone in the parent material whose face locates the interface surface is referred to as a "parent zone". A neighboring zone of the different material, or "target" material, is similarly referred to as a "target zone".

Separation and sliding behavior at the interface is represented by elastic normal and shear springs, respectively, both possessing strength limits. The strength of the shear spring is characterized by Mohr-Coulomb strength parameters c and ϕ, and a tensile strength is assigned to the normal spring, so that if exceeded, separation occurs (compressive strength being unlimited). The shear and normal springs are considered to exist at interface gridpoints that are indicated in Figure 4-18. These interface gridpoints always occupy the same position as their parent zone gridpoints, but are "attached" to the respective target zone gridpoints via the shear and normal springs.

The essence of interface action is illustrated in Figure 4-19, where a typical parent and target zone are depicted together with their interface element. As shown, a "parent face" and "target face" are defined accordingly. Prior to any movement, referred to as "Time Step 0" in Figure 4-19, interface gridpoints and associated parent and target zone gridpoints all occupy the same position. Relative movement between the parent face and target face is then considered to occur as a result of a calculation cycle performed on zone gridpoints, referred to as "Time Step 1" in Figure 4-19. In undergoing the relative movement δ, the shear and normal springs associated with the interface gridpoints are "activated", such that each develop a force (referred to here as $F_{int\text{-}shear}$ and $F_{int\text{-}norm}$, respectively) corresponding to their respective stiffness multiplied by δ.
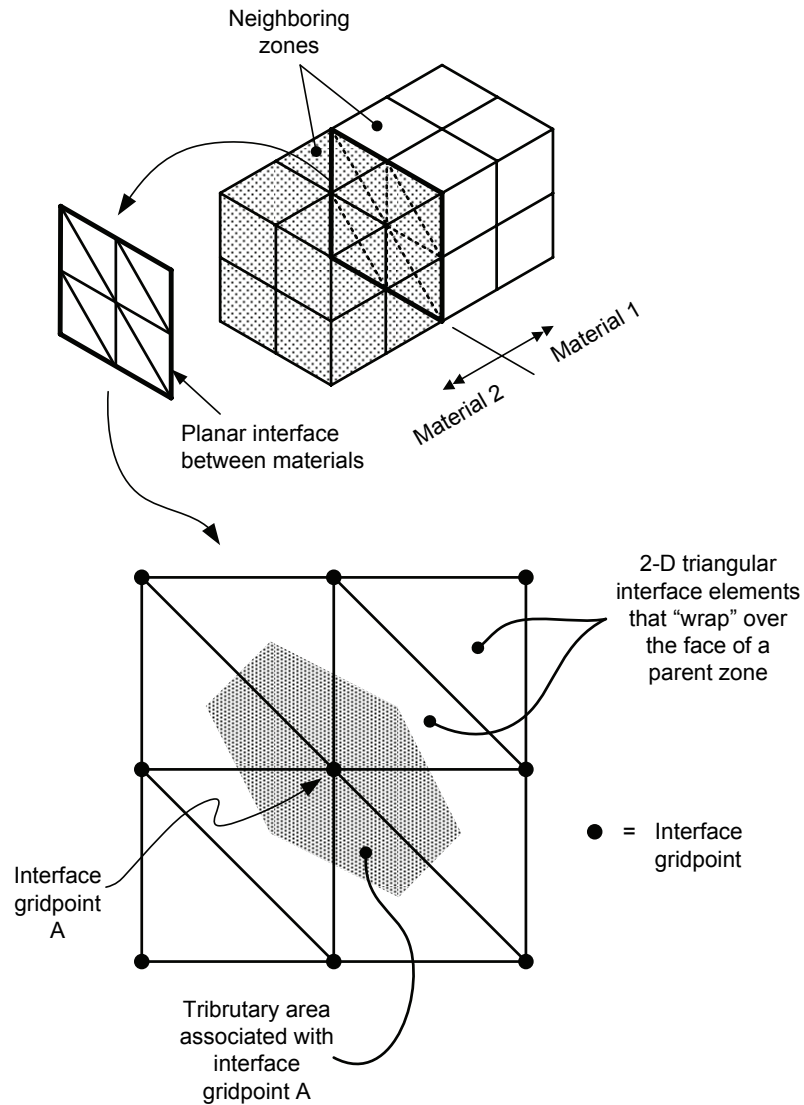
Figure 4-18: 2-D interface elements used in *FLAC*^{3D} (after Itasca, 1997)

Activation causes $F_{\text{int-shear}}$ and $F_{\text{int-norm}}$ to be distributed to both the parent zone and target zone gridpoint associated with the interface gridpoint, the distribution being in an equal an opposite fashion to maintain equilibrium. These forces are then additional forces to be accounted for in the gridpoint formulation represented by (4.62). Furthermore, activation also causes the interface gridpoint spring stiffnesses to be added to the parent zone and target zone gridpoint stiffnesses. Distributing to both maintains numerical stability and enforces a reduced relative-movement regime with subsequent time steps given the greater stiffness inherited by the parent zone and target zone gridpoints. The process of relative movement between parent and target faces, that in turn mobilizes interface forces that are then distributed to attached zone gridpoints, is repeated at each time step with total interface forces constantly monitored against the strength limits assigned.

A) Time Step 0:

Neighboring zones

"Parent face"

Target Zone

Parent Zone

"Target face"

Refer note

Interface that is "wrapped" onto the parent face

Key:

● Parent face gridpoint

○ Target face gridpoint

◉ Interface gridpoint
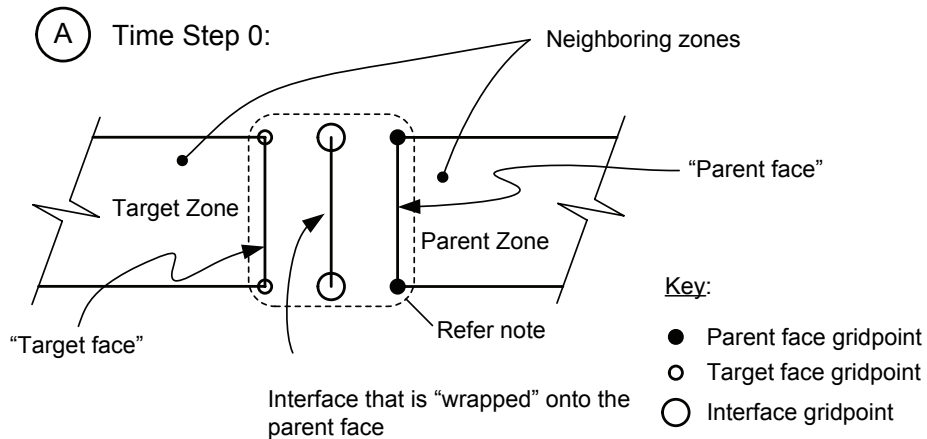
Note:

The zones and interface above have been drawn as separated for clarity only. Initially, the target and parent zones abut each other so that the parent and target face gridpoints, and interface gridpoints, all occupy the same position in space.

B) Time Step 1:

Relative movement equal to δ occurs between parent face and target face, so that the target face can be considered to "penetrate" into the parent face a distance δ

δ
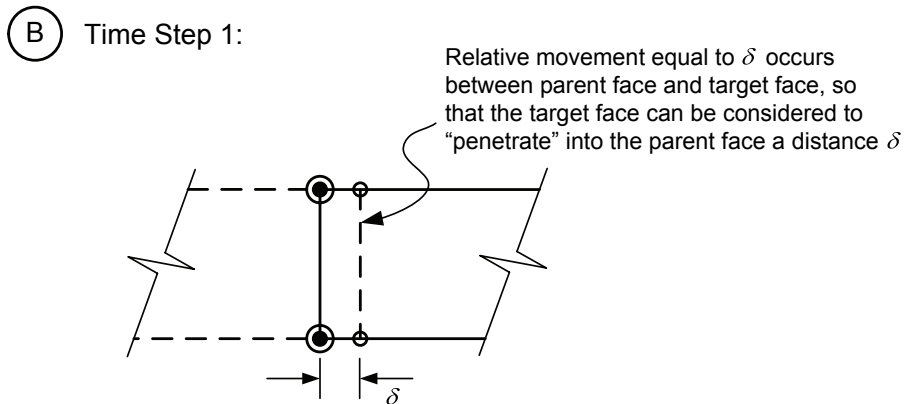
Note:

Interface element remains "glued" to the parent face, moving with it at all times.

Figure 4-19: Essence of interface action in *FLAC*³ᴰ

The magnitude of the stiffnesses assigned to the interface gridpoint springs therefore reflects the type of interface behavior sought: A much greater stiffness compared with that of the zone gridpoint of the associated parent and target zones is akin to a pressure transducer, such that forces are tracked with minimal compliance; whereas a much lesser stiffness compared with that of the zone gridpoint of the associated parent and target zones is akin to a weak discontinuity, such as a clay gouge zone associated with fault movements. In the case of modeling a laterally loaded pile, the interface behavior sought is that akin to a pressure transducer, so that the interface spring stiffnesses must necessarily exceed the zone gridpoint stiffnesses by an appreciable amount. To this end an "apparent stiffness" of a zone gridpoint in the direction normal to the interface plane is defined as

124

$$\frac{K + \frac{4}{3}G}{\Delta z_{min}} \qquad (4.67)$$

where $K \& G$ = bulk and shear moduli of zone, respectively, and

Δz_{min} = the smallest dimension of the zone.

The apparent stiffness measure accounts for the normal stiffness of a zone as this is a function of its elastic properties and its size. An apparent stiffness value is therefore calculated for the parent and target zones associated with the interface gridpoint, and the maximum value used as a benchmark for characterizing the interface spring stiffness. An interface stiffness that provides at least ten times the maximum apparent stiffness is recommended in $FLAC^{3D}$.

4.3   Application to Research

The above review indicates the capabilities but uniqueness of $FLAC^{3D}$ as an analysis tool. In the context of the current research, namely static, monotonic lateral loading of piles, the $FLAC^{3D}$ formulation provides the necessary modeling requirements to undertake a numerical 3-D assessment of pile-soil interaction. However, a qualification is necessary in terms of the way it is applied to simulate the static, monotonic lateral loading. It is apparent from section 4.2.4 and section 4.2.5 that $FLAC^{3D}$ is attempting to approximate the physical disturbance to a soil system brought about by forces imposed on it and manifested as deformation. As with laboratory experiments on soil, such disturbance can be applied via load ("stress control") or movement ("strain control").

Applying load in $FLAC^{3D}$ is a matter of applying forces to gridpoints, either through specifying an external stress on a face that is then converted into gridpoint forces, or by specifying external gridpoint forces directly. Applying movement in $FLAC^{3D}$ is a matter of specifying velocity at a gridpoint, and then stepping through computational time to obtain the specified movement. The amount of stress/force or velocity that is applied to gridpoints is important in that too much can initiate a dynamic "shock" to the system that is unreasonable from a real physical standpoint. A typical $FLAC^{3D}$ pile-soil model is shown in Figure 4-20, comprising a pile constructed of elastic zones, surrounding soil constructed of elastic-plastic zones, and an interface element wrapped over the soil zone faces that cover the pile-soil interface area.

To apply the loading in the direction shown, very small velocity increments were applied to the gridpoints located on the top surface of the pile. These velocity increments were controlled to minimize incremental forces developed in the pile-soil system so as not to pollute the solution with inertial tendencies. Simulation of lateral loading in $FLAC^{3D}$ was therefore achieved by performing what is essentially a very slow dynamic test. Given the in-built restrictions to ensure numerical stability throughout the system, and the inference to physical propagation of a disturbance that this implies (refer section 4.2.5.1), a mathematical model favoring a wave propagation solution approach to the laterally loaded pile problem was therefore realized.
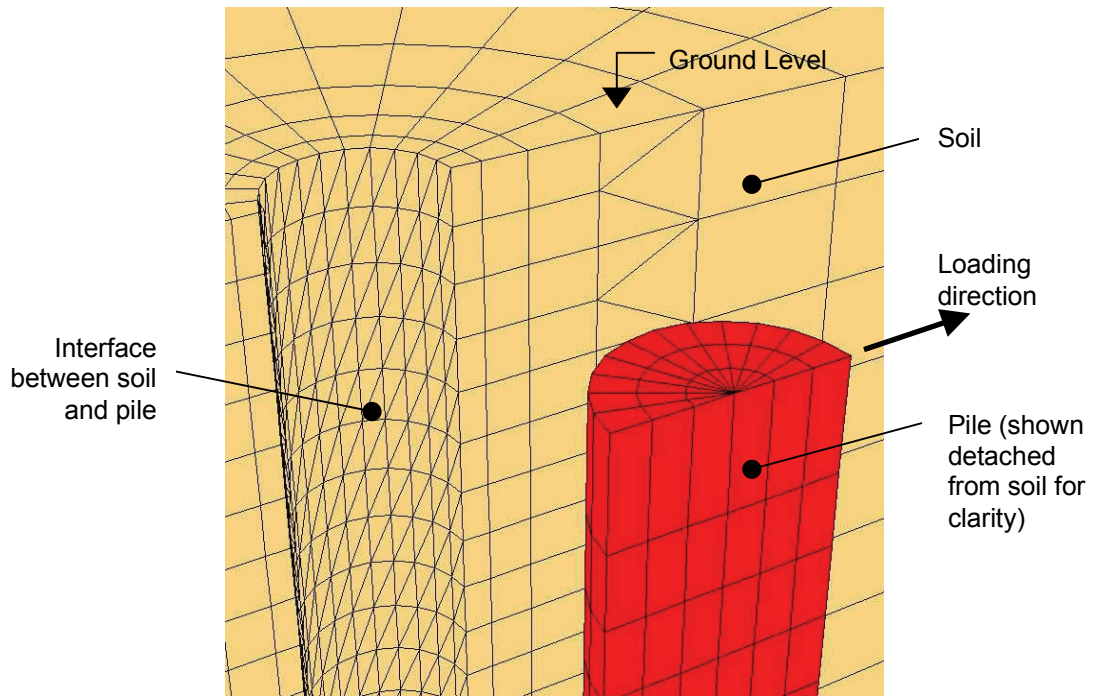
Figure 4-20: Typical *FLAC*^{3D} pile-soil model

SECTION 5
VERIFICATION, VALIDATION AND CALIBRATION

5.1   Introduction

Numerical modeling of geotechnical problems requires cognizance of various issues associated with numerical methods, constitutive models, idealization, discretization, and prediction capabilities. Wood (2004) provided a storehouse of information in this respect, and defined the conduct of numerical modeling in terms of three aspects posed as questions one should ask oneself when embarking on a numerical analysis:

1. Verification: Is the program doing what it claims to be doing?
2. Are we getting the answers that we think we are getting?
3. Validation: Are we getting the answers that we need?

Such questions are the topic of the current section, and are especially relevant in the case of $FLAC^{3D}$ given the rather unique formulation evident from Section 4, and its relative infancy in practice compared with the finite element approach.

A major implication of the $FLAC^{3D}$ approach is an ever-present dynamic tendency of the modeling system, stemming from the use of Newton's Second Law of Motion to convey a solution. This requires particular vigilance on the modeler's part, given the relative ease with which forces can be overestimated for a given deformation (velocity dependence). Construction wise, the low-order constant strain tetrahedra used in $FLAC^{3D}$ somewhat compound the possibility of excessive system stiffness if proper consideration to spatial discretization is not given. The presence of very stiff material, such as a pile, also demands particular care given the sensitivity to movement and dynamic "noise" that can be generated as a result.

The documentation for $FLAC^{3D}$ includes comparisons with analytical solutions for various problems that serve to address verification in a general sense. In the case of the laterally loaded single pile problem, specific consideration as to the model behavior of the pile, the soil, the pile-soil interface, and the pile-soil system combined (i.e., interaction behavior), is required. Extending the problem to that of a group configuration must then consider modeled group effects. In order to seek assurance of the capabilities of $FLAC^{3D}$ to adequately perform in these respects, a series of analyses were undertaken to provide confirmation prior to the research proper. These are documented herein, and serve to address the verification, validation and calibration aspects of the numerical approach utilized in the current research.

5.2   Linear Elastic Analyses

5.2.1   Pile Discretization

An issue that demanded attention first was the behavior of the numerical 3-D pile constructed of elemental zones. Modeling of reinforced concrete piles ("bored" piles or "drilled shafts") and steel pipe piles ("driven" piles) was required for the research analyses, and that these achieved appropriate curvature under lateral loading was of primary concern. Inspection of case histories, and consideration of theoretical solutions discussed in Section 2, suggested strong similarities between a bending moment curve exhibited by a laterally loaded free-head pile, and the bending

moment curve for the triangular-loaded case shown in Figure 5-1. This is evident from the comparisons shown in Figure 5-2 and Figure 5-3, where the bending moment curve for each triangular load case was derived by back-calculating an equivalent total load (W) using the maximum moment measured in the field (M_{max}) as a benchmark i.e., $W = M_{max} \times 6/L$.

w = load per unit length

W = total load $= w_{max} \times L/2$

w_{max}

a) Loading

Structural Member:
EI = bending stiffness
A_s = shear area
G = shear modulus
L = length

$L/2$ $L/2$

L

$\dfrac{W}{2}$

$V_x = \dfrac{W}{2L^2}\left(L^2 - 4x^2\right)$

for $x < L/2$

b) Shear

x

$M_x = Wx\left(\dfrac{1}{2} - \dfrac{2x^2}{3L^2}\right)$ for $x < L/2$

$\dfrac{WL}{6}$

c) Bending Moment

$\Delta_b = \dfrac{Wx}{(480EI)L^2}\left(5L^2 - 4x^2\right)^2$ for $x < \dfrac{L}{2}$

$\Delta_s = \dfrac{Wx}{2A_sG}\left(1 - \dfrac{4}{3}\left(\dfrac{x}{L}\right)^2\right)$ for $x < \dfrac{L}{2}$

x

$(\Delta_b)_{max}$
$= \dfrac{WL^3}{60EI}$

$(\Delta_s)_{max}$
$= \dfrac{WL}{6A_sG}$

d) Deflection

Note :

Δ_b = bending deflection

Δ_s = shear deflection
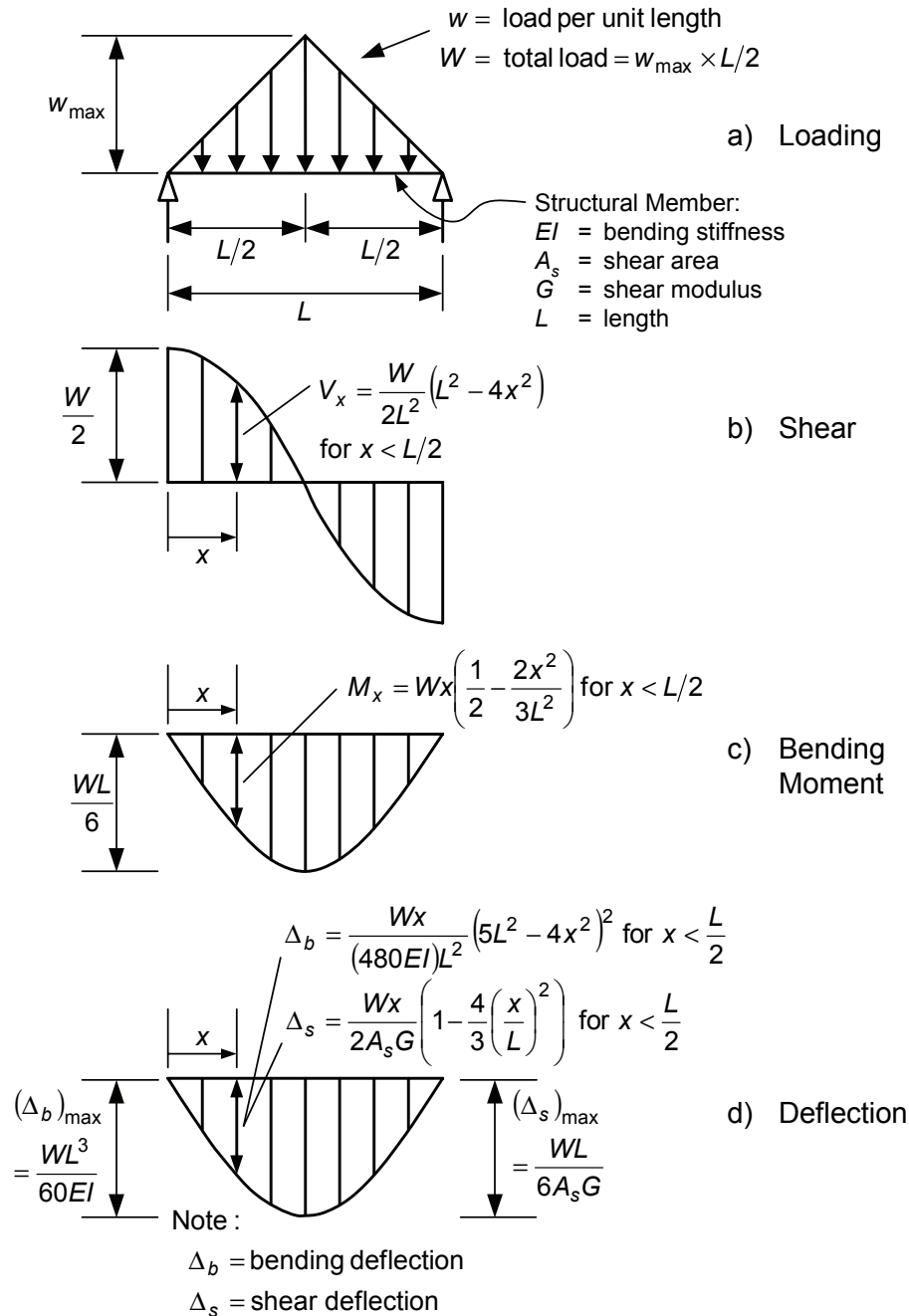
Figure 5-1: Analytical solutions for simply supported structural member with triangular loading
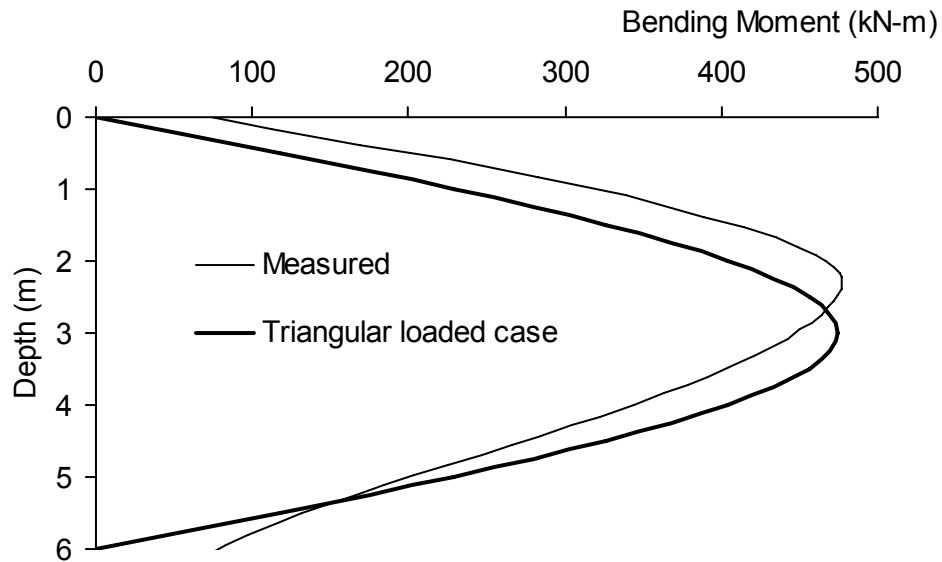
Figure 5-2: Comparison of bending moment distribution for Mustang Island (Reese et al., 1974) case history, lateral load = 266.9 kN
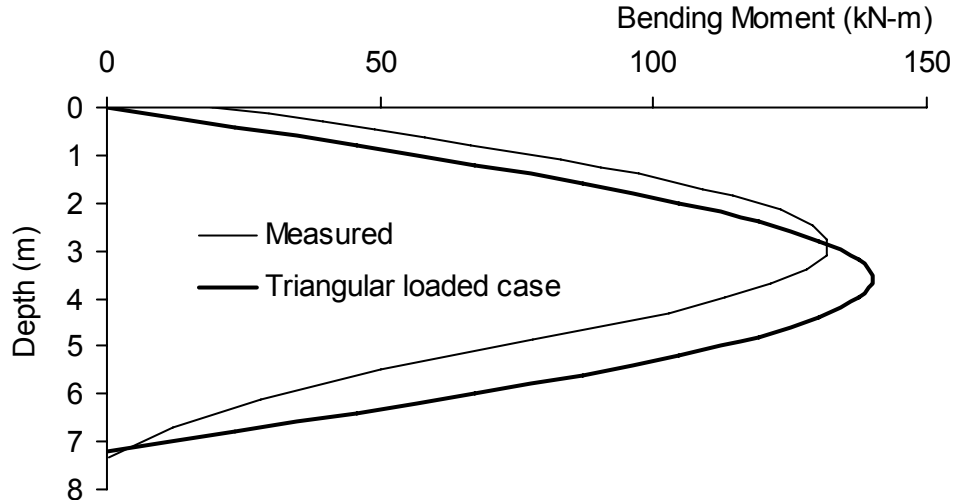
Figure 5-3: Comparison of bending moment distribution for Sabine River (Matlock, 1970) case history, lateral load = 71.2 kN

A means of establishing pile discretization needs in $FLAC^{3D}$ was therefore provided by modeling the simply-supported triangular-loaded case with different discretized pile configurations and assessing the accuracy of results in terms of the analytical solutions given in Figure 5-1. Trial models tested different discretization densities along the length of the pile as well as in a cross-

sectional sense, given the three-dimensional nature of the pile in $FLAC^{3D}$. The terminology adopted for this purpose is indicated in Figure 5-4, consisting of three variables (n, s and t) representing discretization density in a lengthwise, circumferential, and radial sense, respectively. In all cases a solid circular pile section of the form shown in Figure 5-4(a) was modeled in $FLAC^{3D}$, so that an equivalent modulus measure ($E_{p\text{-}equiv.}$) was required when modeling hollow pile sections (i.e., steel pipe piles), defined as

$$E_{p-equiv.} = \frac{E_p I_p}{\left(\pi d_o^4 / 64\right)} \tag{5.1}$$

where $E_p I_p$ = flexural rigidity of actual pile,

d_o = outside diameter of actual pile.
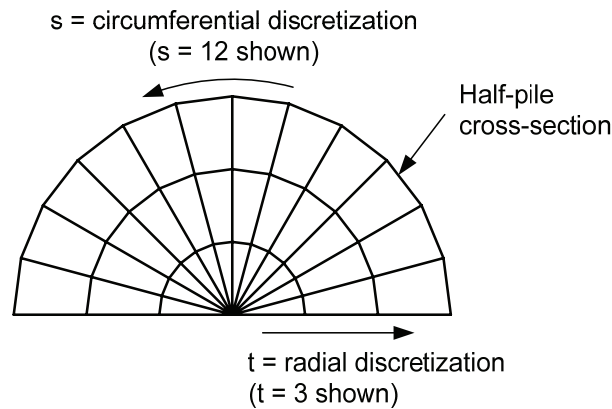
a) Cross-sectional discretization
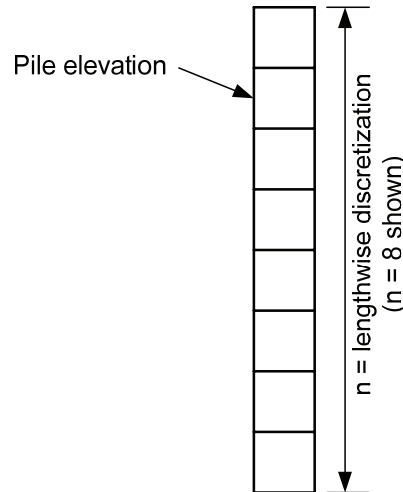
b) Lengthwise discretization

Figure 5-4: Pile discretization variables

Pile dimensions were chosen according to the case histories used for validation and calibration purposes, general details of which are shown in Figure 5-5. Each case history was assigned a name for ease of reference (refer Figure 5-5), and this naming convention is used hereafter (it is to be noted that the piles in Figure 5-5 are drawn to the same scale, emphasizing the variations in piles that occur in practice). Simply-supported configurations were established by first determining W (as previously described), then a trial and error procedure adopted to find a simply supported length that provided a bending moment distribution most similar to that observed. In all cases advantage was taken of symmetry such that only half the pile was actually modeled in a cross-sectional sense.
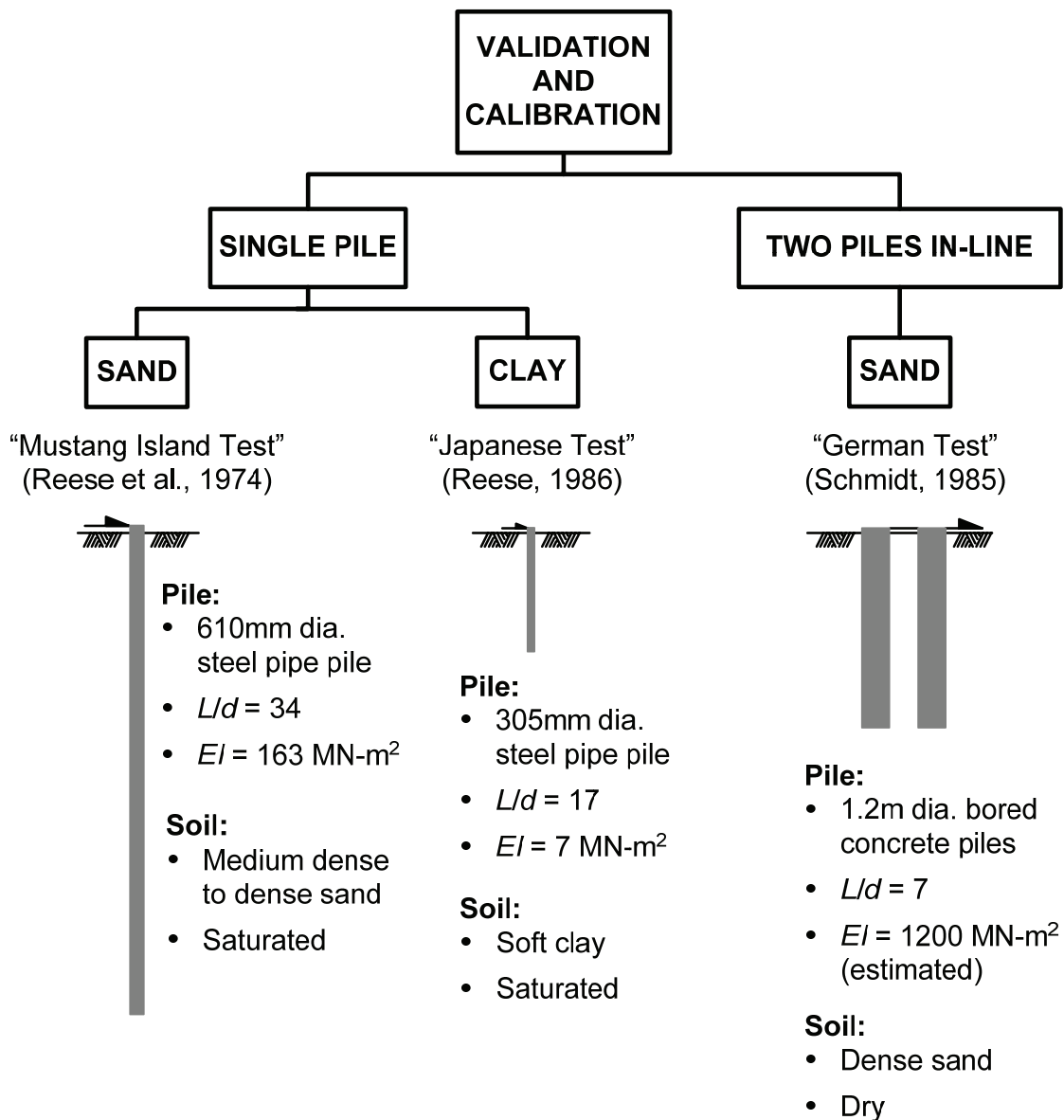
Figure 5-5: Configurations of case histories selected for validation and calibration purposes (piles drawn to same scale)

In the case of the German Test, the small length to diameter ratio of the simply supported configuration (L/d = 5) required the additional consideration of shear deflection in the analytical solution. The expression for shearing deflection given in Figure 5-1 was established using the energy method utilizing a dummy unit load approach, defined as follows:

$$\Delta_s = \int_0^L \frac{Vv}{A_s G} dx \tag{5.2}$$

where v = shear due to unit dummy load and remaining terms were as defined in Figure 5-1.

Bending moment values in $FLAC^{3D}$ were calculated by summing the moments of axial forces mobilized in each zone of a cross-section, where axial forces were calculated by multiplying the axial stress for a zone by the area of the zone face parallel to the plane of the cross-section. Shear forces were similarly derived by summing the shear forces mobilized in each zone of a cross-section, where a zone shear force was calculated by multiplying the shear stress acting in the plane of the cross-section by the area of the zone face parallel to the plane of the cross-section. Thus bending moment and shear force values were defined at points along a pile that were midway between gridpoint locations (i.e., at centroid locations). Deflection values were obtained directly from gridpoints located along the centerline of the pile, so that these applied at gridpoint locations.

Results of the simply-supported analyses are shown in Figure 5-6 (Mustang Island Test), Figure 5-7 (Japanese Test) and Figure 5-8 (German Test). These correspond to the cross-sectional discretization configurations adopted for subsequent pile-soil analyses.

The discretization assessment results indicate that shear force behavior performed exceptionally well, whereas the performance of deflection and bending moment behavior was strongly dependent on lengthwise discretization and, to a lesser extent, cross-sectional discretization. Satisfactory shear force behavior reflects the ease in which zones can respond in shear to the transverse (shear) loading imposed, whereas bending moment and deflection behavior rely on other zone actions that are not so compatible with the loading regime. Higher gradients of axial stress distribution over the cross-section of a pile with increased bending also accentuate discretization deficiencies, given that centroid values can only depict such gradients in a step-wise fashion. Overestimation of deflection in the German Test case (refer Figure 5-8) also suggests possible numerical bias towards shearing action for that particular pile configuration. Overall, the trends in behavior are a reminder of the sensitivity of any numerical solution to the discretization employed, and indicate that appreciable detail is required in the case of $FLAC^{3D}$ when modeling stiff elements such as structural piles.

5.2.2 Pile-Soil Discretization

Following the assessment of pile performance, attention turned to discretization requirements when modeling a pile-soil system and the assessment of respective linear interaction performance. To this end recourse to linear subgrade reaction, boundary element and finite element based solutions provided a means of assessing $FLAC^{3D}$ performance. Analytical solutions for a laterally loaded elastic pile embedded in a soil represented by subgrade reaction models were used as the primary assessment tools: Reese and Van Impe (2001, p. 25) document the solution for the case of a horizontal subgrade modulus (k_h) that is constant with depth, and Poulos and Davis (1980, chap. 8, section 8.2.2.2) document the solution for the case of a

132

horizontal subgrade modulus increasing linearly with depth. These solutions were developed in Excel spreadsheet form using Visual Basic for Applications (VBA) programming support, and an example of the spreadsheet solution is shown in Figure 5-9.
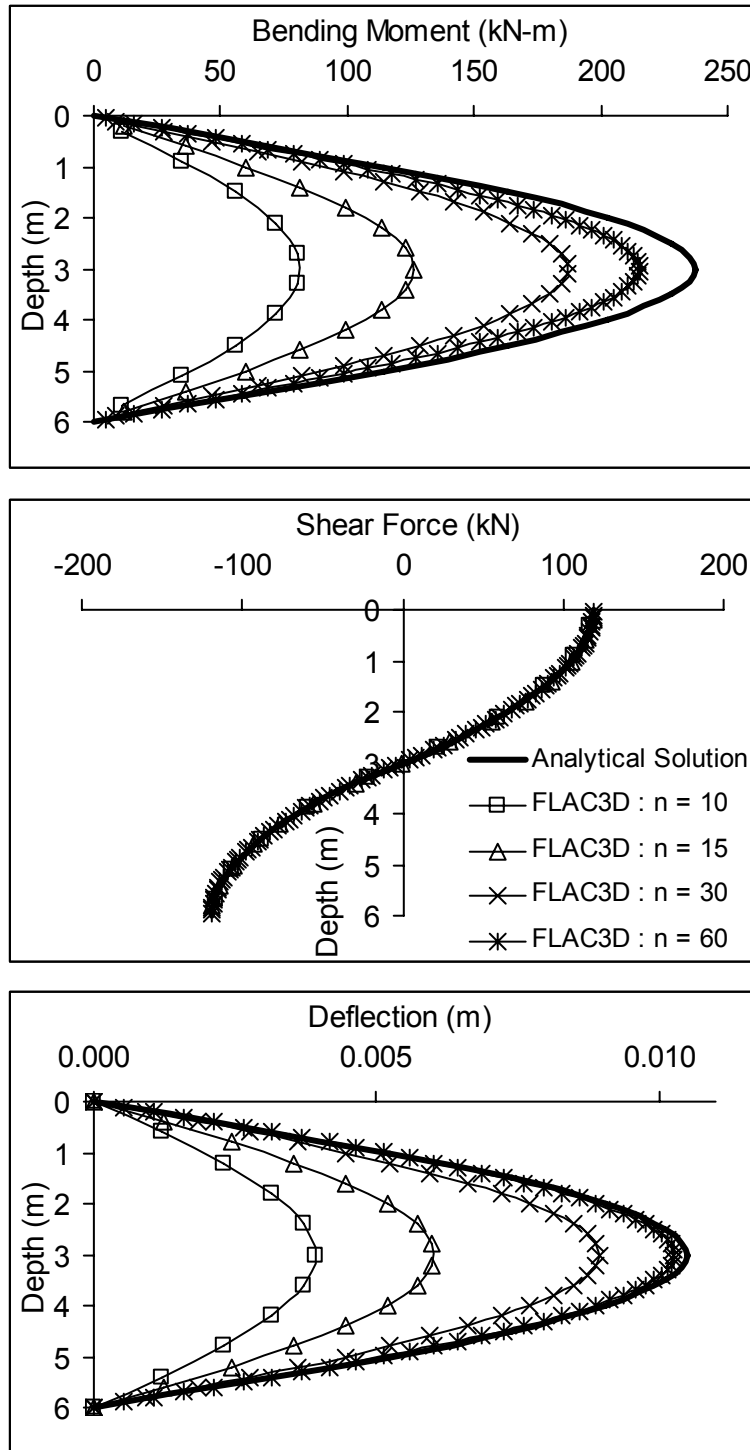
Figure 5-6: Discretization assessment results for Mustang Island Test simply-supported, triangular-loaded pile configuration (s = 12, t = 3)
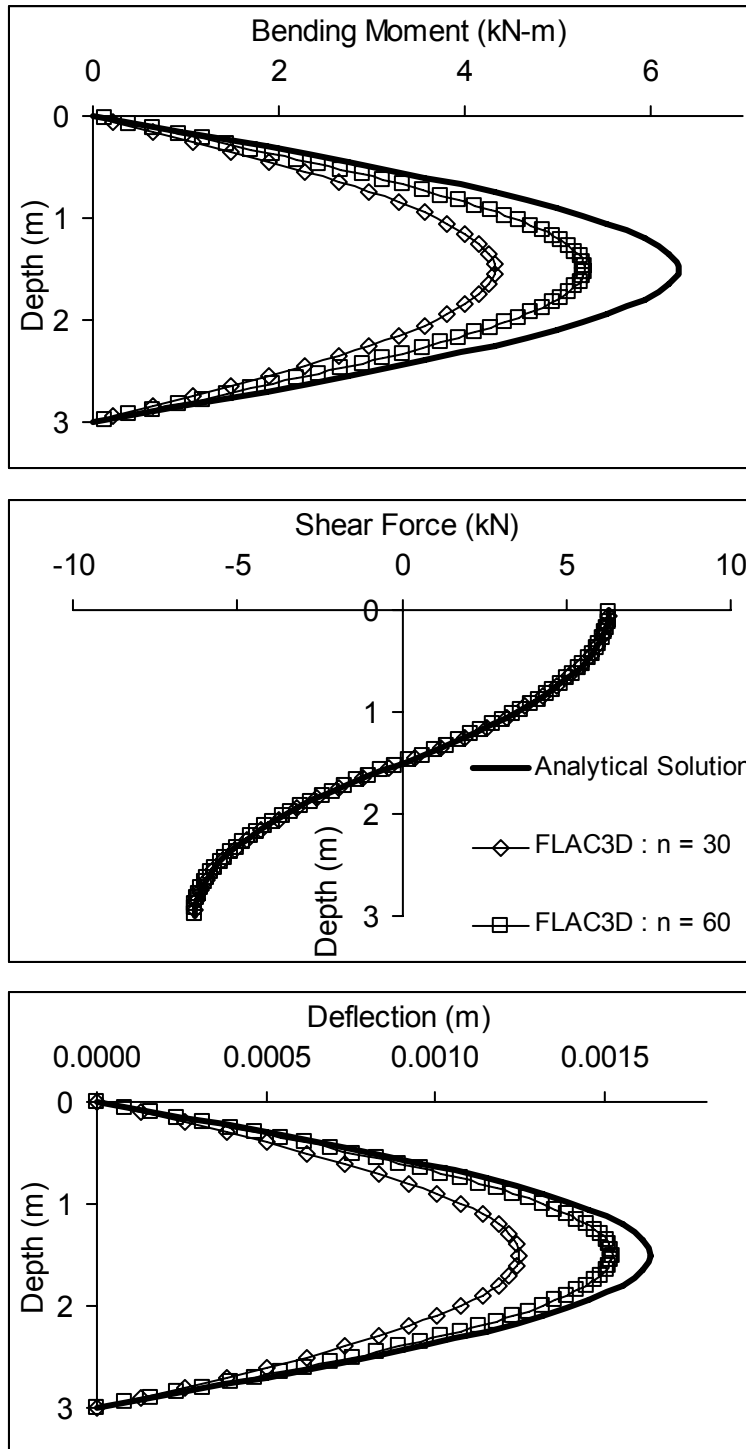
Figure 5-7: Discretization assessment results for Japanese Test simply-supported, triangular-loaded pile configuration (s = 12, t = 2)
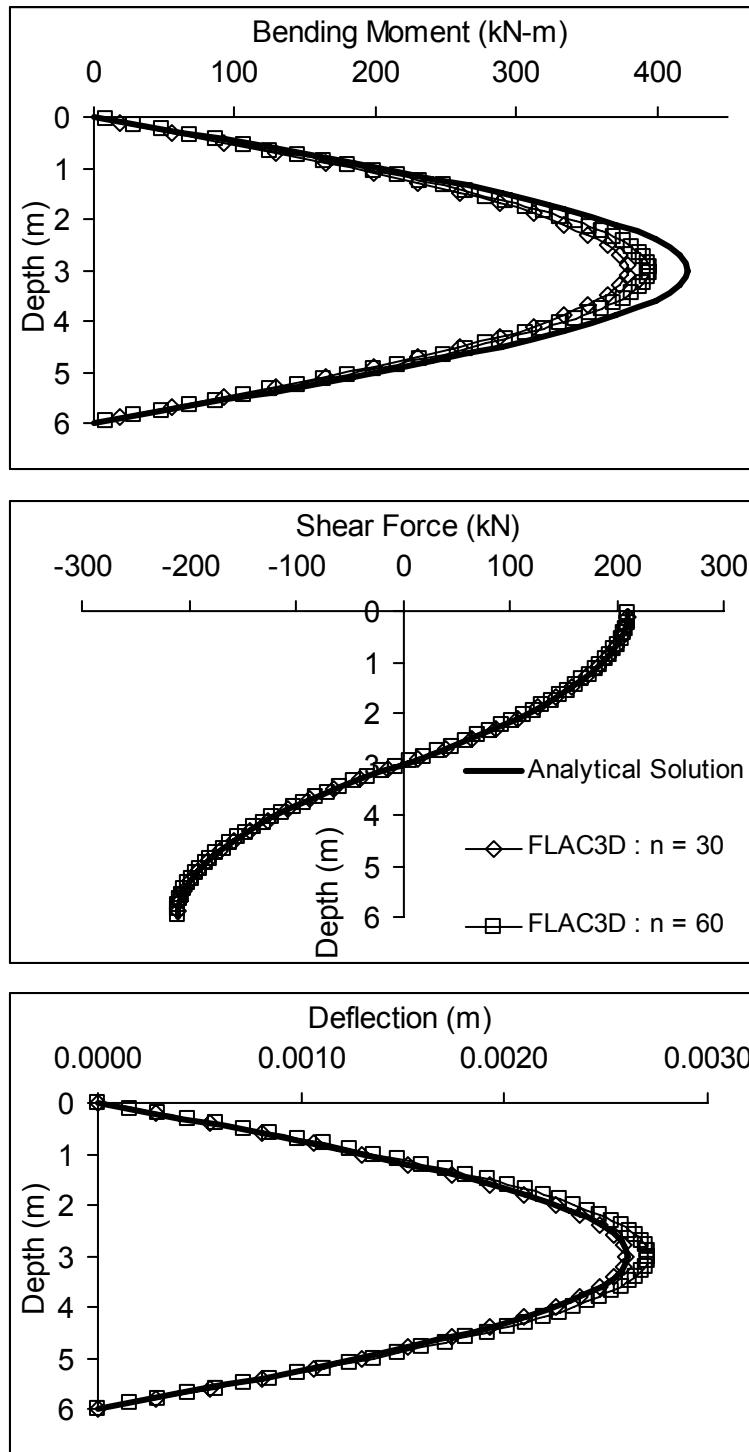
Figure 5-8: Discretization assessment results for German Test simply-supported, triangular-loaded pile configuration (s = 12, t = 3)

Input:

Pile Head Loading:
Moment = 0 kN-m
Horizontal Force = 100 kN

Units: SI (SI or fps)

Pile Data:
E_p = 2.40E+07 kN/m^2
I_p = 0.006797 m^4
L = 21 m
d = 0.61 m
Note: d is not used in L modulus case

Pile Head Restraint: Free (Free or Fixed)

Soil Data:
k_h or n_h = 50000 kN/m^3

Modulus Case: L
Constant, or Linearly increasing ?

k_h $k_h = n_h\left(\dfrac{z}{d}\right)$

Constant   Linearly increasing
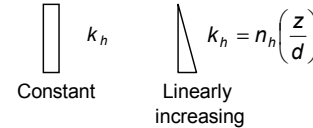
Action[a]: D

[a] *Options:* Constant Modulus: Deflection, Slope, Moment, V (Shear), or P (Soil Pressure)
Linear Modulus: Deflection or Moment (V for Free-Head only)

Calculated Parameters:

Plot:

Value at top of pile = 3.03 mm

Linear Modulus Case:

T = 1.267 m, where $T = \left(\dfrac{E_p I_p}{n_h}\right)^{1/5}$
$4T$ = 5.066 m

Check: Pile is long (L > 4T) thus can proceed.

Constant Modulus Case:

β = N/A 1/m where $\beta = \sqrt[4]{\dfrac{k_h d}{4 E_p I_p}}$
βL = N/A

Check: N/A

Additional Note for Constant Modulus Case:

Long Beams	βL > 5.00
Moderately Long Beams*	2.25 < βL < 5.00

* Error less than 2.5% if assume long beams
Source: Vesic (1961)

Deflection vs. Depth

Defl. (mm)

-1.0   0.0   1.0   2.0   3.0   4.0

Depth (m): 0.0, 1.0, 2.0, 3.0, 4.0, 5.0, 6.0

♦ Linearly Incr. Subgrade
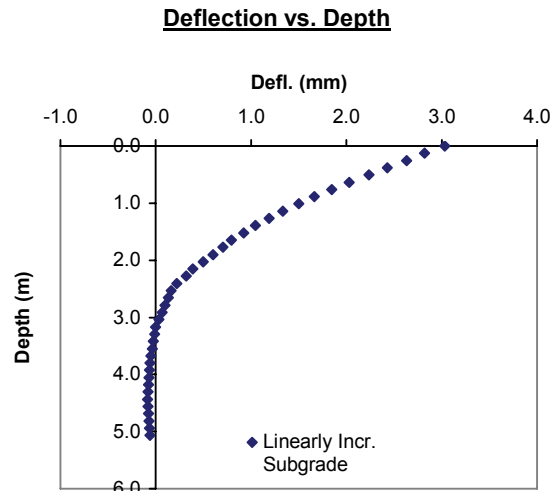
Figure 5-9: Example of spreadsheet solution for subgrade reaction models

Elastic continuum-based solutions obtained using the boundary element approach (Davies and Budhu, 1986; Budhu and Davies, 1987) were used to supplement linear subgrade reaction solutions in that they provided a check on the value of displacement at the pile-head, and also some assurance that equivalency between subgrade reaction and continuum solutions was being achieved. The required solutions for the case of a soil represented by an elastic modulus (E_s) constant with depth and linearly increasing with depth were given in Table 2-2. Elastic continuum-based solutions based on finite element modeling (Randolph, 1981) were also utilized as another check on pile-head behavior and to provide more assurance of subgrade reaction and continuum equivalency. Similar to the linear subgrade reaction solutions, the Randolph solutions were developed into spreadsheet form with VBA support.

In addition to providing an assessment basis for $FLAC^{3D}$ pile-soil models, the subgrade reaction, boundary element and finite element solutions also helped to define discretization needs of the pile-soil model through the calculation of theoretical critical lengths of piles that assisted in establishing the discretization of the pile over its total length, which in turn dictated the discretization of adjacent soil zones. Pile discretization details for the Mustang Island Test and Japanese Test pile-soil models, established from consideration of both critical length values and the findings of the simply-supported discretization assessment exercise, are shown in Figure 5-10.

A subtle aspect to be noted at this point was the assumption of perfect bonding of the pile to the soil, requiring some thought as to the behavioral consequences of the various modeling options. These are illustrated in Figure 5-11, serving as a reminder that the perfect bonding between pile and soil is an idealized concept. Use of a subgrade reaction model for this case implicitly lumps three-dimensional compressive and tensile continuum resistance into a one-dimensional (horizontal) subgrade modulus form of resistance. Conversion between subgrade modulus values and continuum values therefore utilized the relationship determined by Vesić (1961), as discussed in Section 2, but the modulus value was doubled for the laterally loaded pile case to account for the perfect tensile and compressive resistances acting on both sides of the pile, i.e.

$$ k_h = 2 \times \left(\frac{0.65 E_s}{1 - v_s^2} \sqrt[12]{\frac{E_s d^4}{E_p I_p}} \right) \tag{5.3}$$
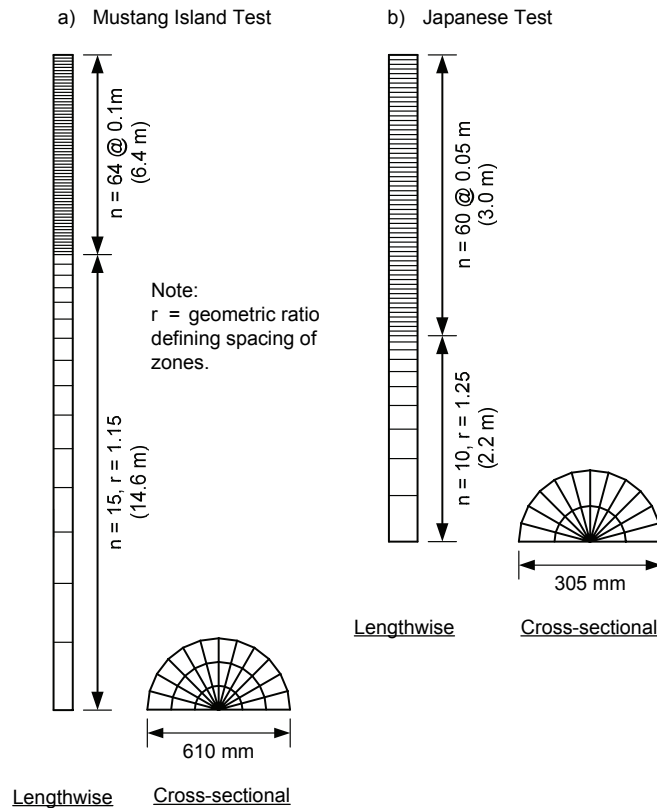
Figure 5-10: Pile discretization for Mustang Island Test and Japanese Test pile-soil models
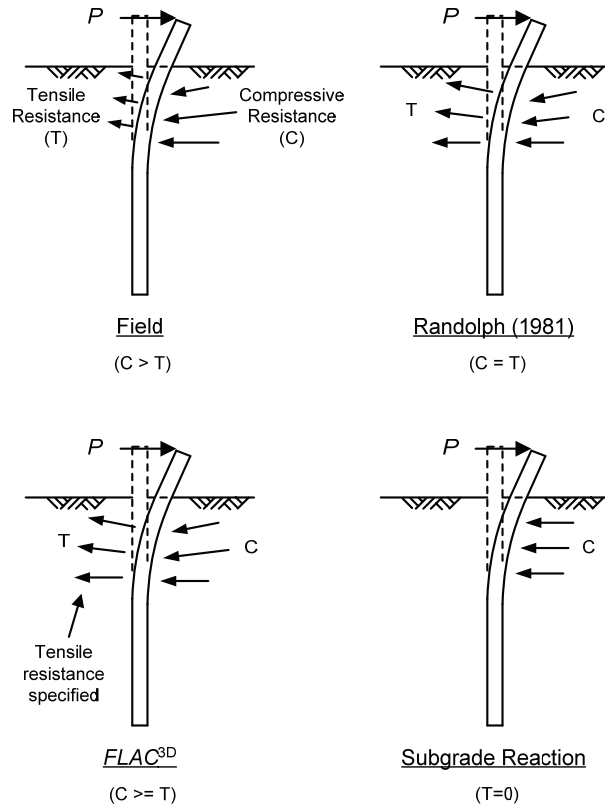
Figure 5-11: Differences in lateral resistance for field and model experiments

Overall dimensions of pile-soil models were established in part by inspection of model dimensions used in prior numerical studies, and through inspection of model behavior at extremities once analyses were completed. In regards to prior numerical studies, Baguelin et al. (1977) used distances to lateral boundaries of between $10d$ and $15d$ when undertaking plane strain analyses of a laterally loaded pile using circular boundaries (refer Figure 2-21 in Section 2), and Bransby (1999) found good agreement with the Baguelin et al. solution when using plane strain analyses with rectangular boundaries located $25d$ from the pile center. Trochanis et al. (1988), utilizing a 3-D axisymmetric finite element mesh constructed of 27-node isoparametric brick elements to model a laterally loaded square pile ($d = 0.5$ m, $L = 10$ m), considered it sufficiently accurate to place the lateral boundary at a distance of $12d$ from the pile center, and the bottom boundary a distance of 0.6 to 0.7 times the pile length from the pile tip. Guided by this information, pile-soil model geometries were established as shown in Figure 5-12 and Figure 5-13. It should be noted that while the base of the Mustang Island Test model is only located a distance 0.38 times the pile length from the pile tip, the length of the pile far exceeded its critical length.

Discretization of the soil region of the pile-soil models was very much a trial and error procedure, with a number of different configurations tested in the initial stages. Vertical discretization was largely controlled by the pile discretization, as matching pile and soil (and interface) gridpoints were required for gridpoints located at pile-soil boundaries. Horizontal discretization of the soil was also controlled by pile discretization to some extent, given that soil immediately adjacent to and in the vicinity of the pile was subject to high stress gradients in the horizontal direction. A

138

very detailed, or dense, pattern of soil zones surrounding the pile was therefore required, followed by a gradual reduction in both vertical and horizontal density towards model boundaries. The reduction in density was driven not only by the less demanding physical behavior with distance and depth requiring less detail, but also the need to minimize the number of zones to avoid excessive computation time.

The discretization employed for the Mustang Island Test pile-soil model is indicated in Figure 5-14 (front elevation), Figure 5-15 (side elevation) and Figure 5-16 (plan). This is representative of the typical discretization layout employed in all pile-soil models developed for isolated pile analyses, including research analyses. Transitioning from regions of higher to lower zone densities was achieved through use of transition annuli in the horizontal case, and use of an attachment feature available in $FLAC^{3D}$ in the vertical case. Transition annuli consisted of brick zones constructed from three triangular (degenerate) zones, as apparent in Figure 5-14. The attachment feature served to appropriately apportion[‡] forces from a "lone" gridpoint, associated with zones in a higher density configuration, to adjacent gridpoints also belonging to neighboring zones in a lower density configuration. Higher and lower zone density configuration transitions in the vertical direction were in almost all cases a 2:1 transition, with some 3:1 transitions provided in isolated cases.
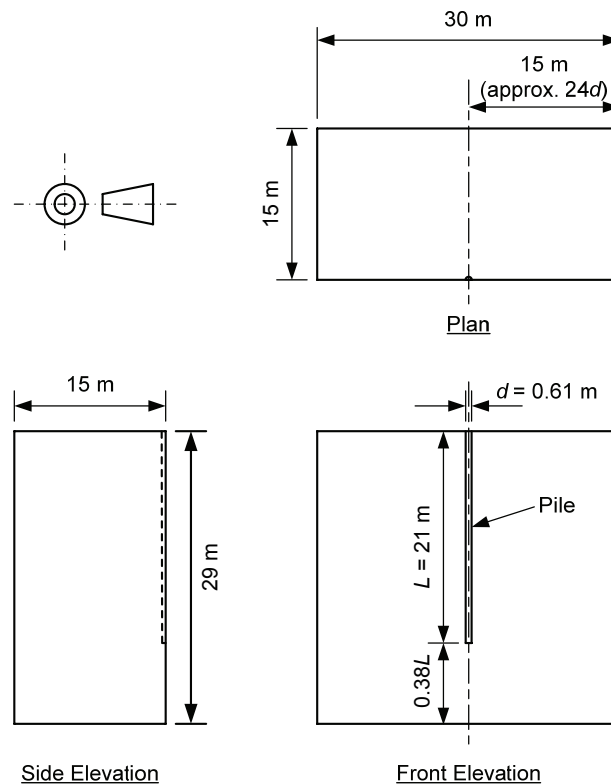
Figure 5-12: Mustang Island Test pile-soil model geometry

[‡] Apportionment uses a weighting scheme based on tributary areas of gridpoints.
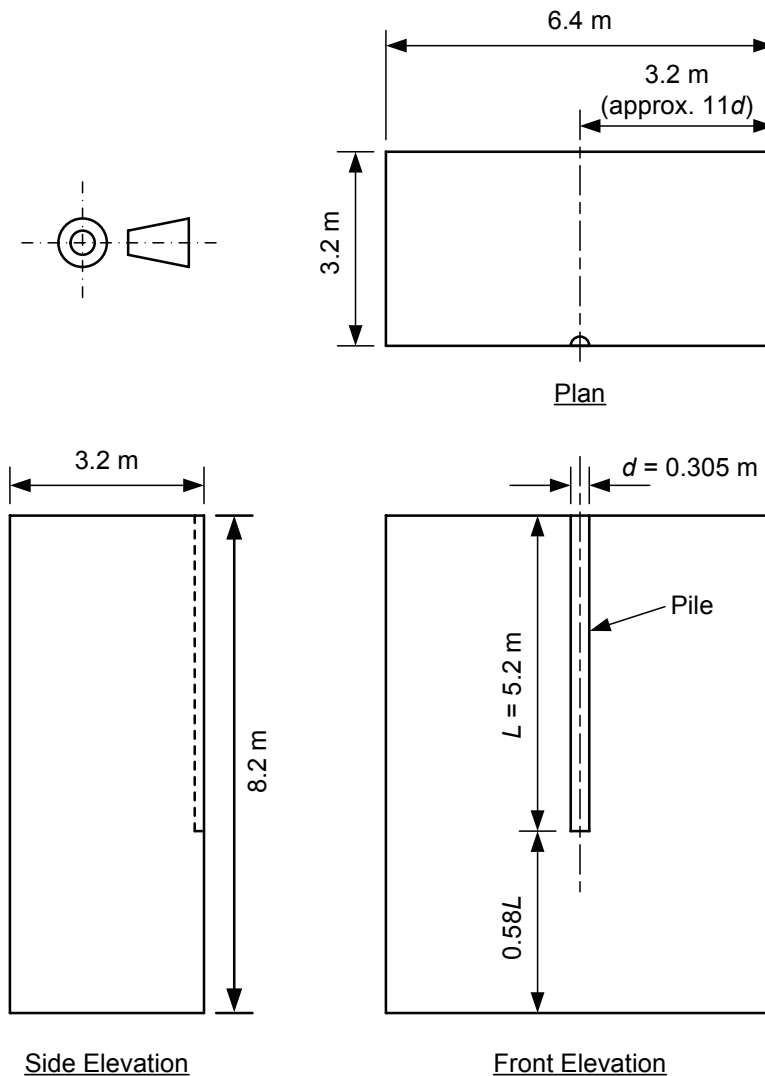
Figure 5-13: Japanese Test pile-soil model geometry

Modeling properties for the linear $FLAC^{3D}$ pile-soil models are given in Table 5-1, where inclusion of an interface component is as discussed in Section 4. Each pile-soil model was assigned a Young's modulus for the soil in accordance with the respective subgrade reaction soil model: In the Mustang Island Test case a Young's modulus increasing linearly with depth was specified, while in the Japanese Test case a Young's modulus constant with depth was specified (E_s and k_h values at each depth satisfying the relation given by Equation 5.3 in each case). Details on how elastic soil values were derived are left for the following section, as there they served the specific purpose of approximating the "elastic" properties of the ground conditions in which each pile was tested, instead of currently serving as just a computational vehicle to assess discretization demands. An equivalent Young's modulus for each pile followed reported flexural stiffness values and the relation given by (5.1), and Poisson's ratio followed the standard value for structural steel. Interface stiffness values were based on ten times the maximum apparent stiffness present in each case (as discussed in Section 4), and a very large tensile strength was assigned to mimic perfect bonding of the pile and soil.

140
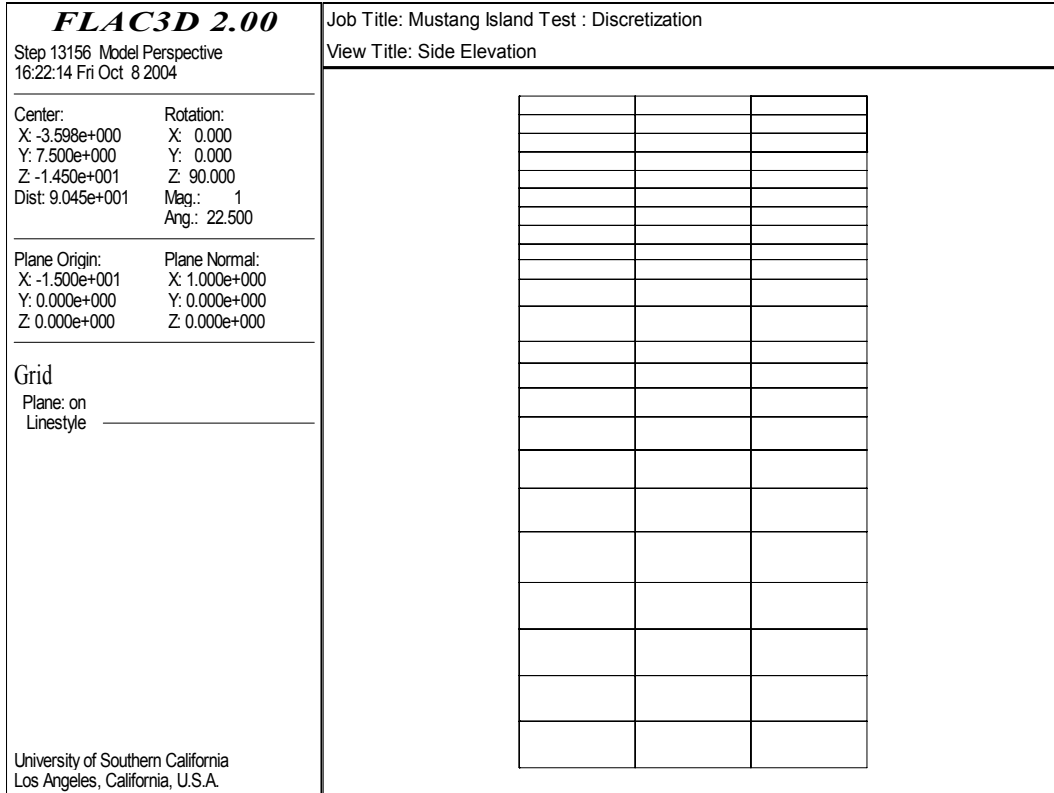
Figure 5-14: Front elevation discretization for Mustang Island Test pile-soil model
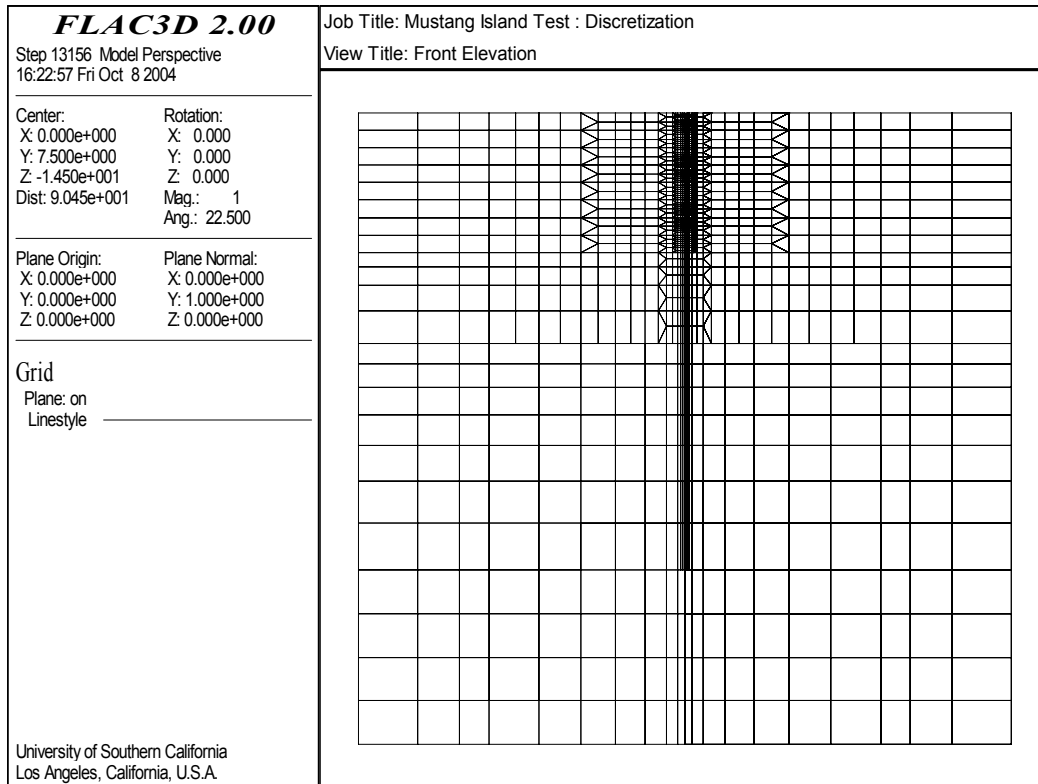
Figure 5-15: Side elevation discretization for Mustang Island Test pile-soil model
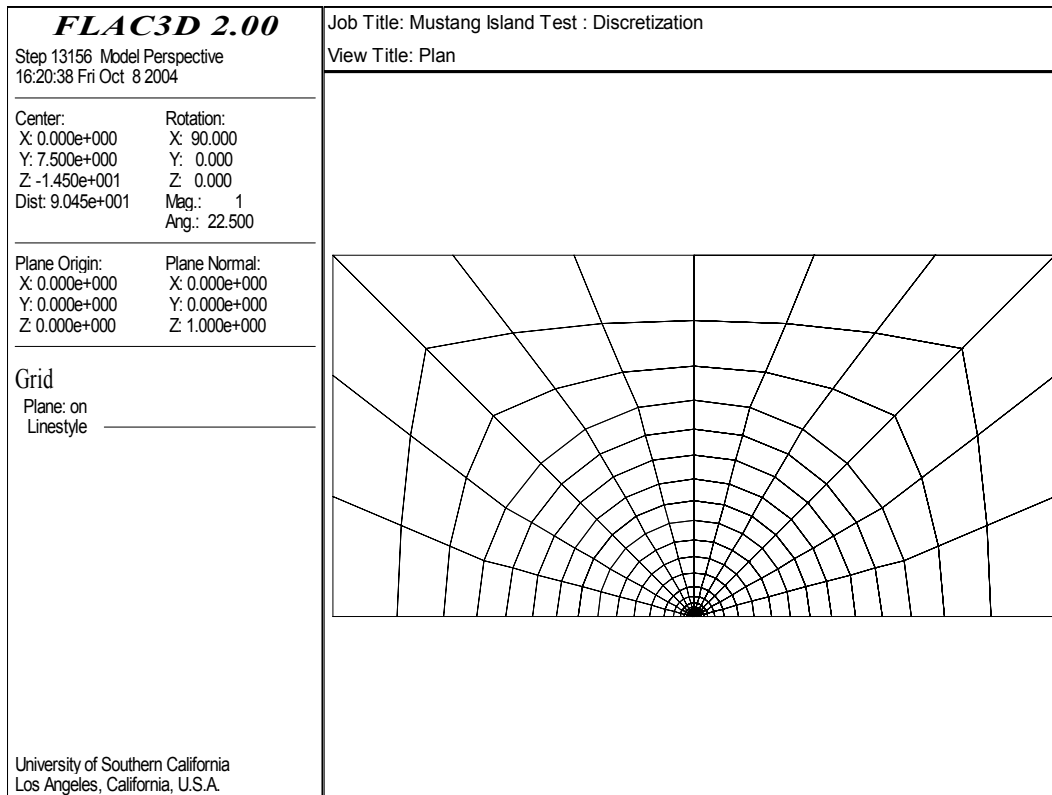
Figure 5-16: Plan discretization for Mustang Island Test pile-soil model

Table 5-1: Modeling properties for linear single pile-soil models

Elastic Properties	Case History	
	Mustang Island Test	**Japanese Test**
Pile:		
Young's modulus, $E_{p\text{-}equiv.}$	23.983 GPa	16.478 GPa
Poisson's ratio, v_p	0.25	0.25
Soil:		
Young's modulus, E_s	$25000z^{(1)}$ kPa	4095 kPa
Poisson's ratio, v_s	0.3	0.5
Interface[2]**:**		
Normal spring stiffness, k_n	2.9 x 10^9 kPa/m	2.6 x 10^9 kPa/m
Shear spring stiffness, k_s	2.9 x 10^9 kPa/m	2.6 x 10^9 kPa/m
Notes: 1. z refers to depth in meters. 2. Interface stiffness units refer to the spring stiffness per unit of tributary area associated with each interface gridpoint.		

Boundary conditions in all analyses consisted of preventing movement of side boundaries in the direction perpendicular to their plane, and preventing movement in the vertical direction at the base. The pile-head was located at the groundline to be consistent with the subgrade reaction, boundary element and finite element based solutions, and both stress control and velocity (displacement) control were used to effect lateral loading on piles. The velocity control analyses applied a constant velocity to the pile-head equal to 2.5e-8 m/s in the Mustang Island Test case and 8e-9 m/s in the Japanese Test case. These values were established by trial so as to restrict the maximum force developed in the model at each time step to small values, and thus realize a very slow dynamic lateral loading process as discussed in Section 4. Both free-head and fixed-head pile-head conditions were also assessed.

Comparative results for lateral loading achieved by velocity control for a fixed-head pile-head condition (the terminology used here being "fixed-head/velocity control", and similarly for other analysis conditions) are shown in Figure 5-17 (Mustang Island Test) and Figure 5-18 (Japanese Test).

The analysis results indicated satisfactory interaction trends but appreciable differences in magnitudes of structural actions for some cases. Overestimation of pile-head shear values when using velocity control analysis conditions was noteworthy, whereas underestimation of pile-head displacement values was the case when stress control analysis conditions were applied. Poor performance of bending moment and shear force behavior in regions of high curvature was apparent in the stress controlled analyses.

In deliberating these findings in the context of the intended research on large pile group effects, several matters were taken into consideration:

1. Linear elastic analyses of pile-soil interaction represent the extreme from a stiffness perspective, translating in $FLAC^{3D}$ terms to a system that is especially sensitive to movement, irrespective of the level of loading.
2. Considering a pile-soil system in terms of p-y curves and their derivation from the structural actions of a pile, accurate measurement of pile displacement (y) is foremost, whereas measurement of the soil reaction (p) is more tolerant given that it corresponds to either the rate of change of shear in the pile or the rate of change of slope of the moment curve.
3. As discussed in Section 2, assessing pile group effects from a p-y curve point of view is primarily concerned with relative differences between isolated pile behavior and the same pile in a group, so that the effect of errors in an absolute sense is more a secondary concern.

With these considerations in mind, the linear interaction performance in $FLAC^{3D}$ using velocity controlled lateral loading was deemed acceptable for the purpose at hand, and as a consequence the discretization used in each model considered sufficiently detailed. Besides exhibiting poor bending moment and shear force performance, stress controlled analyses were not considered further given load path dependency concerns with elastic-plastic analyses, as discussed in Section 4.
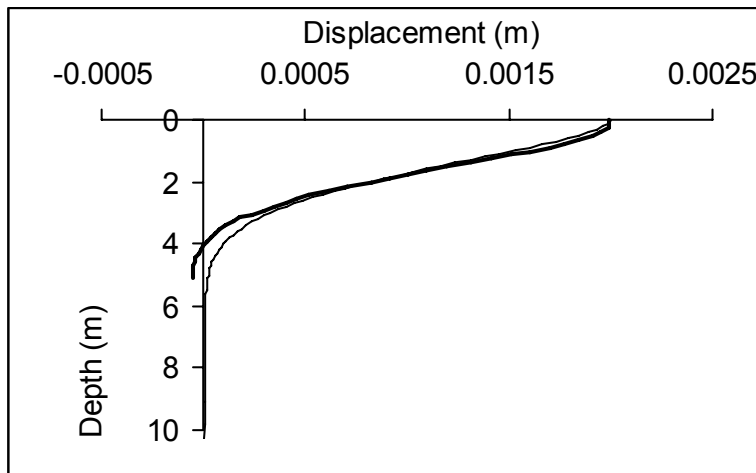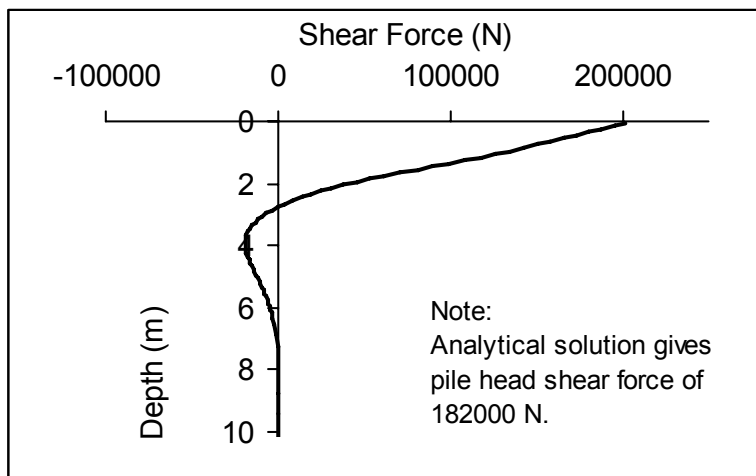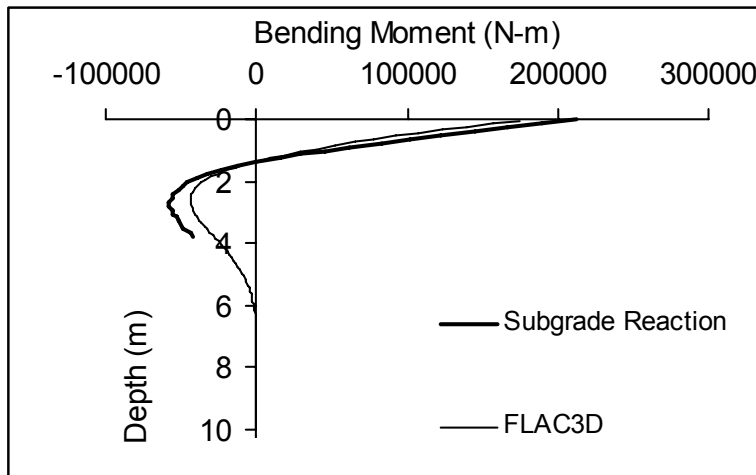
Figure 5-17: Comparative *FLAC*³ᴰ and subgrade reaction linear elastic results for Mustang Island Test using fixed-head/velocity control analysis conditions
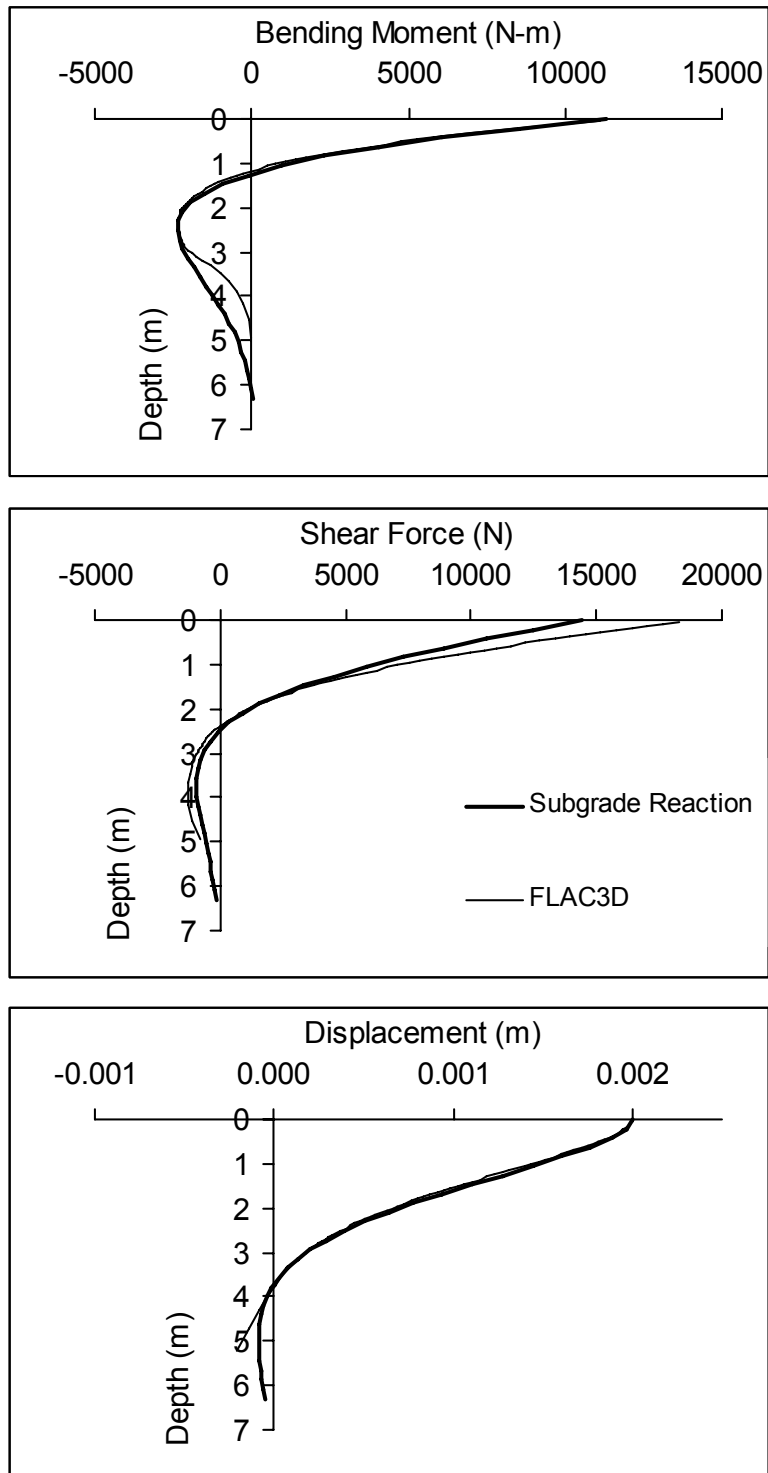
Figure 5-18: Comparative _FLAC_^{3D} and subgrade reaction linear elastic results for Japanese Test using fixed-head/velocity control analysis conditions

Overall, it was considered that the linear nature of the pile-soil system tended to exaggerate possible errors in structural values given the sustained stiffness of the system, causing problematic vibration "noise" brought about from forces induced through mobilization of the extremely stiff interface springs as relative pile-soil movements took place. This highlighted the sensitivity of $FLAC^{3D}$ to stiffness and the need for care in mobilizing the very stiff interface springs. Indeed, velocity control that was applied by starting at zero and then linearly increasing velocity to a constant (but still small) value over a sufficient amount of fictitious time, later proved very effective in minimizing unwanted dynamic "noise".

A final point of note was the significant lateral movement of the pile tip that took place in $FLAC^{3D}$ when modeling the Japanese Test. Such movement was consistent with subgrade reaction theory that predicted a critical length of 6.3 m, a value greater than the actual length of 5.2 m and thus indicative of rigid rather than flexible behavior. However, both the boundary element (Davies and Budhu, 1986) and finite element (Randolph, 1981) based approaches were indicative of flexible behavior, predicting a critical length of 3.1 m and 4.1 m, respectively. An explanation as to the cause of this discrepancy was not forthcoming, but suggests differences in relative stiffness characteristics are at play, due to differences in the way the pile, soil or pile-soil modeling components of the problem were modeled in each case.

5.2.3   Interface Performance

An important aspect of the interface component was its ability to transfer lateral forces between the pile and soil with minimal compliance, as discussed in Section 4. Evidence that the performance of the interface was satisfactory in this regard was obtained indirectly from the fact that satisfactory agreement between the linear elastic $FLAC^{3D}$ pile-soil models and subgrade reaction models was achieved. This confirmed that the recommended stiffness of interface springs (ten times the apparent stiffness as defined by Equation 4.67 in Section 4) was adequate in limiting interface spring displacements to relatively insignificant amounts. In addition to this indirect check on interface performance, sliding block models were developed to provide a direct check on forces mobilized at interface springs.

The sliding block models are shown in Figure 5-19 and included both horizontal and vertical interface elements to check gravity loading and applied horizontal loading, respectively. In each case the forces mobilized at each of the interface gridpoints were summed and compared with the acting forces to ensure equilibrium existed. In addition to force checks, the right-angled sliding block was used to monitor force-displacement (stiffness) behavior of the gridpoints indicated in Figure 5-19(b). This provided another check on interface stiffness requirements to ensure that the interface formulation achieved load transferal between target and parent zone gridpoints with inconsequential compliance.

5.3   Elastic-Plastic Analyses

Given satisfactory performance of $FLAC^{3D}$ with linear elastic models of pile-soil systems and establishment of appropriate discretization, efforts were then directed to modeling the observed behavior of the piles in the selected case histories using the nonlinear elastic-plastic Base Soil Model (described in Appendix B) to model soil behavior. Single pile behavior (Mustang Island Test and Japanese Test) was considered first, followed by the German Test to consider group effects in terms of the in-line two-pile configuration tested. The Mustang Island Test and German Test were considered to be representative of typical "sand" sites, and the Japanese Test considered representative of a typical "clay" site. As it served the specific purpose of establishing

p-y recommendations for cohesionless (sand) soils, the Mustang Island Test provided the best data with which to make comparisons with *FLAC*³ᴰ behavior for validation and calibration purposes.

a)   Angled sliding block model

b)   Right-angled sliding block model
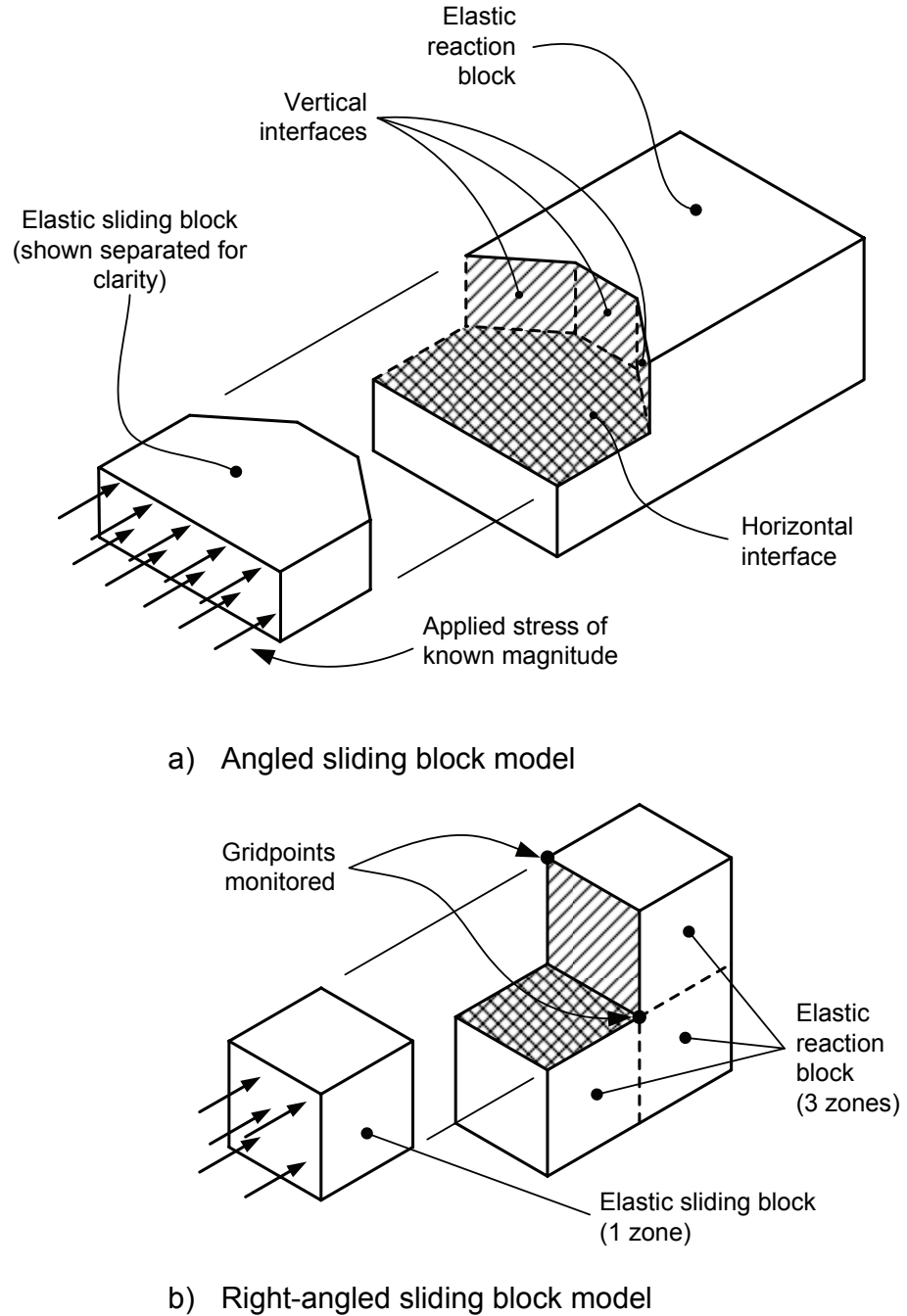
Figure 5-19: Models used to assess interface behavior

5.3.1 Single Pile Behavior

5.3.1.1 Mustang Island Test Simulation

Analysis Details

Cox, Reese and Grubbs (1974) described the field testing undertaken for the Mustang Island Test, and Reese et al. (1974) analyzed the field data in order to establish recommendations for *p-y* criteria to be used with laterally loaded single (isolated) piles in cohesionless soil conditions. Reese and Van Impe (2001, pp. 319-346) also used the Mustang Island Test as an example of a field-research investigation on *p-y* curves, providing more detailed and additional information than that given in the 1974 publications. Pile, soil and loading information garnered from these sources are indicated in Figure 5-20, where it is noted that the upper medium dense sand and dense sand layers represented soil conditions over the depth of interest for lateral loading (i.e., the "active" zone).
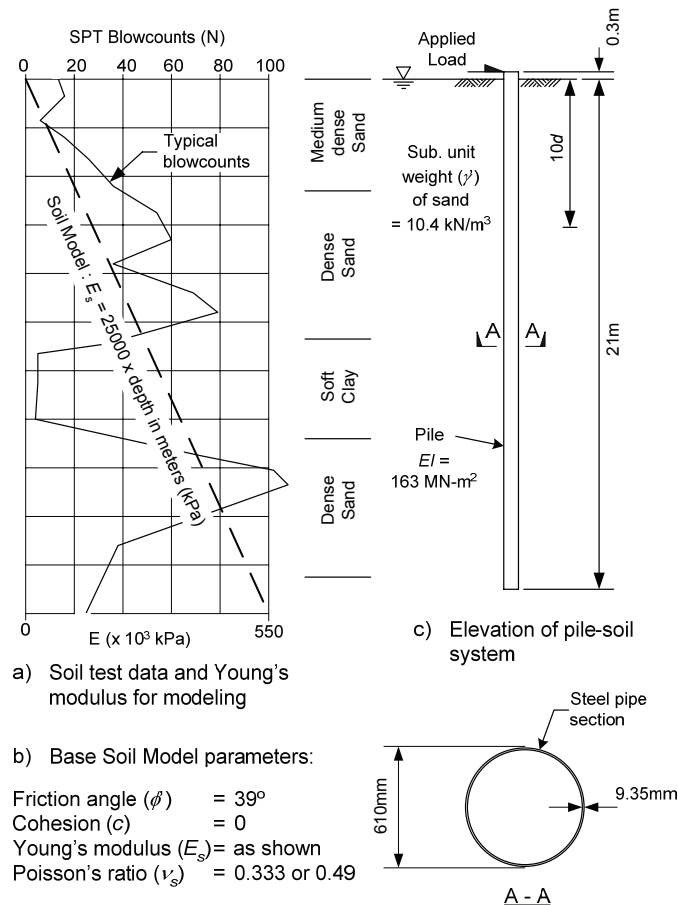
Figure 5-20: Field and modeling details for Mustang Island Test

Mohr-Coulomb (M-C) friction angle and cohesion parameters for the Base Soil Model were as reported, while the isotropic linear elastic (ILE) soil parameters were established as follows. Poisson's ratio was dictated by the ratio of initial horizontal stress to initial vertical stress (denoted by K_h) that was sought in the model, defined according to the theoretical elastic relationship

$$K_h = \frac{\nu_s}{1 - \nu_s} \quad\quad\quad\quad\quad (5.4)$$

Establishment of a Young's modulus first considered typical k_{py} values for sands (as discussed in Section 2), tabulated in Table 5-2.

Table 5-2: Recommended k_{py} values for submerged sand (from Reese and Van Impe, 2001)

Relative Density	Loose	Medium	Dense
k_{py} (MN/m³)	5.432	16.292	33.942

Making the assumption that the stiffness of the sand was zero at the surface and then increased linearly with depth (i.e., a Gibson soil), the k_{py} measure was then interpreted as a rate of increase of Young's modulus with depth, according to the relationship $E_s = k_{py} z$, where z denoted depth in consistent units. This suggested a rate of increase of Young's modulus of between 16.292 MN/m³ and 33.942 MN/m³ for the Mustang Island Test case. To establish a more specific rate of increase, the Randolph (1981) solution for a Gibson soil was used to assess the value of 25 MN/m³ that best-fitted observed pile-head load versus deflection and pile-head load versus slope behavior at a pile-head load of 22.248 kN (5 kips). This pile-head load was sufficiently small for the assumption of elastic conditions and lack of separation between pile and soil to be not unreasonable.

The same pile properties, model geometry and discretization as used for the linear Mustang Island Test pile-soil model described in section 5.2.2 applied. Interface stiffness also remained as per Table 5-1 because the maximum apparent stiffness was governed by the pile zones whose properties had not changed (in fact the higher stiffness of the pile material governed interface spring stiffness requirements in all analyses undertaken). A frictional M-C shear strength equal to that of the adjacent sand was assigned to each interface shear spring, and a tensile strength of zero was assigned to normal springs to account for possible separation between the pile and soil. As stated previously, velocity control was always used as the numerical means of applying lateral load to the pile in all analyses undertaken. To this end, a numerical algorithm was implemented to control the loading process as follows:

- Upper and lower limits to the applied velocity and unbalanced force[§] were first set by the user, together with the initial velocity to be applied to the pile gridpoints locating the point of load application.
- Velocity controlled loading proceeded by applying the initial velocity to the assigned gridpoints, then at each subsequent time step the unbalanced force was checked against the upper and lower force limits.
- If the unbalanced force was greater than its upper limit the velocity to be applied to the assigned gridpoints in the next time step was first decreased by 25%, then this new velocity checked against the upper and lower velocity limits and set at the upper limit if it exceeded it, or set at the lower limit if it was below it.

[§] *FLAC*[3D] automatically tracks the maximum force induced in a model at each time step, referred to as the "unbalanced" force, and this is used to help assess solution performance.

- Conversely, if the unbalanced force was less than its lower limit the velocity to be applied in the next time step was first increased by 25%, then this new velocity checked against its upper and lower limits in the same manner as above.

The algorithm enabled servo-control within the limits specified, allowing increases in the applied velocity in a controlled manner and thus helping to reduce running times.

Various analyses of the Mustang Island Test were undertaken as described in Table 5-3. The majority of these analyses served to assess variations of modeling parameters to help improve the understanding of $FLAC^{3D}$ pile-soil behavior, and such analyses were assigned a "parametric" status as indicated. The "simulation" status referred to those analyses undertaken as legitimate attempts at simulating the observed behavior. Uncertainty regarding the initial stress state of the soil meant that both Run 1 and Run 8 were assigned this status.

Table 5-3: Nonlinear analyses undertaken for Mustang Island Test

ID No.	Analysis Status	Description
Run 1	Simulation	Soil[1]: $K_h = 0.96$ Load[2]: $v_{min} = 1.5e-8$ m/s; $v_{max} = 1.9e-8$ m/s; $\Delta H_{min} = 10$ N; $\Delta H_{max} = 100$ N Other: -
Run 2	Parametric	Soil: $K_h = 0.96$ Load: No servo-control, constant velocity = 1.5e-8 m/s applied Other: -
Run 3	Parametric	Soil: $K_h = 0.96$ Load: No servo-control, constant velocity = 2e-8 m/s applied Other: Interface stiffness decreased to 1.6e12 (average of 2.9e12 & 2.9e11)
Run 4	Parametric	Soil: $K_h = 0.96$ Load: No servo-control, constant velocity = 2e-8 m/s applied Other: Larger annulus of dense soil discretization around pile
Run 5	Parametric	Soil: $K_h = 0.96$ Load: No servo-control, constant velocity = 2e-8 m/s applied Other: As per Run 4 and friction angle for sand decreased to 35 degrees
Run 6	Parametric	Soil: $K_h = 0.96$ Load: No servo-control, constant velocity = 1e-7 m/s applied Other: Friction angle for sand decreased to 35 degrees
Run 7	Parametric	Soil: $K_h = 0.96$ Load: No servo-control, constant velocity = 2e-8 m/s applied Other: Friction angle for sand decreased to 35 degrees
Run 8	Simulation	Soil: $K_h = 0.50$ Load: No servo-control, constant velocity = 2e-8 m/s applied Other: -
Notes:		1. K_h = ratio of horizontal to vertical stress assigned to soil zones under gravity loading. 2. v_{min} = minimum velocity, v_{max} = maximum velocity, ΔH_{min} = minimum unbalanced force and ΔH_{max} = maximum unbalanced force (used with servo-control algorithm).

Data Smoothing

Evident in all the nonlinear analyses undertaken was the ever-present issue of "noise" in $FLAC^{3D}$ (as previously discussed in connection with the linear pile-soil analyses), and a typical example is shown in Figure 5-21 regarding pile load-deflection behavior. As was the case with the linear pile-soil models, the very high stiffness of the interface springs gave rise to a system sensitive to

even the smallest of movements, causing the generation of abrupt forces each time interface springs were activated and culminating in the observed vibrational characteristics. However, unlike the linear model case, occurrence of plastic behavior in soil zones helped to alleviate the "noise" by converting some of the vibration energy into a form of energy dissipation. Nevertheless, smoothing of recorded behavior in *FLAC*[3D] was still necessary and thus data was fitted to a sixth order polynomial curve using the LINEST function available in Excel. The resultant smoothed curve is also indicated in Figure 5-21, and unless indicated otherwise, all data presented henceforth refers to smoothed data.
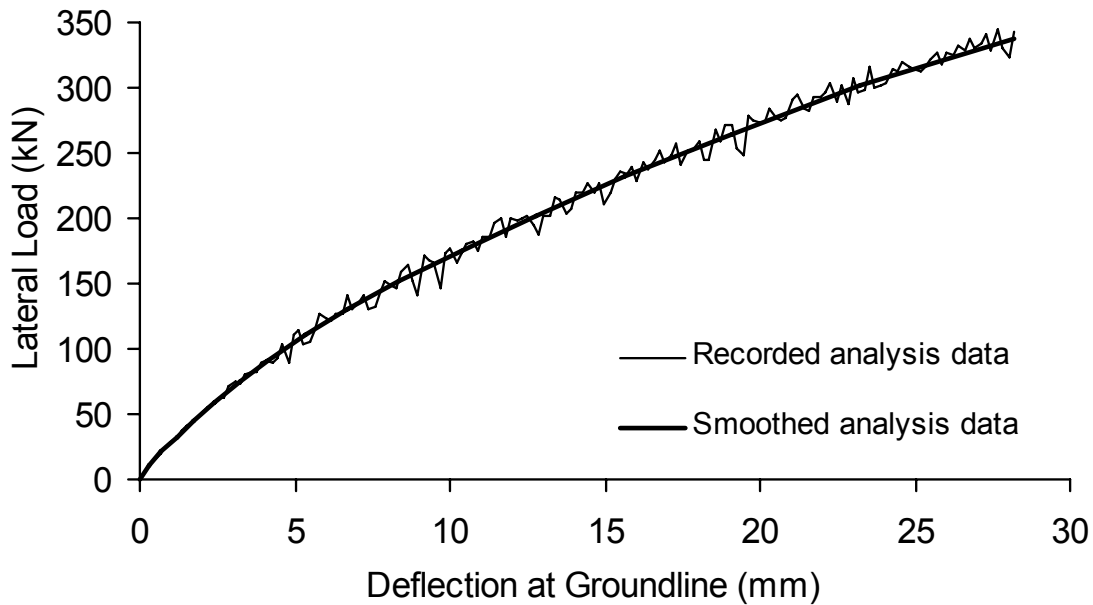
Figure 5-21: Example of dynamic "noise" generated in static *FLAC*[3D] analyses and corresponding smoothed curve

Pile-Head Behavior

Simulated versus observed pile load-deflection behavior at the groundline is shown in Figure 5-22. The excellent agreement between LPILE and observed behavior follows the fact that the Mustang Island Test provided the basis for sand *p-y* curves used in LPILE, and for this reason LPILE results were also used as a basis for comparison. Immediately apparent from Figure 5-22 was the overestimation of lateral load at a given deflection, equating to an additional load of approximately 35% of that observed for the case of an isotropic initial soil stress condition, and approximately 20% for the case where initial horizontal stresses in the soil were half the initial vertical stresses. In both simulation analysis cases, a generally constant unbalanced force equal to 2 kN was observed during time stepping, representing a very small percentage of the forces developed against the pile.
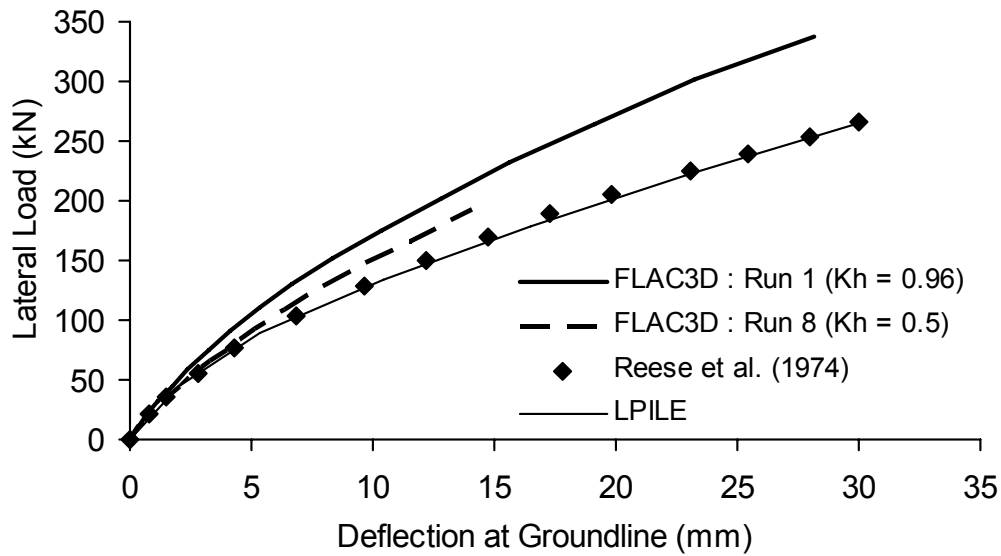
Figure 5-22: Comparison of pile load-deflection behavior for Mustang Island Test simulation analyses

The difference between $FLAC^{3D}$ and observed pile load-deflection behavior was considered to be the result of any or a combination of the following possible reasons:

- A discretized elastic-plastic soil continuum is likely to exhibit stiffer response given that real soil behavior is notorious for finding an easier path of resistance for a given deflection, or in other words nature is a far more efficient system.
- The $FLAC^{3D}$ force derived from a velocity controlled analysis must err on the high side because no matter how small the value of velocity applied, it is still a dynamic solution containing dynamic energy in addition to static energy.
- It is not for certain that the reported soil properties were representative of the soil mass contributing to the observed pile behavior, that the characterization of strength or stiffness was appropriate for the site, and what initial stress state actually existed at the site.

Differences aside, the agreement in the trend of decreasing rate of load increase with increasing deflection was encouraging from a mechanistic standpoint, indicating that the $FLAC^{3D}$ model was capturing the appropriate mode of pile-soil interaction behavior.

Results of pile load-deflection behavior from the parametric analyses are indicated in Figure 5-23 through Figure 5-26, using Run 1 and LPILE results as references. In Figure 5-23 the response curve for Run 7 refers to recorded (rather than smoothed) data, exhibiting significant scatter that was not apparent in other analyses. This behavior demonstrated a somewhat extreme example of velocity dependence in $FLAC^{3D}$, where the increase in velocity to 1e-7 m/s resulted in unrealistic force fluctuations caused by the generation of large unbalanced forces during time stepping. A concern would be use of a smoothed version of this response curve, lying closer to the observed behavior but obviously in error.
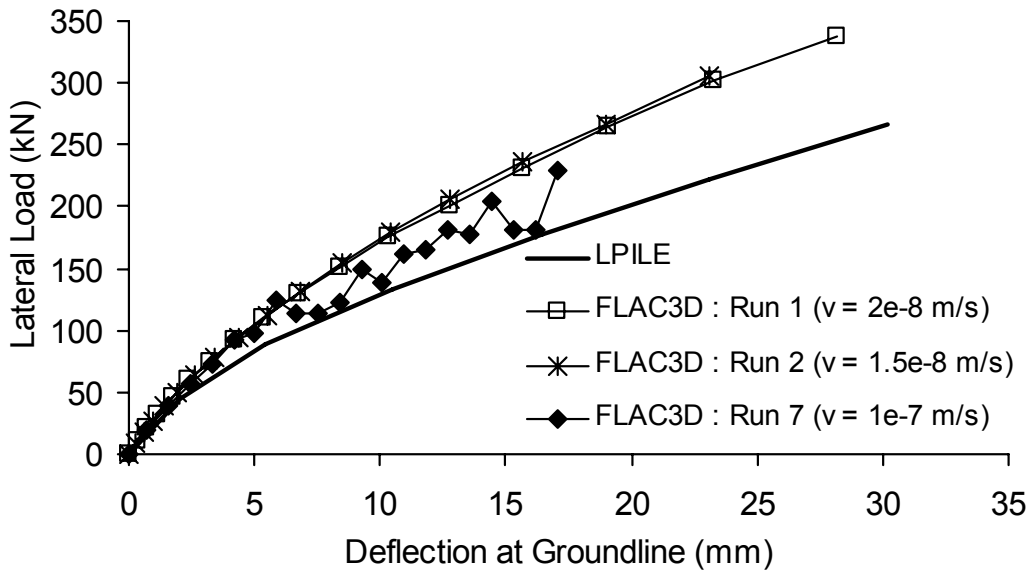
Figure 5-23: Assessment of applied velocity on pile load-deflection behavior for Mustang Island Test
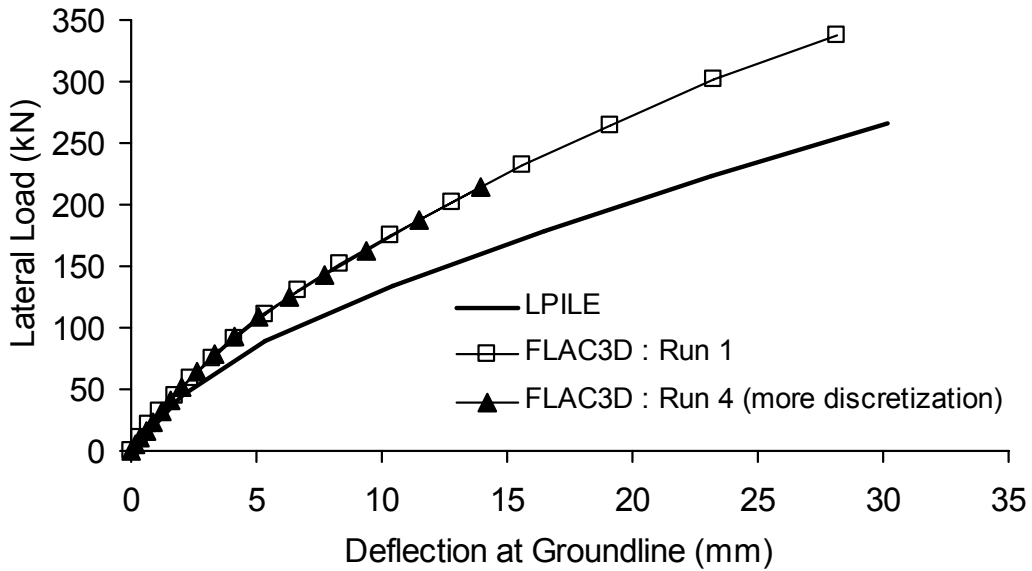
Figure 5-24: Assessment of discretization on pile load-deflection behavior for Mustang Island Test
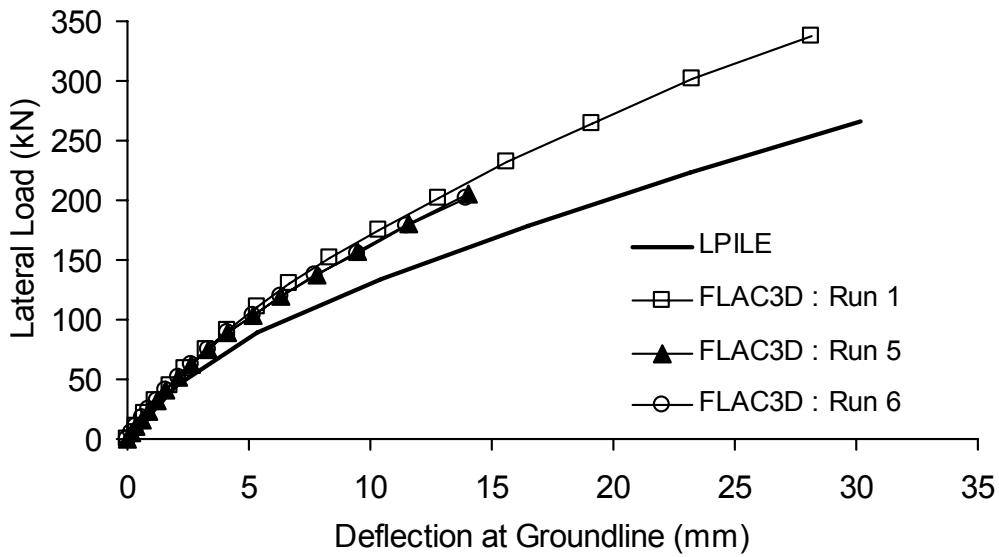
Figure 5-25: Assessment of soil strength on pile load-deflection behavior for Mustang Island Test
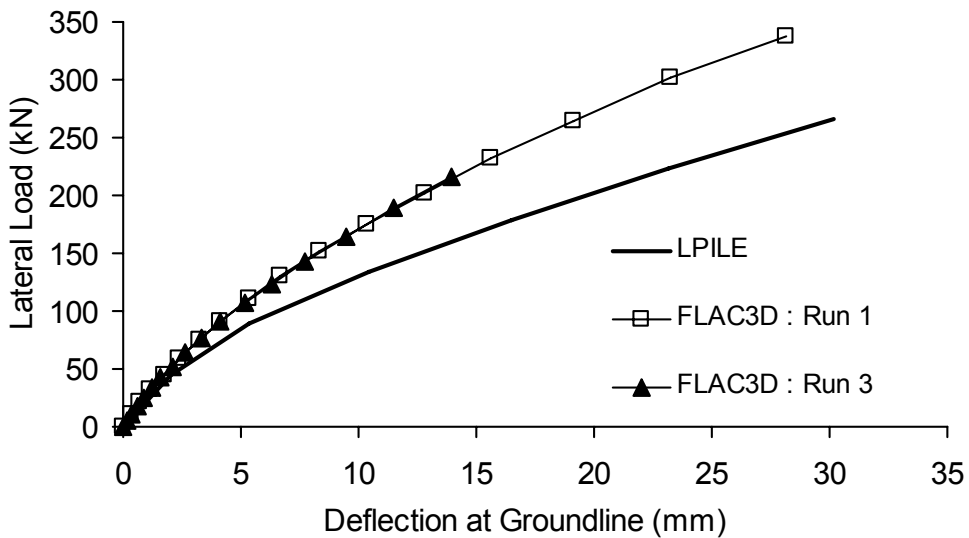
Figure 5-26: Assessment of interface stiffness on pile load-deflection behavior for Mustang Island Test

Figure 5-24 indicates no change in behavior occurred as a result of providing more discretization to the soil in the active zone, confirming the adequacy of discretization in the simulation analyses. Figure 5-25 indicates the reduced friction angle produced percentage changes in force at a given deflection less than half the percentage change in frictional strength, suggesting sensitivity to

154

strength changes was not high in this case. Figure 5-26 indicates no change in behavior occurred when the interface stiffness was reduced to a value halfway between the maximum apparent stiffness and the recommended value of ten times the maximum apparent stiffness. This provided the justification to relax the recommended interface stiffness value in later analyses to help reduce model sensitivity without compromising solution accuracy.

Lengthwise Behavior

A comparison of $FLAC^{3D}$ and LPILE structural actions developed along the pile with increasing load level is shown in Figure 5-27, where H denotes the lateral load applied to the pile. Although only shown for the Run 1 simulation analysis, $FLAC^{3D}$ results for the other analyses were very similar as suggested by the closeness in pile load-deflection behavior results. The discrepancy in pile shear values at the groundline was due to differences in the way pile shear and pile loading was calculated: In the case of pile shear the procedure as described in section 5.2.1 applied, whereas pile loading was calculated by summing the horizontal force components mobilized at each interface spring. The pile loading therefore represented the total lateral resistance mobilized against the deflected pile by the surrounding soil continuum, equilibrium demanding that this be equal and opposite to the lateral load applied to the pile. In the $FLAC^{3D}$ model this was not quite the case because the velocity controlled loading induced a total unbalanced force at the point of load application (0.3 m above the groundline) that was inevitably higher due to dynamic effects. Thus pile shear in the vicinity was locally elevated above "normal" values.

p-y Behavior

In conjunction with the structural actions developed along the pile, *p-y* curves were extracted from the $FLAC^{3D}$ analysis using three methods of obtaining the soil resistance *p* mobilized against the pile: (a) Using the interface, which enabled the soil resistance at a given deflection to be calculated directly by summing the horizontal components of shear and normal forces mobilized in the interface springs around the discretized pile circumference, (b) derived from the bending moment values calculated along the pile by fitting a sixth-order polynomial equation to the data and differentiating twice to obtain soil resistance, and (c) derived from the shear force values calculated along the pile by fitting a sixth-order polynomial equation to the data and differentiating once to obtain soil resistance. Pile deflection was obtained directly from the gridpoints located along the centerline of the modeled pile. In this way a check on the consistency of structural actions was possible through inspection of how close in agreement the differently derived *p-y* curves were to each other.

Comparative *p-y* curves according to $FLAC^{3D}$ (Run 1 simulation analysis) and the Reese et al. (1974) criteria are indicated in Figure 5-28. These show good agreement in the initial portions of the curves, but with increasing deflection a far more stiff response is apparent in the $FLAC^{3D}$ case. Such behavior reflects the differences seen with the pile load-deflection behavior, again emphasizing the limitations of any continuum-based discretization method in capturing all behavioral mechanisms, and the uncertainties in actual values of strength parameters including initial lateral stress conditions.

$FLAC^{3D}$ Performance

The simulation and parametric analyses undertaken for the Mustang Island Test indicated that $FLAC^{3D}$ produced a stiffer response than what was observed, but overall trends in pile-soil interaction behavior with increasing load levels agreed with those observed. Thus $FLAC^{3D}$ performed satisfactorily from a qualitative standpoint, but was less so from a quantitative

standpoint. Given the intended application of *FLAC*[3D] to assess pile group effects and the associated emphasis on relative behavior as discussed in section 5.2.2, the poor quantitative performance was not considered to be a serious limitation. Thus the overall performance of *FLAC*[3D] in connection with isolated pile behavior was judged to be sufficiently accurate for the research purposes at hand.
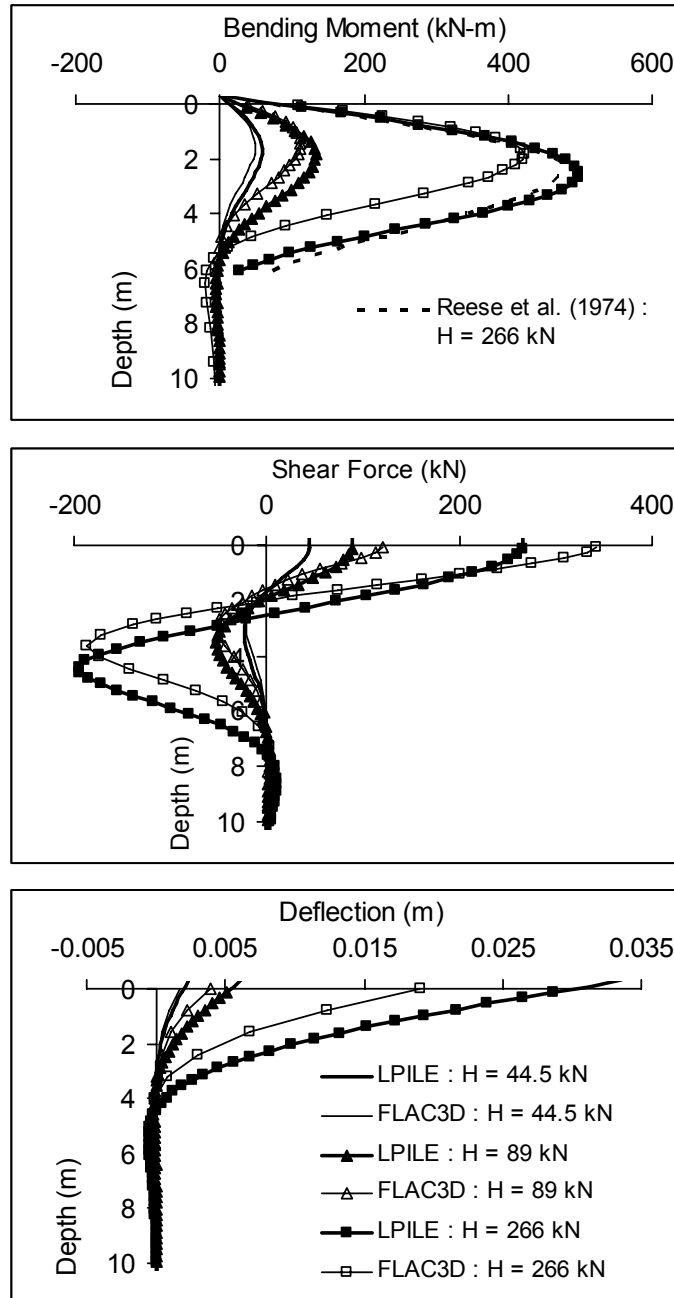
Figure 5-27: Comparison of Run 1 simulation analysis and LPILE bending moment, shear force and deflection behavior for Mustang Island Test

156
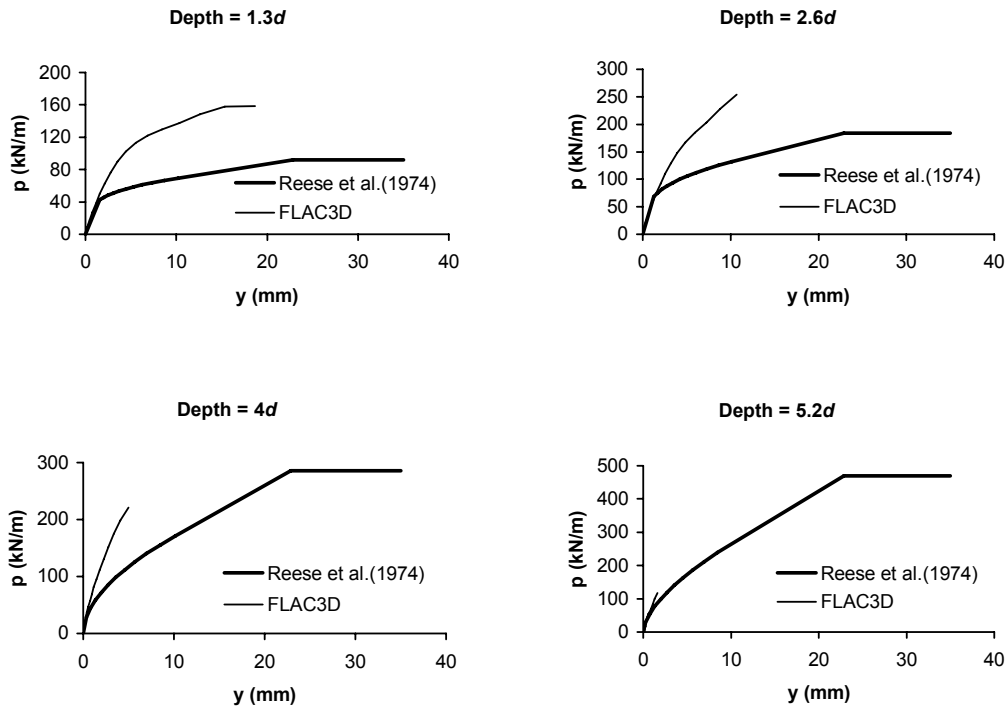
Figure 5-28: Comparison of Run 1 simulation analysis and Reese et al. *p-y* curves for the Mustang Island Test

5.3.1.2   Japanese Test Simulation

The sufficient success achieved with the Mustang Island Test provided a validation of $FLAC^{3D}$ for isolated pile behavior, but additional assurance was sought for the case of cohesive (clay) soil conditions. The *p-y* research test undertaken on a steel pipe pile ($d = 320$ mm, $L/d = 39$) installed in soft clay at Sabine, Texas (Matlock, 1970), was initially chosen for this purpose. However, as is discussed in section 5.4, this proved unsuccessful given practical limitations resulting from the high stiffness of the Sabine pile in $FLAC^{3D}$. The Japanese Test case history was therefore utilized, consisting of a free-head lateral load test undertaken in Japan (circa 1965) and reported in Reese (1986, pp. 215-216) and Reese and Van Impe (2001, pp. 267-269). Pile, soil and loading information obtained from these sources are shown in Figure 5-29.

Analysis Details

Details of pile properties, interface stiffness, and pile-soil model geometry for the $FLAC^{3D}$ simulation of the Japanese Test were given in section 5.2.2. Shear strength mobilized at the interface of the pile and soil in the test was assumed to be equal to the shear strength of the soil. Interface shear springs were therefore assigned a cohesive shear strength increasing with depth in accordance with soil strength. A tensile strength of zero was assigned to the normal springs to account for possible separation between the pile and soil. In terms of the elastic-plastic Base Soil Model, M-C parameters were as shown in Figure 5-29, and followed the reported field values.

Determination of ILE parameters were as follows. Poisson's ratio of 0.49 followed the assumption of undrained soil behavior, noting that a value of 0.5 could not be specified in $FLAC^{3D}$ given that this corresponded to an infinite bulk modulus. Young's modulus was established by drawing on the typical correlation between undrained shear strength and stiffness for soft (normally consolidated) clay. To this end three different correlation relationships were assessed: $E_s = 150s_u$, $E_s = 200s_u$ and $E_s = 250s_u$. The assessment procedure used the Randolph (1981) elastic pile-soil model to test each correlation relationship for goodness of fit with observed pile-head load-deflection values. In this way the correlation relationship $E_s = 150s_u$ was determined to be the best estimate for modeling purposes. Loading was applied using the servo-control algorithm with v_{min} = 5e-9 m/s, v_{max} = 1e-6 m/s, ΔH_{min} = 150 N and ΔH_{max} = 200 N (a description of the servo-control algorithm and definition of parameters was given in section 5.3.1.1).
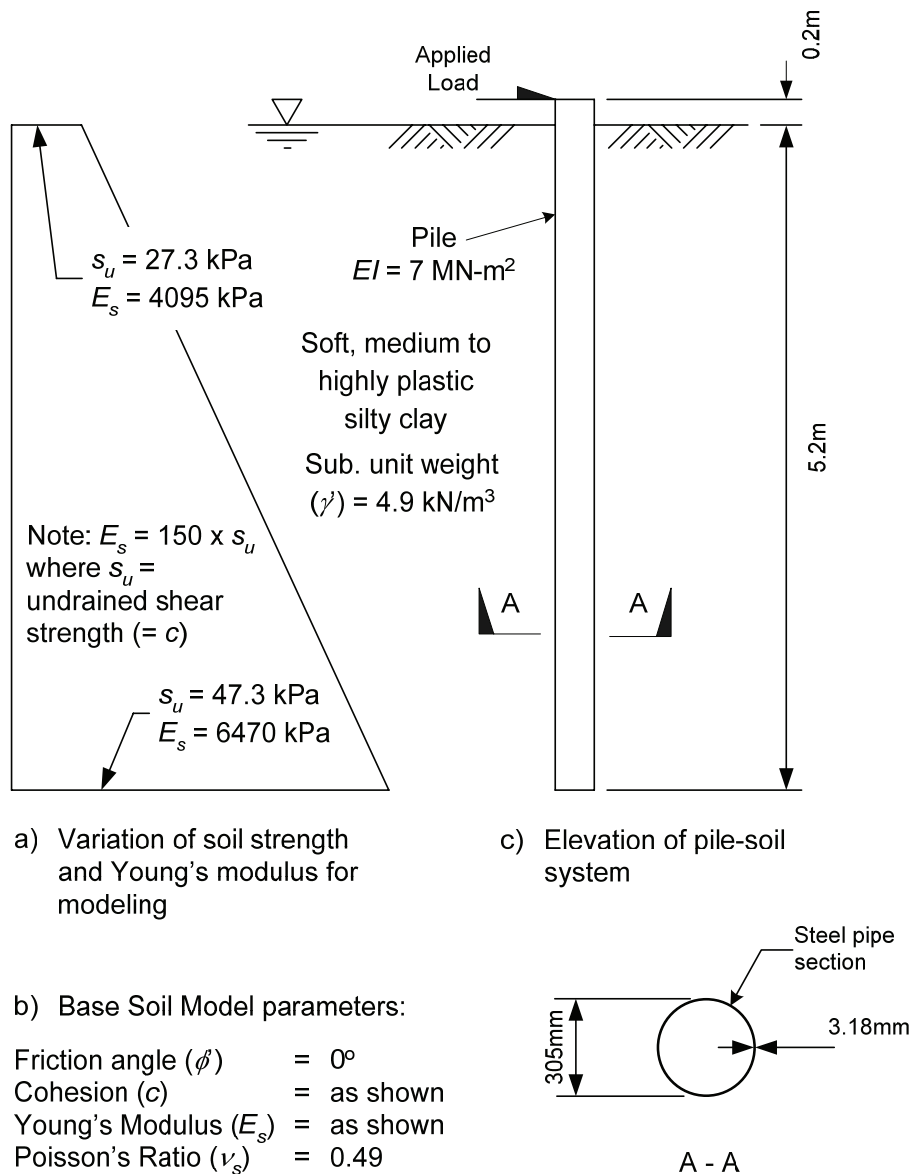
Figure 5-29: Field and modeling details for Japanese Test

158

FLAC^3D Performance

Confirmation that *FLAC*^3D performed adequately in the cohesive soil case is apparent from the comparisons shown in Figure 5-30 through Figure 5-32. As expected the *FLAC*^3D simulation exhibited stiffer response and under-predicted maximum bending moments, but the trends in behavior portrayed appropriate interaction characteristics. It is apparent from Figure 5-31 that pile behavior at depth was less satisfactory, attributed to the coarse discretization provided at this location (refer Figure 5-10) enforcing behavior that was too rigid. This again highlighted the need for appropriate discretization of the pile over its length, particularly in cases like the Japanese Test where the pile length was not overly greater than its critical length.
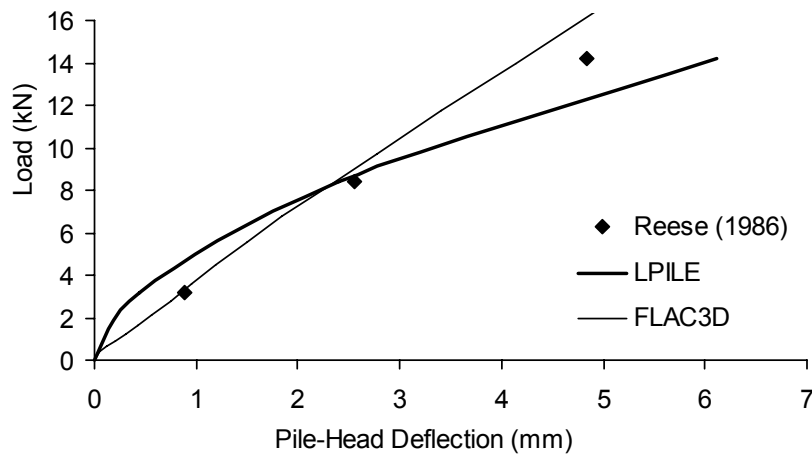
Figure 5-30: Comparison of *FLAC*^3D, LPILE and observed pile-head load-deflection behavior for Japanese Test
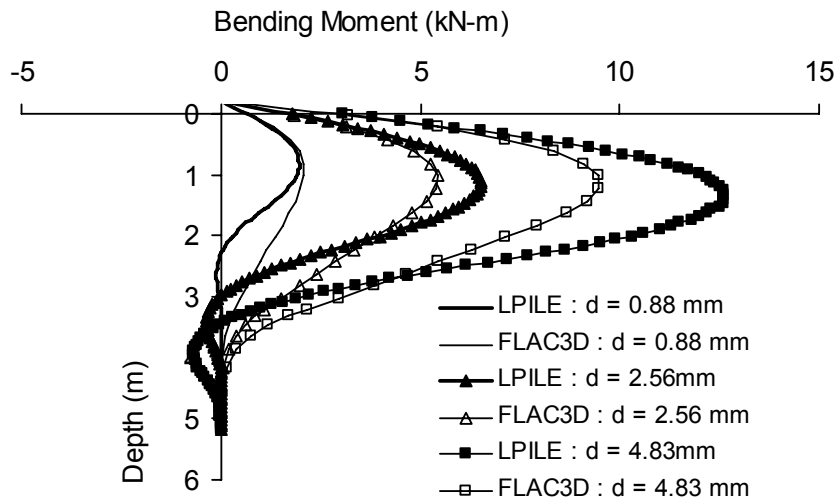
Figure 5-31: Comparison of *FLAC*^3D and LPILE bending moment behavior with increasing pile-head deflection (d) for Japanese Test

159
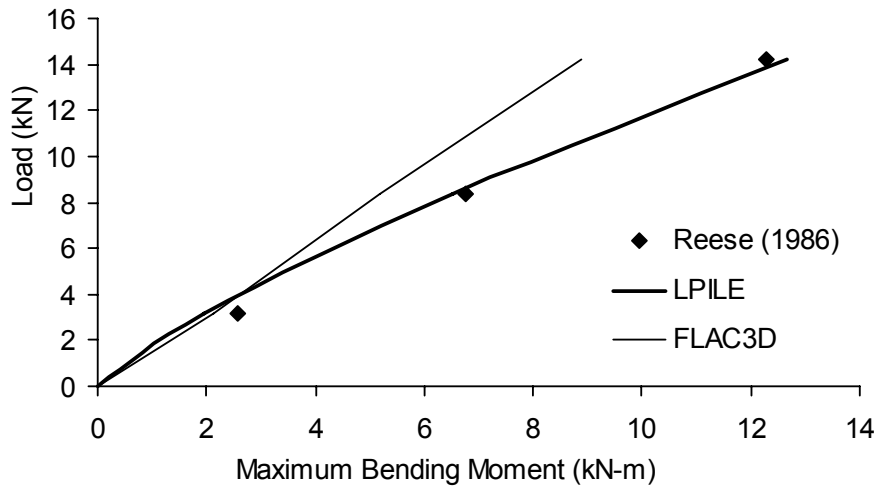
Figure 5-32: Comparison of *FLAC*[3D], LPILE and observed pile-head load versus maximum bending moment behavior for Japanese Test

a) Variation of Young's modulus for modeling

c) Elevation of pile-soil system

b) Base Soil Model parameters:

Friction angle (ϕ) = 39°
Cohesion (c) = 0
Young's modulus (E_s) = as shown
Poisson's ratio (v_s) = 0.333 or 0.49
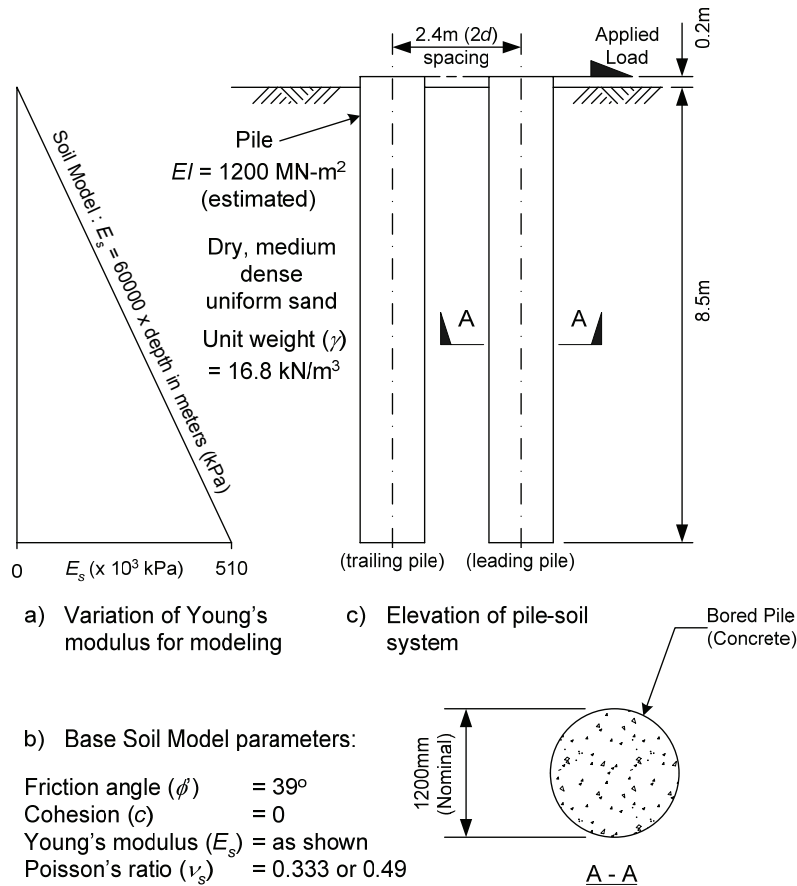
Figure 5-33: Field and modeling details for German Test

$\Sigma H = H_1 + H_2$

d — Leading pile

H_1 = loading applied to leading pile

$2d$

Trailing pile

H_2 = loading applied to trailing pile

Plan View
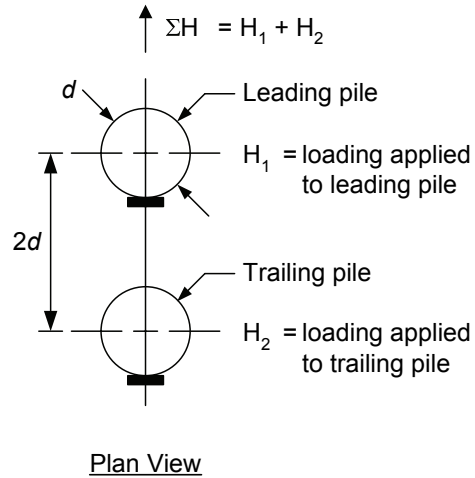
Figure 5-34: Loading configuration and terminology for German Test

5.3.2   In-Line Two-Pile Group Behavior

An assessment of group behavior performance in $FLAC^{3D}$ was predicated on a lateral load test undertaken on relatively short ($L/d = 7$) bored piles consisting of a leading and trailing pile configuration loaded "in-line", as reported in Schmidt (1985). The group test (designated "C 2/2" by Schmidt but referred to here as the German Test) was one in a series of three tests on in-line group configurations. Details of pile, soil and loading conditions for the test are shown in Figure 5-33 and Figure 5-34.

Analysis Details

Figure 5-35 through Figure 5-39 provide details of model geometry and discretization, where procedures to establish these have been discussed previously.

$n = 43 @ 0.2\ m$
$(8.6\ m)$

1.2 m

Cross-sectional

Lengthwise
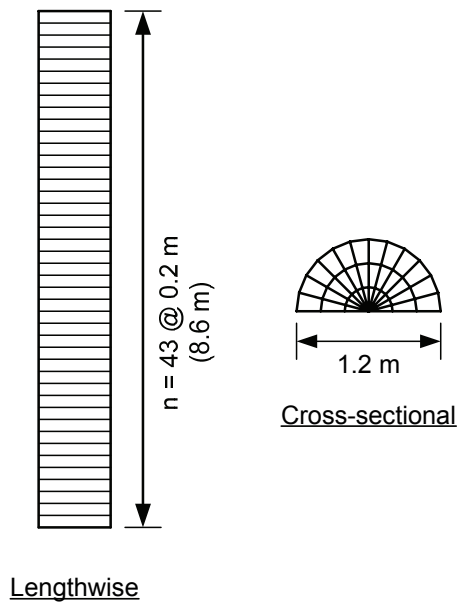
Figure 5-35: Pile discretization for German Test pile-soil model
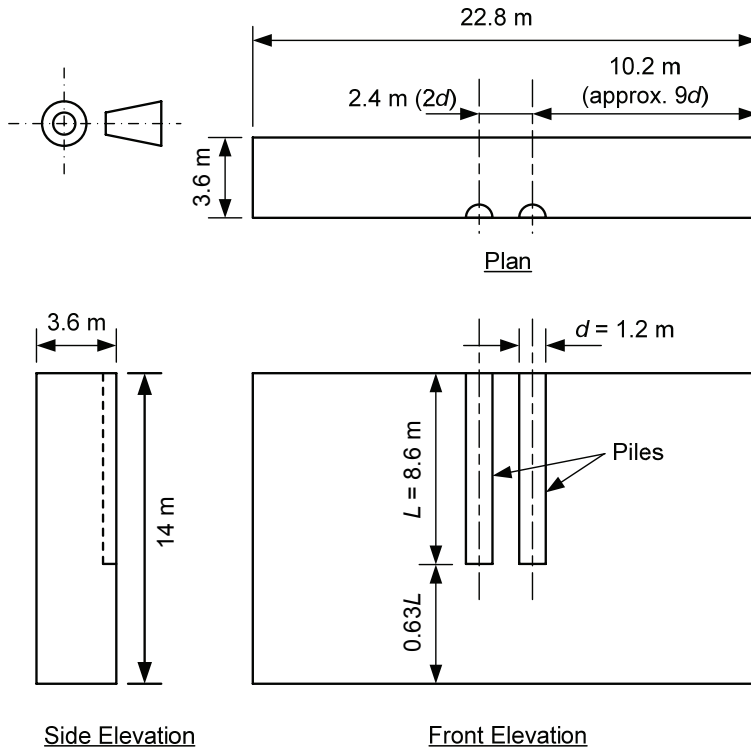
Figure 5-36: German Test pile-soil model geometry
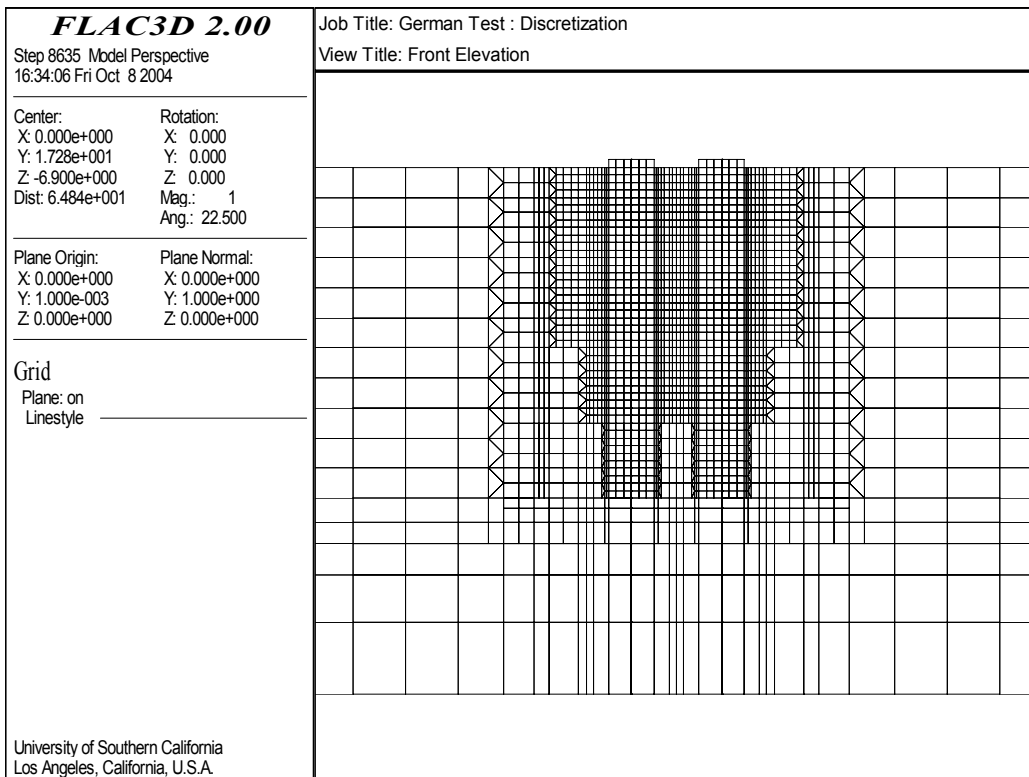
Figure 5-37: Front elevation discretization for German Test pile-soil model

162
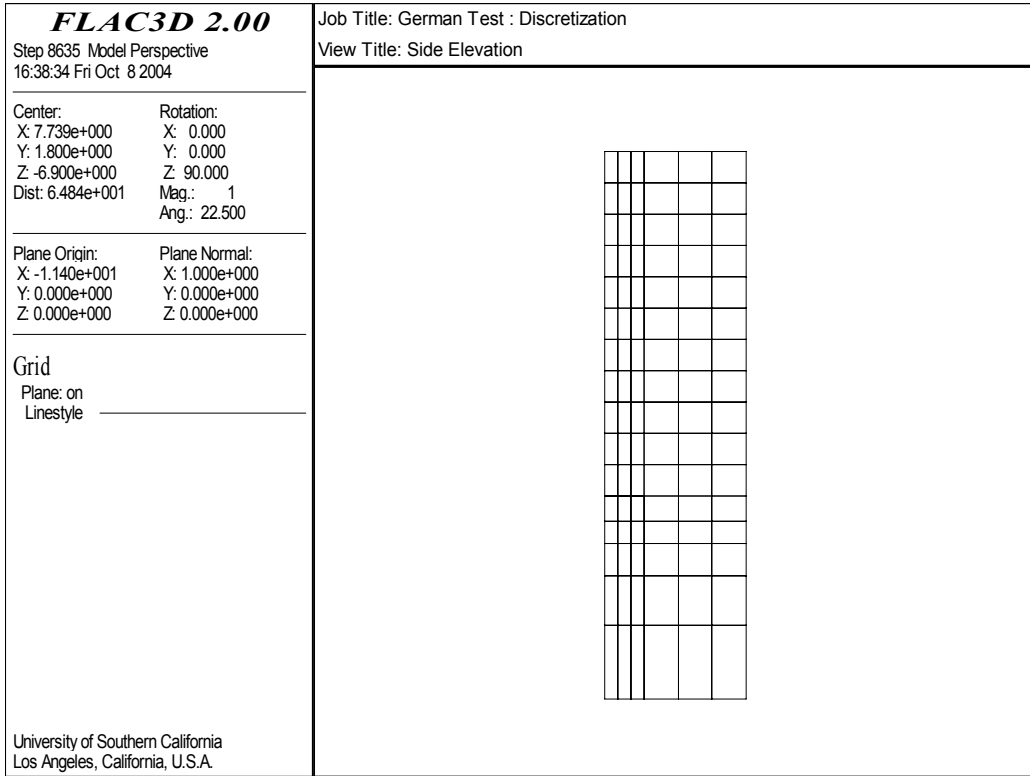
Figure 5-38: Side elevation discretization for German Test pile-soil model
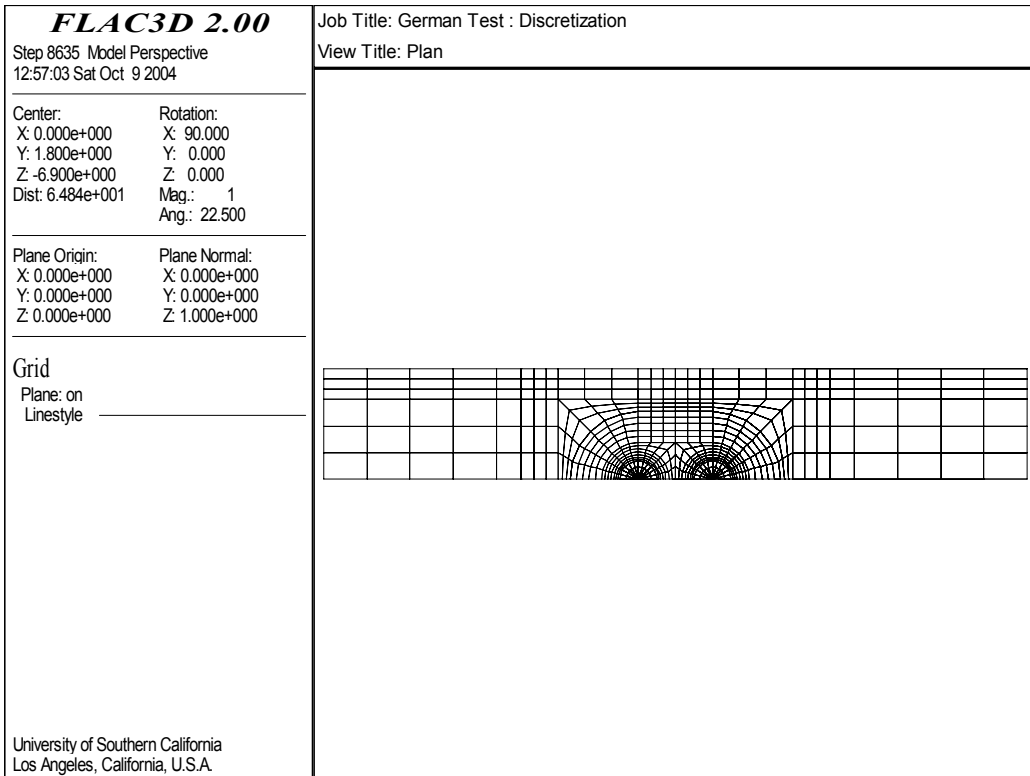
Figure 5-39: Plan discretization for German Test pile-soil model

Base Soil Model parameters are indicated in Figure 5-33, and elastic modeling properties are given in Table 5-4. Soil and pile properties were assessed from information provided in Schmidt (1985), noting the following:

1. A flexural stiffness for the bored pile was not given in Schmidt, but structural actions (deflection and bending moment), together with a characterization of the soil in terms of linear subgrade moduli at three load levels, were provided. This information was utilized to estimate a flexural stiffness of the pile as described in Dodds (2005).

2. The soil was described in Schmidt as dry, medium dense uniform sand, and k_{py} values for medium and dense sand above the watertable (Reese and Van Impe, 2001, p. 87) are 24.4 MN/m^3 and 61 MN/m^3, respectively. Apparent k_{py} values varied between 24.6 MN/m^3 and 127.2 MN/m^3.

3. Typical dry densities for medium dense and dense sands are 1,500 – 1,800 kg/m^3 and 1,700 – 2,000 kg/m^3, respectively (Carter and Bentley, 1991, p. 40).

Two simulation analyses were undertaken to assess initial stress conditions corresponding to an isotropic stress state ($K_h = 0.96 \approx 1.0$), and a stress state where horizontal stresses were set equal to half the vertical stresses ($K_h = 0.5$). The $K_h = 0.5$ simulation utilized the servo-control algorithm to apply loading with v_{min} = 5e-9 m/s, v_{max} = 1e-7 m/s, ΔH_{min} = 150 N and ΔH_{max} = 1000 N, while the $K_h = 0.96$ simulation applied loading with a constant velocity equal to 4e-8 m/s.

Table 5-4: Elastic properties for German Test pile-soil model

Elastic Properties	Value
Pile:	
Young's modulus, E_p	11.789[1] GPa
Poisson's ratio, v_p	0.2
Soil:	
Young's modulus, E_s	60000z[2] kPa
Poisson's ratio, v_s	0.333 or 0.49
Interface:	
Normal spring stiffness, k_n	1.63 x 10^6 kPa/m
Shear spring stiffness, k_s	1.63 x 10^6 kPa/m
Notes: 1. Estimated value as detailed in Dodds (2005). 2. z refers to depth in meters.	

FLAC³D Performance

Comparisons between *FLAC³D* and observed behavior of the piles at the point of load application (0.2 m above the ground surface) are shown in Figure 5-40 and Figure 5-41. The greater differences with load-deflection values apparent in Figure 5-41 compared with Figure 5-40 suggest a $K_h = 0.5$ soil condition existed at the site, which is a condition that one would tend to expect given the minimal disturbance afforded by the pile installation procedure. Less smoothness in the $K_h = 0.96$ curves was the result of the constant velocity loading inducing greater unbalanced forces during the analysis (up to 10 kN), compared with the servo-controlled $K_h = 0.5$ analysis that only recorded a maximum unbalanced force of 1.5 kN. Most important to note, however, is the correct trend of decreasing trailing pile resistance with increasing deflection in both cases, and the lesser sensitivity of the H_2/H_1 ratio value to absolute errors in load-deflection behavior. This provided a validation of the ability of *FLAC³D* to reproduce the type of group effects that have been repeatedly observed in field tests on pile groups.
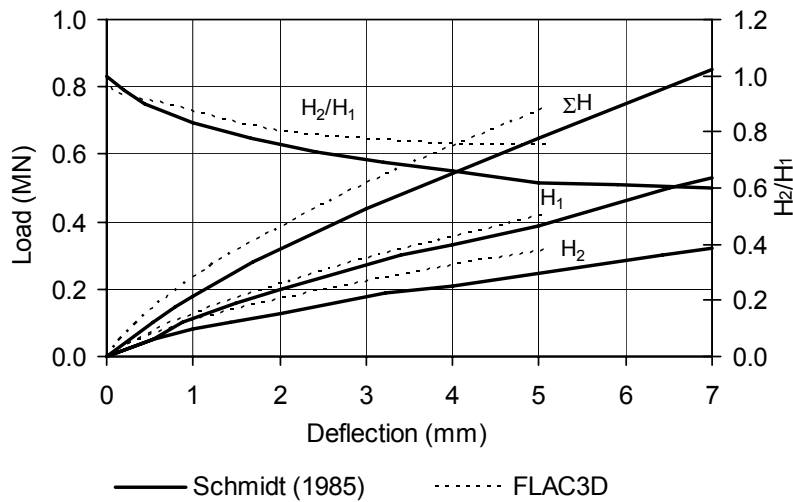
Figure 5-40: Comparison of FLAC3D simulation (Kh = 0.5) and observed behavior for German Test
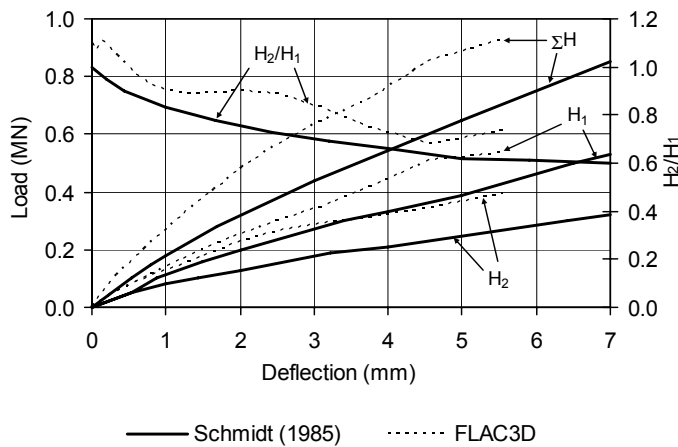
Figure 5-41: Comparison of *FLAC³D* simulation ($K_h = 0.96$) and observed behavior for German Test

5.4   Limitations

The assessment undertaken to address the verification, validation and calibration aspects of the research revealed $FLAC^{3D}$ to be a numerical tool certainly capable of performing the task required of it, but not without limitations. Such was the case when attempts were made to simulate the lateral load test on an instrumented steel pipe pile (d = 0.33 m, L/d = 39) at a soft clay site near the mouth of the Sabine River in Texas (Matlock, 1970). Initially chosen as the case history to assess the performance of $FLAC^{3D}$ isolated pile behavior in clay, numerous analysis attempts were made but all proved inadequate. The cause of the problem was finally attributed to the high stiffness of the $FLAC^{3D}$ pile and associated extreme sensitivity of the numerical pile-soil system to movement.

In order to quantify the problem, the stiffness characteristics of the Sabine pile-soil system were compared with those of the Mustang Island Test pile-soil system using the flexibility ratio (K_R) measure (Poulos, 1971a). Stiffness characteristics are shown in Figure 5-42. The flexural stiffness of the Sabine River pile was based on the pile properties reported in Matlock (1970), in conjunction with information reported in Reese and Van Impe (2001, p. 269). Soil stiffness was assessed using the Randolph (1981) elastic pile-soil model to back-calculate a best-fit distribution at a pile deflection of 5 mm (0.015d), using a stiffness increase with depth based on the increase of the initial stiffness of soft clay p-y curves with depth. Mustang Island Test characteristics were as discussed in section 5.3.1.1.
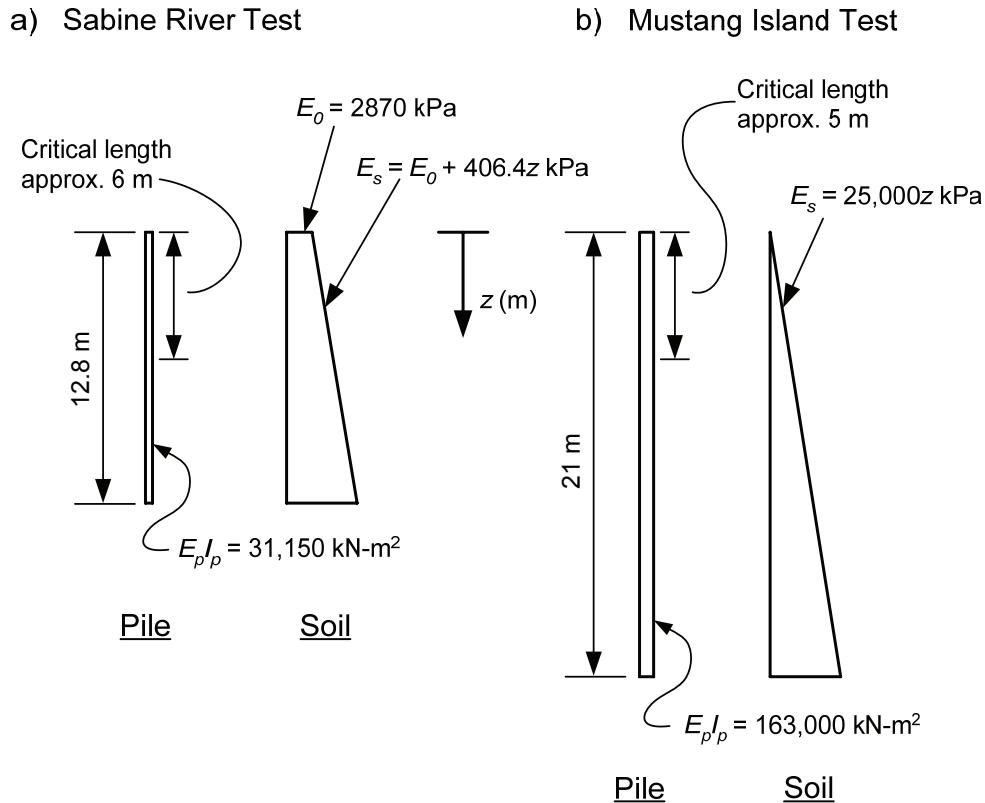
Figure 5-42: Estimated soil stiffness characteristics and pile flexural stiffness values for Sabine River and Mustang Island test pile-soil systems

166

A unique soil stiffness value for each site was established by using the average stiffness over the critical length of the pile, defined in accordance with Randolph (1981). These values were 5,680 kPa in the Sabine case, and 60,070 kPa in the Mustang Island case. Resultant K_R values were thus

$$\text{Sabine:} \quad K_R = \frac{31150}{5680 \times 6^4} = 0.0042 \tag{5.5}$$

$$\text{Mustang Island:} \quad K_R = \frac{163000}{60070 \times 5^4} = 0.0043 \tag{5.6}$$

This indicated that the Mustang Island pile was slightly less flexible compared with the Sabine pile, but certainly not so different as to be a problem. Inspection of the equivalent modulus ($E_{p\text{-}equiv.}$) values for each pile, however, revealed the root of the problem:

$$\text{Sabine:} \quad E_{p-equiv.} = \frac{31150}{\pi \times 0.33^4 / 64} = 53.51 \times 10^6 \ \text{kPa} \tag{5.7}$$

$$\text{Mustang Island:} \quad E_{p-equiv.} = \frac{163000}{\pi \times 0.61^4 / 64} = 23.98 \times 10^6 \ \text{kPa} \tag{5.8}$$

This indicated that the numerical stiffness of the Sabine pile was over twice that of the Mustang Island pile, necessitating an interface stiffness of 1.3e13 compared with 2.9e12 specified in the Mustang Island simulations.

Possessing such a high stiffness is problematic on several accounts: (a) Extremely long computation times in real time are required, given the extremely small velocity increments required to push the numerical pile; (b) introduction of errors into the analysis is facilitated through the inherent velocity dependence; and (c) discretization needs are amplified due to the high stiffness of the numerical pile. Such problems were evident in the Sabine analysis attempts, beginning with pile discretization needs that are indicated in Figure 5-43. Very dense lengthwise discretization requirements are apparent, with n = 72 discretization (corresponding to 0.1 m thick zones) still not ideal.

In terms of simulation problems, applied velocities in the order of 1e-9 m/s were typical for the Sabine pile-soil model, corresponding to computation times of almost a day of real time to move the pile two-tenths of a millimeter. Obviously this is impractical, and attempts to speed up the process by increasing the applied velocity invited more problems. This is indicated in Figure 5-44, where a local jump in pile load-deflection behavior manifested itself from a seemingly innocuous "ramping" of the velocity from 1e-9 m/s up to 1e-8 m/s over 100,000 time steps. Extreme sensitivity was clearly exhibited by the pile-soil system in $FLAC^{3D}$, eventually forcing the abandonment of the test in favor of the Japanese Test.
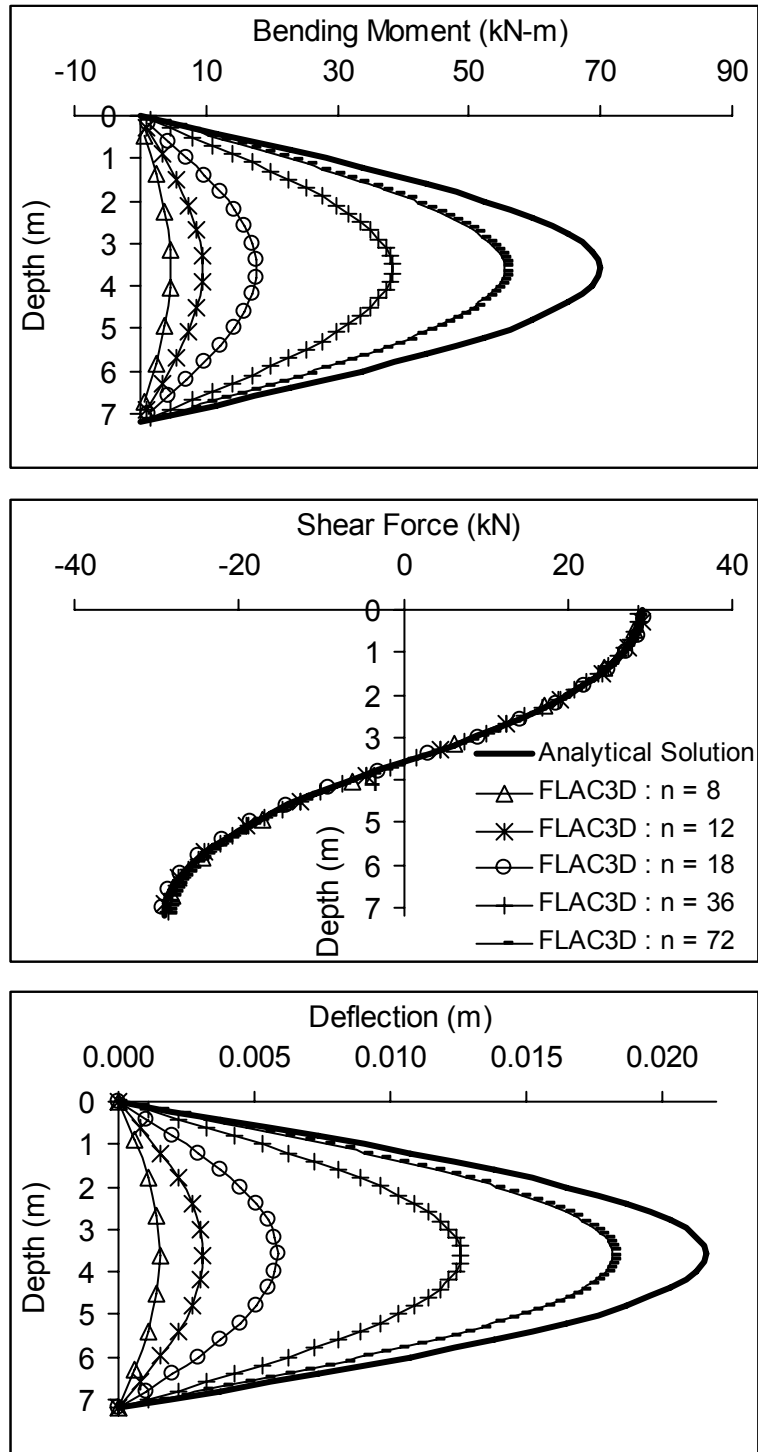
Figure 5-43: Discretization assessment results for Sabine Rive Test simply-supported, triangular-loaded pile configuration (s = 12, t = 3)
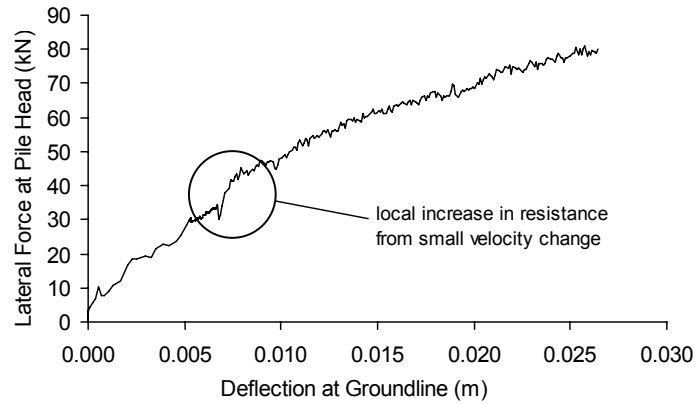
Figure 5-44: Example of sensitivity due to high stiffness of system

Given the problems encountered with the Sabine River analyses, a restriction on piles analyzed in *FLAC*³ᴰ was necessary. The limitation in this respect is evident from Figure 5-45, presenting equivalent modulus values for standard steel pipe sections together with appropriate modulus values for various piles used in reported case histories, including those used for the purpose of the current research. The much higher stiffness of the Sabine case compared with other case histories is clearly seen, and the trend of the data suggests a limitation in terms of the diameter of the pile to be modeled in *FLAC*³ᴰ. Steel pipe piles analyzed in the research were restricted to a diameter no less than 500 mm for this reason.
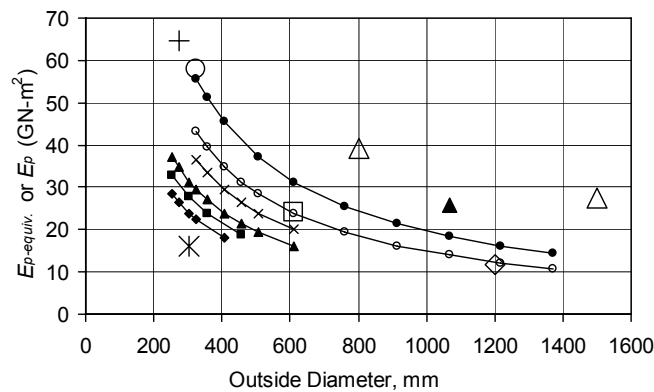
Legend:

— Steel pipe thickness = 4.775 mm
— Stee pipe thickness = 5.563 mm
— Steet pipe thickness = 6.350 mm
— Steel pipe thickness = 7.925 mm
— Steel pipe thickness = 9.525 mm
— Steel pipe thickness = 12.700 mm
▲ Steel pipe thickness = 18 mm
✳ Japanese Test - Soft Clay (Reese, 1986)
○ Sabine River Test - Soft Clay (Matlock, 1970)
□ Mustang Island Test - Med. to Dense Sand (Reese et al., 1974)
◇ German Test - Dense Sand (Schmidt, 1985)
+ NCHRP 24-9 - Sand and Clay (Brown et al., 2001)
△ Taiwan - Loose to Med. Dense Sand (Huang et al., 2001)

Figure 5-45: Pile modulus versus outside pile diameter for standard pipe pile sections and various field case-histories

169

SECTION 6
LARGE PILE GROUP STUDY

6.1   Introduction

Various aspects to consider when undertaking a numerical study of large pile group behavior are now apparent. Many issues involved with observed isolated and group pile-soil behavior are evident in the review of lateral pile-soil interaction provided in Sections 2 and 3, presenting a subject rich in empirical content and masked by its complexity. This in itself presents numerous modeling facets to appreciate and overcome, including the formidable challenge of soil behavior that has been discussed in Dodds (2005). Modeling capabilities are no less demanding, requiring a three-dimensional framework to properly assess the mechanics of interaction, and a formulation able to account for geometric and material nonlinearities as a matter of course.

In respect to modeling capabilities, the formulation of $FLAC^{3D}$ presented in Section 4 indicates the program is an able tool. However, as was demonstrated in Section 5, the performance of $FLAC^{3D}$ is not without its limitations from both an accuracy and practicable capability standpoint. Inherent with any three-dimensional continuum-based numerical approach is the tendency for less flexible behavior than actually exists, but this is exacerbated in $FLAC^{3D}$ by the restriction to constant-strain elemental components used in constructing pile and soil entities. Furthermore, the dynamic nature of $FLAC^{3D}$ asserts additional influences through forces induced as a result of the sensitivity of the pile-soil system to movement. Attention to providing sufficient detail in order to obtain sufficient accuracy is therefore of utmost importance in $FLAC^{3D}$, but this must be tempered with practicable considerations to limit the stiffness of elemental components so as not to pollute results or impede analysis progress.

The physical extent of a large pile group also imposes limits when using $FLAC^{3D}$, given that the computational environment in which $FLAC^{3D}$ operates is simply unable to cope with the computational burden that a fully three-dimensional model of the entire group would present. This is a limitation that applies to three-dimensional numerical programs in general, the review of lateral group effects suggesting that a 3 x 3 pile group is likely to be the largest configuration so far to have been modeled in such a way. A modeling economy, be it representation of piles as line elements or depicting behavior within the group using simplified models of group piles, is therefore a commonplace technique applied in numerical studies of pile groups. The periodic boundary concept developed for large pile groups (Law and Lam, 2001), as discussed in Section 3, is just an example of such a technique, and represents the essence of large pile group behavior investigated in this study.

6.2   Research Methodology

6.2.1   General Strategy

The basic precept of the research was use of numerical pile-soil models to investigate pile-soil-pile interaction of large pile groups. This was undertaken on the basis of a rationalization of a large pile group subject to lateral loading using two pile-soil model configurations: The first consisted of a two-pile configuration loaded in-line and representing leading and trailing piles of rows of infinite number of piles at a given center to center spacing (the spacing perpendicular to the direction of loading being the same as the spacing in the direction of loading). This was utilized to approximate typical leading and immediately trailing piles of a large pile group. The second consisted of a periodic (single) pile model configuration to represent typical interior piles, where the periodic assumption of recurring rows of infinite number of piles at a given center to center spacing is a reasonable approximation (once again the spacing being the same in the directions parallel and perpendicular to the direction of loading). A schematic of this large pile group rationalization is shown in Figure 6-1.
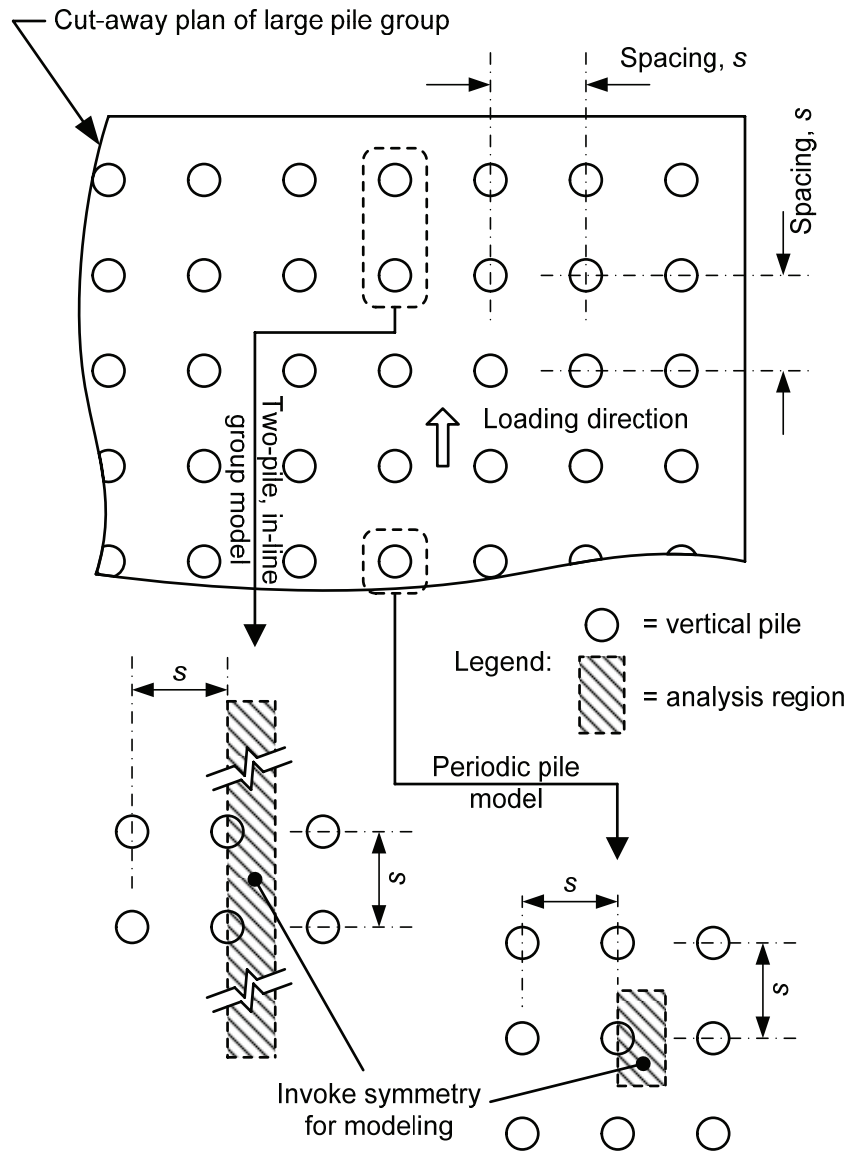
Figure 6-1: Large pile group rationalization using in-line and periodic pile-soil models

Accompanying the large pile group models was a pile-soil model simulating the same pile and soil as used in the group models, but assuming the pile to be laterally loaded in isolation. This was used to assess group effects through examination of the difference in behavior between the group and isolated pile-soil models. The assessment was limited to the case of a horizontal shear load applied to the pile head, where the pile head was located at the groundline. Equal displacement of pile heads was also specified for the in-line group model case. Hence the research analyses represented the case of a large pile group subject to only translational loading at the groundline, and with a rigid pile cap present to enforce equal horizontal displacement of all pile heads[‡].

[‡] Note that pile cap resistance could contribute to lateral stiffness but is not addressed in the current research.

The general process developed to undertake the research analyses is illustrated in Figure 6-2. As indicated, research analyses proceeded on the basis of the preceding sections that served as guides in developing appropriate pile and soil configurations. Pile shapes were restricted to circular sections only and pile types limited to steel pipe piles (representing driven piles) and a reinforced concrete pile (representing a bored pile). Following the approach taken in Section 5, pipe piles were modeled with equivalent solid section properties, and elastic pile behavior assumed in all pile cases. No attempt at modeling the installation process of a pile was made, however the effect of the installation procedure was considered in terms of the initial stress state assigned to the soil: In the driven pile case an isotropic initial effective stress state was considered to be the most appropriate stress state existing in the soil ($K_h = 1.0$), while in the bored pile case an initial horizontal effective stress equal to half the initial vertical effective stress was considered to be the most appropriate stress state ($K_h = 0.5$).
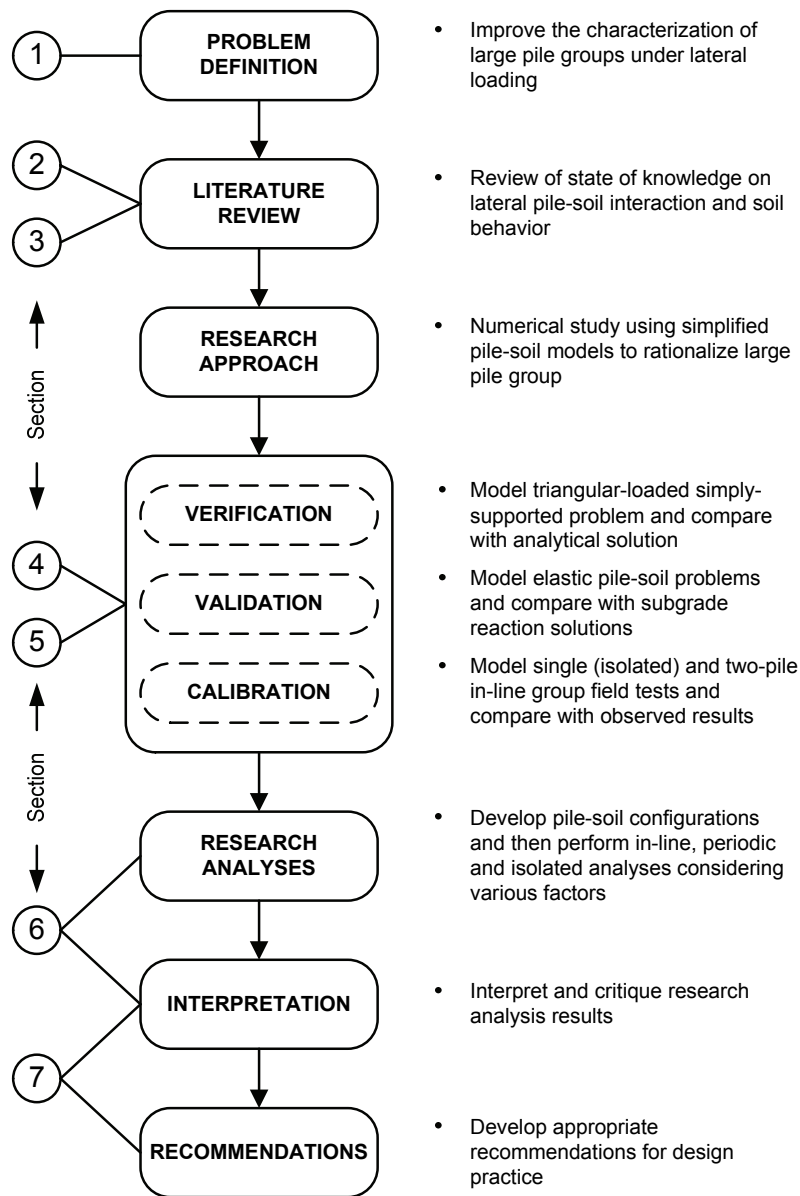
Figure 6-2: General research process

173

Soil models reflected the general classification of sand and clay adopted for research purposes, and this aspect of the research is discussed fully in Dodds (2005). Details of the constitutive models utilized for research purposes are provided in Appendix B. Given the emphasis on long span bridges and the marine type of environment this usually entails, a soft to medium consistency was considered appropriate for the clay soil (normally consolidated), while a medium dense relative density was adopted for the sand soil. In assigning soil properties, a strategy of obtaining "typical" values was attempted through inspection of case histories and using engineering judgment. In particular, strength and stiffness profiles in the clay soil were based on a ratio of undrained shear strength to vertical effective stress (i.e., s_u / σ_v') of between 0.2 and 0.25, and a strength-stiffness correlation corresponding to $E_s \approx 200 s_u$. The strength and stiffness profiles for the sand soil were based on the Mustang Island Test site conditions, considered to be a reasonably typical sand site.

6.2.2 Model Details

Details of soil and pile configurations established for research purposes are shown in Figure 6-3. Moduli values for the steel pipe piles, intended to represent driven piles as noted previously, were based on a pipe thickness of 9.525 mm for the 500 mm diameter pile, and 18 mm for the 1000 mm diameter pile. These corresponded to equivalent pile modulus ($E_{p\text{-}equiv.}$) values of 30 GPa and 25 GPa, respectively. A pile modulus of 15 GPa was adopted for the bored pile, assuming a cracked section applied. This was based on the flexibility assessment for the German Test (refer Dodds, 2005 for workings, indicating a modulus of approximately 12 GPa), and the bored pile test reported by Huang et al. (2001), where a cracked modulus of approximately 16.8 GPa was assessed for the 1500 mm diameter bored piles tested.
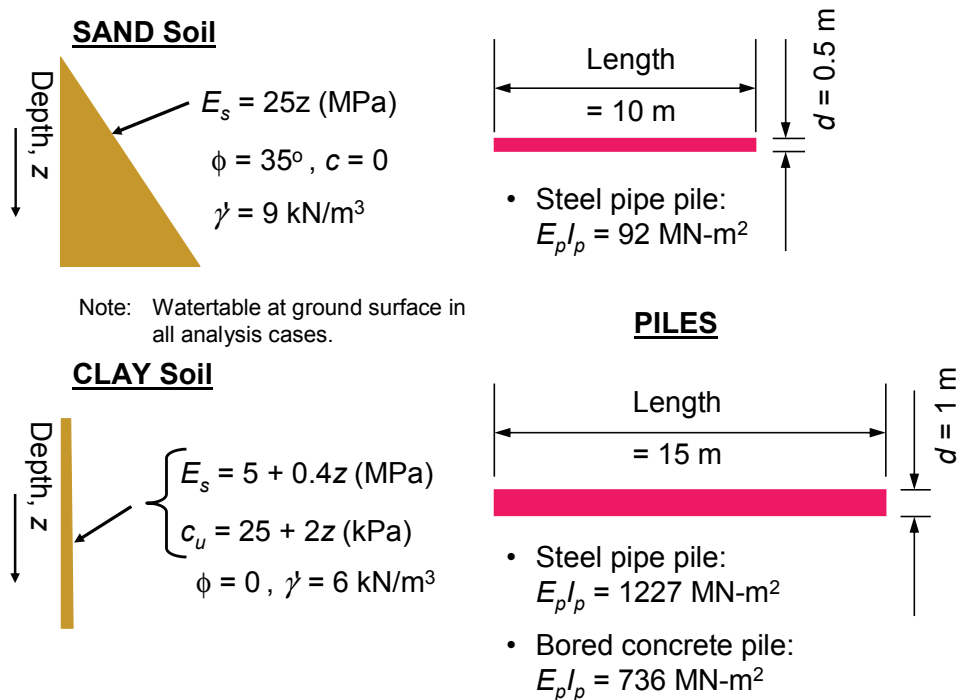
Figure 6-3: Soil and pile configurations adopted for research purposes

A summary of the elastic properties used for the research pile-soil models is given in Table 6-1. As discussed in Section 5, Poisson's ratio for the soil was dictated by the initial stress state assigned. Interface spring stiffness values were based on the recommended stiffness criteria described in Section 4, but a reduction of between 20% and 30% was applied to derive the values given in Table 6-1. This followed the parametric assessment of interface stiffness for the Mustang Island Test (refer Section 5), where a stiffness value approximately 50% of the recommended value resulted in no change to model behavior. Strength parameters assigned to the interface shear springs were such that the shear strength equaled that mobilized by the surrounding soil, according to the Mohr-Coulomb strength criterion. A zero tensile strength ("cut-off" value) was assigned to the interface normal spring to account for possible separation between the pile and soil.

Table 6-1 :   Elastic modeling properties for research analyses

Component	Description of Elastic Property	Pile Type		
		Steel Pipe d = 500 mm L = 10 m	Steel Pipe d = 1000 mm L = 15 m	Reinforced Concrete d = 1000 mm L = 15 m
Pile	Pile modulus ($E_{p\text{-}equiv.}$ or E_p)	30 GPa	25 GPa	15 GPa
Pile	Poisson's ratio, ν_p	0.25	0.25	0.2
Soil	Young's modulus, E_s	Refer Figure 6-3		
Soil	Poisson's ratio, ν_s	0.333 & 0.49	0.49	0.333
Interface[1]	Normal spring stiffness, k_n	2.0 x 10^9 kPa/m	1.44 x 10^9 kPa/m	0.8 x 10^9 kPa/m
Interface[1]	Shear spring stiffness, k_s	2.0 x 10^9 kPa/m	1.44 x 10^9 kPa/m	0.8 x 10^9 kPa/m
Notes:	1. Interface stiffness units refer to the spring stiffness per unit of tributary area associated with each interface gridpoint.			

Pile-soil model geometries for the periodic, isolated and in-line cases are shown in Figure 6-4, Figure 6-5 and Figure 6-6, respectively. For the isolated and in-line cases, a generous distance of 20d to the side boundaries perpendicular to the direction of loading[§] was provided to ensure any boundary effects were insignificant, as was required in order to simulate the unlimited extent of soil actually existing at these locations. This also applied to the outer side boundary parallel to the direction of loading in the isolated model case. Boundary conditions were of the displacement type, as follows: Movement of side boundaries was prevented in the direction perpendicular to their plane, while the base of each model was prevented from moving in the vertical direction (the same boundary conditions as used for the pile-soil models presented in Section 5). An exception was the periodic model, where the side boundaries running perpendicular to the direction of loading were slaved together in the horizontal direction over the depth of the pile in order to realize the assumption of periodic displacement boundaries described in Section 3.

[§] The direction of loading being from left to right when considering the front elevation or plan views.
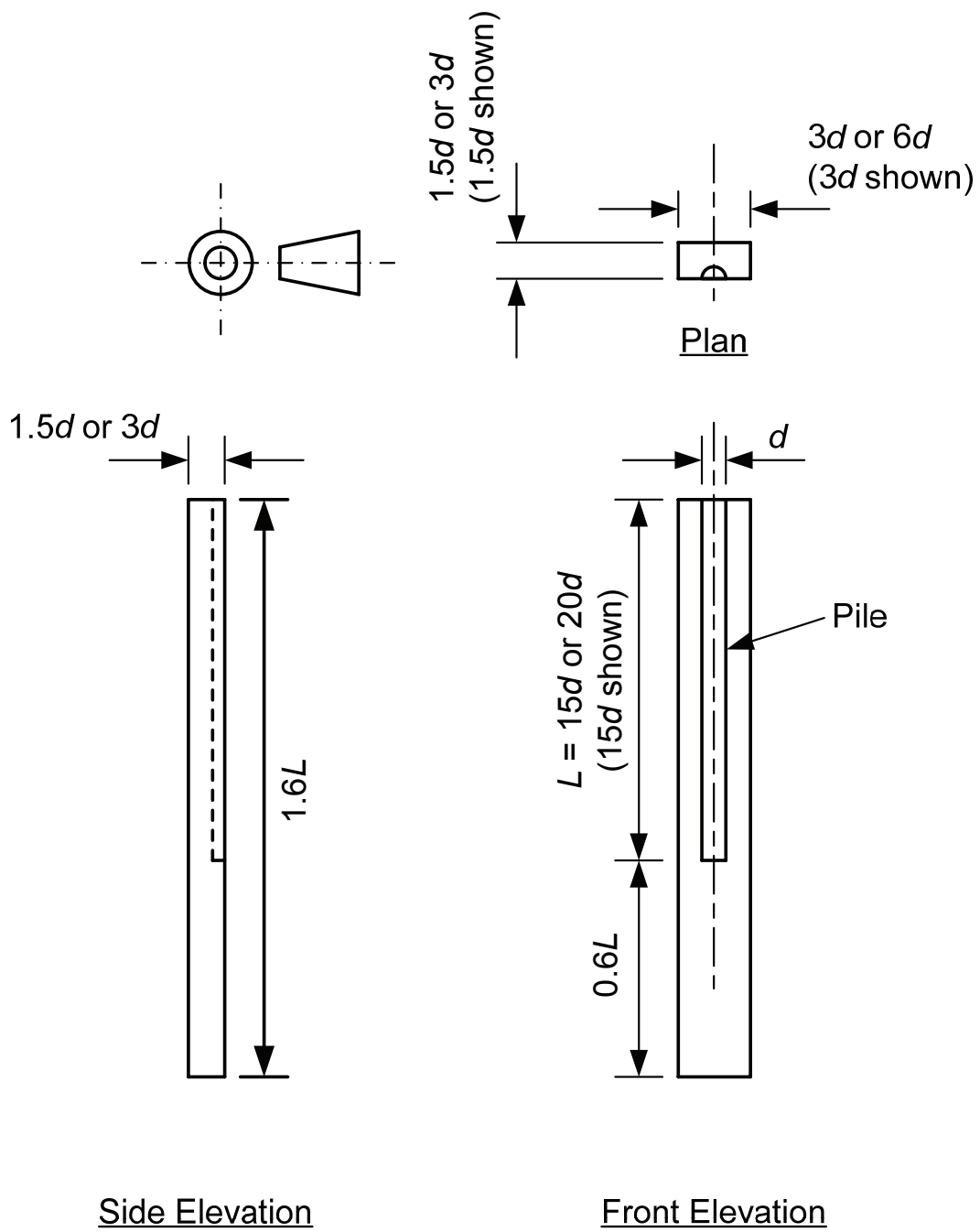
Figure 6-4: Periodic pile-soil model geometry

Plan

20*d*

20*d*

L = 15*d* or 20*d*
(20*d* shown)

0.6L

1.6L

20*d*

d

Pile

Side Elevation

Front Elevation
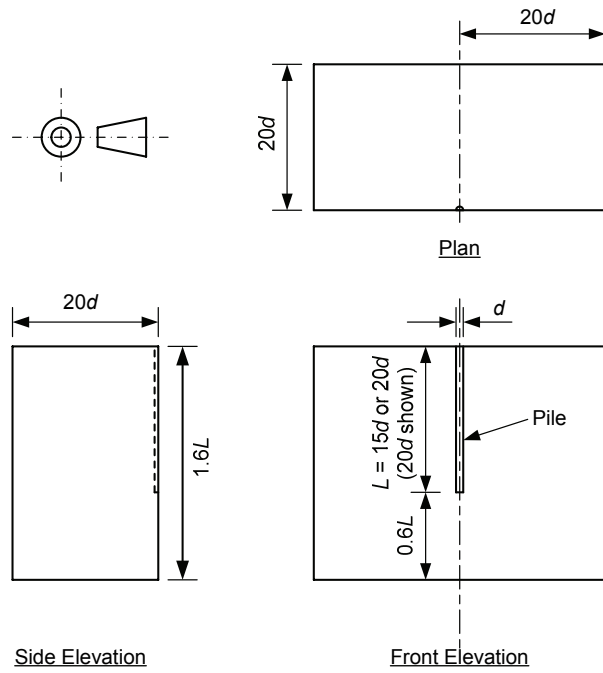
Figure 6-5: Isolated pile-soil model geometry

Plan

3*d*

20*d*

1.5*d*

1.5*d*

L = 15*d* or 20*d*
(20*d* shown)

0.6L

1.6L

d

Piles

Side Elevation

Front Elevation
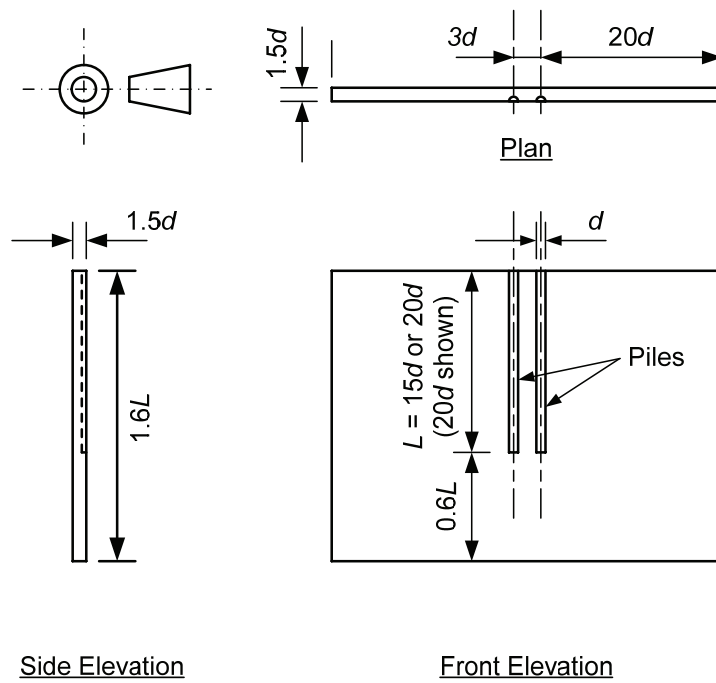
Figure 6-6: In-line pile-soil model geometry

177

Pile discretization is shown in Figure 6-7, and pile-soil discretization indicated in Figure 6-8 through Figure 6-13, where pile-soil discretization followed the same pattern for the two pile sizes. Discretization needs for the research models were established following the same procedures used in Section 5. LPILE (Ensoft, 1999) models of the isolated research cases were used to assess maximum bending moment demands in order to determine vertical discretization needs via the triangular-loaded simply-supported procedure. The LPILE assessment also helped to determine pile lengths sufficient for flexible pile behavior through inspection of pile deflection profiles in LPILE to ensure pile tip movement was negligible under the range of pile head deflection investigated. Linear elastic results supporting the pile and soil discretization used in the research models are provided in Dodds (2005).
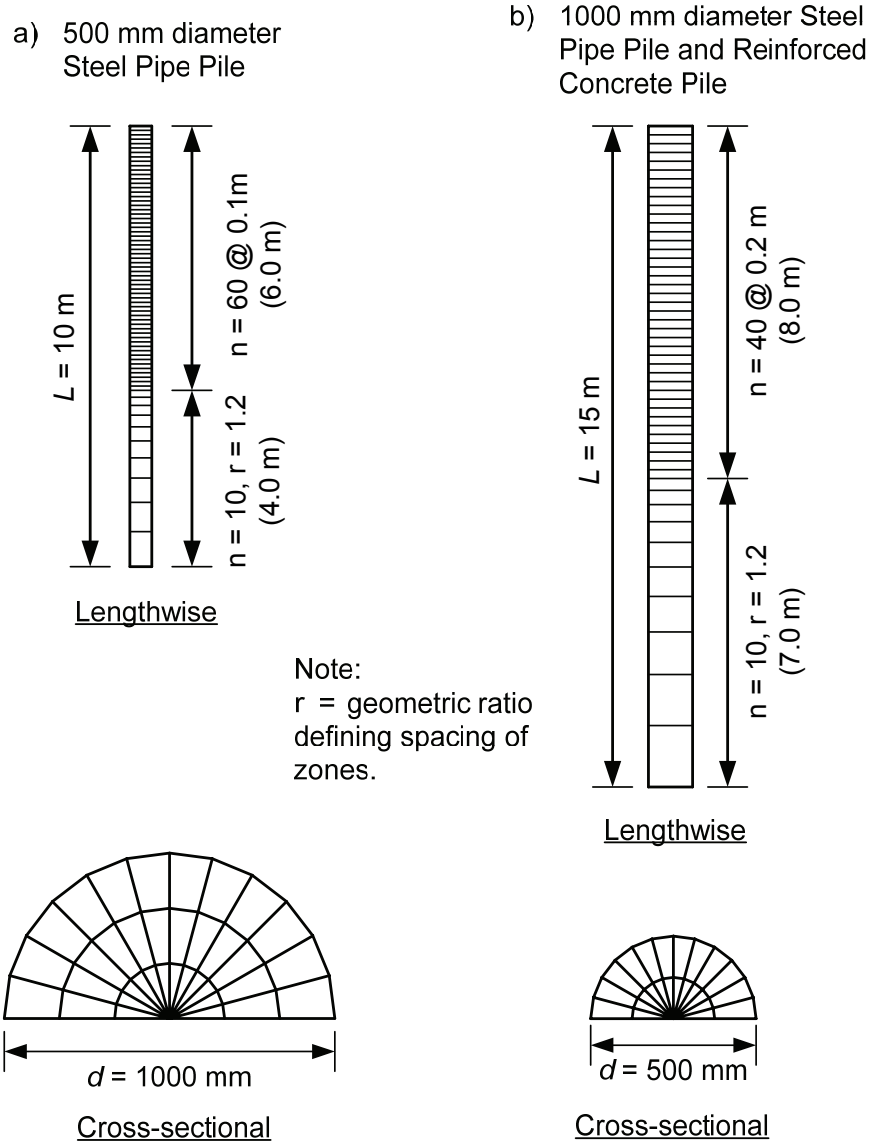
Figure 6-7: Pile discretization for research pile-soil models
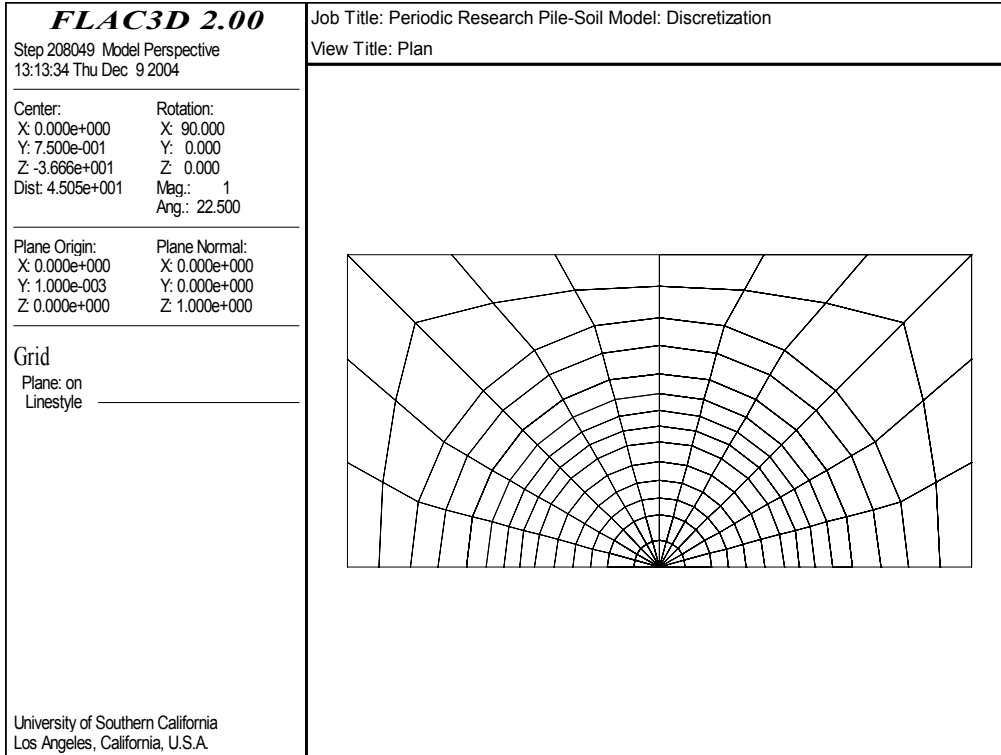
Figure 6-8: Typical front elevation discretization for periodic pile-soil model
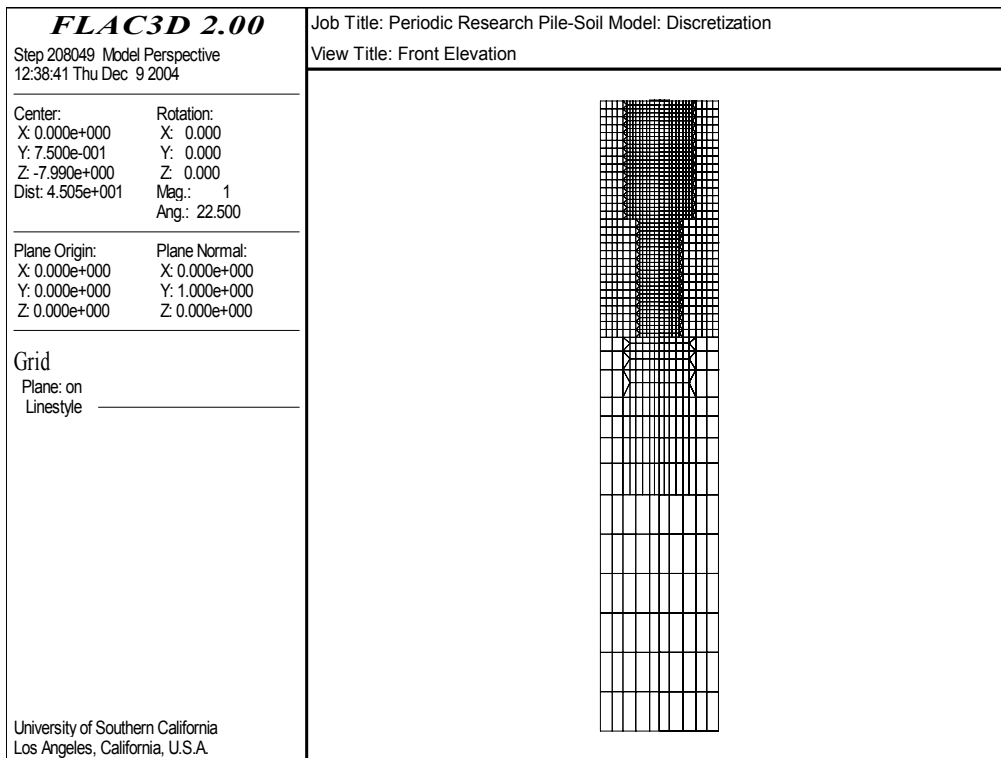
Figure 6-9: Typical plan discretization for periodic pile-soil model

179
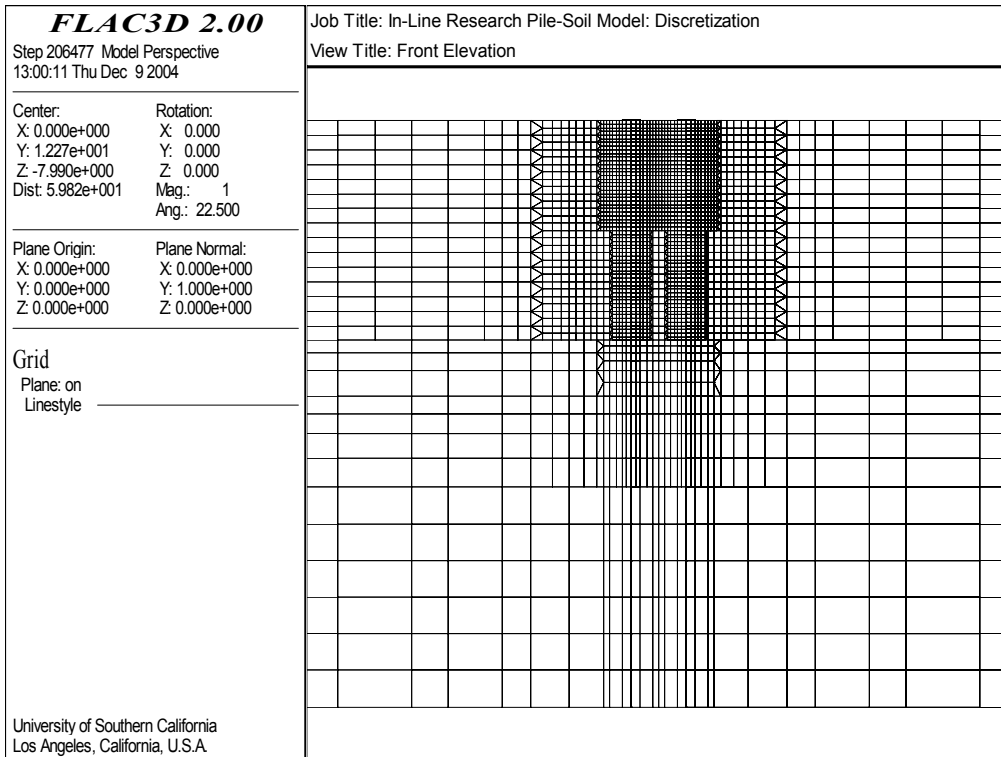
Figure 6-10: Typical front elevation discretization for in-line pile-soil model
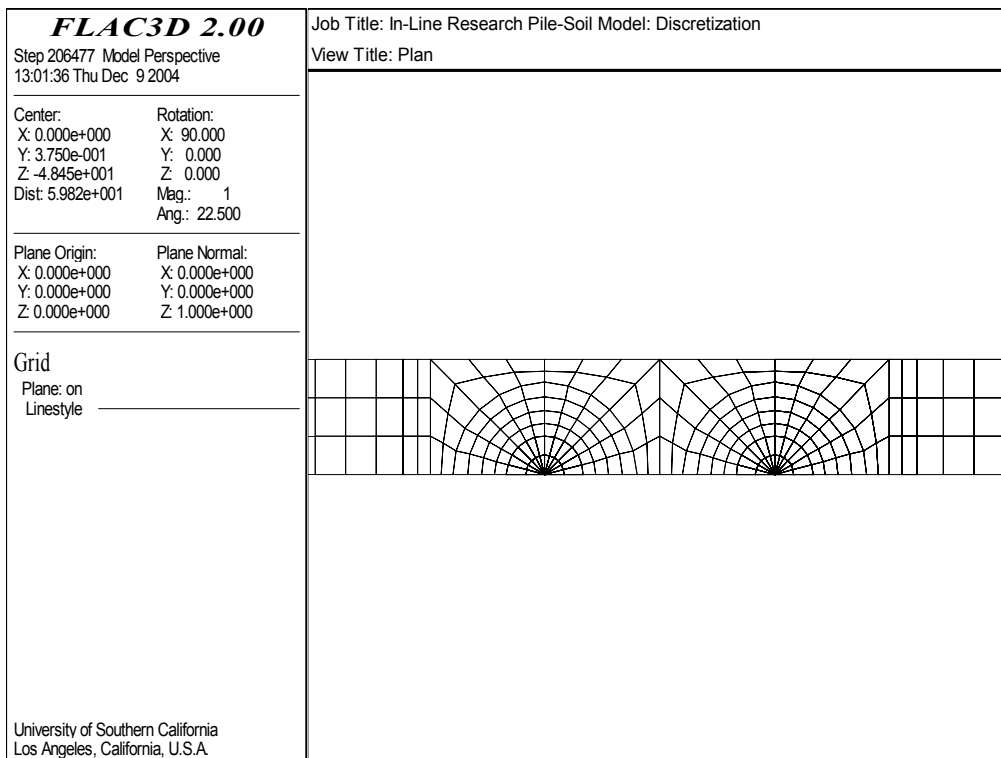
Figure 6-11: Typical plan discretization for in-line pile-soil model
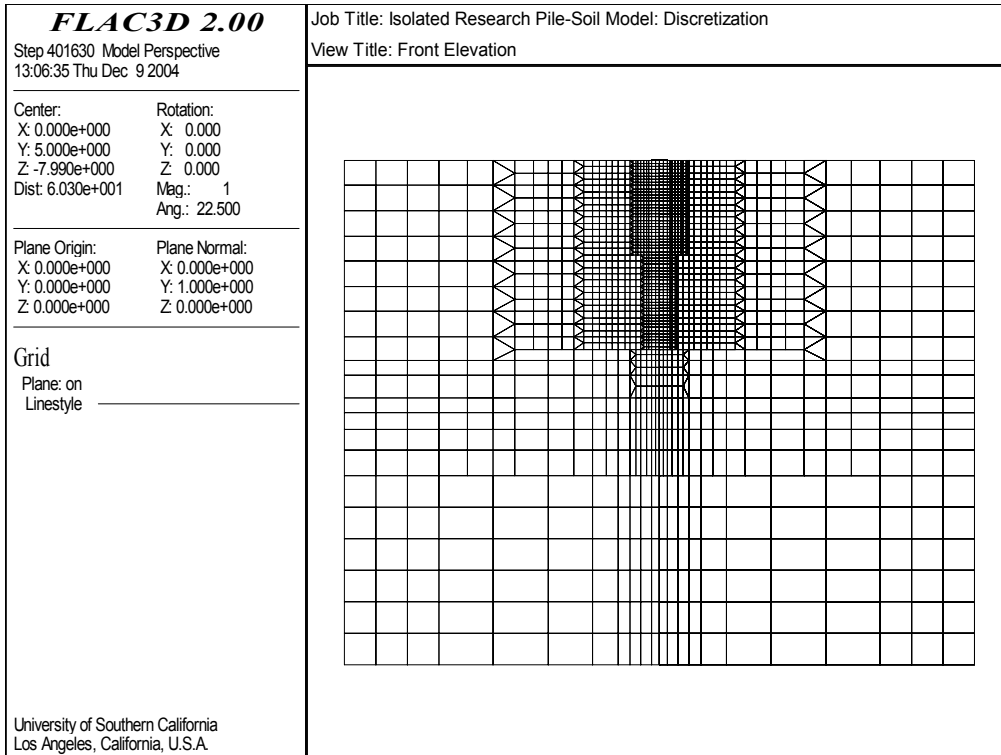
Figure 6-12: Typical front elevation discretization for isolated pile-soil model
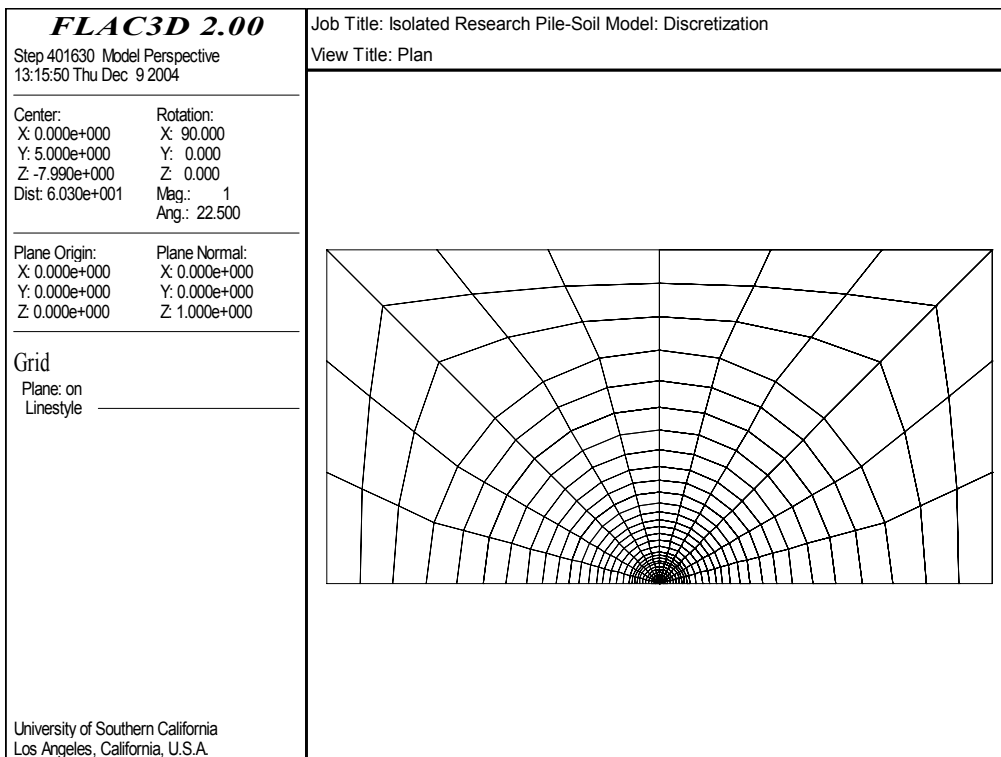
Figure 6-13: Typical plan discretization for isolated pile-soil model

6.2.3   Study Factors

The various factors that were considered in the research are indicated in Figure 6-14, namely: (a) pile type, (b) initial stress state, (c) pile head restraint, (d) pile spacing, and (e) soil type. As noted previously, details of the soil models are given in Appendix B. The Base Soil Model, utilizing the established isotropic linear elastic stiffness model and Mohr-Coulomb strength model to represent elastic and plastic qualities of soil, respectively, formed the basis for assessing the influence of sand and clay soils. Exclusion of the advanced Manzari and Dafalias Sand (MDS) and Cam Clay models (indicated by the crosses in Figure 6-14) followed difficulties encountered when performing pile-soil analyses with these soil models, as discussed in section 6.3.1.3. The schedule of research analyses performed is indicated in Table 6-2, consisting of a total of 30 analyses.

6.2.4   Lateral Loading

Lateral loading was simulated in all research analyses using velocity control procedures noted previously in Sections 4 and 5. Velocity increments were applied to the top of the pile using either the servo-control algorithm described in Section 5, or using a "ramping" algorithm that linearly increased velocity increments from zero to a specified constant value over the first 200,000 to 300,000 steps. In one case, the ramping and servo-control algorithms were used as a combination. The analysis settings and the extent of pile head deflections undertaken for the research analyses are indicated in Table 6-3.
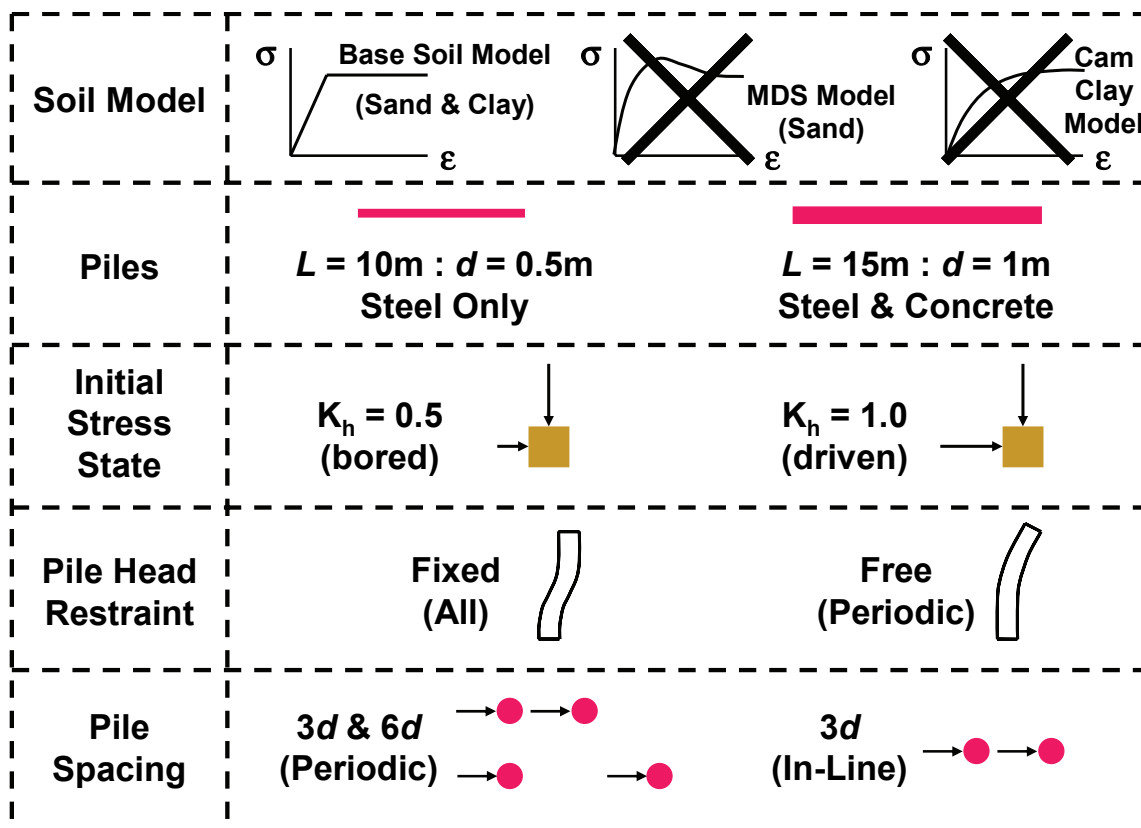
Figure 6-14: Research analysis factors

Table 6-2 :   Schedule of research analyses performed

Analysis Identification	Analysis Model			Fixity Condition		Soil Model		Pile Diameter		Pile Modulus			Pile Spacing		K$_h$ Value	
	Isolated	In-Line	Periodic	Fixed Head	Free Head	BSM Sand	BSM Clay	500 mm	1000 mm	15 GPa - Conc.	25 GPa - Steel	30 GPa - Steel	3*d*	6*d*	0.5	1.0
RA1	█			█		█		█				█			█	
RA2	█			█		█		█				█				█
RA3	█			█			█	█				█			█	
RA4	█			█			█	█				█				█
RA5	█			█		█			█	█	█				█	
RA6	█			█			█		█	█					█	
RA7	█			█		█			█		█				█	
RA8			█	█			█		█		█					█
RA9			█	█		█		█				█				█
RA10			█	█		█		█				█		█		█
RA11			█	█					█		█		█			█
RA13			█	█				█		█			█		█	
RA14			█	█				█				█		█		█
RA17			█	█				█				█	█			█
RA18			█	█				█				█		█		█
RA19			█	█			█		█		█		█			█
RA21			█	█			█	█					█		█	
RA22			█	█			█							█		█
RA25			█		█	█		█				█	█			█
RA27			█		█				█	█	█		█		█	
RA29			█		█	█			█			█	█			█
RA33			█		█		█		█			█	█			█
RA35			█		█		█		█		█		█			█
RA37		█			█		█		█			█	█		█	
RA41		█		█		█		█				█	█		█	
RA42		█		█		█		█								█
RA43		█		█		█			█	█			█		█	
RA44		█		█		█		█				█	█			█
RA45		█		█		█		█				█				█
RA46		█		█		█		█				█	█		█	

Note: █ = item analyzed; BSM = Base Soil Model

Table 6-3 :   Lateral loading parameters

| Analysis ID | Velocity Control Parameters for Lateral Loading | | | | | Pile Head Deflection | |
| | Servo-Control Algorithm Settings | | | | Constant Velocity | | |
	v_{min} (m/s)	v_{max} (m/s)	ΔH_{min} (N)	ΔH_{max} (N)	(m/s)	(mm)	(%d)
RA1	8e-9	8e-8	100	750	-	32	6.3
RA2	8e-9	8e-8	100	750	-	26	5.1
RA3	8e-9	8e-8	100	350	-	31	6.2
RA4	8e-9	8e-8	100	350	-	40	8.0
RA5	5e-8	8e-7	100	750	-	50	5.0
RA6	5e-8	8e-7	100	350	-	52	5.2
RA7	2.5e-8	8e-8	100	1500	-	50	5.0
RA8	2.5e-8	8e-8	100	2000	-	48	4.9
RA9	8e-9	8e-8	100	750	-	30	6.0
RA10	-	-	-	-	2.5e-8	36	7.3
RA11	-	-	-	-	5e-8	52	5.2
RA13	-	-	-	-	5e-8	52	5.2
RA14	-	-	-	-	5e-8	52	5.2
RA17	1e-8	3.5e-8	100	350	2e-8	30	6.0
RA18	-	-	-	-	2.5e-8	36	7.2
RA19	-	-	-	-	2.5e-8	46	4.6
RA21	-	-	-	-	5e-8	52	5.2
RA22	-	-	-	-	5e-8	52	5.2
RA25	-	-	-	-	2e-8	29	5.8
RA27	-	-	-	-	3.75e-8	51	5.1
RA29	-	-	-	-	4e-8	50	5.0
RA33	-	-	-	-	2e-8	29	5.8
RA35	-	-	-	-	2.5e-8	51	5.1
RA37	-	-	-	-	4e-8	50	5.0
RA41	8e-9	8e-8	100	750	-	32	6.4
RA42	8e-9	8e-8	100	750	-	21	4.1
RA43	8e-8	8e-7	100	750	-	50	5.0
RA44	5e-8	8e-7	100	350	-	50	5.0
RA45	8e-9	8e-8	100	350	-	33	6.6
RA46	8e-9	8e-8	100	350	-	31	6.3

6.2.5   Analysis Procedure

The research analyses were undertaken following an analysis procedure developed specifically for the pile-soil models, details of which are provided in Dodds (2005). The procedure, documented in the form of an analysis checklist and accompanying notes evolved from the validation/calibration analysis work, was followed with the construction of each model to ensure consistency of results. This included the assignment of calculation points for recording pile and soil behavior, as indicated in Figure 6-15.
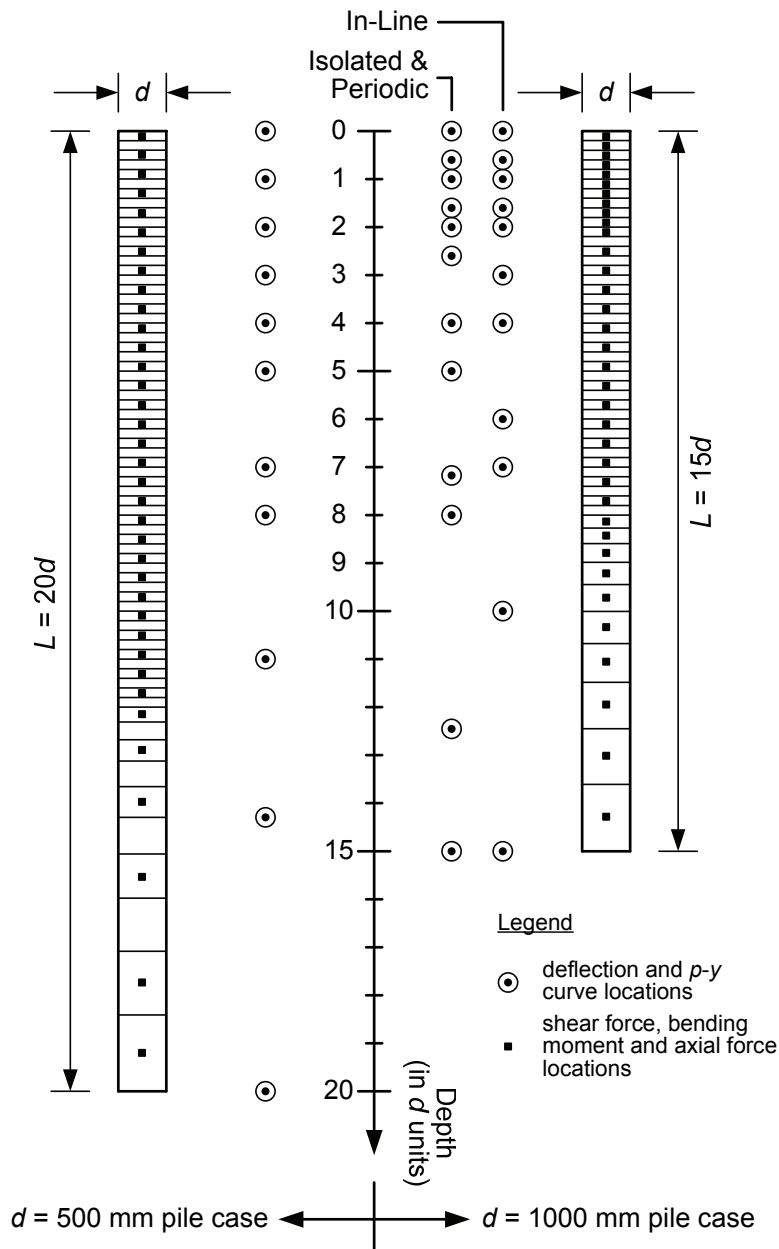
Figure 6-15: Locations of calculation points for recording structural actions and p-y curves

Extensive use of *FISH*[**] was employed for tracking and storing data at calculation points, and required appreciable efforts to develop the various subroutines performing these tasks. Data processing was equally challenging given the substantial amount of data recorded during each analysis and the need to sort and organize this into a format suitable for interpretation. Data management and post-processing were therefore issues with the same importance as undertaking the analysis itself. To this end a computational framework was developed to (a) assess the integrity of data, and (b) interpret the data. Excel with VBA support was used as the computational tool to undertake this task.

[**] *FISH* is a programming language that accompanies *FLAC*[3D] to assist with analysis and processing needs.

6.2.5.1   Data Integrity

Several routine checks of analysis data were conducted with each research analysis to provide an assurance that pile-soil behavior was reasonable and structural actions consistent. Profiles of pile deflection, shear force and bending moment at a given pile head deflection were first plotted and inspected to check for reasonableness including flexible pile behavior in the case of the isolated models, agreement with boundary conditions assigned, and consistency between shear force and bending moment plots. Such inspections were undertaken at pile head deflection values uniformly spread over the entire range of pile head deflection by dividing the total pile head deflection up into ten increments, and plotting structural actions at each increment. In this way the continuity of structural behavior with increased loading was also checked.

Another check on pile behavior was through inspection of axial forces developed in the pile. This followed from the calculation of bending moment as the summation of elementary internal moments, where an elementary internal moment was defined as the product of the axial force developed in each zone forming the cross-section of the pile, and the distance between the centroid of such a zone and the neutral axis (the neutral axis being the pile center given the elastic behavior prescribed to the pile). Such structural behavior demands that the total axial forces developed in the tension and compression side of the cross-section are equal and opposite. Hence the summation of tension and compression forces acting at the cross-section at each calculation point was plotted against pile deflection in order to check that this type of behavior was indeed occurring.

Finally, as discussed in Section 5, the soil resistance p mobilized against the pile was calculated directly from the forces mobilized in the interface springs, and indirectly in two ways by fitting a sixth-order polynomial equation to bending moment data and shear force data, and differentiating twice and once, respectively. Hence three independent methods of deriving p-y curves were possible, drawing on different structural actions in the process. In this way the consistency of data could be assessed by considering how well these p-y curves compared with each other. The three independent p-y curves were therefore plotted together for each p-y calculation point in each analysis case and inspected.

These various checks made in relation to data integrity are illustrated in Figure 6-16. Additional assurance of data integrity was also obtained through comparison of $FLAC^{3D}$ and LPILE structural actions for isolated pile cases, details of which are provided in Dodds (2005).

6.2.5.2   Data Interpretation

The interpretation of the research results was primarily concerned with p-y behavior given the use of p-y curves as the primary assessment tool. In terms of group effects the means of interpretation was through use of p-multipliers so as to compare with the empirically-based p-multipliers developed from field observations. It is to be noted that while the research approach determined p-multipliers dependent on depth and pile deflection, the empirically-based p-multiplier database assumed p-multiplier values constant with depth and pile deflection. Attention to this fact was required when interpreting results, in that research p-multipliers were considered on an average basis for comparative purposes.
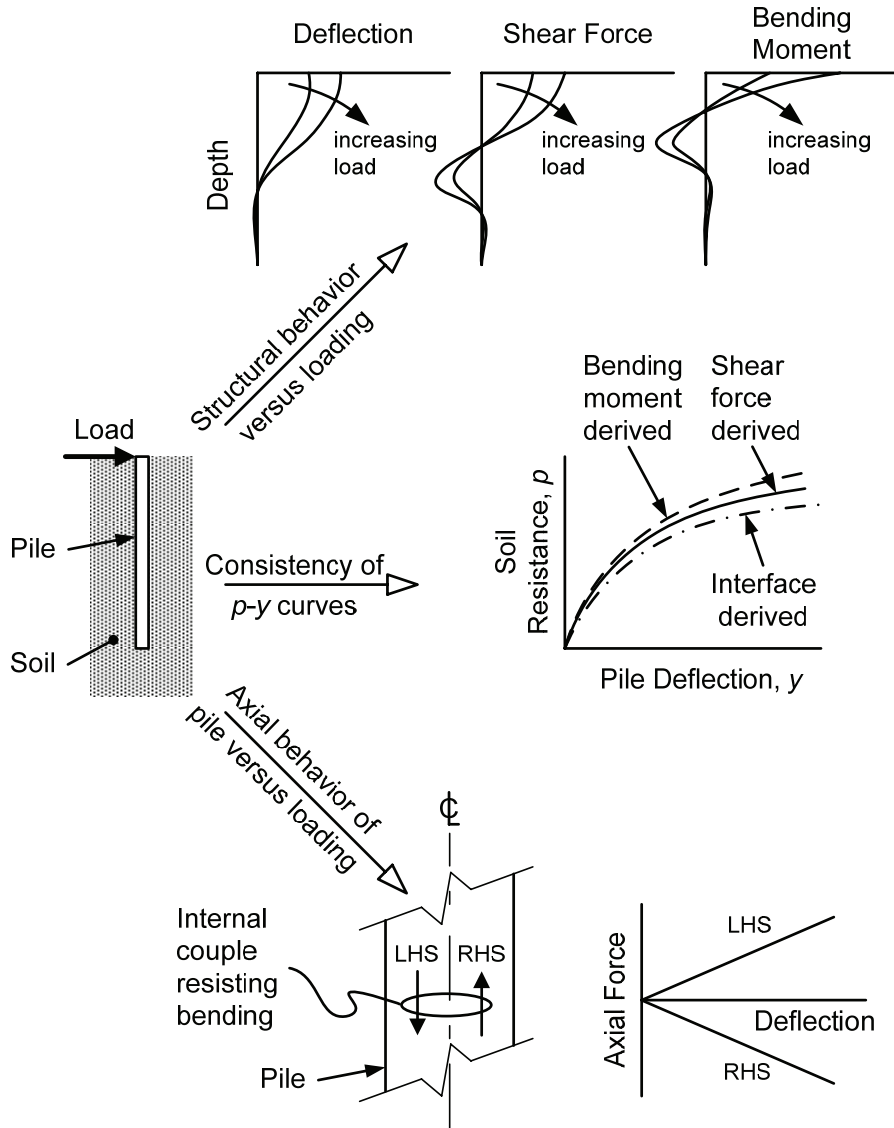
Figure 6-16: Illustration of data integrity checks

Complimenting the *p*-multiplier plots was an assessment of pile-head load-deflection behavior. This consisted of comparing load-deflection curves for group pile cases against isolated pile cases in two ways: Firstly, by simply plotting the curves together to enable a visual assessment of response characteristics; and secondly, through calculation of the pile head ratio defined as

$$\text{Pile Head Ratio} = \frac{\text{Lateral load of group pile at groundline deflection } x}{\text{Lateral load of isolated pile at groundline deflection } x}. \qquad (6.1)$$

Various other forms of data interpretation that assisted with assessing behavioral trends included:

- Distribution of pile deflection, bending moment and shear force with depth.
- Numerical failure pattern in the soil continuum.
- Distribution of p around the pile (refer Figure 6-17 for definition of terms used).
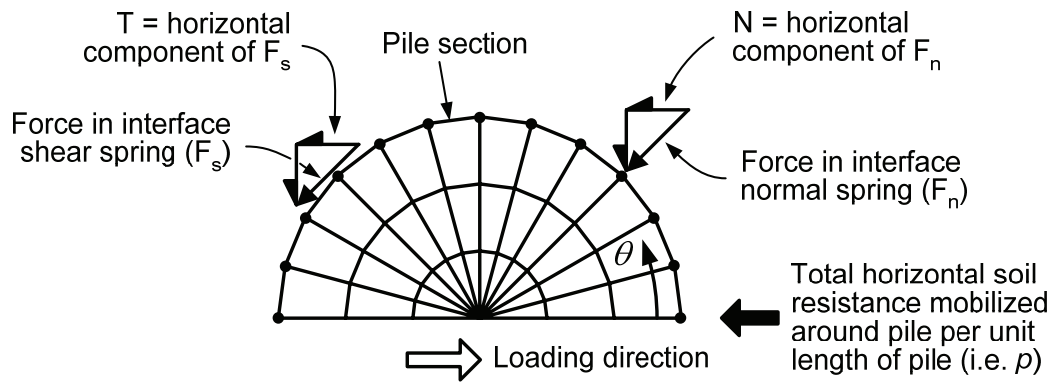
a) Definitions of forces developed around pile
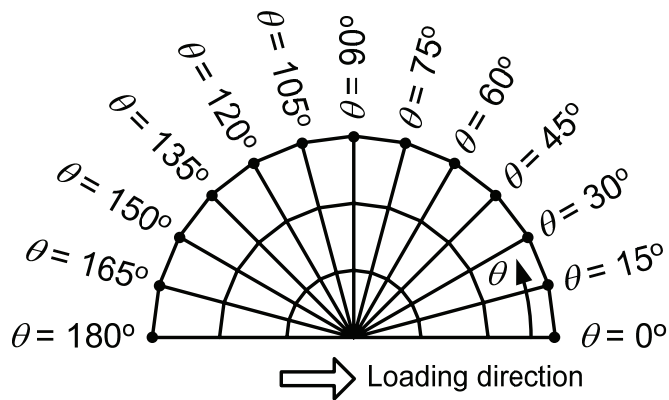
b) Circumferential geometry

Figure 6-17: Definition of terms used for interpreting circumferential behavior

6.3   Research Results

The results of the research analyses are presented in terms of sand and clay soil model classifications, given distinct differences in group pile model behavior that were observed in this respect. Given the voluminous results produced from the research analyses, only typical behavior is reported here in the interest of illustrating the various behavioral trends and issues identified in a clear and concise manner. A record of the research results in their entirety is provided in Dodds (2005).

6.3.1   Base Soil Model Analyses

6.3.1.1   Sand

LPILE Comparison: Typical comparative LPILE and *FLAC*^{3D} behavior for the case of a laterally loaded isolated pile in sand is shown in Figure 6-18, Figure 6-19 and Figure 6-20.

p-y Behavior: A typical comparison of empirical and research sand *p-y* curves at a depth of two pile diameters is shown in Figure 6-21.

p-Multiplier Behavior: Typical *p*-multiplier behavior in sand is shown in Figure 6-22 through Figure 6-25, where f_m denotes a *p*-multiplier value, z denotes depth, d denotes pile diameter, s denotes pile spacing, and pile deflection is given as a percentage of the pile diameter.

Pile Behavior: Typical pile behavior exhibited for isolated and group pile cases in sand is shown in Figure 6-26.

Pile Head Behavior: Typical pile head behavior exhibited by the group pile cases in sand is shown in Figure 6-27.

Failure Patterns: Typical plastic failure patterns (indicated by the darker zones) exhibited in the three research analysis cases for sand are shown in Figure 6-28.

Circumferential Behavior: The typical distribution of *p* around the pile circumference at a depth equal to two pile diameters for the sand research analysis cases is shown in Figure 6-29.

Depth = 0.6*d*

Depth = *d*

Depth = 1.6*d*

Depth = 2*d*

Depth = 2.6*d*

Depth = 4*d*
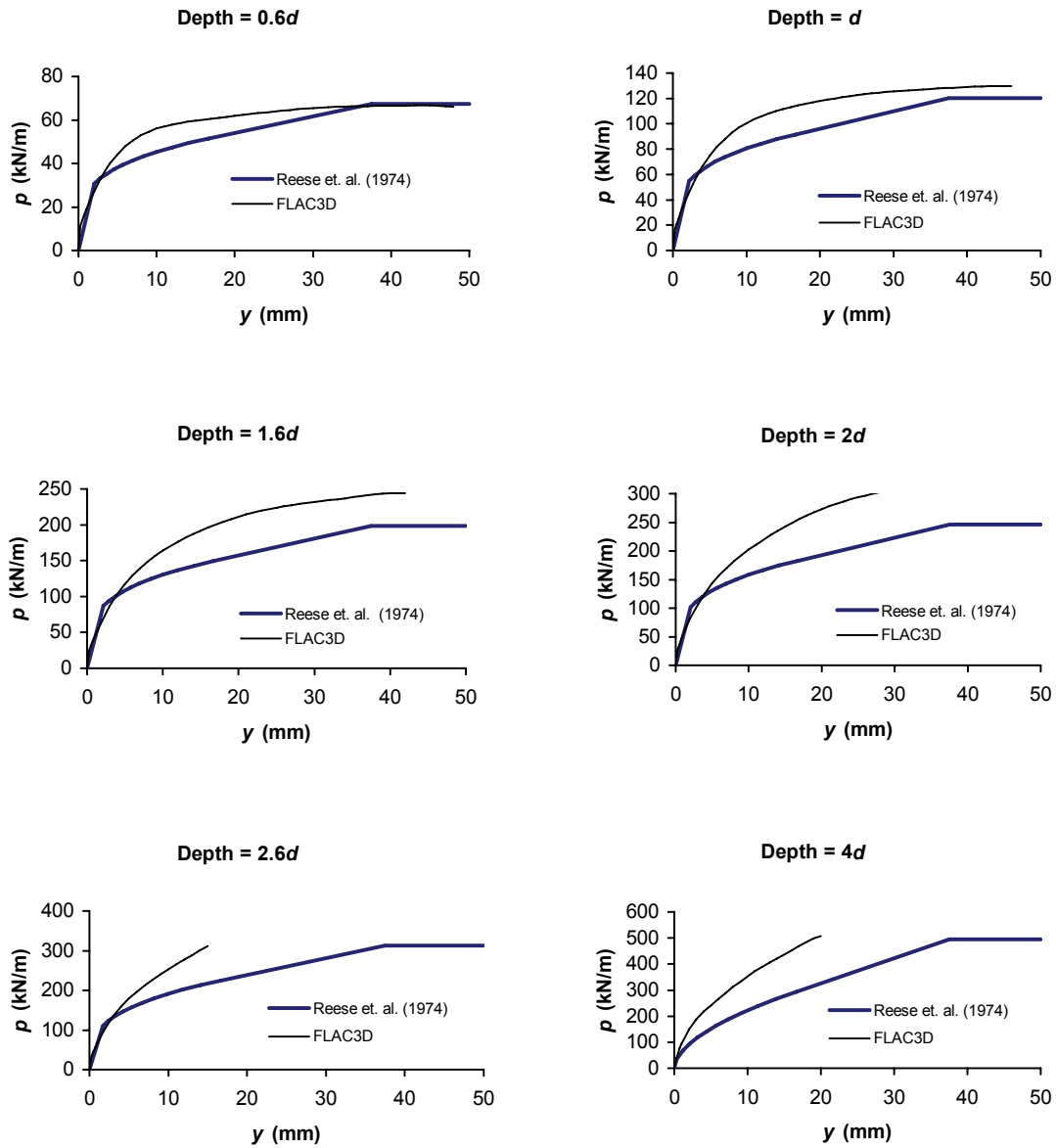
Figure 6-18: Typical comparison between empirical and research sand *p-y* curves
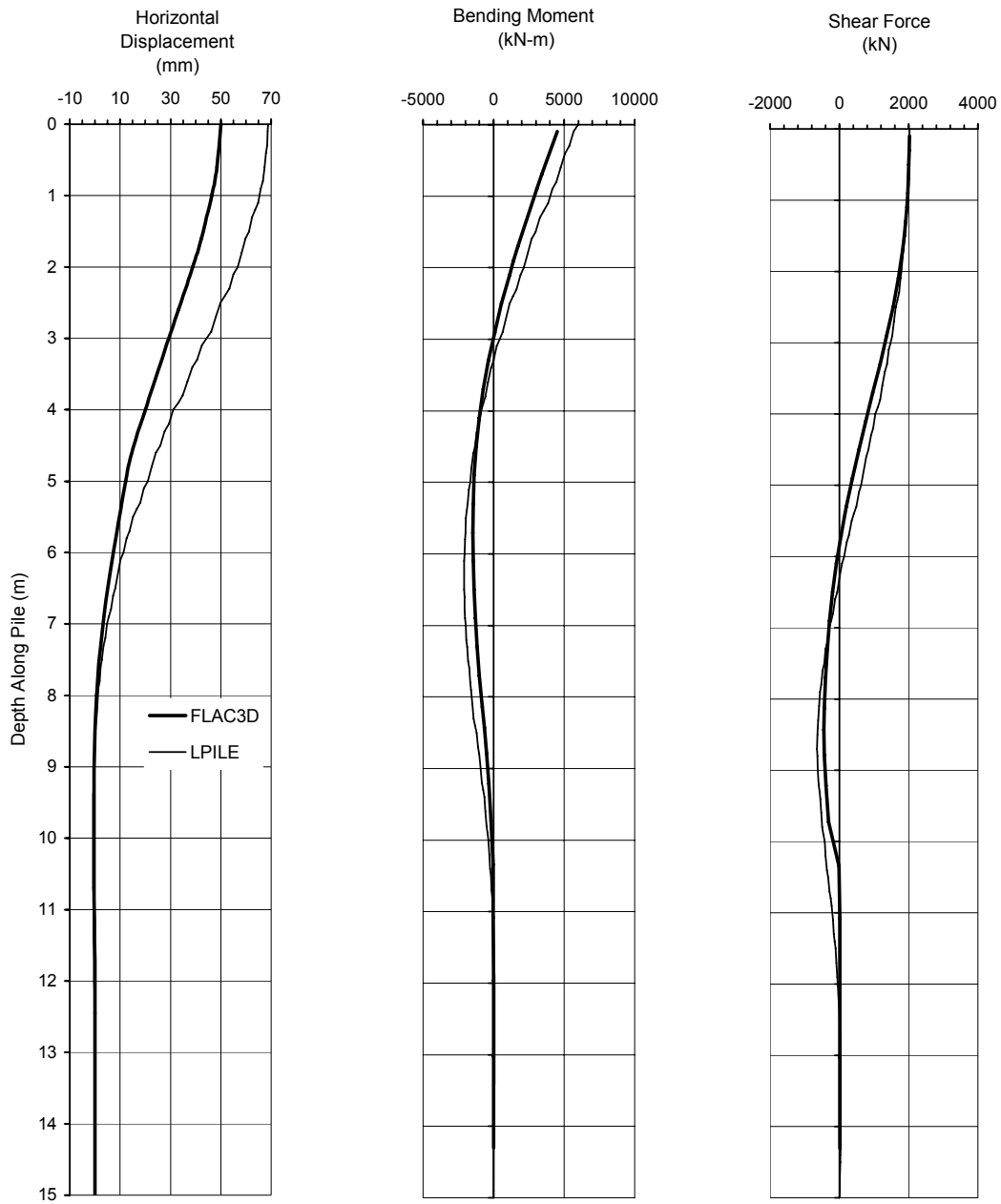
Figure 6-19: Typical comparison between LPILE and research pile behavior for laterally loaded isolated pile in sand
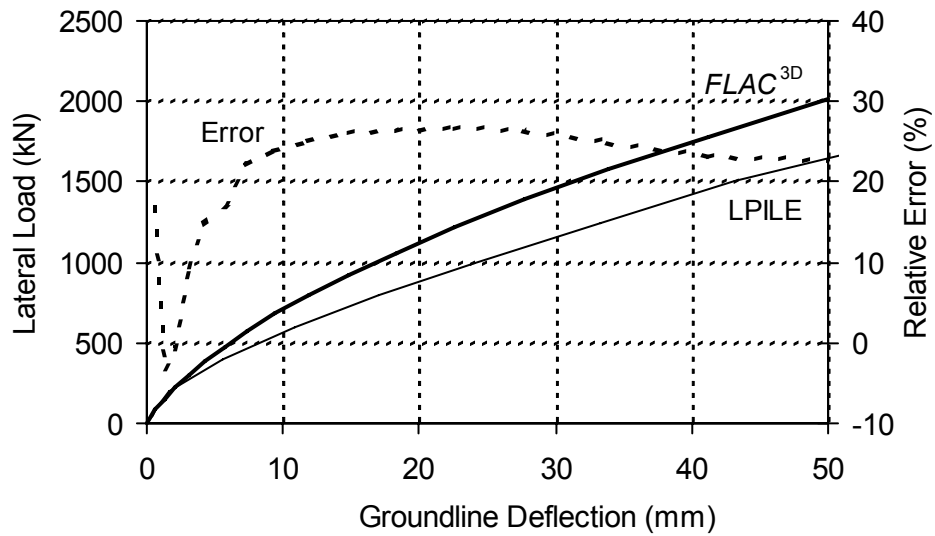
Figure 6-20: Typical comparison between LPILE and research pile head behavior for laterally loaded isolated pile in sand
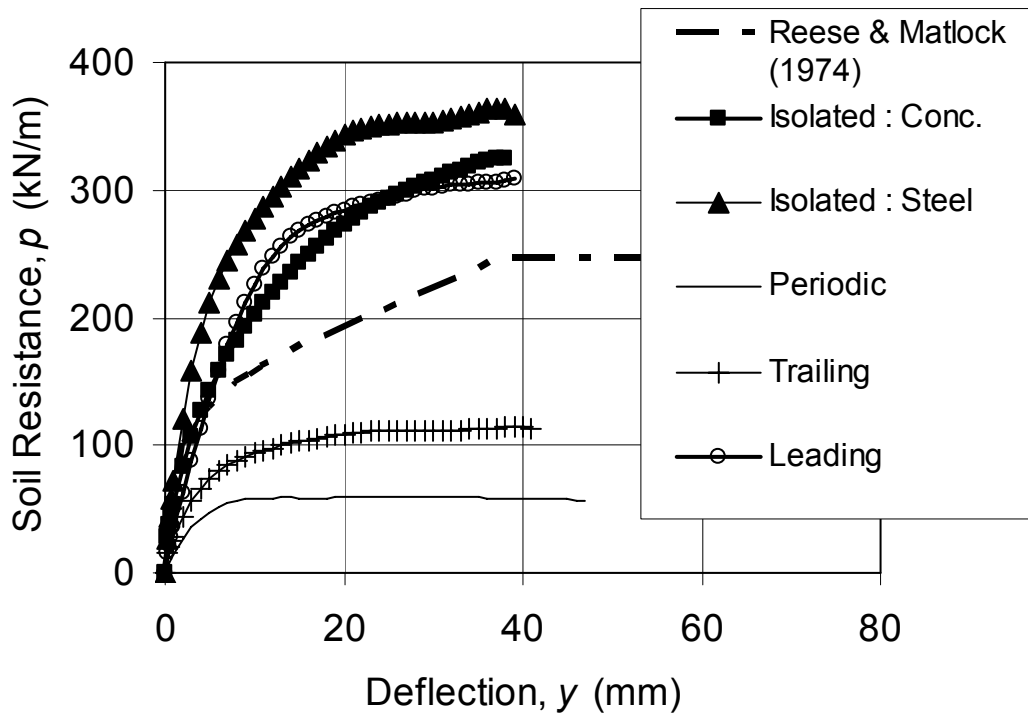
Figure 6-21: Typical comparison of empirical and research sand p-y curves at a depth equal to two pile diameters
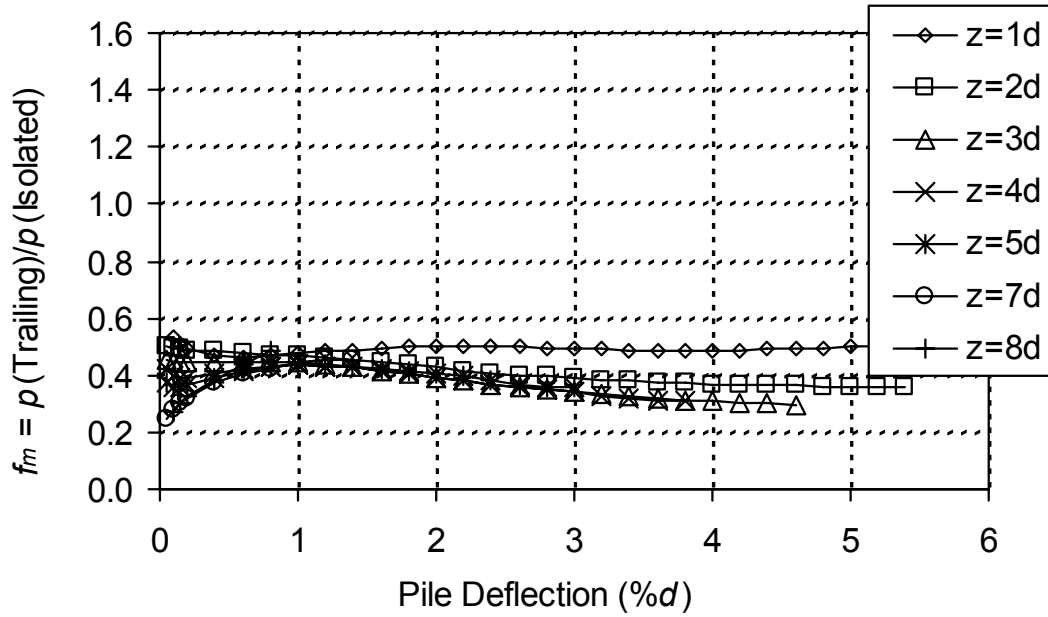
Figure 6-22: Typical variation of f_m for trailing piles in sand, $s = 3d$
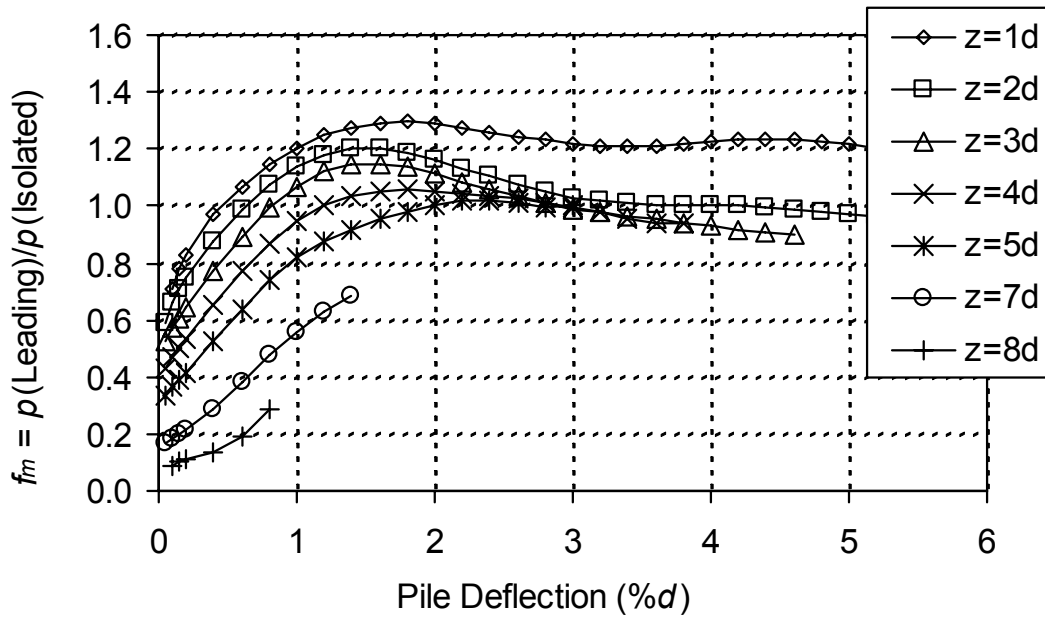
Figure 6-23: Typical variation of f_m for leading piles in sand, $s = 3d$
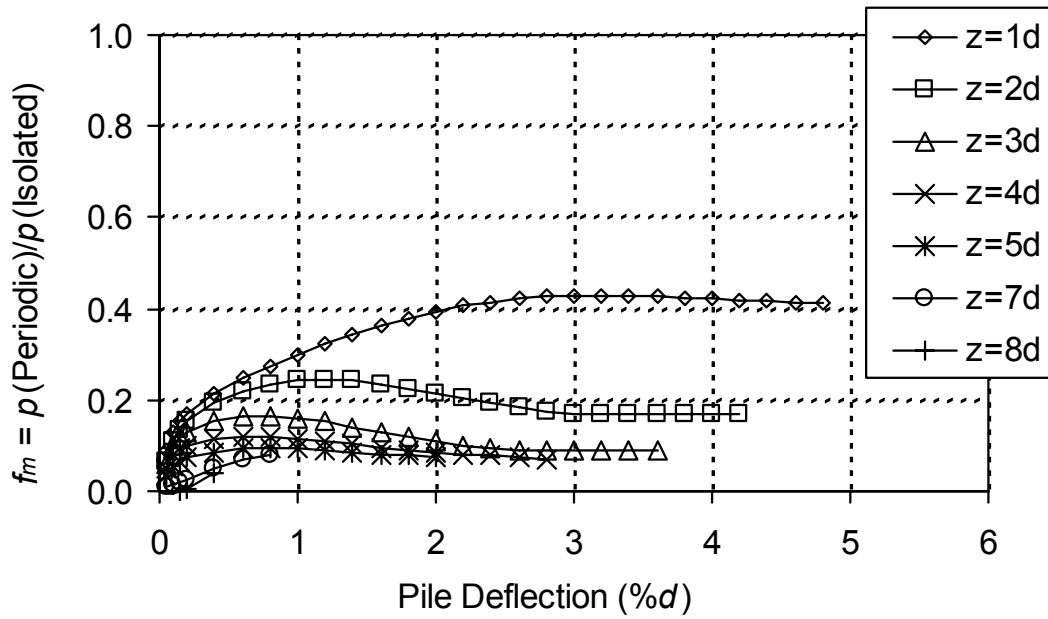
Figure 6-24: Typical variation of f_m for periodic piles in sand, $s = 3d$
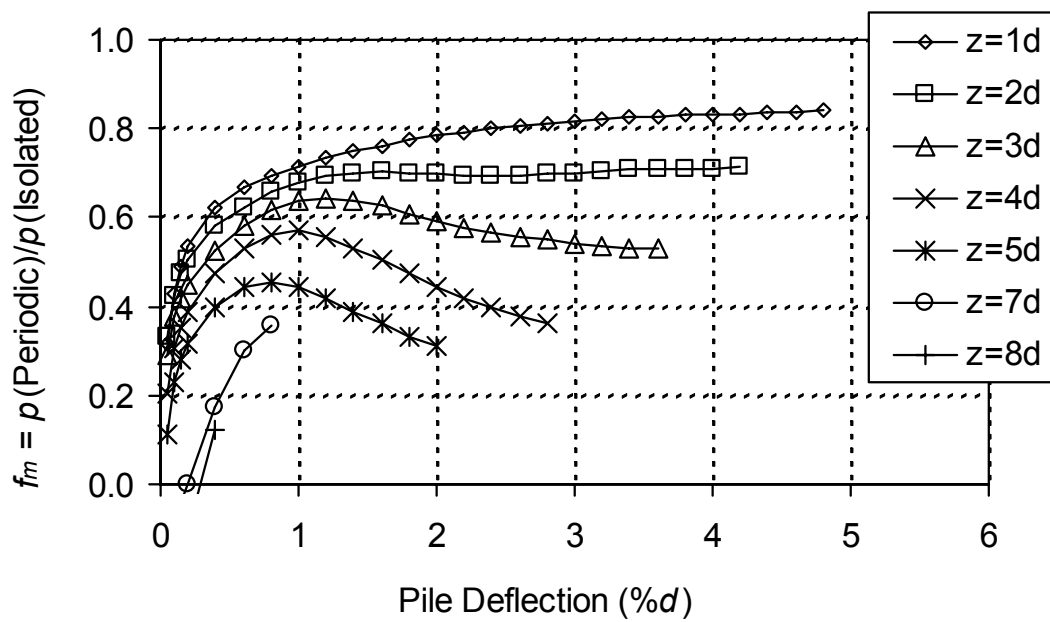
Figure 6-25: Typical variation of f_m for periodic piles in sand, $s = 6d$
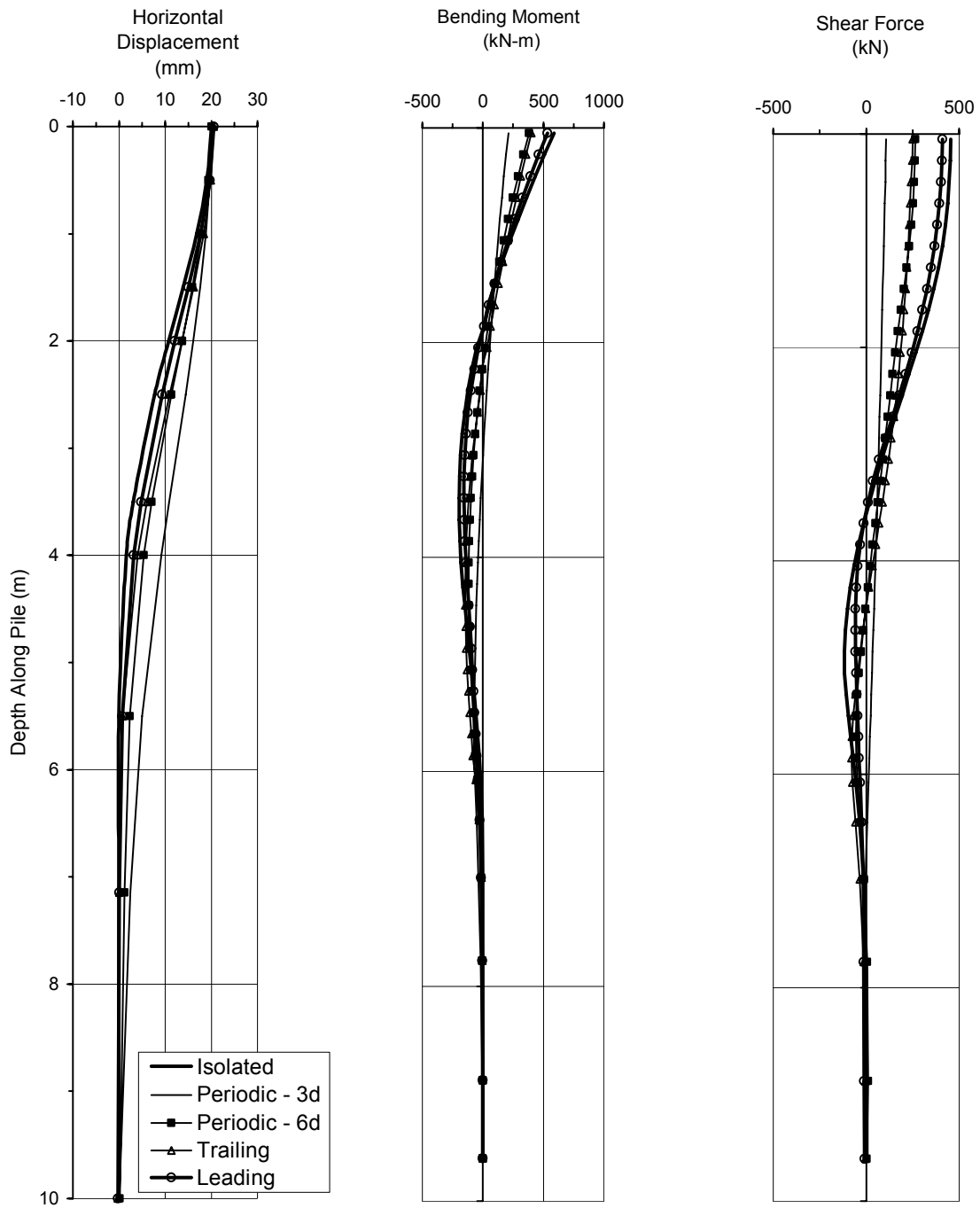
Figure 6-26: Typical pile behavior for isolated and group piles laterally loaded in sand
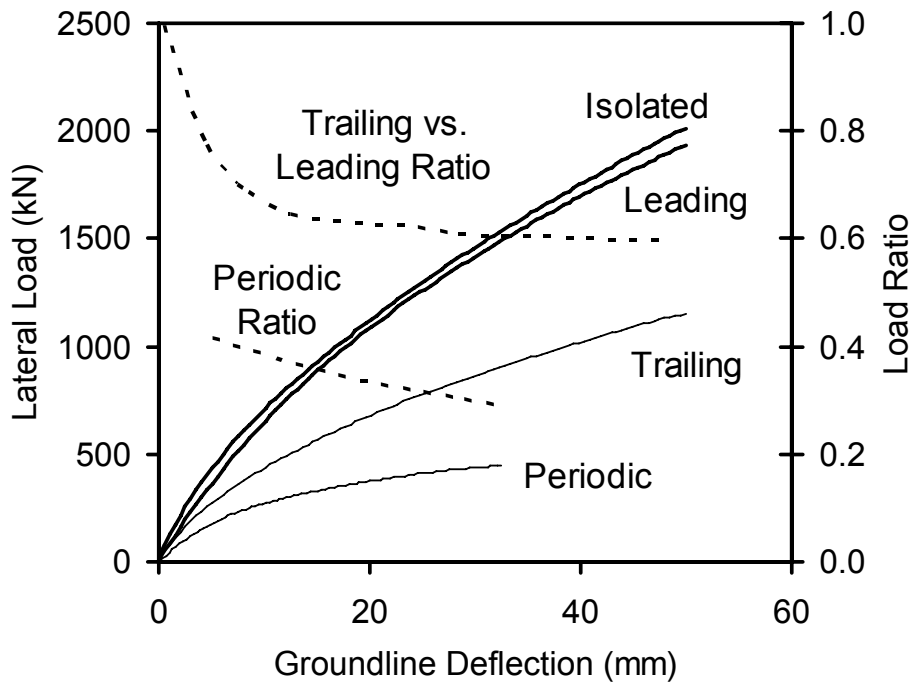
Figure 6-27: Typical pile head behavior for group piles laterally loaded in sand
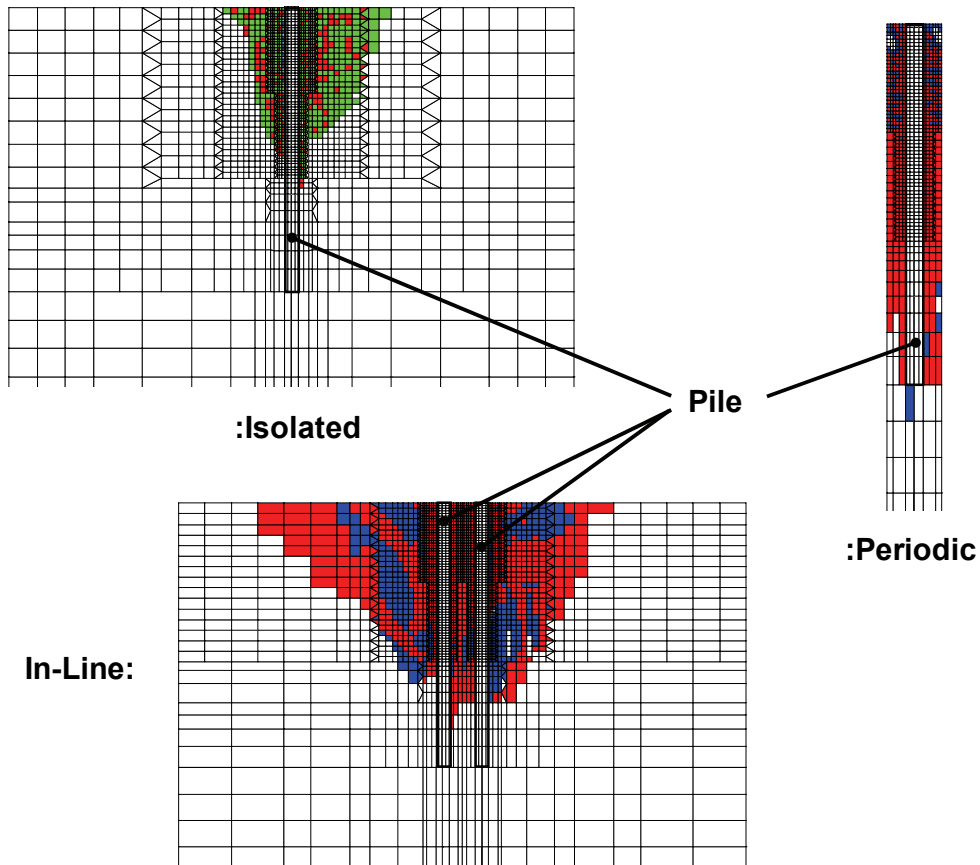
Figure 6-28: Typical plastic failure patterns exhibited in the sand research models
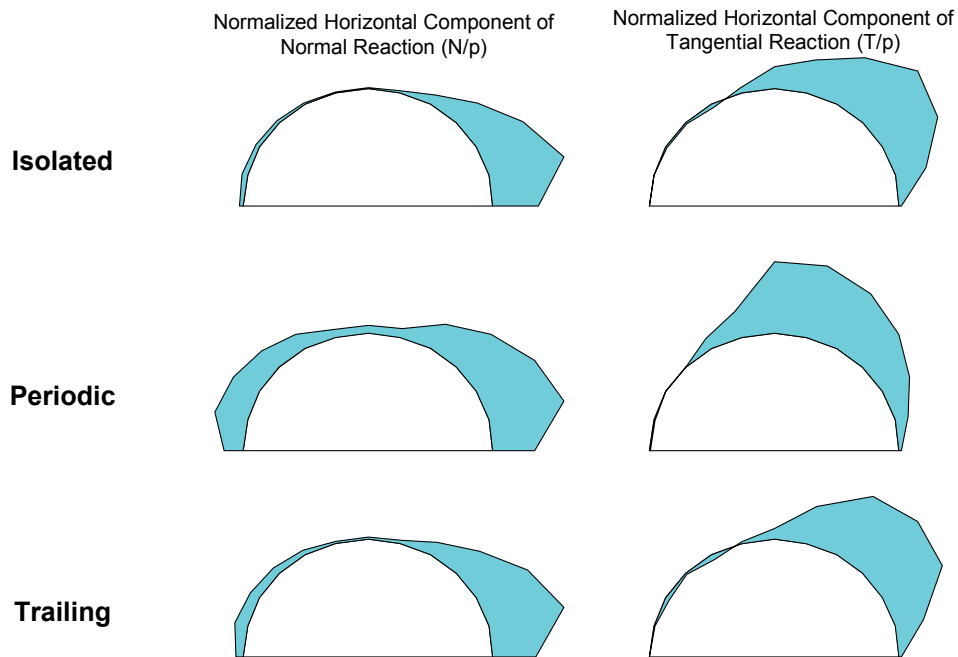
Figure 6-29: **Typical distribution of *p* around the pile for sand research cases**

6.3.1.2   Clay

LPILE Comparison: Typical comparative LPILE and *FLAC*[3D] behavior for the case of a laterally loaded isolated pile in clay is shown in Figure 6-30, Figure 6-31 and Figure 6-32.

p-y Behavior: A typical comparison of empirical and research clay *p-y* curves at a depth of two pile diameters is shown in Figure 6-33.

p-Multiplier Behavior: Typical *p*-multiplier behavior in clay is shown in Figure 6-34 through Figure 6-37.

Pile Behavior: Typical pile behavior exhibited for isolated and group pile cases in clay is shown in Figure 6-38.

Pile Head Behavior: Typical pile head behavior exhibited by the group pile cases in clay is shown in Figure 6-39.

Failure Patterns: Typical plastic failure patterns (failure indicated by the darker zones) exhibited in the three research analysis cases for clay are shown in Figure 6-40.

Circumferential Behavior: The typical distribution of *p* around the pile circumference at a depth equal to two pile diameters for the clay research analysis cases is shown in Figure 6-41.
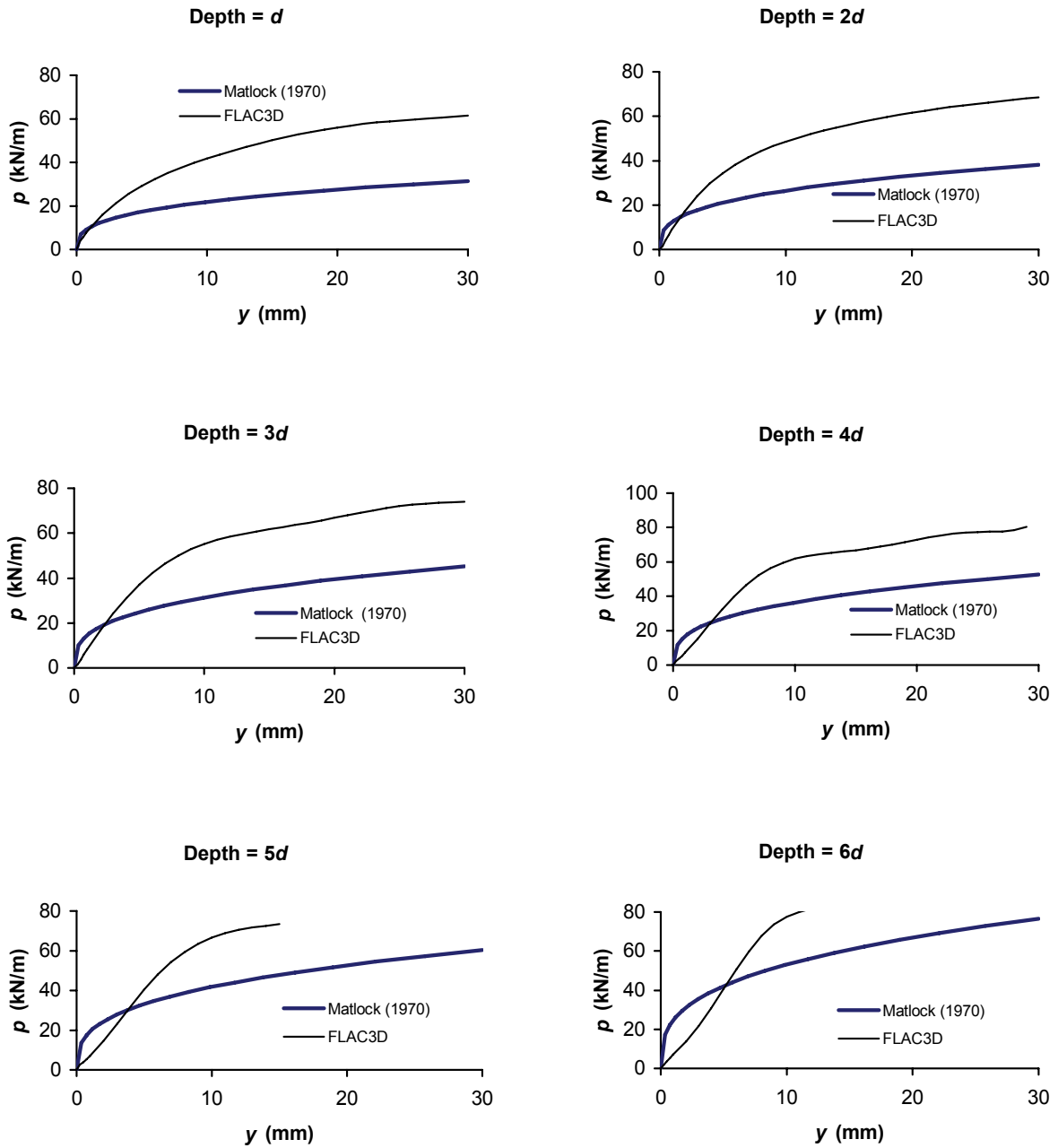
Figure 6-30: Typical comparison between empirical and research clay *p-y* curves
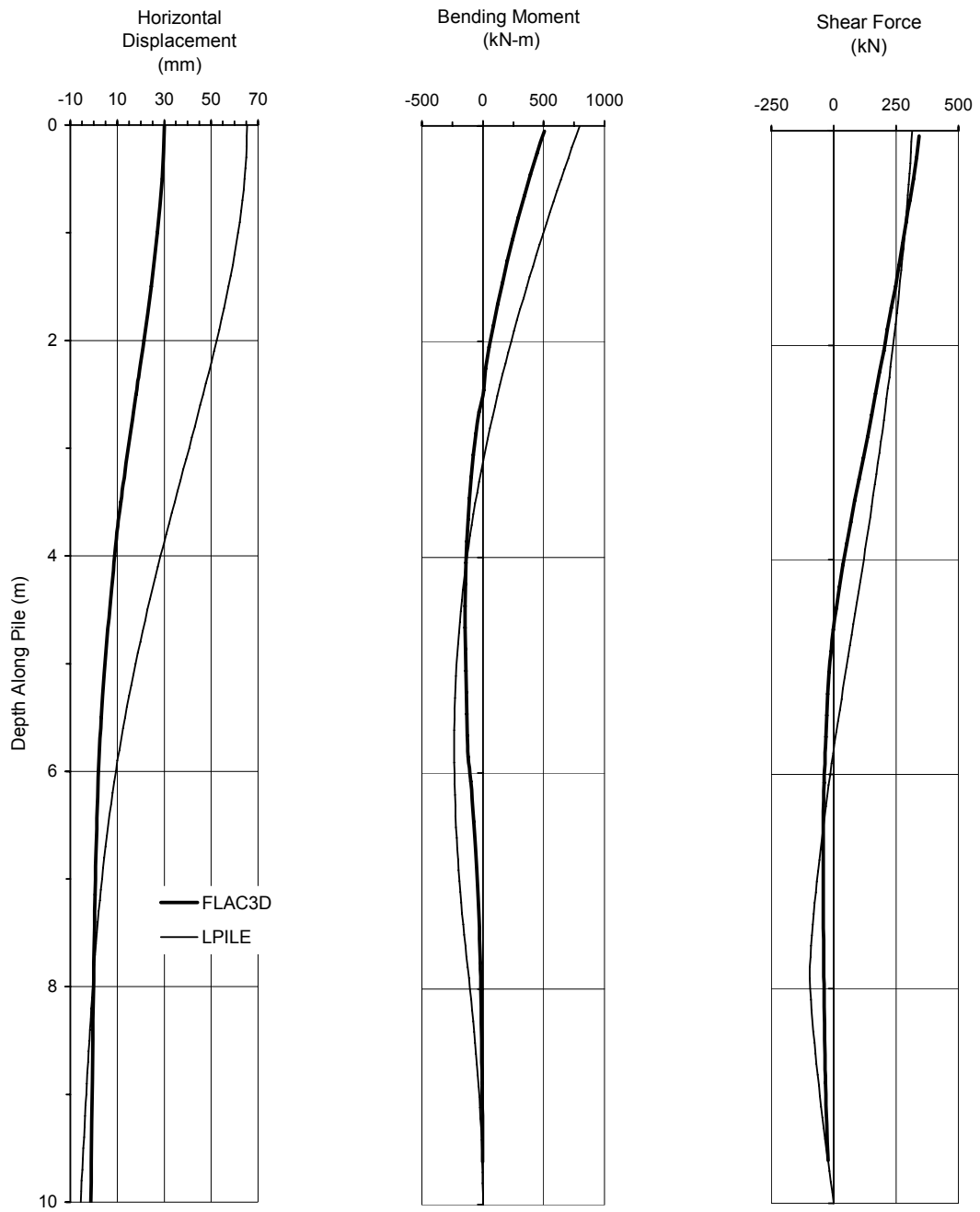
Figure 6-31: Typical comparison between LPILE and research pile behavior for laterally loaded isolated pile in clay
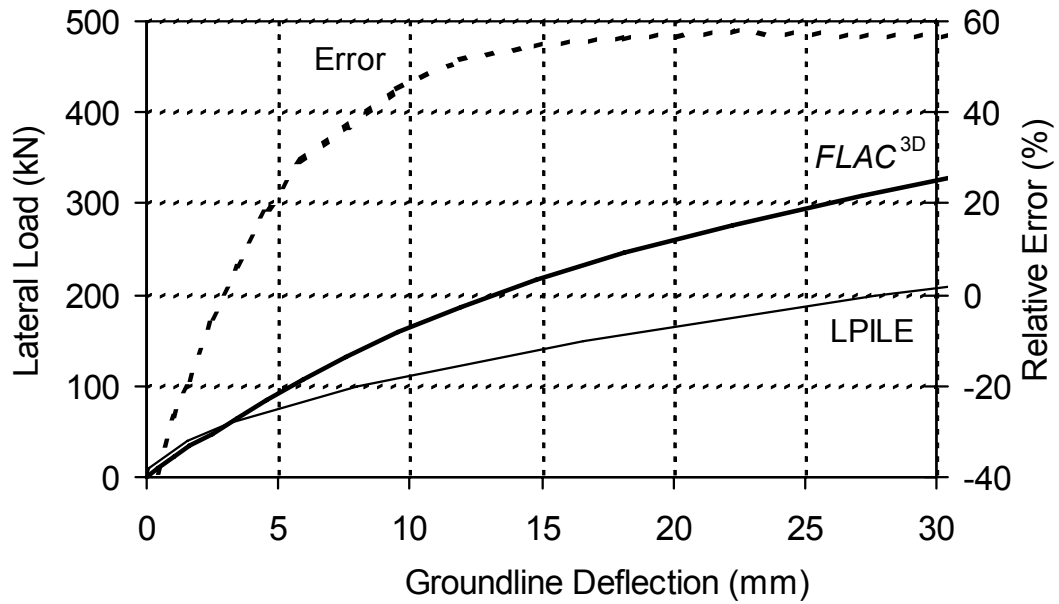
Figure 6-32: Typical comparison between LPILE and research pile head behavior for laterally loaded isolated pile in clay
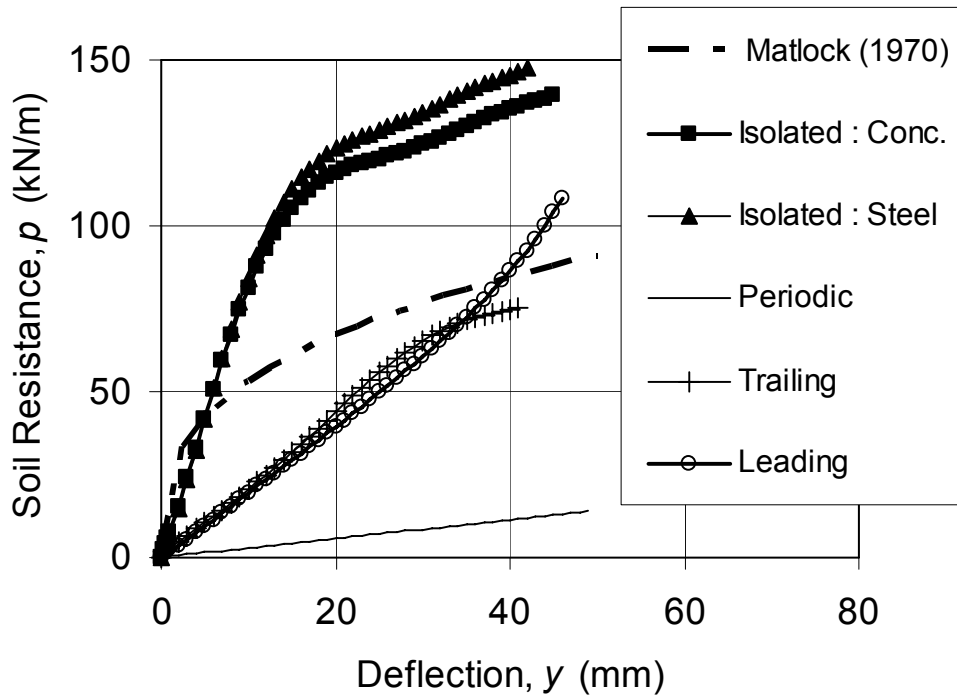
Figure 6-33: Typical comparison of empirical and research clay *p-y* curves at a depth equal to two pile diameters
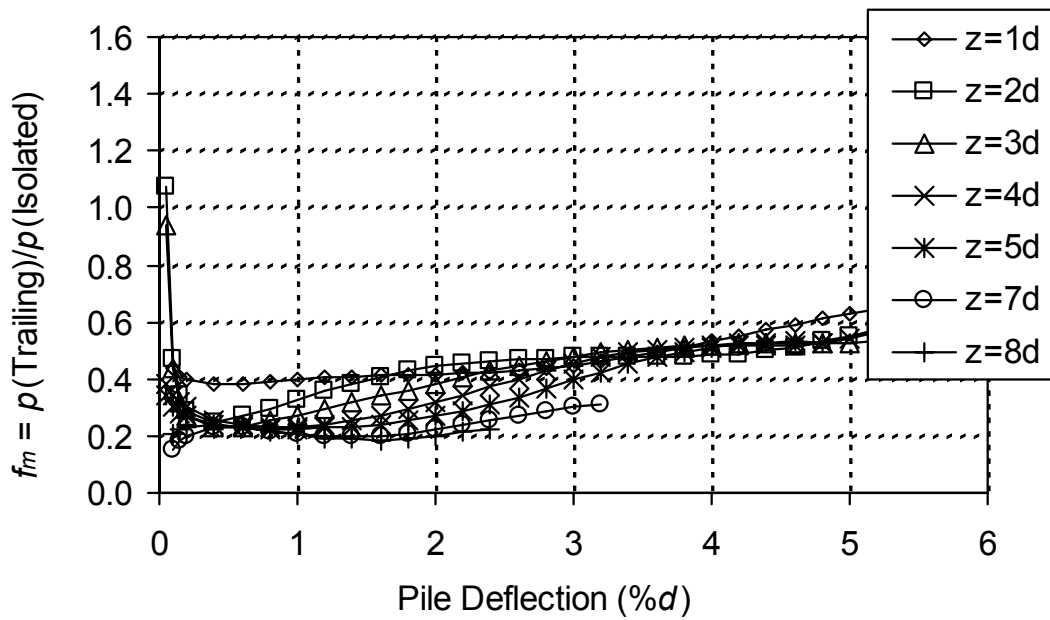
Figure 6-34: Typical variation of f_m for trailing piles in clay, $s = 3d$
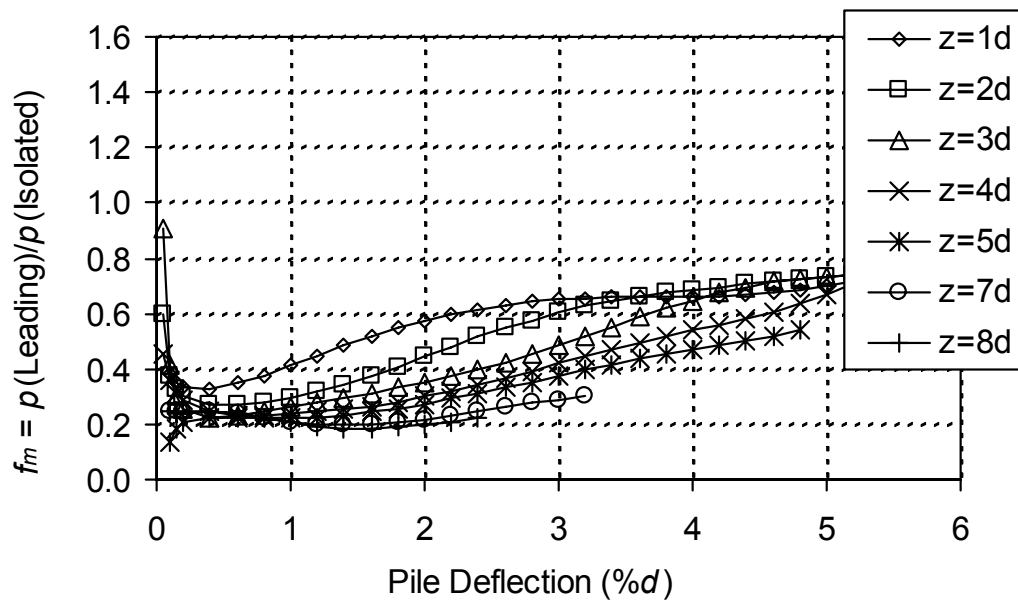
Figure 6-35: Typical variation of f_m for leading piles in clay, $s = 3d$
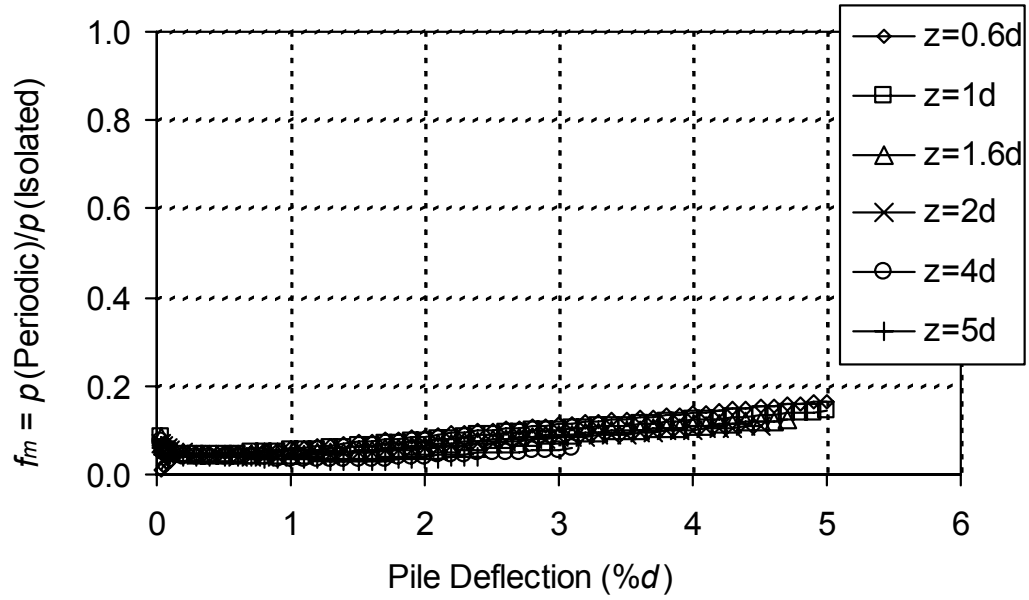
Figure 6-36: Typical variation of f_m for periodic piles in clay, $s = 3d$
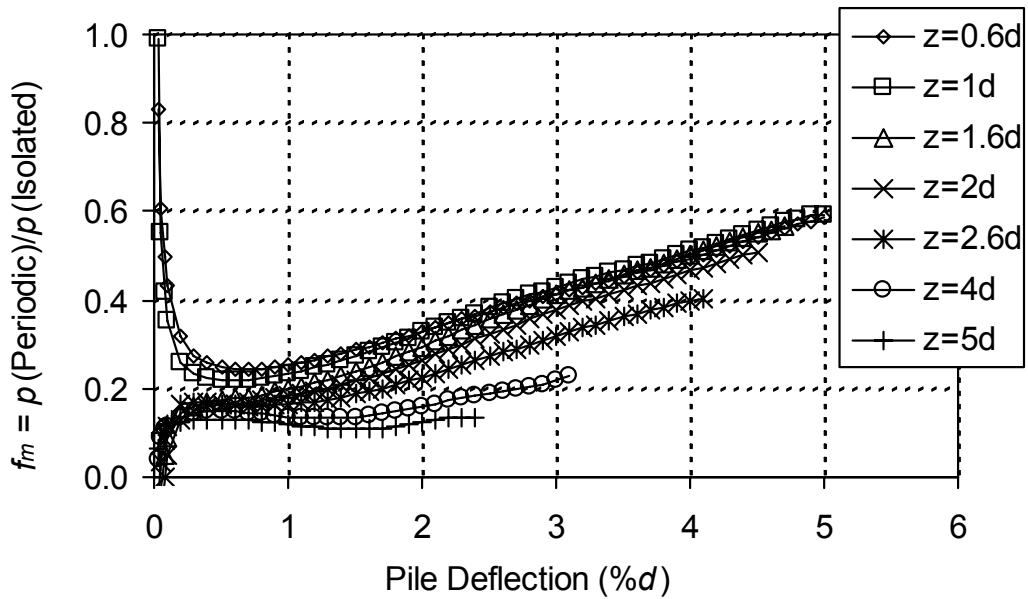
Figure 6-37: Typical variation of f_m for periodic piles in clay, $s = 6d$
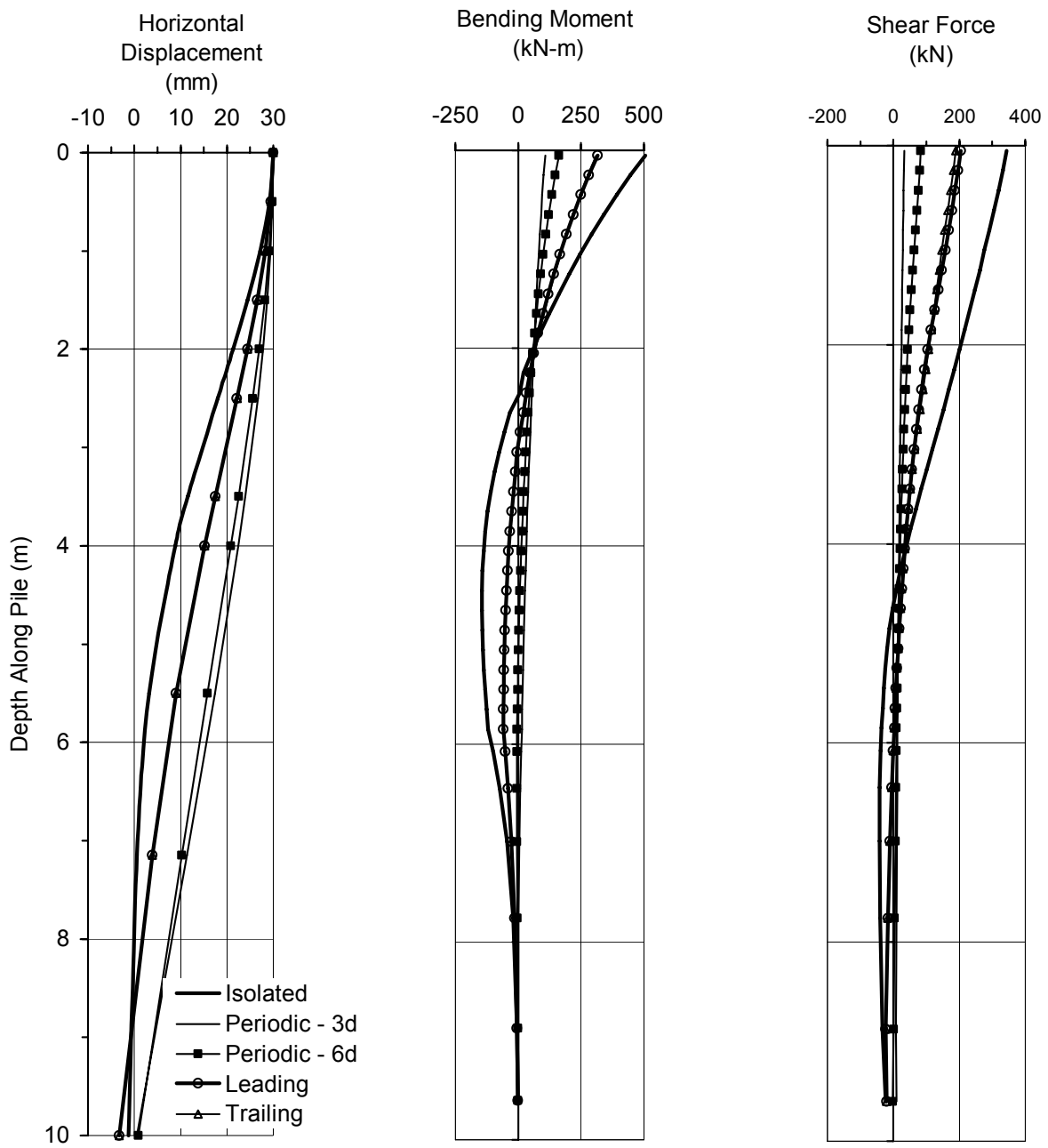
Figure 6-38: Typical pile behavior for isolated and group piles laterally loaded in clay
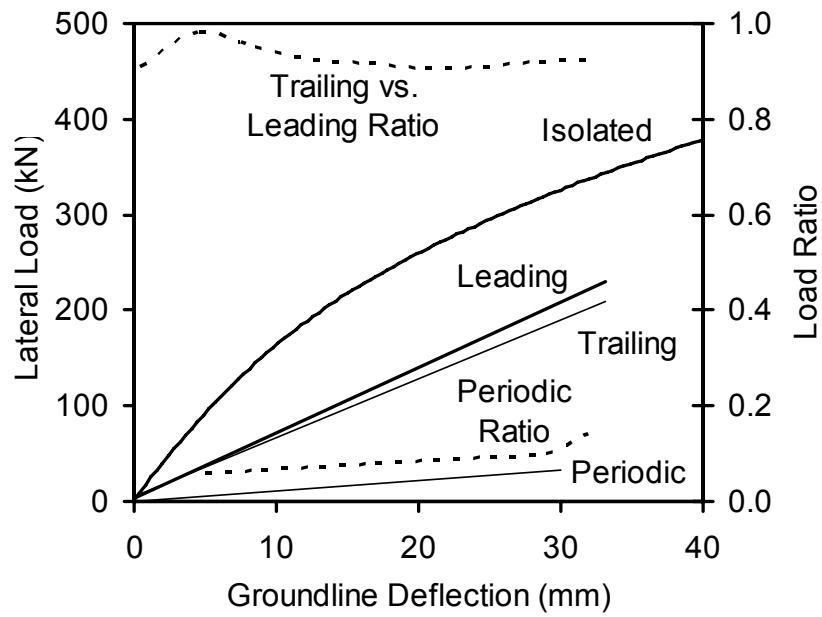
Figure 6-39: Typical pile head behavior for group piles laterally loaded in clay
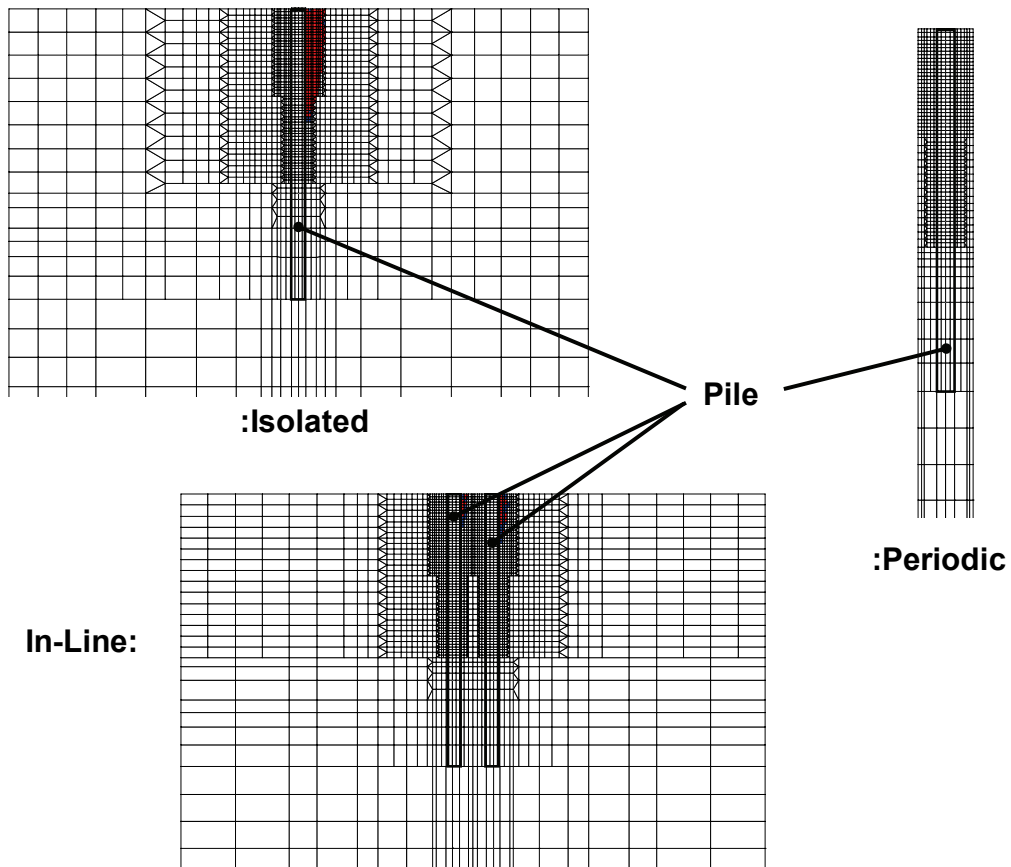
Figure 6-40: Typical plastic failure patterns exhibited in the clay research models
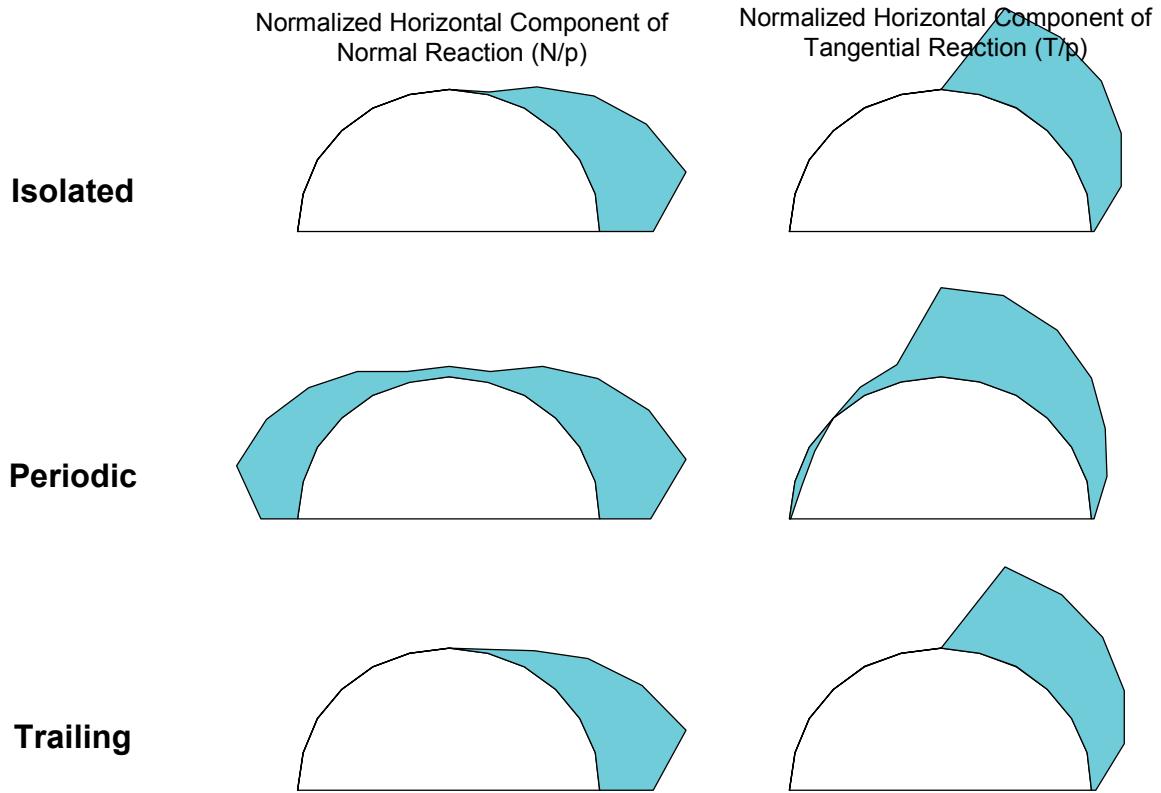
Figure 6-41: Typical distribution of *p* around the pile for clay research cases

6.3.1.3   Pile Head Ratio Results

To assist with the interpretation of the research results, an assessment of pile head resistance developed by the group piles relative to their respective isolated resistance was undertaken, using the so called pile head load ratio measure defined previously as

Pile Head Load Ratio =

$$\frac{\text{Lateral load applied at pile head of group pile at deflection } x}{\text{Lateral load applied at pile head of respective isolated pile at deflection } x}. \qquad (6.1) \text{ (ibid.)}$$

A summary of this behavior is given in Table 6-4.   The pile head ratio measure was considered a reasonable indicator of *p*-multiplier behavior, albeit on the high side.

Table 6-4: Summary of pile head ratio results

Ratio Case (/ Isolated Pile)	BSM Clay		BSM Sand		K_h
	$s = 3d$	$s = 6d$	$s = 3d$	$s = 6d$	
Leading Pile	0.4-0.6		0.95		0.5
	0.3-0.6		0.9		1.0
	0.4-0.6		0.95		0.5
Trailing Pile	0.4-0.6		0.55		0.5
	0.35-0.5		0.55		1.0
	0.35-0.5		0.6		0.5
Periodic Pile (Fixed Head)	0.1	0.2-0.3	0.2-0.4	0.4-0.8	1.0
	0.1	0.3-0.6	0.3-0.6	0.6-0.8	0.5
Periodic Pile (Free Head)	<0.05		0.1		1.0
	0.05		0.2		0.5

Note: ▢ = 1000 mm diameter pile (otherwise 500 mm)

6.3.2 Advanced Soil Models

Research analyses using the advanced Cam Clay and MDS soil models, representing more sophisticated elastic-plastic soil models for modeling clay and sand soils, respectively, were abandoned as a result of encountering numerical difficulties when attempting to execute lateral pile-soil analyses. Specifically, persistent numerical errors occurred in soil zones when velocity increments were applied to the numerical pile to simulate lateral loading. These errors occurred in association with the calculation of the magnitude of the proportionality factor (λ) associated with plastic behavior, and the source of the error was attributed to the solving for the root of the quadratic equation in λ, as required by both the Cam Clay and MDS model formulations. Complete details of the formulation for the MDS model and its implementation into $FLAC^{3D}$ are provided in Dodds (2005), including the derivation of the quadratic equation as just mentioned. A similar quadratic derivation applied to the Cam Clay model provided within $FLAC^{3D}$, details of which are given in the $FLAC^{3D}$ documentation ($FLAC^{3D}$, 1997).

It was suspected that the quadratic solution requirement was too onerous for the stress fluctuations occurring as a result of the sensitivity of the pile-soil system to movement. Successive reductions in the applied velocity increments reduced errors but did not remove them completely. Furthermore, these improvements were at the cost of excessively small velocities that proved too prohibitive in terms of computation time. Analysis attempts were therefore abandoned in favor of the more productive Base Soil Model analyses.

SECTION 7
DISCUSSION, CONCLUSIONS AND RECOMMENDATIONS

7.1   Discussion

7.1.1   General Performance

7.1.1.1   Numerical Comparisons

Comparison of the research results with results from previous three-dimensional finite-element studies on lateral pile-soil interaction, as described in Sections 2 and 3, indicates $FLAC^{3D}$ is comparable performance wise. Specifically, development of a wedge-shaped zone of plastic deformation in front of isolated research piles, deepening and extending outwards with increasing load level, agreed with the findings of Brown and Shie (1990a). Furthermore, the differing extent of plastic deformation when using constant failure strength ("clay") and pressure-dependent strength ("sand") soil models, as noted by Brown and Shie, was also apparent from the research results. Separation of the isolated research piles from the modeled soil to depths between approximately $6d$ and $8d$ compares with the depth of $6d$ reported by Trochanis et al. (1988, 1991a, 1991b) for their isolated pile configuration. In terms of group behavior, similar trends of reduced shears and occurrence of maximum bending moment at greater depths in trailing piles of two-pile in-line configurations, as noted by Brown and Shie (1990b, 1991a), was also observed from the in-line research results.

While the research results are comparable with previous work, it is important to note that the $FLAC^{3D}$ formulation demanded some provisos. The difficulties when attempting to model the Matlock (1970) isolated pile-soil configuration were discussed in Section 5, resulting in the restriction to only modeling steel pipe piles with diameters greater than 500 mm. Otherwise, smaller diameter piles demand a numerical stiffness associated with the equivalent solid section in $FLAC^{3D}$ that is problematic. Also, use of only velocity-control to apply lateral loads to piles in $FLAC^{3D}$ cannot be overstated, as discussed in Sections 4 and 5. This demands velocity increments that are small enough so as to contain unwanted inertial tendencies, and preferably applied in a gradual fashion (i.e., "ramped") to minimize shock effects.

7.1.1.2   Empirical Comparisons

A general observation that can be drawn from the results of the research analyses is that good agreement was achieved with behavioral trends observed in the field for both isolated and group pile cases, but poor quantitative predictions of pile and soil response was apparent. This was also noted with the case history comparisons undertaken in Section 5, and indicates differences in detail but similar overall trends compared with field test data. A particular difference in detail that was evident in several of the research cases was the appearance of an oscillatory form of p-y response, generally near or at the surface. Such behavior was attributed to the dynamic tendencies of $FLAC^{3D}$, where it is suspected that the relatively low stiffness and confinement provided by the soil continuum in the surficial region surrounding the pile tended to promote vibration of the modeled pile. The progressive nature of plastic failure in this region with increasing load may have also been a contributing factor. While the oscillatory behavior was not considered to have had any serious influence on overall behavior, it is suggestive of a dynamic inclination that could present itself in the field.

Performance of the isolated analyses was also defined by a general over-prediction of LPILE resistance at a given pile deflection. Reasons for this were attributed to several factors as discussed in Section 5: a) Differences between elastic-plastic continuum behavior and real soil behavior; b) velocity dependence inherent with the $FLAC^{3D}$ formulation; and c) the issue of initial soil conditions. In the case of the research models, initial soil conditions were characterized by the isotropic linear elastic (ILE) stiffness

model and initial stress conditions assigned to the soil continuum. The influence of the stiffness model was certainly apparent with the clay models, in that under-prediction of LPILE resistance at a given deflection was noticeable at small pile deflections. This early disparity clearly indicated an issue with the stiffness models used in each case.

In the LPILE case the stiffness of the clay was characterized by the ε_{50} value assigned to the soft clay p-y curves. The value of 0.02 used to compare LPILE with the research models is, according to Matlock (1970), appropriate to clays with undrained shear strengths less than 50 kPa, representing the range in strength intended for research purposes. It is to be noted, however, that various other recommendations have been made regarding initial p-y stiffness characteristics for such clay soils (refer Section 2). Furthermore, as discussed in Section 2, establishment of an accurate initial p-y stiffness value is subject to various issues that are generally poorly quantified. Thus the LPILE characterization of soil stiffness cannot be considered as an absolute benchmark.

In the research case the characterization of soil stiffness using the ILE model is certainly a compromise between ideals and material necessity. Nevertheless, consideration of a soft clay soil as an elastic continuum is not a bad approximation, and as evidenced by the numerical work discussed in Section 2, has provided a working basis for assessing lateral pile response for some time. To be noted is the importance of modeling an appropriate distribution of stiffness with depth (Pender, 2004), but in the active region of pile-soil interaction the research assumption of a linearly increasing stiffness with a non-zero value at the ground surface was reasonably compatible with the distribution afforded by the soft clay p-y curves. Thus the issue was not so much the stiffness models themselves, but achieving equivalency in their behavior.

Key aspects in this regard are the progression from elastic to plastic behavior from a modeling standpoint, and sufficient knowledge of initial soil conditions from a field testing standpoint. Elastic as well as plastic parameters dictate the nonlinear behavior that is manifested from an elastic-plastic material model, because the amount of strain prior to reaching an ultimate (plastic) state is controlled by the elastic stiffness of the material. Hence the extent of plastic failure occurring in the soil continuum of the research models was a function of both the elastic parameters (Young's modulus and Poisson's ratio, or alternatively shear modulus and bulk modulus) and plastic parameters (cohesion and friction angle) assigned to the soil zones. Given the Base Soil Model (BSM) strength characterization of clay and sand (i.e., c-soil and ϕ-soil failure qualities, respectively), this meant that potential for plastic failure focused more on elastic parameters in the clay cases, while the frictional strength (plastic) qualities of the ϕ-soil largely influenced nonlinear behavior in the sand cases.

Considering the emphasis on elastic parameters for the clay research models, improvement in performance could have been achieved by adopting a value of zero for Young's modulus at the ground surface, instead of the non-zero value of 5000 kPa used in the research cases. Use of the more advanced Cam Clay soil model may also have improved performance since its stress-strain qualities are continuously nonlinear[§] for a normally consolidated condition. The initial stress state can also play a part here, as was demonstrated by the differences in response for the $K_h = 0.5$ and $K_h = 1.0$ stress states investigated in the research – in the sand case up to a 20 percent difference in lateral load resistance for a given deflection. However, these arguments hold no basis if the actual initial soil conditions in the ground are unknown, a state of affairs that is unfortunately more often the case than not.

Interconnected with initial soil conditions are various construction-related effects that contribute to what is observed in field tests, as discussed in Sections 2 and 3. Not the least of these is the effect from installing a pile into the ground, an issue that has only recently begun to have been considered in

---

[§] At least until a critical state is achieved.

208

sufficient detail for it to be adequately quantified for lateral pile analysis purposes (e.g., Huang et al., 2001; Brown et al., 2001). Thus fitting elastic-plastic soil models to observed pile response is not only a matter of numerical adequacy and refinement, but also an exercise in site characterization in order that numerical models can be utilized meaningfully. Characterization of initial stiffness and its distribution with depth is particularly important given that this is a key parameter controlling nonlinear response of a modeled pile when using an elastic-plastic representation of the soil.

7.1.2   Observed Trends

Observed trends in group behavior compared well with field observations, and this supports the position advanced in Sections 2 and 3 that normalizing behavior in terms of isolated behavior to assess group effects is tolerant of the quantitative shortcomings discussed above. Pronounced reduction in lateral load capacity for a given deflection featured with both the trailing pile and periodic piles compared with leading and isolated piles. Such results reflect similar field observations of reduced soil resistance at a given deflection for group piles that is a function of row position. Deepening of the location of maximum bending moment in the trailing pile compared with leading pile, and thus deepening of the zone of pile-soil interaction was also apparent, as also observed in the field (e.g., Schmidt, 1985; Meimon, Baguelin and Jezequel, 1986; Brown et al., 1987; Brown et al., 2001).

The marked differences in pile responses with depth indicated by the research, however, is an aspect not so well appreciated from field observations, if at all. While the research plots of typical comparative pile head behavior (refer Figure 6-27 and Figure 6-39) clearly indicate reduced group pile resistance, they do little to explain the reasons for such behavior. Upon inspection of the typical deflected pile shapes (refer Figure 6-26 and Figure 6-38), the suggestion of behavior akin to rigid pile behavior is immediately apparent with the periodic pile cases, and to a lesser extent with the trailing piles. This is a direct consequence of the geometrical implications of group behavior, in that soil surrounding a pile will tend to move with the pile given the similar movement of surrounding piles (assuming a rigid pile cap applies).

The periodic boundary assumption represents the extreme of this type of behavior, so that the trend of reduced resistance is simply the result of lack of relative lateral pile-soil movement. In addition, however, the different modeling attributes of the BSM sand and clay, as discussed in the previous section, also imparted an influence. This was apparent from the highly linear (elastic) response of both the in-line and periodic clay cases, whereas the in-line and periodic sand cases exhibited appreciable nonlinear (plastic) response. The preponderance of elastic behavior in the in-line clay case was attributed to the fairly constant strength profile assigned, promoting elastic-based interaction over the entire pile length. In the periodic clay case it was attributed to the simple shear action in the soil continuum surrounding the pile, allowing elastic movements with ease.

In comparison with the fairly uniform strength and stiffness provided by the BSM clay, the BSM sand provided strength and stiffness that was highly variable with depth. Although much greater in strength and stiffness at-depth compared with the BSM clay, the specification of zero strength and stiffness at the ground surface resulted in a comparatively weaker and softer soil continuum in the upper regions of interest. Such reduced surficial strength promoted the wedge-shaped zone of plastic failure seen in the sand cases, given that resistance to lateral loading is mobilized mainly from within this region. Thus a distinctly different form of pile-soil response was apparent with the BSM sand, resembling the type of free-body wedge mechanism that has been used to describe soil resistance against a pile in various instances (e.g., Reese, 1958; Norris, 1986).

Distribution of the soil resistance (p) around the pile with depth is an aspect without empirical comparison, given the difficulty of measuring such behavior in the field. Nevertheless, the relative success of the research models in simulating observed behavior gives some credence to the

circumferential action recorded (refer Dodds, 2005), albeit for specific interface parameters only. Inspection of the circumferential behavior indicated that the distribution of p with depth varied according to the pile-soil model and study factors, but the distribution of p around the pile was less sensitive to such changes. This provides some justification to the two-dimensional simplification of pile-soil interaction using line elements to represent the pile and p-y curves to represent the soil resistance, as is commonly the case in practice.

7.1.3   Comments

The research undertaken has served to provide more insight into the mechanics of lateral pile-soil interaction, and certainly emphasizes the need for an assessment of pile-soil systems in their entirety in order to fully appreciate the observed pile response. Perhaps the most noteworthy of findings is the capability of producing numerical pile-soil systems with distinctly different response and interaction characteristics, depending on the constitutive formulation used to model the soil, the initial stress and stiffness conditions assigned to such a soil, and the boundary conditions applied to the pile-soil model. In terms of the pile-soil models utilized in the immediate research, these factors were evident to differing degrees when considering their effect on pile behavior. Specifically, isolated pile-soil models exhibited more sensitivity to the constitutive formulation and initial conditions assigned to the soil continuum, compared with the periodic pile-soil models where the effect of the boundary conditions negating resistance by reducing relative pile-soil movement was far more evident.

This suggests that for the purely translational resistance of interior piles in large pile groups, the role of soil in providing resistance is somewhat diminished compared with an isolated pile case. The basis for p-y curve representation in the interior pile case is therefore weakened, given that lack of relative pile-soil movement and elastic interaction is not within the realm of p-y curve behavior from a strictly mechanistic point of view. However, when viewed as just a convenient mathematical parameter expressing the ratio of a soil reaction to pile deflection relationship, as appreciated by Jamiolkowski and Garassino (1977) and as is applied in practice, the p-y curve and group adjustment factors in the form of p- and y-multipliers are appropriate. It is noted that given the mechanistic focus on boundary movements rather than loss of soil resistance for the periodic pile-soil model, arguing a case for use of y-multipliers rather than p-multipliers to represent translational large pile group effects in the current study certainly has merit. However, considering lateral group resistance on the whole, and the difficulty of extracting the translational component from this overall behavior in practice, using either a p-multiplier or y-multiplier is neither here nor there.

The various factors and conditions that can influence pile group behavior were discussed in Section 3, where it was apparent that characterization of lateral pile group behavior is a multifaceted task. Thus characterization of translational pile-soil-pile interaction is but one step in the process of characterizing the lateral stiffness of a pile group. Other issues that a designer will be faced with, as discussed in Section 3, are repeated as bulleted items below, serving as a reminder of the complexity of the task ahead:

- Installation effects.
- Structural properties of the piles and pile-head conditions.
- Cross-coupling of lateral and axial stiffness modes.
- Soil conditions.

The last bulleted item is the subject of a final comment to note concerning real soil behavior. Zhang and McVay (1999) considered that gaps and cracks in clay prevent transfer of stresses and thus deny stress overlap leading to diminished shadowing effects. Another real soil condition is the development of shear bands. Bardet and Proubet (1991) undertook a discrete numerical investigation of these failure mechanisms and implied that periodic boundaries reflected shear bands, allowing for collapse

mechanisms different from those had the shear bands not been reflected. Thus modeling such behavior in the context of periodic pile-soil models used for the current research may not be appropriate, sounding a note of caution for the use of modeling economies when utilizing more sophisticated modeling approaches.

7.2   Conclusions

The capability of $FLAC^{3D}$ to assess group effects was confirmed, both in qualitative and quantitative terms. Utilizing elastic piles, elastic-plastic soil models, and simplified representations of group piles, large pile group effects were studied and from the standpoint of pile head response, results are generally in good agreement with field observations on small pile groups, although they are suggestive of lower row multipliers, particularly for clay. Soil resistance versus pile deflection (i.e., *p-y*) behavior for the group piles compliments the pile head response behavior in a general sense, however variation of *p*-multipliers with depth was apparent as a result of different deflected pile shapes and soil resistance patterns compared with isolated piles. Overall, the large pile group study indicated that initial stress state, pile type and pile-head restraint resulted in some differences, but these were relatively weak compared with the influence of soil behavior.

Marked differences in soil response against the piles were primarily associated with the different failure criteria employed for the sand and clay models, and effects resulting from the boundary condition employed for the group models. These factors are interdependent and demonstrate a need to appreciate a relative pile-soil stiffness influence brought about by group effects. The periodic piles in clay clearly illustrated this influence by exhibiting behavior akin to rigid rather than flexible pile behavior. This is particularly the case for interior piles of large pile groups, where much lower *p*-multipliers are considered appropriate. Thus significantly softer translational stiffnesses for large pile groups, compared with current recommendations, should be applied.

In terms of design, the research has enabled greater insight into the mechanics of large pile group lateral stiffness due to horizontal translation, providing appropriate magnitudes of *p*-multipliers to be applied to *p-y* curves for clay and sand conditions. However, the research has also emphasized the fact that characterization of lateral pile group behavior is a multifaceted task that is rich in empirical content and masked by its complexity. Translational stiffness is also just one lateral design mode to contend with, rocking stiffness being another that raises the important issue of cross-coupling between lateral and axial pile behavior. Issues surrounding installation effects, pile, pile head and soil conditions also feature, ensuring that the task of assessing lateral group stiffness remains a challenging endeavor.

7.3   Recommendations

A behavioral trend that is clear from the research results is the significantly reduced translational resistance of periodic piles compared with isolated and leading piles. Accordingly, design recommendations are provided for *p*-multiplier values that characterize the translational resistance of large pile groups. These are based on a practically-orientated assessment of the pile head ratio and *p*-multiplier research results for periodic piles, and are appropriate to typical interior piles of large pile groups. The design recommendations are indicated on Figure 7-1, where they are shown relative to the current design recommendations for smaller pile groups that were discussed in Section 3.

The design recommendations are also tabulated in Table 7-1 for record purposes, together with the large pile group recommendations made by Law and Lam (2001). Given that the Law and Lam recommendations also included respective *y*-multipliers, it is not possible to make a direct comparison. However, the *y*-multiplier values recommended by Law and Lam suggest overall reductions in lateral resistance of the same order as found in the current study.

Table 7-1: Record of large pile group recommendations

Large Pile Group Study	Soil Condition	Center to Center Spacing (*s*)	
		s = 3d	*s = 6d*
Law and Lam (2001)	Soft clay	0.5[1]	0.75[2]
Current Study	Soft clay	0.1	0.5
	Medium dense sand	0.2	0.7
Notes: (1) *y*-multiplier of 4 also applies. (2) *y*-multiplier of 2 also applies.			
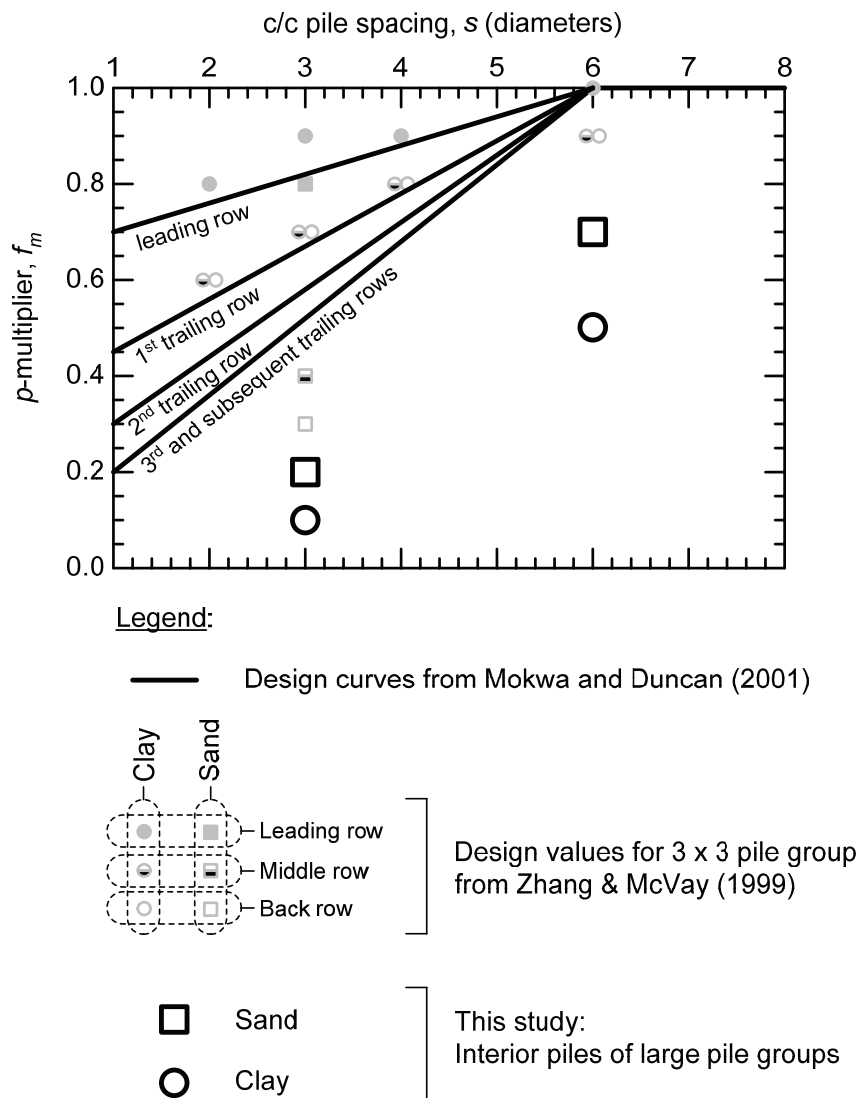
Figure 7-1: Recommended *p*-multiplier design values for the translational mode of lateral resistance of large pile groups

7.4   Further Studies

While the research has achieved greater insight into the mechanics of large pile group pile-soil-pile interaction under lateral loading, it is clear that further studies are required to better understand the lateral stiffness of large pile groups. Improvement on the characterization of field conditions for modeling purposes is considered the greatest need, given that lateral behavior of any pile-soil system, be it an isolated or group configuration, is contingent on appropriate modeling of such field conditions. Given the complexity afforded by the various factors contributing to observed group behavior, research efforts aimed at assessing the effect of a range of values is considered a shrewd investment of time. Greater appreciation of the behavior of a large pile group in its entirety is also a definite need, calling for research into rocking behavior and its importance relative to the translational mode of lateral resistance. Suggested topics of further studies are listed below accordingly.

- Field studies in conjunction with numerical modeling to characterize soil and pile conditions.
- Parametric numerical 3-D studies to establish trends and identify relative effects.
- Assessment of coupling between translational and rocking modes of resistance.

SECTION 8
REFERENCES

Allen, J. D. (1985). "*p-y Curves in Layered Soils*." Doctor of Philosophy Thesis, The University of Texas at Austin, Texas.

American Petroleum Institute (1993). "Section 6 : Foundation Design." In *Recommended Practice for Planning, Designing and Constructing Fixed Offshore Platforms - Working Stress Design*, API Recommended Practice 2A-WSD (RP 2A-WSD), Twentieth Edition, July 1, American Petroleum Institute, Washington, D.C. 20005, 57-71.

Anderson, J. B., Townsend, F. C., and Grajales, B. (2003). "Case history evaluation of laterally loaded piles." *J. Geotech. Geoenvir. Eng.,* ASCE, 129(3), March, 187-196.

Ashford, S. A. and Juirnarongrit, T. (2003). "Evaluation of pile diameter effect on initial modulus of subgrade reaction." *J. Geotech. Geoenvir. Eng.,* ASCE, 129(3), March, 234-242.

Ashour, M. and Norris, G. (2000). "Modeling lateral soil-pile response based on soil-pile interaction." *J. Geotech. Geoenvir. Eng.,* ASCE, 126(5), May, 420-428.

Ashour, M., Norris, G., and Pilling, P. (1998). "Lateral loading of a pile in layered soil using the strain wedge model." *J. Geotech. Geoenvir. Eng.,* ASCE, 124(4), April, 303-315.

Ashour, M., Norris, G., and Shamsabadi, A. (2001). "Effect of the non-linear behavior of pile material on the response of laterally loaded piles." In *Proceedings, Fourth International Conference on Recent Advances in Geotechnical Earthquake Engineering and Soil Dynamics and Symposium in Honor of Professor W.D. Liam Finn*, San Diego, California, March 26-31, 2001, Paper No. 6.10, 1-8.

Ashour, M., Pilling, P., and Norris, G. (1997). "Documentation of the strain wedge model program for analyzing laterally loaded piles and pile groups." In *Proceedings of the 32nd Symposium on Engineering Geology and Geotechnical Engineering*, held at the Owyhee Plaza Hotel, Boise, Idaho, March 26-28, 1997, 141-156.

Ashour, M., Pilling, P., and Norris, G. (2001). "Assessment of pile group response under lateral load." In *Proceedings, Fourth International Conference on Recent Advances in Geotechnical Earthquake Engineering and Soil Dynamics and Symposium in Honor of Professor W.D. Liam Finn*, San Diego, California, March 26-31, 2001, Paper No. 6.11, 1-6.

Ashour, M., Pilling, P., and Norris, G. (2004). "Lateral behavior of pile groups in layered soils." *J. Geotech. Geoenvir. Eng.,* ASCE, 130(6), June, 280-292.

Baguelin, F. and Frank, R. (1980). "Theoretical studies of piles using the finite element method." In *Proceedings of the Conference on Numerical Methods in Offshore Piling,* London, England: 22-23 May, 1979, T.-P. E. Darwent (ed.), Institution of Civil Engineers, London, 83-91.

Baguelin, F., Frank, R., and Saïd, Y. H. (1977). "Theoretical study of lateral reaction mechanism of piles." *Géotechnique*, 27(3), 405-434.

Banerjee, P. K. (1976). "Integral equation methods for analysis of piece-wise non-homogeneous three-dimensional elastic solid of arbitrary shape." *Int. J. Mech. Sci.*, 18(6), 293-303.

Banerjee, P. K. (1978). "Analysis of axially and laterally loaded pile groups." In *Developments in Soil Mechanics - 1*, C. R. Scott (ed.), Applied Science Publishers Ltd., London, 317-346.

Banerjee, P. K. and Davies, T. G. (1978). "The behavior of axially and laterally loaded single piles embedded in non-homogoneous soils." *Géotechnique*, 28(3), 309-326.

Banerjee, P. K. and Driscoll, R. M. (1976a). "Three-dimensional analysis of raked pile groups." *Proc. Instn Civ. Engrs*, 61, 653-671.

Banerjee, P. K. and Driscoll, R. M. (1976b). "Three-dimensional analysis of vertical pile groups." In *Proceedings, Second International Conference on Numerical Methods in Geomechanics,* held at Virginia Polytechnic, Blacksburg, Virginia in June, 1976, C. S. Desai (ed.), ASCE, New York, NY 10017, 438-450.

Bardet, J.P. and Proubet, J. (1991). "A numerical investigation of the structure of persistent shear bands in granular media." *Géotechnique*, 41(4), 599-613.

Bathe, K.-J. (1996). *Finite Element Procedures*, Prentice Hall, Upper Saddle River, New Jersey 07458.

Been, K. and Jefferies, M. G. (1985). "A state parameter for sands." *Géotechnique*, 35(2), 99-112.

Bhowmik, S. K. and Long, J. H. (1991). "An Analytical Investigation of the Behavior of Laterally Loaded Piles." In *Geotechnical Engineering Congress 1991, Boulder, Colorado; June 10-12, 1991 (Geotechnical Special Publication No. 27)*, Vol. II, Proceedings of the Congress sponsored by the Geotechnical Engineering Division, A.S.C.E. in cooperation with the University of Colorado, U.S. Bureau of Reclamation, F. G. McLean, DeW. A. Campbell, & D. W. Harris (eds.), American Society of Civil Engineers, New York, New York 10017-2398, 1307-1318.

Biot, M. A. (1937). "Bending of an infinite beam on an elastic foundation." *J. Appl. Mech.,* ASME, 59, A1-A7.

Bransby, M. F. (1999). "Selection of *p-y* curves for the design of single laterally loaded piles." *Int. J. Numer. Anal. Methods Geomech.*, 23, 1909-1926.

Brettmann, T. and Duncan, J. M. (1996). "Computer application of CLM lateral load analysis to piles and drilled shafts." *J. Geotech. Eng.,* ASCE, 122(6), 496-498.

Briaud, J.-L. (1984). "Panel Discussion." In *Laterally Loaded Deep Foundations: Analysis and Performance*, A symposium sponsored by ASTM Committen D-18 on Soil and Rock, Kansas City, MO, 22 June 1983, J. A. Langer, E. T. Mosley, & C. D. Thompson (eds.), ASTM, Philadelphia, PA 19103, 239-243.

Briaud, J.-L., Smith, T., and Meyer, B. (1984). "Laterally loaded piles and the pressuremeter: comparison of existing methods." In *Laterally Loaded Deep Foundations: Analysis and Performance (ASTM STP 835)*, A symposium sponsored by ASTM Committee D-18 on Soil and Rock, Kansas City, MO, 22 June 1983, J. A. Langer, E. T. Mosley, & C. D. Thompson (eds.), American Society for Testing and Materials, Philadelphia, PA 19103, 97-111.

Briaud, J. L., Smith, T. D., and Tucker, L. M. (1985). "A pressuremeter method for laterally loaded piles." In *Proceedings of the Eleventh International Conference on Soil Mechanics and Foundation Engineering*, Publications Committee of XI ICSMFE (ed.), A.A. Balkema, Boston, 1353-1356.

Broms, B. B. (1964a). "Lateral resistance of piles in cohesionless soils." *J. Soil Mechanics and Foundations Division,* ASCE, 90(SM3), 123-156.

Broms, B. B. (1964b). "Lateral resistance of piles in cohesive soils." *J. Soil Mechanics and Foundations Division,* ASCE, 90(SM2), 27-63.

Broms, B. B. (1965). "Design of laterally loaded piles." *J. Soil Mechanics and Foundations Division,* ASCE, 91(SM3), 79-99.

Brown, D. A., Morrison, C., and Reese, L. C. (1988). "Lateral load behavior of pile group in sand." *J. Geotech. Eng.,* ASCE, 114(11), 1261-1276.

Brown, D. A., Morrison, C., and Reese, L. C. (1990). Closure to discussion: Lateral Load Behavior of Pile Group in Sand. *J. Geotech. Eng.,* ASCE, 116(8), 1282-1283.

Brown, D. A. and Reese, L. C. (1985). *Behavior of a large-scale pile group subjected to cyclic lateral loading*, Report to the Minerals Management Services, U.S. Dept. of Interior, Reston, VA. Dept. of Research, FHWA, Washington D.C. and US Army Engineer Waterways Experiment Station, Vicksburg, Mississippi.

Brown, D. A., Reese, L. C., and O'Neill, M. W. (1987). "Cyclic lateral loading of a large-scale pile group." *J. Geotech. Eng.,* ASCE, 113(11), 1326-1343.

Brown, D. A. and Shie, C.-F. (1990a). "Three-dimensional finite element model of laterally loaded piles." *Comp. and Geotechnics*, 10, 59-79.

Brown, D. A. and Shie, C.-F. (1990b). "Numerical experiments into group effects on the response of piles to lateral loading." *Comp. and Geotechnics*, 10, 211-230.

Brown, D. A. and Shie, C.-F. (1991a). "Modifications of *p-y* curves to account for group effects on laterally loaded piles." In *Geotechnical Engineering Congress 1991, Boulder, Colorado; June 10-12, 1991 (Geotechnical Special Publication No. 27)*, Vol. II, Proceedings of the Congress sponsored by the Geotechnical Engineering Division, A.S.C.E. in cooperation with the University of Colorado, U.S. Bureau of Reclamation, F. G. McLean, DeW. A. Campbell, & D. H. Harris (eds.), American Society of Civil Engineers, New York, New York 10017-2398, 479-490.

Brown, D. A. and Shie, C.-F. (1991b). "Some numerical experiments with a three-dimensional finite element model of a laterally loaded pile." *Comp. and Geotechnics*, 12, 149-162.

Brown, D. A., Shie, C.-F., and Kumar, M. (1989). "*p-y* curves for laterally loaded piles derived from three-dimensional finite element model." In *Proceedings, Third International Symposium, Numerical Models in Geomechanics (NUMOG III)*, S. Pietruszczak & G. N. Pande (eds.), Elsevier Applied Science, New York, 683-690.

Brown, D. A., O'Neill, M. W., Hoit, M., McVay, M., El Naggar, M. H., and Chakraborty, S. (2001). *Static and Dynamic Lateral Loading of Pile Groups,* National Cooperative Highway Research Program, NCHRP Report 461, National Academy Press, Washington, D.C.

Budhu, M. and Davies, T. G. (1987). "Nonlinear analysis of laterally loaded piles in cohesionless soils." *Can. Geotech. J.*, 24, 289-296.

Budhu, M. and Davies, T. G. (1988). "Analysis of laterally loaded piles in soft clay." *J. Geotech. Eng.,* ASCE, 114(1), 21-39.

Carter, J. P., Desai, C. S., Potts, D. M., Schweiger, H. F., and Sloan, S. W. (2000). "Computing and computer modelling in geotechnical engineering." In *Proceedings of GeoEng 2000, An International Conference on Geotechnical and Geological Engineering,* 19-24 November 2000, Melbourne Exhibition and Convention Centre, Melbourne Australia, Vol. 1, GeoEng 2000 (ed.), Technomic, Melbourne, Australia, 1157-1252.

Carter, M. and Bentley, S. P. (1991). *Correlations of Soil Properties*, Pentech Press, London.

Chen, W.-F. and Saleeb, A. F. (1982). *Constitutive Equations for Engineering Materials, Volume 1 - Elasticity and Modeling*, John Wiley Interscience, New York, NY.

Cox, W. R., Reese, L. C., and Grubbs, B. R. (1974). "Field testing of laterally loaded piles in sand." In *Proceedings, Sixth Annual Offshore Technology Conference, 6-8 May, 1974, Houston Texas*, Paper No. 2079, Offshore Technology Conference, Houston, Texas, 459-472.

Cundall, P. (1976). "Explicit finite-difference methods in geomechanics." In *Proceedings of the Second International Conference on Numerical Methods in Geomechanics held at Virginia Polytechnic Institute and State University,* Blacksburg, Virginia, U.S.A., in June, 1976, Vol. 1, C. S. Desai (ed.), ASCE, New York NY 10017, 132-150.

Cundall, P. (1982). "Adaptive density-scaling for time-explicit calculations." In *Proceedings of the Fourth International Conference on Numerical Methods in Geomechanics,* May 31-June 4, 1982, Edmonton, Canada, Z. Eisenstein (ed.), 23-26.

Cundall, P. A. (1987). "Chapter 4: Distinct element models of rock and soil structure." In *Analytical and Computational Methods in Engineering Rock Mechanics*, E. T. Brown (ed.), Allen & Unwin, London, 129-163.

Cundall, P. A. (2001). "*Explicit solution of nonlinear, path-dependent and unstable processes in geomechanics*." [On-Line], GeoMath2 PowerPoint Presentation, 16th February 2001, Available: www.itascacg.com, Itasca Consulting Group Inc., Minneapolis, Minnesota.

Curras, C. J., Hutchinson, T. C., Boulanger, R. W., Chai, Y.-H., and Idriss, I. M. (2001). "Lateral loading & seismic response of CIDH pile supported bridge structures." In *Foundations and Ground Improvement,* Proceedings of a Specialty Conference : June 9-13, Blacksburg, Virginia (Geotechnical Special Publication No. 113), T. L. Brandon (ed.), ASCE, Reston, VA, 260-275.

Davies, T. G. and Budhu, M. (1986). "Non-linear analysis of laterally loaded piles in heavily overconsolidated clays." *Géotechnique*, 36(4), 527-538.

Dodds, A. M. (2005). "*A Numerical Study of Pile Behavior in Large Pile Groups Under Lateral Loading*." Doctor of Philosophy Dissertation, University of Southern California, Los Angeles, California, 639 p.

Duncan, J. M. and Chang, C. (1970). "Nonlinear analysis of stress and strain in soils." *J. Soil Mechanics and Foundations Division,* ASCE, 96(5), 1629-1653.

Duncan, J. M., Evans, L. T. J., and Ooi, P. S. K. (1994). "Lateral load analysis of single piles and drilled shafts." *J. Geotech. Eng.,* ASCE, 120(5), 1018-1033.

Dunnavant, T. W. and O'Neill, M. W. (1989). "Experimental *p-y* model for submerged stiff clay." *J. Geotech. Eng.,* ASCE, 115(1), 95-114.

Dyson, D. J. and Randolph, M. F. (2001). "Monotonic lateral loading of piles in calcareous sand." *J. Geotech. Geoenvir. Eng.,* ASCE, 127(4), April, 346-352.

Ensoft (1999). *LPILE Plus 3.0 - A Program for the Analysis of Piles and Drilled Shafts Under Lateral Loads* [Computer Program], Ensoft Inc., Houston,Texas.

Ensoft (2004). *GROUP Plus 5.0 for Windows - A Program for the Analysis of Piles and Drilled Shafts Under Lateral Loads* [Computer Program], Available: www.ensoftinc.com, Ensoft Inc., Houston, Texas.

Esteva, L. and Ruiz, S. E. (1982). "Reliability of offshore piling: a bayesian approach." In *Proceedings, 2nd International Conference on Numerical Methods in Offshore Piling,* April 29-30, 1982, The University of Texas at Austin, Austin, Texas, 617-632.

Evans, L. T., Jr. and Duncan, J. M. (1982). *Simplified Analysis of Laterally Loaded Piles*, Report No. UCB/GT/82-04, Department of Civil Engineering, University of California, Berkeley, California.

Fedorovsky, V. G., Kurillo, S. V., Levachev, S. N., and Kolesnikov, Y. M. (1986). "Design method for laterally loaded pile groups and its experimental and theoretical background." In *Proceedings, 3rd International Conference on Numerical Methods in Offshore Piling,* Nantes, France, 21-22 May, Editions Technip, Paris, France, 333-347.

$FLAC^{3D}$ (1997). "Appendix G: Modified cam-clay model." In $FLAC^{3D}$ *Version 2.0 User Manual: Volume IV – Appendices A to H*, Itasca Consulting Group, Minneapolis, MN, 55-71.

Focht, J. A., Jr. and Koch, K. J. (1973). "Rational analysis of the lateral performance of offshore pile groups." In *Proceedings, Fifth Annual Offshore Technology Conference,* Houston, Texas, April 29 - May 2, Vol. II, Paper No. 1896, OTC, Houston, Texas, 701-708.

Foray, P., Balachowski, L., and Rault, G. (1998). "Scale effect in shaft friction due to the localisation of deformations." In *Proceedings of the International Conference Centrifuge 98,* 23-25 September 1998, Tokyo, Japan, Vol. 1, T. Kimuara, O. Kusakabe, & J. Takemura (eds.), A. A. Balkema, Rotterdam, 211-216.

Gabr, M. A., Lunne, T., and Powell, J. J. (1994). "*p-y* analysis of laterally loaded piles in clay using DMT." *J. Geotech. Engrg. Div.,* ASCE, 120(5), 816-837.

Garnier, J. and König, D. (1998). "Scale effects in piles and nails loading tests in sand." In *Proceedings of the International Conference Centrifuge 98,* 23-25 September 1998, Tokyo, Japan, Vol. 1, T. Kimuara, O. Kusakabe, & J. Takemura (eds.), A. A. Balkema, Rotterdam, 205-210.

Gazetas, G. (1991). "Foundation vibrations." In *Foundation Engineering Handbook,* Second Ed., H.-Y. Fang (ed.), Van Nostrand Reinhold, New York, 553-593.

Gazioglu, S. M. and O'Neill, M., W (1984). "Evaluation of *p-y* relationships in cohesive soils." In *Analysis and Design of Pile Foundations*, Proceedings of a Symposium sponsored by the ASCE Geotechnical

Engineering Division and a Session sponsored by the ASCE Technical Council on Codes and Standards in conjunction with the ASCE National Convention, San Francisco, J. R. Meyer (ed.), ASCE, New York, 192-213.

Griffiths, D. V. (1990). "Failure criteria interpretation based on Mohr-Coulomb friction." *J. Geotech. Eng., ASCE,* 116(6), 986-999.

Hansen, J. B. (1961). "The ultimate resistance of rigid piles against transversal forces." *Bulletin*, Danish Geotechnical Institue, Copenhagen, Denmark, 11, 5-9.

Hariharan, M. and Kumarasamy, K. (1982). "Analysis of pile groups subjected to lateral loads." In *Proceedings, 3rd International Conference on Behavior of Offshore Structures*, Vol. 2, Hemisphere Publishing Corp., Washington, D.C., 383-390.

Holloway, D. M., Moriwaki, Y., Finno, R. J., and Green, R. K. (1982). "Lateral load response of a pile group in sand." In *Proceedings, 2nd International Conference on Numerical Methods in Offshore Piling,* April 29-30, 1982, The University of Texas at Austin, Austin, Texas, 441-456.

Horsnell, M. R., Aldridge, T. R., and Erbrich, C. (1990). "Lateral group behavior of piles in offshore soil conditions." In *Proceedings, 22nd Offshore Technology Conference,* Houston, Texas: May 7-10, Paper No. 6246, OTC, Houston, Texas, 417-424.

Huang, A.-B., Hsueh, C.-K., O'Neill, M. W., Chern, S., and Chen, C. (2001). "Effects of construction on laterally loaded pile groups." *J. Geotech. Geoenvir. Eng.,* ASCE, 127(5), May, 385-397.

Hunt, C. E., Pestana, J. M., Bray, J. D., and Riemer, M. (2002). "Effect of pile driving on static and dynamic properties of soft clay." *J. Geotech. Geoenvir. Eng.,* ASCE, 128(1), January, 13-24.

Hwang, J.-H., Liang, N., and Chen, C.-H. (2001). "Ground response during pile driving." *J. Geotech. Geoenvir. Eng.,* ASCE, 127(11), November, 939-949.

Ilyas, T., Leung, C. F., Chow, Y. K., and Budi, S. S. (2004). "Centrifuge model study of laterally loaded pile groups in clay." *J. Geotech. Geoenvir. Eng.,* ASCE, 130(3), March, 274-283.

Itasca (1997). FLAC^{3D} *Version 2.0, Fast Lagrangian Analysis of Continua in Three Dimensions* [Computer Program], Itasca Consulting Group, Minneapolis, Minnesota 55415.

Jamiolkowski, M. and Garassino, A. (1977). "Soil modulus for laterally loaded piles." In *Proceedings of the Specialty Session 10, Ninth International Conference on Soil Mechanics and Foundation Engineering,* 14th July, IX ICSMFE Publications Committee (ed.), ICSMFE, Tokyo, 43-58.

Kishida, H. and Nakai, S. (1977). "Large deflection of a single pile under horizontal load." In *Proceedings of the Specialty Session 10, Ninth International Conference on Soil Mechanics and Foundation Engineering,* 14th July, IX ICSMFE Publications Committee (ed.), ICSMFE, Tokyo, 87-92.

Kramer, S. L. and Heavey, E. J. (1988). "Lateral load analysis of nonlinear piles." *J. Geotech. Eng.,* ASCE, 114(9), 1045-1049.

Kuhlemeyer, R. L. (1979). "Static and dynamic laterally loaded floating piles." *J. Geotech. Engrg. Div.,* ASCE, 105(GT2), 289-304.

Kulhawy, F. H. and Chen, Y. J. (1995). "A thirty year perspective of Broms' lateral loading models, as applied to drilled shafts." In *Proceedings, Bengt B. Broms Symposium in Geotechnical Engineering,* 13-15 December, Singapore, 225-240.

Kulhawy, F. H. and Mayne, P. W. (1990). *Manual on Estimating Soil Properties for Foundation Design,* Final Report, Project 1493-6, EL-6800, Electric Power Research Institute, Palo Alto, CA.

Lam, I. P. and Cheang, L. (1995). "Dynamic soil-pile interaction behavior in submerged sands." In *Proceedings, Earthquake-Induced Movements and Seismic Remediation of Existing Foundations and Abutments,* ASCE Convention, San Diego, California: October 23-27, Geotechnical Special Publication No. 55, American Society of Civil Engineers, 1-26.

Lam, I. P., Kapuskar, M. M., and Chaudari, D. (1998). *Modeling of Pile Footings and Drilled Shafts for Seismic Design*, MCEER 98-0018, Multidisciplinary Center for Earthquake Engineering Research, Buffalo, N.Y.

Lam, I. P. and Martin, G. R. (1986). *Seismic Design of Highway Bridge Foundations. Design Procedures and Guidelines*, Vol. 2, Report No. FHWA/RD-86/102, U.S. Department of Transportation, Federal Highway Administration, Springfield, Virginia, U.S.A.

Law, H. and Lam, I. P. (2001). "Application of periodic boundary for large pile group." *J. Geotech. Geoenvir. Eng.,* ASCE, 127(10), October, 889-892.

Lundgren, R. (1958). Discussion: Soil Modulus for Laterally Loaded Piles. *Trans.,* A.S.C.E., 123, 1069-1071.

Manzari, M. T. and Dafalias, Y. F. (1997). "A critical state two-surface plasticity model for sands." *Géotechnique*, 47(2), 255-272.

Margason, E. and Holloway, M. (1977). "Pile bending during earthquakes." In *Proceedings, 6th World Conference on Earthquake Engineering*, Vol. 2, New Delhi, India, 1690-1696.

Marti, J. and Cundall, P. (1982). "Mixed discretization procedure for accurate modelling of plastic collapse." *Int. J. Numer. Anal. Methods Geomech.*, 6, 129-139.

Matlock, H. (1958). Discussion: Soil Modulus for Laterally Loaded Piles. *Trans.,* A.S.C.E., 123, 1077-1081.

Matlock, H. (1970). "Correlations for Design of Laterally Loaded Piles in Soft Clay." In *Proceedings, 2nd Annual Offshore Technology Conference*, Paper No. 1204, OTC, Houston, Texas, 577-594.

Matlock, H. and Grubbs, B. R. (1965). Discussion: Lateral Resistance of Piles in Cohesive Soils. *J. Soil Mechanics and Foundations Division,* ASCE, 91(SM 1), 183-188.

Matlock, H. and Reese, L. C. (1960). "Generalized solutions for laterally loaded piless." *J. Soil Mechanics and Foundations Division,* ASCE, 86(SM5), 63-91.

Matlock, H., Ingram, W. B., Kelley, A. E., and Bogard, D. (1980). "Field tests of the lateral-load behavior of pile groups in soft clay." In *Proceedings, 12th Annual Offshore Technology Conference*, Paper No. 3871, OTC, Houston, Texas, 163-174.

McClelland, B. and Focht, J. A., Jr. (1958a). "Soil modulus for laterally loaded piles." *Trans.,* A.S.C.E., Paper No. 2954, 123, 1049-1063.

McClelland, B. and Focht, J. A., Jr. (1958b). Reply to discussion: Soil Modulus for Laterally Loaded Piles. *Trans.,* A.S.C.E., 123, 1081-1086.

McVay, M., Casper, R., and Shang, T.-I. (1995). "Lateral response of three-row groups in loose to dense sands at 3D and 5D pile spacing." *J. Geotech. Geoenvir. Eng.,* ASCE, 121(5), May, 436-441.

McVay, M., Hays, C., and Hoit, M. (1996). *FLPIER User's Manual* [Computer Program], University of Florida, Gainesville.

McVay, M., Shang, T.-I., and Casper, R. (1996). "Centrifuge testing of fixed-head laterally loaded battered and plumb pile groups in sand." *Geotech. Testing J.,* 19(1), March, 41-50.

McVay, M., Zhang, L., Molnit, T., and Lai, P. (1998). "Centrifuge testing of large laterally loaded pile groups in sands." *J. Geotech. Geoenvir. Eng.,* ASCE, 124(10), October, 1016-1026.

Meimon, Y., Baguelin, F., and Jezequel, J.-F. (1986). "Pile group behaviour under long time lateral monotonic and cyclic loading." In *Proceedings, 3rd International Conference on Numerical Methods in Offshore Piling,* Nantes, France, 21-22 May, Editions Technip, Paris, France, 285-302.

Meyer, B. J. (1979). "*Analysis of Single Piles Under Lateral Loading.*" Master of Science in Engineering Thesis, The University of Texas at Austin.

Mindlin, R. D. (1936). "Force at a point in the interior of a semi-infinite solid." *J. Physics*, 7, 195-202.

Mokwa, R. L. (1999). "*Investigation of the Resistance of Pile Caps to Lateral Loading.*" Doctor of Philosophy Thesis, Virginia Polytechnic Institute and State University, Blacksburg, Virginia.

Mokwa, R. L. and Duncan, J. M. (2001). "Laterally loaded pile group effects and *p-y* multipliers." In *Foundations and Ground Improvement,* Proceedings of a Specialty Conference : June 9-13, Blacksburg, Virginia (Geotechnical Special Publication No. 113), T. L. Brandon (ed.), ASCE, Reston, VA, 728-742.

Mokwa, R. L., Duncan, J. M., and Helmers, M. J. (2001). "Development of *p-y* curves for partly saturated silts and clays." In *New Technological and Design Developments in Deep Foundations,* Geotechnical Special Publication No. 100, Proceedings of Sessions of Geo-Denver 2000, 5-8 August, 2000, Denver, Colorado, N. D. J. Dennis, R. Castelli, & M. W. O'Neill (eds.), ASCE, Reston, Virginia 20191-4400, 224-239.

Morrison, C. and Reese, L. C. (1986). *A Lateral-Load Test of Full-Scale Pile Group in Sand*, GR86-1, FHWA, Washington, D.C.

Murchison, J. M. and O'Neill, M. W. (1984). "Evaluation of *p-y* relationships in cohesionless soils." In *Analysis and Design of Pile Foundations*, Proceedings of a Symposium sponsored by the ASCE Geotechnical Engineering Division and a Session sponsored by the ASCE Technical Council on Codes and Standards in conjunction with the ASCE National Convention, San Francisco, J. R. Meyer (ed.), ASCE, New York, 174-191.

Nagtegaal, J. C., Parks, D. M., and Rice, J. R. (1974). "On numerically accurate finite element solutions in the fully plastic range." *Comput. Methods Appl. Mech. Eng.*, 4, 153-177.

Ng, C. W. W., Zhang, L., and Nip, D. C. N. (2001). "Response of laterally loaded large-diameter bored pile groups." *J. Geotech. Geoenvir. Eng.,* ASCE, 127(8), August, 658-669.

Nogami, T. and Paulson, S. K. (1985). "Transfer matrix approach for nonlinear pile group response analysis." *Int. J. Numer. Anal. Methods Geomech.*, 9, 299-316.

Norris, G. (1986). "Theoretically Based BEF Laterally Loaded Pile Analysis." In *Proceedings, 3rd International Conference on Numerical Methods in Offshore Piling,* Nantes, France, 21-22 May, Editions Technip, Paris, France, 361-386.

Ochoa, M. and O'Neill, M. W. (1989). "Lateral pile interaction factors in submerged sand." *J. Geotech. Eng.,* ASCE, 115(3), 359-378.

O'Neill, M. W. (1983). "Group Action in Offshore Piles." In *Proceedings of the Conference on Geotechnical Practice In Offshore Engineering.* University of Texas at Austin, Austin, Texas: April 27-29, 1983, S. G. Wright (ed.), American Society of Civil Engineers, New York, New York, USA., 25-64.

O'Neill, M. W., Ghazzaly, O. I., and Ha, H. B. (1977). "Analysis of three-dimensional pile groups with non-linear soil response and pile-soil-pile interaction." In *Proceedings, Ninth Annual Offshore Technology Conference*, Vol. II, Paper No. 2838, OTC, Houston, Texas, 245-256.

O'Neill, M. W., Brown, D. A., Anderson, D. G., El Naggar, M. H., Townsend, F. C., and McVay, M. C. (1997). "Appendix C: Current methods for design of laterally loaded pile groups for extreme events." In *Static and Dynamic Lateral Loading of Pile Groups (NCHRP 24-9): Interim Report*, Highway Research Center, Harbert Engineering Center, Auburn University, Alabama 36849-5337.

Ono, K., Shimamura, S., Kasai, H., and Omoto, O. (1991). "Behavior of group pile subjected to lateral force - a 3-d FEM analysis (in Japanese)." In *Proceedings of the 26th Soil Engineering Meeting,* Nagano, July, 1991, 1443-1444.

Otter, J. R. H., Cassell, A. C., and Hobbs, R. E. (1966). "Dynamic relaxation." *Proc. Instn Civ. Engrs*, Paper No. 6986, 35, 633-656.

Peck, R. B., Davisson, M. T., and Hansen, V. (1958). Discussion: Soil Modulus for Laterally Loaded Piles. *Trans.,* A.S.C.E., 123, 1065-1069.

Pecker, A. and Pender, M. J. (2000). "Earthquake resistant design of foundations: new construction (Invited Paper)." In *Proceedings of GeoEng 2000, An International Conference on Geotechnical and Geological Engineering,* 19-24 November 2000, Melbourne Exhibition and Convention Centre, Melbourne Australia, Vol. 1, Technomic, Melbourne, Australia, 313-332.

Pender, M. J. (1993). "Aseismic pile foundation design analysis." *Bull. NZ Nat. Soc. Earthquake Eng.*, 26(1), 49-160.

Pender, M. J. (2004). Discussion: Evaluation of Pile Diameter Effect on Initial Modulus of Subgrade Reaction. *J. Geotech. Geoenvir. Eng.,* ASCE, 130(9), September, 981-982.

Pestana, J. M., Hunt, C. E., and Bray, J. D. (2002). "Soil deformation and excess pore pressure field around a closed-ended pile." *J. Geotech. Geoenvir. Eng.,* ASCE, 128(1), January, 1-12.

Poulos, H. G. (1971a). "Behavior of laterally loaded piles: I - single piles." *J. Soil Mechanics and Foundations Division,* ASCE, 97(SM5), 711-731.

Poulos, H. G. (1971b). "Behavior of laterally loaded piles: II-pile groups." *J. Soil Mechanics and Foundations Division,* ASCE, 97(SM5), 733-751.

Poulos, H. G. (1972). "Behavior of laterally loaded piles: III-socketed piles." *J. Soil Mechanics and Foundations Division,* ASCE, 98(SM4), 341-360.

Poulos, H. G. (1975). "Lateral load-deflection prediction for pile groups." *J. Geotech. Engrg. Div.,* ASCE, 101(GT1), 19-34.

Poulos, H. G. (1979). "Group factors for pile-deflection estimation." *J. Geotech. Engrg. Div.,* ASCE, 105(GT12), 1489-1509.

Poulos, H. G. (1980). "An approach for the analysis of offshore pile groups." In *Proceedings of the Conference on Numerical Methods in Offshore Piling,* London, England: 22-23 May, 1979, Vol. 2, T.-P. E. Darwent (ed.), Institution of Civil Engineers, London, 119-126.

Poulos, H. G. and Davis, E. H. (1980). *Pile foundation analysis and design*, Wiley, New York.

Poulos, H. G. and Randolph, M. F. (1983). "Pile group analysis: a study of two methods." *J. Geotech. Eng.,* ASCE, 109(3), 355-372.

Prevost, J. H. (1982). "Panel Discussion - Pile Load Testing: How, What, Where, When, and Why." In *Proceedings, 2nd International Conference on Numerical Methods in Offshore Piling,* April 29-30, 1982, The University of Texas at Austin, Austin, Texas, 639-670.

Pyke, R. and Beikae, M. (1984). "A new solution for the resistance of single piles to lateral loading." In *Laterally Loaded Deep Foundations: Analysis and Performance, ASTM STP 835*, J. A. Langer, E. T. Mosley, & C. D. Thompson (eds.), American Society for Testing and Materials, Philadelphia, PA, USA, 3-20.

Rajashree, S. S. and Sitharam, T. G. (2001). "Nonlinear finite-element modeling of batter piles under lateral load." *J. Geotech. Geoenvir. Eng.,* ASCE, 127(7), July, 604-612.

Randolph, M. F. (1981). "The response of flexible piles to lateral loading." *Géotechnique*, 31(2), 247-259.

Randolph, M. F. and Houlsby, G. T. (1984). "The limiting pressure on a circular pile loaded laterally in cohesive soil." *Géotechnique*, 34(4), 613-623.

Randolph, M. F. and Poulos, H. G. (1982). "Estimating the flexibility of offshore pile groups." In *Proceedings, 2nd International Conference on Numerical Methods in Offshore Piling,* April 29-30, 1982, The University of Texas at Austin (ed.), 313-328.

Reddick, H. W. and Miller, F. H. (1955). *Advanced Mathematics for Engineers*, Third Ed., John Wiley & Sons, Inc., New York.

Reese, L. C. (1958). Discussion: Soil Modulus for Laterally Loaded Piles. *Trans.,* A.S.C.E., 123, 1071-1074.

Reese, L. C. (1986). *Behavior of Piles and Pile Groups Under Lateral Load,* Report No. FHWA/RD-85/106, Federal Highway Administration, Washington, D.C.

Reese, L. C., Cox, W. R., and Koop, F. D. (1974). "Analysis of laterally loaded piles in sand." In *Proceedings, Sixth Annual Offshore Technology Conference*, Paper No. 2080, OTC, Houston, Texas, 473-483.

Reese, L. C., Cox, W. R., and Koop, F. D. (1975). "Field testing and analysis of laterally loaded piles in stiff clay." In *Proceedings, Seventh Annual Offshore Technology Conference*, Paper No. 2312, OTC, Houston, Texas, 671-690.

Reese, L. C. and Van Impe, W. F. (2001). *Single Piles and Pile Groups under Lateral Loading*, A. A. Balkema, Brookfield, VT.

Reese, L. C. and Welch, R. C. (1975). "Laterally loading of deep foundations in stiff clay." *J. Geotech. Engrg. Div.,* ASCE, 101(GT7), 633-649.

Reese, L. C., Wright, S. G., and Aurora, R. P. (1984). "Analysis of a pile group under lateral loading." In *Laterally Loaded Deep Foundations: Analysis and Performance* (ASTM STP 835), A symposium sponsored by ASTM Committee D-18 on Soil and Rock, Kansas City, MO: 22 June 1983, J. A. Langer, E. T. Mosley, & C. D. Thompson (eds.), American Society for Testing and Materials, Philadelphia, PA, USA, 56-71.

Robertson, P. K., Davies, M. P., and Campanella, R. G. (1989). "Design of laterally loaded driven piles using the flat dilatometer." *Geotech. Testing J.*, 12(1), March, 30-38.

Robertson, P. K., Hughes, J. M. O., Campanella, R. G., and Sy, A. (1984). "Design of laterally loaded displacement piles using a driven pressuremeter." In *Laterally Loaded Deep Foundations: Analysis and Performance* (ASTM STP 835), A symposium sponsored by ASTM Committee D-18 on Soil and Rock, Kansas City, MO, 22 June 1983, J. A. Langer, E. T. Mosley, & C. D. Thompson (eds.), ASTM, Philadelphia, PA 19103, 229-238.

Rollins, K. M., Peterson, K. T., and Weaver, T. J. (1998). "Lateral load behavior of full-scale pile group in clay." *J. Geotech. Geoenvir. Eng.,* ASCE, 124(6), June, 468-478.

Rollins, K. M., Sparks, A. E., and Peterson, K. T. (2000). "Lateral load capacity and passive resistance of a full-scale pile group and cap [CD-ROM]." In *Proceedings of the Transportation Research Board 79th Annual Meeting,* January 9-13, 2000, Washington, D.C, Transportation Research Board, Washington, D.C., 19.

Roscoe, K. H. and Burland, J. B. (1968). "On the generalized stress-strain behaviour of 'wet' clay." In *Engineering Plasticity : Papers for a Conference held in Cambridge,* March 1968, J. Heyman & F. A. Leckie (eds.), Cambridge University Press, Cambridge, 535-609.

Rowe, P. W. (1956). "The single pile subject to horizontal force." *Géotechnique*, 6, 70-85.

Ruesta, P. F. and Townsend, F. C. (1997a). "Evaluation of laterally loaded pile group at Roosevelt Bridge." *J. Geotech. Geoenvir. Eng.,* ASCE, 123(No. 12), December, 1153-1161.

Ruesta, P. F. and Townsend, F. C. (1997b). "Prediction of Lateral Load Response for a Pile Group." In *Proceedings, Transportation Research Board 76th Annual Meeting,* January 12-16, Washington D.C, Preprint Paper No. 970053, Transportation Research Board, Washington, D.C., 30.

Ruiz, S. E. (1986). "Uncertainty about *p-y* curves for piles in soft clays." *J. Geotech. Eng.,* ASCE, 112(6), 594-607.

Schmidt, H. G. (1981). "Group action of laterally loaded bored piles." In *Proceedings, Tenth International Conference on Soil Mechanics and Foundation Engineering--Dixieme congres internationale de Mecanique des sols et des travaux de fondations.* Stockholm, Sweden: June 15-19, 1981, Vol. 8, A.A. Balkema, Rotterdam-Boston, International, 833-837.

Schmidt, H. G. (1985). "Horizontal load tests on files of large diameter bored piles." In *Proceedings of the Eleventh International Conference on Soil Mechanics and Foundation Engineering,* 12-16 August 1985, San Francisco, Vol. 1, Publications Committee of XI ICSMFE (ed.), A. A. Balkema, Boston, 1569-1573.

Scott, R. F. (1980). "*Analysis of centrifuge pile tests, Report of American Petroleum Institute*." Dallas, Texas, June.

Scott, R. F. (1981). *Foundation Analysis*, Prentice-Hall, Engelwood Ciffs, NJ.

Skempton, A. W. (1951). "The bearing capacity of clays." In *Proceedings*, Building Research Congress, Division 1, Part III, London, England, 180-189.

Smith, T. D. (1989). "Fact or fiction: a review of soil response to a laterally moving pile." In *Foundation Engineering: Current Principles and Practices,* Evanston, Illinois, June 25-29, 1989, Vol. 2, Proceedings of the Congress sponsored by the Geotechnical Engineering Division and the Construction Division of the American Society of Civil Engineers, F. H. Kulhawy (ed.), ASCE, New York, New York 10017-2398, 588-599.

Spillers, W. R. and Stoll, R. D. (1964). "Lateral response of piles." *J. Soil Mechanics and Foundations Division,* ASCE, 90(SM6), 1-9.

Stevens, J. B. and Audibert, J. M. E. (1979). "Re-examination of *p-y* curve formulations." In *Proceedings, 11th Annual Offshore Technology Conference*, Paper No. 3402, OTC, Houston, Texas, 397-403.

Structural Research & Analysis Corporation (1999). *COSMOS 2.5 Finite Element Analysis System* [Computer Program], Structural Research & Analysis Corp., Los Angeles, CA 90025.

Sullivan, W. R., Reese, L. C., and Fenske, C. W. (1980). "Unified method for analysis of laterally loaded piles in clay." In *Numerical Methods in Offshore Piling*, Proceedings of a conference organized by The Institution of Civil Engineers, 22-23 May 1979, Institution of Civil Engineers, London, 135-146.

Tamura, A., Sunami, S., Ozawa, Y., and Murakami, S. (1982). "Reduction in horizontal bearing capacity of pile group." In *Proceedings of the Fourth International Conference on Numerical Methods in Geomechanics,* May 31-June 4, 1982, Edmonton, Canada, Z. Eisenstein (ed.), 865-874.

Taylor, D. W. (1948). *Fundamentals of Soil Mechanics*, John Wiley & Sons, Inc., New York.

Terzaghi, K. (1955). "Evaluation of coefficients of subgrade reaction." *Géotechnique*, 5, 297-326.

Thompson, G. R. (1977). "*Application of the Finite Element Method to the Development of p-y curves for Saturated Clays*." Master of Science in Engineering Thesis, The University of Texas at Austin, Austin, Texas.

Ting, J. M. (1987). "Full-scale cyclic dynamic lateral pile responses." *J. Geotech. Eng.,* ASCE, 113(1), 30-45.

Trochanis, A. M., Bielak, J., and Christiano, P. (1988). *A Three-Dimensional Nonlinear Study of Piles Leading to the Development of a Simplified Model*, Department of Civil Engineering, Carnegie Institue of Technology, Carnegie Mellon University, Pittsburgh, PA 15213.

Trochanis, A. M., Bielak, J., and Christiano, P. (1991a). "Three-dimensional nonlinear study of piles." *J. Geotech. Eng.,* ASCE, 117(3), 429-447.

Trochanis, A. M., Bielak, J., and Christiano, P. (1991b). "Three-Dimensional Nonlinear Study of Piles and Simplified Models." In *Geotechnical Engineering Congress 1991,* Boulder, Colorado; June 10-12, 1991 (Geotechnical Special Publication No. 27), Vol. II, F. G. McLean, DeW. A. Campbell, & D. H. Harris (eds.), American Society of Civil Engineers, New York, New York 10017-2398, 356-366.

Underwood, P. (1983). "Dynamic relaxation." In *Computational Methods for Transient Analysis, Volume 1 in Computational Methods in Mechanics*, T. Belytschko & T. J. R. Hughes (eds.), Elsevier Science Publishers B. V., New York, NY 10017, 245-265.

Vesić, A. B. (1961a). "Beams on Elastic Subgrade and Winkler's Hypothesis." *ISMFE*, 1, 845-850.

Vesić, A. B. (1961b). "Bending of beams resting on isotropic elastic solid." *J. Eng. Mech. Div.,* ASCE, 87(EM 2), 35-53.

Vesić, A. S. (1977). "Design of Pile Foundations." In *National Cooperative Highway Research Program Synthesis of Highway Practice No. 42*, Research Sponsored by the American Association of State Highway and Transportation Officials in Cooperation with Federal Highway Administration, Transportation Research Board, National Research Council, Washington, D.C., 68.

Wakai, A., Gose, S., and Ugai, K. (1999). "3-d elasto-plastic finite element analyses of pile foundations subjected to lateral loading." *Soils and Found.*, 39(1), February, 97-111.

Walsh, K. D., Fréchette, D. N., Houston, W. N., and Houston, S. L. (2000). "The State of the Practice for the Design of Groups of Laterally Loaded Drilled Shafts." In *Proceedings of the Transporation Research Board 79th Annual Meeting,* January 9-13, Washington, D.C, Preprint Paper No. 001306, Transportation Research Board, Washington, D.C., 23.

Wood, D. M. (1990). *Soil Behaviour and Critical State Soil Mechanics*, Cambridge University Press, New York.

Wood, D. M. (2004). *Geotechnical Modelling*, Spon Press, New York, NY 10001.

Wood, D. M., Belkheir, K., and Liu, D. F. (1994). "Strain softening and state parameters for sand modelling." *Géotechnique*, 44(2), 335-339.

WSDOT (1997). *Design Manual for Foundation Stiffnesses Under Seismic Loading*. Prepared for Washington State Department of Transportation by Geospectra, A Division of Kleinfelder Incorporated, California 94566.

Wu, D., Broms, B. B., and Choa, V. (1998). "Design of laterally loaded piles in cohesive soils using *p-y* curves." *Soils and Found.*, 38(2), June, 17-26.

Yang, Z. and Jeremić, B. (2002). "Numerical analysis of pile behavior under lateral loads in layered elastic-plastic soils." *Int. J. Numer. Anal. Methods Geomech.*, 26, 1385-1406.

Yegian, M. and Wright, S. G. (1973). "Lateral soil resistance - displacement relationships for pile foundations in soft clays." In *Proceedings, Fifth Annual Offshore Technology Conference*, Vol. II, Paper No. 1893, OTC, Houston, Texas, 663-676.

Zhang, L. and McVay, M. C. (1999). "*p*-multiplier factors for group interactions in laterally loaded pile groups." In *Computational Mechanics for the Next Millenium*, Vol. 2, Geomechanics, Model and Techniques, Proceedings of APCOM '99, C. M. Wang, K. H. Lee, & K. K. Ang (eds.), Elsevier Science Ltd, New York, 867-872.

APPENDIX A
PILE GROUP OBSERVATIONS

A.1 Full-Scale Lateral Load Tests

The following tables provide pertinent test details and observations from published full-scale lateral load tests undertaken on a variety of pile group configurations. These tests are considered to have served a key role in the current understanding of small pile group behavior under lateral loads. A dash (-) indicates that the information was not given or insufficient detail was provided. The length to diameter ratio (L/d) refers to the in-ground portion of a typical pile in the group (for circular hollow sections d refers to the outside diameter, and for square sections d refers to the dimension perpendicular to direction of loading). The group configuration designation (a x b) refers to a rows perpendicular to the direction of loading, and b columns parallel to the direction of loading (both referring to the configuration in plan).

Table A-1:   Group test from Matlock, Ingram, Kelley and Bogard (1980)

Location:	Harvey, Louisiana
Setting:	-
Soil Type:	Very soft clay
Water Level:	-
Configuration:	Five-pile and ten-pile circular groups
Pile Type:	Steel pipe section
Pile Geometry:	d = 168 mm, $L/d \approx 70$
Pile Top:	Test setup applied the equivalent of partial restraint at top of piles
Installation:	Driven open ended (most under hammer weight only)
Pile Spacing:	3.4d and 1.8d
Tests:	Static and slow cyclic
Key Observations:	• Cyclic degradation of lateral resistance. • Greater deflections compared with single piles. • Lesser average lateral load capacity per pile, more so for closer spacing. • Gapping around individual piles, and entire group for close spacing.

Table A-2:   Group test from Schmidt (1981, 1985)

Location:	-
Setting:	-
Soil Type:	Uniform, medium dense sand
Water Level:	Below test depth
Configuration:	In-line or "pile files" (2 x 1) two-pile groups
Pile Type:	Bored (drilled shafts)
Pile Geometry:	d = 1.0 m and 1.2 m, $L/d \approx$ 5 to 7
Pile Top:	Free to rotate
Installation:	Cased, uncased with bentonite slurry, cased with bentonite slurry
Pile Spacing:	2d, 2.2d and 3d
Tests:	Static
Key Observations:	• Reduction in soil resistance for the rear pile in the upper region compared with front pile (both experiencing same deflection). • Maximum bending moment in rear pile slightly deeper than maximum bending moment in front pile. • Group effects affected by relative pile-soil stiffness.

Table A-3:   Group test from Holloway, Moriwaki, Finno and Green (1982)

Location:	Near Alton, Illinois
Setting:	Flood plain of river
Soil Type:	Dense to very dense sand
Water Level:	150 mm below test surface
Configuration:	Eight-pile (4 x 2) rectangular group
Pile Type:	Timber
Pile Geometry:	d =356 mm (butt diameter), $L/d \approx$ 30
Pile Top:	Piles embedded 0.6 m into pile cap, but "less than full fixity" noted
Installation:	Jetted and then driven final 1.5 m
Pile Spacing:	2.6d
Tests:	Static and slow cyclic
Key Observations:	• Rear piles encountered less lateral resistance compared with front piles. • Cyclic degradation of lateral resistance. • Installation vibrations influenced behavior.

Table A-4:   Group test from Meimon, Baguelin and Jezequel (1986)

Location:	Brittany, France
Setting:	-
Soil Type:	≈ 4 m (≈ 14d thick) of soft clay (CL) overlying silty sand (SM)
Water Level:	Site test pit submerged
Configuration:	Six-pile (2 x 3) rectangular group
Pile Type:	Steel H section closed with welded plates (also at pile tip)
Pile Geometry:	Width = 284 mm and web height = 270 mm, , $L/d ≈ 20$ (load direction perpendicular to width)
Pile Top:	Piles hinged into a rigid pile cap above groundline (i.e. free head)
Installation:	Driven closed-ended
Pile Spacing:	3d in load direction, 2d in perpendicular direction
Tests:	Static, creep and slow one-way cyclic
Key Observations:	• Response affected by rest period between driving and testing. • Displacement under sustained loading (i.e. creep) significant (between 40% to 50% of total displacement). • Behavior of piles in the same row identical, but front row the most loaded. • Cyclic loading caused migration of pile-soil load transfer downwards and led to a more uniform response.

Table A-5:   Group test from Brown, Reese and O'Neill (1987)

Location:	Houston, Texas
Setting:	National Geotechnical Experiment Site, University of Houston
Soil Type:	Stiff, overconsolidated clay
Water Level:	0.5 m above the test surface
Configuration:	Nine-pile (3 x 3) square group
Pile Type:	Steel pipe section
Pile Geometry:	$d = 273$ mm, $L/d ≈ 46$
Pile Top:	Load frame provided moment-free connections (i.e. free head)
Installation:	Driven closed-ended with prior pilot hole (203 mm in diameter) to aid in maintaining vertical alignment
Pile Spacing:	3d
Tests:	Static and slow cyclic
Key Observations:	• Load distribution within group primarily a function of row position, with leading (front) row taking greater portion of total lateral load (contrary to elasticity-based predictions). • Reduction in ultimate lateral resistance noted for middle and rear (i.e. trailing) piles in the "shadow" of leading piles. • Zone of soil-pile interaction deeper for trailing piles.

Table A-6:   Group test from Brown, Morrison and Reese (1988)

Location:	Houston, Texas
Setting:	National Geotechnical Experiment Site, University of Houston
Soil Type:	Medium dense sand ($\approx 11d$ thick) overlying stiff clay
Water Level:	≈ 0.1 m above test surface
Configuration:	Nine-pile (3 x 3) square group
Pile Type:	Steel pile section
Pile Geometry:	$d = 273$ mm, $L/d \approx 46$
Pile Top:	Load frame provided moment-free connections (i.e. free head)
Installation:	As per Brown et al. (1987), then 3.0 m of clay removed ($\approx 11d$) and backfilled with sand compacted to relative density = 50%
Pile Spacing:	$3d$
Tests:	Static and slow cyclic
Key Observations:	• Shadowing effect more pronounced with dense sand compared with stiff clay. • p-multiplier introduced to account for shadowing effect, reducing resistance for given deflection rather than increasing deflection for given load. • Densification of compacted sand around piles due to cyclic loading.

Table A-7:   Group test from Ochoa and O'Neill (1989)

Location:	Houston, Texas
Setting:	National Geotechnical Experiment Site, University of Houston
Soil Type:	Medium dense to dense sand ($\approx 11d$ thick) overlying stiff clay
Water Level:	≈ 0.1 m above test surface
Configuration:	Nine-pile (3 x 3) square group
Pile Type:	Steel pile section
Pile Geometry:	$d = 273$ mm, $L/d \approx 46$
Pile Top:	Load frame provided moment-free connections (i.e. free head)
Installation:	As per Brown et al. (1988) but with additional compacted sand added to surface (up to 0.3 m thick) due to settlement from prior testing
Pile Spacing:	$3d$
Tests:	Slow cyclic
Key Observations:	• Elastic-based interaction factors increased with increasing load and decreased with increasing number of cyclic loads. • Cyclic effect predominantly a local phenomenon, concerning pile flexibility changes due to nonlinear soil behavior close to the pile. • Influence of trailing piles on leading piles was affected by load path dependencies of the soil.

Table A-8:   Group test from Ruesta and Townsend (1997a, b)

Location:	Stuart, Florida
Setting:	River site
Soil Type:	Medium dense sand
Water Level:	≈ 2 m above test surface
Configuration:	Sixteen-pile (4 x 4) square group
Pile Type:	Prestressed concrete
Pile Geometry:	0.76 m square, $L/d \approx 22$
Pile Top:	Free-headed
Installation:	Jetted and then driven
Pile Spacing:	$3d$
Tests:	Static
Key Observations:	• Pile driving sequence may be an important factor. • Construction "multiplier" suggested for installation effects. • Outer piles took more load than inner piles within each row, "possibly due to a shadow effect and pile driving sequence". • Nonlinear pile behavior dominated analysis assessment. • Overall p-multiplier successful in predicting group behavior.

Table A-9:   Group test from Rollins, Peterson and Weaver (1998)

Location:	Salt Lake City, Utah
Setting:	Salt Lake International Airport
Soil Type:	Soft to medium-stiff clays and silts
Water Level:	Near the ground surface
Configuration:	Nine-pile (3 x 3) square group
Pile Type:	Steel pipe section
Pile Geometry:	$d = 324$ mm, $L/d \approx 28$
Pile Top:	Load frame provided moment-free connections (i.e. free head)
Installation:	Driven closed-ended
Pile Spacing:	$3d$
Tests:	Static
Key Observations:	• Pore pressure effects (dilation and contraction) may influence load distribution between rows. • Comparison with previous tests suggests soil type appears to have a relatively small effect on p-mutlipliers on a row by row basis.

Table A-10: Group test from Rollins, Sparks and Peterson (2000)

Location:	Salt Lake City, Utah
Setting:	Salt Lake International Airport
Soil Type:	Soft to medium-stiff clays and silts
Water Level:	Near the ground surface
Configuration:	Nine-pile (3 x 3) square group
Pile Type:	Steel pipe section
Pile Geometry:	d = 324 mm, $L/d \approx 28$
Pile Top:	Piles connected into 1.22 m thick reinforced concrete pile cap by embedding 8 x 2.3 m long No. 8 (25 mm diam.) reinforcing bars 1.22 m into each pile (steel pipe terminated at the bottom of the pile cap) – considered to provide fixed-head conditions
Installation:	As per Rollins et al. (1998)
Pile Spacing:	$3d$
Tests:	Static
Key Observations:	• p-multipliers based on a prior free-head test (Rollins et al., 1998) predicted "reasonable estimates" of total load versus displacement behavior. • Computed resistances with and without gapping around piles at group deflections less than $0.07d$ differed by 35 to 55%. • Pile cap resistance was estimated to be 40% of total resistance.

Table A-11:   Group tests from Huang, Hsueh, O'Neill, Chern and Chen (2001)

Location:	Taiwan
Setting:	Flat coastal plain, 5 km west of Chaiyi township
Soil Type:	Predominantly loose to medium dense silty sand
Water Level:	Approximately 1 m below ground surface
Configuration:	a) Six-pile (3 x 2) rectangular group b) Twelve-pile (4 x 3) rectangular group
Pile Type:	a) Bored b) Hollow prestressed concrete section
Pile Geometry:	a) $d = 1.5$ m, $L/d \approx 22$ b) $d = 0.8$ m, $L/d \approx 42$
Pile Top:	a) Piles embedded 0.3 m into 2 m reinforced concrete pile cap with 32 mm diam. re-bars extending 1.35 m into cap – considered fixed for loads up to 9.6 MN, then partially restrained thereafter (1.7 x 10^7 kN-m/radian rotational restraint) b) Piles embedded 150 mm into 2 m thick reinforced concrete pile cap with 26 mm diam. re-bars extending ≈ 0.8 m into cap, considered partially restrained with varying rotational stiffness - between 4.5 x 10^5 (low load levels) and 3.2 x 10^4 (high load levels) kN-m/radian
Installation:	a) Bentonite slurry displacement; b) Driven closed-ended
Pile Spacing:	$3d$
Tests:	Static
Key Observations:	• Bored pile construction softened the pile-soil system, whereas driven pile construction stiffened the pile-soil system. • p-multipliers were dependent on soil conditions, installation (construction) procedures, and the modeling method used to simulate pile group behavior. • Rigidity of the piles and pile-cap connection played significant roles in establishing appropriate p-multipliers.

Table A-12: Group test from Ng, Zhang and Nip (2001)

Location:	Hong Kong
Setting:	-
Soil Type:	Clayey/silty alluvium
Water Level:	1 m below ground surface
Configuration:	a) Two-pile (2 x 1) in-line group; b) Three-pile (triangular) group
Pile Type:	Bored
Pile Geometry:	d = 1.5 m, $L/d \approx 20$
Pile Top:	1.2 m thick reinforced concrete pile caps indicated
Installation:	Temporary casing, soil removed, reinforcing cage placed, concrete tremied in while casing extracted
Pile Spacing:	$3d$
Tests:	Static
Key Observations:	• Changes in pile-cap performance with increasing load levels modified leading and trailing pile behavior.

Table A-13: Group test from Ng et al. (2001)

Location:	Hong Kong
Setting:	-
Soil Type:	Silty and sandy fill/marine deposit/alluvium
Water Level:	2 m below ground surface
Configuration:	Two-pile (2 x 1) in-line group
Pile Type:	Bored
Pile Geometry:	d = 1.5 m, $L/d \approx 14$
Pile Top:	2 m thick reinforced concrete pile cap provided restraint
Installation:	Temporary casing inserted full length of pile, soil inside removed with grab, concrete tremied while casing extracted
Pile Spacing:	$6d$
Tests:	Static
Key Observations:	• Negligible group effects observed.

Table A-14:   Group test from Brown, O'Neill, Hoit, McVay, El Naggar and Chakraborty (2001)

Location:	Cape Fear River, Wilmington, North Carolina
Setting:	Shore of land area known as Ratt Island
Soil Type:	Very soft clay ($\approx 9d$ thick) overlaying loose sandy silts and silty sands
Water Level:	-
Configuration:	Reusable twelve-pile (4 x 3) rectangular group
Pile Type:	Steel pipe section
Pile Geometry:	$d = 273$ mm, $L/d \approx 34$
Pile Top:	305 mm diam. steel pipe-pile guides connected rigidly to load frame provided rotational restraint to pile heads (i.e. fixed-head)
Installation:	Driven
Pile Spacing:	$3d$
Tests:	Static
Key Observations:	• Large variations of pile-head shear forces amongst individual piles in each row (up to a factor of 2), possibly due to soil variability or inaccuracy of shear values derived from discrete experimental bending moment measurements. • Row dependence of load distribution was only obvious on an average basis.

Table A-15:   Group tests from Brown et al. (2001)

Location:	Near Opelika, Alabama (near Auburn University)
Setting:	Spring Villa National Geotechnical Experimentation Site
Soil Type:	Stiff micaceous sandy silts (CL/ML and SM material)
Water Level:	3 m to 4 m below ground surface
Configuration:	a) Reusable twelve-pile (4 x 3) rectangular group b) Reusable nine-pile (3 x 3) square group
Pile Type:	Steel pipe section
Pile Geometry:	$d = 273$ mm, $L/d \approx 35$
Pile Top:	a) As per Wilmington test but "less than full fixity" noted b) 0.9 m thick heavily reinforced concrete cap cast around piles, considered to provide a "strongly fixed" pile-head connection
Installation:	Driven
Pile Spacing:	a) $3d$ and b) $4d$
Tests:	Static
Key Observations:	• Group effects apparent with both $3d$ and $4d$ configurations. • Load distribution by row less varied but scatter of individual pile-head shears greater c.f. Wilmington site (apparent random variability of soil conditions suspected once again).

A.2   Selected Centrifuge Group Tests

Table A-16:   Group test by McVay, Casper and Shang (1995)

Soil Type:	Medium loose and medium dense sand
Configuration:	Nine-pile (3 x 3) square group
Simulated Pile Type:	Steel pipe section
Simulated Pile Geometry:	d = 430 mm, $L/d \approx 27$
Pile Top:	Free-head
Installation:	Driven open-ended (in flight)
Pile Spacing:	$3d$ and $5d$
Tests:	Static
Key Observations:	• Load distribution amongst rows becomes more uniform with decreasing soil density. • Shadowing effect appeared to be a function of both pile spacing and soil density.

Table A-17:   Group test from McVay, Shang and Casper (1996)

Soil Type:	Medium loose and medium dense sand
Configuration:	Nine-pile (3 x 3) square group
Simulated Pile Type:	Steel pipe section
Simulated Pile Geometry:	d = 430 mm, $L/d \approx 27$
Pile Top:	Fixed-head
Installation:	Driven open-ended (in flight)
Pile Spacing:	$3d$ and $5d$
Tests:	Static
Key Observations:	• Fixed-head pile groups mobilized a greater lateral resistance compared with the free-head pile groups tested by McVay et al. (1995), and appeared to be a function of both soil density and pile spacing. • Tension capacity of piles was a controlling factor for lateral resistance, associated with rocking of the pile cap.

Table A-18:   Group tests by McVay, Zhang, Molnit, and Lai (1998)

Soil Type:	Loose and medium dense sand
Configuration:	Nine through twenty-one pile (3 x 3; 4 x 3; 5 x 3; 6 x 3; 7 x 3) square group and rectangular groups
Simulated Pile Type:	Solid square section
Simulated Pile Geometry:	d = 430 mm, $L/d \approx 32$
Pile Top:	Fixed-head
Installation:	Hydraulically jacked (in flight)
Pile Spacing:	$3d$
Tests:	Static
Key Observations:	• Increment in group resistance increased with the addition of rows up until the five row group, after which it remained constant. • p-multipliers were independent of soil density and very similar after the third-trailing row.

Table A-19:   Group tests from Ilyas, Leung, Chow and Budi (2004)

Soil Type:	Soft kaolin clay (reconstituted)
Configuration:	Two through sixteen-pile (2 x 1; 2 x 2; 3 x 2; 3 x 3; 4 x 4) rectangular and square groups
Simulated Pile Type:	Hollow square section
Simulated Pile Geometry:	d = 840 mm, $L/d \approx 17$
Pile Top:	Free-head (lateral load and moment applied at groundline)
Installation:	Jacked into the soil at $1g$ (prior to spinning)
Pile Spacing:	$3d$ (2 x 1; 2 x 2; 3 x 3; 4 x 4) $5d$ (3 x 2; 3 x 3)
Tests:	Static
Key Observations:	• Increasing the strength of surficial clay by preloading improved group efficiency. • Interior rows exhibited greater differences in shear and bending moment magnitudes between outer and inner piles compared with leading and back rows. • Load distribution amongst trailing rows was very similar for the 3 x 3 and 4 x 4 groups.

APPENDIX B
CONSTITUTIVE MODELS

B.1   Introduction

Soil behavior involves appreciable physical complexity that calls for equally complex soil models. Providing a comprehensive soil model is obviously the ideal research solution, but in doing so there must be assurance of realistic behavior at the prototype scale. Given the unavoidable uncertainties associated with soil in situ, such assurance must come from comparison with other soil models where the numerical behavior has been verified. The isotropic-linear-elastic (ILE) and Mohr-Coulomb (M-C) models fall into this category, being the most common models to have represented the elastic and plastic components, respectively, of elastic-plastic soil models used in past research.

The current research adopted a combined ILE and M-C soil model, herein referred to as the Base Soil Model, to serve as a basis for assessing lateral group effects. Use of advanced soil models were limited to selected analyses to assess any possible additional influences due to soil modeling refinements. To simplify matters, soil was characterized as simply clay or sand for analysis purposes. In the Base Soil Model case, distinction between sand and clay was achieved by assigning just a c' value to model clay (implying undrained conditions) and just a ϕ' value to model sand (implying drained conditions). The more sophisticated soil models consisted of advanced clay and sand models, namely the Modified Cam Clay model to represent clay, and a bounding surface model to represent sand. The following describes the constitutive models used, beginning with a brief description of the Base Soil Model, then descriptions of the advanced clay and sand models.

B.1.1   Base Soil Model

An elastic-perfectly plastic constitutive formulation was utilized for the Base Soil Model, neglecting any hardening effects such that strength parameters remained constant regardless of volumetric and shear strain magnitudes. The elastic behavior was modeled using isotropic, linear elastic theory that can be expressed in terms of deviatoric and volumetric components as follows (using index notation and the summation convention):

$$\sigma_{ij} = 2Ge_{ij} + K\varepsilon_{kk}\delta_{ij} \tag{B.1}$$

where $e_{ij} = \varepsilon_{ij} - \dfrac{\varepsilon_{kk}}{3}\delta_{ij} =$ deviatoric strain,

$\varepsilon_{kk} = \varepsilon_{11} + \varepsilon_{22} + \varepsilon_{33} =$ volumetric strain,

$G =$ shear modulus,

$K =$ bulk modulus, and

$\delta_{ij} =$ Kronecker delta.

Plastic behavior utilized a yield (failure) surface defined in principal stress space by a M-C shear surface combined with a tension surface depicting a limiting tensile "cut-off" value. Figure B-1 indicates the M-C shear yield surface in $\tau - \sigma_n$ space.
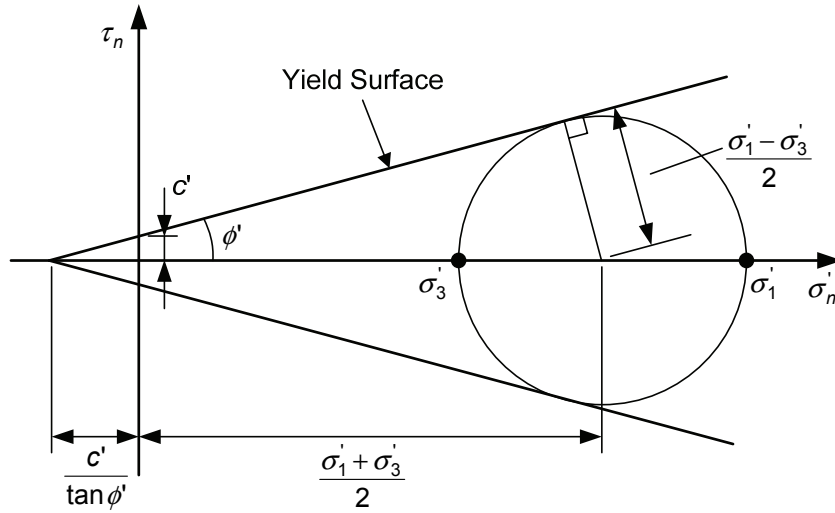
Figure B-1: Mohr-Coulomb yield surface in $\tau - \sigma_n'$ space

Apparent from Figure B-1 is the following trigonometric relationship:

$$\left(\frac{\sigma_1' - \sigma_3'}{2}\right) \bigg/ \left[c' \cot \phi' + \left(\frac{\sigma_1' + \sigma_3'}{2}\right)\right] = \sin \phi' \tag{B.2}$$

Rearranging this expression and using trigonometric identities leads to

$$\sigma_1' = 2c\sqrt{N_\phi} + \sigma_3' N_\phi \tag{B.3}$$

where $N_\phi = \dfrac{1 + \sin \phi'}{1 - \sin \phi'}$ and adopting $\sigma_1' \geq \sigma_2' \geq \sigma_3'$ (compression positive).

A tensile yield surface is simply expressed by

$$\sigma_1' - \sigma_3' = \sigma_t \tag{B.4}$$

where $\sigma_t = $ specified tension cut - off value.

A section of the combined yield surface given by (B.3) and (B.4) is shown in biaxial stress space in Figure B-2, plotted in the plane $\sigma_2' = 0$ (i.e., plane stress conditions). Two yield surfaces are shown corresponding to clay and sand strength parameters used in the current research. Also shown are the same yield surfaces viewed in the deviatoric plane. The yield surfaces as shown correspond to $p' = 30\,\text{kPa}$, where 30 kPa corresponds to an average soil depth equal to approximately one-third the pile

lengths considered for the research analyses. This represented a typical soil element located within the mobilized depth of lateral soil resistance.

a) Biaxial stress space

σ_3' (kPa)

Sand
$c' = 0 \, \text{kPa}$
$\phi' = 35°$
$\sigma_t = 0 \, \text{kPa}$

$\boxed{\sigma_2' = 0}$

$\sigma_1' = \sigma_3'$

$\sigma_t = -70 \, \text{kPa}$

σ_1' (kPa)

Clay
$c' = 35 \, \text{kPa}$
$\phi' = 0°$
$\sigma_t = -70 \, \text{kPa}$

b) Deviatoric plane

σ_1'

Sand Model

Clay Model

$\boxed{p' = 30 \, \text{kPa}}$

σ_3'

σ_2'
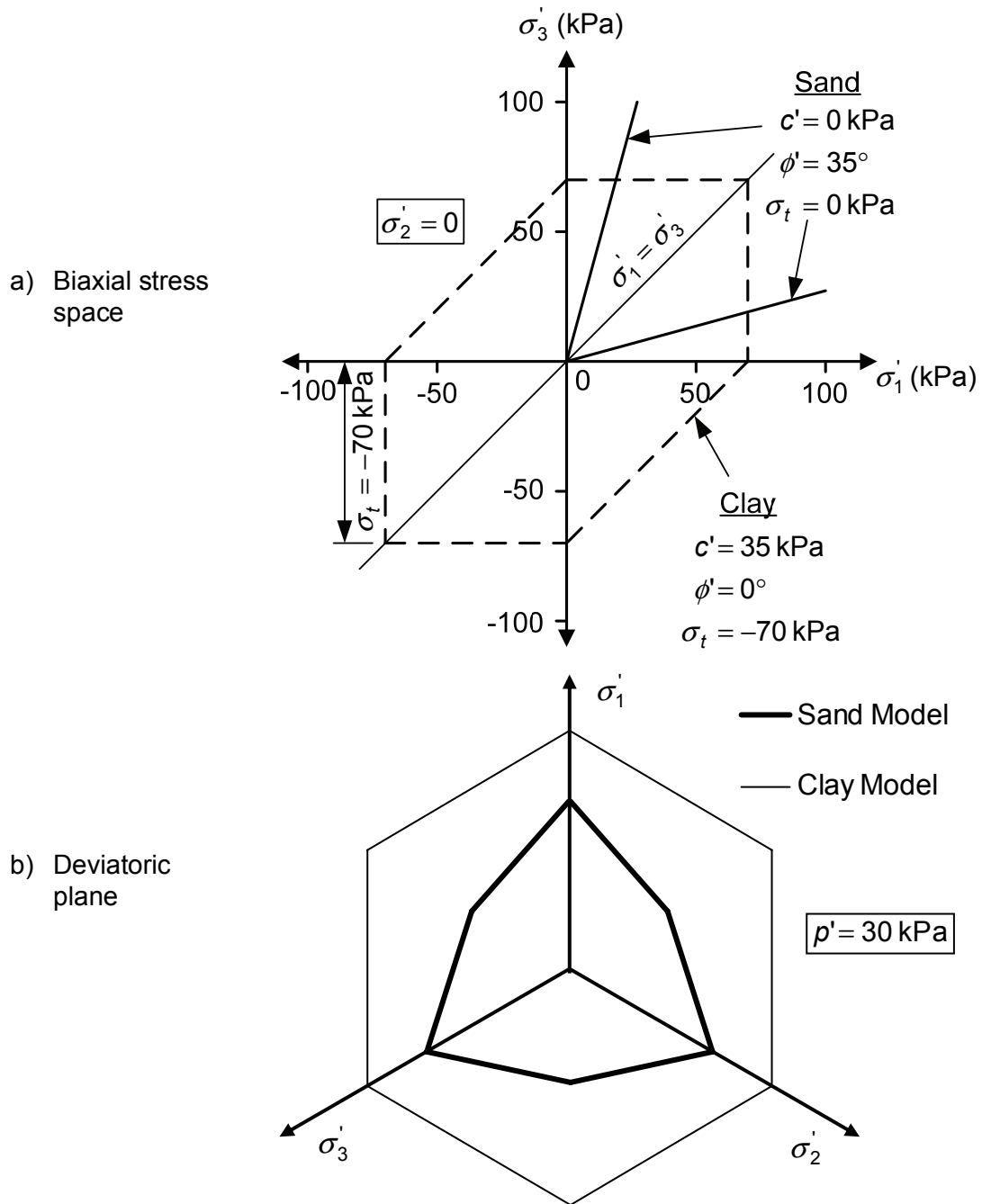
Figure B-2: Base soil model yield surface configurations

Chen and Saleeb (1982) noted two main shortcomings concerning the M-C failure criterion: a) It takes no account of the intermediate principal stress ($\sigma_2^{'}$) when determining failure; and b) it does not take into account curvature of the failure surface with increasing mean effective stress. The latter can be a concern over a wide range of mean effective stresses, but for the lateral pile loading conditions investigated in the current research, the range was considered to be small enough for curvature to be neglected. The influence of $\sigma_2^{'}$, however, cannot be discounted, particularly in terms of shear strength. Griffiths (1990) examined this issue through numerical comparison with other more realistic strength criteria, concluding that the M-C criterion generally underestimates strength for all modes of loading except compression (i.e., when $\sigma_2^{'} = \sigma_3^{'}$). Friction angles measured in plane strain compression, for example, are about 10 percent higher than those measured in triaxial compression (Kulhawy and Mayne, 1990), whereas the M-C criterion predicts the same friction angle regardless of loading condition (i.e., $\phi' = \text{constant}$).

In addition to conservative soil strength values, the base soil model possesses limited capabilities given the bilinear depiction of soil stress-strain behavior and imposition of constant volume conditions (perfect plasticity). The latter issue is likely to have little impact on the clay base model given that constant volume conditions are appropriate for undrained behavior, but in the sand base model case, where a medium-dense relative density applies, this is an obvious limitation. An associated flow rule was also adopted (as was the case for both the sand and clay base models), and in the sand case this implies too much dilative plastic strain tendencies at the expense of too little plastic shear strain. Such limitations must be kept in mind when assessing results, but are a necessary compromise for having the attractive model qualities of simplicity and a well proven track record.

B.1.2   Advanced Clay Model

The Base Soil Model idealization of undrained clay behavior may not be a bad approximation of actual undrained behavior. However, the demarcation of elastic and plastic behavior, as well as the use of a sole strength parameter c', does not truly reflect the various factors that contribute to the observed behavior. Not the least of these factors is volume-change tendencies and the affect they have in establishing the undrained shear strength. An advanced clay model should recognize such volume effects, and to this end the Modified Cam Clay (MCC) model (Roscoe and Burland, 1968) was chosen to serve the more advanced modeling role for clay.

The MCC model constitutes a volumetric-hardening elastic-plastic soil model entrenched in the critical state framework. In this way the model behaves in accordance with the volume versus mean effective pressure (i.e., $e - \log p'$) behavior, but is distinguished by a particular elastic and plastic formulation that defines the stress-strain response. Elastic deviatoric behavior draws on isotropic, linear elastic theory as per the Base Soil Model, but elastic volumetric behavior is defined via the unload-reload line (url) in $e - \log p'$ space. This defines an increment in elastic (recoverable) volume as

$$\delta v^e = -\kappa \frac{\delta p'}{p'} \tag{B.5}$$

which gives an increment of elastic volumetric strain

$$\delta\varepsilon_p^e = \kappa\frac{\delta p'}{vp'} \tag{B.6}$$

where the superscript e in (B.5) denotes elastic action (and similarly a superscript p would denote plastic action), and the subscript p in (B.6) indicates that p'-q (triaxial) stress space applies.

Plastic behavior in the MCC model adopts an ellipse-shaped surface serving as both a yield and plastic potential surface, with an associated flow rule assumed. Plastic volumetric strains are derived using the $e - \log p'$ deformation behavior, and denoting mean effective pressures on the normal compression line (iso-ncl) with the subscript "o", are given by (Wood, 1990)

$$\delta\varepsilon_p^p = (\lambda - \kappa)\frac{\delta p_o'}{vp_o'} \tag{B.7}$$

Plastic deviatoric strains are determined with knowledge of plastic volumetric strain magnitude (Equation B.7) and the ratio of plastic volumetric to plastic shear strain as provided by the flow rule direction. The size of the ellipse-shaped yield and plastic potential surface is controlled by plastic volumetric hardening alone, which from (B.7) is described by the following relationship:

$$\frac{\partial p_o'}{\partial\varepsilon_p^p} = \frac{vp_o'}{\lambda - \kappa} \tag{B.8}$$

Resultant undrained behavior predicted by the MCC model, and appropriate to the current research, is shown in Figure B-3.
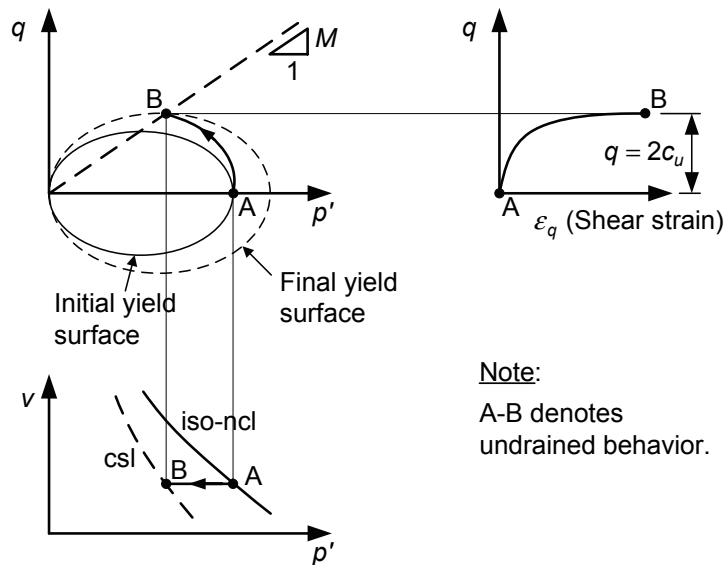
Figure B-3: Undrained behavior from MCC model

245

This indicates the stress-strain response and stress path taken upon loading, starting from a normally consolidated state (point A) then proceeding towards the critical state (point B). Between points A and B the requirement of zero volume change demands counterbalancing dilative elastic volumetric strain increments and contractive plastic volumetric strain increments, given by (B.6) and (B.7) respectively. Given the contractive plastic volumetric strains, the yield-plastic potential surface must increase in size according to the change in p_o' as defined by (B.8). Thus the p_o' value defines the size of the yield-plastic potential surface, and given the geometry of an ellipse corresponds to a critical state at a mean effective pressure equal to $p_o'/2$.

Although originally developed to predict the response of remolded clays in the triaxial test apparatus, the MCC model has had particular success in modeling the response of uncemented, normally consolidated and lightly overconsolidated clay deposits (Chen and Saleeb, 1982; Wood, 1990). A particular strength of the model is its ability to provide for continuous yielding in response to loading (as is evident from the nonlinear stress-strain response indicated in Figure B-3), rather than being limited to a bilinear elastic-plastic idealization as with the Base Soil Model. Important shortcomings include a circular trace of the failure surface in the deviatoric plane, implying stress-path independent strength, and neglecting to provide for deviatoric plastic strain hardening (Carter, Desai, Potts, Schweiger and Sloan, 2000). It is also to be noted that the model is not defined for negative p' values, which is in effect the equivalent of a zero tension cut-off value.

B.1.3   Advanced Sand Model

Modeling the drained behavior of sand presents a far more formidable task compared with undrained clay behavior, given the greater significance of both volume (density) and stress states. Both of these factors contribute to a variable pattern of contractive or dilative response dependent on the level of stress imposed and the current volume state. This type of behavior is beyond the capabilities of the Base Soil Model depiction of sand behavior, and calls for more sophisticated modeling techniques. To address this more sophisticated need in the current research, a bounding surface sand model presented by Manzari and Dafalias (1997) was selected, herein referred to as the Manzari and Dafalias Sand (MDS) model.

Motivation for the MDS model concerned two problems in particular: (a) monotonic versus cyclic loading behavior, where Manzari and Dafalias (1997) considered that existing models had difficulty in being able to accurately model one without loss of accuracy to the other; and (b) the strong dependence of sand behavior on density, often requiring sands at different densities to be treated as different materials for modeling purposes. The MDS model therefore sought to predict monotonic and cyclic behavior with equal capabilities, and at the same time take into account the influence of differing densities as a matter of course. The critical state concept was chosen as the basic behavioral framework in which to portray such behavior, but with added complexity to emulate contractive and dilative characteristics as a function of stress and density state.

Treatment of contractive and dilative tendencies uses a parameter that appears to capture both the density and confining stress influence on behavior. This parameter has been termed the "state parameter" (Been and Jefferies, 1985), and is shown on Figure B-4 denoted by the symbol ψ. The state parameter is simply the difference between the current void ratio of the sand at a given mean effective stress (e), and the void ratio corresponding to the critical state at the same mean effective stress (e_c) i.e., $\psi = e - e_c$. Hence, dilative behavior occurs when $\psi < 0$ and contractive behavior occurs when $\psi > 0$. The MDS model utilizes ψ to provide a necessary link between the current state and loading abilities of sand, drawing on a method developed by Wood, Belkheir and Liu (1994).
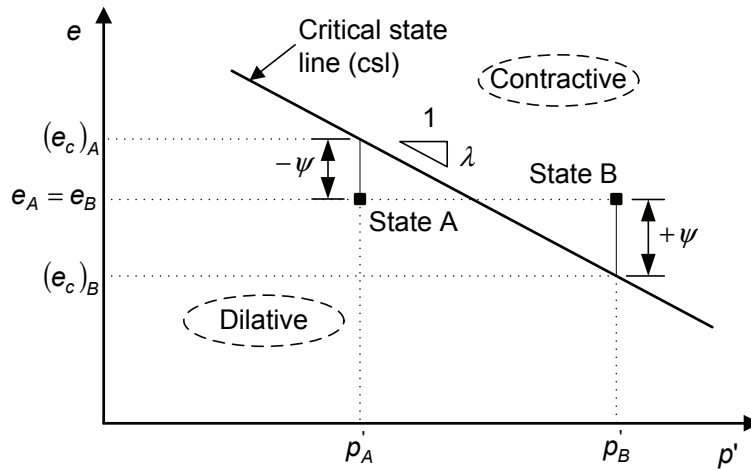
Figure B-4: Definition of state parameter

The essence of the Wood et al. (1994) method is use of an approximately linear relationship between the peak friction angle and state parameter, as obtained by Been and Jefferies (1985) and shown in Figure 6-5.
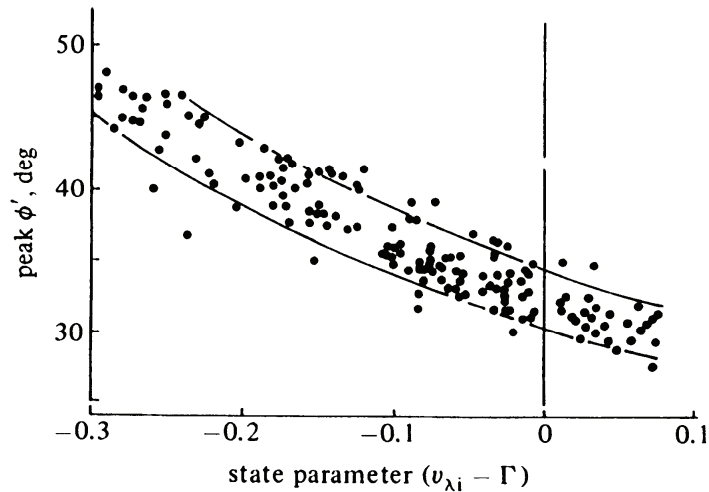
Figure B-5: Peak friction angle versus state parameter relationship (from Wood, 1990)

Using this relationship between stress ratio (i.e., $\eta = q/p'$ for triaxial test conditions) and friction angle, the following approximate relationship is implied:

$$\eta_p = \eta_{cs} - k\psi \tag{B.9}$$

247

where η_p = peak stress ratio for triaxial test conditions,

η_{cs} = critical state stress ratio for triaxial test conditions, and

k = positive constant.

Adopting the following flow rule based on Rowe's stress-dilatancy theory (ignoring elastic strains such that plastic strain = total strain),

$$\frac{\delta\varepsilon_p}{\delta\varepsilon_q} = A(\eta_{cs} - \eta) \tag{B.10}$$

where A = positive constant,

a means of linking the current state of sand (ψ) with loading abilities (η) was made possible through interaction of (B.9) and (B.10). However, the Wood et al. (1994) method was limited to triaxial compression loading conditions, and in order to provide a more general loading framework, the MDS model extends the concept to compression and extension loading in all principal directions. This is undertaken within the context of bounding surface theory, whereby the existence of two main surfaces are proposed: (a) a yielding surface, defining the boundary of elastic and plastic behavior; and (b) a bounding surface that constitutes the limit of possible stress states (i.e., a failure surface). The yield surface takes the form of a circular open-ended inner cone, while the bounding surface takes the form of a smooth triangular-shaped open-ended outer cone. The basic two-surface configuration is illustrated in Figure B-6.
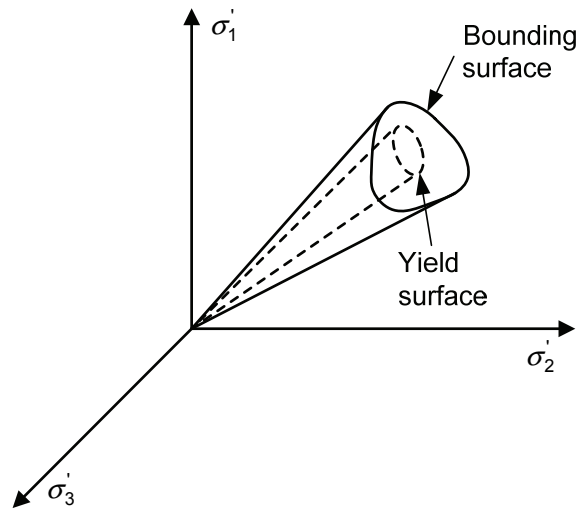
Figure B-6: Basic two-surface configuration for the MDS model

Working within this basic two-surface configuration and employing the interactive volume and strength mechanism put forward by Wood et al. (1994), the MDS model offers complete strain hardening and softening capabilities that are typical of sand response at varying density and stress states. In doing so the model encompasses stress-dependent elastic moduli, non-associated plastic behavior, and realistic stress-path dependent strength behavior. Complete details of the model and the elastic-plastic formulation are given in Dodds (2005). An example of the capabilities of the model is illustrated in Figure B-7, depicting undrained triaxial tests (i.e., single element tests) of Nevada Sand for various initial void ratios.
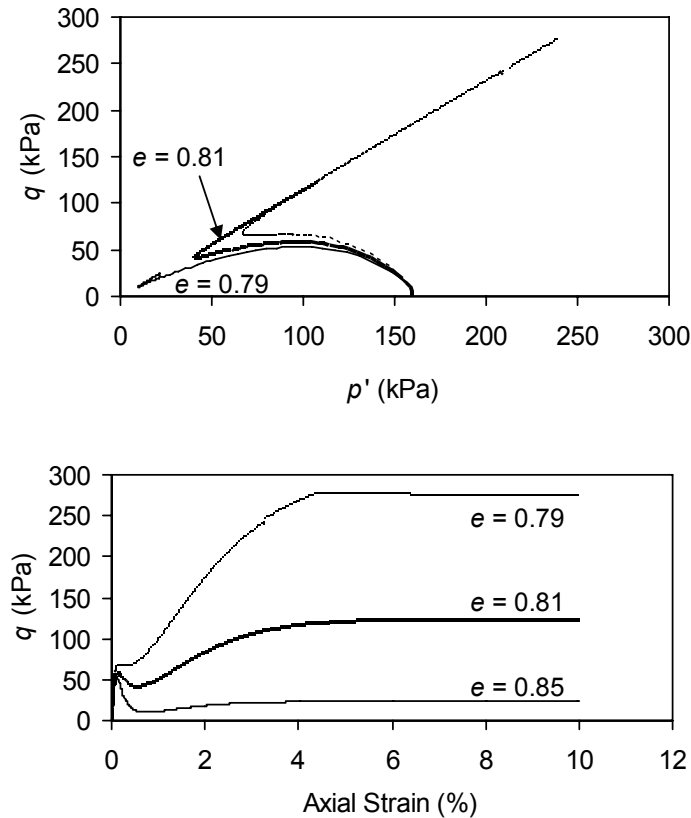
Figure B-7: MDS model single element simulations of undrained triaxial tests

MCEER Technical Reports

MCEER publishes technical reports on a variety of subjects written by authors funded through MCEER. These reports are available from both MCEER Publications and the National Technical Information Service (NTIS). Requests for reports should be directed to MCEER Publications, MCEER, University at Buffalo, State University of New York, Red Jacket Quadrangle, Buffalo, New York 14261. Reports can also be requested through NTIS, 5285 Port Royal Road, Springfield, Virginia 22161. NTIS accession numbers are shown in parenthesis, if available.

NCEER-87-0001   "First-Year Program in Research, Education and Technology Transfer," 3/5/87, (PB88-134275, A04, MF-A01).

NCEER-87-0002   "Experimental Evaluation of Instantaneous Optimal Algorithms for Structural Control," by R.C. Lin, T.T. Soong and A.M. Reinhorn, 4/20/87, (PB88-134341, A04, MF-A01).

NCEER-87-0003   "Experimentation Using the Earthquake Simulation Facilities at University at Buffalo," by A.M. Reinhorn and R.L. Ketter, to be published.

NCEER-87-0004   "The System Characteristics and Performance of a Shaking Table," by J.S. Hwang, K.C. Chang and G.C. Lee, 6/1/87, (PB88-134259, A03, MF-A01). This report is available only through NTIS (see address given above).

NCEER-87-0005   "A Finite Element Formulation for Nonlinear Viscoplastic Material Using a Q Model," by O. Gyebi and G. Dasgupta, 11/2/87, (PB88-213764, A08, MF-A01).

NCEER-87-0006   "Symbolic Manipulation Program (SMP) - Algebraic Codes for Two and Three Dimensional Finite Element Formulations," by X. Lee and G. Dasgupta, 11/9/87, (PB88-218522, A05, MF-A01).

NCEER-87-0007   "Instantaneous Optimal Control Laws for Tall Buildings Under Seismic Excitations," by J.N. Yang, A. Akbarpour and P. Ghaemmaghami, 6/10/87, (PB88-134333, A06, MF-A01). This report is only available through NTIS (see address given above).

NCEER-87-0008   "IDARC: Inelastic Damage Analysis of Reinforced Concrete Frame - Shear-Wall Structures," by Y.J. Park, A.M. Reinhorn and S.K. Kunnath, 7/20/87, (PB88-134325, A09, MF-A01). This report is only available through NTIS (see address given above).

NCEER-87-0009   "Liquefaction Potential for New York State: A Preliminary Report on Sites in Manhattan and Buffalo," by M. Budhu, V. Vijayakumar, R.F. Giese and L. Baumgras, 8/31/87, (PB88-163704, A03, MF-A01). This report is available only through NTIS (see address given above).

NCEER-87-0010   "Vertical and Torsional Vibration of Foundations in Inhomogeneous Media," by A.S. Veletsos and K.W. Dotson, 6/1/87, (PB88-134291, A03, MF-A01). This report is only available through NTIS (see address given above).

NCEER-87-0011   "Seismic Probabilistic Risk Assessment and Seismic Margins Studies for Nuclear Power Plants," by Howard H.M. Hwang, 6/15/87, (PB88-134267, A03, MF-A01). This report is only available through NTIS (see address given above).

NCEER-87-0012   "Parametric Studies of Frequency Response of Secondary Systems Under Ground-Acceleration Excitations," by Y. Yong and Y.K. Lin, 6/10/87, (PB88-134309, A03, MF-A01). This report is only available through NTIS (see address given above).

NCEER-87-0013   "Frequency Response of Secondary Systems Under Seismic Excitation," by J.A. HoLung, J. Cai and Y.K. Lin, 7/31/87, (PB88-134317, A05, MF-A01). This report is only available through NTIS (see address given above).

NCEER-87-0014   "Modelling Earthquake Ground Motions in Seismically Active Regions Using Parametric Time Series Methods," by G.W. Ellis and A.S. Cakmak, 8/25/87, (PB88-134283, A08, MF-A01). This report is only available through NTIS (see address given above).

NCEER-87-0015   "Detection and Assessment of Seismic Structural Damage," by E. DiPasquale and A.S. Cakmak, 8/25/87, (PB88-163712, A05, MF-A01). This report is only available through NTIS (see address given above).

NCEER-87-0016   "Pipeline Experiment at Parkfield, California," by J. Isenberg and E. Richardson, 9/15/87, (PB88-163720, A03, MF-A01). This report is available only through NTIS (see address given above).

NCEER-87-0017   "Digital Simulation of Seismic Ground Motion," by M. Shinozuka, G. Deodatis and T. Harada, 8/31/87, (PB88-155197, A04, MF-A01). This report is available only through NTIS (see address given above).

NCEER-87-0018   "Practical Considerations for Structural Control: System Uncertainty, System Time Delay and Truncation of Small Control Forces," J.N. Yang and A. Akbarpour, 8/10/87, (PB88-163738, A08, MF-A01). This report is only available through NTIS (see address given above).

NCEER-87-0019   "Modal Analysis of Nonclassically Damped Structural Systems Using Canonical Transformation," by J.N. Yang, S. Sarkani and F.X. Long, 9/27/87, (PB88-187851, A04, MF-A01).

NCEER-87-0020   "A Nonstationary Solution in Random Vibration Theory," by J.R. Red-Horse and P.D. Spanos, 11/3/87, (PB88-163746, A03, MF-A01).

NCEER-87-0021   "Horizontal Impedances for Radially Inhomogeneous Viscoelastic Soil Layers," by A.S. Veletsos and K.W. Dotson, 10/15/87, (PB88-150859, A04, MF-A01).

NCEER-87-0022   "Seismic Damage Assessment of Reinforced Concrete Members," by Y.S. Chung, C. Meyer and M. Shinozuka, 10/9/87, (PB88-150867, A05, MF-A01). This report is available only through NTIS (see address given above).

NCEER-87-0023   "Active Structural Control in Civil Engineering," by T.T. Soong, 11/11/87, (PB88-187778, A03, MF-A01).

NCEER-87-0024   "Vertical and Torsional Impedances for Radially Inhomogeneous Viscoelastic Soil Layers," by K.W. Dotson and A.S. Veletsos, 12/87, (PB88-187786, A03, MF-A01).

NCEER-87-0025   "Proceedings from the Symposium on Seismic Hazards, Ground Motions, Soil-Liquefaction and Engineering Practice in Eastern North America," October 20-22, 1987, edited by K.H. Jacob, 12/87, (PB88-188115, A23, MF-A01). This report is available only through NTIS (see address given above).

NCEER-87-0026   "Report on the Whittier-Narrows, California, Earthquake of October 1, 1987," by J. Pantelic and A. Reinhorn, 11/87, (PB88-187752, A03, MF-A01). This report is available only through NTIS (see address given above).

NCEER-87-0027   "Design of a Modular Program for Transient Nonlinear Analysis of Large 3-D Building Structures," by S. Srivastav and J.F. Abel, 12/30/87, (PB88-187950, A05, MF-A01). This report is only available through NTIS (see address given above).

NCEER-87-0028   "Second-Year Program in Research, Education and Technology Transfer," 3/8/88, (PB88-219480, A04, MF-A01).

NCEER-88-0001   "Workshop on Seismic Computer Analysis and Design of Buildings With Interactive Graphics," by W. McGuire, J.F. Abel and C.H. Conley, 1/18/88, (PB88-187760, A03, MF-A01). This report is only available through NTIS (see address given above).

NCEER-88-0002   "Optimal Control of Nonlinear Flexible Structures," by J.N. Yang, F.X. Long and D. Wong, 1/22/88, (PB88-213772, A06, MF-A01).

NCEER-88-0003   "Substructuring Techniques in the Time Domain for Primary-Secondary Structural Systems," by G.D. Manolis and G. Juhn, 2/10/88, (PB88-213780, A04, MF-A01).

NCEER-88-0004   "Iterative Seismic Analysis of Primary-Secondary Systems," by A. Singhal, L.D. Lutes and P.D. Spanos, 2/23/88, (PB88-213798, A04, MF-A01).

NCEER-88-0005   "Stochastic Finite Element Expansion for Random Media," by P.D. Spanos and R. Ghanem, 3/14/88, (PB88-213806, A03, MF-A01).

NCEER-88-0006   "Combining Structural Optimization and Structural Control," by F.Y. Cheng and C.P. Pantelides, 1/10/88, (PB88-213814, A05, MF-A01).

NCEER-88-0007   "Seismic Performance Assessment of Code-Designed Structures," by H.H-M. Hwang, J-W. Jaw and H-J. Shau, 3/20/88, (PB88-219423, A04, MF-A01). This report is only available through NTIS (see address given above).

NCEER-88-0008   "Reliability Analysis of Code-Designed Structures Under Natural Hazards," by H.H-M. Hwang, H. Ushiba and M. Shinozuka, 2/29/88, (PB88-229471, A07, MF-A01). This report is only available through NTIS (see address given above).

NCEER-88-0009   "Seismic Fragility Analysis of Shear Wall Structures," by J-W Jaw and H.H-M. Hwang, 4/30/88, (PB89-102867, A04, MF-A01).

NCEER-88-0010   "Base Isolation of a Multi-Story Building Under a Harmonic Ground Motion - A Comparison of Performances of Various Systems," by F-G Fan, G. Ahmadi and I.G. Tadjbakhsh, 5/18/88, (PB89-122238, A06, MF-A01). This report is only available through NTIS (see address given above).

NCEER-88-0011   "Seismic Floor Response Spectra for a Combined System by Green's Functions," by F.M. Lavelle, L.A. Bergman and P.D. Spanos, 5/1/88, (PB89-102875, A03, MF-A01).

NCEER-88-0012   "A New Solution Technique for Randomly Excited Hysteretic Structures," by G.Q. Cai and Y.K. Lin, 5/16/88, (PB89-102883, A03, MF-A01).

NCEER-88-0013   "A Study of Radiation Damping and Soil-Structure Interaction Effects in the Centrifuge," by K. Weissman, supervised by J.H. Prevost, 5/24/88, (PB89-144703, A06, MF-A01).

NCEER-88-0014   "Parameter Identification and Implementation of a Kinematic Plasticity Model for Frictional Soils," by J.H. Prevost and D.V. Griffiths, to be published.

NCEER-88-0015   "Two- and Three- Dimensional Dynamic Finite Element Analyses of the Long Valley Dam," by D.V. Griffiths and J.H. Prevost, 6/17/88, (PB89-144711, A04, MF-A01).

NCEER-88-0016   "Damage Assessment of Reinforced Concrete Structures in Eastern United States," by A.M. Reinhorn, M.J. Seidel, S.K. Kunnath and Y.J. Park, 6/15/88, (PB89-122220, A04, MF-A01). This report is only available through NTIS (see address given above).

NCEER-88-0017   "Dynamic Compliance of Vertically Loaded Strip Foundations in Multilayered Viscoelastic Soils," by S. Ahmad and A.S.M. Israil, 6/17/88, (PB89-102891, A04, MF-A01).

NCEER-88-0018   "An Experimental Study of Seismic Structural Response With Added Viscoelastic Dampers," by R.C. Lin, Z. Liang, T.T. Soong and R.H. Zhang, 6/30/88, (PB89-122212, A05, MF-A01). This report is available only through NTIS (see address given above).

NCEER-88-0019   "Experimental Investigation of Primary - Secondary System Interaction," by G.D. Manolis, G. Juhn and A.M. Reinhorn, 5/27/88, (PB89-122204, A04, MF-A01).

NCEER-88-0020   "A Response Spectrum Approach For Analysis of Nonclassically Damped Structures," by J.N. Yang, S. Sarkani and F.X. Long, 4/22/88, (PB89-102909, A04, MF-A01).

NCEER-88-0021   "Seismic Interaction of Structures and Soils: Stochastic Approach," by A.S. Veletsos and A.M. Prasad, 7/21/88, (PB89-122196, A04, MF-A01). This report is only available through NTIS (see address given above).

NCEER-88-0022   "Identification of the Serviceability Limit State and Detection of Seismic Structural Damage," by E. DiPasquale and A.S. Cakmak, 6/15/88, (PB89-122188, A05, MF-A01). This report is available only through NTIS (see address given above).

NCEER-88-0023   "Multi-Hazard Risk Analysis: Case of a Simple Offshore Structure," by B.K. Bhartia and E.H. Vanmarcke, 7/21/88, (PB89-145213, A05, MF-A01).

NCEER-88-0024   "Automated Seismic Design of Reinforced Concrete Buildings," by Y.S. Chung, C. Meyer and M. Shinozuka, 7/5/88, (PB89-122170, A06, MF-A01). This report is available only through NTIS (see address given above).

NCEER-88-0025   "Experimental Study of Active Control of MDOF Structures Under Seismic Excitations," by L.L. Chung, R.C. Lin, T.T. Soong and A.M. Reinhorn, 7/10/88, (PB89-122600, A04, MF-A01).

NCEER-88-0026   "Earthquake Simulation Tests of a Low-Rise Metal Structure," by J.S. Hwang, K.C. Chang, G.C. Lee and R.L. Ketter, 8/1/88, (PB89-102917, A04, MF-A01).

NCEER-88-0027   "Systems Study of Urban Response and Reconstruction Due to Catastrophic Earthquakes," by F. Kozin and H.K. Zhou, 9/22/88, (PB90-162348, A04, MF-A01).

NCEER-88-0028   "Seismic Fragility Analysis of Plane Frame Structures," by H.H-M. Hwang and Y.K. Low, 7/31/88, (PB89-131445, A06, MF-A01).

NCEER-88-0029   "Response Analysis of Stochastic Structures," by A. Kardara, C. Bucher and M. Shinozuka, 9/22/88, (PB89-174429, A04, MF-A01).

NCEER-88-0030   "Nonnormal Accelerations Due to Yielding in a Primary Structure," by D.C.K. Chen and L.D. Lutes, 9/19/88, (PB89-131437, A04, MF-A01).

NCEER-88-0031   "Design Approaches for Soil-Structure Interaction," by A.S. Veletsos, A.M. Prasad and Y. Tang, 12/30/88, (PB89-174437, A03, MF-A01). This report is available only through NTIS (see address given above).

NCEER-88-0032   "A Re-evaluation of Design Spectra for Seismic Damage Control," by C.J. Turkstra and A.G. Tallin, 11/7/88, (PB89-145221, A05, MF-A01).

NCEER-88-0033   "The Behavior and Design of Noncontact Lap Splices Subjected to Repeated Inelastic Tensile Loading," by V.E. Sagan, P. Gergely and R.N. White, 12/8/88, (PB89-163737, A08, MF-A01).

NCEER-88-0034   "Seismic Response of Pile Foundations," by S.M. Mamoon, P.K. Banerjee and S. Ahmad, 11/1/88, (PB89-145239, A04, MF-A01).

NCEER-88-0035   "Modeling of R/C Building Structures With Flexible Floor Diaphragms (IDARC2)," by A.M. Reinhorn, S.K. Kunnath and N. Panahshahi, 9/7/88, (PB89-207153, A07, MF-A01).

NCEER-88-0036   "Solution of the Dam-Reservoir Interaction Problem Using a Combination of FEM, BEM with Particular Integrals, Modal Analysis, and Substructuring," by C-S. Tsai, G.C. Lee and R.L. Ketter, 12/31/88, (PB89-207146, A04, MF-A01).

NCEER-88-0037   "Optimal Placement of Actuators for Structural Control," by F.Y. Cheng and C.P. Pantelides, 8/15/88, (PB89-162846, A05, MF-A01).

NCEER-88-0038   "Teflon Bearings in Aseismic Base Isolation: Experimental Studies and Mathematical Modeling," by A. Mokha, M.C. Constantinou and A.M. Reinhorn, 12/5/88, (PB89-218457, A10, MF-A01). This report is available only through NTIS (see address given above).

NCEER-88-0039   "Seismic Behavior of Flat Slab High-Rise Buildings in the New York City Area," by P. Weidlinger and M. Ettouney, 10/15/88, (PB90-145681, A04, MF-A01).

NCEER-88-0040   "Evaluation of the Earthquake Resistance of Existing Buildings in New York City," by P. Weidlinger and M. Ettouney, 10/15/88, to be published.

NCEER-88-0041   "Small-Scale Modeling Techniques for Reinforced Concrete Structures Subjected to Seismic Loads," by W. Kim, A. El-Attar and R.N. White, 11/22/88, (PB89-189625, A05, MF-A01).

NCEER-88-0042   "Modeling Strong Ground Motion from Multiple Event Earthquakes," by G.W. Ellis and A.S. Cakmak, 10/15/88, (PB89-174445, A03, MF-A01).

NCEER-88-0043   "Nonstationary Models of Seismic Ground Acceleration," by M. Grigoriu, S.E. Ruiz and E. Rosenblueth, 7/15/88, (PB89-189617, A04, MF-A01).

NCEER-88-0044   "SARCF User's Guide: Seismic Analysis of Reinforced Concrete Frames," by Y.S. Chung, C. Meyer and M. Shinozuka, 11/9/88, (PB89-174452, A08, MF-A01).

NCEER-88-0045   "First Expert Panel Meeting on Disaster Research and Planning," edited by J. Pantelic and J. Stoyle, 9/15/88, (PB89-174460, A05, MF-A01).

NCEER-88-0046   "Preliminary Studies of the Effect of Degrading Infill Walls on the Nonlinear Seismic Response of Steel Frames," by C.Z. Chrysostomou, P. Gergely and J.F. Abel, 12/19/88, (PB89-208383, A05, MF-A01).

NCEER-88-0047   "Reinforced Concrete Frame Component Testing Facility - Design, Construction, Instrumentation and Operation," by S.P. Pessiki, C. Conley, T. Bond, P. Gergely and R.N. White, 12/16/88, (PB89-174478, A04, MF-A01).

NCEER-89-0001   "Effects of Protective Cushion and Soil Compliancy on the Response of Equipment Within a Seismically Excited Building," by J.A. HoLung, 2/16/89, (PB89-207179, A04, MF-A01).

NCEER-89-0002   "Statistical Evaluation of Response Modification Factors for Reinforced Concrete Structures," by H.H-M. Hwang and J-W. Jaw, 2/17/89, (PB89-207187, A05, MF-A01).

NCEER-89-0003   "Hysteretic Columns Under Random Excitation," by G-Q. Cai and Y.K. Lin, 1/9/89, (PB89-196513, A03, MF-A01).

NCEER-89-0004   "Experimental Study of `Elephant Foot Bulge' Instability of Thin-Walled Metal Tanks," by Z-H. Jia and R.L. Ketter, 2/22/89, (PB89-207195, A03, MF-A01).

NCEER-89-0005   "Experiment on Performance of Buried Pipelines Across San Andreas Fault," by J. Isenberg, E. Richardson and T.D. O'Rourke, 3/10/89, (PB89-218440, A04, MF-A01). This report is available only through NTIS (see address given above).

NCEER-89-0006   "A Knowledge-Based Approach to Structural Design of Earthquake-Resistant Buildings," by M. Subramani, P. Gergely, C.H. Conley, J.F. Abel and A.H. Zaghw, 1/15/89, (PB89-218465, A06, MF-A01).

NCEER-89-0007   "Liquefaction Hazards and Their Effects on Buried Pipelines," by T.D. O'Rourke and P.A. Lane, 2/1/89, (PB89-218481, A09, MF-A01).

NCEER-89-0008   "Fundamentals of System Identification in Structural Dynamics," by H. Imai, C-B. Yun, O. Maruyama and M. Shinozuka, 1/26/89, (PB89-207211, A04, MF-A01).

NCEER-89-0009   "Effects of the 1985 Michoacan Earthquake on Water Systems and Other Buried Lifelines in Mexico," by A.G. Ayala and M.J. O'Rourke, 3/8/89, (PB89-207229, A06, MF-A01).

NCEER-89-R010   "NCEER Bibliography of Earthquake Education Materials," by K.E.K. Ross, Second Revision, 9/1/89, (PB90-125352, A05, MF-A01). This report is replaced by NCEER-92-0018.

NCEER-89-0011   "Inelastic Three-Dimensional Response Analysis of Reinforced Concrete Building Structures (IDARC-3D), Part I - Modeling," by S.K. Kunnath and A.M. Reinhorn, 4/17/89, (PB90-114612, A07, MF-A01). This report is available only through NTIS (see address given above).

NCEER-89-0012   "Recommended Modifications to ATC-14," by C.D. Poland and J.O. Malley, 4/12/89, (PB90-108648, A15, MF-A01).

NCEER-89-0013   "Repair and Strengthening of Beam-to-Column Connections Subjected to Earthquake Loading," by M. Corazao and A.J. Durrani, 2/28/89, (PB90-109885, A06, MF-A01).

NCEER-89-0014   "Program EXKAL2 for Identification of Structural Dynamic Systems," by O. Maruyama, C-B. Yun, M. Hoshiya and M. Shinozuka, 5/19/89, (PB90-109877, A09, MF-A01).

NCEER-89-0015   "Response of Frames With Bolted Semi-Rigid Connections, Part I - Experimental Study and Analytical Predictions," by P.J. DiCorso, A.M. Reinhorn, J.R. Dickerson, J.B. Radziminski and W.L. Harper, 6/1/89, to be published.

NCEER-89-0016   "ARMA Monte Carlo Simulation in Probabilistic Structural Analysis," by P.D. Spanos and M.P. Mignolet, 7/10/89, (PB90-109893, A03, MF-A01).

NCEER-89-P017   "Preliminary Proceedings from the Conference on Disaster Preparedness - The Place of Earthquake Education in Our Schools," Edited by K.E.K. Ross, 6/23/89, (PB90-108606, A03, MF-A01).

NCEER-89-0017   "Proceedings from the Conference on Disaster Preparedness - The Place of Earthquake Education in Our Schools," Edited by K.E.K. Ross, 12/31/89, (PB90-207895, A012, MF-A02). This report is available only through NTIS (see address given above).

NCEER-89-0018   "Multidimensional Models of Hysteretic Material Behavior for Vibration Analysis of Shape Memory Energy Absorbing Devices, by E.J. Graesser and F.A. Cozzarelli, 6/7/89, (PB90-164146, A04, MF-A01).

NCEER-89-0019   "Nonlinear Dynamic Analysis of Three-Dimensional Base Isolated Structures (3D-BASIS)," by S. Nagarajaiah, A.M. Reinhorn and M.C. Constantinou, 8/3/89, (PB90-161936, A06, MF-A01). This report has been replaced by NCEER-93-0011.

NCEER-89-0020   "Structural Control Considering Time-Rate of Control Forces and Control Rate Constraints," by F.Y. Cheng and C.P. Pantelides, 8/3/89, (PB90-120445, A04, MF-A01).

NCEER-89-0021   "Subsurface Conditions of Memphis and Shelby County," by K.W. Ng, T-S. Chang and H-H.M. Hwang, 7/26/89, (PB90-120437, A03, MF-A01).

NCEER-89-0022   "Seismic Wave Propagation Effects on Straight Jointed Buried Pipelines," by K. Elhmadi and M.J. O'Rourke, 8/24/89, (PB90-162322, A10, MF-A02).

NCEER-89-0023   "Workshop on Serviceability Analysis of Water Delivery Systems," edited by M. Grigoriu, 3/6/89, (PB90-127424, A03, MF-A01).

NCEER-89-0024   "Shaking Table Study of a 1/5 Scale Steel Frame Composed of Tapered Members," by K.C. Chang, J.S. Hwang and G.C. Lee, 9/18/89, (PB90-160169, A04, MF-A01).

NCEER-89-0025   "DYNA1D: A Computer Program for Nonlinear Seismic Site Response Analysis - Technical Documentation," by Jean H. Prevost, 9/14/89, (PB90-161944, A07, MF-A01). This report is available only through NTIS (see address given above).

NCEER-89-0026   "1:4 Scale Model Studies of Active Tendon Systems and Active Mass Dampers for Aseismic Protection," by A.M. Reinhorn, T.T. Soong, R.C. Lin, Y.P. Yang, Y. Fukao, H. Abe and M. Nakai, 9/15/89, (PB90-173246, A10, MF-A02). This report is available only through NTIS (see address given above).

NCEER-89-0027   "Scattering of Waves by Inclusions in a Nonhomogeneous Elastic Half Space Solved by Boundary Element Methods," by P.K. Hadley, A. Askar and A.S. Cakmak, 6/15/89, (PB90-145699, A07, MF-A01).

NCEER-89-0028   "Statistical Evaluation of Deflection Amplification Factors for Reinforced Concrete Structures," by H.H.M. Hwang, J-W. Jaw and A.L. Ch'ng, 8/31/89, (PB90-164633, A05, MF-A01).

NCEER-89-0029   "Bedrock Accelerations in Memphis Area Due to Large New Madrid Earthquakes," by H.H.M. Hwang, C.H.S. Chen and G. Yu, 11/7/89, (PB90-162330, A04, MF-A01).

NCEER-89-0030   "Seismic Behavior and Response Sensitivity of Secondary Structural Systems," by Y.Q. Chen and T.T. Soong, 10/23/89, (PB90-164658, A08, MF-A01).

NCEER-89-0031   "Random Vibration and Reliability Analysis of Primary-Secondary Structural Systems," by Y. Ibrahim, M. Grigoriu and T.T. Soong, 11/10/89, (PB90-161951, A04, MF-A01).

NCEER-89-0032   "Proceedings from the Second U.S. - Japan Workshop on Liquefaction, Large Ground Deformation and Their Effects on Lifelines, September 26-29, 1989," Edited by T.D. O'Rourke and M. Hamada, 12/1/89, (PB90-209388, A22, MF-A03).

NCEER-89-0033   "Deterministic Model for Seismic Damage Evaluation of Reinforced Concrete Structures," by J.M. Bracci, A.M. Reinhorn, J.B. Mander and S.K. Kunnath, 9/27/89, (PB91-108803, A06, MF-A01).

NCEER-89-0034   "On the Relation Between Local and Global Damage Indices," by E. DiPasquale and A.S. Cakmak, 8/15/89, (PB90-173865, A05, MF-A01).

NCEER-89-0035   "Cyclic Undrained Behavior of Nonplastic and Low Plasticity Silts," by A.J. Walker and H.E. Stewart, 7/26/89, (PB90-183518, A10, MF-A01).

NCEER-89-0036   "Liquefaction Potential of Surficial Deposits in the City of Buffalo, New York," by M. Budhu, R. Giese and L. Baumgrass, 1/17/89, (PB90-208455, A04, MF-A01).

NCEER-89-0037   "A Deterministic Assessment of Effects of Ground Motion Incoherence," by A.S. Veletsos and Y. Tang, 7/15/89, (PB90-164294, A03, MF-A01).

NCEER-89-0038   "Workshop on Ground Motion Parameters for Seismic Hazard Mapping," July 17-18, 1989, edited by R.V. Whitman, 12/1/89, (PB90-173923, A04, MF-A01).

NCEER-89-0039   "Seismic Effects on Elevated Transit Lines of the New York City Transit Authority," by C.J. Costantino, C.A. Miller and E. Heymsfield, 12/26/89, (PB90-207887, A06, MF-A01).

NCEER-89-0040   "Centrifugal Modeling of Dynamic Soil-Structure Interaction," by K. Weissman, Supervised by J.H. Prevost, 5/10/89, (PB90-207879, A07, MF-A01).

NCEER-89-0041   "Linearized Identification of Buildings With Cores for Seismic Vulnerability Assessment," by I-K. Ho and A.E. Aktan, 11/1/89, (PB90-251943, A07, MF-A01).

NCEER-90-0001   "Geotechnical and Lifeline Aspects of the October 17, 1989 Loma Prieta Earthquake in San Francisco," by T.D. O'Rourke, H.E. Stewart, F.T. Blackburn and T.S. Dickerman, 1/90, (PB90-208596, A05, MF-A01).

NCEER-90-0002   "Nonnormal Secondary Response Due to Yielding in a Primary Structure," by D.C.K. Chen and L.D. Lutes, 2/28/90, (PB90-251976, A07, MF-A01).

NCEER-90-0003   "Earthquake Education Materials for Grades K-12," by K.E.K. Ross, 4/16/90, (PB91-251984, A05, MF-A05). This report has been replaced by NCEER-92-0018.

NCEER-90-0004   "Catalog of Strong Motion Stations in Eastern North America," by R.W. Busby, 4/3/90, (PB90-251984, A05, MF-A01).

NCEER-90-0005   "NCEER Strong-Motion Data Base: A User Manual for the GeoBase Release (Version 1.0 for the Sun3)," by P. Friberg and K. Jacob, 3/31/90 (PB90-258062, A04, MF-A01).

NCEER-90-0006   "Seismic Hazard Along a Crude Oil Pipeline in the Event of an 1811-1812 Type New Madrid Earthquake," by H.H.M. Hwang and C-H.S. Chen, 4/16/90, (PB90-258054, A04, MF-A01).

NCEER-90-0007   "Site-Specific Response Spectra for Memphis Sheahan Pumping Station," by H.H.M. Hwang and C.S. Lee, 5/15/90, (PB91-108811, A05, MF-A01).

NCEER-90-0008   "Pilot Study on Seismic Vulnerability of Crude Oil Transmission Systems," by T. Ariman, R. Dobry, M. Grigoriu, F. Kozin, M. O'Rourke, T. O'Rourke and M. Shinozuka, 5/25/90, (PB91-108837, A06, MF-A01).

NCEER-90-0009   "A Program to Generate Site Dependent Time Histories: EQGEN," by G.W. Ellis, M. Srinivasan and A.S. Cakmak, 1/30/90, (PB91-108829, A04, MF-A01).

NCEER-90-0010   "Active Isolation for Seismic Protection of Operating Rooms," by M.E. Talbott, Supervised by M. Shinozuka, 6/8/9, (PB91-110205, A05, MF-A01).

NCEER-90-0011 "Program LINEARID for Identification of Linear Structural Dynamic Systems," by C-B. Yun and M. Shinozuka, 6/25/90, (PB91-110312, A08, MF-A01).

NCEER-90-0012 "Two-Dimensional Two-Phase Elasto-Plastic Seismic Response of Earth Dams," by A.N. Yiagos, Supervised by J.H. Prevost, 6/20/90, (PB91-110197, A13, MF-A02).

NCEER-90-0013 "Secondary Systems in Base-Isolated Structures: Experimental Investigation, Stochastic Response and Stochastic Sensitivity," by G.D. Manolis, G. Juhn, M.C. Constantinou and A.M. Reinhorn, 7/1/90, (PB91-110320, A08, MF-A01).

NCEER-90-0014 "Seismic Behavior of Lightly-Reinforced Concrete Column and Beam-Column Joint Details," by S.P. Pessiki, C.H. Conley, P. Gergely and R.N. White, 8/22/90, (PB91-108795, A11, MF-A02).

NCEER-90-0015 "Two Hybrid Control Systems for Building Structures Under Strong Earthquakes," by J.N. Yang and A. Danielians, 6/29/90, (PB91-125393, A04, MF-A01).

NCEER-90-0016 "Instantaneous Optimal Control with Acceleration and Velocity Feedback," by J.N. Yang and Z. Li, 6/29/90, (PB91-125401, A03, MF-A01).

NCEER-90-0017 "Reconnaissance Report on the Northern Iran Earthquake of June 21, 1990," by M. Mehrain, 10/4/90, (PB91-125377, A03, MF-A01).

NCEER-90-0018 "Evaluation of Liquefaction Potential in Memphis and Shelby County," by T.S. Chang, P.S. Tang, C.S. Lee and H. Hwang, 8/10/90, (PB91-125427, A09, MF-A01).

NCEER-90-0019 "Experimental and Analytical Study of a Combined Sliding Disc Bearing and Helical Steel Spring Isolation System," by M.C. Constantinou, A.S. Mokha and A.M. Reinhorn, 10/4/90, (PB91-125385, A06, MF-A01). This report is available only through NTIS (see address given above).

NCEER-90-0020 "Experimental Study and Analytical Prediction of Earthquake Response of a Sliding Isolation System with a Spherical Surface," by A.S. Mokha, M.C. Constantinou and A.M. Reinhorn, 10/11/90, (PB91-125419, A05, MF-A01).

NCEER-90-0021 "Dynamic Interaction Factors for Floating Pile Groups," by G. Gazetas, K. Fan, A. Kaynia and E. Kausel, 9/10/90, (PB91-170381, A05, MF-A01).

NCEER-90-0022 "Evaluation of Seismic Damage Indices for Reinforced Concrete Structures," by S. Rodriguez-Gomez and A.S. Cakmak, 9/30/90, PB91-171322, A06, MF-A01).

NCEER-90-0023 "Study of Site Response at a Selected Memphis Site," by H. Desai, S. Ahmad, E.S. Gazetas and M.R. Oh, 10/11/90, (PB91-196857, A03, MF-A01).

NCEER-90-0024 "A User's Guide to Strongmo: Version 1.0 of NCEER's Strong-Motion Data Access Tool for PCs and Terminals," by P.A. Friberg and C.A.T. Susch, 11/15/90, (PB91-171272, A03, MF-A01).

NCEER-90-0025 "A Three-Dimensional Analytical Study of Spatial Variability of Seismic Ground Motions," by L-L. Hong and A.H.-S. Ang, 10/30/90, (PB91-170399, A09, MF-A01).

NCEER-90-0026 "MUMOID User's Guide - A Program for the Identification of Modal Parameters," by S. Rodriguez-Gomez and E. DiPasquale, 9/30/90, (PB91-171298, A04, MF-A01).

NCEER-90-0027 "SARCF-II User's Guide - Seismic Analysis of Reinforced Concrete Frames," by S. Rodriguez-Gomez, Y.S. Chung and C. Meyer, 9/30/90, (PB91-171280, A05, MF-A01).

NCEER-90-0028 "Viscous Dampers: Testing, Modeling and Application in Vibration and Seismic Isolation," by N. Makris and M.C. Constantinou, 12/20/90 (PB91-190561, A06, MF-A01).

NCEER-90-0029 "Soil Effects on Earthquake Ground Motions in the Memphis Area," by H. Hwang, C.S. Lee, K.W. Ng and T.S. Chang, 8/2/90, (PB91-190751, A05, MF-A01).

NCEER-91-0001   "Proceedings from the Third Japan-U.S. Workshop on Earthquake Resistant Design of Lifeline Facilities and Countermeasures for Soil Liquefaction, December 17-19, 1990," edited by T.D. O'Rourke and M. Hamada, 2/1/91, (PB91-179259, A99, MF-A04).

NCEER-91-0002   "Physical Space Solutions of Non-Proportionally Damped Systems," by M. Tong, Z. Liang and G.C. Lee, 1/15/91, (PB91-179242, A04, MF-A01).

NCEER-91-0003   "Seismic Response of Single Piles and Pile Groups," by K. Fan and G. Gazetas, 1/10/91, (PB92-174994, A04, MF-A01).

NCEER-91-0004   "Damping of Structures: Part 1 - Theory of Complex Damping," by Z. Liang and G. Lee, 10/10/91, (PB92-197235, A12, MF-A03).

NCEER-91-0005   "3D-BASIS - Nonlinear Dynamic Analysis of Three Dimensional Base Isolated Structures: Part II," by S. Nagarajaiah, A.M. Reinhorn and M.C. Constantinou, 2/28/91, (PB91-190553, A07, MF-A01). This report has been replaced by NCEER-93-0011.

NCEER-91-0006   "A Multidimensional Hysteretic Model for Plasticity Deforming Metals in Energy Absorbing Devices," by E.J. Graesser and F.A. Cozzarelli, 4/9/91, (PB92-108364, A04, MF-A01).

NCEER-91-0007   "A Framework for Customizable Knowledge-Based Expert Systems with an Application to a KBES for Evaluating the Seismic Resistance of Existing Buildings," by E.G. Ibarra-Anaya and S.J. Fenves, 4/9/91, (PB91-210930, A08, MF-A01).

NCEER-91-0008   "Nonlinear Analysis of Steel Frames with Semi-Rigid Connections Using the Capacity Spectrum Method," by G.G. Deierlein, S-H. Hsieh, Y-J. Shen and J.F. Abel, 7/2/91, (PB92-113828, A05, MF-A01).

NCEER-91-0009   "Earthquake Education Materials for Grades K-12," by K.E.K. Ross, 4/30/91, (PB91-212142, A06, MF-A01). This report has been replaced by NCEER-92-0018.

NCEER-91-0010   "Phase Wave Velocities and Displacement Phase Differences in a Harmonically Oscillating Pile," by N. Makris and G. Gazetas, 7/8/91, (PB92-108356, A04, MF-A01).

NCEER-91-0011   "Dynamic Characteristics of a Full-Size Five-Story Steel Structure and a 2/5 Scale Model," by K.C. Chang, G.C. Yao, G.C. Lee, D.S. Hao and Y.C. Yeh," 7/2/91, (PB93-116648, A06, MF-A02).

NCEER-91-0012   "Seismic Response of a 2/5 Scale Steel Structure with Added Viscoelastic Dampers," by K.C. Chang, T.T. Soong, S-T. Oh and M.L. Lai, 5/17/91, (PB92-110816, A05, MF-A01).

NCEER-91-0013   "Earthquake Response of Retaining Walls; Full-Scale Testing and Computational Modeling," by S. Alampalli and A-W.M. Elgamal, 6/20/91, to be published.

NCEER-91-0014   "3D-BASIS-M: Nonlinear Dynamic Analysis of Multiple Building Base Isolated Structures," by P.C. Tsopelas, S. Nagarajaiah, M.C. Constantinou and A.M. Reinhorn, 5/28/91, (PB92-113885, A09, MF-A02).

NCEER-91-0015   "Evaluation of SEAOC Design Requirements for Sliding Isolated Structures," by D. Theodossiou and M.C. Constantinou, 6/10/91, (PB92-114602, A11, MF-A03).

NCEER-91-0016   "Closed-Loop Modal Testing of a 27-Story Reinforced Concrete Flat Plate-Core Building," by H.R. Somaprasad, T. Toksoy, H. Yoshiyuki and A.E. Aktan, 7/15/91, (PB92-129980, A07, MF-A02).

NCEER-91-0017   "Shake Table Test of a 1/6 Scale Two-Story Lightly Reinforced Concrete Building," by A.G. El-Attar, R.N. White and P. Gergely, 2/28/91, (PB92-222447, A06, MF-A02).

NCEER-91-0018   "Shake Table Test of a 1/8 Scale Three-Story Lightly Reinforced Concrete Building," by A.G. El-Attar, R.N. White and P. Gergely, 2/28/91, (PB93-116630, A08, MF-A02).

NCEER-91-0019   "Transfer Functions for Rigid Rectangular Foundations," by A.S. Veletsos, A.M. Prasad and W.H. Wu, 7/31/91, to be published.

NCEER-91-0020   "Hybrid Control of Seismic-Excited Nonlinear and Inelastic Structural Systems," by J.N. Yang, Z. Li and A. Danielians, 8/1/91, (PB92-143171, A06, MF-A02).

NCEER-91-0021   "The NCEER-91 Earthquake Catalog: Improved Intensity-Based Magnitudes and Recurrence Relations for U.S. Earthquakes East of New Madrid," by L. Seeber and J.G. Armbruster, 8/28/91, (PB92-176742, A06, MF-A02).

NCEER-91-0022   "Proceedings from the Implementation of Earthquake Planning and Education in Schools: The Need for Change - The Roles of the Changemakers," by K.E.K. Ross and F. Winslow, 7/23/91, (PB92-129998, A12, MF-A03).

NCEER-91-0023   "A Study of Reliability-Based Criteria for Seismic Design of Reinforced Concrete Frame Buildings," by H.H.M. Hwang and H-M. Hsu, 8/10/91, (PB92-140235, A09, MF-A02).

NCEER-91-0024   "Experimental Verification of a Number of Structural System Identification Algorithms," by R.G. Ghanem, H. Gavin and M. Shinozuka, 9/18/91, (PB92-176577, A18, MF-A04).

NCEER-91-0025   "Probabilistic Evaluation of Liquefaction Potential," by H.H.M. Hwang and C.S. Lee," 11/25/91, (PB92-143429, A05, MF-A01).

NCEER-91-0026   "Instantaneous Optimal Control for Linear, Nonlinear and Hysteretic Structures - Stable Controllers," by J.N. Yang and Z. Li, 11/15/91, (PB92-163807, A04, MF-A01).

NCEER-91-0027   "Experimental and Theoretical Study of a Sliding Isolation System for Bridges," by M.C. Constantinou, A. Kartoum, A.M. Reinhorn and P. Bradford, 11/15/91, (PB92-176973, A10, MF-A03).

NCEER-92-0001   "Case Studies of Liquefaction and Lifeline Performance During Past Earthquakes, Volume 1: Japanese Case Studies," Edited by M. Hamada and T. O'Rourke, 2/17/92, (PB92-197243, A18, MF-A04).

NCEER-92-0002   "Case Studies of Liquefaction and Lifeline Performance During Past Earthquakes, Volume 2: United States Case Studies," Edited by T. O'Rourke and M. Hamada, 2/17/92, (PB92-197250, A20, MF-A04).

NCEER-92-0003   "Issues in Earthquake Education," Edited by K. Ross, 2/3/92, (PB92-222389, A07, MF-A02).

NCEER-92-0004   "Proceedings from the First U.S. - Japan Workshop on Earthquake Protective Systems for Bridges," Edited by I.G. Buckle, 2/4/92, (PB94-142239, A99, MF-A06).

NCEER-92-0005   "Seismic Ground Motion from a Haskell-Type Source in a Multiple-Layered Half-Space," A.P. Theoharis, G. Deodatis and M. Shinozuka, 1/2/92, to be published.

NCEER-92-0006   "Proceedings from the Site Effects Workshop," Edited by R. Whitman, 2/29/92, (PB92-197201, A04, MF-A01).

NCEER-92-0007   "Engineering Evaluation of Permanent Ground Deformations Due to Seismically-Induced Liquefaction," by M.H. Baziar, R. Dobry and A-W.M. Elgamal, 3/24/92, (PB92-222421, A13, MF-A03).

NCEER-92-0008   "A Procedure for the Seismic Evaluation of Buildings in the Central and Eastern United States," by C.D. Poland and J.O. Malley, 4/2/92, (PB92-222439, A20, MF-A04).

NCEER-92-0009   "Experimental and Analytical Study of a Hybrid Isolation System Using Friction Controllable Sliding Bearings," by M.Q. Feng, S. Fujii and M. Shinozuka, 5/15/92, (PB93-150282, A06, MF-A02).

NCEER-92-0010   "Seismic Resistance of Slab-Column Connections in Existing Non-Ductile Flat-Plate Buildings," by A.J. Durrani and Y. Du, 5/18/92, (PB93-116812, A06, MF-A02).

NCEER-92-0011   "The Hysteretic and Dynamic Behavior of Brick Masonry Walls Upgraded by Ferrocement Coatings Under Cyclic Loading and Strong Simulated Ground Motion," by H. Lee and S.P. Prawel, 5/11/92, to be published.

NCEER-92-0012   "Study of Wire Rope Systems for Seismic Protection of Equipment in Buildings," by G.F. Demetriades, M.C. Constantinou and A.M. Reinhorn, 5/20/92, (PB93-116655, A08, MF-A02).

NCEER-92-0013   "Shape Memory Structural Dampers: Material Properties, Design and Seismic Testing," by P.R. Witting and F.A. Cozzarelli, 5/26/92, (PB93-116663, A05, MF-A01).

NCEER-92-0014   "Longitudinal Permanent Ground Deformation Effects on Buried Continuous Pipelines," by M.J. O'Rourke, and C. Nordberg, 6/15/92, (PB93-116671, A08, MF-A02).

NCEER-92-0015   "A Simulation Method for Stationary Gaussian Random Functions Based on the Sampling Theorem," by M. Grigoriu and S. Balopoulou, 6/11/92, (PB93-127496, A05, MF-A01).

NCEER-92-0016   "Gravity-Load-Designed Reinforced Concrete Buildings: Seismic Evaluation of Existing Construction and Detailing Strategies for Improved Seismic Resistance," by G.W. Hoffmann, S.K. Kunnath, A.M. Reinhorn and J.B. Mander, 7/15/92, (PB94-142007, A08, MF-A02).

NCEER-92-0017   "Observations on Water System and Pipeline Performance in the Limón Area of Costa Rica Due to the April 22, 1991 Earthquake," by M. O'Rourke and D. Ballantyne, 6/30/92, (PB93-126811, A06, MF-A02).

NCEER-92-0018   "Fourth Edition of Earthquake Education Materials for Grades K-12," Edited by K.E.K. Ross, 8/10/92, (PB93-114023, A07, MF-A02).

NCEER-92-0019   "Proceedings from the Fourth Japan-U.S. Workshop on Earthquake Resistant Design of Lifeline Facilities and Countermeasures for Soil Liquefaction," Edited by M. Hamada and T.D. O'Rourke, 8/12/92, (PB93-163939, A99, MF-E11).

NCEER-92-0020   "Active Bracing System: A Full Scale Implementation of Active Control," by A.M. Reinhorn, T.T. Soong, R.C. Lin, M.A. Riley, Y.P. Wang, S. Aizawa and M. Higashino, 8/14/92, (PB93-127512, A06, MF-A02).

NCEER-92-0021   "Empirical Analysis of Horizontal Ground Displacement Generated by Liquefaction-Induced Lateral Spreads," by S.F. Bartlett and T.L. Youd, 8/17/92, (PB93-188241, A06, MF-A02).

NCEER-92-0022   "IDARC Version 3.0: Inelastic Damage Analysis of Reinforced Concrete Structures," by S.K. Kunnath, A.M. Reinhorn and R.F. Lobo, 8/31/92, (PB93-227502, A07, MF-A02).

NCEER-92-0023   "A Semi-Empirical Analysis of Strong-Motion Peaks in Terms of Seismic Source, Propagation Path and Local Site Conditions, by M. Kamiyama, M.J. O'Rourke and R. Flores-Berrones, 9/9/92, (PB93-150266, A08, MF-A02).

NCEER-92-0024   "Seismic Behavior of Reinforced Concrete Frame Structures with Nonductile Details, Part I: Summary of Experimental Findings of Full Scale Beam-Column Joint Tests," by A. Beres, R.N. White and P. Gergely, 9/30/92, (PB93-227783, A05, MF-A01).

NCEER-92-0025   "Experimental Results of Repaired and Retrofitted Beam-Column Joint Tests in Lightly Reinforced Concrete Frame Buildings," by A. Beres, S. El-Borgi, R.N. White and P. Gergely, 10/29/92, (PB93-227791, A05, MF-A01).

NCEER-92-0026   "A Generalization of Optimal Control Theory: Linear and Nonlinear Structures," by J.N. Yang, Z. Li and S. Vongchavalitkul, 11/2/92, (PB93-188621, A05, MF-A01).

NCEER-92-0027   "Seismic Resistance of Reinforced Concrete Frame Structures Designed Only for Gravity Loads: Part I - Design and Properties of a One-Third Scale Model Structure," by J.M. Bracci, A.M. Reinhorn and J.B. Mander, 12/1/92, (PB94-104502, A08, MF-A02).

NCEER-92-0028   "Seismic Resistance of Reinforced Concrete Frame Structures Designed Only for Gravity Loads: Part II - Experimental Performance of Subassemblages," by L.E. Aycardi, J.B. Mander and A.M. Reinhorn, 12/1/92, (PB94-104510, A08, MF-A02).

NCEER-92-0029   "Seismic Resistance of Reinforced Concrete Frame Structures Designed Only for Gravity Loads: Part III - Experimental Performance and Analytical Study of a Structural Model," by J.M. Bracci, A.M. Reinhorn and J.B. Mander, 12/1/92, (PB93-227528, A09, MF-A01).

NCEER-92-0030   "Evaluation of Seismic Retrofit of Reinforced Concrete Frame Structures: Part I - Experimental Performance of Retrofitted Subassemblages," by D. Choudhuri, J.B. Mander and A.M. Reinhorn, 12/8/92, (PB93-198307, A07, MF-A02).

NCEER-92-0031   "Evaluation of Seismic Retrofit of Reinforced Concrete Frame Structures: Part II - Experimental Performance and Analytical Study of a Retrofitted Structural Model," by J.M. Bracci, A.M. Reinhorn and J.B. Mander, 12/8/92, (PB93-198315, A09, MF-A03).

NCEER-92-0032   "Experimental and Analytical Investigation of Seismic Response of Structures with Supplemental Fluid Viscous Dampers," by M.C. Constantinou and M.D. Symans, 12/21/92, (PB93-191435, A10, MF-A03). This report is available only through NTIS (see address given above).

NCEER-92-0033   "Reconnaissance Report on the Cairo, Egypt Earthquake of October 12, 1992," by M. Khater, 12/23/92, (PB93-188621, A03, MF-A01).

NCEER-92-0034   "Low-Level Dynamic Characteristics of Four Tall Flat-Plate Buildings in New York City," by H. Gavin, S. Yuan, J. Grossman, E. Pekelis and K. Jacob, 12/28/92, (PB93-188217, A07, MF-A02).

NCEER-93-0001   "An Experimental Study on the Seismic Performance of Brick-Infilled Steel Frames With and Without Retrofit," by J.B. Mander, B. Nair, K. Wojtkowski and J. Ma, 1/29/93, (PB93-227510, A07, MF-A02).

NCEER-93-0002   "Social Accounting for Disaster Preparedness and Recovery Planning," by S. Cole, E. Pantoja and V. Razak, 2/22/93, (PB94-142114, A12, MF-A03).

NCEER-93-0003   "Assessment of 1991 NEHRP Provisions for Nonstructural Components and Recommended Revisions," by T.T. Soong, G. Chen, Z. Wu, R-H. Zhang and M. Grigoriu, 3/1/93, (PB93-188639, A06, MF-A02).

NCEER-93-0004   "Evaluation of Static and Response Spectrum Analysis Procedures of SEAOC/UBC for Seismic Isolated Structures," by C.W. Winters and M.C. Constantinou, 3/23/93, (PB93-198299, A10, MF-A03).

NCEER-93-0005   "Earthquakes in the Northeast - Are We Ignoring the Hazard? A Workshop on Earthquake Science and Safety for Educators," edited by K.E.K. Ross, 4/2/93, (PB94-103066, A09, MF-A02).

NCEER-93-0006   "Inelastic Response of Reinforced Concrete Structures with Viscoelastic Braces," by R.F. Lobo, J.M. Bracci, K.L. Shen, A.M. Reinhorn and T.T. Soong, 4/5/93, (PB93-227486, A05, MF-A02).

NCEER-93-0007   "Seismic Testing of Installation Methods for Computers and Data Processing Equipment," by K. Kosar, T.T. Soong, K.L. Shen, J.A. HoLung and Y.K. Lin, 4/12/93, (PB93-198299, A07, MF-A02).

NCEER-93-0008   "Retrofit of Reinforced Concrete Frames Using Added Dampers," by A. Reinhorn, M. Constantinou and C. Li, to be published.

NCEER-93-0009   "Seismic Behavior and Design Guidelines for Steel Frame Structures with Added Viscoelastic Dampers," by K.C. Chang, M.L. Lai, T.T. Soong, D.S. Hao and Y.C. Yeh, 5/1/93, (PB94-141959, A07, MF-A02).

NCEER-93-0010   "Seismic Performance of Shear-Critical Reinforced Concrete Bridge Piers," by J.B. Mander, S.M. Waheed, M.T.A. Chaudhary and S.S. Chen, 5/12/93, (PB93-227494, A08, MF-A02).

NCEER-93-0011   "3D-BASIS-TABS: Computer Program for Nonlinear Dynamic Analysis of Three Dimensional Base Isolated Structures," by S. Nagarajaiah, C. Li, A.M. Reinhorn and M.C. Constantinou, 8/2/93, (PB94-141819, A09, MF-A02).

NCEER-93-0012   "Effects of Hydrocarbon Spills from an Oil Pipeline Break on Ground Water," by O.J. Helweg and H.H.M. Hwang, 8/3/93, (PB94-141942, A06, MF-A02).

NCEER-93-0013   "Simplified Procedures for Seismic Design of Nonstructural Components and Assessment of Current Code Provisions," by M.P. Singh, L.E. Suarez, E.E. Matheu and G.O. Maldonado, 8/4/93, (PB94-141827, A09, MF-A02).

NCEER-93-0014   "An Energy Approach to Seismic Analysis and Design of Secondary Systems," by G. Chen and T.T. Soong, 8/6/93, (PB94-142767, A11, MF-A03).

NCEER-93-0015   "Proceedings from School Sites: Becoming Prepared for Earthquakes - Commemorating the Third Anniversary of the Loma Prieta Earthquake," Edited by F.E. Winslow and K.E.K. Ross, 8/16/93, (PB94-154275, A16, MF-A02).

NCEER-93-0016   "Reconnaissance Report of Damage to Historic Monuments in Cairo, Egypt Following the October 12, 1992 Dahshur Earthquake," by D. Sykora, D. Look, G. Croci, E. Karaesmen and E. Karaesmen, 8/19/93, (PB94-142221, A08, MF-A02).

NCEER-93-0017   "The Island of Guam Earthquake of August 8, 1993," by S.W. Swan and S.K. Harris, 9/30/93, (PB94-141843, A04, MF-A01).

NCEER-93-0018   "Engineering Aspects of the October 12, 1992 Egyptian Earthquake," by A.W. Elgamal, M. Amer, K. Adalier and A. Abul-Fadl, 10/7/93, (PB94-141983, A05, MF-A01).

NCEER-93-0019   "Development of an Earthquake Motion Simulator and its Application in Dynamic Centrifuge Testing," by I. Krstelj, Supervised by J.H. Prevost, 10/23/93, (PB94-181773, A-10, MF-A03).

NCEER-93-0020   "NCEER-Taisei Corporation Research Program on Sliding Seismic Isolation Systems for Bridges: Experimental and Analytical Study of a Friction Pendulum System (FPS)," by M.C. Constantinou, P. Tsopelas, Y-S. Kim and S. Okamoto, 11/1/93, (PB94-142775, A08, MF-A02).

NCEER-93-0021   "Finite Element Modeling of Elastomeric Seismic Isolation Bearings," by L.J. Billings, Supervised by R. Shepherd, 11/8/93, to be published.

NCEER-93-0022   "Seismic Vulnerability of Equipment in Critical Facilities: Life-Safety and Operational Consequences," by K. Porter, G.S. Johnson, M.M. Zadeh, C. Scawthorn and S. Eder, 11/24/93, (PB94-181765, A16, MF-A03).

NCEER-93-0023   "Hokkaido Nansei-oki, Japan Earthquake of July 12, 1993, by P.I. Yanev and C.R. Scawthorn, 12/23/93, (PB94-181500, A07, MF-A01).

NCEER-94-0001   "An Evaluation of Seismic Serviceability of Water Supply Networks with Application to the San Francisco Auxiliary Water Supply System," by I. Markov, Supervised by M. Grigoriu and T. O'Rourke, 1/21/94, (PB94-204013, A07, MF-A02).

NCEER-94-0002   "NCEER-Taisei Corporation Research Program on Sliding Seismic Isolation Systems for Bridges: Experimental and Analytical Study of Systems Consisting of Sliding Bearings, Rubber Restoring Force Devices and Fluid Dampers," Volumes I and II, by P. Tsopelas, S. Okamoto, M.C. Constantinou, D. Ozaki and S. Fujii, 2/4/94, (PB94-181740, A09, MF-A02 and PB94-181757, A12, MF-A03).

NCEER-94-0003   "A Markov Model for Local and Global Damage Indices in Seismic Analysis," by S. Rahman and M. Grigoriu, 2/18/94, (PB94-206000, A12, MF-A03).

NCEER-94-0004   "Proceedings from the NCEER Workshop on Seismic Response of Masonry Infills," edited by D.P. Abrams, 3/1/94, (PB94-180783, A07, MF-A02).

NCEER-94-0005   "The Northridge, California Earthquake of January 17, 1994: General Reconnaissance Report," edited by J.D. Goltz, 3/11/94, (PB94-193943, A10, MF-A03).

NCEER-94-0006   "Seismic Energy Based Fatigue Damage Analysis of Bridge Columns: Part I - Evaluation of Seismic Capacity," by G.A. Chang and J.B. Mander, 3/14/94, (PB94-219185, A11, MF-A03).

NCEER-94-0007   "Seismic Isolation of Multi-Story Frame Structures Using Spherical Sliding Isolation Systems," by T.M. Al-Hussaini, V.A. Zayas and M.C. Constantinou, 3/17/94, (PB94-193745, A09, MF-A02).

NCEER-94-0008   "The Northridge, California Earthquake of January 17, 1994: Performance of Highway Bridges," edited by I.G. Buckle, 3/24/94, (PB94-193851, A06, MF-A02).

NCEER-94-0009   "Proceedings of the Third U.S.-Japan Workshop on Earthquake Protective Systems for Bridges," edited by I.G. Buckle and I. Friedland, 3/31/94, (PB94-195815, A99, MF-A06).

NCEER-94-0010   "3D-BASIS-ME: Computer Program for Nonlinear Dynamic Analysis of Seismically Isolated Single and Multiple Structures and Liquid Storage Tanks," by P.C. Tsopelas, M.C. Constantinou and A.M. Reinhorn, 4/12/94, (PB94-204922, A09, MF-A02).

NCEER-94-0011   "The Northridge, California Earthquake of January 17, 1994: Performance of Gas Transmission Pipelines," by T.D. O'Rourke and M.C. Palmer, 5/16/94, (PB94-204989, A05, MF-A01).

NCEER-94-0012   "Feasibility Study of Replacement Procedures and Earthquake Performance Related to Gas Transmission Pipelines," by T.D. O'Rourke and M.C. Palmer, 5/25/94, (PB94-206638, A09, MF-A02).

NCEER-94-0013   "Seismic Energy Based Fatigue Damage Analysis of Bridge Columns: Part II - Evaluation of Seismic Demand," by G.A. Chang and J.B. Mander, 6/1/94, (PB95-18106, A08, MF-A02).

NCEER-94-0014   "NCEER-Taisei Corporation Research Program on Sliding Seismic Isolation Systems for Bridges: Experimental and Analytical Study of a System Consisting of Sliding Bearings and Fluid Restoring Force/Damping Devices," by P. Tsopelas and M.C. Constantinou, 6/13/94, (PB94-219144, A10, MF-A03).

NCEER-94-0015   "Generation of Hazard-Consistent Fragility Curves for Seismic Loss Estimation Studies," by H. Hwang and J-R. Huo, 6/14/94, (PB95-181996, A09, MF-A02).

NCEER-94-0016   "Seismic Study of Building Frames with Added Energy-Absorbing Devices," by W.S. Pong, C.S. Tsai and G.C. Lee, 6/20/94, (PB94-219136, A10, A03).

NCEER-94-0017   "Sliding Mode Control for Seismic-Excited Linear and Nonlinear Civil Engineering Structures," by J. Yang, J. Wu, A. Agrawal and Z. Li, 6/21/94, (PB95-138483, A06, MF-A02).

NCEER-94-0018   "3D-BASIS-TABS Version 2.0: Computer Program for Nonlinear Dynamic Analysis of Three Dimensional Base Isolated Structures," by A.M. Reinhorn, S. Nagarajaiah, M.C. Constantinou, P. Tsopelas and R. Li, 6/22/94, (PB95-182176, A08, MF-A02).

NCEER-94-0019   "Proceedings of the International Workshop on Civil Infrastructure Systems: Application of Intelligent Systems and Advanced Materials on Bridge Systems," Edited by G.C. Lee and K.C. Chang, 7/18/94, (PB95-252474, A20, MF-A04).

NCEER-94-0020   "Study of Seismic Isolation Systems for Computer Floors," by V. Lambrou and M.C. Constantinou, 7/19/94, (PB95-138533, A10, MF-A03).

NCEER-94-0021   "Proceedings of the U.S.-Italian Workshop on Guidelines for Seismic Evaluation and Rehabilitation of Unreinforced Masonry Buildings," Edited by D.P. Abrams and G.M. Calvi, 7/20/94, (PB95-138749, A13, MF-A03).

NCEER-94-0022   "NCEER-Taisei Corporation Research Program on Sliding Seismic Isolation Systems for Bridges: Experimental and Analytical Study of a System Consisting of Lubricated PTFE Sliding Bearings and Mild Steel Dampers," by P. Tsopelas and M.C. Constantinou, 7/22/94, (PB95-182184, A08, MF-A02).

NCEER-94-0023   "Development of Reliability-Based Design Criteria for Buildings Under Seismic Load," by Y.K. Wen, H. Hwang and M. Shinozuka, 8/1/94, (PB95-211934, A08, MF-A02).

NCEER-94-0024   "Experimental Verification of Acceleration Feedback Control Strategies for an Active Tendon System," by S.J. Dyke, B.F. Spencer, Jr., P. Quast, M.K. Sain, D.C. Kaspari, Jr. and T.T. Soong, 8/29/94, (PB95-212320, A05, MF-A01).

NCEER-94-0025   "Seismic Retrofitting Manual for Highway Bridges," Edited by I.G. Buckle and I.F. Friedland, published by the Federal Highway Administration (PB95-212676, A15, MF-A03).

NCEER-94-0026   "Proceedings from the Fifth U.S.-Japan Workshop on Earthquake Resistant Design of Lifeline Facilities and Countermeasures Against Soil Liquefaction," Edited by T.D. O'Rourke and M. Hamada, 11/7/94, (PB95-220802, A99, MF-E08).

NCEER-95-0001 "Experimental and Analytical Investigation of Seismic Retrofit of Structures with Supplemental Damping: Part 1 - Fluid Viscous Damping Devices," by A.M. Reinhorn, C. Li and M.C. Constantinou, 1/3/95, (PB95-266599, A09, MF-A02).

NCEER-95-0002 "Experimental and Analytical Study of Low-Cycle Fatigue Behavior of Semi-Rigid Top-And-Seat Angle Connections," by G. Pekcan, J.B. Mander and S.S. Chen, 1/5/95, (PB95-220042, A07, MF-A02).

NCEER-95-0003 "NCEER-ATC Joint Study on Fragility of Buildings," by T. Anagnos, C. Rojahn and A.S. Kiremidjian, 1/20/95, (PB95-220026, A06, MF-A02).

NCEER-95-0004 "Nonlinear Control Algorithms for Peak Response Reduction," by Z. Wu, T.T. Soong, V. Gattulli and R.C. Lin, 2/16/95, (PB95-220349, A05, MF-A01).

NCEER-95-0005 "Pipeline Replacement Feasibility Study: A Methodology for Minimizing Seismic and Corrosion Risks to Underground Natural Gas Pipelines," by R.T. Eguchi, H.A. Seligson and D.G. Honegger, 3/2/95, (PB95-252326, A06, MF-A02).

NCEER-95-0006 "Evaluation of Seismic Performance of an 11-Story Frame Building During the 1994 Northridge Earthquake," by F. Naeim, R. DiSulio, K. Benuska, A. Reinhorn and C. Li, to be published.

NCEER-95-0007 "Prioritization of Bridges for Seismic Retrofitting," by N. Basöz and A.S. Kiremidjian, 4/24/95, (PB95-252300, A08, MF-A02).

NCEER-95-0008 "Method for Developing Motion Damage Relationships for Reinforced Concrete Frames," by A. Singhal and A.S. Kiremidjian, 5/11/95, (PB95-266607, A06, MF-A02).

NCEER-95-0009 "Experimental and Analytical Investigation of Seismic Retrofit of Structures with Supplemental Damping: Part II - Friction Devices," by C. Li and A.M. Reinhorn, 7/6/95, (PB96-128087, A11, MF-A03).

NCEER-95-0010 "Experimental Performance and Analytical Study of a Non-Ductile Reinforced Concrete Frame Structure Retrofitted with Elastomeric Spring Dampers," by G. Pekcan, J.B. Mander and S.S. Chen, 7/14/95, (PB96-137161, A08, MF-A02).

NCEER-95-0011 "Development and Experimental Study of Semi-Active Fluid Damping Devices for Seismic Protection of Structures," by M.D. Symans and M.C. Constantinou, 8/3/95, (PB96-136940, A23, MF-A04).

NCEER-95-0012 "Real-Time Structural Parameter Modification (RSPM): Development of Innervated Structures," by Z. Liang, M. Tong and G.C. Lee, 4/11/95, (PB96-137153, A06, MF-A01).

NCEER-95-0013 "Experimental and Analytical Investigation of Seismic Retrofit of Structures with Supplemental Damping: Part III - Viscous Damping Walls," by A.M. Reinhorn and C. Li, 10/1/95, (PB96-176409, A11, MF-A03).

NCEER-95-0014 "Seismic Fragility Analysis of Equipment and Structures in a Memphis Electric Substation," by J-R. Huo and H.H.M. Hwang, 8/10/95, (PB96-128087, A09, MF-A02).

NCEER-95-0015 "The Hanshin-Awaji Earthquake of January 17, 1995: Performance of Lifelines," Edited by M. Shinozuka, 11/3/95, (PB96-176383, A15, MF-A03).

NCEER-95-0016 "Highway Culvert Performance During Earthquakes," by T.L. Youd and C.J. Beckman, available as NCEER-96-0015.

NCEER-95-0017 "The Hanshin-Awaji Earthquake of January 17, 1995: Performance of Highway Bridges," Edited by I.G. Buckle, 12/1/95, to be published.

NCEER-95-0018 "Modeling of Masonry Infill Panels for Structural Analysis," by A.M. Reinhorn, A. Madan, R.E. Valles, Y. Reichmann and J.B. Mander, 12/8/95, (PB97-110886, MF-A01, A06).

NCEER-95-0019 "Optimal Polynomial Control for Linear and Nonlinear Structures," by A.K. Agrawal and J.N. Yang, 12/11/95, (PB96-168737, A07, MF-A02).

NCEER-95-0020 "Retrofit of Non-Ductile Reinforced Concrete Frames Using Friction Dampers," by R.S. Rao, P. Gergely and R.N. White, 12/22/95, (PB97-133508, A10, MF-A02).

NCEER-95-0021 "Parametric Results for Seismic Response of Pile-Supported Bridge Bents," by G. Mylonakis, A. Nikolaou and G. Gazetas, 12/22/95, (PB97-100242, A12, MF-A03).

NCEER-95-0022 "Kinematic Bending Moments in Seismically Stressed Piles," by A. Nikolaou, G. Mylonakis and G. Gazetas, 12/23/95, (PB97-113914, MF-A03, A13).

NCEER-96-0001 "Dynamic Response of Unreinforced Masonry Buildings with Flexible Diaphragms," by A.C. Costley and D.P. Abrams," 10/10/96, (PB97-133573, MF-A03, A15).

NCEER-96-0002 "State of the Art Review: Foundations and Retaining Structures," by I. Po Lam, to be published.

NCEER-96-0003 "Ductility of Rectangular Reinforced Concrete Bridge Columns with Moderate Confinement," by N. Wehbe, M. Saiidi, D. Sanders and B. Douglas, 11/7/96, (PB97-133557, A06, MF-A02).

NCEER-96-0004 "Proceedings of the Long-Span Bridge Seismic Research Workshop," edited by I.G. Buckle and I.M. Friedland, to be published.

NCEER-96-0005 "Establish Representative Pier Types for Comprehensive Study: Eastern United States," by J. Kulicki and Z. Prucz, 5/28/96, (PB98-119217, A07, MF-A02).

NCEER-96-0006 "Establish Representative Pier Types for Comprehensive Study: Western United States," by R. Imbsen, R.A. Schamber and T.A. Osterkamp, 5/28/96, (PB98-118607, A07, MF-A02).

NCEER-96-0007 "Nonlinear Control Techniques for Dynamical Systems with Uncertain Parameters," by R.G. Ghanem and M.I. Bujakov, 5/27/96, (PB97-100259, A17, MF-A03).

NCEER-96-0008 "Seismic Evaluation of a 30-Year Old Non-Ductile Highway Bridge Pier and Its Retrofit," by J.B. Mander, B. Mahmoodzadegan, S. Bhadra and S.S. Chen, 5/31/96, (PB97-110902, MF-A03, A10).

NCEER-96-0009 "Seismic Performance of a Model Reinforced Concrete Bridge Pier Before and After Retrofit," by J.B. Mander, J.H. Kim and C.A. Ligozio, 5/31/96, (PB97-110910, MF-A02, A10).

NCEER-96-0010 "IDARC2D Version 4.0: A Computer Program for the Inelastic Damage Analysis of Buildings," by R.E. Valles, A.M. Reinhorn, S.K. Kunnath, C. Li and A. Madan, 6/3/96, (PB97-100234, A17, MF-A03).

NCEER-96-0011 "Estimation of the Economic Impact of Multiple Lifeline Disruption: Memphis Light, Gas and Water Division Case Study," by S.E. Chang, H.A. Seligson and R.T. Eguchi, 8/16/96, (PB97-133490, A11, MF-A03).

NCEER-96-0012 "Proceedings from the Sixth Japan-U.S. Workshop on Earthquake Resistant Design of Lifeline Facilities and Countermeasures Against Soil Liquefaction, Edited by M. Hamada and T. O'Rourke, 9/11/96, (PB97-133581, A99, MF-A06).

NCEER-96-0013 "Chemical Hazards, Mitigation and Preparedness in Areas of High Seismic Risk: A Methodology for Estimating the Risk of Post-Earthquake Hazardous Materials Release," by H.A. Seligson, R.T. Eguchi, K.J. Tierney and K. Richmond, 11/7/96, (PB97-133565, MF-A02, A08).

NCEER-96-0014 "Response of Steel Bridge Bearings to Reversed Cyclic Loading," by J.B. Mander, D-K. Kim, S.S. Chen and G.J. Premus, 11/13/96, (PB97-140735, A12, MF-A03).

NCEER-96-0015 "Highway Culvert Performance During Past Earthquakes," by T.L. Youd and C.J. Beckman, 11/25/96, (PB97-133532, A06, MF-A01).

NCEER-97-0001 "Evaluation, Prevention and Mitigation of Pounding Effects in Building Structures," by R.E. Valles and A.M. Reinhorn, 2/20/97, (PB97-159552, A14, MF-A03).

NCEER-97-0002 "Seismic Design Criteria for Bridges and Other Highway Structures," by C. Rojahn, R. Mayes, D.G. Anderson, J. Clark, J.H. Hom, R.V. Nutt and M.J. O'Rourke, 4/30/97, (PB97-194658, A06, MF-A03).

NCEER-97-0003   "Proceedings of the U.S.-Italian Workshop on Seismic Evaluation and Retrofit," Edited by D.P. Abrams and G.M. Calvi, 3/19/97, (PB97-194666, A13, MF-A03).

NCEER-97-0004   "Investigation of Seismic Response of Buildings with Linear and Nonlinear Fluid Viscous Dampers," by A.A. Seleemah and M.C. Constantinou, 5/21/97, (PB98-109002, A15, MF-A03).

NCEER-97-0005   "Proceedings of the Workshop on Earthquake Engineering Frontiers in Transportation Facilities," edited by G.C. Lee and I.M. Friedland, 8/29/97, (PB98-128911, A25, MR-A04).

NCEER-97-0006   "Cumulative Seismic Damage of Reinforced Concrete Bridge Piers," by S.K. Kunnath, A. El-Bahy, A. Taylor and W. Stone, 9/2/97, (PB98-108814, A11, MF-A03).

NCEER-97-0007   "Structural Details to Accommodate Seismic Movements of Highway Bridges and Retaining Walls," by R.A. Imbsen, R.A. Schamber, E. Thorkildsen, A. Kartoum, B.T. Martin, T.N. Rosser and J.M. Kulicki, 9/3/97, (PB98-108996, A09, MF-A02).

NCEER-97-0008   "A Method for Earthquake Motion-Damage Relationships with Application to Reinforced Concrete Frames," by A. Singhal and A.S. Kiremidjian, 9/10/97, (PB98-108988, A13, MF-A03).

NCEER-97-0009   "Seismic Analysis and Design of Bridge Abutments Considering Sliding and Rotation," by K. Fishman and R. Richards, Jr., 9/15/97, (PB98-108897, A06, MF-A02).

NCEER-97-0010   "Proceedings of the FHWA/NCEER Workshop on the National Representation of Seismic Ground Motion for New and Existing Highway Facilities," edited by I.M. Friedland, M.S. Power and R.L. Mayes, 9/22/97, (PB98-128903, A21, MF-A04).

NCEER-97-0011   "Seismic Analysis for Design or Retrofit of Gravity Bridge Abutments," by K.L. Fishman, R. Richards, Jr. and R.C. Divito, 10/2/97, (PB98-128937, A08, MF-A02).

NCEER-97-0012   "Evaluation of Simplified Methods of Analysis for Yielding Structures," by P. Tsopelas, M.C. Constantinou, C.A. Kircher and A.S. Whittaker, 10/31/97, (PB98-128929, A10, MF-A03).

NCEER-97-0013   "Seismic Design of Bridge Columns Based on Control and Repairability of Damage," by C-T. Cheng and J.B. Mander, 12/8/97, (PB98-144249, A11, MF-A03).

NCEER-97-0014   "Seismic Resistance of Bridge Piers Based on Damage Avoidance Design," by J.B. Mander and C-T. Cheng, 12/10/97, (PB98-144223, A09, MF-A02).

NCEER-97-0015   "Seismic Response of Nominally Symmetric Systems with Strength Uncertainty," by S. Balopoulou and M. Grigoriu, 12/23/97, (PB98-153422, A11, MF-A03).

NCEER-97-0016   "Evaluation of Seismic Retrofit Methods for Reinforced Concrete Bridge Columns," by T.J. Wipf, F.W. Klaiber and F.M. Russo, 12/28/97, (PB98-144215, A12, MF-A03).

NCEER-97-0017   "Seismic Fragility of Existing Conventional Reinforced Concrete Highway Bridges," by C.L. Mullen and A.S. Cakmak, 12/30/97, (PB98-153406, A08, MF-A02).

NCEER-97-0018   "Loss Asssessment of Memphis Buildings," edited by D.P. Abrams and M. Shinozuka, 12/31/97, (PB98-144231, A13, MF-A03).

NCEER-97-0019   "Seismic Evaluation of Frames with Infill Walls Using Quasi-static Experiments," by K.M. Mosalam, R.N. White and P. Gergely, 12/31/97, (PB98-153455, A07, MF-A02).

NCEER-97-0020   "Seismic Evaluation of Frames with Infill Walls Using Pseudo-dynamic Experiments," by K.M. Mosalam, R.N. White and P. Gergely, 12/31/97, (PB98-153430, A07, MF-A02).

NCEER-97-0021   "Computational Strategies for Frames with Infill Walls: Discrete and Smeared Crack Analyses and Seismic Fragility," by K.M. Mosalam, R.N. White and P. Gergely, 12/31/97, (PB98-153414, A10, MF-A02).

NCEER-97-0022 "Proceedings of the NCEER Workshop on Evaluation of Liquefaction Resistance of Soils," edited by T.L. Youd and I.M. Idriss, 12/31/97, (PB98-155617, A15, MF-A03).

MCEER-98-0001 "Extraction of Nonlinear Hysteretic Properties of Seismically Isolated Bridges from Quick-Release Field Tests," by Q. Chen, B.M. Douglas, E.M. Maragakis and I.G. Buckle, 5/26/98, (PB99-118838, A06, MF-A01).

MCEER-98-0002 "Methodologies for Evaluating the Importance of Highway Bridges," by A. Thomas, S. Eshenaur and J. Kulicki, 5/29/98, (PB99-118846, A10, MF-A02).

MCEER-98-0003 "Capacity Design of Bridge Piers and the Analysis of Overstrength," by J.B. Mander, A. Dutta and P. Goel, 6/1/98, (PB99-118853, A09, MF-A02).

MCEER-98-0004 "Evaluation of Bridge Damage Data from the Loma Prieta and Northridge, California Earthquakes," by N. Basoz and A. Kiremidjian, 6/2/98, (PB99-118861, A15, MF-A03).

MCEER-98-0005 "Screening Guide for Rapid Assessment of Liquefaction Hazard at Highway Bridge Sites," by T. L. Youd, 6/16/98, (PB99-118879, A06, not available on microfiche).

MCEER-98-0006 "Structural Steel and Steel/Concrete Interface Details for Bridges," by P. Ritchie, N. Kauhl and J. Kulicki, 7/13/98, (PB99-118945, A06, MF-A01).

MCEER-98-0007 "Capacity Design and Fatigue Analysis of Confined Concrete Columns," by A. Dutta and J.B. Mander, 7/14/98, (PB99-118960, A14, MF-A03).

MCEER-98-0008 "Proceedings of the Workshop on Performance Criteria for Telecommunication Services Under Earthquake Conditions," edited by A.J. Schiff, 7/15/98, (PB99-118952, A08, MF-A02).

MCEER-98-0009 "Fatigue Analysis of Unconfined Concrete Columns," by J.B. Mander, A. Dutta and J.H. Kim, 9/12/98, (PB99-123655, A10, MF-A02).

MCEER-98-0010 "Centrifuge Modeling of Cyclic Lateral Response of Pile-Cap Systems and Seat-Type Abutments in Dry Sands," by A.D. Gadre and R. Dobry, 10/2/98, (PB99-123606, A13, MF-A03).

MCEER-98-0011 "IDARC-BRIDGE: A Computational Platform for Seismic Damage Assessment of Bridge Structures," by A.M. Reinhorn, V. Simeonov, G. Mylonakis and Y. Reichman, 10/2/98, (PB99-162919, A15, MF-A03).

MCEER-98-0012 "Experimental Investigation of the Dynamic Response of Two Bridges Before and After Retrofitting with Elastomeric Bearings," by D.A. Wendichansky, S.S. Chen and J.B. Mander, 10/2/98, (PB99-162927, A15, MF-A03).

MCEER-98-0013 "Design Procedures for Hinge Restrainers and Hinge Sear Width for Multiple-Frame Bridges," by R. Des Roches and G.L. Fenves, 11/3/98, (PB99-140477, A13, MF-A03).

MCEER-98-0014 "Response Modification Factors for Seismically Isolated Bridges," by M.C. Constantinou and J.K. Quarshie, 11/3/98, (PB99-140485, A14, MF-A03).

MCEER-98-0015 "Proceedings of the U.S.-Italy Workshop on Seismic Protective Systems for Bridges," edited by I.M. Friedland and M.C. Constantinou, 11/3/98, (PB2000-101711, A22, MF-A04).

MCEER-98-0016 "Appropriate Seismic Reliability for Critical Equipment Systems: Recommendations Based on Regional Analysis of Financial and Life Loss," by K. Porter, C. Scawthorn, C. Taylor and N. Blais, 11/10/98, (PB99-157265, A08, MF-A02).

MCEER-98-0017 "Proceedings of the U.S. Japan Joint Seminar on Civil Infrastructure Systems Research," edited by M. Shinozuka and A. Rose, 11/12/98, (PB99-156713, A16, MF-A03).

MCEER-98-0018 "Modeling of Pile Footings and Drilled Shafts for Seismic Design," by I. PoLam, M. Kapuskar and D. Chaudhuri, 12/21/98, (PB99-157257, A09, MF-A02).

MCEER-99-0001   "Seismic Evaluation of a Masonry Infilled Reinforced Concrete Frame by Pseudodynamic Testing," by S.G. Buonopane and R.N. White, 2/16/99, (PB99-162851, A09, MF-A02).

MCEER-99-0002   "Response History Analysis of Structures with Seismic Isolation and Energy Dissipation Systems: Verification Examples for Program SAP2000," by J. Scheller and M.C. Constantinou, 2/22/99, (PB99-162869, A08, MF-A02).

MCEER-99-0003   "Experimental Study on the Seismic Design and Retrofit of Bridge Columns Including Axial Load Effects," by A. Dutta, T. Kokorina and J.B. Mander, 2/22/99, (PB99-162877, A09, MF-A02).

MCEER-99-0004   "Experimental Study of Bridge Elastomeric and Other Isolation and Energy Dissipation Systems with Emphasis on Uplift Prevention and High Velocity Near-source Seismic Excitation," by A. Kasalanati and M. C. Constantinou, 2/26/99, (PB99-162885, A12, MF-A03).

MCEER-99-0005   "Truss Modeling of Reinforced Concrete Shear-flexure Behavior," by J.H. Kim and J.B. Mander, 3/8/99, (PB99-163693, A12, MF-A03).

MCEER-99-0006   "Experimental Investigation and Computational Modeling of Seismic Response of a 1:4 Scale Model Steel Structure with a Load Balancing Supplemental Damping System," by G. Pekcan, J.B. Mander and S.S. Chen, 4/2/99, (PB99-162893, A11, MF-A03).

MCEER-99-0007   "Effect of Vertical Ground Motions on the Structural Response of Highway Bridges," by M.R. Button, C.J. Cronin and R.L. Mayes, 4/10/99, (PB2000-101411, A10, MF-A03).

MCEER-99-0008   "Seismic Reliability Assessment of Critical Facilities: A Handbook, Supporting Documentation, and Model Code Provisions," by G.S. Johnson, R.E. Sheppard, M.D. Quilici, S.J. Eder and C.R. Scawthorn, 4/12/99, (PB2000-101701, A18, MF-A04).

MCEER-99-0009   "Impact Assessment of Selected MCEER Highway Project Research on the Seismic Design of Highway Structures," by C. Rojahn, R. Mayes, D.G. Anderson, J.H. Clark, D'Appolonia Engineering, S. Gloyd and R.V. Nutt, 4/14/99, (PB99-162901, A10, MF-A02).

MCEER-99-0010   "Site Factors and Site Categories in Seismic Codes," by R. Dobry, R. Ramos and M.S. Power, 7/19/99, (PB2000-101705, A08, MF-A02).

MCEER-99-0011   "Restrainer Design Procedures for Multi-Span Simply-Supported Bridges," by M.J. Randall, M. Saiidi, E. Maragakis and T. Isakovic, 7/20/99, (PB2000-101702, A10, MF-A02).

MCEER-99-0012   "Property Modification Factors for Seismic Isolation Bearings," by M.C. Constantinou, P. Tsopelas, A. Kasalanati and E. Wolff, 7/20/99, (PB2000-103387, A11, MF-A03).

MCEER-99-0013   "Critical Seismic Issues for Existing Steel Bridges," by P. Ritchie, N. Kauhl and J. Kulicki, 7/20/99, (PB2000-101697, A09, MF-A02).

MCEER-99-0014   "Nonstructural Damage Database," by A. Kao, T.T. Soong and A. Vender, 7/24/99, (PB2000-101407, A06, MF-A01).

MCEER-99-0015   "Guide to Remedial Measures for Liquefaction Mitigation at Existing Highway Bridge Sites," by H.G. Cooke and J. K. Mitchell, 7/26/99, (PB2000-101703, A11, MF-A03).

MCEER-99-0016   "Proceedings of the MCEER Workshop on Ground Motion Methodologies for the Eastern United States," edited by N. Abrahamson and A. Becker, 8/11/99, (PB2000-103385, A07, MF-A02).

MCEER-99-0017   "Quindío, Colombia Earthquake of January 25, 1999: Reconnaissance Report," by A.P. Asfura and P.J. Flores, 10/4/99, (PB2000-106893, A06, MF-A01).

MCEER-99-0018   "Hysteretic Models for Cyclic Behavior of Deteriorating Inelastic Structures," by M.V. Sivaselvan and A.M. Reinhorn, 11/5/99, (PB2000-103386, A08, MF-A02).

MCEER-99-0019   "Proceedings of the 7th U.S.- Japan Workshop on Earthquake Resistant Design of Lifeline Facilities and Countermeasures Against Soil Liquefaction," edited by T.D. O'Rourke, J.P. Bardet and M. Hamada, 11/19/99, (PB2000-103354, A99, MF-A06).

MCEER-99-0020   "Development of Measurement Capability for Micro-Vibration Evaluations with Application to Chip Fabrication Facilities," by G.C. Lee, Z. Liang, J.W. Song, J.D. Shen and W.C. Liu, 12/1/99, (PB2000-105993, A08, MF-A02).

MCEER-99-0021   "Design and Retrofit Methodology for Building Structures with Supplemental Energy Dissipating Systems," by G. Pekcan, J.B. Mander and S.S. Chen, 12/31/99, (PB2000-105994, A11, MF-A03).

MCEER-00-0001   "The Marmara, Turkey Earthquake of August 17, 1999: Reconnaissance Report," edited by C. Scawthorn; with major contributions by M. Bruneau, R. Eguchi, T. Holzer, G. Johnson, J. Mander, J. Mitchell, W. Mitchell, A. Papageorgiou, C. Scaethorn, and G. Webb, 3/23/00, (PB2000-106200, A11, MF-A03).

MCEER-00-0002   "Proceedings of the MCEER Workshop for Seismic Hazard Mitigation of Health Care Facilities," edited by G.C. Lee, M. Ettouney, M. Grigoriu, J. Hauer and J. Nigg, 3/29/00, (PB2000-106892, A08, MF-A02).

MCEER-00-0003   "The Chi-Chi, Taiwan Earthquake of September 21, 1999: Reconnaissance Report," edited by G.C. Lee and C.H. Loh, with major contributions by G.C. Lee, M. Bruneau, I.G. Buckle, S.E. Chang, P.J. Flores, T.D. O'Rourke, M. Shinozuka, T.T. Soong, C-H. Loh, K-C. Chang, Z-J. Chen, J-S. Hwang, M-L. Lin, G-Y. Liu, K-C. Tsai, G.C. Yao and C-L. Yen, 4/30/00, (PB2001-100980, A10, MF-A02).

MCEER-00-0004   "Seismic Retrofit of End-Sway Frames of Steel Deck-Truss Bridges with a Supplemental Tendon System: Experimental and Analytical Investigation," by G. Pekcan, J.B. Mander and S.S. Chen, 7/1/00, (PB2001-100982, A10, MF-A02).

MCEER-00-0005   "Sliding Fragility of Unrestrained Equipment in Critical Facilities," by W.H. Chong and T.T. Soong, 7/5/00, (PB2001-100983, A08, MF-A02).

MCEER-00-0006   "Seismic Response of Reinforced Concrete Bridge Pier Walls in the Weak Direction," by N. Abo-Shadi, M. Saiidi and D. Sanders, 7/17/00, (PB2001-100981, A17, MF-A03).

MCEER-00-0007   "Low-Cycle Fatigue Behavior of Longitudinal Reinforcement in Reinforced Concrete Bridge Columns," by J. Brown and S.K. Kunnath, 7/23/00, (PB2001-104392, A08, MF-A02).

MCEER-00-0008   "Soil Structure Interaction of Bridges for Seismic Analysis," I. PoLam and H. Law, 9/25/00, (PB2001-105397, A08, MF-A02).

MCEER-00-0009   "Proceedings of the First MCEER Workshop on Mitigation of Earthquake Disaster by Advanced Technologies (MEDAT-1), edited by M. Shinozuka, D.J. Inman and T.D. O'Rourke, 11/10/00, (PB2001-105399, A14, MF-A03).

MCEER-00-0010   "Development and Evaluation of Simplified Procedures for Analysis and Design of Buildings with Passive Energy Dissipation Systems," by O.M. Ramirez, M.C. Constantinou, C.A. Kircher, A.S. Whittaker, M.W. Johnson, J.D. Gomez and C. Chrysostomou, 11/16/01, (PB2001-105523, A23, MF-A04).

MCEER-00-0011   "Dynamic Soil-Foundation-Structure Interaction Analyses of Large Caissons," by C-Y. Chang, C-M. Mok, Z-L. Wang, R. Settgast, F. Waggoner, M.A. Ketchum, H.M. Gonnermann and C-C. Chin, 12/30/00, (PB2001-104373, A07, MF-A02).

MCEER-00-0012   "Experimental Evaluation of Seismic Performance of Bridge Restrainers," by A.G. Vlassis, E.M. Maragakis and M. Saiid Saiidi, 12/30/00, (PB2001-104354, A09, MF-A02).

MCEER-00-0013   "Effect of Spatial Variation of Ground Motion on Highway Structures," by M. Shinozuka, V. Saxena and G. Deodatis, 12/31/00, (PB2001-108755, A13, MF-A03).

MCEER-00-0014   "A Risk-Based Methodology for Assessing the Seismic Performance of Highway Systems," by S.D. Werner, C.E. Taylor, J.E. Moore, II, J.S. Walton and S. Cho, 12/31/00, (PB2001-108756, A14, MF-A03).

MCEER-01-0001	"Experimental Investigation of P-Delta Effects to Collapse During Earthquakes," by D. Vian and M. Bruneau, 6/25/01, (PB2002-100534, A17, MF-A03).

MCEER-01-0002	"Proceedings of the Second MCEER Workshop on Mitigation of Earthquake Disaster by Advanced Technologies (MEDAT-2)," edited by M. Bruneau and D.J. Inman, 7/23/01, (PB2002-100434, A16, MF-A03).

MCEER-01-0003	"Sensitivity Analysis of Dynamic Systems Subjected to Seismic Loads," by C. Roth and M. Grigoriu, 9/18/01, (PB2003-100884, A12, MF-A03).

MCEER-01-0004	"Overcoming Obstacles to Implementing Earthquake Hazard Mitigation Policies: Stage 1 Report," by D.J. Alesch and W.J. Petak, 12/17/01, (PB2002-107949, A07, MF-A02).

MCEER-01-0005	"Updating Real-Time Earthquake Loss Estimates: Methods, Problems and Insights," by C.E. Taylor, S.E. Chang and R.T. Eguchi, 12/17/01, (PB2002-107948, A05, MF-A01).

MCEER-01-0006	"Experimental Investigation and Retrofit of Steel Pile Foundations and Pile Bents Under Cyclic Lateral Loadings," by A. Shama, J. Mander, B. Blabac and S. Chen, 12/31/01, (PB2002-107950, A13, MF-A03).

MCEER-02-0001	"Assessment of Performance of Bolu Viaduct in the 1999 Duzce Earthquake in Turkey" by P.C. Roussis, M.C. Constantinou, M. Erdik, E. Durukal and M. Dicleli, 5/8/02, (PB2003-100883, A08, MF-A02).

MCEER-02-0002	"Seismic Behavior of Rail Counterweight Systems of Elevators in Buildings," by M.P. Singh, Rildova and L.E. Suarez, 5/27/02. (PB2003-100882, A11, MF-A03).

MCEER-02-0003	"Development of Analysis and Design Procedures for Spread Footings," by G. Mylonakis, G. Gazetas, S. Nikolaou and A. Chauncey, 10/02/02, (PB2004-101636, A13, MF-A03, CD-A13).

MCEER-02-0004	"Bare-Earth Algorithms for Use with SAR and LIDAR Digital Elevation Models," by C.K. Huyck, R.T. Eguchi and B. Houshmand, 10/16/02, (PB2004-101637, A07, CD-A07).

MCEER-02-0005	"Review of Energy Dissipation of Compression Members in Concentrically Braced Frames," by K.Lee and M. Bruneau, 10/18/02, (PB2004-101638, A10, CD-A10).

MCEER-03-0001	"Experimental Investigation of Light-Gauge Steel Plate Shear Walls for the Seismic Retrofit of Buildings" by J. Berman and M. Bruneau, 5/2/03, (PB2004-101622, A10, MF-A03, CD-A10).

MCEER-03-0002	"Statistical Analysis of Fragility Curves," by M. Shinozuka, M.Q. Feng, H. Kim, T. Uzawa and T. Ueda, 6/16/03, (PB2004-101849, A09, CD-A09).

MCEER-03-0003	"Proceedings of the Eighth U.S.-Japan Workshop on Earthquake Resistant Design f Lifeline Facilities and Countermeasures Against Liquefaction," edited by M. Hamada, J.P. Bardet and T.D. O'Rourke, 6/30/03, (PB2004-104386, A99, CD-A99).

MCEER-03-0004	"Proceedings of the PRC-US Workshop on Seismic Analysis and Design of Special Bridges," edited by L.C. Fan and G.C. Lee, 7/15/03, (PB2004-104387, A14, CD-A14).

MCEER-03-0005	"Urban Disaster Recovery: A Framework and Simulation Model," by S.B. Miles and S.E. Chang, 7/25/03, (PB2004-104388, A07, CD-A07).

MCEER-03-0006	"Behavior of Underground Piping Joints Due to Static and Dynamic Loading," by R.D. Meis, M. Maragakis and R. Siddharthan, 11/17/03, (PB2005-102194, A13, MF-A03, CD-A00).

MCEER-03-0007	"Seismic Vulnerability of Timber Bridges and Timber Substructures," by A.A. Shama, J.B. Mander, I.M. Friedland and D.R. Allicock, 12/15/03.

MCEER-04-0001	"Experimental Study of Seismic Isolation Systems with Emphasis on Secondary System Response and Verification of Accuracy of Dynamic Response History Analysis Methods," by E. Wolff and M. Constantinou, 1/16/04 (PB2005-102195, A99, MF-E08, CD-A00).

MCEER-04-0002   "Tension, Compression and Cyclic Testing of Engineered Cementitious Composite Materials," by K. Kesner and S.L. Billington, 3/1/04, (PB2005-102196, A08, CD-A08).

MCEER-04-0003   "Cyclic Testing of Braces Laterally Restrained by Steel Studs to Enhance Performance During Earthquakes," by O.C. Celik, J.W. Berman and M. Bruneau, 3/16/04, (PB2005-102197, A13, MF-A03, CD-A00).

MCEER-04-0004   "Methodologies for Post Earthquake Building Damage Detection Using SAR and Optical Remote Sensing: Application to the August 17, 1999 Marmara, Turkey Earthquake," by C.K. Huyck, B.J. Adams, S. Cho, R.T. Eguchi, B. Mansouri and B. Houshmand, 6/15/04, (PB2005-104888, A10, CD-A00).

MCEER-04-0005   "Nonlinear Structural Analysis Towards Collapse Simulation: A Dynamical Systems Approach," by M.V. Sivaselvan and A.M. Reinhorn, 6/16/04, (PB2005-104889, A11, MF-A03, CD-A00).

MCEER-04-0006   "Proceedings of the Second PRC-US Workshop on Seismic Analysis and Design of Special Bridges," edited by G.C. Lee and L.C. Fan, 6/25/04, (PB2005-104890, A16, CD-A00).

MCEER-04-0007   "Seismic Vulnerability Evaluation of Axially Loaded Steel Built-up Laced Members," by K. Lee and M. Bruneau, 6/30/04, (PB2005-104891, A16, CD-A00).

MCEER-04-0008   "Evaluation of Accuracy of Simplified Methods of Analysis and Design of Buildings with Damping Systems for Near-Fault and for Soft-Soil Seismic Motions," by E.A. Pavlou and M.C. Constantinou, 8/16/04, (PB2005-104892, A08, MF-A02, CD-A00).

MCEER-04-0009   "Assessment of Geotechnical Issues in Acute Care Facilities in California," by M. Lew, T.D. O'Rourke, R. Dobry and M. Koch, 9/15/04, (PB2005-104893, A08, CD-A00).

MCEER-04-0010   "Scissor-Jack-Damper Energy Dissipation System," by A.N. Sigaher-Boyle and M.C. Constantinou, 12/1/04 (PB2005-108221).

MCEER-04-0011   "Seismic Retrofit of Bridge Steel Truss Piers Using a Controlled Rocking Approach," by M. Pollino and M. Bruneau, 12/20/04 (PB2006-105795).

MCEER-05-0001   "Experimental and Analytical Studies of Structures Seismically Isolated with an Uplift-Restraint Isolation System," by P.C. Roussis and M.C. Constantinou, 1/10/05 (PB2005-108222).

MCEER-05-0002   "A Versatile Experimentation Model for Study of Structures Near Collapse Applied to Seismic Evaluation of Irregular Structures," by D. Kusumastuti, A.M. Reinhorn and A. Rutenberg, 3/31/05 (PB2006-101523).

MCEER-05-0003   "Proceedings of the Third PRC-US Workshop on Seismic Analysis and Design of Special Bridges," edited by L.C. Fan and G.C. Lee, 4/20/05, (PB2006-105796).

MCEER-05-0004   "Approaches for the Seismic Retrofit of Braced Steel Bridge Piers and Proof-of-Concept Testing of an Eccentrically Braced Frame with Tubular Link," by J.W. Berman and M. Bruneau, 4/21/05 (PB2006-101524).

MCEER-05-0005   "Simulation of Strong Ground Motions for Seismic Fragility Evaluation of Nonstructural Components in Hospitals," by A. Wanitkorkul and A. Filiatrault, 5/26/05 (PB2006-500027).

MCEER-05-0006   "Seismic Safety in California Hospitals: Assessing an Attempt to Accelerate the Replacement or Seismic Retrofit of Older Hospital Facilities," by D.J. Alesch, L.A. Arendt and W.J. Petak, 6/6/05 (PB2006-105794).

MCEER-05-0007   "Development of Seismic Strengthening and Retrofit Strategies for Critical Facilities Using Engineered Cementitious Composite Materials," by K. Kesner and S.L. Billington, 8/29/05 (PB2006-111701).

MCEER-05-0008   "Experimental and Analytical Studies of Base Isolation Systems for Seismic Protection of Power Transformers," by N. Murota, M.Q. Feng and G-Y. Liu, 9/30/05 (PB2006-111702).

MCEER-05-0009   "3D-BASIS-ME-MB: Computer Program for Nonlinear Dynamic Analysis of Seismically Isolated Structures," by P.C. Tsopelas, P.C. Roussis, M.C. Constantinou, R. Buchanan and A.M. Reinhorn, 10/3/05 (PB2006-111703).

MCEER-05-0010   "Steel Plate Shear Walls for Seismic Design and Retrofit of Building Structures," by D. Vian and M. Bruneau, 12/15/05 (PB2006-111704).

MCEER-05-0011   "The Performance-Based Design Paradigm," by M.J. Astrella and A. Whittaker, 12/15/05 (PB2006-111705).

MCEER-06-0001   "Seismic Fragility of Suspended Ceiling Systems," H. Badillo-Almaraz, A.S. Whittaker, A.M. Reinhorn and G.P. Cimellaro, 2/4/06 (PB2006-111706).

MCEER-06-0002   "Multi-Dimensional Fragility of Structures," by G.P. Cimellaro, A.M. Reinhorn and M. Bruneau, 3/1/06 (PB2007-106974, A09, MF-A02, CD A00).

MCEER-06-0003   "Built-Up Shear Links as Energy Dissipators for Seismic Protection of Bridges," by P. Dusicka, A.M. Itani and I.G. Buckle, 3/15/06 (PB2006-111708).

MCEER-06-0004   "Analytical Investigation of the Structural Fuse Concept," by R.E. Vargas and M. Bruneau, 3/16/06 (PB2006-111709).

MCEER-06-0005   "Experimental Investigation of the Structural Fuse Concept," by R.E. Vargas and M. Bruneau, 3/17/06 (PB2006-111710).

MCEER-06-0006   "Further Development of Tubular Eccentrically Braced Frame Links for the Seismic Retrofit of Braced Steel Truss Bridge Piers," by J.W. Berman and M. Bruneau, 3/27/06 (PB2007-105147).

MCEER-06-0007   "REDARS Validation Report," by S. Cho, C.K. Huyck, S. Ghosh and R.T. Eguchi, 8/8/06 (PB2007-106983).

MCEER-06-0008   "Review of Current NDE Technologies for Post-Earthquake Assessment of Retrofitted Bridge Columns," by J.W. Song, Z. Liang and G.C. Lee, 8/21/06 06 (PB2007-106984).

MCEER-06-0009   "Liquefaction Remediation in Silty Soils Using Dynamic Compaction and Stone Columns," by S. Thevanayagam, G.R. Martin, R. Nashed, T. Shenthan, T. Kanagalingam and N. Ecemis, 8/28/06 06 (PB2007-106985).

MCEER-06-0010   "Conceptual Design and Experimental Investigation of Polymer Matrix Composite Infill Panels for Seismic Retrofitting," by W. Jung, M. Chiewanichakorn and A.J. Aref, 9/21/06 (PB2007-106986).

MCEER-06-0011   "A Study of the Coupled Horizontal-Vertical Behavior of Elastomeric and Lead-Rubber Seismic Isolation Bearings," by G.P. Warn and A.S. Whittaker, 9/22/06 (PB2007-108679).

MCEER-06-0012   "Proceedings of the Fourth PRC-US Workshop on Seismic Analysis and Design of Special Bridges: Advancing Bridge Technologies in Research, Design, Construction and Preservation," Edited by L.C. Fan, G.C. Lee and L. Ziang, 10/12/06.

MCEER-06-0013   "Cyclic Response and Low Cycle Fatigue Characteristics of Plate Steels," by P. Dusicka, A.M. Itani and I.G. Buckle, 11/1/06 06 (PB2007-106987).

MCEER-06-0014   "Proceedings of the Second US-Taiwan Bridge Engineering Workshop," edited by W.P. Yen, J. Shen, J-Y. Chen and M. Wang, 11/15/06.

MCEER-06-0015   "User Manual and Technical Documentation for the REDARS™ Import Wizard," by S. Cho, S. Ghosh, C.K. Huyck and S.D. Werner, 11/30/06.

MCEER-06-0016   "Hazard Mitigation Strategy and Monitoring Technologies for Urban and Infrastructure Public Buildings: Proceedings of the China-US Workshops," edited by X.Y. Zhou, A.L. Zhang, G.C. Lee and M. Tong, 12/12/06.

MCEER-07-0001   "Static and Kinetic Coefficients of Friction for Rigid Blocks," by C. Kafali, S. Fathali, M. Grigoriu and A.S. Whittaker, 3/20/07.

MCEER-07-0002   "Hazard Mitigation Investment Decision Making: Organizational Response to Legislative Mandate," by L.A. Arendt, D.J. Alesch and W.J. Petak, 4/9/07.

MCEER-07-0003 "Seismic Behavior of Bidirectional-Resistant Ductile End Diaphragms with Unbonded Braces in Straight or Skewed Steel Bridges," by O. Celik and M. Bruneau, 4/11/07.

MCEER-07-0004 "Modeling Pile Behavior in Large Pile Groups Under Lateral Loading," by A.M. Dodds and G.R. Martin, 4/16/07.